

Syracuse University

SURFACE

Electrical Engineering and Computer Science -
Dissertations

College of Engineering and Computer Science

6-2012

Method of Moment Analysis of Partially Shielded Chiral Bodies of Revolution

Khaja Qutubuddin
Syracuse University

Follow this and additional works at: https://surface.syr.edu/eecs_etd



Part of the [Engineering Commons](#)

Recommended Citation

Qutubuddin, Khaja, "Method of Moment Analysis of Partially Shielded Chiral Bodies of Revolution" (2012). *Electrical Engineering and Computer Science - Dissertations*. 318.
https://surface.syr.edu/eecs_etd/318

This Dissertation is brought to you for free and open access by the College of Engineering and Computer Science at SURFACE. It has been accepted for inclusion in Electrical Engineering and Computer Science - Dissertations by an authorized administrator of SURFACE. For more information, please contact surface@syr.edu.

ABSTRACT

A chiral body of revolution (BOR) which is partially covered by a thin conducting shield is analyzed using the method of moments (MOM). The axisymmetric system is excited by a plane wave. The total internal fields and the far scattered fields are computed. The problem is solved using the surface equivalence principle. The scattered fields outside the structure are assumed to be produced by an equivalent magnetic surface current that exists on the unshielded part of the BOR surface and an external equivalent electric surface current that exists over all of the BOR surface S . These two currents are assumed to radiate in the unbounded external medium. Similarly, the total internal fields are assumed to be produced by the negative of the above magnetic current and an internal equivalent electric surface current that exists over all of the BOR surface, but is the negative of an independent unknown only on the shielded part of S . These two currents radiate in the unbounded internal medium. Enforcing continuity of the tangential components of total electric field (\mathbf{E}) and total magnetic field (\mathbf{H}) on S gives a two coupled integral equations for the two unknown surface currents. The two unknown surface currents are the external equivalent electric surface current and the union of magnetic current (\mathbf{M}) on the unshielded part of S and the negative of the internal equivalent electric surface current on the shielded part of S . The method of moments as applied to bodies of revolution is used to solve these integral equations numerically. Piecewise linear variation of the currents is assumed along the generating curve of the BOR. The variation of the currents along the circumferential direction is represented by Fourier series. An approximate Galerkin's method is used for testing. Conical and spherical BORs are studied. Computed results for the partially shielded spherical chiral body are in excellent agreement with other data.

Theoretical framework developed in chapters two through six factually validated the underlying firm foundation of mathematical physics and sound computational electromagnetic methods of our theory by producing correct scattered fields and radar cross sections of the chiral and perfectly conducting sphere, chiral and perfectly conducting cylinder, chiral and perfectly conducting cone. Chapter seven demonstrates the soundness of the theoretical foundation of this thesis by producing computed results and graphs of not only the case of a perfectly conducting sphere, cylinder and cone but those of the chiral sphere, chiral cylinder, and chiral cone and those of the chiral sphere, chiral cylinder and chiral cone partially covered by rotationally symmetric perfectly conducting surface. The computed results and graphs obtained in chapter seven by the application of our theoretical framework were almost one hundred percent accurate with respect to the conformability of our graph mappings, form of our graphs and accuracy of our graph readings with respect to analytically calculated results and graphs. Our computed results and graphs with respect to the computed results and graphs of early research works that used numerical approach distinctly different than ours were in good agreement.

Partially Shielded Chiral Bodies of Revolution

By

Khaja Qutubuddin

B.Sc. in Mathematics, Osmania University, India

B.E. in Mechanical Engineering, Osmania University, India

M.S. in Engineering Science, Florida State University

Computer Engineer, in Computer Engineering, Syracuse University

DISSERTATION

Submitted in partial fulfillment of the requirements for the degree
of Doctor of Philosophy in Electrical Engineering
in the Graduate School of Syracuse University.

June 2012

© Copyright 2012 Khaja Qutubuddin

All rights reserved.

Acknowledgements

The Electrical Engineering Department of Syracuse University maintains its proud tradition of research in the fields of Electromagnetic theory, Microwave Engineering and Computational Electromagnetics, since the time of esteemed Professor Harrington.

Professor Harrington, who served in the Electrical Engineering Department of Syracuse University for a number of years, pioneered method of moments (MoM) based on sound electromagnetic theory and more generally, method of mathematical physics, in particular, variational calculus. He coined the name 'method of moments (MoM)', and the name caught on quickly. His classic texts on time-harmonic fields titled '*Time-Harmonic Electromagnetic Fields*' and '*Field Computation by Moment Methods*' are still very widely used and referenced all over the world.

Exceptionally erudite professors and researchers, particularly, Dr. Arvas and Dr. Mautz, among others in this department, wrote and published a number of elegant research papers characterized by power of origination which have been widely referenced in the electromagnetic fields of study. They have conducted and supervised many Doctoral researches of their students.

It is humbling to have Dr. Ercument Arvas and Dr. Joseph R. Mautz to be my Doctoral Research advisor and co-advisor.

I owe many debts of gratitude to Dr. Arvas and Dr. Mautz for providing a supportive intellectual environment and so much kindness, patience, guidance, understanding, and encouragement which enabled me to complete this Doctoral research.

I am enormously indebted to Dr. Mautz for skillfully and very patiently guiding me through, what appeared at times to be arduous and insurmountable task, of the programming aspect of this thesis.

Dedication

According to Chinese philosophical thought, blades of grass can never return back warmth of immeasurable radiant sunlight they receive for their nurture and growth.

In complete analogy to this saying, my indebtedness to my parents, who gave me anchors of faith, taught me important moral values, struggled very hard to provide me the best education, empowered me with wings, encouragement, direction and prayers, can never be returned by me. Their endeavors and struggle to see that I could fly aloft to the zenith of the skies and reach the stars remains immeasurable and beyond gratitude.

I also owe profound debt to my remarkable wife as well. Humility, gentleness, patience and serenity were hallmarks of her character. She remained my inspiration, backbone and unfaltering support when my free time turned into research time.

With humble gratitude, I dedicate this Doctoral Dissertation to the loving memory of my father, Khaja Moinuddin, mother, Sardar Begum, and wife Sabiha Sayeed Qutubuddin.

TABLE OF CONTENTS

ACKNOWLEDGEMENTS	IV
DEDICATION	V
LIST OF FIGURES	XIV
Chapter 1	
1- Introduction	1
1.1 Body of revolution (BOR)	3
1.2 Complicated shaped bodies of revolution	4
1.3 Motivation Obtained From Previous Research Work	4
1.4 Organization of the Dissertation	11
Chapter 2	
Integral Equations and the Moment Matrix Equation	15
2.1 Introduction	15
2.2 Integral Equations	15
2.3 Expansion of the electric and magnetic currents	21
2.4 Testing functions	25
Chapter 3	
The Elements of Moment Matrix	30
3.1 Introduction	30

3.2	Analytical Treatment of Expressions (2.51)–(2.53) for the Z 's and Y 's	30
3.3	The Z 's and Y 's Expressed as Summations	38
3.4	Properties of the Z 's and Y 's of (3.74)–(3.81) and (3.109)–(3.112)	42

Chapter 4

	Planer Wave Excitation	46
4.1	Introduction	46
4.2	\vec{V}_{ni}^{pq} and \vec{I}_{ni}^{pq} expressed as integrals	46
4.3	$\vec{V}_{ni}^{t\theta}$	48
4.4	$\vec{V}_{ni}^{\phi\theta}$	50
4.5	$\vec{I}_{ni}^{t\theta}$	51
4.6	$\vec{I}_{ni}^{\phi\theta}$	52
4.7	$\vec{V}_{ni}^{t\phi}$, $\vec{V}_{ni}^{\phi\phi}$, $\vec{I}_{ni}^{t\phi}$, and $\vec{I}_{ni}^{\phi\phi}$	52
4.8	Calculation of $\vec{V}_{ni}^{t\theta}$, $\vec{V}_{ni}^{\phi\theta}$, $\vec{I}_{ni}^{t\theta}$, $\vec{I}_{ni}^{\phi\theta}$, $\vec{V}_{ni}^{t\phi}$, $\vec{V}_{ni}^{\phi\phi}$, $\vec{I}_{ni}^{t\phi}$, and $\vec{I}_{ni}^{\phi\phi}$	53

Chapter 5

	Scattered Field Far from the Scatterer	55
5.1	Introduction	55
5.2	Reciprocity	55

5.3	The θ -Component of the Scattered Field	56
5.4	Evaluation of the First Integral in (5.15)	57
5.5	Evaluation of Second Integral in (5.15)	59
5.6	Evaluation of Third Integral in (5.15)	60
5.7	Evaluation of Fourth Integral in (5.17)	61
5.8	The ϕ -component of the Scattered Field	63
5.9	Use of the Four Integrals That Were Previously Evaluated	63
5.10	Scattering Cross Section	64
Chapter 6		
	The Electromagnetic Field Inside the Scatterer	66
6.1	Introduction	66
6.2	General Form of the Solution for the Electromagnetic Field Inside the Scatterer	66
6.3	Use of the Wavefield Decomposition in (6.3) and (6.4)	67
6.4	Evaluation of the \mathbf{Z} 's and \mathbf{Y} 's of (6.16) and (6.17)	70
6.4.1	The Vectors on the Right-Hand Sides of (6.37)–(6.40)	72
6.4.2	The ρ -, ϕ -, and z -Components of the \mathbf{Z} 's	

and Y 's of (6.37)–(6.40)	76
6.5 The Cylindrical and Rectangular Components of the Electromagnetic Field ($\mathbf{E}_i, \mathbf{H}_i$) Inside the Scatterer	82
6.5.1 The Cylindrical Components of the Inside Electromagnetic Field	82
6.5.2 The Rectangular Components of the Inside Electromagnetic Field	85
6.6 The Special Case Where the Electromagnetic Field Inside the Scatterer is Observed on the z -Axis	86
6.6.1 Properties of the Fourier Coefficients of the Cylindrical and Rectangular Components of the Inside Electromagnetic Field on the z -Axis	88
Chapter 7	
Computed Results	93
7-1 Chiral sphere	93
7-2.1 Computed Results	94
7-2.2 Characteristic Graphs of the Chiral Sphere	94
7-3 Conducting Sphere	102
7-3.1 Characteristic Graphs of the Conducting Sphere	103

7-4	Spherical-shaped Perfectly Conducting BOR	
	enclosing Chiral material with an Aperture	
	of 30 degrees at its bottom	105
7-4.1	Computed Results	106
7-4.2	chirality vs. surface currents	109
7-4.3	Computed results of the Chirality vs. Bistatic RCS	117
7-4.4	Chirality vs. Bistatic Radar	
	Cross Sections (RCS)	117
7-4.5	Computed Results of the Internal fields	121
7-4.6	Internal fields	121
7-5	Cylinder	125
7-5.1	A Cylinder and its Generating Curve	125
7-6	A Chiral Cylinder	126
7-6.1	Computed Results of the Internal Fields	127
7-6.2	Internal Fields	128
7-6.3	Bistatic Radar Cross Sections (RCS)	131
7-6.4	Surface currents	132
7-7	Empty Conductor Cylindrical Shell with an Aperture	136
7-8	Cylinder-shaped Perfectly Conducting Metallic BOR enclosing	
	Chiral material with an Aperture ratio of $b/a = 0.5$ at its top	138
7-8.1	Computed Results	139

7-8.2	Internal fields	141
7-8.3	Chirality versus Bistatic Radar Cross Sections (RCS)	143
7-8.4	Chirality versus Surface Currents	145
7-9	Perfectly Conducting Cylindrical surface of revolution enclosing Chiral material with an Aperture ratio of $b/a = 1$ at its top	149
7-9.1	Computed Results	150
7-9.2	Internal Fields	152
7-9.3	Chirality versus Bistatic Cross Sections (RCS)	154
7-9.4	Chirality versus Surface Currents	156
7-10	Cone	160
7-10.1	Chiral Cone	160
7-10.2	Computed Results	161
7-10.3	Surface currents	161
7-10.4	Bistatic co-polarize and cross polarized RCS	166
7-11.1	Perfectly conducting metallic cone	167
7-11.2	surface currents and radar cross sections	168
7-12.1	Cone-shaped perfectly conducting metallic BOR enclosing chiral material with an Aperture of 0.5 meter at its bottom	169
7-12.2	Computed Results	170
7-12.3	Surface currents	170

7-12.4 Computed Results	174
7-12.5 Radar cross sections	174
7-12.6 Computed Results	175
7-12.7 Internal fields	176
Chapter 8	
Conclusion	179
Appendix A	
A-1.1 Equivalence Principle	183
A-1.1(a) Original Problem	183
A-1.1(b) External Equivalence	183
A-1.1(b) Internal Equivalence	188
Appendix B	
B-1.1 The Method of Moments (MoM)	191
B-1.2 Method of collocation (Point Matching)	192
B-1.3 Method of Weighted residuals	193
B-1.4 Choice of basis (expansion) and weighting (testing) functions	194
B-1.4(a) Piecewise uniform or pulse function	194
B-1.4(b) Triangular basis functions	195
B-1.5 Galerkin's method	200
B-1.6 Point Matching method	205

B-1.7	Triangular function	212
Appendix C		
C 3.1	Chiral media	232
C 3.2	Electromagnetic plane wave scattering and Maxwell's Equations	232
C 3.3	Electric and Magnetic Field Equations And Field Sources in Chiral Media	233
C 3.4	Electric and magnetic fields for electric (J) and magnetic (M) current sources	250
C 3.5	Electric and magnetic fields for electric (J) and magnetic (M) current sources in chiral media	252
Appendix D		266
Appendix E		279
	Interpretation of Any Approximate Solution of (2.5) and (2.6)	280
Bibliography		281
Vita		285

LIST OF FIGURES

Figure 1.1	A chiral body of revolution (BOR) with two apertures.....	1
Figure 1.2	A plane wave incident on a sphere with $\alpha = 30$ (degrees) aperture.....	2
Figure 1.1.1	Typical bodies of revolution.....	3
Figure 2.1	Original problem	16
Figure 2.2	External Equivalenc.	17
Figure 2.3	Internal Equivalence.....	19
Figure 2.4	Generating curve is approximated by seven straight line segments.....	.23
Figure 7.1.1	A chiral sphere is illuminated by a plane electromagnetic wave ($\mathbf{E}^{inc}, \mathbf{H}^{inc}$).....	93
Figure 7-2.2.1	$\sigma_{\theta\theta}$ of the chiral sphere.....	95
Figure 7-2.2.2	$\sigma_{\phi\theta}$ of the chiral sphere.....	95
Figure 7-2.2.3	$\sigma_{\theta\theta}$ of the chiral sphere. (Insert taken from Altunkilic [3]).....	96
Figure 7-2.2.4	$\sigma_{\phi\theta}$ of the chiral sphere. (Insert taken from Altunkilic [3]).....	96
Figure 7-2.2.5	Magnitude of θ -component of the external electric current in the $\phi = 0$ plane.....	97
Figure 7-2.2.6	Magnitude of θ -component of internal electric current in the $\phi = 0$ plane.....	97
Figure 7-2.2.7	Magnitude of θ -component of external and internal equivalent electric currents in the $\phi = 0$ plane (taken from Altunkilic [3]).....	98
Figure 7-2.2.8	Magnitude of θ -component of equivalent magnetic current in the $\phi = 0$ plane.....	99

Figure 7-2.2.9 Magnitude of θ -component of equivalent magnetic current in the $\phi = 0$ plane compared with the exact solution of chiral sphere (taken from Altunkilic [3]).....99

Figure 7-2.2.10 Magnitude of x-component of electric field external to the chiral sphere along the z-axis.....100

Figure 7-2.2.11 Magnitude of x-component of electric field internal to the chiral sphere along the z-axis (taken from Altunkilic [3]).....100

Figure 7-2.2.12 Magnitude of y-component of electric field internal to the chiral sphere along the z-axis (taken from Altunkilic [3])101

Figure 7-2.2.13 Magnitude of y-component of electric field internal to the chiral sphere along the z-axis (taken from Altunkilic [3]).....101

Figure 7-3.1 Perfectly conducting metallic spherical shell. This shell is illuminated b a plane electromagnetic wave.....102

Figure 7-3.2 Magnitude of θ -component of physical electric current in the $\phi = 0$ plane.....103

Figure 7-3.3 Magnitude of θ -component of physical electric current in the $\phi = 0$ plane compared with exact solution of the of conductor sphere (taken from Altunkilic [3])103

Figure 7-3.4 $\sigma_{\theta\theta}$ of the Metallic sphere.....104

Figure 7-4.1 Plane wave incident from the bottom of a perfectly conducting thin metallic shell that encloses chiral material in it.....105

Figure 7-4.2.1 Perfectly conducting metallic shell with an aperture of 30°

	at its bottom.....	108
Figure 7-4.2.2	Magnitude of θ -component of external equivalent current in the $\phi = 0$ plane.....	109
Figure 7-4.2.3	Magnitude of θ -component of external current in the $\phi = 0$ plane (taken from Altunkilic [3]).....	109
Figure 7-4.2.4	Magnitude of θ -component of internal equivalent current in the $\phi = 0$ plane.....	110
Figure 7-4.2.5	Magnitude of θ -component of internal equivalent electric current in the $\phi = 0$ plane (taken from Altunkilic [3]).....	110
Figure 7-4.2.6	Magnitude of θ -component of physical current in the $\phi = 0$ plane.....	111
Figure 7-4.2.7	Magnitude of θ -component of physical current in the $\phi = 0$ plane (taken from Altunkilic [3]).....	111
Figure 7-4.2.8	Magnitude of θ -component of equivalent magnetic current in the $\phi = 0$ plane.....	112
Figure 7-4.2.9	Magnitude of θ -component of equivalent magnetic current in the $\phi = 0$ plane (taken from Altunkilic [3]).....	113
Figure 7-4.2.10	Magnitude of ϕ -component of external equivalent electric current (varying chiralities) in the $\phi = 0$ plane.....	113
Figure 7-4.2.11	Magnitude of ϕ -component of external equivalent current in the $\phi = 0$ plane (taken from Altunkilic [3]).....	114
Figure 7-4.2.12	Magnitude of ϕ -component of internal equivalent electric current (varying chiralities) in the $\phi = 0$ plane.....	114

Figure 7-4.2.13	Magnitude of ϕ -component of internal equivalent electric current (varying chiralities) in the $\phi = 0$ plane (taken from Altunkilic [3])....	115
Figure 7-4.2.14	Magnitude of ϕ -component of physical current (varying chiralities) in the $\phi = 0$ plane.....	115
Figure 7-4.2.15	Magnitude of ϕ -component of physical current (varying chiralities) in the $\phi = 0$ plane (taken from Altunkilic [3])	116
Figure 7-4.2.16	Magnitude of ϕ -component of equivalent magnetic current (varying chiralities) in the $\phi = 0$ plane.....	116
Figure 7-4.2.17	Magnitude of ϕ -component of equivalent magnetic current (varying chiralities) in the $\phi = 0$ plane (taken from Altunkilic).....	117
Figure 7-4.4.1	$\sigma_{\theta\theta}$ of the obstacle (varying chiralities).....	118
Figure 7-4.4.2	$\sigma_{\theta\theta}$ of the obstacle (varying chiralities) (taken from Altunkilic [3]).....	118
Figure 7-4.4.3	$\sigma_{\phi\theta}$ of the obstacle (varying chiralities).....	119
Figure 7-4.4.4	$\sigma_{\theta\theta}$ of the perfectly conducting spherical shell with 30 degrees aperture at its bottom (varying wave numbers).....	119
Figure 7-4.4.5	$\sigma_{\theta\theta}$ of the obstacle (varying wave numbers) (taken from Altunkilic [3]).....	120
Figure7-4.4.6	$\sigma_{\phi\theta}$ of the perfectly conducting spherical shell with 30 degrees aperture at its bottom (varying wave numbers).....	120
Figure 7-4.6.1	Magnitude of x-component of internal electric field along z-axis (varying chiralities).....	121
Figure 7-4.6.2	Magnitude of y-component of internal electric field along z-axis	

	(varying chiralities).....	122
Figure7-4.6.3	Magnitude of x-component of internal electric field along z-axis (varying wave numbers).....	122
Figure 7-4.6.4	Magnitude of y-component of internal electric field along z-axis (varying wave numbers).....	123
Figure 7-4.6.5	Magnitude of x-component of internal electric field along z-axis (varying permittivities).....	123
Figure 7-4.6.6	Magnitude of y-component of internal electric field along z-axis (varying permittivities).....	124
Figure 7-5.1	The Generating Curve of the cylinder in the $\phi = 0$ plane.....	125
Figure 7-6	A Chiral cylinder.....	126
Figure 7-6.2.1	Magnitude of x-component of the internal E-field along z-axis.....	128
Figure 7-6..2.2	Magnitude of x-component of the internal E-field along z-axis (taken from Altunkilic [3]).....	128
Figure 7-6.2.3	Magnitude of y-component of the internal E-field along z-axis.....	129
Figure 7-6.2.4	Magnitude of y-component of the internal E-field along z-axis (taken from Altunkilic [3]).....	129
Figure 7-6.3.1	$\sigma_{\theta\theta}$ of the obstacle.....	130
Figure 7-6.3.2	$\sigma_{\theta\theta}$ of the obstacle (taken from Altunkilic [3]).....	130
Figure 7-6.3.3	$\sigma_{\phi\theta}$ of the obstacle.....	131
Figure 7-6.3.4	$\sigma_{\phi\theta}$ of the obstacle (taken from Altunkilic [3]).....	131
Figure 7-6.4.1	Magnitude of t -component of magnetic current in the $\phi = 0$ plane....	132

Figure 7-6.4.2	Magnitude of t -component of magnetic current in the $\phi = 0$ plane (taken from Altunkilic [3]).....	132
Figure 7-6.4.3	A Cylinder and the readings on its generating curve.....	133
Figure 7-6.4.4	Magnitude of l -component of magnetic current in the $\phi = 0$ plane.....	134
Figure 7-6.4.5	Magnitude of l -component of magnetic current in the $\phi = 0$ plane (taken from Altunkilic).....	134
Figure 7-6.4.6	Magnitude of l -component of equivalent electric current in the $\phi = 0$ plane.....	135
Figure 7-6.4.7	Magnitude of l -component of equivalent electric current in the $\phi = 0$ plane (taken from Altunkilic).....	135
Figure 7-6	Plane wave incident on conducting shell of empty cylinder.....	130
Figure 7-6.1	Amplitude of E -field upon axis of open ended cylinder.....	131
Figure 7-6.2	Amplitude of E -field upon axis of open ended cylinder (taken from Altunkilic).....	131
Figure 7.7	Plane electromagnetic wave impinges from the top of the cylinder.....	136
Figure 7-7.1	Magnitude of x-component of the internal E -field along z-axis.....	137
Figure 7-7.2	Magnitude of x-component of the internal E -field along z-axis (taken from Altunkilic [3]).....	137
Figure 7-8	Plane electromagnetic wave impinges on the top of the cylinder.....	138
Figure 7-8.2.1	Magnitude of x-component of the internal E -field along z-axis.....	141
Figure 7-8.2.2	Magnitude of x-component of the internal E -field along z-axis (taken from Altunkilic [3]).....	141

Figure 7-8.2.3	Magnitude of y-component of the internal E -field along z-axis.....	142
Figure 7-8.2.2	Magnitude of y-component of the internal E -field along z-axis (taken from Altunkilic [3]).....	142
Figure 7-8.3.1	$\sigma_{\theta\theta}$ of the obstacle.....	143
Figure 7-8.3.2	$\sigma_{\theta\theta}$ of the obstacle (taken from Altunkilic [3]).....	143
Figure 7-8.3.3	$\sigma_{\phi\theta}$ of the obstacle.....	144
Figure 7-8.3.4	$\sigma_{\phi\theta}$ of the obstacle (taken from Altunkilic [3]).....	144
Figure 7-8.4.1	Magnitude of l -component of magnetic current in the $\phi = 0$ plane.....	145
Figure 7-8.4.2	Magnitude of l -component of magnetic current in the $\phi = 0$ plane (taken from Altunkilic [3]).....	145
Figure 7-8.4.3	Magnitude of t -component of magnetic current in the $\phi = 0$ plane.....	146
Figure 7-8.4.4	Magnitude of t -component of magnetic current in the $\phi = 0$ plane (taken from Altunkilic [3]).....	146
Figure 7-8.4.5	Magnitude of l -component of physical electric current in the $\phi = 0$ plane.....	147
Figure 7-8.4.6	Magnitude of l -component of physical electric current in the $\phi = 0$ plane (taken from Altunkilic [3]).....	147
Figure 7-8.4.7	Magnitude of t -component of physical electric current in the $\phi = 0$ plane.....	148

Figure 7-8.4.8	Magnitude of t -component of physical electric current in the $\phi = 0$ plane (taken from Altunkilic [3]).....	148
Figure 7.9	Plane electromagnetic wave impinges from the top of the cylinder.....	149
Figure 7.9.2.1	Magnitude of x-component of the internal E -field along z-axis.....	152
Figure 7.9.2.2	Magnitude of x-component of the internal E -field along z-axis (taken from Altunkilic).....	152
Figure 7.9.2.3	Magnitude of y-component of the internal E -field along z-axis.....	153
Figure 7.9.2.4	Magnitude of y-component of the internal E -field along z-axis (taken from Altunkilic).....	153
Figure 7.9.3.1	$\sigma_{\theta\theta}$ of the obstacle.....	154
Figure 7.9.3.2	$\sigma_{\theta\theta}$ of the obstacle (taken from Altunkilic).....	154
Figure 7.9.3.3	$\sigma_{\phi\theta}$ of the obstacle.....	155
Figure 7.9.3.4	$\sigma_{\phi\theta}$ of the obstacle (taken from Altunkilic).....	155
Figure 7.9.4.1	Magnitude of t -component of magnetic current in the $\phi = 0$ plane.....	156
Figure 7.9.4.2	Magnitude of t -component of magnetic current in the $\phi = 0$ plane (taken from Altunkilic).....	156
Figure 7.9.4.3	Magnitude of l -component of magnetic current in the $\phi = 0$ plane.....	157

Figure 7.9.4.4	Magnitude of l -component of magnetic current in the $\phi = 0$ plane (taken from Altunkilic).....	157
Figure 7.9.4.5	Magnitude of t -component of physical electric current in the $\phi = 0$ plane.....	158
Figure 7.9.4.6	Magnitude of t -component of physical electric current in the $\phi = 0$ plane (taken from Altunkilic).....	158
Figure 7.9.4.7	Magnitude of l -component of physical electric current in the $\phi = 0$ plane.....	159
Figure 7.9.4.8	Magnitude of l -component of physical electric current in the $\phi = 0$ plane (taken from Altunkilic).....	159
Figure 7-10.1	Chiral Cone.....	160
Figure 7-10.3.1	Magnitude of t -directed component of external equivalent current.....	162
Figure 7-10.3.2	Magnitude of t -directed component of internal equivalent current.....	162
Figure 7-10.3.3	Magnitude of t -directed component of physical current.....	163
Figure 7-10.3.4	Magnitude of t -directed component of equivalent magnetic current.....	163
Figure 7-10.3.5	Magnitude of ϕ -directed component of external current.....	164
Figure 7-10.3.6	Magnitude of ϕ -directed component of internal current.....	164
Figure 7-10.3.7	Magnitude of ϕ -directed component of physical current.....	165
Figure 7-10.3.8	Magnitude of ϕ -directed component of magnetic current.....	165
Figure 7-10.4.1	$\sigma_{\theta\theta}$ of the obstacle.....	166
Figure 7-10.4.2	$\sigma_{\phi\phi}$ of the obstacle.....	166

Figure 7-11.1	Perfectly conducting metallic cone.....	167
Figure 7-11.2.1	Magnitude of t -component of equivalent external current.....	168
Figure 7-11.2.2	$\sigma_{\theta\theta}$ of the perfectly conducting cone shell.....	168
Figure 7-12.1.1	Perfectly conducting cone with an aperture enclosing chiral material.....	169
Figure 7-12.3.1	Magnitude of t -directed component of external equivalent electric current.....	170
Figure 7-12.3.2	Magnitude of t -directed component of equivalent internal electric current.....	171
Figure 7-12.3.3	Magnitude of t -directed component of physical electric current.....	171
Figure 7-12.3.4	Magnitude of t -directed component of equivalent magnetic current.....	172
Figure 7-12.3.5	Magnitude of ϕ -component of equivalent external electric current.....	172
Figure 7-12.3.6	Magnitude of ϕ -component of equivalent internal electric current.....	173
Figure 7-12.3.7	Magnitude of ϕ -component of physical electric current.....	173
Figure 7-12.3.8	Magnitude of ϕ -component of equivalent magnetic current.....	174
Figure 7-12.5.1	$\sigma_{\theta\theta}$ of the obstacle.....	174
Figure 7-12.5.2	$\sigma_{\phi\theta}$ of the obstacle.....	175
Figure 7-12.7.1	Magnitude of x -component of internal electric field (varying chiralities).....	176

Figure 7-12.7.2	Magnitude of y-component of internal electric field (varying chiralities).....	176
Figure7-12.7.3	Magnitude of x-component of internal electric field (varying permittivities).....	177
Figure 7-12.7.4	Magnitude of y-component of internal electric field (varying permittivities).....	177
Figure 7-12.7.5	Magnitude of x-component of internal electric field (varying wave numbers).....	178
Figure 7-12.7.6	Magnitude of y-component of internal electric field (varying wave numbers).....	178
Figure 8(a)	A rocket-shaped perfectly conducting body of revolution with a single aperture at its bottom which encloses chiral material.....	182
Figure 8(b)	Generating curve of the rocket of the Figure (8a).....	182
Figure 8(c)	A rocket in flight.....	182
Figure A-1.1.1	Original problem.....	184.
Figure A-1.1.2	External Equivalence.....	186
Figure A-1.1.3	Internal Equivalence.....	188
Figure B-1.4.1	Pulse basis functions.....	195
Figure B-1.4.2	Step approximation of a function using pulse functions.....	195
Figure B-1.4.3	Triangular functions and approximations using them; (a) a triangular function (b) piecewise linear approximation of a function using triangular functins.....	196

Figure B-1.5.1	Graph of Exact and Approximate solution (Galerkin's method).....	205
Figure B-1.6.1	Graph of Exact and Approximate solution (Point Matching method).....	212
Figure B-1.7.1	Graph of Exact and Approximate solution (Triangle function method), using five expansion functions.....	217
Figure B-1.7.2	Graph of Exact and Approximate solution (Triangle function method), using ten expansion functions.....	206
Figure B-1.7.3	Graph of Exact and Approximate solution (Triangle function method), using fifteen expansion functions.....	223
Figure B-1.8.1	Graph of Exact and Approximate solution (Galerkin method), using 1, 2, 3, and 5 expansion functions. $\Phi_n(x) = \sin(n\pi x)$ is the expansion function.....	231
Figure D-1	Rectangular and Cylindrical Coordinates.....	266
Figure D-2	Three dimensional directional vector relationships.....	268

Chapter 1

1- Introduction

Figure 1.1 shows the problem considered in this work. It shows a chiral body of revolution (BOR) that is partially covered by perfectly conducting axisymmetric surfaces. The chiral body is characterized by $(\epsilon_2, \mu_2, \xi_2)$, where ξ_2 is the chirality of the material. The partially shielded body is surrounded by a regular dielectric medium with parameters (ϵ_1, μ_1) . It is excited by an incident plane wave $(\mathbf{E}^{inc}, \mathbf{H}^{inc})$. This field penetrates into the chiral body through the apertures on its surface and produces the total field $(\mathbf{E}_2, \mathbf{H}_2)$ at points inside the BOR. The incident field is also

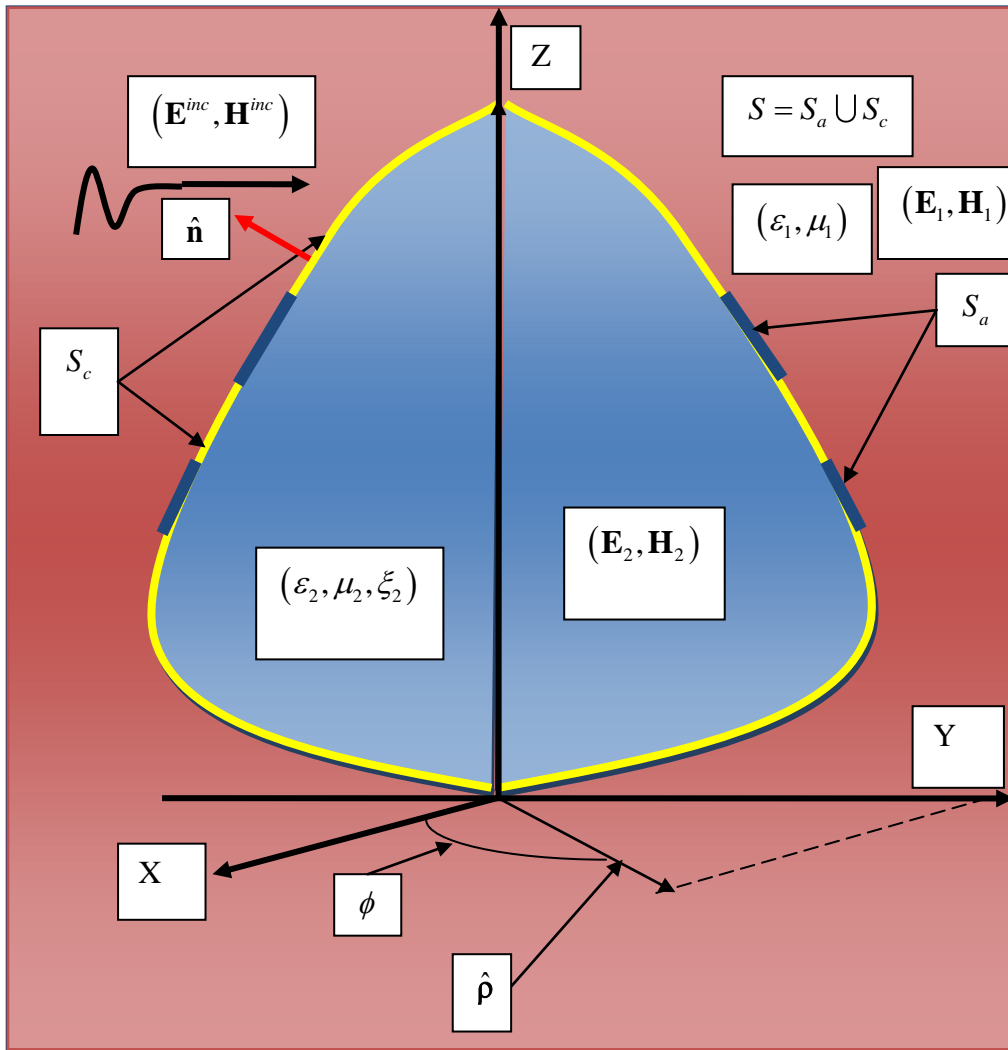


Figure 1.1 A chiral body of revolution (BOR) with two apertures

scattered by the system producing the total field $(\mathbf{E}_1, \mathbf{H}_1)$ at points external to the body. We are interested in finding the field $(\mathbf{E}_2, \mathbf{H}_2)$ at an arbitrary point inside the BOR and the far field scattered by the structure. The problem of electromagnetic penetration into an empty body of revolution that is partially covered by perfectly conducting surface with one aperture in it is analyzed in [1], [2]. The problem of electromagnetic transmission through an arbitrary aperture in an arbitrary 3-D conducting surface enclosing chiral material is analyzed in [3]. The electromagnetic analysis of general bodies of revolution is given in [4]. The work presented in this dissertation is an extension/combination of the work in [1]–[3].

In Fig. 1.1, S_a denotes the unshielded part of the surface of the chiral BOR, and S_c denotes the surface of the conducting shield. The union of these two surfaces is denoted by S . The surface equivalence principle is used to separate the problem of Fig1.1 into two simpler parts, namely, the region external to surface S , and the region internal to S . The scattered field in the external problem is produced by equivalent magnetic surface current \mathbf{M} and equivalent electric surface current \mathbf{J}_e radiating in the unbounded external medium. The current \mathbf{M} exists on only S_a and the current \mathbf{J}_e exists on the whole surface S . The total field in the chiral medium is produced by an equivalent magnetic surface current $-\mathbf{M}$, and an equivalent electric surface current $-\mathbf{J}_i$ radiating in the unbounded chiral medium. $-\mathbf{J}_i$ exists on the whole surface S . There are two unknowns: \mathbf{J}_e on S and the union of \mathbf{M} on S_a and \mathbf{J}_i on S_c . On S_a , \mathbf{J}_i is known to be equal to \mathbf{J}_e . Enforcing continuity of the tangential parts of total \mathbf{E} and \mathbf{H} across S gives two coupled vector integral equations for the two unknown surface currents. The method of moments as applied to bodies of revolution is used to solve the integral equations numerically. Piecewise linear variations of the currents are assumed along the generating curve of the BOR. The variations of the currents along the circumferential direction are represented by Fourier series. Galerkin's method is used for testing. The linear variations of the currents along the generating curve are approximated by Dirac delta functions with special treatment of the "self terms". Numerical results for conical and spherical chiral BORs partially shielded by thin perfect conductors are computed. Results for the sphere shown in Figure 1.2, are in agreement with those computed using other methods.

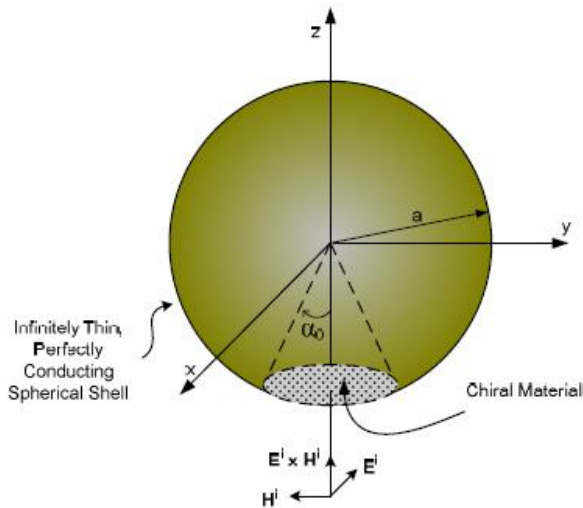
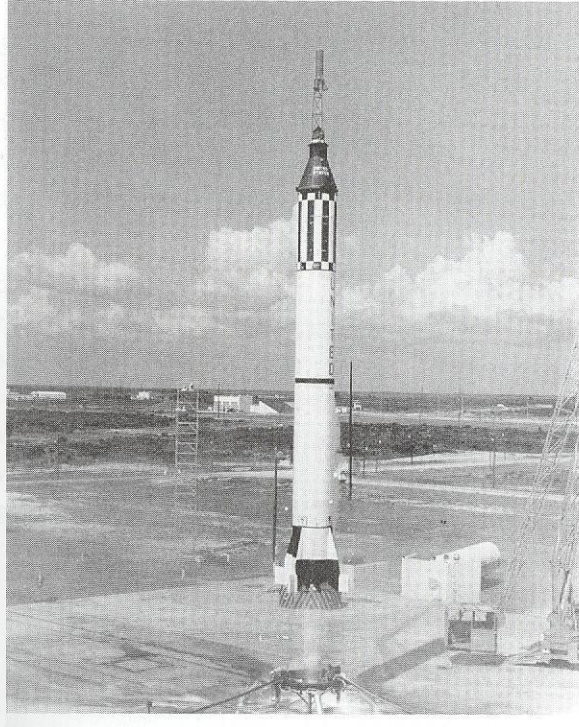
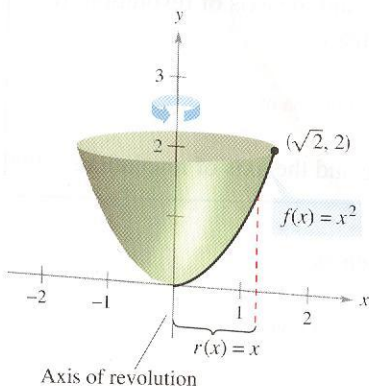


Figure 1.2 A plane wave incident on a sphere with $\alpha = 30$ (degrees) aperture.

1.1 Body of revolution (BOR)

A surface of revolution is formed when a curve is rotated about a line. Such a surface is the lateral boundary of a solid of revolution. At least two chapters are devoted in advanced calculus books [5] to calculation of surfaces and solids of revolution by using integration methods. Figure 1.1.1, shown below, represent typical bodies of revolution.



Almost a BOR

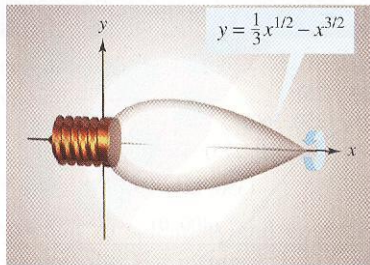


Figure 1.1.1 Typical bodies of revolution

1.2 Complicated shaped bodies of revolution

Unfortunately, bodies of revolution encountered in the real world are complicated shaped. Analytical solution methods in scattering problems are possible only for regularly shaped bodies of revolution necessitating *approximate numerical approaches* in cases of complicated shaped bodies of revolution. This thesis pertains to scattering by *complicated shaped bodies of revolution*. Therefore, integral equations encountered in this research will not lead to elegant analytical solutions. Inherent challenges involving sophisticated computational solutions of great varieties and magnitudes in this research work are tackled by resorting to a numerical technique commonly referred to as the Method of Moments (MoM).

Theoretical framework is developed in Chapters 2–6 that provides conceptual foundation from formulation of integral equations for a metallic perfectly conducting arbitrarily shaped apertured surface of revolution enclosing chiral material to MoM and from MoM to the intricacies of mathematics required to meet the very elaborate and rigorous research goal of this thesis. In order to deal with enormous sizes of matrices (*matrices of size 6000×6000 and inversions of the same size of matrices were required to produce some graphs of Chapter 7*) and vectors met in this research work for obtaining solutions and graphic mappings, we needed to resort to programming in Matlab script.

The mathematical edifice built in Chapters 2–6 is multi-faceted and versatile enough to analyze scattering and radiation by perfectly conducting metallic as well as unshielded dielectric bodies of revolution (BOR's) of complicated shapes.

In Chapter 7, we further this research activity by proving that the theoretical framework developed in Chapters 2–6 is equally applicable to regularly shaped bodies of revolution. We will compare, in the format of graphs, the results of regularly shaped bodies of revolution based on our theoretical formulations to those graphs that are produced analytically by earlier researchers. In cases where integral and other equations pertaining to scattering problems cannot be solved by analytical methods, we will compare our results with those of earlier researches carried out by application of theoretical and numerical approaches different from ours.

1.3 Motivation Obtained From Previous Research Work

Penetration of electromagnetic waves through apertures has been studied extensively. Two-dimensional apertures in thin infinite planes are studied in [6], [7]. Apertures in arbitrarily shaped three dimensional surfaces are studied in [3], [8]. In [3] the internal medium considered was chiral and in [8] both internal and external media were regular dielectrics. Memory and CPU time are the main limitation of analyzing arbitrarily shaped 3-D structures using MOM. However, larger bodies of revolution can be analyzed by the method of moments. Apertures in bodies of revolution were studied first in [1]–[2], where both the internal and external media were the same regular dielectric. In this work, we extend/combine the works in [1]–[3] by considering apertures in partially shielded

chiral bodies of revolution where the external region is a regular dielectric. This way, we are able to study the effect of chirality on the penetration of electromagnetic waves through apertures on the surface of partially shielded chiral bodies of revolution. Restricting ourselves to bodies of revolution allows us to study larger structures given memory and CPU time restrictions.

The problem of electromagnetic transmission through an aperture in a conducting plane [9], is treated by obtaining an operator equation for the equivalent magnetic current, and then reducing it to a matrix equation via the method of moments (MoM). Integral formulations for the matrix elements are given for apertures of arbitrary shape. The problem of electromagnetic scattering from a homogeneous material body of Revolution [10] is formulated in terms of equivalent electric and magnetic currents over the surface which defines the body. Application of the boundary conditions leads to four simultaneous surface integral equations to be satisfied by the two unknown equivalent currents, electric and magnetic. The set of four equations is reduced to a coupled pair of two equations. The latter two equations were solved via the method of moments MoM. The research problem dealt with in [11] relates to a rotationally symmetric aperture on a perfectly conducting BOR surface containing in the interior as well as the exterior the same homogeneous dielectric. In [11], the aperture is closed with a perfect conductor, the electric current that flows on the closed aperture is found to be \mathbf{J} , and the effect of the aperture is obtained by subjecting the perfectly conducting BOR to the additional incident electric field which exists only on the closed aperture and causes $-\mathbf{J}$ to flow on the closed aperture. This method produces good results for small apertures. The research work in [12], deals electromagnetic scattering by a three dimensional homogeneous chiral body. The research work carried out in [13], deals specifically with scattering by a chiral body of revolution.

The problem of scattering of a plane electromagnetic wave from an arbitrarily shaped metallic BOR is solved by an integral equation method which is, in principle, an exact method [14]. In [14], the incident plane electromagnetic wave is expanded in a set of orthogonal modes TE and TM to the axis of the BOR. Each of these incident modes will induce a current distribution on the surface of the body. Due to the mode orthogonality, the total induced current distribution is represented by the sum of the of the induced mode current distributions. Each mode current distribution satisfies two coupled integral equations. These integral equations are reduced to a set of linear complex equations which can be solved by a digital computer. A boundary integral equation is used in [15], for dielectric objects partially coated with a perfectly conductive layer. CAD-generated geometries are accepted in the numerical approach of [15]. The study of scattering of electromagnetic waves by arbitrarily shaped dielectric bodies in [16] uses equivalence principle and spherical vector harmonics in a Green's dyadic based numerical approach. However, this study is limited to the case of arbitrary shaped dielectric bodies only. Study of simple and efficient numerical methods for problems of electromagnetic radiation and scattering in [17], is done for bodies of complex geometries such as bent strips of infinite extent and a bent rectangular plate as well as a conducting body of revolution (BOR) and a dielectric BOR. This study in [17] is significant; however, it eludes the case of a perfectly conducting BOR surface with apertures enclosing chiral or dielectric material.

Diffraction of an electromagnetic plane wave by a rectangular plate and a rectangular hole in the conducting plate [18] is rigorously tackled using the method of the Kobayashi potential (KP

method). The KP method resembles the MoM in its spectrum domain, but the formulation is different. The MoM is based on an integral equation whereas the KP starts from dual integral equations derived from the potential integrals and boundary conditions on the plane where a plate or hole is located. The dual integral equations are solved by applying the properties of the Weber-Schafheitlin's integrals and the solution is obtained in the form of a matrix equation. This approach computes far diffracted field patterns and the current densities induced on the plate. Aside from its rigorous theoretical formulations, this research work, although mentally stimulating has no bearing on MoM. In [19], the scattering of a plane electromagnetic wave by a perfectly conducting disk or a circular hole in a perfectly conducting plane is formulated in a form of the dual integral equations. The unknowns in [19] are the induced surface current (or magnetic field) on the disk and the tangential components of the electric field in the hole. The solution for the surface current on the disk is expanded in terms of a set of functions which satisfy Maxwell's equations for the magnetic field on the disk and the required edge condition. The authors of [19] used the method of the Kobayashi potential and the vector Hankel transform thereby reducing the problem to the matrix equations for the expansion coefficients. The matrix elements are given in terms of the infinite integrals with a single variable and these are transformed into infinite series that are convenient for numerical computation. In [19], numerical results are obtained for far field patterns, current densities induced on the disk, transmission coefficients through the circular aperture, and the radar cross section. Aside from the current densities induced on the perfectly conducting disk and the radar cross section, the research in [19] is not relevant to the work in the present dissertation.

A nonmodal formulation for electromagnetic transmission through a slot of arbitrary cross section cut in a thick conducting screen filled with homogeneous material separating the single thick conducting screen into two [20] uses the equivalence principle to break the original problem into three equivalent parts where postulated equivalent sources radiate into unbounded homogeneous media. The equivalent electric and magnetic currents, in [20], are chosen to ensure continuity of the tangential components of the electric and magnetic fields at each aperture. An integral equation is written for each of the three regions, the slot region and the two half space regions, one on each side of the thick screen with the equivalent currents as unknowns. The resulting set of coupled integral equations is solved by the method of moments. The primary quantities computed in [20] are the equivalent electric and magnetic currents on each aperture and the electric current on the remaining portions of the slot cross section. The two-dimensional nature of the problem enabled the authors of [20] to treat the TE (magnetic field parallel to z-axis) and the TM (electric field parallel to z) polarizations separately. The valuable research work in [20] proved extremely conducive to understanding varied applications of the equivalence principle. In [21], a hybrid numerical technique is used for a characterization of the scattering and transmission properties of a three-dimensional slot in a thick conducting plane. In [22] there are four different surface integral equation formulations for the problem of electromagnetic coupling through an aperture between a cavity and an external region.

Text books [23]–[24], authored by Prof. Harrington of Syracuse University, are considered authoritative and are used and are referenced all over the world. Text book [23] introduces the equivalence principle and [24] introduces field computation by the method of moments (MoM). Graduate level text book [25] on electromagnetic wave theory deals with many electromagnetic theorems and principles including the equivalence principle.

In [26], there is a method applicable to arbitrarily shaped apertures (in particular those not azimuthally symmetric in bodies of revolution) employing the technique of the method of moments. The authors of [26] use an equivalence theorem by which the field inside the BOR is due to the excitation on the closed aperture that causes $-\mathbf{J}$ to flow on the closed aperture where \mathbf{J} is the electric current induced on the closed aperture by the incident field. The method in [26] gives good results for small apertures. This method is not used in the present thesis because the formulation therein was not intended to give good results for small apertures. The problem of the scattering of an electromagnetic plane wave with arbitrary polarization and angle of incidence from a perfectly conducting spherical shell with a circular aperture [27] is solved with a generalized dual series approach. This canonical problem encompasses coupling to an open spherical cavity and scattering from a spherical reflector. In contrast to the closed sphere problem, the electromagnetic boundary conditions couple the TE and TM modes. A pseudodecoupling of the resultant dual series equations system into dual series problems for the TE and TM modal coefficients is accomplished by introducing terms that are proportional to the associated Legendre functions.

A graphical user interface (GUI) for plane-wave scattering from a conducting, dielectric, or chiral sphere [28], obtains scattering from a chiral, dielectric, or a perfectly conducting sphere using a friendly graphical user interface (GUI). This GUI using matlab script enables the user to enter the scattering parameters and to observe the results, and to save the data and displayed figures.

Electromagnetic field penetration into a spherical cavity [29] uses a different numerical approach. In this approach, the authors solve the problem of scattering from a spherical shell with a circular aperture symmetrically illuminated by a plane electromagnetic wave by expanding the fields inside and outside the cavity in terms of spherical vector wave functions and finding the modal coefficients by application of the least squares method to the boundary conditions. From result obtained in [29] in the form of amplitude curves of the interior and aperture fields as functions of position for a variety of cavity and aperture sizes, it appears that the field variations are primarily determined by the cavity size and that the aperture size serves only to scale them.

A hybrid FE–BI method for electromagnetic scattering from dielectric bodies partially covered by conductors [30] uses a hybrid technique that combines the finite element (FEM) and boundary integral (BI) methods to analyze electromagnetic scattering problems from structures consisting of an inhomogeneous dielectric body attached to perfectly conducting bodies. The hybrid approach takes advantage of the strengths of each numerical technique in order to solve problems that neither technique could model efficiently. A new variational direct boundary integral equation approach is presented in [31] for solving the scattering and transmission problem for dielectric objects partially coated with a perfect electric conducting (PEC) layer. The main idea is to use the electromagnetic Calderon projector along with transmission conditions for the electromagnetic fields. This leads to a symmetric variational formulation which lends itself to Galerkin discretization by means of divergence-conforming discrete surface currents.

Closed form modal Green's functions for accelerated computation of bodies of revolution [32] uses MoM and Modal Green's function (MGF). The MGF is defined as the radiation field of a circular loop antenna with sinusoidal current distribution. The authors of [32] proposed closed form expressions for near-axis far-distance modal Green's functions in order to accelerate the

computation of BOR problems. They also presented a criterion based on rigorous error analysis to guarantee MGF's range of applications. Radiation and scattering problems using the MGF approach were solved in this research. Electromagnetic penetration through apertures in conducting surfaces [33] provides a tutorial review of aperture theory in its present state of maturity with emphasis upon those facets of the theory which lead to better understanding of EMP penetration. The authors of [33] discuss the boundary value problem involving an aperture-perforated, planar screen separating two homogeneous half spaces having the same electromagnetic properties, and formulate preliminary integro-differential equations for this problem. They generalize these preliminary concepts and derive equations for the problem of diffraction by a closed conducting surface in which an aperture has been cut.

Radiation and scattering from bi-Isotropic bodies of revolution [34] discusses use of bi-isotropic (BI) media in the fields of millimeter wave and microwave. The BI media is characterized by a bi-isotropic constitutive relation, which complicates the solution of the electromagnetic scattering and radiation problems associated with bi-isotropic medium. The authors of [34] develop a general solution based on surface integral equation (SIE) to analyze the scattering and radiation of arbitrarily shaped BI bodies, which takes both chiral and Tellegen parameters in consideration. They design a dedicated solution for bi-isotropic BOR (BI-BOR). Calculation of the absorption cross section of a partially shielded dielectric sphere [35] solves the problem of a plane electromagnetic wave diffracted from a dielectric sphere partially covered by a thin perfectly conducting spherical surface.

In [36] an improved solution of the E-field integro-differential equation is intended for electromagnetic scattering from a perfectly conducting body of revolution. This solution eliminates an instability of previous solutions which manifested itself by an oscillation of the azimuthal current about its mean value. The authors of [36] present examples of the computed electric current on several bodies of revolution for which many past solutions exhibited an oscillatory instability. In [37] a new method is proposed for the computation of the radar cross section and other associated field quantities arising when a smooth, perfectly conducting obstacle is illuminated by an incident electromagnetic wave. The scattered wave is first represented by a distribution of electric dipoles over the surface in question, with the response from any dipole proportional to the induced surface current density at that point. The surface current is then determined by the "boundary condition" that the scattered wave, through interference, precisely cancels the incident wave on the surface of the largest sphere inscribed in the obstacle. One obtains in this manner a pair of coupled matrix equations for the surface current. Green's identity permits decoupling of the equations, reducing the problem to roughly the equivalent of two independent scalar problems. The authors specialized the equations to axially symmetric obstacles and then solved the equations numerically.

H-Field, E-Field, and Combined Field solutions for bodies of revolution [38] derives formulas for the computation of the electric surface current and far scattered field of a perfectly conducting body of revolution for arbitrary plane wave excitation. Computations in [38] showed that both the H-field solution and the E-field solution deteriorate near internal resonances of the conducting surface, but that the combined field solution does not. The field solutions in [38] are obtained by applying the method of moments (MoM) to the H-field integral equation, the E-field integral equation, and the combined field integral equation for a perfectly conducting body of

revolution. An integral equation method is presented in [39] for the solution of the field scattered by a set of cylinders with arbitrary cross-sectional shape and arbitrarily varying anisotropic surface impedance. The integral equations are given for an arbitrary source with arbitrary harmonic variation along the cylinder axis. The scattering problem can be solved for arbitrary three-dimensional sources by expansion of the sources in a Fourier integral over the axial propagation constant. The author developed a computer program and used it for solving a great variety of scattering, antenna, and propagation problems. In [40] there is a survey of recently developed techniques for solving the rigorous equations that arise in scattering problems. These methods generate a system of linear equations for the unknown current density by enforcing the boundary conditions at discrete points in the scattering body or on its surface. This approach shows promise of leading to a systematic solution for a dielectric or conducting body of arbitrary size and shape. The authors of [40] discuss relative merits of the linear-equation solution and the variational solutions and numerical results, obtained by these two methods, for straight wires of finite length.

Two-dimensional electromagnetic scattering by a dielectric cylinder partially covered by zero-thickness perfect conductors is treated in [41]. The impressed field is either transverse magnetic (TM) or transverse electric (TE) to the cylinder axis. The problem is formulated in terms of two coupled boundary integral equations in each case. For the TM case the unknowns are equivalent electric currents, and for the TE case they are equivalent magnetic currents. In [41] the integral equations are solved by the method of moments (MoM) with pulse functions for expansion and point matching for testing. In [41], numerical solutions are obtained for a thin rectangular dielectric cylinder partially covered by perfectly conducting plates, where the impressed fields is either a TM or a TE plane wave. In [42], scattering from wires and open circular cylinders of finite length is obtained using entire domain Galerkin expansions. The case of a straight wire, viewed as a thin cylinder, is examined in this context. The salient features of this study are a) use of the electric field integral equation (EFIE) as a starting point, b) solution of this equation by Galerkin method, and c) representation of the axial variation of the current on the scatterer by an entire domain (Fourier series) expansion. Edge modes are considered in the expansion set and their effect is examined. The open cylinder backscatter cross section is computed as a function of aspect angle for various radii and lengths and is compared with measured data.

In [43], there is a formulation based on the physical theory of diffraction (PTD) for electromagnetic scattering from finite conical surfaces with circular and elliptic cross sections. The base-rim discontinuity is represented by equivalent currents, including second order terms extended for elliptic boundaries. Tip-rim interactions are examined as a function of the tip-rim distance, cone angle, and illumination angle for circular cones; and their implications for elliptic cones are noted. The diffraction contribution from tip-rim interactions is shown to be dependent on the cone angle and the illumination angle but to be relatively insensitive to the tip-rim distance. The formulation in [43] was applied to cones with varying ellipticity for axial and oblique illumination. Correlation is made with published results for circular cones and with experimental data for an elliptic cone. In [44], the behavior of an electromagnetic field in the neighborhood of the common edge of angular dielectric or conducting regions is determined from the condition that the energy density must be integrable over any finite domain (the so-called edge condition). Two cases are treated in detail. 1) A region consisting of a conducting wedge and two different dielectric wedges with a common edge. 2) A region consisting of two different dielectric wedges with a common edge. It is also

shown that near such edges, electrostatic and magnetostatic fields will exhibit the same behavior as the electromagnetic field.

Books covering important topics in electromagnetic fields and waves [45]–[49] were used to understand the subject, concepts, and terminologies used in this thesis.

In [50], an axisymmetric chiral radome is analyzed via the method of moments (MoM). The chiral body is illuminated by a plane wave and the surface equivalence principle is used to replace the body by equivalent electric and magnetic surface currents. The scattered field outside and the total internal field are produced by these currents. By using the boundary conditions on the surfaces of the bodies, eight simultaneous surface integral equations are obtained for four unknown equivalent surface currents. By taking linear combinations, the eight integral equations are reduced to four integral equations. A matlab computer program is developed for an axisymmetric chiral radome and examples of numerical calculations are given for a chiral spherical radome and chiral Von Karman radome. Numerical results of the chiral spherical radome are in excellent agreement with the exact ones obtained by the eigenfunction solution. In [51], a method of moments (MoM) solution is presented for electromagnetic scattering by a three-dimensional (3-D) inhomogeneous chiral scatterer illuminated by an arbitrary incident field. The volume equivalence principle was used to obtain coupled integral equations for equivalent volume currents. These integral equations were then solved numerically using MoM. The volume of the scatterer was modeled by tetrahedral cells, and face-based expansion functions were used to approximate the equivalent currents. Computed results are in very good agreement with exact data or other published data. In [52], the electric field integral equation (EFIE) with the method of moment (MoM) is used to develop a simple and efficient numerical procedure for treating problems of scattering by arbitrarily shaped objects. For numerical purposes, the objects are modeled using planar triangular surface patches. Because the EFIE formulation is used, the procedure is applicable to both open and closed surfaces. Crucial to the numerical formulation is the development of a set of special subdomain type basis functions which are defined on pairs of adjacent triangular patches and yield a current representation free of line or point charges at sub-domain boundaries. The method is applied to the scattering problems of a plane wave illuminated flat square plate, bent square plate, circular disk, and sphere. Excellent correspondence between the surface current computed via the method [52] and that obtained via earlier approaches or exact formulations is demonstrated in each case.

Going through the cited research works and scores of other research works not enumerated above, led to acquiring a body of knowledge, acquiring inspiration, and acquiring motivation to build a theoretical framework that does not omit any feature and facet of scattering from a BOR of complex geometry. *The theoretical foundation developed in Chapters 2–6 is multi-faceted in that it can be adapted to; (a) the case of a perfectly conducting BOR surface, (b) the case of a chiral BOR, (c) the case of a dielectric BOR, (d) the case of a perfectly conducting BOR surface with aperture that encloses dielectric material, (e) the case of a perfectly conducting BOR surface with apertures that encloses chiral material, and (f) the case of, not just one, but as many apertures as desired in the structure.*

This research work is important because of its significance for numerous applications in radar techniques and for tracking and discriminating between space vehicles and objects. The scope

of the applicability of this research work is important in radar. For example, the transmitting antenna radiates the incident field, which closely approximates a plane wave at the target (BOR), which could very well be a rocket in flight. The current induced on the target (rocket) by the incident wave produces the scattered wave, which is approximately a plane wave at the receiving antenna. The received signal is processed to obtain information about the rocket including its shape and its orientation in space as well as its radar cross section.

1.4 Organization of the Dissertation

In Chapter 2, equivalent electric and magnetic currents on the surface of the chiral body of revolution (BOR) are used to obtain external and internal equivalences. In the external equivalence, the field outside the BOR is the field in the original problem and the field inside the BOR is the null field. In the internal equivalence, the field inside the BOR is the field in the original problem and the field outside the BOR is the null field. Realizing these null fields, two vector integral equations are obtained for the equivalent electric and magnetic currents. The equivalent currents are represented by two unknown vector functions over the entire surface of the BOR. The first unknown vector function is the unknown electric current \mathbf{J}_e of the external equivalence. The second unknown vector function is the union of \mathbf{M} over the part of the surface of the BOR not covered by the conductors and \mathbf{J}_i covered by the conductors. Here, \mathbf{M} is the unknown equivalent magnetic current of the external equivalence on the part of the surface of the BOR not covered by conductors and \mathbf{J}_i is such that $-\mathbf{J}_i$ is the unknown equivalent electric current of the internal equivalence on the part of the surface of the BOR covered by conductors. The unknown equivalent magnetic current of the internal equivalence is $-\mathbf{M}$. Unknown equivalent magnetic current is not needed on the part of the surface of the BOR covered by conductors because the equivalent magnetic current of both external and internal equivalences is zero there. Unknown equivalent electric current of the internal equivalence is not needed on the part of the surface of the BOR not covered by conductors because this equivalent electric current is equal to $-\mathbf{J}_e$ there.

In Chapter 2, applications of the method of moments (MoM) using expansion and testing functions on the surface of the BOR gives the moment matrix equation in which a square matrix called the moment matrix post-multiplied by a column matrix of the unknowns is equal to an excitation column matrix. Because an $e^{jn\phi}$ dependent source current on the surface of the BOR that is symmetric about the z -axis produces only an $e^{jn\phi}$ dependent field, the originally encountered large moment matrix equation decomposes into smaller moment matrix equations, one for each value of n for which $e^{jn\phi}$ dependent equivalent currents are significant. Because each tangential vector on the surface of the BOR has two orthogonal components, each moment matrix that comes from the two vector integral equations is a four by four array of submatrices. The first expressions for the moment matrix elements in Chapter 2 contain integrals over the testing functions of the

fields of the expansion functions for the equivalent electric and magnetic currents. These electric and magnetic current expansion functions radiate both in all space filled with the homogeneous achiral medium outside the BOR in the original problem and in all space filled with the homogeneous chiral medium inside the BOR in the original problem. In Chapter 2, the elements of the excitation column matrix for a particular value of n are expressed in terms of integrals over testing functions of the field of an incident plane wave. Because the surface of the BOR is symmetric about the z -axis, only plane waves that propagate in the xz -plane need to be considered. Solving for the column matrix of unknowns in the moment matrix for a particular value of n amounts to solving for the $e^{jn\phi}$ dependent equivalent electric and magnetic currents. Before the moment matrix equation for a particular value n can be solved for the column matrix of unknowns, the elements of the moment matrix and the elements of the excitation column matrix have to be evaluated.

In Chapter 2, the fields in the previously-mentioned expressions for the moment matrix are dealt with as follows. The field of each equivalent current expansion function radiating in all space filled with the chiral medium is decomposed into the sum of a right-handed field and a left-handed field. The right-handed field is produced by the right-handed source radiating in a hypothetical achiral medium called the right-handed medium and the left-handed field is produced by the left-handed source radiating in a hypothetical achiral medium called the left-handed medium. The right-handed sources are expressed in terms of the equivalent electric and magnetic currents. The left-handed sources are also expressed in terms of the equivalent electric and magnetic currents. The four needed field operators which are electric field of electric current, magnetic field of electric current, electric field of magnetic current, and magnetic field of magnetic current are reduced to two needed field operators by expressing electric field of magnetic current in terms of magnetic field of electric current and by expressing magnetic field of magnetic current in terms of electric field of electric current. Such a treatment of the fields allows the moment matrix elements to be expressed as (2.47)–(2.50) in which the Z 's and Y 's on the right-hand side are given by (2.51)–(2.53). These Z 's and Y 's are proportional to the integrals over the testing functions of the fields of the expansion functions for the equivalent currents radiating in all space filled with the achiral medium outside the BOR in the original problem, in all space filled with the right-handed medium, and in all space filled with the left-handed medium.

In Chapter 3, formulas that can be used to compute the Z 's and Y 's of (2.51)–(2.53) are obtained. The moment matrix elements can be computed by substituting computed values of Z 's and Y 's into expressions (2.47)–(2.50) for the moment matrix elements. Formulas that can be used to compute the Z 's of (2.51) are obtained by first using the mixed potential formulation to expand the fields in (2.51). In this formulation, the electric fields of electric current sources are expressed in terms of magnetic vector potentials and electric scalar potentials. Next, a vector identity and the surface divergence theorem are used to trade the gradient operation on the electric scalar potential for the surface divergence operation on the testing function. The magnetic fields in (2.52) and (2.53) are proportional to the curls of the magnetic vector potentials. Each magnetic vector potential is proportional to an integral. The curl of the integral is replaced by the integral of the curl of the integrand and the limit is taken as the field point approaches the source surface (surface on which the electric current source of the magnetic vector potential resides) from the appropriate side of the source surface. Finally, the piecewise linear approximation of the generating

curve is introduced and each expansion and testing function is approximated by four Dirac delta functions. Except for the "self-term" where the delta function of a testing function coincides with the delta function of an expansion function, the four delta function approximations make the integrals tractable. The equivalent radius [53] is used for the self term.

In Chapter 4, the expressions for the elements of the excitation column matrix that were obtained in Chapter 2 are made amenable to computation by treating the electric and magnetic fields of the incident electromagnetic field. The incident electromagnetic field is the field that its impressed sources would produce if they radiated in all space filled with the homogeneous medium outside the BOR in the original problem. Two kinds of incident waves are considered: one whose electric field is in the θ -direction and one whose electric field is in the ϕ -direction. The incident field whose electric field is θ -polarized is called the θ -polarized incident field and the incident field whose electric vector is ϕ -polarized is called the ϕ -polarized incident field. The integrals with respect to ϕ in the expressions for the elements of the excitation column matrix for the θ -polarized incident field are expressed in terms of integral representations of the cylindrical Bessel functions J_{n-1} , J_n , J_{n+1} . Because the electric field of the ϕ -polarized incident field is proportional to the magnetic field of the θ -polarized incident field and because the magnetic field of the ϕ -polarized incident field is proportional to the electric field of the θ -polarized incident field, each element of the excitation column matrix for the ϕ -polarized incident field is proportional to one of the elements of the excitation column matrix for the θ -polarized incident field. The remaining integrals, those with respect to t , are done by approximating the t -dependence of each testing function by four Dirac delta functions.

In Chapter 5, the scattered electric field far from the scatterer is expressed as a summation with respect to n where the term characterized by n in the summation is the matrix product of a measurement row matrix and a column matrix T multiplied by $e^{jn\phi_{rec}}$, where, from reciprocity, each element of the measurement row matrix is either an element of or the negative of an element of the excitation column matrix with the angle θ of the direction from which the incident field comes replaced by the angle θ of the radius vector from the origin in the vicinity of the scatterer to the location where the scattered field is observed. Also each element of T is a coefficient of an expansion function in the solution for the equivalent currents that radiate the scattered field. In Chapter 5, the definition of the bistatic radar cross section per square wavelength in the exterior medium (the exterior medium is the medium outside the BOR in the original problem) is used to express the bistatic radar cross section as a normalized square of the magnitude of the scattered electric field.

In Chapter 6, expressions are obtained for the six field components $E_x, E_y, E_z, H_x, H_y,$ and H_z inside the BOR. The field inside the BOR is the field of the equivalent electric and magnetic currents of the internal equivalence radiating in all space filled with the homogeneous chiral medium inside the BOR in the original problem. The field of each equivalent current is expressed as the sum of the right-handed field and the left-handed field. The right-handed field is radiated by the right-handed sources in the right-handed achiral medium and the left-handed field is radiated by the left-handed sources in the left-handed achiral medium. The right-handed sources are expressed

in terms of the equivalent electric and magnetic currents. The left-handed sources are also expressed in terms of the equivalent electric and magnetic currents. Because the electric field of a magnetic current is proportional to the magnetic field of an electric current and because the magnetic field of a magnetic current is proportional to the electric field of an electrical current, all fields can be expressed in terms of Z 's and Y 's where each Z is the electric field of an electric current and each Y is the magnetic field of an electric current. Each Z is expressed in terms of a magnetic vector potential and an electric scalar potential. Each Y is proportional to the curl of a magnetic vector potential. The magnetic vector potential is proportional to an integral. The curl of the integral is replaced by the integral of the curl of the integrand. Numerical integrations over the source coordinate ϕ' are done first. Integrations over the source coordinate t' are done by approximating the t' dependence of each expansion function by four Dirac delta functions. Expressions for the ρ -, ϕ -, and z -components of the fields are obtained and then the expressions for the ρ - and ϕ -components of the fields are used to obtain expressions for the x - and y -components of the fields. For field evaluation on the z -axis, the distance between source and field points does not depend on ϕ' so that the integrands of the integrals with respect to ϕ' are trigonometric functions that can be integrated analytically instead of numerically, thereby saving computer time.

The mathematical edifice built in Chapters 2–6 is multi-faceted and versatile enough to analyze scattering and radiation by perfectly conducting metallic as well as unshielded dielectric bodies of revolution of complicated shapes. Chapter 7, furthers this research activity by proving that the theoretical formulations developed in Chapters 2–6 are equally applicable to cases of regular-shaped bodies of revolution. Comparison, of the graphs of results for regular-shaped bodies of revolution based on our theoretical formulations with those graphs that were produced analytically by earlier researchers showed almost one hundred percent conformability of graph mappings, form and accuracy of graph readings with our graphs. In cases where integral and other equations pertaining to scattering problems could not be solved by analytical methods we compared our results with those earlier researches carried out by application of theoretical and numerical approaches different than ours. Chapter 8 presents the conclusion reached based on the systematic theoretical structure presented in Chapters 2–6 which led to the numerical results and graphs, presented in Chapter 7, that conformed to an agreeable extent with the results and graphs obtained by early researchers using distinctly different numerical approaches than ours.

There are five appendices. Appendix A gives clear, uncluttered presentation of the Equivalence Principle, Appendix B presents analysis of the MoM technique, Appendix C presents comprehensive exploration of electric and magnetic field equations and field sources in chiral media, Appendix D explains formulations not fully explained in Chapters 2–3 and Appendix E elucidates derivations of important equations of Chapter 2.

Chapter 2

Integral Equations and the Moment Matrix Equation

2.1 Introduction

In Chapter 2, the fields inside and outside the body of revolution are simulated by using unknown equivalent electric and magnetic currents. Integral equations for these equivalent currents are derived. Expansion and testing functions are used in the method of moments to discretize these integral equations. The discretization yields the moment matrix equation where a square matrix called the moment matrix multiplied by a column matrix of unknown elements is equal to a column matrix of known elements called the excitation column matrix. If the elements of the moment matrix and the elements of the excitation column matrix can be computed, then the moment matrix equation can be solved to obtain an approximate numerical solution for the equivalent currents. In Chapter 2, the elements of the excitation column matrix are given by (2.28) and (2.29) which contain the incident electromagnetic field, and the elements of the moment matrix are given by (2.47)–(2.50) whose right-hand sides contain Z 's and Y 's. Computation of the Z 's and Y 's is described in Chapter 3. Computation of the elements of the excitation column matrix for plane wave excitation is described in Chapter 4.

2.2 Integral Equations

Let S_c be the part of the surface of the chiral body (scatterer) covered by rotational symmetric perfect conductors, let S_a be the part of the surface of the scatterer not covered by the rotationally symmetric conductors, and let S be the entire surface of the scatterer as shown in Fig. 2.1. Here, the subscript c stands for conductor, and, because S_a is an aperture or apertures, the subscript “ a ” stands for aperture.

The electromagnetic field outside the scatterer is simulated as the electromagnetic field produced by the combination of the impressed source of the plane wave, the electric current \mathbf{J}_e on S and the magnetic current \mathbf{M} on S_a , both radiating in all space filled with the homogeneous achiral medium that is outside the scatterer in the original problem. This simulation, where e in \mathbf{J}_e stands for external, is called the external equivalence (see Fig. 2.2).

The electromagnetic field inside the scatterer is simulated as the electromagnetic field produced by the combination of the electric current $-\mathbf{J}_i$ on S_c , the electric current $-\mathbf{J}_e$ on S_a , and the magnetic current $-\mathbf{M}$ on S_a , all radiating in all space filled with the homogeneous

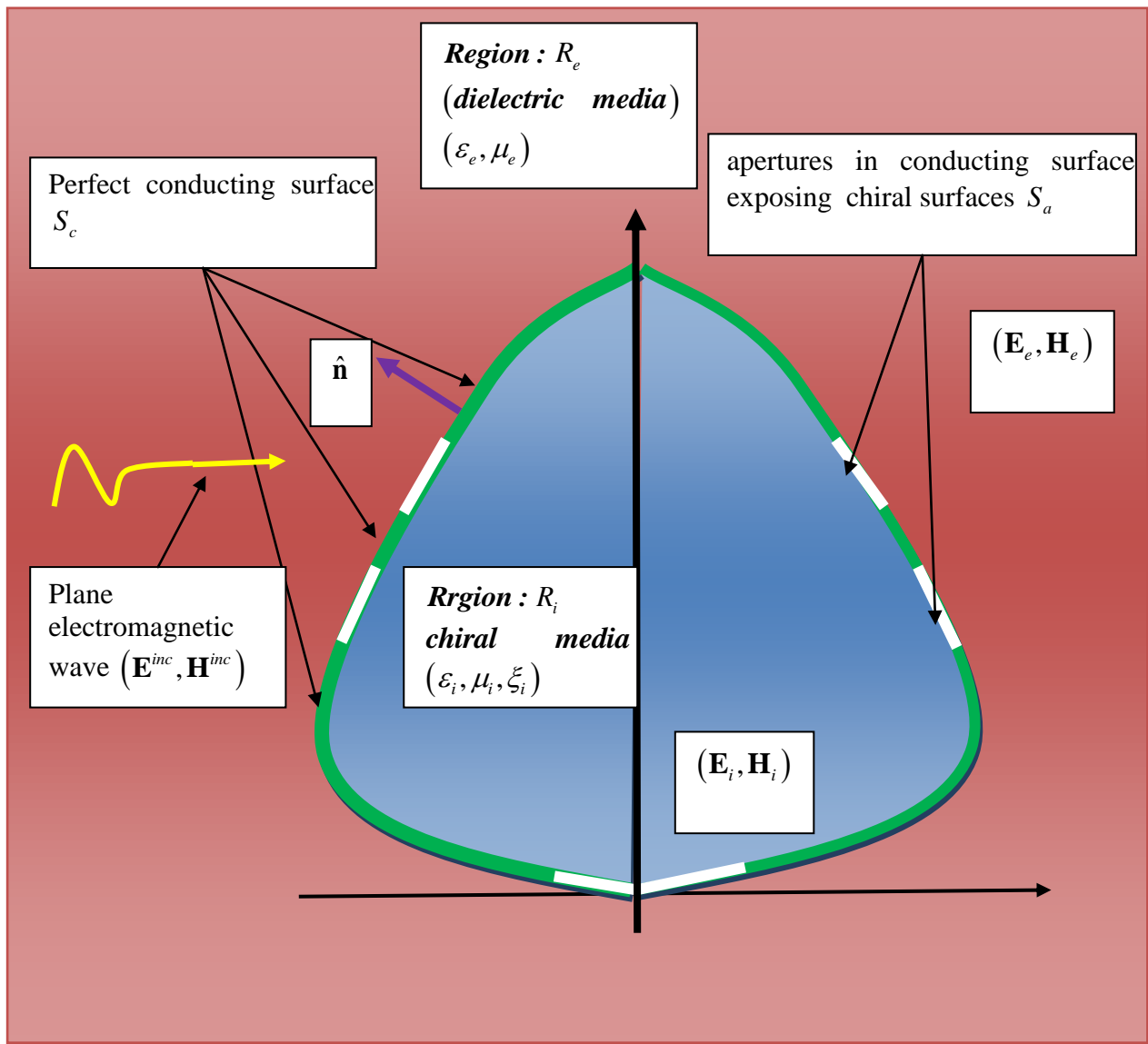


Figure 2.1 Original problem

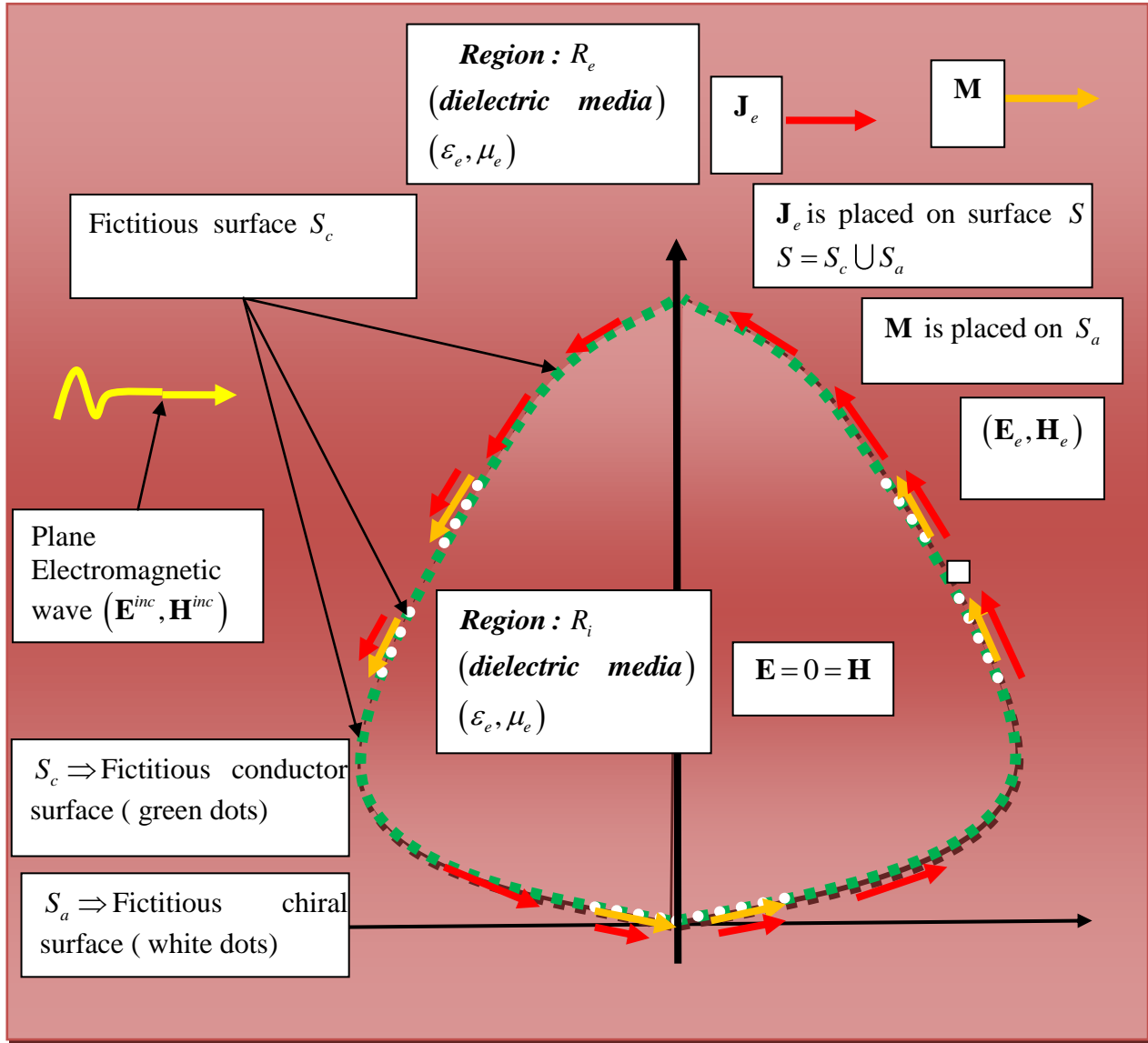


Figure 2.2 External Equivalence



chiral medium that is inside the scatterer in the original problem. This simulation, where i in $-\mathbf{J}_i$ stands for internal, is called the internal equivalence (see Fig. Fig. 2.3).

The boundary conditions are that the part of the electric field that is tangent to S_a is continuous across S_a , that the part of the electric field that is tangent to S_c is zero on both sides of S_c (the side facing outside the scatterer and the side facing inside the scatterer), and that the part of the magnetic field that is tangent to S_a is continuous across S_a . Hence, there are two boundary conditions everywhere on S .

Let “just outside S ” refer to the side of S facing outside the scatterer and let “just inside S ” refer to the side of S facing inside the scatterer. If \mathbf{J}_e , \mathbf{J}_i , and \mathbf{M} can be determined such that the tangential electric and magnetic fields of the external equivalence are zero just inside S and the tangential electric and magnetic fields of the internal equivalence are zero just outside S , then all boundary conditions on S in the original problem will be satisfied. The tangential electric field will be continuous across S_a because the magnetic current on S_a in the internal equivalence is the negative of the magnetic current on S_a in the external equivalence. The tangential electric field will be zero on both sides of S_c because there is no magnetic current on S_c in both external and internal equivalences. The tangential magnetic field will be continuous across S_a because the electric current on S_a in the internal equivalence is the negative of the electric current on S_a in the external equivalence.

The requirement that the tangential electric field of the external equivalence be zero just inside S is expressed as

$$-\frac{1}{\eta_e} [\mathbf{E}_e(\mathbf{J}_e, \mathbf{M})]_{S^-} = \frac{1}{\eta_e} [\mathbf{E}^{\text{inc}}]_S \quad (2.1)$$

where $\eta_e = \sqrt{\mu_e/\varepsilon_e}$ is the intrinsic impedance of the homogeneous achiral medium outside the scatterer in the original problem. Also, $\mathbf{E}_e(\mathbf{J}_e, \mathbf{M})$ is the electric field of the combination of \mathbf{J}_e and \mathbf{M} , both radiating in all space filled with the homogeneous achiral medium that is outside the scatterer in the original problem. The e in \mathbf{E}_e indicates radiation in all space filled with the external medium of the original problem. The first argument of \mathbf{E}_e is an electric current and the second argument of \mathbf{E}_e is a magnetic current. In (2.1), S^- indicates the tangential part of the enclosed field on the side of S facing inside the scatterer. Moreover, \mathbf{E}^{inc} is the incident electric field. The incident electric field is the electric field that would exist if the scatterer was removed and if the resulting empty space was filled with the homogeneous achiral medium outside the scatterer in the original problem. The subscript S indicates the tangential part of the enclosed field on S . There is no need to specify the side of S where \mathbf{E}^{inc} is evaluated because \mathbf{E}^{inc} is continuous across S .

The requirement that the tangential magnetic field of the external equivalence be zero just inside S is expressed as

$$-[\mathbf{H}_e(\mathbf{J}_e, \mathbf{M})]_{S^-} = [\mathbf{H}^{\text{inc}}]_S \quad (2.2)$$

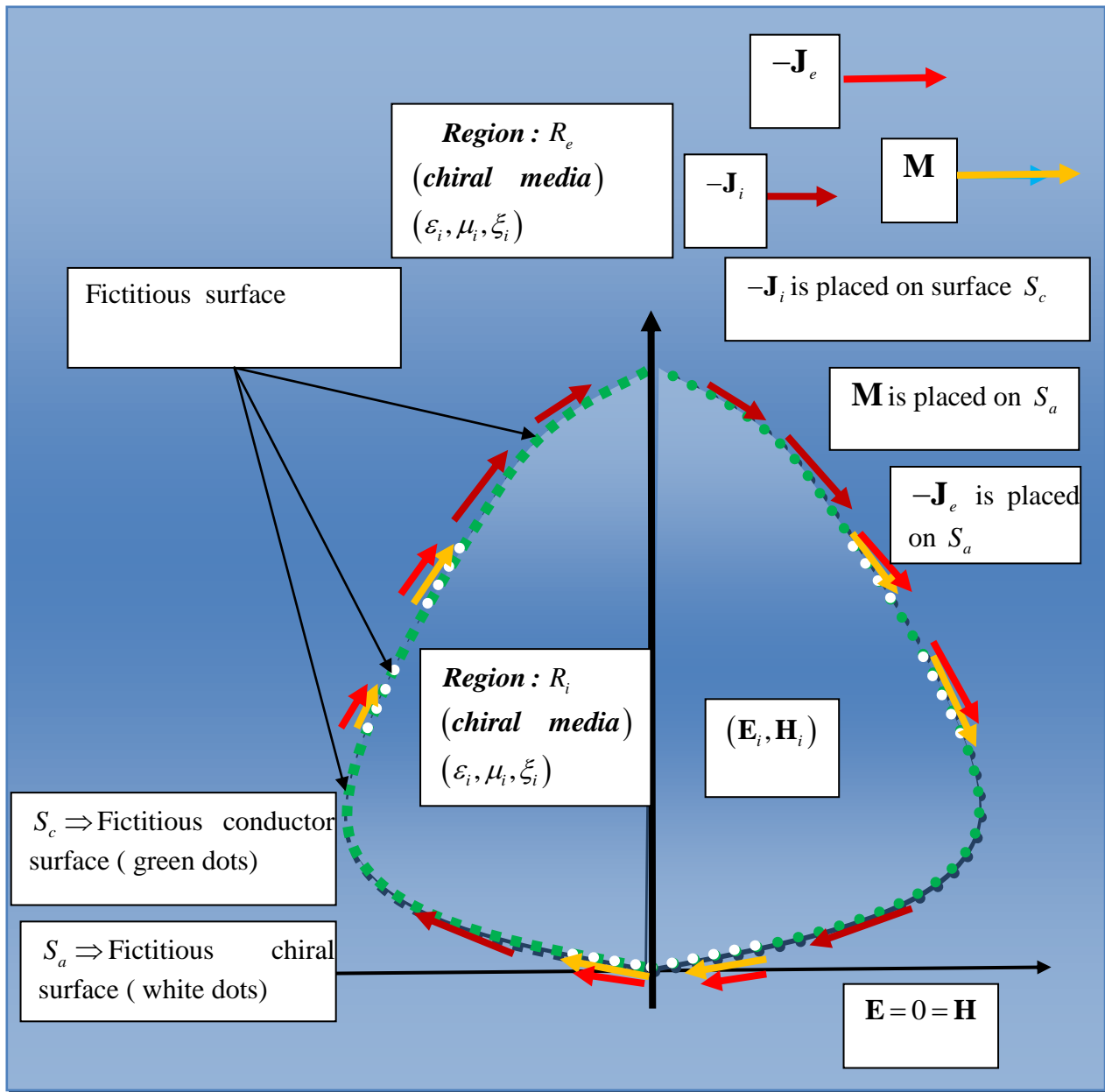


Figure 2.3 Internal Equivalence



where $\mathbf{H}^e(\mathbf{J}_e, \mathbf{M})$ is the magnetic field of the combination of \mathbf{J}_e and \mathbf{M} , both radiating in all space filled with the homogeneous achiral medium that is outside the scatterer in the original problem. The e in \mathbf{H}_e indicates radiation in all space filled with the external medium of the original problem. The first argument of \mathbf{H}_e is an electric current and the second argument of \mathbf{H}_e is a magnetic current. As in (2.1), S^- indicates the tangential part of the enclosed field on the side of S facing inside the scatterer. Moreover, \mathbf{H}^{inc} is the incident magnetic field. The incident magnetic field is the magnetic field that would exist if the scatterer was removed and if the resulting empty space was filled with the homogeneous achiral medium outside the scatterer in the original problem. The subscript S indicates the tangential part of the enclosed field on S . There is no need to specify the side of S where \mathbf{H}^{inc} is evaluated because \mathbf{H}^{inc} is continuous across S .

The requirement that the tangential electric field of the internal equivalence be zero just outside S is expressed as

$$-\frac{1}{\eta_e} [\mathbf{E}_i(\mathbf{J}_{ie}, \mathbf{M})]_{S^+} = \mathbf{0} \quad (2.3)$$

where $\mathbf{E}_i(\mathbf{J}_{ie}, \mathbf{M})$ is the electric field of the combination of \mathbf{J}_{ie} and \mathbf{M} , both radiating in all space filled with the homogeneous chiral medium that is inside the scatterer in the original problem. Here, \mathbf{J}_{ie} is the combination of \mathbf{J}_i on S_c and \mathbf{J}_e on S_a . In (2.3), the i in \mathbf{E}_i indicates radiation in all space filled with the internal medium of the original problem. The first argument of \mathbf{E}_i is an electric current and the second argument of \mathbf{E}_i is a magnetic current. In (2.3), S^+ indicates the tangential part of the enclosed field on the side of S facing outside the scatterer. Although the sources on S in the internal equivalence are $-\mathbf{J}_{ie}$ and $-\mathbf{M}$, it was possible to employ \mathbf{J}_{ie} and \mathbf{M} in (2.3) because (2.3) is equivalent to itself with \mathbf{J}_{ie} and \mathbf{M} replaced by $-\mathbf{J}_{ie}$ and $-\mathbf{M}$, respectively.

The requirement that the tangential magnetic field of the internal equivalence be zero just outside S is expressed as

$$-[\mathbf{H}_i(\mathbf{J}_{ie}, \mathbf{M})]_{S^+} = \mathbf{0} \quad (2.4)$$

where $\mathbf{H}_i(\mathbf{J}_{ie}, \mathbf{M})$ is the magnetic field of the combination of \mathbf{J}_{ie} and \mathbf{M} , both radiating in all space filled with the homogeneous chiral medium that is inside the scatterer in the original problem. The i in \mathbf{H}_i indicates radiation in all space filled with the internal medium of the original problem. The first argument of \mathbf{H}_i is an electric current and the second argument of \mathbf{H}_i is a magnetic current. The subscript S^+ indicates the tangential part of the enclosed field on the side of S facing outside the scatterer. Although the sources on S in the internal equivalence are $-\mathbf{J}_{ie}$ and $-\mathbf{M}$, it was possible to employ \mathbf{J}_{ie} and \mathbf{M} in (2.4) because (2.4) is equivalent to itself with \mathbf{J}_{ie} and \mathbf{M} replaced by $-\mathbf{J}_{ie}$ and $-\mathbf{M}$, respectively.

The product of an arbitrary constant α with (2.3) is added to (2.1) to obtain

$$-\frac{1}{\eta_e} ([\mathbf{E}_e(\mathbf{J}_e, \mathbf{M})]_{S^-} + \alpha [\mathbf{E}_i(\mathbf{J}_{ie}, \mathbf{M})]_{S^+}) = \frac{1}{\eta_e} [\mathbf{E}^{\text{inc}}]_S \quad (2.5)$$

and the product of an arbitrary constant β with (2.4) is added to (2.2) to obtain

$$-([\mathbf{H}_e(\mathbf{J}_e, \mathbf{M})]_{S^-} + \beta [\mathbf{H}_i(\mathbf{J}_{ie}, \mathbf{M})]_{S^+}) = [\mathbf{H}^{\text{inc}}]_S \quad (2.6)$$

where, in Chapter 3, the \mathbf{E} 's and the \mathbf{H} 's will be expressed in terms of integrals over their arguments. Equations (2.5) and (2.6) are the integral equations that will be solved by the method of moments. If $\alpha\beta^*$ is real and positive where $*$ denotes the complex conjugate, then it can be shown that (2.5) and (2.6) imply (2.1)–(2.4) [10, Section 2]. Equations (2.5) and (2.6) are two vector equations on S . The unknowns in (2.5) and (2.6) are \mathbf{J}_e on S and the composite unknown consisting of \mathbf{J}_i on S_c and \mathbf{M} on S_a . Hence, the unknowns in the two vector equations (2.5) and (2.6) on S are two vector unknowns on S . Therefore, it should be possible to solve (2.5) and (2.6) by the method of moments.

2.3 Expansion of the electric and magnetic currents

The electric and magnetic currents in (2.5) and (2.6) are expanded as

$$\mathbf{J}_e = \sum_{n=-N}^N \sum_{j=1}^{N_t} \left(I_{nj}^t \mathbf{J}_{nj}^t + I_{nj}^\phi \mathbf{J}_{nj}^\phi \right) \quad (2.7)$$

$$\mathbf{J}_{ie} = \sum_{n=-N}^N \sum_{j=1}^{N_t} \left((L'_j V_{nj}^t + L_j I_{nj}^t) \mathbf{J}_{nj}^t + (L'_j V_{nj}^\phi + L_j I_{nj}^\phi) \mathbf{J}_{nj}^\phi \right) \quad (2.8)$$

$$\mathbf{M} = \eta_e \sum_{n=-N}^N \sum_{j=1}^{N_t} L_j \left(V_{nj}^t \mathbf{J}_{nj}^t + V_{nj}^\phi \mathbf{J}_{nj}^\phi \right) \quad (2.9)$$

where I_{nj}^t , I_{nj}^ϕ , V_{nj}^t and V_{nj}^ϕ are complex constants to be determined and \mathbf{J}_{nj}^t and \mathbf{J}_{nj}^ϕ are expansion functions given by

$$\mathbf{J}_{nj}^t = \hat{\mathbf{t}} \frac{T_j(t)}{\rho} e^{jn\phi} \quad (2.10)$$

$$\mathbf{J}_{nj}^\phi = \hat{\boldsymbol{\phi}} \frac{T_j(t)}{\rho} e^{jn\phi} \quad (2.11)$$

where t is the arc length along the generating curve C of the body of revolution (BOR), $\rho = \rho(t)$ is the distance from the z -axis of the BOR, ϕ is the angle measured from the positive x -axis toward the y -axis in the xy -plane, and $T_j(t)$ is the triangular function defined by

$$T_j(t) = \begin{cases} \frac{t - t_{2j-1}}{d_j}, & t_{2j-1} \leq t < t_{2j+1} \\ \frac{t_{2j+3} - t}{d_{j+1}}, & t_{2j+1} \leq t < t_{2j+3} \\ 0, & \text{elsewhere} \end{cases} \quad (2.12)$$

where

$$d_j = \Delta_{2j-1} + \Delta_{2j} \quad (2.13)$$

$$\Delta_j = t_{j+1} - t_j. \quad (2.14)$$

In (2.10) and (2.11), $\hat{\mathbf{t}}$ and $\hat{\boldsymbol{\phi}}$ are the unit vectors in the t - and ϕ -directions, respectively. The t -direction is such that

$$\hat{\boldsymbol{\phi}} \times \hat{\mathbf{t}} = \hat{\mathbf{n}} \quad (2.15)$$

where $\hat{\mathbf{n}}$ is the unit vector that is perpendicular to S and point outwards from chiral BOR.

The generating curve C consists of the straight line segment from $t = t_1$ to $t = t_2$, that from t_2 to t_3, \dots , that from t_{2N_t+2} to t_{2N_t+3} where, as in (2.7), N_t is the number of triangles on C . A generating curve for $N_t = 3$ is shown in Fig. 2.4. In (2.8) and (2.9),

$$L_j = \begin{cases} 1, & T_j(t) \text{ is in an aperture} \\ 0, & T_j(t) \text{ is on a conductor} \end{cases} \quad (2.16)$$

$$L'_j = \begin{cases} 1, & T_j(t) \text{ is on a conductor} \\ 0, & T_j(t) \text{ is in an aperture.} \end{cases} \quad (2.17)$$

The combination of the triangular functions in the apertures and the triangular functions on the conductors has to cover C exactly. Actually, the terms in (2.8) and (2.9) are more easily controlled by a single logical variable rather than the two numerical variables L_j and L'_j . In (2.8), \mathbf{J}_{ie} on S_c consists of the terms multiplied by L'_j and \mathbf{J}_{ie} on S_a consists of the terms multiplied by L_j . The j in $jn\phi$ in (2.10) and (2.11) is $\sqrt{-1}$, not to be confused with the other j in (2.10) and (2.11).

Each triangular function on C has to be identified as either a triangular function in the apertures or a triangular function on the conductors. Because the combination of the

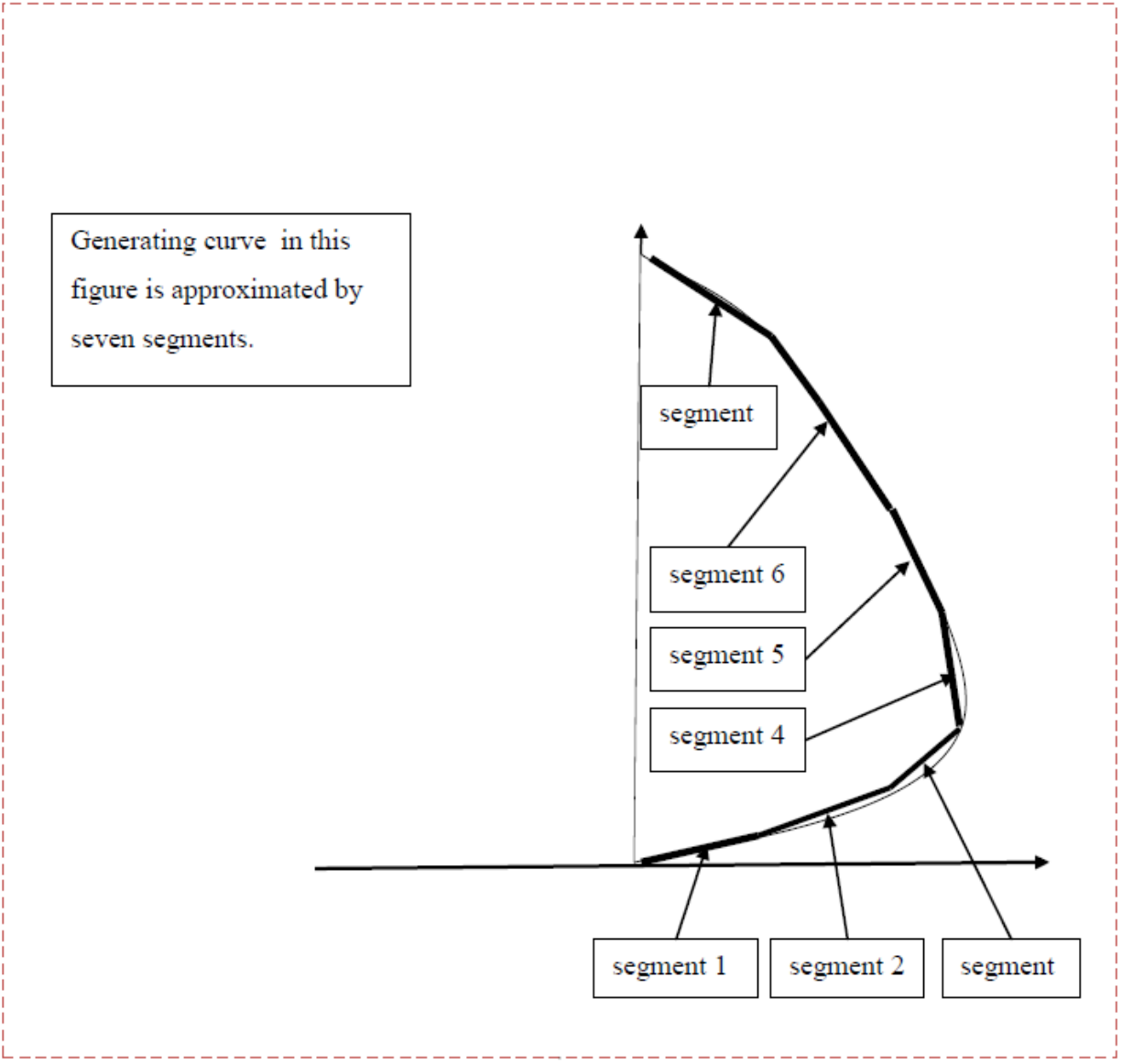


Figure 2.4 Generating curve is approximated by seven straight line segments

triangular functions in the apertures and the triangular functions on the conductors has to cover C exactly, the last triangular function on a conductor must overlap with the first triangular function in the aperture at the end of the conductor. Unfortunately, identification of the first triangular function in the aperture at the end of a conductor is not precise. This triangular function could be chosen such that all of it is in the aperture or such that only part of it is in the aperture. For example, if the aperture begins at t_{2j+1} , then the first triangular function in the aperture could, with reference to (2.12), be either T_j or T_{j+1} . If the aperture begins at t_{2j} , then the first triangular function in the aperture could be T_{j-1} , T_j , or T_{j+1} . Because of this uncertainty, the number of triangles in the apertures is not known exactly. This number can be made known exactly by deciding whether to put the beginning of each aperture at an even or odd point and deciding whether to require the first and last triangular functions in each aperture to be either entirely in the aperture or only partly in the aperture.

Due to possible singular behavior of the fields at the edge of a conductor [44], equivalent currents that are perpendicular to the edge could be proportional to \sqrt{d} near the edge and equivalent currents that are parallel to the edge could be proportional to $1/\sqrt{d}$ near the edge where d is the distance from the edge. The expansions (2.7)–(2.9) do not allow for such behavior near the edge.

Substitution of (2.7)–(2.9) into (2.5) and (2.6) gives

$$\begin{aligned}
& \sum_{n=-N}^N \left\{ \sum_{j=1}^{N_t} \left(I_{nj}^t \left[-\frac{1}{\eta_e} \mathbf{E}_e(\mathbf{J}_{nj}^t, \mathbf{0}) \right]_{S^-} + I_{nj}^\phi \left[-\frac{1}{\eta_e} \mathbf{E}_e(\mathbf{J}_{nj}^\phi, \mathbf{0}) \right]_{S^-} \right) \right. \\
& \quad \left. + \sum_{j=1}^{N_t} L_j \left(V_{nj}^t \left[-\mathbf{E}_e(\mathbf{0}, \mathbf{J}_{nj}^t) \right]_{S^-} + V_{nj}^\phi \left[-\mathbf{E}_e(\mathbf{0}, \mathbf{J}_{nj}^\phi) \right]_{S^-} \right) \right. \\
& + \sum_{j=1}^{N_t} \left((L'_j V_{nj}^t + L_j I_{nj}^t) \left[-\frac{\alpha}{\eta_e} \mathbf{E}_i(\mathbf{J}_{nj}^t, \mathbf{0}) \right]_{S^+} + (L'_j V_{nj}^\phi + L_j I_{nj}^\phi) \left[-\frac{\alpha}{\eta_e} \mathbf{E}_i(\mathbf{J}_{nj}^\phi, \mathbf{0}) \right]_{S^+} \right) \\
& \quad \left. + \sum_{j=1}^{N_t} L_j \left(V_{nj}^t \left[-\alpha \mathbf{E}_i(\mathbf{0}, \mathbf{J}_{nj}^t) \right]_{S^+} + V_{nj}^\phi \left[-\alpha \mathbf{E}_i(\mathbf{0}, \mathbf{J}_{nj}^\phi) \right]_{S^+} \right) \right\} = \left[\frac{1}{\eta_e} \mathbf{E}^{\text{inc}} \right]_S \quad (2.18) \\
& \sum_{n=-N}^N \left\{ \sum_{j=1}^{N_t} \left(I_{nj}^t \left[-\mathbf{H}_e(\mathbf{J}_{nj}^t, \mathbf{0}) \right]_{S^-} + I_{nj}^\phi \left[-\mathbf{H}_e(\mathbf{J}_{nj}^\phi, \mathbf{0}) \right]_{S^-} \right) \right. \\
& \quad \left. + \sum_{j=1}^{N_t} L_j \left(V_{nj}^t \left[-\eta_e \mathbf{H}_e(\mathbf{0}, \mathbf{J}_{nj}^t) \right]_{S^-} + V_{nj}^\phi \left[-\eta_e \mathbf{H}_e(\mathbf{0}, \mathbf{J}_{nj}^\phi) \right]_{S^-} \right) \right.
\end{aligned}$$

$$\begin{aligned}
& + \sum_{j=1}^{N_t} \left((L'_j V_{nj}^t + L_j I_{nj}^t) [-\beta \mathbf{H}_i(\mathbf{J}_{nj}^t, \mathbf{0})]_{S^+} + (L'_j V_{nj}^\phi + L_j I_{nj}^\phi) [-\beta \mathbf{H}_i(\mathbf{J}_{nj}^\phi, \mathbf{0})]_{S^+} \right) \\
& + \sum_{j=1}^{N_t} L_j \left(V_{nj}^t [-\beta \eta_e \mathbf{H}_i(\mathbf{0}, \mathbf{J}_{nj}^t)]_{S^+} + V_{nj}^\phi [-\beta \eta_e \mathbf{H}_i(\mathbf{0}, \mathbf{J}_{nj}^\phi)]_{S^+} \right) \Big\} = [\mathbf{H}^{\text{inc}}]_S. \quad (2.19)
\end{aligned}$$

2.4 Testing functions

Testing functions \mathbf{J}_{-mi}^t and \mathbf{J}_{-mi}^ϕ are defined by

$$\mathbf{J}_{-mi}^t = \hat{\mathbf{t}} \frac{T_i(t)}{\rho} e^{-jm\phi} \quad (2.20)$$

$$\mathbf{J}_{-mi}^\phi = \hat{\boldsymbol{\phi}} \frac{T_i(t)}{\rho} e^{-jm\phi}. \quad (2.21)$$

The symmetric product of two vector functions \mathbf{f} and \mathbf{g} on S is $\langle \mathbf{f}, \mathbf{g} \rangle$ given by

$$\langle \mathbf{f}, \mathbf{g} \rangle = \iint_S \mathbf{f} \cdot \mathbf{g} \, ds. \quad (2.22)$$

First taking the symmetric product of \mathbf{J}_{-mi}^t with (2.18), then taking the symmetric product of \mathbf{J}_{-mi}^ϕ with (2.18), next taking the symmetric product of \mathbf{J}_{-mi}^t with (2.19), and finally taking the symmetric product of \mathbf{J}_{-mi}^ϕ with (2.19), one obtains four equations. In (2.18) and (2.19), the term of \sum_{-N}^N whose index is n has, as will be seen later, $e^{jn\phi}$ dependence so that only the term of \sum_{-N}^N whose index is m will survive in the previously mentioned equations. Replacing m by n in these equations, one obtains the matrix equation

$$\begin{bmatrix} Z_n^{tt} & Z_n^{t\phi} & C_n^{tt} & C_n^{t\phi} \\ Z_n^{\phi t} & Z_n^{\phi\phi} & C_n^{\phi t} & C_n^{\phi\phi} \\ D_n^{tt} & D_n^{t\phi} & Y_n^{tt} & Y_n^{t\phi} \\ D_n^{\phi t} & D_n^{\phi\phi} & Y_n^{\phi t} & Y_n^{\phi\phi} \end{bmatrix} \begin{bmatrix} I_n^t \\ I_n^\phi \\ V_n^t \\ V_n^\phi \end{bmatrix} = \begin{bmatrix} \vec{V}_n^t \\ \vec{V}_n^\phi \\ \vec{I}_n^t \\ \vec{I}_n^\phi \end{bmatrix} \quad (2.23)$$

where, for $q = t$ or $q = \phi$, I_n^q and V_n^q are column matrices whose j^{th} elements are I_{nj}^q and V_{nj}^q , respectively. The ij^{th} elements of the members of the 4×4 array in (2.23) are, for $p = t$ or $p = \phi$ and $q = t$ or $q = \phi$,

$$Z_{nij}^{pq} = \iint_S \mathbf{J}_{-ni}^p \cdot \left[-\frac{1}{\eta_e} \mathbf{E}_e(\mathbf{J}_{nj}^q, \mathbf{0}) \right]_{S^-} ds + L_j \iint_S \mathbf{J}_{-ni}^p \cdot \left[-\frac{\alpha}{\eta_e} \mathbf{E}_i(\mathbf{J}_{nj}^q, \mathbf{0}) \right]_{S^+} ds \quad (2.24)$$

$$C_{nij}^{pq} = L_j \left(\iint_S \mathbf{J}_{-ni}^p \cdot [-\mathbf{E}_e(\mathbf{0}, \mathbf{J}_{nj}^q)]_{S^-} ds + \iint_S \mathbf{J}_{-ni}^p \cdot [-\alpha \mathbf{E}_i(\mathbf{0}, \mathbf{J}_{nj}^q)]_{S^+} ds \right) \\ + L'_j \iint_S \mathbf{J}_{-ni}^p \cdot \left[-\frac{\alpha}{\eta_e} \mathbf{E}_i(\mathbf{J}_{nj}^q, \mathbf{0}) \right]_{S^+} ds \quad (2.25)$$

$$D_{nij}^{pq} = \iint_S \mathbf{J}_{-ni}^p \cdot [-\mathbf{H}_e(\mathbf{J}_{nj}^q, \mathbf{0})]_{S^-} ds + L_j \iint_S \mathbf{J}_{-ni}^p \cdot [-\beta \mathbf{H}_i(\mathbf{J}_{nj}^q, \mathbf{0})]_{S^+} ds \quad (2.26)$$

$$Y_{nij}^{pq} = L_j \left(\iint_S \mathbf{J}_{-ni}^p \cdot [-\eta_e \mathbf{H}_e(\mathbf{0}, \mathbf{J}_{nj}^q)]_{S^-} ds + \iint_S \mathbf{J}_{-ni}^p \cdot [-\beta \eta_e \mathbf{H}_i(\mathbf{0}, \mathbf{J}_{nj}^q)]_{S^+} ds \right) \\ + L'_j \iint_S \mathbf{J}_{-ni}^p \cdot [-\beta \mathbf{H}_i(\mathbf{J}_{nj}^q, \mathbf{0})]_{S^+} ds. \quad (2.27)$$

For $p = t$ or $p = \phi$ the i^{th} elements of \vec{V}_n^p and \vec{I}_n^p are, respectively, \vec{V}_{ni}^p and \vec{I}_{ni}^p given by

$$\vec{V}_{ni}^p = \iint_S \mathbf{J}_{-ni}^p \cdot \left[\frac{1}{\eta_e} \mathbf{E}^{\text{inc}} \right]_S ds \quad (2.28)$$

$$\vec{I}_{ni}^p = \iint_S \mathbf{J}_{-ni}^p \cdot [\mathbf{H}^{\text{inc}}]_S ds. \quad (2.29)$$

The electric and magnetic fields of the combination of an electric current \mathbf{J} and a magnetic current \mathbf{M} in the chiral medium are respectively $\mathbf{E}_i(\mathbf{J}, \mathbf{M})$ and $\mathbf{H}_i(\mathbf{J}, \mathbf{M})$ given by [12, (11), (12)]

$$\mathbf{E}_i(\mathbf{J}, \mathbf{M}) = \mathbf{E}_+(\mathbf{J}_+, \mathbf{M}_+) + \mathbf{E}_-(\mathbf{J}_-, \mathbf{M}_-) \quad (2.30)$$

$$\mathbf{H}_i(\mathbf{J}, \mathbf{M}) = \mathbf{H}_+(\mathbf{J}_+, \mathbf{M}_+) + \mathbf{H}_-(\mathbf{J}_-, \mathbf{M}_-) \quad (2.31)$$

where $(\mathbf{E}_\pm(\mathbf{J}_\pm, \mathbf{M}_\pm), \mathbf{H}_\pm(\mathbf{J}_\pm, \mathbf{M}_\pm))$ is the electromagnetic field of the combination of the electric current \mathbf{J}_\pm and the magnetic current \mathbf{M}_\pm in the hypothetical medium whose permittivity and permeability are, respectively, ε_\pm and μ_\pm given by [12, (15), (16)]

$$\varepsilon_\pm = \varepsilon_i(1 \pm \xi_r) \quad (2.32)$$

$$\mu_\pm = \mu_i(1 \pm \xi_r) \quad (2.33)$$

where ε_i , μ_i , and ξ_r are, respectively, the permittivity, permeability, and relative chirality of the chiral medium; $\xi_r = \xi / \sqrt{\varepsilon_i \mu_i}$ where ξ is the chirality of the chiral medium. The intrinsic impedance of the hypothetical medium and the wavenumber in the hypothetical medium are, respectively, η_\pm and k_\pm defined by

$$\eta_\pm = \sqrt{\frac{\mu_\pm}{\varepsilon_\pm}} \quad (2.34)$$

$$k_\pm = \omega \sqrt{\mu_\pm \varepsilon_\pm} \quad (2.35)$$

where ω is the angular frequency. In (2.30) and (2.31) [12, (17), (18)],

$$\mathbf{J}_{\pm} = \frac{1}{2} \left(\mathbf{J} \mp \frac{j}{\eta_i} \mathbf{M} \right) \quad (2.36)$$

$$\mathbf{M}_{\pm} = \frac{1}{2} (\mathbf{M} \pm j\eta_i \mathbf{J}) \quad (2.37)$$

where $\eta_i = \sqrt{\mu_i/\varepsilon_i}$ is the intrinsic impedance of the chiral medium. It can be shown that

$$\eta_{\pm} = \eta_i. \quad (2.38)$$

Substituting (2.36) and (2.37) into (2.30) and (2.31), one obtains

$$\mathbf{E}_i(\mathbf{J}, \mathbf{M}) = \frac{1}{2} \mathbf{E}_+(\mathbf{J} - \frac{j}{\eta_i} \mathbf{M}, \mathbf{M} + j\eta_i \mathbf{J}) + \frac{1}{2} \mathbf{E}_-(\mathbf{J} + \frac{j}{\eta_i} \mathbf{M}, \mathbf{M} - j\eta_i \mathbf{J}) \quad (2.39)$$

$$\mathbf{H}_i(\mathbf{J}, \mathbf{M}) = \frac{1}{2} \mathbf{H}_+(\mathbf{J} - \frac{j}{\eta_i} \mathbf{M}, \mathbf{M} + j\eta_i \mathbf{J}) + \frac{1}{2} \mathbf{H}_-(\mathbf{J} + \frac{j}{\eta_i} \mathbf{M}, \mathbf{M} - j\eta_i \mathbf{J}). \quad (2.40)$$

Substitution of (2.39) and (2.40) into (2.24)–(2.27) gives

$$\begin{aligned} Z_{nij}^{pq} &= \iint_S \mathbf{J}_{-ni}^p \cdot \left[-\frac{1}{\eta_e} \mathbf{E}_e(\mathbf{J}_{nj}^q, \mathbf{0}) \right]_{S^-} ds \\ &\quad + L_j \iint_S \mathbf{J}_{-ni}^p \cdot \left[-\frac{\alpha}{2\eta_e} \mathbf{E}_+(\mathbf{J}_{nj}^q, j\eta_i \mathbf{J}_{nj}^q) - \frac{\alpha}{2\eta_e} \mathbf{E}_-(\mathbf{J}_{nj}^q, -j\eta_i \mathbf{J}_{nj}^q) \right]_{S^+} ds \end{aligned} \quad (2.41)$$

$$\begin{aligned} C_{nij}^{pq} &= L_j \left(\iint_S \mathbf{J}_{-ni}^p \cdot [-\mathbf{E}_e(\mathbf{0}, \mathbf{J}_{nj}^q)]_{S^-} ds \right. \\ &\quad \left. + \iint_S \mathbf{J}_{-ni}^p \cdot \left[-\frac{\alpha}{2} \mathbf{E}_+(\mathbf{J}_{nj}^q, \mathbf{J}_{nj}^q) - \frac{\alpha}{2} \mathbf{E}_-(\mathbf{J}_{nj}^q, \mathbf{J}_{nj}^q) \right]_{S^+} ds \right) \\ &\quad + L'_j \iint_S \mathbf{J}_{-ni}^p \cdot \left[-\frac{\alpha}{2\eta_e} \mathbf{E}_+(\mathbf{J}_{nj}^q, j\eta_i \mathbf{J}_{nj}^q) - \frac{\alpha}{2\eta_e} \mathbf{E}_-(\mathbf{J}_{nj}^q, -j\eta_i \mathbf{J}_{nj}^q) \right]_{S^+} ds \end{aligned} \quad (2.42)$$

$$\begin{aligned} D_{nij}^{pq} &= \iint_S \mathbf{J}_{-ni}^p \cdot [-\mathbf{H}_e(\mathbf{J}_{nj}^q, \mathbf{0})]_{S^-} ds \\ &\quad + L_j \iint_S \mathbf{J}_{-ni}^p \cdot \left[-\frac{\beta}{2} \mathbf{H}_+(\mathbf{J}_{nj}^q, j\eta_i \mathbf{J}_{nj}^q) - \frac{\beta}{2} \mathbf{H}_-(\mathbf{J}_{nj}^q, -j\eta_i \mathbf{J}_{nj}^q) \right]_{S^+} ds \end{aligned} \quad (2.43)$$

$$\begin{aligned} Y_{nij}^{pq} &= L_j \left(\iint_S \mathbf{J}_{-ni}^p \cdot [-\eta_e \mathbf{H}_e(\mathbf{0}, \mathbf{J}_{nj}^q)]_{S^-} ds \right. \\ &\quad \left. + \iint_S \mathbf{J}_{-ni}^p \cdot \left[-\frac{\beta\eta_e}{2} \mathbf{H}_+(\mathbf{J}_{nj}^q, \mathbf{J}_{nj}^q) - \frac{\beta\eta_e}{2} \mathbf{H}_-(\mathbf{J}_{nj}^q, \mathbf{J}_{nj}^q) \right]_{S^+} ds \right) \\ &\quad + L'_j \iint_S \mathbf{J}_{-ni}^p \cdot \left[-\frac{\beta}{2} \mathbf{H}_+(\mathbf{J}_{nj}^q, j\eta_i \mathbf{J}_{nj}^q) - \frac{\beta}{2} \mathbf{H}_-(\mathbf{J}_{nj}^q, -j\eta_i \mathbf{J}_{nj}^q) \right]_{S^+} ds. \end{aligned} \quad (2.44)$$

The electromagnetic field (\mathbf{E}, \mathbf{H}) in any homogeneous medium satisfies [34, (1)]

$$\mathbf{E}(\mathbf{0}, \mathbf{J}) = -\mathbf{H}(\mathbf{J}, \mathbf{0}) \quad (2.45)$$

$$\mathbf{H}(\mathbf{0}, \mathbf{J}) = \frac{1}{\eta^2} \mathbf{E}(\mathbf{J}, \mathbf{0}) \quad (2.46)$$

where η is the intrinsic impedance in the homogeneous medium in question. Using (2.45) and (2.46) to reduce all nonzero magnetic current arguments to zeros in (2.41)–(2.44), next using (2.38), and then suppressing all the zero magnetic current arguments in the resulting equations, one obtains

$$Z_{nij}^{pq} = \frac{1}{2} \left\{ 2Z_{nije}^{pq} + L_j (\alpha\eta_r Z_{nij+}^{pq} - j\alpha\eta_r Y_{nij+}^{pq+} + \alpha\eta_r Z_{nij-}^{pq} + j\alpha\eta_r Y_{nij-}^{pq+}) \right\} \quad (2.47)$$

$$C_{nij}^{pq} = \frac{1}{2} \left\{ L_j (-2Y_{nije}^{pq-} - j\alpha Z_{nij+}^{pq} - \alpha Y_{nij+}^{pq+} + j\alpha Z_{nij-}^{pq} - \alpha Y_{nij-}^{pq+}) \right. \\ \left. + L'_j (\alpha\eta_r Z_{nij+}^{pq} - j\alpha\eta_r Y_{nij+}^{pq+} + \alpha\eta_r Z_{nij-}^{pq} + j\alpha\eta_r Y_{nij-}^{pq+}) \right\} \quad (2.48)$$

$$D_{nij}^{pq} = \frac{1}{2} \left\{ 2Y_{nije}^{pq-} + L_j (\beta Y_{nij+}^{pq+} + j\beta Z_{nij+}^{pq} + \beta Y_{nij-}^{pq+} - j\beta Z_{nij-}^{pq}) \right\} \quad (2.49)$$

$$Y_{nij}^{pq} = \frac{1}{2} \left\{ L_j \left(2Z_{nije}^{pq} - \frac{j\beta}{\eta_r} Y_{nij+}^{pq+} + \frac{\beta}{\eta_r} Z_{nij+}^{pq} + \frac{j\beta}{\eta_r} Y_{nij-}^{pq+} + \frac{\beta}{\eta_r} Z_{nij-}^{pq} \right) \right. \\ \left. + L'_j (\beta Y_{nij+}^{pq+} + j\beta Z_{nij+}^{pq} + \beta Y_{nij-}^{pq+} - j\beta Z_{nij-}^{pq}) \right\} \quad (2.50)$$

where $\eta_r = \eta_i/\eta_e$ is the relative intrinsic impedance of the chiral medium and

$$Z_{nij(e,+, -)}^{pq} = -\frac{1}{\eta_{(e,+, -)}} \iint_S \mathbf{J}_{-ni}^p \cdot \mathbf{E}_{(e,+, -)}(\mathbf{J}_{nj}^q) ds \quad (2.51)$$

$$Y_{nije}^{pq-} = -\iint_S \mathbf{J}_{-ni}^p \cdot \mathbf{H}_e^-(\mathbf{J}_{nj}^q) ds \quad (2.52)$$

$$Y_{nij\pm}^{pq+} = -\iint_S \mathbf{J}_{-ni}^p \cdot \mathbf{H}_\pm^+(\mathbf{J}_{nj}^q) ds \quad (2.53)$$

where η_\pm is given by (4.38). Because \mathbf{J}_{-ni}^p is on S , each field in (2.51)–(2.53) is automatically evaluated on S . The electric field $\mathbf{E}_{(e,+, -)}$ in (2.51) is continuous across S . However, the magnetic field $\mathbf{H}_{(e,+, -)}$ is not continuous across S . In (2.52), \mathbf{H}_e^- is \mathbf{H}_e evaluated on the side of S facing inside the scatterer. In (2.53), \mathbf{H}_\pm^+ is \mathbf{H}_\pm evaluated on the side of S facing outside the scatterer.

Equations (2.47)–(2.50) are recast as

$$Z_{nij}^{pq} = Z_{nije}^{pq} + L_j \alpha \eta_r Z_{ny}^{pq} \quad (2.54)$$

$$C_{nij}^{pq} = L_j (-Y_{nije}^{pq-} - \alpha Y_{nz}^{pq}) + L'_j \alpha \eta_r Z_{ny}^{pq} \quad (2.55)$$

$$D_{nij}^{pq} = Y_{nije}^{pq-} + L_j \beta Y_{nz}^{pq} \quad (2.56)$$

$$Y_{nij}^{pq} = L_j \left(Z_{nije}^{pq} + \frac{\beta}{\eta_r} Z_{ny}^{pq} \right) + L'_j \beta Y_{nz}^{pq} \quad (2.57)$$

where

$$Z_{ny}^{pq} = 0.5 \left\{ Z_{nij+}^{pq} + Z_{nij-}^{pq} - j \left(Y_{nij+}^{pq+} - Y_{nij-}^{pq+} \right) \right\} \quad (2.58)$$

$$Y_{nz}^{pq} = 0.5 \left\{ Y_{nij+}^{pq+} + Y_{nij-}^{pq+} + j \left(Z_{nij+}^{pq} - Z_{nij-}^{pq} \right) \right\}. \quad (2.59)$$

Replacing n by $-n$ in(2.54)–(2.59) and taking advantage of the even or odd property with respect to n of each quantity on the right-hand side, one obtains

$$Z_{-nij}^{pq} = Z_{-nije}^{pq} + L_j \alpha \eta_r Z_{-ny}^{pq} \quad (2.60)$$

$$C_{-nij}^{pq} = L_j \left(-Y_{-nije}^{pq-} - \alpha Y_{-nz}^{pq} \right) + L'_j \alpha \eta_r Z_{-ny}^{pq} \quad (2.61)$$

$$D_{-nij}^{pq} = Y_{-nije}^{pq-} + L_j \beta Y_{-nz}^{pq} \quad (2.62)$$

$$Y_{-nij}^{pq} = L_j \left(Z_{-nije}^{pq} + \frac{\beta}{\eta_r} Z_{-ny}^{pq} \right) + L'_j \beta Y_{-nz}^{pq} \quad (2.63)$$

where, for $pq = tt$ or $pq = \phi\phi$,

$$Z_{-nije}^{pq} = Z_{nije}^{pq} \quad (2.64)$$

$$Y_{-nije}^{pq-} = -Y_{nije}^{pq-} \quad (2.65)$$

$$Z_{-ny}^{pq} = 0.5 \left\{ Z_{nij+}^{pq} + Z_{nij-}^{pq} + j \left(Y_{nij+}^{pq+} - Y_{nij-}^{pq+} \right) \right\} \quad (2.66)$$

$$Y_{-nz}^{pq} = -0.5 \left\{ Y_{nij+}^{pq+} + Y_{nij-}^{pq+} - j \left(Z_{nij+}^{pq} - Z_{nij-}^{pq} \right) \right\} \quad (2.67)$$

and, for $pq = t\phi$ or $pq = \phi t$,

$$Z_{-nije}^{pq} = -Z_{nije}^{pq} \quad (2.68)$$

$$Y_{-nije}^{pq-} = Y_{nije}^{pq-} \quad (2.69)$$

$$Z_{-ny}^{pq} = -0.5 \left\{ Z_{nij+}^{pq} + Z_{nij-}^{pq} + j \left(Y_{nij+}^{pq+} - Y_{nij-}^{pq+} \right) \right\} \quad (2.70)$$

$$Y_{-nz}^{pq} = 0.5 \left\{ Y_{nij+}^{pq+} + Y_{nij-}^{pq+} - j \left(Z_{nij+}^{pq} - Z_{nij-}^{pq} \right) \right\}. \quad (2.71)$$

Chapter 3

The Elements of the Moment Matrix

3.1 Introduction

In Chapter 2, the elements of the moment matrix are given by (2.47)–(2.50) whose right-hand sides contain Z 's and Y 's. In Chapter 3, the Z 's and Y 's are given by (3.74)–(3.81) and (3.109)–(3.112). These Z 's and Y 's can be substituted into (2.47)–(2.50) to obtain expressions that can be used to compute the elements of the moment matrix.

3.2 Analytical Treatment of Expressions (2.51)–(2.53) for the Z 's and Y 's

The moment matrix is the square matrix in (2.23). Its elements are given by (2.47)–(2.50) where $Z_{nij(e,+,-)}^{pq}$, Y_{nije}^{pq-} , and $Y_{nij\pm}^{pq+}$ are given by (2.51)–(2.53) where [4, (2)]

$$-\frac{1}{\eta_{(e,+,-)}} \mathbf{E}_{(e,+,-)}(\mathbf{J}_{nj}^q) = \frac{1}{\eta_{(e,+,-)}} (j\omega \mathbf{A}_{(e,+,-)}(\mathbf{r}) + \nabla V_{(e,+,-)}(\mathbf{r})) \quad (3.1)$$

$$-\mathbf{H}_e^-(\mathbf{J}_{nj}^q) = -\frac{1}{\mu_e} \nabla^- \times \mathbf{A}_e(\mathbf{r}) \quad (3.2)$$

$$-\mathbf{H}_\pm^+(\mathbf{J}_{nj}^q) = -\frac{1}{\mu_\pm} \nabla^+ \times \mathbf{A}_\pm(\mathbf{r}) \quad (3.3)$$

where

$$\mathbf{A}_{(e,+,-)}(\mathbf{r}) = \frac{\mu_{(e,+,-)}}{4\pi} \iint_S \mathbf{J}_{nj}^q(\mathbf{r}') G_{(e,+,-)}(R) ds' \quad (3.4)$$

$$V_{(e,+,-)}(\mathbf{r}) = \frac{j}{4\pi\omega\epsilon_{(e,+,-)}} \iint_S (\nabla'_s \cdot \mathbf{J}_{nj}^q(\mathbf{r}')) G_{(e,+,-)}(R) ds' \quad (3.5)$$

$$G_{(e,+,-)}(R) = \frac{e^{-jk_{(e,+,-)}R}}{R} \quad (3.6)$$

$$R = |\mathbf{r} - \mathbf{r}'| \quad (3.7)$$

where $k_{(e,+,-)}$ is the wavenumber in the external medium, the “+” hypothetical medium, or the “-” hypothetical medium. In (3.2), the “-” in ∇^- indicates evaluation on the side of S facing inside the scatterer. In (3.3), the “+” in ∇^+ indicates evaluation on the side of S facing outside the scatterer.

Substitution (3.1) into (2.51) gives

$$Z_{nij(e,+,-)}^{pq} = \frac{1}{\eta_{(e,+,-)}} \iint_S \mathbf{J}_{-ni}^p(\mathbf{r}) \cdot (j\omega \mathbf{A}_{(e,+,-)}(\mathbf{r}) + \nabla V_{(e,+,-)}(\mathbf{r})) ds. \quad (3.8)$$

In view of the vector identity

$$\nabla_s \cdot (\mathbf{J}_{-ni}^p V_{(e,+,-)}) = (\nabla_s \cdot \mathbf{J}_{-ni}^p) V_{(e,+,-)} + \mathbf{J}_{-ni}^p \cdot \nabla V_{(e,+,-)} \quad (3.9)$$

and the surface divergence theorem, (3.8) becomes

$$Z_{nij(e,+,-)}^{pq} = \frac{j\omega}{\eta_{(e,+,-)}} \iint_S \mathbf{J}_{-ni}^p(\mathbf{r}) \cdot \mathbf{A}_{(e,+,-)}(\mathbf{r}) ds - \frac{1}{\eta_{(e,+,-)}} \iint_S (\nabla_s \cdot \mathbf{J}_{-ni}^p(\mathbf{r})) V_{(e,+,-)}(\mathbf{r}) ds. \quad (3.10)$$

Substituting (3.4) and (3.5) into (3.10), one obtains

$$\begin{aligned} Z_{nij(e,+,-)}^{pq} &= \frac{jk_{(e,+,-)}}{4\pi} \iint_S ds \iint_S ds' (\mathbf{J}_{-ni}^p(\mathbf{r}) \cdot \mathbf{J}_{nj}^q(\mathbf{r}')) G_{(e,+,-)}(R) \\ &\quad - \frac{j}{4\pi k_{(e,+,-)}} \iint_S ds \iint_S ds' (\nabla_s \cdot \mathbf{J}_{-ni}^p(\mathbf{r})) (\nabla'_s \cdot \mathbf{J}_{nj}^q(\mathbf{r}')) G_{(e,+,-)}(R). \end{aligned} \quad (3.11)$$

Substitution of the “e” part of (3.4) into (3.2) gives

$$-\mathbf{H}_e^-(\mathbf{J}_{nj}^q) = -\frac{1}{4\pi} \nabla^- \times \iint_S \mathbf{J}_{nj}^q(\mathbf{r}') G_e(R) ds'. \quad (3.12)$$

Taking the curl of the integrand instead of the integral in (3.12) and then taking the limit as \mathbf{r} approaches S from inside the scatterer, one obtains [54, Section 3.1.1]

$$-\mathbf{H}_e^-(\mathbf{J}_{nj}^q) = -\frac{1}{4\pi} \iint_S \mathbf{J}_{nj}^q(\mathbf{r}') \times \nabla' G_e(R) ds' + \frac{1}{2} \mathbf{J}_{nj}^q(\mathbf{r}) \times \hat{\mathbf{n}}. \quad (3.13)$$

Substitution of the “±” part of (3.4) into (3.3) gives

$$-\mathbf{H}_\pm^+(\mathbf{J}_{nj}^q) = -\frac{1}{4\pi} \nabla^+ \times \iint_S \mathbf{J}_{nj}^q(\mathbf{r}') G_\pm(R) ds'. \quad (3.14)$$

Taking the curl of the integrand instead of the integral in (3.14) and then taking the limit as \mathbf{r} approaches S from outside the scatterer, one obtains [54, Section 3.1.1]

$$-\mathbf{H}_\pm^+(\mathbf{J}_{nj}^q) = -\frac{1}{4\pi} \iint_S \mathbf{J}_{nj}^q(\mathbf{r}') \times \nabla' G_\pm(R) ds' - \frac{1}{2} \mathbf{J}_{nj}^q(\mathbf{r}) \times \hat{\mathbf{n}}. \quad (3.15)$$

In the integrands in (3.13) and (3.15), \mathbf{r} is exactly on S and the principal values of the integrals are taken if necessary to obtain convergence of the integrals. Because R is given by (3.7),

$$\nabla' G_{(e,+,-)}(R) = G'_{(e,+,-)}(R)(\mathbf{r} - \mathbf{r}') \quad (3.16)$$

where

$$G'_{(e,+,-)}(R) = \frac{1 + jk_{(e,+,-)}R}{R^3} e^{-jk_{(e,+,-)}R}. \quad (3.17)$$

Substitution of the “ e ” part of (3.16) into (3.13) gives

$$-\mathbf{H}_e^-(\mathbf{J}_{nj}^q) = -\frac{1}{4\pi} \iint_S (\mathbf{J}_{nj}^q(\mathbf{r}') \times (\mathbf{r} - \mathbf{r}')) G'_e(R) ds' + \frac{1}{2} \mathbf{J}_{nj}^q(\mathbf{r}) \times \hat{\mathbf{n}}. \quad (3.18)$$

Substitution of the “ \pm ” part of (3.16) into (3.15) gives

$$-\mathbf{H}_{\pm}^+(\mathbf{J}_{nj}^q) = -\frac{1}{4\pi} \iint_S (\mathbf{J}_{nj}^q(\mathbf{r}') \times (\mathbf{r} - \mathbf{r}')) G'_{\pm}(R) ds' - \frac{1}{2} \mathbf{J}_{nj}^q(\mathbf{r}) \times \hat{\mathbf{n}}. \quad (3.19)$$

Substituting (3.18) into (3.52), one obtains

$$\begin{aligned} Y_{nije}^{pq-} &= -\frac{1}{4\pi} \iint_S ds \iint_S ds' \mathbf{J}_{-ni}^p(\mathbf{r}) \cdot (\mathbf{J}_{nj}^q(\mathbf{r}') \times (\mathbf{r} - \mathbf{r}')) G'_e(R) \\ &\quad + \frac{1}{2} \iint_S \mathbf{J}_{-ni}^p(\mathbf{r}) \cdot (\mathbf{J}_{nj}^q(\mathbf{r}) \times \hat{\mathbf{n}}) ds. \end{aligned} \quad (3.20)$$

Substituting (3.19) into (3.53), one obtains

$$\begin{aligned} Y_{nij\pm}^{pq+} &= -\frac{1}{4\pi} \iint_S ds \iint_S ds' \mathbf{J}_{-ni}^p(\mathbf{r}) \cdot (\mathbf{J}_{nj}^q(\mathbf{r}') \times (\mathbf{r} - \mathbf{r}')) G'_{\pm}(R) \\ &\quad - \frac{1}{2} \iint_S \mathbf{J}_{-ni}^p(\mathbf{r}) \cdot (\mathbf{J}_{nj}^q(\mathbf{r}) \times \hat{\mathbf{n}}) ds. \end{aligned} \quad (3.21)$$

The t and ϕ dependences of $\mathbf{J}_{-ni}^p(\mathbf{r})$ and the t' and ϕ' dependences of $\mathbf{J}_{nj}^q(\mathbf{r}')$ are needed in expression (3.11) for $Z_{nij(e,+,-)}^{pq}$. Replacing (t, ϕ) by (t', ϕ') in (2.10) and (2.11) and replacing m by n in (2.20) and (2.21), one obtains

$$\mathbf{J}_{nj}^q(\mathbf{r}') = \hat{\mathbf{t}}' \frac{T_j(t')}{\rho'} e^{jn\phi'} \quad (3.22)$$

$$\mathbf{J}_{nj}^\phi(\mathbf{r}') = \hat{\phi}' \frac{T_j(t')}{\rho'} e^{jn\phi'} \quad (3.23)$$

$$\mathbf{J}_{-ni}^t(\mathbf{r}) = \hat{\mathbf{t}} \frac{T_i(t)}{\rho} e^{-jn\phi} \quad (3.24)$$

$$\mathbf{J}_{-ni}^\phi(\mathbf{r}) = \hat{\phi} \frac{T_i(t)}{\rho} e^{-jn\phi} \quad (3.25)$$

where $\hat{\mathbf{t}}'$, $\hat{\phi}'$, and ρ' are, respectively, $\hat{\mathbf{t}}$, $\hat{\phi}$, and ρ at $t = t'$. The surface divergence of a vector function $\hat{\mathbf{t}}f_t(t, \phi) + \hat{\phi}f_\phi(t, \phi)$ is $\nabla_s \cdot (\hat{\mathbf{t}}f_t(t, \phi) + \hat{\phi}f_\phi(t, \phi))$ given by

$$\nabla_s \cdot (\hat{\mathbf{t}}f_t(t, \phi) + \hat{\phi}f_\phi(t, \phi)) = \frac{1}{\rho} \frac{\partial}{\partial t} (\rho f_t(t, \phi)) + \frac{1}{\rho} \frac{\partial}{\partial \phi} f_\phi(t, \phi) \quad (3.26)$$

so that the the surface divergences of (3.22)–(3.25) are

$$\nabla'_s \cdot \mathbf{J}_{nj}^t(\mathbf{r}') = \frac{1}{\rho'} \left(\frac{d}{dt'} T_j(t') \right) e^{jn\phi'} \quad (3.27)$$

$$\nabla'_s \cdot \mathbf{J}_{nj}^\phi(\mathbf{r}') = \frac{jn}{\rho'^2} T_j(t') e^{jn\phi'} \quad (3.28)$$

$$\nabla_s \cdot \mathbf{J}_{-ni}^t(\mathbf{r}) = \frac{1}{\rho} \left(\frac{d}{dt} T_i(t) \right) e^{-jn\phi} \quad (3.29)$$

$$\nabla_s \cdot \mathbf{J}_{-ni}^\phi(\mathbf{r}) = \frac{-jn}{\rho^2} T_i(t) e^{-jn\phi}. \quad (3.30)$$

Taking the derivative with respect to t of (2.12) and then replacing t by t' in the resulting equation, one obtains

$$\frac{d}{dt'} T_j(t') = \frac{P_j(t')}{d_j} - \frac{P_{j+1}(t')}{d_{j+1}} \quad (3.31)$$

where $P_j(t)$ is the pulse function defined by

$$P_j(t) = \begin{cases} 1, & t_{2j-1} \leq t < t_{2j+1} \\ 0, & \text{elsewhere.} \end{cases} \quad (3.32)$$

Equation (3.31) with j replaced by i and t' replaced by t is

$$\frac{d}{dt} T_i(t) = \frac{P_i(t)}{d_i} - \frac{P_{i+1}(t)}{d_{i+1}}. \quad (3.33)$$

Substitution of (3.31) into (3.27) and substitution of (3.33) into (3.29) give

$$\nabla'_s \cdot \mathbf{J}_{nj}^t(\mathbf{r}') = \frac{1}{\rho'} \left(\frac{P_j(t')}{d_j} - \frac{P_{j+1}(t')}{d_{j+1}} \right) e^{jn\phi'} \quad (3.34)$$

$$\nabla_s \cdot \mathbf{J}_{-ni}^t(\mathbf{r}) = \frac{1}{\rho} \left(\frac{P_i(t)}{d_i} - \frac{P_{i+1}(t)}{d_{i+1}} \right) e^{-jn\phi}. \quad (3.35)$$

In view of (3.22)–(3.25), the dot products $\hat{\mathbf{t}} \cdot \hat{\mathbf{t}}'$, $\hat{\mathbf{t}} \cdot \hat{\boldsymbol{\phi}}'$, $\hat{\boldsymbol{\phi}} \cdot \hat{\mathbf{t}}'$, and $\hat{\boldsymbol{\phi}} \cdot \hat{\boldsymbol{\phi}}'$ are needed to evaluate $\mathbf{J}_{-ni}^p(\mathbf{r}) \cdot \mathbf{J}_{nj}^q(\mathbf{r}')$ in (3.11). These dot products are given by

$$\hat{\mathbf{t}} \cdot \hat{\mathbf{t}}' = \sin v \sin v' \cos(\phi' - \phi) + \cos v \cos v' \quad (3.36)$$

$$\hat{\mathbf{t}} \cdot \hat{\boldsymbol{\phi}}' = -\sin v \sin(\phi' - \phi) \quad (3.37)$$

$$\hat{\boldsymbol{\phi}} \cdot \hat{\mathbf{t}}' = \sin v' \sin(\phi' - \phi) \quad (3.38)$$

$$\hat{\boldsymbol{\phi}} \cdot \hat{\boldsymbol{\phi}}' = \cos(\phi' - \phi) \quad (3.39)$$

where v is the angle between $\hat{\mathbf{t}}$ and the z -axis and v' is the angle between $\hat{\mathbf{t}}'$ and the z -axis; v is positive if ρ increases with t and v' is positive if ρ' increases with t' . Replacing ds by $dt \rho d\phi$ and ds' by $dt' \rho' d\phi'$ in (3.11), letting p be either t or ϕ and q be either t or ϕ in (3.11), and then substituting (3.22)–(3.25), (3.28), (3.30), (3.34), and (3.35) into the resulting equations, one obtains, upon use of (3.36)–(3.39),

$$\begin{aligned} Z_{nij(e,+,-)}^{tt} &= \frac{jk_{(e,+,-)}}{4\pi} \int dt T_i(t) \int dt' T_j(t') \int_0^{2\pi} d\phi \\ &\quad \cdot \int_0^{2\pi} d\phi' G_{(e,+,-)}(R) (\sin v \sin v' \cos(\phi' - \phi) + \cos v \cos v') e^{jn(\phi' - \phi)} \\ &\quad - \frac{j}{4\pi k_{(e,+,-)}} \int dt \left(\frac{P_i(t)}{d_i} - \frac{P_{i+1}(t)}{d_{i+1}} \right) \int dt' \left(\frac{P_j(t')}{d_j} - \frac{P_{j+1}(t')}{d_{j+1}} \right) \int_0^{2\pi} d\phi \\ &\quad \cdot \int_0^{2\pi} d\phi' G_{(e,+,-)}(R) e^{jn(\phi' - \phi)} \end{aligned} \quad (3.40)$$

$$\begin{aligned} Z_{nij(e,+,-)}^{t\phi} &= -\frac{jk_{(e,+,-)}}{4\pi} \int dt T_i(t) \int dt' T_j(t') \int_0^{2\pi} d\phi \\ &\quad \cdot \int_0^{2\pi} d\phi' G_{(e,+,-)}(R) \sin v \sin(\phi' - \phi) e^{jn(\phi' - \phi)} \\ &\quad + \frac{n}{4\pi k_{(e,+,-)}} \int dt \left(\frac{P_i(t)}{d_i} - \frac{P_{i+1}(t)}{d_{i+1}} \right) \int dt' \frac{T_j(t')}{\rho'} \int_0^{2\pi} d\phi \int_0^{2\pi} d\phi' G_{(e,+,-)}(R) e^{jn(\phi' - \phi)} \end{aligned} \quad (3.41)$$

$$\begin{aligned}
Z_{nij(e,+,-)}^{\phi t} &= \frac{jk_{(e,+,-)}}{4\pi} \int dt T_i(t) \int dt' T_j(t') \int_0^{2\pi} d\phi \\
&\quad \cdot \int_0^{2\pi} d\phi' G_{(e,+,-)}(R) \sin v' \sin(\phi' - \phi) e^{jn(\phi' - \phi)} \\
&\quad - \frac{n}{4\pi k_{(e,+,-)}} \int dt \frac{T_i(t)}{\rho} \int dt' \left(\frac{P_j(t')}{d_j} - \frac{P_{j+1}(t')}{d_{j+1}} \right) \int_0^{2\pi} d\phi \\
&\quad \cdot \int_0^{2\pi} d\phi' G_{(e,+,-)}(R) e^{jn(\phi' - \phi)} \tag{3.42}
\end{aligned}$$

$$\begin{aligned}
Z_{nij(e,+,-)}^{\phi\phi} &= \frac{jk_{(e,+,-)}}{4\pi} \int dt T_i(t) \int dt' T_j(t') \int_0^{2\pi} d\phi \\
&\quad \cdot \int_0^{2\pi} d\phi' G_{(e,+,-)}(R) \cos(\phi' - \phi) e^{jn(\phi' - \phi)} \\
&\quad - \frac{jn^2}{4\pi k_{(e,+,-)}} \int dt \frac{T_i(t)}{\rho} \int dt' \frac{T_j(t')}{\rho'} \int_0^{2\pi} d\phi \int_0^{2\pi} d\phi' G_{(e,+,-)}(R) e^{jn(\phi' - \phi)}. \tag{3.43}
\end{aligned}$$

In view of (3.22)–(3.25), the scalar triple products $\hat{\mathbf{t}} \cdot (\hat{\mathbf{t}}' \times (\mathbf{r} - \mathbf{r}'))$, $\hat{\mathbf{t}} \cdot (\hat{\boldsymbol{\phi}}' \times (\mathbf{r} - \mathbf{r}'))$, $\hat{\boldsymbol{\phi}} \cdot (\hat{\mathbf{t}}' \times (\mathbf{r} - \mathbf{r}'))$, and $\hat{\boldsymbol{\phi}} \cdot (\hat{\boldsymbol{\phi}}' \times (\mathbf{r} - \mathbf{r}'))$ are needed in expression (3.20) for Y_{nije}^{pq-} . These scalar triple products are given by

$$\hat{\mathbf{t}} \cdot (\hat{\mathbf{t}}' \times (\mathbf{r} - \mathbf{r}')) = (\rho' \sin v \cos v' - \rho \sin v' \cos v - (z' - z) \sin v \sin v') \sin(\phi' - \phi) \tag{3.44}$$

$$\hat{\mathbf{t}} \cdot (\hat{\boldsymbol{\phi}}' \times (\mathbf{r} - \mathbf{r}')) = \rho' \cos v + (-\rho \cos v - (z' - z) \sin v) \cos(\phi' - \phi) \tag{3.45}$$

$$\hat{\boldsymbol{\phi}} \cdot (\hat{\mathbf{t}}' \times (\mathbf{r} - \mathbf{r}')) = \rho \cos v' + (-\rho' \cos v' + (z' - z) \sin v') \cos(\phi' - \phi) \tag{3.46}$$

$$\hat{\boldsymbol{\phi}} \cdot (\hat{\boldsymbol{\phi}}' \times (\mathbf{r} - \mathbf{r}')) = -(z' - z) \sin(\phi' - \phi). \tag{3.47}$$

Other scalar triple products needed in (3.20) are, using (3.15), evaluated as

$$\hat{\mathbf{t}} \cdot (\hat{\mathbf{t}} \times \hat{\mathbf{n}}) = 0 \tag{3.48}$$

$$\hat{\mathbf{t}} \cdot (\hat{\boldsymbol{\phi}} \times \hat{\mathbf{n}}) = -1 \tag{3.49}$$

$$\hat{\boldsymbol{\phi}} \cdot (\hat{\mathbf{t}} \times \hat{\mathbf{n}}) = 1 \tag{3.50}$$

$$\hat{\boldsymbol{\phi}} \cdot (\hat{\boldsymbol{\phi}} \times \hat{\mathbf{n}}) = 0. \tag{3.51}$$

Replacing ds by $dt \rho d\phi$ and ds' by $dt' \rho' d\phi'$ in (3.20), letting p be either t or ϕ and q be either t or ϕ in (3.20), and then substituting (3.22)–(3.25) into the resulting equations, one obtains, upon use of (3.44)–(3.51),

$$Y_{nije}^{tt-} = -\frac{1}{4\pi} \int dt T_i(t) \int dt' T_j(t') \int_0^{2\pi} d\phi$$

$$\cdot \int_0^{2\pi} d\phi' (\rho' \sin v \cos v' - \rho \sin v' \cos v - (z' - z) \sin v \sin v') \sin(\phi' - \phi) G'_e(R) e^{jn(\phi' - \phi)} \quad (3.52)$$

$$\begin{aligned} Y_{nije}^{t\phi-} &= -\frac{1}{4\pi} \int dt T_i(t) \int dt' T_j(t') \int_0^{2\pi} d\phi \\ &\cdot \int_0^{2\pi} d\phi' \{ \rho' \cos v + (-\rho \cos v - (z' - z) \sin v) \cos(\phi' - \phi) \} G'_e(R) e^{jn(\phi' - \phi)} \\ &- \frac{1}{2} \int dt \frac{T_i(t) T_j(t)}{\rho} \int_0^{2\pi} d\phi \end{aligned} \quad (3.53)$$

$$\begin{aligned} Y_{nije}^{\phi t-} &= -\frac{1}{4\pi} \int dt T_i(t) \int dt' T_j(t') \int_0^{2\pi} d\phi \\ &\cdot \int_0^{2\pi} d\phi' \{ \rho \cos v' + (-\rho' \cos v' + (z' - z) \sin v') \cos(\phi' - \phi) \} G'_e(R) e^{jn(\phi' - \phi)} \\ &+ \frac{1}{2} \int dt \frac{T_i(t) T_j(t)}{\rho} \int_0^{2\pi} d\phi \end{aligned} \quad (3.54)$$

$$\begin{aligned} Y_{nije}^{\phi\phi-} &= \frac{1}{4\pi} \int dt T_i(t) \int dt' T_j(t') \int_0^{2\pi} d\phi \\ &\cdot \int_0^{2\pi} d\phi' (z' - z) \sin(\phi' - \phi) G'_e(R) e^{jn(\phi' - \phi)}. \end{aligned} \quad (3.55)$$

Because $Y_{nij\pm}^{pq+}$ of (3.21) is similar to Y_{nije}^{pq-} of (3.20), $Y_{nij\pm}^{tt+}$, $Y_{nij\pm}^{t\phi+}$, $Y_{nij\pm}^{\phi t+}$, and $Y_{nij\pm}^{\phi\phi+}$, are given by expressions similar to the right-hand sides of (3.52)–(3.55).

With the help of the cosine law and the trigonometric identity [55, Formulas 410.01 and 404.12]

$$\cos \phi = 1 - 2 \sin^2 \frac{\phi}{2}, \quad (3.56)$$

expression (3.7) for R expands to

$$R = \sqrt{(\rho - \rho')^2 + (z - z')^2 + 4\rho\rho' \sin^2 \frac{\phi' - \phi}{2}}. \quad (3.57)$$

Because each integrand of each integral with respect to ϕ' in (3.40)–(3.43) and (3.52)–(3.55) is a periodic function of ϕ' with the period 2π , ϕ' can be replaced by $\phi' + \phi$ in each integrand without changing the value of the integral. The replacement of ϕ' by $\phi' + \phi$ eliminates the ϕ -dependence of each integrand so that each integration with respect to ϕ can be replaced by the factor 2π . Integrating from $-\pi$ to π with respect to ϕ' instead of from 0 to 2π , replacing

$e^{jn\phi'}$ by $\cos(n\phi') + j \sin(n\phi')$, and then exploiting the evenness of $\cos(n\phi')$ about $\phi' = 0$ and the oddness of $\sin(n\phi')$ about $\phi' = 0$, one reduces (3.40)–(3.43) and (3.52)–(3.55) to

$$\begin{aligned} Z_{nij(e,+,-)}^{tt} &= jk_{(e,+,-)} \int dt T_i(t) \int dt' T_j(t') (G_{2(e,+,-)} \sin v \sin v' + G_{1(e,+,-)} \cos v \cos v') \\ &\quad - \frac{j}{k_{(e,+,-)}} \int dt \left(\frac{P_i(t)}{d_i} - \frac{P_{i+1}(t)}{d_{i+1}} \right) \int dt' \left(\frac{P_j(t')}{d_j} - \frac{P_{j+1}(t')}{d_{j+1}} \right) G_{1(e,+,-)} \end{aligned} \quad (3.58)$$

$$\begin{aligned} Z_{nij(e,+,-)}^{t\phi} &= k_{(e,+,-)} \int dt T_i(t) \int dt' T_j(t') G_{3(e,+,-)} \sin v \\ &\quad + \frac{n}{k_{(e,+,-)}} \int dt \left(\frac{P_i(t)}{d_i} - \frac{P_{i+1}(t)}{d_{i+1}} \right) \int dt' \frac{T_j(t')}{\rho'} G_{1(e,+,-)} \end{aligned} \quad (3.59)$$

$$\begin{aligned} Z_{nij(e,+,-)}^{\phi t} &= -k_{(e,+,-)} \int dt T_i(t) \int dt' T_j(t') G_{3(e,+,-)} \sin v' \\ &\quad - \frac{n}{k_{(e,+,-)}} \int dt \frac{T_i(t)}{\rho} \int dt' \left(\frac{P_j(t')}{d_j} - \frac{P_{j+1}(t')}{d_{j+1}} \right) G_{1(e,+,-)} \end{aligned} \quad (3.60)$$

$$\begin{aligned} Z_{nij(e,+,-)}^{\phi\phi} &= jk_{(e,+,-)} \int dt T_i(t) \int dt' T_j(t') G_{2(e,+,-)} \\ &\quad - \frac{jn^2}{k_{(e,+,-)}} \int dt \frac{T_i(t)}{\rho} \int dt' \frac{T_j(t')}{\rho'} G_{1(e,+,-)} \end{aligned} \quad (3.61)$$

$$Y_{nije}^{tt-} = -j \int dt T_i(t) \int dt' T_j(t') (\rho' \sin v \cos v' - \rho \sin v' \cos v - (z' - z) \sin v \sin v') G'_{3e} \quad (3.62)$$

$$\begin{aligned} Y_{nije}^{t\phi-} &= - \int dt T_i(t) \int dt' T_j(t') \{ (\rho' - \rho) \cos v - (z' - z) \sin v \} G'_{2e} + G'_{1e} \rho' \cos v \} \\ &\quad - \pi \int \frac{T_i(t) T_j(t)}{\rho} dt \end{aligned} \quad (3.63)$$

$$\begin{aligned} Y_{nije}^{\phi t-} &= - \int dt T_i(t) \int dt' T_j(t') \{ (\rho - \rho') \cos v' + (z' - z) \sin v' \} G'_{2e} + G'_{1e} \rho \cos v' \} \\ &\quad + \pi \int \frac{T_i(t) T_j(t)}{\rho} dt \end{aligned} \quad (3.64)$$

$$Y_{nije}^{\phi\phi-} = j \int dt T_i(t) \int dt' T_j(t') (z' - z) G'_{3e} \quad (3.65)$$

where

$$G_{1(e,+,-)} = \int_0^\pi G_{(e,+,-)}(\check{R}) \cos(n\phi') d\phi' \quad (3.66)$$

$$G_{2(e,+, -)} = \int_0^\pi G_{(e,+, -)}(\check{R}) \cos \phi' \cos(n\phi') d\phi' \quad (3.67)$$

$$G_{3(e,+, -)} = \int_0^\pi G_{(e,+, -)}(\check{R}) \sin \phi' \sin(n\phi') d\phi' \quad (3.68)$$

$$G'_{1(e,+, -)} = 2 \int_0^\pi G'_{(e,+, -)}(\check{R}) \sin^2\left(\frac{\phi'}{2}\right) \cos(n\phi') d\phi' \quad (3.69)$$

$$G'_{2(e,+, -)} = \int_0^\pi G'_{(e,+, -)}(\check{R}) \cos \phi' \cos(n\phi') d\phi' \quad (3.70)$$

$$G'_{3(e,+, -)} = \int_0^\pi G'_{(e,+, -)}(\check{R}) \sin \phi' \sin(n\phi') d\phi'. \quad (3.71)$$

where

$$\check{R} = \sqrt{(\rho - \rho')^2 + (z - z')^2 + 4\rho\rho' \sin^2 \frac{\phi'}{2}}. \quad (3.72)$$

The quantities $G'_{1\pm}$, $G'_{2\pm}$, and $G'_{3\pm}$ will be needed later. In obtaining (3.63), the trigonometric identity (3.56) was used to replace $\rho' \cos v$ in (3.53) by $\rho' \cos v (\cos(\phi' - \phi) + 2 \sin^2 \frac{\phi' - \phi}{2})$. Similarly, $\rho \cos v'$ in (3.54) was replaced by $\rho \cos v' (\cos(\phi' - \phi) + 2 \sin^2 \frac{\phi' - \phi}{2})$ in order to obtain (3.64). It is apparent that, as foreseen in the sentence before that which contains (2.23), the fields of $e^{jn\phi}$ dependent electric and magnetic current expansion functions have $e^{jn\phi}$ dependence.

3.3 The Z 's and Y 's Expressed as Summations

Points

$$t = \bar{t}_p = \frac{1}{2}(t_p + t_{p+1}), \quad p = 1, 2, \dots, 2N_t + 2 \quad (3.73)$$

are defined on the generating curve of the BOR. The integrals with respect to t and t' in (3.58)–(3.65) are approximated by sampling at these points. Thus, (3.58)–(3.65) become

$$\begin{aligned} Z_{nij(e,+, -)}^{tt} &= jk_{(e,+, -)} \sum_{p=2i-1}^{2i+2} \sum_{q=2j-1}^{2j+2} T_{p'} T_{q'} (G_{2(e,+, -)}^{pq} \sin v_p \sin v_q + G_{1(e,+, -)}^{pq} \cos v_p \cos v_q) \\ &\quad - \frac{j}{k_{(e,+, -)}} \sum_{p=2i-1}^{2i+2} \sum_{q=2j-1}^{2j+2} T_{p'} T_{q'} G_{1(e,+, -)}^{pq} \end{aligned} \quad (3.74)$$

$$\begin{aligned}
Z_{nij(e,+,-)}^{t\phi} &= k_{(e,+,-)} \sum_{p=2i-1}^{2i+2} \sum_{q=2j-1}^{2j+2} T_{p'} T_{q'} G_{3(e,+,-)}^{pq} \sin v_p \\
&\quad + \frac{n}{k_{(e,+,-)}} \sum_{p=2i-1}^{2i+2} \sum_{q=2j-1}^{2j+2} T_{p'} T_{q'} G_{1(e,+,-)}^{pq}
\end{aligned} \tag{3.75}$$

$$\begin{aligned}
Z_{nij(e,+,-)}^{\phi t} &= -k_{(e,+,-)} \sum_{p=2i-1}^{2i+2} \sum_{q=2j-1}^{2j+2} T_{p'} T_{q'} G_{3(e,+,-)}^{pq} \sin v_q \\
&\quad - \frac{n}{k_{(e,+,-)}} \sum_{p=2i-1}^{2i+2} \sum_{q=2j-1}^{2j+2} T_{p'} T_{q'} G_{1(e,+,-)}^{pq}
\end{aligned} \tag{3.76}$$

$$\begin{aligned}
Z_{nij(e,+,-)}^{\phi\phi} &= jk_{(e,+,-)} \sum_{p=2i-1}^{2i+2} \sum_{q=2j-1}^{2j+2} T_{p'} T_{q'} G_{2(e,+,-)}^{pq} \\
&\quad - \frac{jn^2}{k_{(e,+,-)}} \sum_{p=2i-1}^{2i+2} \sum_{q=2j-1}^{2j+2} T_{p'} T_{q'} G_{1(e,+,-)}^{pq}
\end{aligned} \tag{3.77}$$

$$\begin{aligned}
Y_{nije}^{tt-} &= -j \sum_{p=2i-1}^{2i+2} \sum_{q=2j-1}^{2j+2} T_{p'} T_{q'} (\bar{\rho}_q \sin v_p \cos v_q - \bar{\rho}_p \sin v_q \cos v_p \\
&\quad - (\bar{z}_q - \bar{z}_p) \sin v_p \sin v_q) G_{3e}^{'pq}
\end{aligned} \tag{3.78}$$

$$Y_{nije}^{t\phi-} = - \sum_{p=2i-1}^{2i+2} \sum_{q=2j-1}^{2j+2} T_{p'} T_{q'} \{ ((\bar{\rho}_q - \bar{\rho}_p) \cos v_p - (\bar{z}_q - \bar{z}_p) \sin v_p) G_{2e}^{'pq} + G_{1e}^{'pq} \bar{\rho}_q \cos v_p \} - Y_{ij} \tag{3.79}$$

$$Y_{nije}^{\phi t-} = - \sum_{p=2i-1}^{2i+2} \sum_{q=2j-1}^{2j+2} T_{p'} T_{q'} \{ ((\bar{\rho}_p - \bar{\rho}_q) \cos v_q + (\bar{z}_q - \bar{z}_p) \sin v_q) G_{2e}^{'pq} + G_{1e}^{'pq} \bar{\rho}_p \cos v_q \} + Y_{ij} \tag{3.80}$$

$$Y_{nije}^{\phi\phi-} = j \sum_{p=2i-1}^{2i+2} \sum_{q=2j-1}^{2j+2} T_{p'} T_{q'} (\bar{z}_q - \bar{z}_p) G_{3e}^{'pq} \tag{3.81}$$

where

$$Y_{ij} = \pi \left(\delta_{i-1,j} \sum_{p=2i-1}^{2i} \frac{T_{p+2i-4} T_{p+2i-2}}{\bar{\rho}_p \Delta_p} + \delta_{ij} \sum_{p=2i-1}^{2i+2} \frac{T_{p+2i-2}^2}{\bar{\rho}_p \Delta_p} + \delta_{i+1,j} \sum_{p=2i+1}^{2i+2} \frac{T_{p+2i} T_{p+2i-2}}{\bar{\rho}_p \Delta_p} \right), \tag{3.82}$$

δ_{ij} is the Kronecker delta function given by

$$\delta_{ij} = \begin{cases} 1, & i = j \\ 0, & i \neq j, \end{cases} \quad (3.83)$$

and

$$p' = p + 2(i - 1) \quad (3.84)$$

$$q' = q + 2(j - 1) \quad (3.85)$$

$$T_{4i-3} = \frac{\Delta_{2i-1}^2}{2d_i} \quad (3.86)$$

$$T_{4i-2} = \frac{(\Delta_{2i-1} + \frac{1}{2}\Delta_{2i})\Delta_{2i}}{d_i} \quad (3.87)$$

$$T_{4i-1} = \frac{(\Delta_{2i+2} + \frac{1}{2}\Delta_{2i+1})\Delta_{2i+1}}{d_{i+1}} \quad (3.88)$$

$$T_{4i} = \frac{\Delta_{2i+2}^2}{2d_{i+1}} \quad (3.89)$$

$$T'_{4i-3} = \frac{\Delta_{2i-1}}{d_i} \quad (3.90)$$

$$T'_{4i-2} = \frac{\Delta_{2i}}{d_i} \quad (3.91)$$

$$T'_{4i-1} = -\frac{\Delta_{2i+1}}{d_{i+1}} \quad (3.92)$$

$$T'_{4i} = -\frac{\Delta_{2i+2}}{d_{i+1}} \quad (3.93)$$

$$T'_{4i-3}{}^\phi = \frac{T_{4i-3}}{\bar{\rho}_{2i-1}} \quad (3.94)$$

$$T'_{4i-2}{}^\phi = \frac{T_{4i-2}}{\bar{\rho}_{2i}} \quad (3.95)$$

$$T'_{4i-1}{}^\phi = \frac{T_{4i-1}}{\bar{\rho}_{2i+1}} \quad (3.96)$$

$$T'_{4i}{}^\phi = \frac{T_{4i}}{\bar{\rho}_{2i+2}} \quad (3.97)$$

$$\bar{\rho}_p = \rho(\bar{t}_p) \quad (3.98)$$

$$\bar{z}_p = z(\bar{t}_p) \quad (3.99)$$

$$v_p = v(t), \quad t_p \leq t < t_{p+1} \quad (3.100)$$

$$G_{1(e,+,-)}^{pq} = \int_0^\pi G_{(e,+,-)}(R^{pq}) \cos(n\phi') d\phi' \quad (3.101)$$

$$G_{2(e,+,-)}^{pq} = \int_0^\pi G_{(e,+,-)}(R^{pq}) \cos \phi' \cos(n\phi') d\phi' \quad (3.102)$$

$$G_{3(e,+,-)}^{pq} = \int_0^\pi G_{(e,+,-)}(R^{pq}) \sin \phi' \sin(n\phi') d\phi' \quad (3.103)$$

$$G_{1(e,+,-)}^{\prime pq} = 2 \int_0^\pi G'_{(e,+,-)}(R^{pq}) \sin^2\left(\frac{\phi'}{2}\right) \cos(n\phi') d\phi' \quad (3.104)$$

$$G_{2(e,+,-)}^{\prime pq} = \int_0^\pi G'_{(e,+,-)}(R^{pq}) \cos \phi' \cos(n\phi') d\phi' \quad (3.105)$$

$$G_{3(e,+,-)}^{\prime pq} = \int_0^\pi G'_{(e,+,-)}(R^{pq}) \sin \phi' \sin(n\phi') d\phi' \quad (3.106)$$

$$R^{pq} = \sqrt{(\bar{\rho}_p - \bar{\rho}_q)^2 + (\bar{z}_p - \bar{z}_q)^2 + 4\bar{\rho}_p\bar{\rho}_q \sin^2 \frac{\phi'}{2}}. \quad (3.107)$$

If $p = q$, none of the integrals in (3.101)–(3.107) except that in (3.103) converge. Convergence is obtained for $p = q$ by replacing R^{pp} by the equivalent radius R_e^{pp} given by [53]

$$R_e^{pp} = \sqrt{\left(\frac{\Delta_p}{4}\right)^2 + 4\bar{\rho}_p^2 \sin^2 \frac{\phi'}{2}}. \quad (3.108)$$

The quantities $G_{1\pm}^{\prime pq}$, $G_{2\pm}^{\prime pq}$, and $G_{3\pm}^{\prime pq}$ defined by (3.104)–(3.106) are needed to evaluate $Y_{nij\pm}^{pq+}$ of (3.21). Because $Y_{nij\pm}^{pq+}$ of (3.21) is equal to the right-hand side of (3.20) with e replaced by \pm and $\frac{1}{2}$ replaced by $-\frac{1}{2}$, $Y_{nij\pm}^{tt+}$, $Y_{nij\pm}^{t\phi+}$, $Y_{nij\pm}^{\phi t+}$, and $Y_{nij\pm}^{\phi\phi+}$, are given by the right-hand sides of (3.78)–(3.81) with e replaced by \pm and with the opposite sign of what came from the term containing the factor $\frac{1}{2}$ in (3.20):

$$Y_{nij\pm}^{tt+} = -j \sum_{p=2i-1}^{2i+2} \sum_{q=2j-1}^{2j+2} T_{p'} T_{q'} (\bar{\rho}_q \sin v_p \cos v_q - \bar{\rho}_p \sin v_q \cos v_p - (\bar{z}_q - \bar{z}_p) \sin v_p \sin v_q) G_{3\pm}^{\prime pq} \quad (3.109)$$

$$Y_{nij\pm}^{t\phi+} = - \sum_{p=2i-1}^{2i+2} \sum_{q=2j-1}^{2j+2} T_{p'} T_{q'} \{ ((\bar{\rho}_q - \bar{\rho}_p) \cos v_p - (\bar{z}_q - \bar{z}_p) \sin v_p) G_{2\pm}^{\prime pq} + G_{1\pm}^{\prime pq} \bar{\rho}_q \cos v_p \} + Y_{ij} \quad (3.110)$$

$$Y_{nij\pm}^{\phi t+} = - \sum_{p=2i-1}^{2i+2} \sum_{q=2j-1}^{2j+2} T_{p'} T_{q'} \{ ((\bar{\rho}_p - \bar{\rho}_q) \cos v_q + (\bar{z}_q - \bar{z}_p) \sin v_q) G_{2\pm}^{\prime pq} + G_{1\pm}^{\prime pq} \bar{\rho}_p \cos v_q \} - Y_{ij} \quad (3.111)$$

$$Y_{nij\pm}^{\phi\phi+} = j \sum_{p=2i-1}^{2i+2} \sum_{q=2j-1}^{2j+2} T_{p'} T_{q'} (\bar{z}_q - \bar{z}_p) G_{3\pm}^{\prime pq}. \quad (3.112)$$

3.4 Properties of the Z 's and Y 's of (3.74)–(3.81) and (3.109)–(3.112)

Because $G_{(e,+,-)}(R^{pq})$ and $G'_{(e,+,-)}(R^{pq})$ do not depend on n , it is evident from (3.101)–(3.106) that $G_{1(e,+,-)}^{pq}$, $G_{2(e,+,-)}^{pq}$, $G'_{1(e,+,-)}{}^{pq}$, and $G'_{2(e,+,-)}{}^{pq}$ are even functions of n and that $G_{3(e,+,-)}^{pq}$, and $G'_{3(e,+,-)}{}^{pq}$ are odd functions of n . Therefore, inspection of (3.74)–(3.82) and (3.109)–(3.112) reveals that $Z_{nij(e,+,-)}^{tt}$, $Z_{nij(e,+,-)}^{\phi\phi}$, $Y_{nije}^{t\phi-}$, $Y_{nij\pm}^{t\phi+}$, $Y_{nije}^{\phi t-}$, and $Y_{nij\pm}^{\phi t+}$ are even functions of n and that $Z_{nij(e,+,-)}^{t\phi}$, $Z_{nij(e,+,-)}^{\phi t}$, Y_{nije}^{tt-} , $Y_{nij\pm}^{tt+}$, $Y_{nije}^{\phi\phi-}$, and $Y_{nij\pm}^{\phi\phi+}$ are odd functions of n .

Equations (3.74)–(3.81) with i and j interchanged are

$$\begin{aligned} Z_{nji(e,+,-)}^{tt} &= j k_{(e,+,-)} \sum_{p=2j-1}^{2j+2} \sum_{q=2i-1}^{2i+2} T_{p'} T_{q'} (G_{2(e,+,-)}^{pq} \sin v_p \sin v_q + G_{1(e,+,-)}^{pq} \cos v_p \cos v_q) \\ &\quad - \frac{j}{k_{(e,+,-)}} \sum_{p=2j-1}^{2j+2} \sum_{q=2i-1}^{2i+2} T_{p'} T_{q'} G_{1(e,+,-)}^{pq} \end{aligned} \quad (3.113)$$

$$\begin{aligned} Z_{nji(e,+,-)}^{t\phi} &= k_{(e,+,-)} \sum_{p=2j-1}^{2j+2} \sum_{q=2i-1}^{2i+2} T_{p'} T_{q'} G_{3(e,+,-)}^{pq} \sin v_p \\ &\quad + \frac{n}{k_{(e,+,-)}} \sum_{p=2j-1}^{2j+2} \sum_{q=2i-1}^{2i+2} T_{p'} T_{q'} G_{1(e,+,-)}^{pq} \end{aligned} \quad (3.114)$$

$$\begin{aligned} Z_{nji(e,+,-)}^{\phi t} &= -k_{(e,+,-)} \sum_{p=2j-1}^{2j+2} \sum_{q=2i-1}^{2i+2} T_{p'} T_{q'} G_{3(e,+,-)}^{pq} \sin v_q \\ &\quad - \frac{n}{k_{(e,+,-)}} \sum_{p=2j-1}^{2j+2} \sum_{q=2i-1}^{2i+2} T_{p'} T_{q'} G_{1(e,+,-)}^{pq} \end{aligned} \quad (3.115)$$

$$\begin{aligned} Z_{nji(e,+,-)}^{\phi\phi} &= j k_{(e,+,-)} \sum_{p=2j-1}^{2j+2} \sum_{q=2i-1}^{2i+2} T_{p'} T_{q'} G_{2(e,+,-)}^{pq} \\ &\quad - \frac{j n^2}{k_{(e,+,-)}} \sum_{p=2j-1}^{2j+2} \sum_{q=2i-1}^{2i+2} T_{p'} T_{q'} G_{1(e,+,-)}^{pq} \end{aligned} \quad (3.116)$$

$$Y_{nje}^{tt-} = -j \sum_{p=2j-1}^{2j+2} \sum_{q=2i-1}^{2i+2} T_{p'} T_{q'} (\bar{\rho}_q \sin v_p \cos v_q - \bar{\rho}_p \sin v_q \cos v_p - (\bar{z}_q - \bar{z}_p) \sin v_p \sin v_q) G_{3e}'^{tpq} \quad (3.117)$$

$$Y_{nje}^{t\phi-} = - \sum_{p=2j-1}^{2j+2} \sum_{q=2i-1}^{2i+2} T_{p'} T_{q'} \{ ((\bar{\rho}_q - \bar{\rho}_p) \cos v_p - (\bar{z}_q - \bar{z}_p) \sin v_p) G_{2e}'^{tpq} + G_{1e}'^{tpq} \bar{\rho}_q \cos v_p \} - Y_{ji} \quad (3.118)$$

$$Y_{nje}^{\phi t-} = - \sum_{p=2j-1}^{2j+2} \sum_{q=2i-1}^{2i+2} T_{p'} T_{q'} \{ ((\bar{\rho}_p - \bar{\rho}_q) \cos v_q + (\bar{z}_q - \bar{z}_p) \sin v_q) G_{2e}'^{tpq} + G_{1e}'^{tpq} \bar{\rho}_p \cos v_q \} + Y_{ji} \quad (3.119)$$

$$Y_{nje}^{\phi\phi-} = j \sum_{p=2j-1}^{2j+2} \sum_{q=2i-1}^{2i+2} T_{p'} T_{q'} (\bar{z}_q - \bar{z}_p) G_{3e}'^{tpq} \quad (3.120)$$

where p' and q' are given, not by (3.84) and (3.85), but by

$$p' = p + 2(j - 1) \quad (3.121)$$

$$q' = q + 2(i - 1). \quad (3.122)$$

In view of (3.101)–(3.107), (3.6), and (3.17), each G^{pq} in (3.113)–(3.120) is equal to itself with p and q interchanged. Therefore, (3.113)–(3.120) with their dummy indices of summation p and q interchanged (this interchange is accompanied by p' of (3.121) $\rightarrow q + 2(j - 1) = q'$ of (3.85) and q' of (3.122) $\rightarrow p + 2(i - 1) = p'$ of (3.84)) are

$$Z_{nji(e,+,-)}^{tt} = jk_{(e,+,-)} \sum_{q=2j-1}^{2j+2} \sum_{p=2i-1}^{2i+2} T_{q'} T_{p'} (G_{2(e,+,-)}^{pq} \sin v_q \sin v_p + G_{1(e,+,-)}^{pq} \cos v_q \cos v_p) - \frac{j}{k_{(e,+,-)}} \sum_{q=2j-1}^{2j+2} \sum_{p=2i-1}^{2i+2} T_{q'} T_{p'} G_{1(e,+,-)}^{pq} \quad (3.123)$$

$$Z_{nji(e,+,-)}^{t\phi} = k_{(e,+,-)} \sum_{q=2j-1}^{2j+2} \sum_{p=2i-1}^{2i+2} T_{q'} T_{p'} G_{3(e,+,-)}^{pq} \sin v_q + \frac{n}{k_{(e,+,-)}} \sum_{q=2j-1}^{2j+2} \sum_{p=2i-1}^{2i+2} T_{q'} T_{p'} G_{1(e,+,-)}^{pq} \quad (3.124)$$

$$Z_{nji(e,+,-)}^{\phi t} = -k_{(e,+,-)} \sum_{q=2j-1}^{2j+2} \sum_{p=2i-1}^{2i+2} T_{q'} T_{p'} G_{3(e,+,-)}^{pq} \sin v_p$$

$$-\frac{n}{k_{(e,+,-)}} \sum_{q=2j-1}^{2j+2} \sum_{p=2i-1}^{2i+2} T_{q'}^{\prime\phi} T_{p'}^{\prime\phi} G_{1(e,+,-)}^{pq} \quad (3.125)$$

$$\begin{aligned} Z_{nji(e,+,-)}^{\phi\phi} &= j k_{(e,+,-)} \sum_{q=2j-1}^{2j+2} \sum_{p=2i-1}^{2i+2} T_{q'} T_{p'} G_{2(e,+,-)}^{pq} \\ &\quad - \frac{j n^2}{k_{(e,+,-)}} \sum_{q=2j-1}^{2j+2} \sum_{p=2i-1}^{2i+2} T_{q'}^{\prime\phi} T_{p'}^{\prime\phi} G_{1(e,+,-)}^{pq} \end{aligned} \quad (3.126)$$

$$\begin{aligned} Y_{nje}^{tt-} &= -j \sum_{q=2j-1}^{2j+2} \sum_{p=2i-1}^{2i+2} T_{q'} T_{p'} (\bar{\rho}_p \sin v_q \cos v_p - \bar{\rho}_q \sin v_p \cos v_q \\ &\quad - (\bar{z}_p - \bar{z}_q) \sin v_q \sin v_p) G_{3e}^{\prime pq} \end{aligned} \quad (3.127)$$

$$Y_{nje}^{t\phi-} = - \sum_{q=2j-1}^{2j+2} \sum_{p=2i-1}^{2i+2} T_{q'} T_{p'} \{ ((\bar{\rho}_p - \bar{\rho}_q) \cos v_q - (\bar{z}_p - \bar{z}_q) \sin v_q) G_{2e}^{\prime pq} + G_{1e}^{\prime pq} \bar{\rho}_p \cos v_q \} - Y_{ji} \quad (3.128)$$

$$Y_{nje}^{\phi t-} = - \sum_{q=2j-1}^{2j+2} \sum_{p=2i-1}^{2i+2} T_{q'} T_{p'} \{ ((\bar{\rho}_p - \bar{\rho}_q) \cos v_p + (\bar{z}_p - \bar{z}_q) \sin v_p) G_{2e}^{\prime pq} + G_{1e}^{\prime pq} \bar{\rho}_q \cos v_p \} + Y_{ji} \quad (3.129)$$

$$Y_{nje}^{\phi\phi-} = j \sum_{q=2j-1}^{2j+2} \sum_{p=2i-1}^{2i+2} T_{q'} T_{p'} (\bar{z}_p - \bar{z}_q) G_{3e}^{\prime pq} \quad (3.130)$$

where p' and q' are given by (3.84) and (3.85).

Comparison of (3.123) with (3.74), (3.124) with (3.76), (3.125) with (3.75), (3.126) with (3.77), (3.127) with (3.78), (3.128) with (3.80), (3.129) with (3.79), and (3.130) with (3.81) reveal that

$$Z_{nji(e,+,-)}^{tt} = Z_{nij(e,+,-)}^{tt} \quad (3.131)$$

$$Z_{nji(e,+,-)}^{t\phi} = -Z_{nij(e,+,-)}^{\phi t} \quad (3.132)$$

$$Z_{nji(e,+,-)}^{\phi t} = -Z_{nij(e,+,-)}^{t\phi} \quad (3.133)$$

$$Z_{nji(e,+,-)}^{\phi\phi} = Z_{nij(e,+,-)}^{\phi\phi} \quad (3.134)$$

$$Y_{nje}^{tt-} = -Y_{nije}^{tt-} \quad (3.135)$$

$$Y_{nje}^{t\phi-} + Y_{ji} = Y_{nije}^{\phi t-} - Y_{ij} \quad (3.136)$$

$$Y_{nje}^{\phi t-} - Y_{ji} = Y_{nije}^{t\phi-} + Y_{ij} \quad (3.137)$$

$$Y_{nje}^{\phi\phi-} = -Y_{nije}^{\phi\phi-} \quad (3.138)$$

Equation (3.82) with i and j interchanged is

$$Y_{ji} = \pi \left(\delta_{j-1,i} \sum_{p=2j-1}^{2j} \frac{T_{p+2j-4} T_{p+2j-2}}{\bar{\rho}_p \Delta_p} + \delta_{ji} \sum_{p=2j-1}^{2j+2} \frac{T_{p+2j-2}^2}{\bar{\rho}_p \Delta_p} + \delta_{j+1,i} \sum_{p=2j+1}^{2j+2} \frac{T_{p+2j} T_{p+2j-2}}{\bar{\rho}_p \Delta_p} \right). \quad (3.139)$$

Because $\delta_{j-1,i}$ is not zero only when $j = i + 1$, j can be set equal to $i + 1$ in the first summation in (3.139). Because δ_{ji} is not zero only when $j = i$, j can be set equal to i in the second summation in (3.139). Because $\delta_{j+1,i}$ is not zero only when $j = i - 1$, j can be set equal to $i - 1$ in the third summation in (3.139). Setting $j = i + 1$ in the first summation in (3.139), setting $j = i$ in the second summation in (3.139), and setting $j = i - 1$ in the third summation in (3.139), one obtains

$$Y_{ji} = \pi \left(\delta_{j-1,i} \sum_{p=2i+1}^{2i+2} \frac{T_{p+2i-2} T_{p+2i}}{\bar{\rho}_p \Delta_p} + \delta_{ji} \sum_{p=2i-1}^{2i+2} \frac{T_{p+2i-2}^2}{\bar{\rho}_p \Delta_p} + \delta_{j+1,i} \sum_{p=2i-1}^{2i} \frac{T_{p+2i-2} T_{p+2i-4}}{\bar{\rho}_p \Delta_p} \right). \quad (3.140)$$

Since δ_{ij} is given by (3.83), it is evident that the right-hand side of (3.140) is equal to the right-hand side of (3.82) so that

$$Y_{ji} = Y_{ij}. \quad (3.141)$$

Substitution of (3.141) into (3.136) and (3.137) gives

$$Y_{nje}^{t\phi-} = \left(Y_{nije}^{\phi t-} - Y_{ij} \right) - Y_{ij} \quad (3.142)$$

$$Y_{nje}^{\phi t-} = \left(Y_{nije}^{t\phi-} + Y_{ij} \right) + Y_{ij}. \quad (3.143)$$

The quantity in the parentheses in (3.142) is the negative of the double summation in (3.80) and the quantity in the parentheses in (3.143) is the negative of the double summation in (3.79).

Because (3.109)–(3.112) are similar to (3.78)–(3.81), $Y_{nji\pm}^{tt+}$, $Y_{nji\pm}^{t\phi+}$, $Y_{nji\pm}^{\phi t+}$, and $Y_{nji\pm}^{\phi\phi+}$ are given by expressions similar to the right-hand sides of (3.135), (3.142), (3.143), and (3.138), respectively.

$$Y_{nji\pm}^{tt+} = -Y_{nji\pm}^{tt+} \quad (3.144)$$

$$Y_{nji\pm}^{t\phi+} = \left(Y_{nji\pm}^{\phi t+} + Y_{ij} \right) + Y_{ij} \quad (3.145)$$

$$Y_{nji\pm}^{\phi t+} = \left(Y_{nji\pm}^{t\phi+} - Y_{ij} \right) - Y_{ij} \quad (3.146)$$

$$Y_{nji\pm}^{\phi\phi+} = -Y_{nji\pm}^{\phi\phi+}. \quad (3.147)$$

Chapter 4

Plane Wave Excitation

4.1 Introduction

In Chapter 2, the elements of \vec{V}_{ni}^p and \vec{I}_{ni}^p of the excitation vector for plane wave excitation are given by (2.28) and (2.29) where $p = t$ for the t -directed testing function and $p = \phi$ for the ϕ -directed testing function. In Chapter 4, \vec{V}_{ni}^p and \vec{I}_{ni}^p are specialized to \vec{V}_{ni}^{pq} and \vec{I}_{ni}^{pq} where $q = \theta$ for the incident electromagnetic field whose electric field is θ -polarized and $q = \phi$ for the incident electromagnetic field whose electric field is ϕ -polarized. In Chapter 4, expressions amenable to computation are given for \vec{V}_{ni}^{pq} and \vec{I}_{ni}^{pq} .

4.2 \vec{V}_{ni}^{pq} and \vec{I}_{ni}^{pq} expressed as integrals

Two incident plane waves whose propagation vectors are in the xz -plane are considered. The electromagnetic fields of these plane waves are $(\mathbf{E}^\theta, \mathbf{H}^\theta)$ and $(\mathbf{E}^\phi, \mathbf{H}^\phi)$ where

$$\mathbf{E}^\theta = \hat{\boldsymbol{\theta}}^{\text{inc}} k_e \eta_e e^{-j\mathbf{k}^{\text{inc}} \cdot \mathbf{r}} \quad (4.1)$$

$$\mathbf{H}^\theta = -\hat{\mathbf{y}} k_e e^{-j\mathbf{k}^{\text{inc}} \cdot \mathbf{r}} \quad (4.2)$$

$$\mathbf{E}^\phi = \hat{\mathbf{y}} k_e \eta_e e^{-j\mathbf{k}^{\text{inc}} \cdot \mathbf{r}} \quad (4.3)$$

$$\mathbf{H}^\phi = \hat{\boldsymbol{\theta}}^{\text{inc}} k_e e^{-j\mathbf{k}^{\text{inc}} \cdot \mathbf{r}} \quad (4.4)$$

where

$$\mathbf{k}^{\text{inc}} = -k_e(\hat{\mathbf{x}} \sin \theta^{\text{inc}} + \hat{\mathbf{z}} \cos \theta^{\text{inc}}) \quad (4.5)$$

$$\hat{\boldsymbol{\theta}}^{\text{inc}} = \hat{\mathbf{x}} \cos \theta^{\text{inc}} - \hat{\mathbf{z}} \sin \theta^{\text{inc}} \quad (4.6)$$

$$\mathbf{r} = \hat{\mathbf{x}} \rho \cos \phi + \hat{\mathbf{y}} \rho \sin \phi + \hat{\mathbf{z}} z \quad (4.7)$$

where $\hat{\mathbf{x}}$, $\hat{\mathbf{y}}$, and $\hat{\mathbf{z}}$ are the unit vectors in the x -, y -, and z -directions, respectively. The electric field of $(\mathbf{E}^\theta, \mathbf{H}^\theta)$ is θ -polarized and the electric field of $(\mathbf{E}^\phi, \mathbf{H}^\phi)$ is ϕ -polarized. The dot product of (4.5) and (4.7) is

$$\mathbf{k}^{\text{inc}} \cdot \mathbf{r} = -k_e(\rho \sin \theta^{\text{inc}} \cos \phi + z \cos \theta^{\text{inc}}). \quad (4.8)$$

Substitution of (4.6) and (4.8) into (4.1)–(4.4) gives

$$\mathbf{E}^\theta = (\hat{\mathbf{x}} \cos \theta^{\text{inc}} - \hat{\mathbf{z}} \sin \theta^{\text{inc}}) k_e \eta_e e^{jk_e(\rho \sin \theta^{\text{inc}} \cos \phi + z \cos \theta^{\text{inc}})} \quad (4.9)$$

$$\mathbf{H}^\theta = -\hat{\mathbf{y}} k_e e^{jk_e(\rho \sin \theta^{\text{inc}} \cos \phi + z \cos \theta^{\text{inc}})} \quad (4.10)$$

$$\mathbf{E}^\phi = \hat{\mathbf{y}} k_e \eta_e e^{jk_e(\rho \sin \theta^{\text{inc}} \cos \phi + z \cos \theta^{\text{inc}})} \quad (4.11)$$

$$\mathbf{H}^\phi = (\hat{\mathbf{x}} \cos \theta^{\text{inc}} - \hat{\mathbf{z}} \sin \theta^{\text{inc}}) k_e e^{jk_e(\rho \sin \theta^{\text{inc}} \cos \phi + z \cos \theta^{\text{inc}})}. \quad (4.12)$$

The column matrix elements \vec{V}_{ni}^t , \vec{V}_{ni}^ϕ , \vec{I}_{ni}^t , and \vec{I}_{ni}^ϕ , due to the incident electromagnetic field ($\mathbf{E}^{\text{inc}}, \mathbf{H}^{\text{inc}}$) are given by

$$\vec{V}_{ni}^t = \langle \mathbf{J}_{-ni}^t, \frac{1}{\eta_e} [\mathbf{E}^{\text{inc}}]_S \rangle \quad (4.13)$$

$$\vec{V}_{ni}^\phi = \langle \mathbf{J}_{-ni}^\phi, \frac{1}{\eta_e} [\mathbf{E}^{\text{inc}}]_S \rangle \quad (4.14)$$

$$\vec{I}_{ni}^t = \langle \mathbf{J}_{-ni}^t, [\mathbf{H}^{\text{inc}}]_S \rangle \quad (4.15)$$

$$\vec{I}_{ni}^\phi = \langle \mathbf{J}_{-ni}^\phi, [\mathbf{H}^{\text{inc}}]_S \rangle \quad (4.16)$$

where

$$\mathbf{J}_{-ni}^t = \hat{\mathbf{t}} \frac{T_i(t)}{\rho} e^{-jn\phi} \quad (4.17)$$

$$\mathbf{J}_{-ni}^\phi = \hat{\phi} \frac{T_i(t)}{\rho} e^{-jn\phi} \quad (4.18)$$

and, given two vector functions \mathbf{f} and \mathbf{g} , $\langle \mathbf{f}, \mathbf{g} \rangle$ is the symmetric product of \mathbf{f} and \mathbf{g} given by

$$\langle \mathbf{f}, \mathbf{g} \rangle = \int dt \rho \int_0^{2\pi} d\phi (\mathbf{f} \cdot \mathbf{g}) \quad (4.19)$$

where the double integration is over the surface S of the body of revolution (BOR). In view of (4.19), substitution of (4.17) into (4.13) and (6.15) and substitution of (4.18) into (4.14), and (4.16) give

$$\vec{V}_{ni}^t = \int dt T_i(t) \int_0^{2\pi} d\phi \hat{\mathbf{t}} \cdot \frac{1}{\eta_e} [\mathbf{E}^{\text{inc}}]_S e^{-jn\phi} \quad (4.20)$$

$$\vec{V}_{ni}^\phi = \int dt T_i(t) \int_0^{2\pi} d\phi \hat{\phi} \cdot \frac{1}{\eta_e} [\mathbf{E}^{\text{inc}}]_S e^{-jn\phi} \quad (4.21)$$

$$\vec{I}_{ni}^t = \int dt T_i(t) \int_0^{2\pi} d\phi \hat{\mathbf{t}} \cdot [\mathbf{H}^{\text{inc}}]_S e^{-jn\phi} \quad (4.22)$$

$$\vec{I}_{ni}^\phi = \int dt T_i(t) \int_0^{2\pi} d\phi \hat{\boldsymbol{\phi}} \cdot [\mathbf{H}^{\text{inc}}]_S e^{-jn\phi}. \quad (4.23)$$

For the incident electromagnetic field $(\mathbf{E}^\theta, \mathbf{H}^\theta)$, the column matrix elements \vec{V}_{ni}^t , \vec{V}_{ni}^ϕ , \vec{I}_{ni}^t , and \vec{I}_{ni}^ϕ , of (4.20)–(4.23) specialize to $\vec{V}_{ni}^{t\theta}$, $\vec{V}_{ni}^{\phi\theta}$, $\vec{I}_{ni}^{t\theta}$, and $\vec{I}_{ni}^{\phi\theta}$, respectively, given by

$$\vec{V}_{ni}^{t\theta} = \int dt T_i(t) \int_0^{2\pi} d\phi \hat{\mathbf{t}} \cdot \frac{1}{\eta_e} [\mathbf{E}^\theta]_S e^{-jn\phi} \quad (4.24)$$

$$\vec{V}_{ni}^{\phi\theta} = \int dt T_i(t) \int_0^{2\pi} d\phi \hat{\boldsymbol{\phi}} \cdot \frac{1}{\eta_e} [\mathbf{E}^\theta]_S e^{-jn\phi} \quad (4.25)$$

$$\vec{I}_{ni}^{t\theta} = \int dt T_i(t) \int_0^{2\pi} d\phi \hat{\mathbf{t}} \cdot [\mathbf{H}^\theta]_S e^{-jn\phi} \quad (4.26)$$

$$\vec{I}_{ni}^{\phi\theta} = \int dt T_i(t) \int_0^{2\pi} d\phi \hat{\boldsymbol{\phi}} \cdot [\mathbf{H}^\theta]_S e^{-jn\phi}. \quad (4.27)$$

For the incident electromagnetic field $(\mathbf{E}^\phi, \mathbf{H}^\phi)$, the column matrix elements \vec{V}_{ni}^t , \vec{V}_{ni}^ϕ , \vec{I}_{ni}^t , and \vec{I}_{ni}^ϕ of (4.20)–(4.23) specialize to $\vec{V}_{ni}^{t\phi}$, $\vec{V}_{ni}^{\phi\phi}$, $\vec{I}_{ni}^{t\phi}$, and $\vec{I}_{ni}^{\phi\phi}$, respectively, given by

$$\vec{V}_{ni}^{t\phi} = \int dt T_i(t) \int_0^{2\pi} d\phi \hat{\mathbf{t}} \cdot \frac{1}{\eta_e} [\mathbf{E}^\phi]_S e^{-jn\phi} \quad (4.28)$$

$$\vec{V}_{ni}^{\phi\phi} = \int dt T_i(t) \int_0^{2\pi} d\phi \hat{\boldsymbol{\phi}} \cdot \frac{1}{\eta_e} [\mathbf{E}^\phi]_S e^{-jn\phi} \quad (4.29)$$

$$\vec{I}_{ni}^{t\phi} = \int dt T_i(t) \int_0^{2\pi} d\phi \hat{\mathbf{t}} \cdot [\mathbf{H}^\phi]_S e^{-jn\phi} \quad (4.30)$$

$$\vec{I}_{ni}^{\phi\phi} = \int dt T_i(t) \int_0^{2\pi} d\phi \hat{\boldsymbol{\phi}} \cdot [\mathbf{H}^\phi]_S e^{-jn\phi}. \quad (4.31)$$

4.3 $\vec{V}_{ni}^{t\theta}$

Substitution of (4.9) into (4.24) gives

$$\vec{V}_{ni}^{t\theta} = k_e \int dt T_i(t) \int_0^{2\pi} d\phi \hat{\mathbf{t}} \cdot (\hat{\mathbf{x}} \cos \theta^{\text{inc}} - \hat{\mathbf{z}} \sin \theta^{\text{inc}}) e^{jk_e(\rho \sin \theta^{\text{inc}} \cos \phi + z \cos \theta^{\text{inc}})} e^{-jn\phi}. \quad (4.32)$$

Because the dot product with $\hat{\mathbf{t}}$ in (4.32) samples only a tangential component of the incident electric field on S , the subscript S , which indicates evaluation of the tangential part of the incident electric field on S , does not have to appear in (4.32). Use of

$$\hat{\mathbf{t}} = \hat{\mathbf{x}} \sin v \cos \phi + \hat{\mathbf{y}} \sin v \sin \phi + \hat{\mathbf{z}} \cos v \quad (4.33)$$

leads to

$$\hat{\mathbf{t}} \cdot (\hat{\mathbf{x}} \cos \theta^{\text{inc}} - \hat{\mathbf{z}} \sin \theta^{\text{inc}}) = \cos \theta^{\text{inc}} \sin v \cos \phi - \sin \theta^{\text{inc}} \cos v. \quad (4.34)$$

Substitution of (4.34) into (4.32) gives

$$\vec{V}_{ni}^{t\theta} = k_e \int dt T_i(t) e^{jk_e z \cos \theta^{\text{inc}}} \int_0^{2\pi} d\phi (\cos \theta^{\text{inc}} \sin v \cos \phi - \sin \theta^{\text{inc}} \cos v) e^{j(k_e \rho \sin \theta^{\text{inc}} \cos \phi - n\phi)}. \quad (4.35)$$

Equation (4.35) is recast as

$$\begin{aligned} \vec{V}_{ni}^{t\theta} = k_e \int T_i(t) e^{jk_e z \cos \theta^{\text{inc}}} \left\{ \cos \theta^{\text{inc}} \sin v \int_0^{2\pi} \cos \phi e^{j(k_e \rho \sin \theta^{\text{inc}} \cos \phi - n\phi)} d\phi \right. \\ \left. - \sin \theta^{\text{inc}} \cos v \int_0^{2\pi} e^{j(k_e \rho \sin \theta^{\text{inc}} \cos \phi - n\phi)} d\phi \right\} dt. \end{aligned} \quad (4.36)$$

In regard to (4.36), consider

$$\int_0^{2\pi} e^{j(k_e \rho \sin \theta^{\text{inc}} \cos \phi - n\phi)} d\phi = 2\pi j^n J_n(k_e \rho \sin \theta^{\text{inc}}) \quad (4.37)$$

where

$$J_n(x) = \frac{j^{-n}}{2\pi} \int_0^{2\pi} e^{j(x \cos \phi - n\phi)} d\phi. \quad (4.38)$$

Later, it will be shown that J_n of (4.38) is the Bessel function of the first kind of order n . Use of the complex exponential representation of the first $\cos \phi$ in the first integral with respect to ϕ in (4.36) gives

$$\begin{aligned} \int_0^{2\pi} \cos \phi e^{j(k_e \rho \sin \theta^{\text{inc}} \cos \phi - n\phi)} d\phi = \frac{1}{2} \int_0^{2\pi} e^{j(k_e \rho \sin \theta^{\text{inc}} \cos \phi - (n+1)\phi)} d\phi \\ + \frac{1}{2} \int_0^{2\pi} e^{j(k_e \rho \sin \theta^{\text{inc}} \cos \phi - (n-1)\phi)} d\phi. \end{aligned} \quad (4.39)$$

Equation (4.39) is rewritten as

$$\int_0^{2\pi} \cos \phi e^{j(k_e \rho \sin \theta^{\text{inc}} \cos \phi - n\phi)} d\phi = \pi j^{n+1} (J_{n+1}(k_e \rho \sin \theta^{\text{inc}}) - J_{n-1}(k_e \rho \sin \theta^{\text{inc}})) \quad (4.40)$$

where J_n is given by (4.38). Substitution of (4.37) and (4.40) into (4.36) produces

$$\begin{aligned} \vec{V}_{ni}^{t\theta} = & j^n \pi k_e \int T_i(t) e^{jk_e z \cos \theta^{\text{inc}}} \{j \cos \theta^{\text{inc}} \sin v (J_{n+1}(k_e \rho \sin \theta^{\text{inc}}) - J_{n-1}(k_e \rho \sin \theta^{\text{inc}})) \\ & - 2 \sin \theta^{\text{inc}} \cos v J_n(k_e \rho \sin \theta^{\text{inc}})\} dt. \end{aligned} \quad (4.41)$$

It will now be shown that J_n of (4.38) is the Bessel function of the first kind of order n . Because the integrand in (4.38) is periodic with the period 2π , (4.38) can, upon replacement of $e^{-jn\phi}$ by $\cos(n\phi) - j \sin(n\phi)$, be written as

$$J_n(x) = \frac{j^{-n}}{2\pi} \int_{-\pi}^{\pi} e^{jx \cos \phi} (\cos(n\phi) - j \sin(n\phi)) d\phi. \quad (4.42)$$

Because the cosines are even functions of ϕ and because $\sin(n\phi)$ is an odd function of ϕ , (4.42) reduces to

$$J_n(x) = \frac{j^{-n}}{\pi} \int_0^{\pi} e^{jx \cos \phi} \cos(n\phi) d\phi. \quad (4.43)$$

Now, $J_n(x)$ of (4.43) is the Bessel function of the first kind of order n given by formula 9.1.21 in [56].

4.4 $\vec{V}_{ni}^{\phi\theta}$

Substitution of (4.9) into (4.25) gives

$$\vec{V}_{ni}^{\phi\theta} = k_e \int dt T_i(t) \int_0^{2\pi} d\phi \hat{\phi} \cdot (\hat{\mathbf{x}} \cos \theta^{\text{inc}} - \hat{\mathbf{z}} \sin \theta^{\text{inc}}) e^{jk_e(\rho \sin \theta^{\text{inc}} \cos \phi + z \cos \theta^{\text{inc}})} e^{-jn\phi}. \quad (4.44)$$

Use of

$$\hat{\phi} = -\hat{\mathbf{x}} \sin \phi + \hat{\mathbf{y}} \cos \phi \quad (4.45)$$

leads to

$$\hat{\phi} \cdot (\hat{\mathbf{x}} \cos \theta^{\text{inc}} - \hat{\mathbf{z}} \sin \theta^{\text{inc}}) = -\cos \theta^{\text{inc}} \sin \phi. \quad (4.46)$$

Substitution of (4.46) into (4.44) gives

$$\vec{V}_{ni}^{\phi\theta} = -k_e \int dt T_i(t) e^{jk_e z \cos \theta^{\text{inc}}} \cos \theta^{\text{inc}} \int_0^{2\pi} d\phi \sin \phi e^{j(k_e \rho \sin \theta^{\text{inc}} \cos \phi - n\phi)}. \quad (4.47)$$

Use of the complex exponential representation of $\sin \phi$ gives

$$\int_0^{2\pi} \sin \phi e^{j(k_e \rho \sin \theta^{\text{inc}} \cos \phi - n\phi)} d\phi = \frac{j}{2} \left(\int_0^{2\pi} e^{j(k_e \rho \sin \theta^{\text{inc}} \cos \phi - (n+1)\phi)} d\phi - \int_0^{2\pi} e^{j(k_e \rho \sin \theta^{\text{inc}} \cos \phi - (n-1)\phi)} d\phi \right). \quad (4.48)$$

Equation (4.48) is rewritten as

$$\int_0^{2\pi} \sin \phi e^{j(k_e \rho \sin \theta^{\text{inc}} \cos \phi - n\phi)} d\phi = -\pi j^n (J_{n+1}(k_e \rho \sin \theta^{\text{inc}}) + J_{n-1}(k_e \rho \sin \theta^{\text{inc}})) \quad (4.49)$$

where J_n is given by (4.38). Substitution of (4.49) into (4.47) produces

$$\vec{V}_{ni}^{\phi\theta} = j^n \pi k_e \int T_i(t) e^{jk_e z \cos \theta^{\text{inc}}} \cos \theta^{\text{inc}} (J_{n+1}(k_e \rho \sin \theta^{\text{inc}}) + J_{n-1}(k_e \rho \sin \theta^{\text{inc}})) dt. \quad (4.50)$$

4.5 $\vec{I}_{ni}^{t\theta}$

Substitution of (4.10) into (4.26) gives

$$\vec{I}_{ni}^{t\theta} = -k_e \int dt T_i(t) \int_0^{2\pi} d\phi (\hat{\mathbf{t}} \cdot \hat{\mathbf{y}}) e^{jk_e(\rho \sin \theta^{\text{inc}} \cos \phi + z \cos \theta^{\text{inc}})} e^{-jn\phi}. \quad (4.51)$$

Use of (4.33) leads to

$$\hat{\mathbf{t}} \cdot \hat{\mathbf{y}} = \sin v \sin \phi. \quad (4.52)$$

Substitution of (4.52) into (4.51) gives

$$\vec{I}_{ni}^{t\theta} = -k_e \int dt T_i(t) e^{jk_e z \cos \theta^{\text{inc}}} \sin v \int_0^{2\pi} d\phi \sin \phi e^{j(k_e \rho \sin \theta^{\text{inc}} \cos \phi - n\phi)}. \quad (4.53)$$

Substitution of (4.49) into (4.53) produces

$$\vec{I}_{ni}^{t\theta} = j^n \pi k_e \int T_i(t) e^{jk_e z \cos \theta^{\text{inc}}} \sin v (J_{n+1}(k_e \rho \sin \theta^{\text{inc}}) + J_{n-1}(k_e \rho \sin \theta^{\text{inc}})) dt. \quad (4.54)$$

4.6 $\vec{I}_{ni}^{\phi\theta}$

Substitution of (4.10) into (4.27) gives

$$\vec{I}_{ni}^{\phi\theta} = -k_e \int dt T_i(t) \int_0^{2\pi} d\phi (\hat{\phi} \cdot \hat{\mathbf{y}}) e^{jk_e(\rho \sin \theta^{\text{inc}} \cos \phi + z \cos \theta^{\text{inc}})} e^{-jn\phi}. \quad (4.55)$$

The dot product of $\hat{\phi}$ of (4.45) with $\hat{\mathbf{y}}$ is

$$\hat{\phi} \cdot \hat{\mathbf{y}} = \cos \phi. \quad (4.56)$$

Substitution of (4.56) into (4.55) gives

$$\vec{I}_{ni}^{\phi\theta} = -k_e \int dt T_i(t) e^{jk_e z \cos \theta^{\text{inc}}} \int_0^{2\pi} d\phi \cos \phi e^{j(k_e \rho \sin \theta^{\text{inc}} \cos \phi - n\phi)}. \quad (4.57)$$

Substitution of (4.40) into (4.57) produces

$$\vec{I}_{ni}^{\phi\theta} = -j^{n+1} \pi k_e \int T_i(t) e^{jk_e z \cos \theta^{\text{inc}}} (J_{n+1}(k_e \rho \sin \theta^{\text{inc}}) - J_{n-1}(k_e \rho \sin \theta^{\text{inc}})) dt. \quad (4.58)$$

4.7 $\vec{V}_{ni}^{t\phi}$, $\vec{V}_{ni}^{\phi\phi}$, $\vec{I}_{ni}^{t\phi}$, and $\vec{I}_{ni}^{\phi\phi}$

In expressions (4.28)–(4.31) for $(\vec{V}_{ni}^{t\phi}, \vec{V}_{ni}^{\phi\phi}, \vec{I}_{ni}^{t\phi}, \vec{I}_{ni}^{\phi\phi})$, \mathbf{E}^ϕ and \mathbf{H}^ϕ are given by (4.11) and (4.12), respectively. Comparison of (4.11) with (4.10) and comparison of (4.12) with (4.9) reveal that

$$\frac{1}{\eta_e} \mathbf{E}^\phi = -\mathbf{H}^\theta \quad (4.59)$$

$$\mathbf{H}^\phi = \frac{1}{\eta_e} \mathbf{E}^\theta. \quad (4.60)$$

Substituting (4.59) into (4.28) and (4.29) and substituting (4.60) into (4.30) and (4.31), one obtains

$$\vec{V}_{ni}^{t\phi} = - \int dt T_i(t) \int_0^{2\pi} d\phi \hat{\mathbf{t}} \cdot [\mathbf{H}^\theta]_S e^{-jn\phi} \quad (4.61)$$

$$\vec{V}_{ni}^{\phi\phi} = - \int dt T_i(t) \int_0^{2\pi} d\phi \hat{\phi} \cdot [\mathbf{H}^\theta]_S e^{-jn\phi} \quad (4.62)$$

$$\vec{I}_{ni}^{t\phi} = \int dt T_i(t) \int_0^{2\pi} d\phi \hat{\mathbf{t}} \cdot \frac{1}{\eta_e} [\mathbf{E}^\theta]_S e^{-jn\phi} \quad (4.63)$$

$$\vec{I}_{ni}^{\phi\phi} = \int dt T_i(t) \int_0^{2\pi} d\phi \hat{\phi} \cdot \frac{1}{\eta_e} [\mathbf{E}^\theta]_S e^{-jn\phi}. \quad (4.64)$$

Recognizing that the right-hand sides of (4.61) and (4.62) are the negatives of the right-hand sides of (4.26) and (4.27), respectively, one obtains

$$\vec{V}_{ni}^{t\phi} = -\vec{I}_{ni}^{t\theta} \quad (4.65)$$

$$\vec{V}_{ni}^{\phi\phi} = -\vec{I}_{ni}^{\phi\theta}. \quad (4.66)$$

Recognizing that the right-hand sides of (4.63) and (4.64) are identical to the right-hand sides of (4.24) and (4.25), respectively, one obtains

$$\vec{I}_{ni}^{t\phi} = \vec{V}_{ni}^{t\theta} \quad (4.67)$$

$$\vec{I}_{ni}^{\phi\phi} = \vec{V}_{ni}^{\phi\theta}. \quad (4.68)$$

4.8 Calculation of $\vec{V}_{ni}^{t\theta}$, $\vec{V}_{ni}^{\phi\theta}$, $\vec{I}_{ni}^{t\theta}$, $\vec{I}_{ni}^{\phi\theta}$, $\vec{V}_{ni}^{t\phi}$, $\vec{V}_{ni}^{\phi\phi}$, $\vec{I}_{ni}^{t\phi}$, and $\vec{I}_{ni}^{\phi\phi}$

As given by (4.41) and (4.58), $\vec{V}_{ni}^{t\theta}$ and $\vec{I}_{ni}^{\phi\theta}$ are even functions of n . As given by (4.50) and (4.54), $\vec{V}_{ni}^{\phi\theta}$ and $\vec{I}_{ni}^{t\theta}$ are odd functions of n . Also, $\vec{V}_{ni}^{t\phi}$, $\vec{V}_{ni}^{\phi\phi}$, $\vec{I}_{ni}^{t\phi}$, and $\vec{I}_{ni}^{\phi\phi}$ are, by (4.65)–(4.68), simply related to $\vec{V}_{ni}^{t\theta}$, $\vec{V}_{ni}^{\phi\theta}$, $\vec{I}_{ni}^{t\theta}$, and $\vec{I}_{ni}^{\phi\theta}$. Therefore, it is sufficient to calculate $\vec{V}_{ni}^{t\theta}$, $\vec{V}_{ni}^{\phi\theta}$, $\vec{I}_{ni}^{t\theta}$, and $\vec{I}_{ni}^{\phi\theta}$ for $n \geq 0$.

The integrals with respect to t in (4.41), (4.50), (4.54), and (4.58) are evaluated by sampling at $\{\bar{t} = \bar{t}_p, p = 2i - 1, 2i, 2i + 1, 2i + 2\}$. Thus, (4.41), (4.50), (4.54), and (4.58) become

$$\begin{aligned} \vec{V}_{ni}^{t\theta} = j^n \pi k_e \sum_{p=2i-1}^{2i+2} T_{p+2i-2} e^{jk_e \bar{z}_p \cos \theta^{\text{inc}}} \{ & j \cos \theta^{\text{inc}} \sin v_p (J_{n+1}(k_e \bar{\rho}_p \sin \theta^{\text{inc}}) \\ & - J_{n-1}(k_e \bar{\rho}_p \sin \theta^{\text{inc}})) - 2 \sin \theta^{\text{inc}} \cos v_p J_n(k_e \bar{\rho}_p \sin \theta^{\text{inc}}) \} \end{aligned} \quad (4.69)$$

$$\vec{V}_{ni}^{\phi\theta} = j^n \pi k_e \sum_{p=2i-1}^{2i+2} T_{p+2i-2} e^{jk_e \bar{z}_p \cos \theta^{\text{inc}}} \cos \theta^{\text{inc}} (J_{n+1}(k_e \bar{\rho}_p \sin \theta^{\text{inc}}) + J_{n-1}(k_e \bar{\rho}_p \sin \theta^{\text{inc}})) \quad (4.70)$$

$$\vec{I}_{ni}^{t\theta} = j^n \pi k_e \sum_{p=2i-1}^{2i+2} T_{p+2i-2} e^{jk_e \bar{z}_p \cos \theta^{\text{inc}}} \sin v_p (J_{n+1}(k_e \bar{\rho}_p \sin \theta^{\text{inc}}) + J_{n-1}(k_e \bar{\rho}_p \sin \theta^{\text{inc}})) \quad (4.71)$$

$$\vec{I}_{ni}^{\phi\theta} = -j^{n+1} \pi k_e \sum_{p=2i-1}^{2i+2} T_{p+2i-2} e^{jk_e \bar{z}_p \cos \theta^{\text{inc}}} (J_{n+1}(k_e \bar{\rho}_p \sin \theta^{\text{inc}}) - J_{n-1}(k_e \bar{\rho}_p \sin \theta^{\text{inc}})) \quad (4.72)$$

where T_{4i-3} , T_{4i-2} , T_{4i-1} , and T_{4i} are given by (3.86)–(3.89). Also, $\bar{\rho}_p$, \bar{z}_p , and v_p are, respectively, ρ at $t = \bar{t}_p$, z at $t = \bar{t}_p$, and v for $t_p \leq t < t_{p+1}$.

From (4.69)–(4.72),

$$\vec{V}_{-ni}^{t\theta} = \vec{V}_{ni}^{t\theta} \quad (4.73)$$

$$\vec{V}_{-ni}^{\phi\theta} = -\vec{V}_{ni}^{\phi\theta} \quad (4.74)$$

$$\vec{I}_{-ni}^{t\theta} = -\vec{I}_{ni}^{t\theta} \quad (4.75)$$

$$\vec{I}_{-ni}^{\phi\theta} = \vec{I}_{ni}^{\phi\theta}. \quad (4.76)$$

Chapter 5

Scattered Field Far from the Scatterer

5.1 Introduction

In Chapter 5, reciprocity is used to obtain an expression for the scattered electric field $\mathbf{E}_{pq}^{\text{scat}}$ far from the scatterer. Here, $p = \theta$ for reception of the θ -polarized scattered electric field and $p = \phi$ for reception of the ϕ -polarized scattered electric field. Also, $q = \theta$ for excitation by an incident electromagnetic field whose electric field is θ -polarized and $q = \phi$ for excitation by an electromagnetic field whose electric field is ϕ -polarized. As given by (5.56), the expression for $\mathbf{E}_{pq}^{\text{scat}}$ contains elements of column vectors that are solutions of two moment matrix equations and contains elements of excitation column vectors with the angle θ^{inc} replaced by θ^{scat} . Here, θ^{inc} is the angle that the radius vector from the origin in the vicinity of the scatterer to the distant source of the incident field makes with the z -axis, and θ^{scat} is the angle that the radius vector from the origin to the location of the receiver makes with the z -axis. Expressed in terms of $\mathbf{E}_{pq}^{\text{scat}}$ and the q -component of the incident electric field, the radar cross section σ^{pq} is given by (5.61).

5.2 Reciprocity

The scattered field far from the scatterer is obtained by using the reciprocity theorem [23, Section 3-8]. The reciprocity theorem for the two sets of electric and magnetic current sources $(\mathbf{J}^a, \mathbf{M}^a)$ and $(\mathbf{J}^b, \mathbf{M}^b)$ is

$$\int_{V_b} (\mathbf{E}^a \cdot \mathbf{J}^b - \mathbf{H}^a \cdot \mathbf{M}^b) d\tau = \int_{V_a} (\mathbf{E}^b \cdot \mathbf{J}^a - \mathbf{H}^b \cdot \mathbf{M}^a) d\tau \quad (5.1)$$

where $(\mathbf{E}^a, \mathbf{H}^a)$ is the electromagnetic field of $(\mathbf{J}^a, \mathbf{M}^a)$, $(\mathbf{E}^b, \mathbf{H}^b)$ is the electromagnetic field of $(\mathbf{J}^b, \mathbf{M}^b)$, V_a is the volume where $(\mathbf{J}^a, \mathbf{M}^a)$ exists, V_b is the volume where $(\mathbf{J}^b, \mathbf{M}^b)$ exists, and $d\tau$ is the differential element of volume.

Let

$$(\mathbf{J}^a, \mathbf{M}^a) = (\mathbf{J}_e, \mathbf{M}) \quad (5.2)$$

$$(\mathbf{J}^b, \mathbf{M}^b) = (\mathcal{I}\ell, \mathbf{0}) \quad (5.3)$$

where \mathbf{J}_e and \mathbf{M} are the equivalent electric and magnetic currents that radiate the scattered electromagnetic field $(\mathbf{E}^{\text{scat}}, \mathbf{H}^{\text{scat}})$ and $\mathcal{I}\ell$ is an electric current element located at the point

where the scattered field is observed. Here, \mathcal{I} is a finite vector that represents a very small vector length ℓ of very large electric current I at the point where the scattered field is observed. Substitution of (5.2) and (5.3) into (5.1) gives

$$\mathcal{I} \cdot \mathbf{E}(\mathbf{J}_e, \mathbf{M}) = \int_S (\mathbf{E}(\mathcal{I}, \mathbf{0}) \cdot \mathbf{J}_e - \mathbf{H}(\mathcal{I}, \mathbf{0}) \cdot \mathbf{M}) ds \quad (5.4)$$

where the first argument of an electric field \mathbf{E} or a magnetic field \mathbf{H} is its electric current source and the second argument is its magnetic current source. In the transition from (5.1) to (5.4), the volume integral on the left-hand side of (5.1) reduces to the left-hand side of (5.4) where $\mathbf{E}(\mathbf{J}_e, \mathbf{M})$ is the scattered electric field \mathbf{E}^{scat} evaluated at the point where \mathcal{I} is located and the volume integral on the right-hand side of (5.1) becomes the surface integral over the surface S where \mathbf{J}_e and \mathbf{M} exist. The electric current element \mathcal{I} has no radial component and is located far from S so that its electric and magnetic fields on S are given by

$$\mathbf{E}(\mathcal{I}, \mathbf{0}) = -jk_e \eta_e \frac{e^{-jk_e r^{\text{rec}}}}{4\pi r^{\text{rec}}} \mathcal{I} e^{jk_e \mathbf{r} \cdot \hat{\mathbf{r}}^{\text{rec}}} \quad (5.5)$$

$$\mathbf{H}(\mathcal{I}, \mathbf{0}) = -\frac{1}{\eta_e} \hat{\mathbf{r}}^{\text{rec}} \times \mathbf{E}(\mathcal{I}, \mathbf{0}) \quad (5.6)$$

where \mathbf{r} is the radius vector from the origin to the point where ds in (5.4) is located, r^{rec} is the distance from the origin in the vicinity of S to the location of \mathcal{I} , and $\hat{\mathbf{r}}^{\text{rec}}$ is the unit vector that points from the origin toward the location of \mathcal{I} . Therefore, the radius vector from the origin to the location of \mathcal{I} is \mathbf{r}^{rec} given by

$$\mathbf{r}^{\text{rec}} = r^{\text{rec}} \hat{\mathbf{r}}^{\text{rec}}. \quad (5.7)$$

Given that the location of \mathcal{I} is where the scattered field is received, the superscript *rec* in r^{rec} , $\hat{\mathbf{r}}^{\text{rec}}$ and \mathbf{r}^{rec} stands for receiver. Substitution of (5.5) and (5.6) into (5.4) and subsequent replacement of $\mathbf{E}(\mathbf{J}_e, \mathbf{M})$ by the scattered electric field \mathbf{E}^{scat} give

$$\mathcal{I} \cdot \mathbf{E}^{\text{scat}} = -\frac{jk_e \eta_e e^{-jk_e r^{\text{rec}}}}{4\pi r^{\text{rec}}} \left\{ \int_S (\mathcal{I} \cdot \mathbf{J}_e) e^{jk_e \mathbf{r} \cdot \hat{\mathbf{r}}^{\text{rec}}} ds + \int_S \left((\hat{\mathbf{r}}^{\text{rec}} \times \mathcal{I}) \cdot \frac{\mathbf{M}}{\eta_e} \right) e^{jk_e \mathbf{r} \cdot \hat{\mathbf{r}}^{\text{rec}}} ds \right\}. \quad (5.8)$$

5.3 The θ -Component of the Scattered Field

Let $\hat{\boldsymbol{\theta}}^{\text{rec}}$ be $\hat{\boldsymbol{\theta}}$ at \mathbf{r}^{rec} . Substitution of $\hat{\boldsymbol{\theta}}^{\text{rec}}$ for \mathcal{I} in (5.8) produces

$$E_{\theta}^{\text{scat}} = -\frac{jk_e \eta_e e^{-jk_e r^{\text{rec}}}}{4\pi r^{\text{rec}}} \left\{ \int_S (\hat{\boldsymbol{\theta}}^{\text{rec}} \cdot \mathbf{J}_e) e^{jk_e \mathbf{r} \cdot \hat{\mathbf{r}}^{\text{rec}}} ds + \int_S \left(\hat{\boldsymbol{\phi}}^{\text{rec}} \cdot \frac{\mathbf{M}}{\eta_e} \right) e^{jk_e \mathbf{r} \cdot \hat{\mathbf{r}}^{\text{rec}}} ds \right\} \quad (5.9)$$

where

$$E_{\theta}^{\text{scat}} = \hat{\boldsymbol{\theta}}^{\text{rec}} \cdot \mathbf{E}^{\text{scat}} \quad (5.10)$$

is the θ -component of the scattered field at \mathbf{r}^{rec} and

$$\hat{\boldsymbol{\phi}}^{\text{rec}} = \hat{\mathbf{r}}^{\text{rec}} \times \hat{\boldsymbol{\theta}}^{\text{rec}} \quad (5.11)$$

is $\hat{\boldsymbol{\phi}}$ at \mathbf{r}^{rec} . As given by (2.7) and (2.9), the method of moments solution for \mathbf{J}_e and \mathbf{M}/η_e is

$$\mathbf{J}_e = \sum_{n=-N}^N \sum_{j=1}^{N_t} \left(I_{nj}^{tq} \mathbf{J}_{nj}^t + I_{nj}^{\phi q} \mathbf{J}_{nj}^{\phi} \right) \quad (5.12)$$

$$\frac{\mathbf{M}}{\eta_e} = \sum_{n=-N}^N \sum_{j=1}^{N_t} L_j \left(V_{nj}^{tq} \mathbf{J}_{nj}^t + V_{nj}^{\phi q} \mathbf{J}_{nj}^{\phi} \right) \quad (5.13)$$

where the extra superscript $q = \theta$ for the θ -polarized incident electric field and $q = \phi$ for the ϕ -polarized incident electric field. Also,

$$L_j = \begin{cases} 1, & \mathbf{J}_{nj}^t \text{ and } \mathbf{J}_{nj}^{\phi} \text{ are in an aperture} \\ 0, & \mathbf{J}_{nj}^t \text{ and } \mathbf{J}_{nj}^{\phi} \text{ are on a conductor.} \end{cases} \quad (5.14)$$

Substitution of (5.12) and (5.13) into (5.9) gives

$$\begin{aligned} E_{\theta q}^{\text{scat}} = & -\frac{j\eta_e e^{-jk_e r^{\text{rec}}}}{4\pi r^{\text{rec}}} \sum_{n=-N}^N \sum_{j=1}^{N_t} \left\{ I_{nj}^{tq} \int_S k_e \left(\mathbf{J}_{nj}^t \cdot \hat{\boldsymbol{\theta}}^{\text{rec}} \right) e^{jk_e \mathbf{r} \cdot \hat{\mathbf{r}}^{\text{rec}}} ds \right. \\ & + I_{nj}^{\phi q} \int_S k_e \left(\mathbf{J}_{nj}^{\phi} \cdot \hat{\boldsymbol{\theta}}^{\text{rec}} \right) e^{jk_e \mathbf{r} \cdot \hat{\mathbf{r}}^{\text{rec}}} ds + L_j V_{nj}^{tq} \int_S k_e \left(\mathbf{J}_{nj}^t \cdot \hat{\boldsymbol{\phi}}^{\text{rec}} \right) e^{jk_e \mathbf{r} \cdot \hat{\mathbf{r}}^{\text{rec}}} ds \\ & \left. + L_j V_{nj}^{\phi q} \int_S k_e \left(\mathbf{J}_{nj}^{\phi} \cdot \hat{\boldsymbol{\phi}}^{\text{rec}} \right) e^{jk_e \mathbf{r} \cdot \hat{\mathbf{r}}^{\text{rec}}} ds \right\}. \end{aligned} \quad (5.15)$$

The extra subscript q in $E_{\theta q}^{\text{scat}}$ indicates the polarization of the incident electric field. The factor k_e in the integrands in (5.15) will simplify relations between these integrals and the plane wave excitation quantities (4.69)–(4.72).

5.4 Evaluation of the First Integral in (5.15)

The first integral in (5.15) is iterated as

$$\int_S k_e \left(\mathbf{J}_{nj}^t \cdot \hat{\boldsymbol{\theta}}^{\text{rec}} \right) e^{jk_e \mathbf{r} \cdot \hat{\mathbf{r}}^{\text{rec}}} ds = k_e \int dt \rho \int_0^{2\pi} d\phi \left(\mathbf{J}_{nj}^t \cdot \hat{\boldsymbol{\theta}}^{\text{rec}} \right) e^{jk_e \mathbf{r} \cdot \hat{\mathbf{r}}^{\text{rec}}}. \quad (5.16)$$

Substitution of

$$\mathbf{J}_{nj}^t = \hat{\mathbf{t}} \frac{T_j(t)}{\rho} e^{jn\phi} \quad (5.17)$$

into (5.16) gives

$$\int_S k_e \left(\mathbf{J}_{nj}^t \cdot \hat{\boldsymbol{\theta}}^{\text{rec}} \right) e^{jk_e \mathbf{r} \cdot \hat{\mathbf{r}}^{\text{rec}}} ds = k_e \int dt T_j(t) \int_0^{2\pi} d\phi \left(\hat{\mathbf{t}} \cdot \hat{\boldsymbol{\theta}}^{\text{rec}} \right) e^{jk_e \mathbf{r} \cdot \hat{\mathbf{r}}^{\text{rec}}} e^{jn\phi}. \quad (5.18)$$

In (5.18),

$$\hat{\boldsymbol{\theta}}^{\text{rec}} = \hat{\mathbf{x}} \cos \theta^{\text{rec}} \cos \phi^{\text{rec}} + \hat{\mathbf{y}} \cos \theta^{\text{rec}} \sin \phi^{\text{rec}} - \hat{\mathbf{z}} \sin \theta^{\text{rec}}. \quad (5.19)$$

The dot product of (4.33) with (5.19) is

$$\left(\hat{\mathbf{t}} \cdot \hat{\boldsymbol{\theta}}^{\text{rec}} \right) = \cos \theta^{\text{rec}} \sin v \cos(\phi - \phi^{\text{rec}}) - \sin \theta^{\text{rec}} \cos v. \quad (5.20)$$

In (5.18),

$$\hat{\mathbf{r}}^{\text{rec}} = \hat{\mathbf{x}} \sin \theta^{\text{rec}} \cos \phi^{\text{rec}} + \hat{\mathbf{y}} \sin \theta^{\text{rec}} \sin \phi^{\text{rec}} + \hat{\mathbf{z}} \cos \theta^{\text{rec}}. \quad (5.21)$$

The dot product of (4.7) with (5.21) is

$$\mathbf{r} \cdot \hat{\mathbf{r}}^{\text{rec}} = \rho \sin \theta^{\text{rec}} \cos(\phi - \phi^{\text{rec}}) + z \cos \theta^{\text{rec}}. \quad (5.22)$$

Substitution of (5.20) and (5.22) into (5.18) gives

$$\int_S k_e \left(\mathbf{J}_{nj}^t \cdot \hat{\boldsymbol{\theta}}^{\text{rec}} \right) e^{jk_e \mathbf{r} \cdot \hat{\mathbf{r}}^{\text{rec}}} ds = k_e \int dt T_j(t) e^{jk_e z \cos \theta^{\text{rec}}} \int_0^{2\pi} d\phi \cdot (\cos \theta^{\text{rec}} \sin v \cos(\phi - \phi^{\text{rec}}) - \sin \theta^{\text{rec}} \cos v) e^{j(k_e \rho \sin \theta^{\text{rec}} \cos(\phi - \phi^{\text{rec}}) + n\phi)}. \quad (5.23)$$

The integrand of the integral with respect to ϕ in (5.23) is a periodic function of ϕ with the period 2π . Therefore, ϕ can be replaced by $\phi + \phi^{\text{rec}}$ in the integrand without changing the value of the integral. Replacing ϕ by $\phi + \phi^{\text{rec}}$ in this integrand, one obtains

$$\int_S k_e \left(\mathbf{J}_{nj}^t \cdot \hat{\boldsymbol{\theta}}^{\text{rec}} \right) e^{jk_e \mathbf{r} \cdot \hat{\mathbf{r}}^{\text{rec}}} ds = e^{jn\phi^{\text{rec}}} k_e \int dt T_j(t) e^{jk_e z \cos \theta^{\text{rec}}} \int_0^{2\pi} d\phi \cdot (\cos \theta^{\text{rec}} \sin v \cos \phi - \sin \theta^{\text{rec}} \cos v) e^{j(k_e \rho \sin \theta^{\text{rec}} \cos \phi + n\phi)}. \quad (5.24)$$

Replacing i by j in (4.35) and replacing n by $-n$ in (4.35), one obtains

$$\vec{V}_{-nj}^{t\theta} = k_e \int dt T_j(t) e^{jk_e z \cos \theta^{\text{inc}}} \int_0^{2\pi} d\phi (\cos \theta^{\text{inc}} \sin v \cos \phi - \sin \theta^{\text{inc}} \cos v) e^{j(k_e \rho \sin \theta^{\text{inc}} \cos \phi + n\phi)}. \quad (5.25)$$

Note that what multiplies $e^{jn\phi^{\text{rec}}}$ on the right-hand side of (5.24) is the right-hand side of (5.25) with θ^{inc} replaced by θ^{rec} . Therefore, what multiplies $e^{jn\phi^{\text{rec}}}$ on the right-hand side of (5.24) is $\vec{V}_{-nj}^{t\theta}$ with θ^{inc} replaced by θ^{rec} . Furthermore, because it can be shown that $\vec{V}_{nj}^{t\theta}$ is an even function of n , it follows that

$$\int_S k_e (\mathbf{J}_{nj}^t \cdot \hat{\boldsymbol{\theta}}^{\text{rec}}) e^{jk_e \mathbf{r} \cdot \hat{\mathbf{r}}^{\text{rec}}} ds = e^{jn\phi^{\text{rec}}} \left[\vec{V}_{nj}^{t\theta} \right]_{\theta^{\text{inc}} \rightarrow \theta^{\text{rec}}} \quad (5.26)$$

where the notation $\theta^{\text{inc}} \rightarrow \theta^{\text{rec}}$ means that θ^{inc} is replaced by θ^{rec} .

5.5 Evaluation of the Second Integral in (5.15)

The second integral in (7.15) is iterated as

$$\int_S k_e (\mathbf{J}_{nj}^\phi \cdot \hat{\boldsymbol{\theta}}^{\text{rec}}) e^{jk_e \mathbf{r} \cdot \hat{\mathbf{r}}^{\text{rec}}} ds = k_e \int dt \rho \int_0^{2\pi} d\phi (\mathbf{J}_{nj}^\phi \cdot \hat{\boldsymbol{\theta}}^{\text{rec}}) e^{jk_e \mathbf{r} \cdot \hat{\mathbf{r}}^{\text{rec}}}. \quad (5.27)$$

Substitution of

$$\mathbf{J}_{nj}^\phi = \hat{\boldsymbol{\phi}} \frac{T_j(t)}{\rho} e^{jn\phi} \quad (5.28)$$

into (5.27) gives

$$\int_S k_e (\mathbf{J}_{nj}^\phi \cdot \hat{\boldsymbol{\theta}}^{\text{rec}}) e^{jk_e \mathbf{r} \cdot \hat{\mathbf{r}}^{\text{rec}}} ds = k_e \int dt T_j(t) \int_0^{2\pi} d\phi (\hat{\boldsymbol{\phi}} \cdot \hat{\boldsymbol{\theta}}^{\text{rec}}) e^{jk_e \mathbf{r} \cdot \hat{\mathbf{r}}^{\text{rec}}} e^{jn\phi}. \quad (5.29)$$

The dot product of (4.45) with (5.19) is

$$\hat{\boldsymbol{\phi}} \cdot \hat{\boldsymbol{\theta}}^{\text{rec}} = -\cos \theta^{\text{rec}} \sin(\phi - \phi^{\text{rec}}). \quad (5.30)$$

Substitution of (5.22) and (5.30) into (5.29) gives

$$\int_S k_e (\mathbf{J}_{nj}^\phi \cdot \hat{\boldsymbol{\theta}}^{\text{rec}}) e^{jk_e \mathbf{r} \cdot \hat{\mathbf{r}}^{\text{rec}}} ds = -k_e \int dt T_j(t) e^{jk_e z \cos \theta^{\text{rec}}} \cos \theta^{\text{rec}} \int_0^{2\pi} d\phi \sin(\phi - \phi^{\text{rec}}) e^{j(k_e \rho \sin \theta^{\text{rec}} \cos(\phi - \phi^{\text{rec}}) + n\phi)}. \quad (5.31)$$

The integrand of the integral with respect to ϕ in (5.31) is a periodic function of ϕ with the period 2π . Therefore, ϕ can be replaced by $\phi + \phi^{\text{rec}}$ in the integrand without changing the value of the integral. Replacing ϕ by $\phi + \phi^{\text{rec}}$ in this integrand, one obtains

$$\int_S k_e \left(\mathbf{J}_{nj}^\phi \cdot \hat{\boldsymbol{\theta}}^{\text{rec}} \right) e^{jk_e \mathbf{r} \cdot \hat{\mathbf{r}}^{\text{rec}}} ds = -k_e e^{jn\phi^{\text{rec}}} \int dt T_j(t) e^{jk_e z \cos \theta^{\text{rec}}} \cos \theta^{\text{rec}} \cdot \int_0^{2\pi} d\phi \sin \phi e^{j(k_e \rho \sin \theta^{\text{rec}} \cos \phi + n\phi)}. \quad (5.32)$$

Replacing i by j in (4.47) and replacing n by $-n$ in (4.47), one obtains

$$\vec{V}_{-nj}^{\phi\theta} = -k_e \int dt T_j(t) e^{jk_e z \cos \theta^{\text{inc}}} \cos \theta^{\text{inc}} \int_0^{2\pi} d\phi \sin \phi e^{j(k_e \rho \sin \theta^{\text{inc}} \cos \phi + n\phi)}. \quad (5.33)$$

Note that what multiplies $e^{jn\phi^{\text{rec}}}$ on the right-hand side of (5.32) is the right-hand side of (5.33) with θ^{inc} replaced by θ^{rec} . Therefore, what multiplies $e^{jn\phi^{\text{rec}}}$ on the right-hand side of (5.32) is $\vec{V}_{-nj}^{\phi\theta}$ with θ^{inc} replaced by θ^{rec} . Furthermore, because it can be shown that $\vec{V}_{nj}^{\phi\theta}$ is an odd function of n , it follows that

$$\int_S k_e \left(\mathbf{J}_{nj}^\phi \cdot \hat{\boldsymbol{\theta}}^{\text{rec}} \right) e^{jk_e \mathbf{r} \cdot \hat{\mathbf{r}}^{\text{rec}}} ds = -e^{jn\phi^{\text{rec}}} \left[\vec{V}_{nj}^{\phi\theta} \right]_{\theta^{\text{inc}} \rightarrow \theta^{\text{rec}}} \quad (5.34)$$

where the notation $\theta^{\text{inc}} \rightarrow \theta^{\text{rec}}$ means that θ^{inc} is replaced by θ^{rec} .

5.6 Evaluation of the Third Integral in (5.15)

The third integral in (5.15) is iterated as

$$\int_S k_e \left(\mathbf{J}_{nj}^t \cdot \hat{\boldsymbol{\phi}}^{\text{rec}} \right) e^{jk_e \mathbf{r} \cdot \hat{\mathbf{r}}^{\text{rec}}} ds = k_e \int dt \rho \int_0^{2\pi} d\phi \left(\mathbf{J}_{nj}^t \cdot \hat{\boldsymbol{\phi}}^{\text{rec}} \right) e^{jk_e \mathbf{r} \cdot \hat{\mathbf{r}}^{\text{rec}}}. \quad (5.35)$$

Substitution of (5.17) into (5.35) gives

$$\int_S k_e \left(\mathbf{J}_{nj}^t \cdot \hat{\boldsymbol{\phi}}^{\text{rec}} \right) e^{jk_e \mathbf{r} \cdot \hat{\mathbf{r}}^{\text{rec}}} ds = k_e \int dt T_j(t) \int_0^{2\pi} d\phi \left(\hat{\mathbf{t}} \cdot \hat{\boldsymbol{\phi}}^{\text{rec}} \right) e^{jk_e \mathbf{r} \cdot \hat{\mathbf{r}}^{\text{rec}}} e^{jn\phi}. \quad (5.36)$$

In (5.36),

$$\hat{\boldsymbol{\phi}}^{\text{rec}} = -\hat{\mathbf{x}} \sin \phi^{\text{rec}} + \hat{\mathbf{y}} \cos \phi^{\text{rec}}. \quad (5.37)$$

The dot product of (4.33) with (5.37) is

$$(\hat{\mathbf{t}} \cdot \hat{\boldsymbol{\phi}}^{\text{rec}}) = \sin v \sin(\phi - \phi^{\text{rec}}). \quad (5.38)$$

Substitution of (5.22) and (5.38) into (5.36) gives

$$\int_S k_e \left(\mathbf{J}_{nj}^t \cdot \hat{\boldsymbol{\phi}}^{\text{rec}} \right) e^{jk_e \mathbf{r} \cdot \hat{\mathbf{r}}^{\text{rec}}} ds = k_e \int dt T_j(t) e^{jk_e z \cos \theta^{\text{rec}}} \sin v \int_0^{2\pi} d\phi \sin(\phi - \phi^{\text{rec}}) e^{j(k_e \rho \sin \theta^{\text{rec}} \cos(\phi - \phi^{\text{rec}}) + n\phi)}. \quad (5.39)$$

The integrand of the integral with respect to ϕ in (5.39) is a periodic function of ϕ with the period 2π . Therefore, ϕ can be replaced by $\phi + \phi^{\text{rec}}$ in the integrand without changing the value of the integral. Replacing ϕ by $\phi + \phi^{\text{rec}}$ in this integrand, one obtains

$$\int_S k_e \left(\mathbf{J}_{nj}^t \cdot \hat{\boldsymbol{\phi}}^{\text{rec}} \right) e^{jk_e \mathbf{r} \cdot \hat{\mathbf{r}}^{\text{rec}}} ds = e^{jn\phi^{\text{rec}}} k_e \int dt T_j(t) e^{jk_e z \cos \theta^{\text{rec}}} \sin v \int_0^{2\pi} d\phi \sin \phi e^{j(k_e \rho \sin \theta^{\text{rec}} \cos \phi + n\phi)}. \quad (5.40)$$

Replacing i by j in (4.53), replacing n by $-n$ in (4.53), and changing the signs of both sides of (4.53), one obtains

$$-\vec{I}_{-nj}^{t\theta} = k_e \int dt T_j(t) e^{jk_e z \cos \theta^{\text{inc}}} \sin v \int_0^{2\pi} d\phi \sin \phi e^{j(k_e \rho \sin \theta^{\text{inc}} \cos \phi + n\phi)}. \quad (5.41)$$

Note that what multiplies $e^{jn\phi^{\text{rec}}}$ on the right-hand side of (5.40) is the right-hand side of (5.41) with θ^{inc} replaced by θ^{rec} . Therefore, what multiplies $e^{jn\phi^{\text{rec}}}$ on the right-hand side of (5.40) is $-\vec{I}_{-nj}^{t\theta}$ with θ^{inc} replaced by θ^{rec} . Furthermore, because it can be shown that $\vec{I}_{nj}^{t\theta}$ is an odd function of n , it follows that

$$\int_S k_e \left(\mathbf{J}_{nj}^t \cdot \hat{\boldsymbol{\phi}}^{\text{rec}} \right) e^{jk_e \mathbf{r} \cdot \hat{\mathbf{r}}^{\text{rec}}} ds = e^{jn\phi^{\text{rec}}} \left[\vec{I}_{nj}^{t\theta} \right]_{\theta^{\text{inc}} \rightarrow \theta^{\text{rec}}} \quad (5.42)$$

where the notation $\theta^{\text{inc}} \rightarrow \theta^{\text{rec}}$ means that θ^{inc} is replaced by θ^{rec} .

5.7 Evaluation of the Fourth Integral in (7.15)

The fourth integral in (5.15) is iterated as

$$\int_S k_e \left(\mathbf{J}_{nj}^\phi \cdot \hat{\boldsymbol{\phi}}^{\text{rec}} \right) e^{jk_e \mathbf{r} \cdot \hat{\mathbf{r}}^{\text{rec}}} ds = k_e \int dt \rho \int_0^{2\pi} d\phi \left(\mathbf{J}_{nj}^\phi \cdot \hat{\boldsymbol{\phi}}^{\text{rec}} \right) e^{jk_e \mathbf{r} \cdot \hat{\mathbf{r}}^{\text{rec}}}. \quad (5.43)$$

Substitution of (5.28) into (5.43) gives

$$\int_S k_e \left(\mathbf{J}_{nj}^\phi \cdot \hat{\boldsymbol{\phi}}^{\text{rec}} \right) e^{jk_e \mathbf{r} \cdot \hat{\mathbf{r}}^{\text{rec}}} ds = k_e \int dt T_j(t) \int_0^{2\pi} d\phi \left(\hat{\boldsymbol{\phi}} \cdot \hat{\boldsymbol{\phi}}^{\text{rec}} \right) e^{jk_e \mathbf{r} \cdot \hat{\mathbf{r}}^{\text{rec}}} e^{jn\phi}. \quad (5.44)$$

The dot product of (4.45) with (5.37) is

$$\hat{\boldsymbol{\phi}} \cdot \hat{\boldsymbol{\phi}}^{\text{rec}} = \cos(\phi - \phi^{\text{rec}}). \quad (5.45)$$

Substitution of (5.22) and (5.45) into (5.44) gives

$$\int_S k_e \left(\mathbf{J}_{nj}^\phi \cdot \hat{\boldsymbol{\phi}}^{\text{rec}} \right) e^{jk_e \mathbf{r} \cdot \hat{\mathbf{r}}^{\text{rec}}} ds = k_e \int dt T_j(t) e^{jk_e z \cos \theta^{\text{rec}}} \int_0^{2\pi} d\phi \cos(\phi - \phi^{\text{rec}}) \cdot e^{j(k_e \rho \sin \theta^{\text{rec}} \cos(\phi - \phi^{\text{rec}}) + n\phi)}. \quad (5.46)$$

The integrand of the integral with respect to ϕ in (5.46) is a periodic function of ϕ with the period 2π . Therefore, ϕ can be replaced by $\phi + \phi^{\text{rec}}$ in the integrand without changing the value of the integral. Replacing ϕ by $\phi + \phi^{\text{rec}}$ in this integrand, one obtains

$$\int_S k_e \left(\mathbf{J}_{nj}^\phi \cdot \hat{\boldsymbol{\phi}}^{\text{rec}} \right) e^{jk_e \mathbf{r} \cdot \hat{\mathbf{r}}^{\text{rec}}} ds = e^{jn\phi^{\text{rec}}} k_e \int dt T_j(t) e^{jk_e z \cos \theta^{\text{rec}}} \cdot \int_0^{2\pi} d\phi \cos \phi e^{j(k_e \rho \sin \theta^{\text{rec}} \cos \phi + n\phi)}. \quad (5.47)$$

Replacing i by j in (4.57), replacing n by $-n$ in (4.57), and changing the signs of both sides of (4.57), one obtains

$$-\vec{I}_{-nj}^{\phi\theta} = k_e \int dt T_j(t) e^{jk_e z \cos \theta^{\text{inc}}} \int_0^{2\pi} d\phi \cos \phi e^{j(k_e \rho \sin \theta^{\text{inc}} \cos \phi + n\phi)}. \quad (5.48)$$

Note that what multiplies $e^{jn\phi^{\text{rec}}}$ on the right-hand side of (5.47) is the right-hand side of (5.48) with θ^{inc} replaced by θ^{rec} . Therefore, what multiplies $e^{jn\phi^{\text{rec}}}$ on the right-hand side of (5.47) is $-\vec{I}_{-nj}^{\phi\theta}$ with θ^{inc} replaced by θ^{rec} . Furthermore, because it can be shown that $\vec{I}_{nj}^{\phi\theta}$ is an even function of n , it follows that

$$\int_S k_e \left(\mathbf{J}_{nj}^\phi \cdot \hat{\boldsymbol{\phi}}^{\text{rec}} \right) e^{jk_e \mathbf{r} \cdot \hat{\mathbf{r}}^{\text{rec}}} ds = -e^{jn\phi^{\text{rec}}} \left[\vec{I}_{nj}^{\phi\theta} \right]_{\theta^{\text{inc}} \rightarrow \theta^{\text{rec}}} \quad (5.49)$$

where the notation $\theta^{\text{inc}} \rightarrow \theta^{\text{rec}}$ means that θ^{inc} is replaced by θ^{rec} .

5.8 The ϕ -Component of the Scattered Field

Recall that $\hat{\phi}^{\text{rec}}$ is $\hat{\phi}$ at \mathbf{r}^{rec} . Substitution of $\hat{\phi}^{\text{rec}}$ for \mathcal{I} in (5.8) produces

$$E_{\phi}^{\text{scat}} = -\frac{jk_e\eta_e e^{-jk_e r^{\text{rec}}}}{4\pi r^{\text{rec}}} \left\{ \int_S \left(\hat{\phi}^{\text{rec}} \cdot \mathbf{J}_e \right) e^{jk_e \mathbf{r} \cdot \hat{\mathbf{r}}^{\text{rec}}} ds - \int_S \left(\hat{\boldsymbol{\theta}}^{\text{rec}} \cdot \frac{\mathbf{M}}{\eta_e} \right) e^{jk_e \mathbf{r} \cdot \hat{\mathbf{r}}^{\text{rec}}} ds \right\} \quad (5.50)$$

where

$$E_{\phi}^{\text{scat}} = \hat{\phi}^{\text{rec}} \cdot \mathbf{E}^{\text{scat}} \quad (5.51)$$

is the ϕ -component of the scattered field at \mathbf{r}^{rec} and

$$\hat{\boldsymbol{\theta}}^{\text{rec}} = -\mathbf{r}^{\text{rec}} \times \hat{\phi}^{\text{rec}}. \quad (5.52)$$

Substitution of (5.12) and (5.13) into (5.50) gives

$$\begin{aligned} E_{\phi q}^{\text{scat}} = & -\frac{j\eta_e e^{-jk_e r^{\text{rec}}}}{4\pi r^{\text{rec}}} \sum_{n=-N}^N \sum_{j=1}^{N_t} \left\{ I_{nj}^{tq} \int_S k_e \left(\mathbf{J}_{nj}^t \cdot \hat{\phi}^{\text{rec}} \right) e^{jk_e \mathbf{r} \cdot \hat{\mathbf{r}}^{\text{rec}}} ds \right. \\ & + I_{nj}^{\phi q} \int_S k_e \left(\mathbf{J}_{nj}^{\phi} \cdot \hat{\phi}^{\text{rec}} \right) e^{jk_e \mathbf{r} \cdot \hat{\mathbf{r}}^{\text{rec}}} ds - L_j \left(V_{nj}^{tq} \int_S k_e \left(\mathbf{J}_{nj}^t \cdot \hat{\boldsymbol{\theta}}^{\text{rec}} \right) e^{jk_e \mathbf{r} \cdot \hat{\mathbf{r}}^{\text{rec}}} ds \right. \\ & \left. \left. + V_{nj}^{\phi q} \int_S k_e \left(\mathbf{J}_{nj}^{\phi} \cdot \hat{\boldsymbol{\theta}}^{\text{rec}} \right) e^{jk_e \mathbf{r} \cdot \hat{\mathbf{r}}^{\text{rec}}} ds \right) \right\} \quad (5.53) \end{aligned}$$

where the extra subscript q in $E_{\phi q}^{\text{scat}}$ indicates the polarization of the incident electric field.

The first, second, third, and fourth integrals in (5.53) are given by (5.42), (5.49), (5.26), and (5.34), respectively.

5.9 Use of the Four Integrals That Were Previously Evaluated

Substitution of (5.26), (5.34), (5.42), and (5.49) into (5.15) produces

$$\begin{aligned} E_{\theta q}^{\text{scat}} = & -\frac{j\eta_e e^{-jk_e r^{\text{rec}}}}{4\pi r^{\text{rec}}} \sum_{n=-N}^N e^{jn\phi^{\text{rec}}} \sum_{j=1}^{N_t} \left\{ \left[\vec{V}_{nj}^{t\theta} \right]_{\theta^{\text{inc}} \rightarrow \theta^{\text{rec}}} I_{nj}^{tq} - \left[\vec{V}_{nj}^{\phi\theta} \right]_{\theta^{\text{inc}} \rightarrow \theta^{\text{rec}}} I_{nj}^{\phi q} \right. \\ & \left. + L_j \left(\left[\vec{I}_{nj}^{t\theta} \right]_{\theta^{\text{inc}} \rightarrow \theta^{\text{rec}}} V_{nj}^{tq} - \left[\vec{I}_{nj}^{\phi\theta} \right]_{\theta^{\text{inc}} \rightarrow \theta^{\text{rec}}} V_{nj}^{\phi q} \right) \right\}. \quad (5.54) \end{aligned}$$

Substitution of (5.42), (5.49), (5.26), and (5.34) into (5.53) produces

$$E_{\phi q}^{\text{scat}} = -\frac{j\eta_e e^{-jk_e r^{\text{rec}}}}{4\pi r^{\text{rec}}} \sum_{n=-N}^N e^{jn\phi^{\text{rec}}} \sum_{j=1}^{N_t} \left\{ \left[\tilde{I}_{nj}^{t\theta} \right]_{\theta^{\text{inc}} \rightarrow \theta^{\text{rec}}} I_{nj}^{tq} - \left[\tilde{I}_{nj}^{\phi\theta} \right]_{\theta^{\text{inc}} \rightarrow \theta^{\text{rec}}} I_{nj}^{\phi q} \right. \\ \left. - L_j \left(\left[\tilde{V}_{nj}^{t\theta} \right]_{\theta^{\text{inc}} \rightarrow \theta^{\text{rec}}} V_{nj}^{tq} - \left[\tilde{V}_{nj}^{\phi\theta} \right]_{\theta^{\text{inc}} \rightarrow \theta^{\text{rec}}} V_{nj}^{\phi q} \right) \right\}. \quad (5.55)$$

Equations (5.54) and (5.55) are written in matrix form as

$$E_{pq}^{\text{scat}} = -\frac{j\eta_e e^{-jk_e r^{\text{rec}}}}{4\pi r^{\text{rec}}} \sum_{n=-N}^N \left(\tilde{R}_n^p T_n^q \right) e^{jn\phi^{\text{rec}}}, \quad p, q = \theta, \phi \quad (5.56)$$

where

$$\tilde{R}_n^\theta = \left[\tilde{V}_n^{t\theta} \quad -\tilde{V}_n^{\phi\theta} \quad \tilde{I}_n^{t\theta} \quad -\tilde{I}_n^{\phi\theta} \right]_{\theta^{\text{inc}} \rightarrow \theta^{\text{rec}}} \quad (5.57)$$

$$\tilde{R}_n^\phi = \left[\tilde{I}_n^{t\theta} \quad -\tilde{I}_n^{\phi\theta} \quad -\tilde{V}_n^{t\theta} \quad \tilde{V}_n^{\phi\theta} \right]_{\theta^{\text{inc}} \rightarrow \theta^{\text{rec}}} \quad (5.58)$$

$$\tilde{T}_n^q = \left[\tilde{I}_n^{tq} \quad \tilde{I}_n^{\phi q} \quad \tilde{V}_n^{tq} L \quad \tilde{V}_n^{\phi q} L \right], \quad q = \theta, \phi. \quad (5.59)$$

where L is the diagonal matrix whose j^{th} diagonal element is L_j given by (5.14). The tilde on the right-hand sides of (5.57)–(5.59) indicates the transpose of a column matrix so that $\tilde{V}_n^{t\theta}$, $\tilde{V}_n^{\phi\theta}$, $\tilde{I}_n^{t\theta}$, $\tilde{I}_n^{\phi\theta}$, \tilde{I}_n^{tq} , $\tilde{I}_n^{\phi q}$, \tilde{V}_n^{tq} , and $\tilde{V}_n^{\phi q}$ are row matrices whose j^{th} elements are $\tilde{V}_{nj}^{t\theta}$, $\tilde{V}_{nj}^{\phi\theta}$, $\tilde{I}_{nj}^{t\theta}$, $\tilde{I}_{nj}^{\phi\theta}$, I_{nj}^{tq} , $I_{nj}^{\phi q}$, V_{nj}^{tq} , and $V_{nj}^{\phi q}$, respectively.

5.10 Scattering Cross Section

The scattering cross section σ_{pq} is the area by which the power per unit area of the incident plane wave whose electric field is q -polarized must be multiplied to obtain, by isotropic radiation, the power per unit area of the p -component E_{pq}^{scat} of the scattered electric field [24, p. 76]. Here, p is either θ or ϕ and q is either θ or ϕ . Because the isotropic radiator of power P produces the power per unit area $P/(4\pi (r^{\text{rec}})^2)$ at the distance r^{rec} where a receiver is located, this isotropic radiator will produce the power per unit area $|E_{pq}^{\text{scat}}|^2/\eta_e$ of the p -component of the scattered electric field at the distance r^{rec} if

$$\frac{P}{4\pi (r^{\text{rec}})^2} = \frac{|E_{pq}^{\text{scat}}|^2}{\eta_e} \quad (5.60)$$

where η_e is the intrinsic impedance of the medium. Using the definition of σ_{pq} to set P equal to the product of σ_{pq} with the incident power per unit area $|\mathbf{E}^q|^2/\eta_e$ of the q -polarized incident electric field \mathbf{E}^q , one obtains

$$\sigma_{pq} = \frac{4\pi (r^{\text{rec}})^2 |E_{pq}^{\text{scat}}|^2}{|\mathbf{E}^q|^2}. \quad (5.61)$$

When the incident electric field is \mathbf{E}^θ of (4.1) or \mathbf{E}^ϕ of (4.3),

$$|\mathbf{E}^q|^2 = k_e^2 \eta_e^2, \quad q = \theta, \phi. \quad (5.62)$$

Substitution of (5.56) and (5.62) into (5.61) leads to

$$\sigma_{pq} = \frac{\left| \sum_{n=-N}^N \left(\tilde{R}_n^p T_n^q \right) e^{jn\phi^{\text{rec}}} \right|^2}{4\pi k_e^2}. \quad (5.63)$$

Let $\lambda_e = 2\pi/k_e$ be the wavelength. Dividing both sides of (5.63) by λ_e^2 , one obtains

$$\frac{\sigma_{pq}}{\lambda_e^2} = \frac{\left| \sum_{n=-N}^N \left(\tilde{R}_n^p T_n^q \right) e^{jn\phi^{\text{rec}}} \right|^2}{16\pi^3}. \quad (5.64)$$

Chapter 6

The Electromagnetic Field Inside the Scatterer

6.1 Introduction

As stated in the third paragraph of Section 2.2, the electromagnetic field inside the scatterer is simulated as the electromagnetic field produced by the combination of the electric current $-\mathbf{J}_i$ on S_c , the electric current $-\mathbf{J}_e$ on S_a , and the magnetic current $-\mathbf{M}$ on S_a , all radiating in all space filled with the homogeneous medium that is inside the scatterer in the original problem. The union of \mathbf{J}_i on S_c and \mathbf{J}_e on S_a is called \mathbf{J}_{ie} . Here, \mathbf{J}_{ie} and \mathbf{M} are given by (2.8) and (2.9) where the V 's and I 's are elements of column vectors that are solutions of moment matrix

The general form of the method of moments solution for the electromagnetic field inside the scatterer is obtained in Section 6.2. In Section 6.3, the electric and magnetic fields inside the scatterer are expressed as (6.18) and (6.19) where, for $q = t$ and $z = \phi$, \mathbf{Z}_{ny}^q and \mathbf{Y}_{nz}^q are given by (6.20) and (6.21) where $\mathbf{Z}_{nj\pm}^q$ and $\mathbf{Y}_{nj\pm}^q$ are given by (6.16) and (6.17) in terms of the parts \mathbf{E}_\pm and \mathbf{H}_\pm of the wave decomposition in the chiral medium. In Section 6.4, the cylindrical components of $\mathbf{Z}_{nj\pm}^q$ and $\mathbf{Y}_{nj\pm}^q$ are given by (6.151) and (6.152) where $\check{\mathbf{Z}}_{nj\pm}^q$ and $\check{\mathbf{Y}}_{nj\pm}^q$ are given by (6.153) and (6.154) where the $\check{Z}_{nj\pm}^z$'s and the $\check{Y}_{nj\pm}^z$'s are given by (6.116)–(6.127). In Section 6.5, the cylindrical components of $\mathbf{Z}_{nj\pm}^q$ and $\mathbf{Y}_{nj\pm}^q$ are used to obtain first (6.161)–(6.166) for the cylindrical components of the electromagnetic field inside the scatterer and next (6.188)–(6.193) for the rectangular components of the electromagnetic field inside the scatterer. In Section 6.6 where the field point is assumed to be on the z -axis inside the scatterer, the distance between source and field points does not depend on ϕ' so that integrals with respect to ϕ' reduce to integrals of trigonometric functions that are evaluated analytically to save computation time.

6.2 General Form of the Solution for the Electromagnetic Field Inside the Scatterer

As given by (2.8), the method of moments solution for \mathbf{J}_{ie} is

$$-\mathbf{J}_{ie} = - \sum_{n=-N}^N \sum_{j=1}^{N_t} \left((L'_j V_{nj}^t + L_j I_{nj}^t) \mathbf{J}_{nj}^t + (L'_j V_{nj}^\phi + L_j I_{nj}^\phi) \mathbf{J}_{nj}^\phi \right). \quad (6.1)$$

The method of moments solution for $-\mathbf{M}$ on S_a is $-\mathbf{M}$ where \mathbf{M} is given by (2.9).

$$-\mathbf{M} = -\eta_e \sum_{n=-N}^N \sum_{j=1}^{N_t} L_j \left(V_{nj}^t \mathbf{J}_{nj}^t + V_{nj}^\phi \mathbf{J}_{nj}^\phi \right). \quad (6.2)$$

The electromagnetic field inside the scatterer is therefore $(\mathbf{E}_i, \mathbf{H}_i)$ where

$$\begin{aligned} \mathbf{E}_i = & - \sum_{n=-N}^N \sum_{j=1}^{N_t} \left\{ L'_j \left(V_{nj}^t \mathbf{E}_i(\mathbf{J}_{nj}^t, \mathbf{0}) + \mathbf{V}_{nj}^\phi \mathbf{E}_i(\mathbf{J}_{nj}^\phi, \mathbf{0}) \right) \right. \\ & \left. + L_j \left(I_{nj}^t \mathbf{E}_i(\mathbf{J}_{nj}^t, \mathbf{0}) + I_{nj}^\phi \mathbf{E}_i(\mathbf{J}_{nj}^\phi, \mathbf{0}) \right) + L_j \eta_e \left(V_{nj}^t \mathbf{E}_i(\mathbf{0}, \mathbf{J}_{nj}^t) + V_{nj}^\phi \mathbf{E}_i(\mathbf{0}, \mathbf{J}_{nj}^\phi) \right) \right\} \quad (6.3) \end{aligned}$$

$$\begin{aligned} \mathbf{H}_i = & - \sum_{n=-N}^N \sum_{j=1}^{N_t} \left\{ L'_j \left(V_{nj}^t \mathbf{H}_i(\mathbf{J}_{nj}^t, \mathbf{0}) + \mathbf{V}_{nj}^\phi \mathbf{H}_i(\mathbf{J}_{nj}^\phi, \mathbf{0}) \right) \right. \\ & \left. + L_j \left(I_{nj}^t \mathbf{H}_i(\mathbf{J}_{nj}^t, \mathbf{0}) + I_{nj}^\phi \mathbf{H}_i(\mathbf{J}_{nj}^\phi, \mathbf{0}) \right) + L_j \eta_e \left(V_{nj}^t \mathbf{H}_i(\mathbf{0}, \mathbf{J}_{nj}^t) + V_{nj}^\phi \mathbf{H}_i(\mathbf{0}, \mathbf{J}_{nj}^\phi) \right) \right\} \quad (6.4) \end{aligned}$$

where the subscript i in \mathbf{E}_i and \mathbf{H}_i indicates radiation in all space filled with the medium inside the scatterer in the original problem. The first argument of each of \mathbf{E}_i and \mathbf{H}_i is treated as an electric current and the second argument is treated as a magnetic current.

6.3 Use of the Wavefield Decomposition in (6.3) and (6.4)

Setting $(\mathbf{J}, \mathbf{M}) = (\mathbf{J}_{nj}^q, \mathbf{0})$ in (2.39) and (2.40), one obtains

$$\mathbf{E}_i(\mathbf{J}_{nj}^q, \mathbf{0}) = \frac{1}{2} \left(\mathbf{E}_+(\mathbf{J}_{nj}^q, j\eta_i \mathbf{J}_{nj}^q) + \mathbf{E}_-(\mathbf{J}_{nj}^q, -j\eta_i \mathbf{J}_{nj}^q) \right) \quad (6.5)$$

$$\mathbf{H}_i(\mathbf{J}_{nj}^q, \mathbf{0}) = \frac{1}{2} \left(\mathbf{H}_+(\mathbf{J}_{nj}^q, j\eta_i \mathbf{J}_{nj}^q) + \mathbf{H}_-(\mathbf{J}_{nj}^q, -j\eta_i \mathbf{J}_{nj}^q) \right). \quad (6.6)$$

Setting $(\mathbf{J}, \mathbf{M}) = (\mathbf{0}, \mathbf{J}_{nj}^q)$ in (2.39) and (2.40), one obtains

$$\mathbf{E}_i(\mathbf{0}, \mathbf{J}_{nj}^q) = \frac{1}{2} \left(\mathbf{E}_+\left(-\frac{j}{\eta_i} \mathbf{J}_{nj}^q, \mathbf{J}_{nj}^q\right) + \mathbf{E}_-\left(\frac{j}{\eta_i} \mathbf{J}_{nj}^q, \mathbf{J}_{nj}^q\right) \right) \quad (6.7)$$

$$\mathbf{H}_i(\mathbf{0}, \mathbf{J}_{nj}^q) = \frac{1}{2} \left(\mathbf{H}_+\left(-\frac{j}{\eta_i} \mathbf{J}_{nj}^q, \mathbf{J}_{nj}^q\right) + \mathbf{H}_-\left(\frac{j}{\eta_i} \mathbf{J}_{nj}^q, \mathbf{J}_{nj}^q\right) \right). \quad (6.8)$$

Substituting into (6.3) and (6.4) the equations obtained by replacing q by either t or ϕ in (6.5)–(6.8), one obtains

$$\begin{aligned}
\mathbf{E}_i = & -\frac{1}{2} \sum_{n=-N}^N \sum_{j=1}^{N_t} \left\{ L'_j \left(V_{nj}^t \left(\mathbf{E}_+(\mathbf{J}_{nj}^t, \mathbf{0}) + j\eta_i \mathbf{E}_+(\mathbf{0}, \mathbf{J}_{nj}^t) + \mathbf{E}_-(\mathbf{J}_{nj}^t, \mathbf{0}) - j\eta_i \mathbf{E}_-(\mathbf{0}, \mathbf{J}_{nj}^t) \right) \right. \right. \\
& + V_{nj}^\phi \left(\mathbf{E}_+(\mathbf{J}_{nj}^\phi, \mathbf{0}) + j\eta_i \mathbf{E}_+(\mathbf{0}, \mathbf{J}_{nj}^\phi) + \mathbf{E}_-(\mathbf{J}_{nj}^\phi, \mathbf{0}) - j\eta_i \mathbf{E}_-(\mathbf{0}, \mathbf{J}_{nj}^\phi) \right) \\
& + L_j \left(I_{nj}^t \left(\mathbf{E}_+(\mathbf{J}_{nj}^t, \mathbf{0}) + j\eta_i \mathbf{E}_+(\mathbf{0}, \mathbf{J}_{nj}^t) + \mathbf{E}_-(\mathbf{J}_{nj}^t, \mathbf{0}) - j\eta_i \mathbf{E}_-(\mathbf{0}, \mathbf{J}_{nj}^t) \right) \right. \\
& + I_{nj}^\phi \left(\mathbf{E}_+(\mathbf{J}_{nj}^\phi, \mathbf{0}) + j\eta_i \mathbf{E}_+(\mathbf{0}, \mathbf{J}_{nj}^\phi) + \mathbf{E}_-(\mathbf{J}_{nj}^\phi, \mathbf{0}) - j\eta_i \mathbf{E}_-(\mathbf{0}, \mathbf{J}_{nj}^\phi) \right) \\
& + L_j \eta_e \left(V_{nj}^t \left(-\frac{j}{\eta_i} \mathbf{E}_+(\mathbf{J}_{nj}^t, \mathbf{0}) + \mathbf{E}_+(\mathbf{0}, \mathbf{J}_{nj}^t) + \frac{j}{\eta_i} \mathbf{E}_-(\mathbf{J}_{nj}^t, \mathbf{0}) + \mathbf{E}_-(\mathbf{0}, \mathbf{J}_{nj}^t) \right) \right. \\
& \left. \left. + V_{nj}^\phi \left(-\frac{j}{\eta_i} \mathbf{E}_+(\mathbf{J}_{nj}^\phi, \mathbf{0}) + \mathbf{E}_+(\mathbf{0}, \mathbf{J}_{nj}^\phi) + \frac{j}{\eta_i} \mathbf{E}_-(\mathbf{J}_{nj}^\phi, \mathbf{0}) + \mathbf{E}_-(\mathbf{0}, \mathbf{J}_{nj}^\phi) \right) \right) \right\} \quad (6.9)
\end{aligned}$$

$$\begin{aligned}
\mathbf{H}_i = & -\frac{1}{2} \sum_{n=-N}^N \sum_{j=1}^{N_t} \left\{ L'_j \left(V_{nj}^t \left(\mathbf{H}_+(\mathbf{J}_{nj}^t, \mathbf{0}) + j\eta_i \mathbf{H}_+(\mathbf{0}, \mathbf{J}_{nj}^t) + \mathbf{H}_-(\mathbf{J}_{nj}^t, \mathbf{0}) - j\eta_i \mathbf{H}_-(\mathbf{0}, \mathbf{J}_{nj}^t) \right) \right. \right. \\
& + V_{nj}^\phi \left(\mathbf{H}_+(\mathbf{J}_{nj}^\phi, \mathbf{0}) + j\eta_i \mathbf{H}_+(\mathbf{0}, \mathbf{J}_{nj}^\phi) + \mathbf{H}_-(\mathbf{J}_{nj}^\phi, \mathbf{0}) - j\eta_i \mathbf{H}_-(\mathbf{0}, \mathbf{J}_{nj}^\phi) \right) \\
& + L_j \left(I_{nj}^t \left(\mathbf{H}_+(\mathbf{J}_{nj}^t, \mathbf{0}) + j\eta_i \mathbf{H}_+(\mathbf{0}, \mathbf{J}_{nj}^t) + \mathbf{H}_-(\mathbf{J}_{nj}^t, \mathbf{0}) - j\eta_i \mathbf{H}_-(\mathbf{0}, \mathbf{J}_{nj}^t) \right) \right. \\
& + I_{nj}^\phi \left(\mathbf{H}_+(\mathbf{J}_{nj}^\phi, \mathbf{0}) + j\eta_i \mathbf{H}_+(\mathbf{0}, \mathbf{J}_{nj}^\phi) + \mathbf{H}_-(\mathbf{J}_{nj}^\phi, \mathbf{0}) - j\eta_i \mathbf{H}_-(\mathbf{0}, \mathbf{J}_{nj}^\phi) \right) \\
& + L_j \eta_e \left(V_{nj}^t \left(-\frac{j}{\eta_i} \mathbf{H}_+(\mathbf{J}_{nj}^t, \mathbf{0}) + \mathbf{H}_+(\mathbf{0}, \mathbf{J}_{nj}^t) + \frac{j}{\eta_i} \mathbf{H}_-(\mathbf{J}_{nj}^t, \mathbf{0}) + \mathbf{H}_-(\mathbf{0}, \mathbf{J}_{nj}^t) \right) \right. \\
& \left. \left. + V_{nj}^\phi \left(-\frac{j}{\eta_i} \mathbf{H}_+(\mathbf{J}_{nj}^\phi, \mathbf{0}) + \mathbf{H}_+(\mathbf{0}, \mathbf{J}_{nj}^\phi) + \frac{j}{\eta_i} \mathbf{H}_-(\mathbf{J}_{nj}^\phi, \mathbf{0}) + \mathbf{H}_-(\mathbf{0}, \mathbf{J}_{nj}^\phi) \right) \right) \right\}. \quad (6.10)
\end{aligned}$$

Using (2.45) and (2.46) to reduce all nonzero magnetic current arguments to zeros in (6.9) and (6.10), next using (2.38), and then suppressing all zero magnetic current arguments in the resulting equations, one obtains

$$\begin{aligned}
\mathbf{E}_i = & -\frac{1}{2} \sum_{n=-N}^N \sum_{j=1}^{N_t} \left\{ L'_j \left(V_{nj}^t \left(\mathbf{E}_+(\mathbf{J}_{nj}^t) - j\eta_i \mathbf{H}_+(\mathbf{J}_{nj}^t) + \mathbf{E}_-(\mathbf{J}_{nj}^t) + j\eta_i \mathbf{H}_-(\mathbf{J}_{nj}^t) \right) \right. \right. \\
& \left. \left. + V_{nj}^\phi \left(\mathbf{E}_+(\mathbf{J}_{nj}^\phi) - j\eta_i \mathbf{H}_+(\mathbf{J}_{nj}^\phi) + \mathbf{E}_-(\mathbf{J}_{nj}^\phi) + j\eta_i \mathbf{H}_-(\mathbf{J}_{nj}^\phi) \right) \right) \right\}
\end{aligned}$$

$$\begin{aligned}
& +L_j \left(I_{nj}^t(\mathbf{E}_+(\mathbf{J}_{nj}^t) - j\eta_i \mathbf{H}_+(\mathbf{J}_{nj}^t) + \mathbf{E}_-(\mathbf{J}_{nj}^t) + j\eta_i \mathbf{H}_-(\mathbf{J}_{nj}^t)) \right. \\
& \left. + I_{nj}^\phi(\mathbf{E}_+(\mathbf{J}_{nj}^\phi) - j\eta_i \mathbf{H}_+(\mathbf{J}_{nj}^\phi) + \mathbf{E}_-(\mathbf{J}_{nj}^\phi) + j\eta_i \mathbf{H}_-(\mathbf{J}_{nj}^\phi)) \right) \\
& +L_j \left(V_{nj}^t \left(-\frac{j}{\eta_r} \mathbf{E}_+(\mathbf{J}_{nj}^t) - \eta_e \mathbf{H}_+(\mathbf{J}_{nj}^t) + \frac{j}{\eta_r} \mathbf{E}_-(\mathbf{J}_{nj}^t) - \eta_e \mathbf{H}_-(\mathbf{J}_{nj}^t) \right) \right. \\
& \left. + V_{nj}^\phi \left(-\frac{j}{\eta_r} \mathbf{E}_+(\mathbf{J}_{nj}^\phi) - \eta_e \mathbf{H}_+(\mathbf{J}_{nj}^\phi) + \frac{j}{\eta_r} \mathbf{E}_-(\mathbf{J}_{nj}^\phi) - \eta_e \mathbf{H}_-(\mathbf{J}_{nj}^\phi) \right) \right) \} \quad (6.11)
\end{aligned}$$

$$\begin{aligned}
\mathbf{H}_i = & -\frac{1}{2} \sum_{n=-N}^N \sum_{j=1}^{N_t} \left\{ L_j' \left(V_{nj}^t(\mathbf{H}_+(\mathbf{J}_{nj}^t) + \frac{j}{\eta_i} \mathbf{E}_+(\mathbf{J}_{nj}^t) + \mathbf{H}_-(\mathbf{J}_{nj}^t) - \frac{j}{\eta_i} \mathbf{E}_-(\mathbf{J}_{nj}^t)) \right. \right. \\
& \left. + V_{nj}^\phi(\mathbf{H}_+(\mathbf{J}_{nj}^\phi) + \frac{j}{\eta_i} \mathbf{E}_+(\mathbf{J}_{nj}^\phi) + \mathbf{H}_-(\mathbf{J}_{nj}^\phi) - \frac{j}{\eta_i} \mathbf{E}_-(\mathbf{J}_{nj}^\phi)) \right) \\
& +L_j \left(I_{nj}^t(\mathbf{H}_+(\mathbf{J}_{nj}^t) + \frac{j}{\eta_i} \mathbf{E}_+(\mathbf{J}_{nj}^t) + \mathbf{H}_-(\mathbf{J}_{nj}^t) - \frac{j}{\eta_i} \mathbf{E}_-(\mathbf{J}_{nj}^t)) \right. \\
& \left. + I_{nj}^\phi(\mathbf{H}_+(\mathbf{J}_{nj}^\phi) + \frac{j}{\eta_i} \mathbf{E}_+(\mathbf{J}_{nj}^\phi) + \mathbf{H}_-(\mathbf{J}_{nj}^\phi) - \frac{j}{\eta_i} \mathbf{E}_-(\mathbf{J}_{nj}^\phi)) \right) \\
& +L_j \left(V_{nj}^t \left(-\frac{j}{\eta_r} \mathbf{H}_+(\mathbf{J}_{nj}^t) + \frac{1}{\eta_r \eta_i} \mathbf{E}_+(\mathbf{J}_{nj}^t) + \frac{j}{\eta_r} \mathbf{H}_-(\mathbf{J}_{nj}^t) + \frac{1}{\eta_r \eta_i} \mathbf{E}_-(\mathbf{J}_{nj}^t) \right) \right. \\
& \left. + V_{nj}^\phi \left(-\frac{j}{\eta_r} \mathbf{H}_+(\mathbf{J}_{nj}^\phi) + \frac{1}{\eta_r \eta_i} \mathbf{E}_+(\mathbf{J}_{nj}^\phi) + \frac{j}{\eta_r} \mathbf{H}_-(\mathbf{J}_{nj}^\phi) + \frac{1}{\eta_r \eta_i} \mathbf{E}_-(\mathbf{J}_{nj}^\phi) \right) \right) \} \quad (6.12)
\end{aligned}$$

where

$$\eta_r = \frac{\eta_i}{\eta_e}. \quad (6.13)$$

Equations (6.11) and (6.12) are recast as

$$\begin{aligned}
\mathbf{E}_i = & \frac{1}{2} \sum_{n=-N}^N \sum_{j=1}^{N_t} \left\{ L_j' \eta_i \left(V_{nj}^t(\mathbf{Z}_{nj+}^t - j\mathbf{Y}_{nj+}^t + \mathbf{Z}_{nj-}^t + j\mathbf{Y}_{nj-}^t) \right. \right. \\
& \left. + V_{nj}^\phi(\mathbf{Z}_{nj+}^\phi - j\mathbf{Y}_{nj+}^\phi + \mathbf{Z}_{nj-}^\phi + j\mathbf{Y}_{nj-}^\phi) \right) \\
& +L_j \eta_i \left(I_{nj}^t(\mathbf{Z}_{nj+}^t - j\mathbf{Y}_{nj+}^t + \mathbf{Z}_{nj-}^t + j\mathbf{Y}_{nj-}^t) + I_{nj}^\phi(\mathbf{Z}_{nj+}^\phi - j\mathbf{Y}_{nj+}^\phi + \mathbf{Z}_{nj-}^\phi + j\mathbf{Y}_{nj-}^\phi) \right) \\
& \left. -L_j \eta_e \left(V_{nj}^t(j\mathbf{Z}_{nj+}^t + \mathbf{Y}_{nj+}^t - j\mathbf{Z}_{nj-}^t + \mathbf{Y}_{nj-}^t) + V_{nj}^\phi(j\mathbf{Z}_{nj+}^\phi + \mathbf{Y}_{nj+}^\phi - j\mathbf{Z}_{nj-}^\phi + \mathbf{Y}_{nj-}^\phi) \right) \right\}
\end{aligned}$$

(6.14)

$$\begin{aligned}
\mathbf{H}_i = & \frac{1}{2} \sum_{n=-N}^N \sum_{j=1}^{N_t} \left\{ L'_j \left(V_{nj}^t (\mathbf{Y}_{nj+}^t + j\mathbf{Z}_{nj+}^t + \mathbf{Y}_{nj-}^t - j\mathbf{Z}_{nj-}^t) \right. \right. \\
& \left. \left. + V_{nj}^\phi (\mathbf{Y}_{nj+}^\phi + j\mathbf{Z}_{nj+}^\phi + \mathbf{Y}_{nj-}^\phi - j\mathbf{Z}_{nj-}^\phi) \right) \right. \\
& + L_j \left(I_{nj}^t (\mathbf{Y}_{nj+}^t + j\mathbf{Z}_{nj+}^t + \mathbf{Y}_{nj-}^t - j\mathbf{Z}_{nj-}^t) + I_{nj}^\phi (\mathbf{Y}_{nj+}^\phi + j\mathbf{Z}_{nj+}^\phi + \mathbf{Y}_{nj-}^\phi - j\mathbf{Z}_{nj-}^\phi) \right) \\
& \left. + \frac{L_j}{\eta_r} \left(V_{nj}^t (-j\mathbf{Y}_{nj+}^t + \mathbf{Z}_{nj+}^t + j\mathbf{Y}_{nj-}^t + \mathbf{Z}_{nj-}^t) + V_{nj}^\phi (-j\mathbf{Y}_{nj+}^\phi + \mathbf{Z}_{nj+}^\phi + j\mathbf{Y}_{nj-}^\phi + \mathbf{Z}_{nj-}^\phi) \right) \right\}
\end{aligned} \tag{6.15}$$

where

$$\mathbf{Z}_{nj\pm}^q = -\frac{1}{\eta_i} \mathbf{E}_\pm(\mathbf{J}_{nj}^q), \quad q = t, \phi \tag{6.16}$$

$$\mathbf{Y}_{nj\pm}^q = -\mathbf{H}_\pm(\mathbf{J}_{nj}^q), \quad q = t, \phi. \tag{6.17}$$

Equations (6.14) and (6.15) condense to

$$\begin{aligned}
\mathbf{E}_i = & \sum_{n=-N}^N \sum_{j=1}^{N_t} \left\{ L'_j \eta_i (V_{nj}^t \mathbf{Z}_{ny}^t + V_{nj}^\phi \mathbf{Z}_{ny}^\phi) \right. \\
& \left. + L_j \eta_i (I_{nj}^t \mathbf{Z}_{ny}^t + I_{nj}^\phi \mathbf{Z}_{ny}^\phi) - L_j \eta_e (V_{nj}^t \mathbf{Y}_{nz}^t + V_{nj}^\phi \mathbf{Y}_{nz}^\phi) \right\}
\end{aligned} \tag{6.18}$$

$$\begin{aligned}
\mathbf{H}_i = & \sum_{n=-N}^N \sum_{j=1}^{N_t} \left\{ L'_j (V_{nj}^t \mathbf{Y}_{nz}^t + V_{nj}^\phi \mathbf{Y}_{nz}^\phi) \right. \\
& \left. + L_j (I_{nj}^t \mathbf{Y}_{nz}^t + I_{nj}^\phi \mathbf{Y}_{nz}^\phi) + \frac{L_j}{\eta_r} (V_{nj}^t \mathbf{Z}_{ny}^t + V_{nj}^\phi \mathbf{Z}_{ny}^\phi) \right\}
\end{aligned} \tag{6.19}$$

where

$$\mathbf{Z}_{ny}^q = 0.5 \{ \mathbf{Z}_{nj+}^q + \mathbf{Z}_{nj-}^q - j(\mathbf{Y}_{nj+}^q - \mathbf{Y}_{nj-}^q) \}, \quad q = t, \phi \tag{6.20}$$

$$\mathbf{Y}_{nz}^q = 0.5 \{ \mathbf{Y}_{nj+}^q + \mathbf{Y}_{nj-}^q + j(\mathbf{Z}_{nj+}^q - \mathbf{Z}_{nj-}^q) \}, \quad q = t, \phi. \tag{6.21}$$

6.4 Evaluation of the Z's and Y's of (6.16) and (6.17)

Evaluation of \mathbf{E}_i and \mathbf{H}_i of (6.18) and (6.19) where \mathbf{Z}_{ny}^q and \mathbf{Y}_{nz}^q are given by (6.20) and (6.21) requires evaluation of $\mathbf{Z}_{nj\pm}^q$ and $\mathbf{Y}_{nj\pm}^q$ of (6.16) and (6.17). With reference to (3.1),

(3.3), and (3.4)–(3.7),

$$\mathbf{Z}_{nj\pm}^q = \frac{1}{\eta_i} (j\omega \mathbf{A}_{\pm}^q(\mathbf{r}) + \nabla V_{\pm}^q(\mathbf{r})) \quad (6.22)$$

$$\mathbf{Y}_{nj\pm}^q = -\frac{1}{\mu_{\pm}} \nabla \times \mathbf{A}_{\pm}^q(\mathbf{r}) \quad (6.23)$$

where

$$\mathbf{A}_{\pm}^q(\mathbf{r}) = \frac{\mu_{\pm}}{4\pi} \iint_S \mathbf{J}_{nj}^q(\mathbf{r}') G_{\pm}(R) ds' \quad (6.24)$$

$$V_{\pm}^q(\mathbf{r}) = \frac{j}{4\pi\omega\varepsilon_{\pm}} \iint_S (\nabla'_s \cdot \mathbf{J}_{nj}^q(\mathbf{r}')) G_{\pm}(R) ds' \quad (6.25)$$

$$G_{\pm}(R) = \frac{e^{-jk_{\pm}R}}{R} \quad (6.26)$$

$$R = |\mathbf{r} - \mathbf{r}'|. \quad (6.27)$$

In (6.22)–(6.25), $q = t$ or $q = \phi$.

Substitution of (6.24) and (6.25) into (6.22) and subsequent replacement of $(\omega\mu_{\pm}, \omega\varepsilon_{\pm})$ by $(k_{\pm}\eta_i, \frac{k_{\pm}}{\eta_i})$ give

$$\mathbf{Z}_{nj\pm}^q = \frac{jk_{\pm}}{4\pi} \iint_S \mathbf{J}_{nj}^q(\mathbf{r}') G_{\pm}(R) ds' + \frac{j}{4\pi k_{\pm}} \nabla \iint_S (\nabla'_s \cdot \mathbf{J}_{nj}^q(\mathbf{r}')) G_{\pm}(R) ds'. \quad (6.28)$$

Substitution of (6.24) into (6.23) gives

$$\mathbf{Y}_{nj\pm}^q = -\frac{1}{4\pi} \nabla \times \iint_S \mathbf{J}_{nj}^q(\mathbf{r}') G_{\pm}(R) ds'. \quad (6.29)$$

Taking the gradient of the integrand instead of the integral in (6.28) and taking the curl of the integrand instead of the integral in (6.29), one obtains

$$\mathbf{Z}_{nj\pm}^q = \frac{jk_{\pm}}{4\pi} \iint_S \mathbf{J}_{nj}^q(\mathbf{r}') G_{\pm}(R) ds' - \frac{j}{4\pi k_{\pm}} \iint_S (\nabla'_s \cdot \mathbf{J}^q(\mathbf{r}')) G'_{\pm}(R) (\mathbf{r} - \mathbf{r}') ds' \quad (6.30)$$

$$\mathbf{Y}_{nj\pm}^q = -\frac{1}{4\pi} \iint_S (\mathbf{J}_{nj}^q(\mathbf{r}') \times (\mathbf{r} - \mathbf{r}')) G'_{\pm}(R) ds' \quad (6.31)$$

where, as in (3.17),

$$G'_{\pm}(R) = \frac{1 + jk_{\pm}R}{R^3} e^{-jk_{\pm}R}. \quad (6.32)$$

With reference to (3.22), (3.23), (3.34), and (3.28),

$$\mathbf{J}_{nj}^t(\mathbf{r}') = \hat{\mathbf{t}}' \frac{T_j(t')}{\rho'} e^{jn\phi'} \quad (6.33)$$

$$\mathbf{J}_{nj}^\phi(\mathbf{r}') = \hat{\phi}' \frac{T_j(t')}{\rho'} e^{jn\phi'} \quad (6.34)$$

$$\nabla'_s \cdot \mathbf{J}_{nj}^t(\mathbf{r}') = \frac{1}{\rho'} \left(\frac{P_j(t')}{d_j} - \frac{P_{j+1}(t')}{d_{j+1}} \right) e^{jn\phi'} \quad (6.35)$$

$$\nabla'_s \cdot \mathbf{J}_{nj}^\phi(\mathbf{r}') = \frac{jn}{\rho'^2} T_j(t') e^{jn\phi'}. \quad (6.36)$$

Substituting (6.33)–(6.36) into (6.30) and (6.31) and interating the integrals, one obtains

$$\begin{aligned} \mathbf{Z}_{nj\pm}^t &= \frac{jk_\pm}{4\pi} \int dt' T_j(t') \int_0^{2\pi} d\phi' \hat{\mathbf{t}}' G_\pm(R) e^{jn\phi'} \\ &\quad - \frac{j}{4\pi k_\pm} \int dt' \left(\frac{P_j(t')}{d_j} - \frac{P_{j+1}(t')}{d_{j+1}} \right) \int_0^{2\pi} d\phi' (\mathbf{r} - \mathbf{r}') G'_\pm(R) e^{jn\phi'} \end{aligned} \quad (6.37)$$

$$\begin{aligned} \mathbf{Z}_{nj\pm}^\phi &= \frac{jk_\pm}{4\pi} \int dt' T_j(t') \int_0^{2\pi} d\phi' \hat{\phi}' G_\pm(R) e^{jn\phi'} \\ &\quad + \frac{n}{4\pi k_\pm} \int dt' \frac{T_j(t')}{\rho'} \int_0^{2\pi} d\phi' (\mathbf{r} - \mathbf{r}') G'_\pm(R) e^{jn\phi'} \end{aligned} \quad (6.38)$$

$$\mathbf{Y}_{nj\pm}^t = -\frac{1}{4\pi} \int dt' T_j(t') \int_0^{2\pi} d\phi' (\hat{\mathbf{t}}' \times (\mathbf{r} - \mathbf{r}')) G'_\pm(R) e^{jn\phi'} \quad (6.39)$$

$$\mathbf{Y}_{nj\pm}^\phi = -\frac{1}{4\pi} \int dt' T_j(t') \int_0^{2\pi} d\phi' (\hat{\phi}' \times (\mathbf{r} - \mathbf{r}')) G'_\pm(R) e^{jn\phi'}. \quad (6.40)$$

6.4.1 The Vectors on the Right-Hand Sides of (6.37)–(6.40)

The vectors on the right-hand sides of (6.37)–(6.40) are $\hat{\mathbf{t}}'$, $\hat{\phi}'$, $\mathbf{r} - \mathbf{r}'$, $\hat{\mathbf{t}}' \times (\mathbf{r} - \mathbf{r}')$, and $\hat{\phi}' \times (\mathbf{r} - \mathbf{r}')$.

The vectors $\hat{\mathbf{t}}'$ and $\hat{\phi}'$ are expressed as

$$\hat{\mathbf{t}}' = \hat{\rho}(\hat{\mathbf{t}}' \cdot \hat{\rho}) + \hat{\phi}(\hat{\mathbf{t}}' \cdot \hat{\phi}) + \hat{\mathbf{z}}(\hat{\mathbf{t}}' \cdot \hat{\mathbf{z}}). \quad (6.41)$$

$$\hat{\phi}' = \hat{\rho}(\hat{\phi}' \cdot \hat{\rho}) + \hat{\phi}(\hat{\phi}' \cdot \hat{\phi}). \quad (6.42)$$

Similar to (4.33) and (4.45),

$$\hat{\mathbf{t}}' = \hat{\mathbf{x}} \sin v' \cos \phi' + \hat{\mathbf{y}} \sin v' \sin \phi' + \hat{\mathbf{z}} \cos v'. \quad (6.43)$$

$$\hat{\phi}' = -\hat{\mathbf{x}} \sin \phi' + \hat{\mathbf{y}} \cos \phi'. \quad (6.44)$$

Use of (6.43) and

$$\hat{\boldsymbol{\rho}} = \hat{\mathbf{x}} \cos \phi + \hat{\mathbf{y}} \sin \phi \quad (6.45)$$

gives

$$\hat{\mathbf{t}}' \cdot \hat{\boldsymbol{\rho}} = \sin v' (\cos \phi' \cos \phi + \sin \phi' \sin \phi) \quad (6.46)$$

which reduces to

$$\hat{\mathbf{t}}' \cdot \hat{\boldsymbol{\rho}} = \sin v' \cos(\phi' - \phi). \quad (6.47)$$

Use of (6.43) and (4.45) gives

$$\hat{\mathbf{t}}' \cdot \hat{\boldsymbol{\phi}} = \sin v' (-\cos \phi' \sin \phi + \sin \phi' \cos \phi) \quad (6.48)$$

which reduces to

$$\hat{\mathbf{t}}' \cdot \hat{\boldsymbol{\phi}} = \sin v' \sin(\phi' - \phi). \quad (6.49)$$

From (6.43),

$$\hat{\mathbf{t}}' \cdot \hat{\mathbf{z}} = \cos v'. \quad (6.50)$$

Use of (6.44) and (6.45) gives

$$\hat{\boldsymbol{\phi}}' \cdot \hat{\boldsymbol{\rho}} = -\sin \phi' \cos \phi + \cos \phi' \sin \phi \quad (6.51)$$

which reduces to

$$\hat{\boldsymbol{\phi}}' \cdot \hat{\boldsymbol{\rho}} = -\sin(\phi' - \phi). \quad (6.52)$$

Use of (6.44) and (4.45) leads to

$$\hat{\boldsymbol{\phi}}' \cdot \hat{\boldsymbol{\phi}} = \cos(\phi' - \phi). \quad (6.53)$$

Substitution of (6.47), (6.49), and (6.50) into (6.41) gives

$$\hat{\mathbf{t}}' = \hat{\boldsymbol{\rho}} \sin v' \cos(\phi' - \phi) + \hat{\boldsymbol{\phi}} \sin v' \sin(\phi' - \phi) + \hat{\mathbf{z}} \cos v'. \quad (6.54)$$

Substitution of (6.52) and (6.53) into (6.42) gives

$$\hat{\phi}' = -\hat{\rho} \sin(\phi' - \phi) + \hat{\phi} \cos(\phi' - \phi). \quad (6.55)$$

The vector $\mathbf{r} - \mathbf{r}'$ is expressed as

$$\mathbf{r} - \mathbf{r}' = \hat{\rho}\rho + \hat{\mathbf{z}}z - \hat{\rho}'\rho' - \hat{\mathbf{z}}z'. \quad (6.56)$$

In (6.56),

$$\hat{\rho}' = \hat{\rho}(\hat{\rho}' \cdot \hat{\rho}) + \hat{\phi}(\hat{\rho}' \cdot \hat{\phi}). \quad (6.57)$$

Use of (6.45) and

$$\hat{\rho}' = \hat{\mathbf{x}} \cos \phi' + \hat{\mathbf{y}} \sin \phi' \quad (6.58)$$

leads to

$$\hat{\rho}' \cdot \hat{\rho} = \cos(\phi' - \phi). \quad (6.59)$$

Use of (6.58) and (4.45) leads to

$$(\hat{\rho}' \cdot \hat{\phi}) = \sin(\phi' - \phi). \quad (6.60)$$

Substitution of (6.59) and (6.60) into (6.57) produces

$$\hat{\rho}' = \hat{\rho} \cos(\phi' - \phi) + \hat{\phi} \sin(\phi' - \phi). \quad (6.61)$$

Substituting (6.61) into (6.56), one obtains

$$\mathbf{r} - \mathbf{r}' = \hat{\rho}(\rho - \rho' \cos(\phi' - \phi)) - \hat{\phi}\rho' \sin(\phi' - \phi) + \hat{\mathbf{z}}(z - z'). \quad (6.62)$$

Use of (6.54) and (6.62) gives

$$\begin{aligned} \hat{\mathbf{t}}' \times (\mathbf{r} - \mathbf{r}') &= \left(\hat{\rho} \sin v' \cos(\phi' - \phi) + \hat{\phi} \sin v' \sin(\phi' - \phi) + \hat{\mathbf{z}} \cos v' \right) \\ &\quad \times \left(\hat{\rho}(\rho - \rho' \cos(\phi' - \phi)) - \hat{\phi}\rho' \sin(\phi' - \phi) + \hat{\mathbf{z}}(z - z') \right) \end{aligned} \quad (6.63)$$

which is evaluated as

$$\begin{aligned} \hat{\mathbf{t}}' \times (\mathbf{r} - \mathbf{r}') &= \hat{\rho} \left(\sin v' \sin(\phi' - \phi) (z - z') + \cos v' \rho' \sin(\phi' - \phi) \right) \\ &\quad + \hat{\phi} \left(\cos v' (\rho - \rho' \cos(\phi' - \phi)) - \sin v' \cos(\phi' - \phi) (z - z') \right) \\ &\quad + \hat{\mathbf{z}} \left(-\sin v' \cos(\phi' - \phi) \rho' \sin(\phi' - \phi) - \sin v' \sin(\phi' - \phi) (\rho - \rho' \cos(\phi' - \phi)) \right) \end{aligned} \quad (6.64)$$

which reduces to

$$\begin{aligned} \hat{\mathbf{t}}' \times (\mathbf{r} - \mathbf{r}') &= \hat{\boldsymbol{\rho}}(\rho' \cos v' + (z - z') \sin v') \sin(\phi' - \phi) \\ &\quad + \hat{\boldsymbol{\phi}}(\rho \cos v' - (\rho' \cos v' + (z - z') \sin v') \cos(\phi' - \phi)) - \hat{\mathbf{z}}\rho \sin v' \sin(\phi' - \phi). \end{aligned} \quad (6.65)$$

Use of (6.55) and (6.62) gives

$$\begin{aligned} \hat{\boldsymbol{\phi}}' \times (\mathbf{r} - \mathbf{r}') &= \left(-\hat{\boldsymbol{\rho}} \sin(\phi' - \phi) + \hat{\boldsymbol{\phi}} \cos(\phi' - \phi) \right) \\ &\quad \times \left(\hat{\boldsymbol{\rho}}(\rho - \rho' \cos(\phi' - \phi)) - \hat{\boldsymbol{\phi}}\rho' \sin(\phi' - \phi) + \hat{\mathbf{z}}(z - z') \right) \end{aligned} \quad (6.66)$$

which is evaluated as

$$\begin{aligned} \hat{\boldsymbol{\phi}}' \times (\mathbf{r} - \mathbf{r}') &= \hat{\boldsymbol{\rho}} \cos(\phi' - \phi) (z - z') + \hat{\boldsymbol{\phi}} \sin(\phi' - \phi) (z - z') \\ &\quad + \hat{\mathbf{z}} \left(\sin(\phi' - \phi) \rho' \sin(\phi' - \phi) - \cos(\phi' - \phi) (\rho - \rho' \cos(\phi' - \phi)) \right) \end{aligned} \quad (6.67)$$

which reduces to

$$\hat{\boldsymbol{\phi}}' \times (\mathbf{r} - \mathbf{r}') = \hat{\boldsymbol{\rho}}(z - z') \cos(\phi' - \phi) + \hat{\boldsymbol{\phi}}(z - z') \sin(\phi' - \phi) + \hat{\mathbf{z}}(\rho' - \rho \cos(\phi' - \phi)). \quad (6.68)$$

Replacement of ϕ by $\phi' - \phi$ in (3.56) leads to

$$1 = 2 \sin^2 \left(\frac{\phi' - \phi}{2} \right) + \cos(\phi' - \phi). \quad (6.69)$$

With ρ and $z - z'$ multiplied by the right-hand side of (6.69), (6.62) becomes

$$\begin{aligned} \mathbf{r} - \mathbf{r}' &= \hat{\boldsymbol{\rho}} \left(2\rho \sin^2 \left(\frac{\phi' - \phi}{2} \right) + (\rho - \rho') \cos(\phi' - \phi) \right) - \hat{\boldsymbol{\phi}}\rho' \sin(\phi' - \phi) \\ &\quad + \hat{\mathbf{z}}(z - z') \left(2 \sin^2 \left(\frac{\phi' - \phi}{2} \right) + \cos(\phi' - \phi) \right). \end{aligned} \quad (6.70)$$

With $\rho \cos v'$ multiplied by the right-hand side of (6.69), (6.65) becomes

$$\begin{aligned} \hat{\mathbf{t}}' \times (\mathbf{r} - \mathbf{r}') &= \hat{\boldsymbol{\rho}}(\rho' \cos v' + (z - z') \sin v') \sin(\phi' - \phi) \\ &\quad + \hat{\boldsymbol{\phi}} \left(2\rho \cos v' \sin^2 \left(\frac{\phi' - \phi}{2} \right) + ((\rho - \rho') \cos v' - (z - z') \sin v') \cos(\phi' - \phi) \right) \\ &\quad - \hat{\mathbf{z}}\rho \sin v' \sin(\phi' - \phi). \end{aligned} \quad (6.71)$$

With ρ' multiplied by the the right-hand side of (6.69), (6.68) becomes

$$\begin{aligned} \hat{\boldsymbol{\phi}}' \times (\mathbf{r} - \mathbf{r}') &= \hat{\boldsymbol{\rho}}(z - z') \cos(\phi' - \phi) + \hat{\boldsymbol{\phi}}(z - z') \sin(\phi' - \phi) \\ &\quad + \hat{\mathbf{z}} \left(2\rho' \sin^2 \left(\frac{\phi' - \phi}{2} \right) - (\rho - \rho') \cos(\phi' - \phi) \right). \end{aligned} \quad (6.72)$$

6.4.2 The ρ -, ϕ -, and z -Components of the \mathbf{Z} 's and \mathbf{Y} 's of (6.37)–(6.40)

Substituting (6.54) and (6.70) into (6.37), (6.55) and (6.70) into (6.38), (6.71) into (6.39), and (6.72) into (6.40), one obtains

$$\mathbf{Z}_{nj\pm}^t = \hat{\boldsymbol{\rho}}(Z_{nj\pm}^t)_\rho + \hat{\boldsymbol{\phi}}(Z_{nj\pm}^t)_\phi + \hat{\mathbf{z}}(Z_{nj\pm}^t)_z \quad (6.73)$$

$$\mathbf{Z}_{nj\pm}^\phi = \hat{\boldsymbol{\rho}}(Z_{nj\pm}^\phi)_\rho + \hat{\boldsymbol{\phi}}(Z_{nj\pm}^\phi)_\phi + \hat{\mathbf{z}}(Z_{nj\pm}^\phi)_z \quad (6.74)$$

$$\mathbf{Y}_{nj\pm}^t = \hat{\boldsymbol{\rho}}(Y_{nj\pm}^t)_\rho + \hat{\boldsymbol{\phi}}(Y_{nj\pm}^t)_\phi + \hat{\mathbf{z}}(Y_{nj\pm}^t)_z \quad (6.75)$$

$$\mathbf{Y}_{nj\pm}^\phi = \hat{\boldsymbol{\rho}}(Y_{nj\pm}^\phi)_\rho + \hat{\boldsymbol{\phi}}(Y_{nj\pm}^\phi)_\phi + \hat{\mathbf{z}}(Y_{nj\pm}^\phi)_z \quad (6.76)$$

where

$$\begin{aligned} (Z_{nj\pm}^t)_\rho &= \frac{jk_\pm}{4\pi} \int dt' T_j(t') \sin v' \int_0^{2\pi} d\phi' \cos(\phi' - \phi) G_\pm(R) e^{jn\phi'} - \frac{j}{4\pi k_\pm} \int dt' \\ &\cdot \left(\frac{P_j(t')}{d_j} - \frac{P_{j+1}(t')}{d_{j+1}} \right) \int_0^{2\pi} d\phi' \left(2\rho \sin^2 \left(\frac{\phi' - \phi}{2} \right) + (\rho - \rho') \cos(\phi' - \phi) \right) G'_\pm(R) e^{jn\phi'} \end{aligned} \quad (6.77)$$

$$\begin{aligned} (Z_{nj\pm}^t)_\phi &= \frac{jk_\pm}{4\pi} \int dt' T_j(t') \sin v' \int_0^{2\pi} d\phi' \sin(\phi' - \phi) G_\pm(R) e^{jn\phi'} \\ &+ \frac{j}{4\pi k_\pm} \int dt' \rho' \left(\frac{P_j(t')}{d_j} - \frac{P_{j+1}(t')}{d_{j+1}} \right) \int_0^{2\pi} d\phi' \sin(\phi' - \phi) G'_\pm(R) e^{jn\phi'} \end{aligned} \quad (6.78)$$

$$\begin{aligned} (Z_{nj\pm}^t)_z &= \frac{jk_\pm}{4\pi} \int dt' T_j(t') \cos v' \int_0^{2\pi} d\phi' G_\pm(R) e^{jn\phi'} \\ &- \frac{j}{4\pi k_\pm} \int dt' \left(\frac{P_j(t')}{d_j} - \frac{P_{j+1}(t')}{d_{j+1}} \right) (z - z') \int_0^{2\pi} d\phi' \\ &\cdot \left(2 \sin^2 \left(\frac{\phi' - \phi}{2} \right) + \cos(\phi' - \phi) \right) G'_\pm(R) e^{jn\phi'} \end{aligned} \quad (6.79)$$

$$\begin{aligned} (Z_{nj\pm}^\phi)_\rho &= -\frac{jk_\pm}{4\pi} \int dt' T_j(t') \int_0^{2\pi} d\phi' \sin(\phi' - \phi) G_\pm(R) e^{jn\phi'} \\ &+ \frac{n}{4\pi k_\pm} \int dt' \frac{T_j(t')}{\rho'} \int_0^{2\pi} d\phi' \left(2\rho \sin^2 \left(\frac{\phi' - \phi}{2} \right) + (\rho - \rho') \cos(\phi' - \phi) \right) G'_\pm(R) e^{jn\phi'} \end{aligned} \quad (6.80)$$

$$\begin{aligned} (Z_{nj\pm}^\phi)_\phi &= \frac{jk_\pm}{4\pi} \int dt' T_j(t') \int_0^{2\pi} d\phi' \cos(\phi' - \phi) G_\pm(R) e^{jn\phi'} \\ &- \frac{n}{4\pi k_\pm} \int dt' T_j(t') \int_0^{2\pi} d\phi' \sin(\phi' - \phi) G'_\pm(R) e^{jn\phi'} \end{aligned} \quad (6.81)$$

$$\begin{aligned} (Z_{nj\pm}^\phi)_z &= \frac{n}{4\pi k_\pm} \int dt' \frac{T_j(t')}{\rho'} (z - z') \int_0^{2\pi} d\phi' \\ &\cdot \left(2 \sin^2 \left(\frac{\phi' - \phi}{2} \right) + \cos(\phi' - \phi) \right) G'_\pm(R) e^{jn\phi'} \end{aligned} \quad (6.82)$$

$$(Y_{nj\pm}^t)_\rho = -\frac{1}{4\pi} \int dt' T_j(t') (\rho' \cos v' + (z - z') \sin v') \int_0^{2\pi} d\phi' \sin(\phi' - \phi) G'_\pm(R) e^{jn\phi'} \quad (6.83)$$

$$\begin{aligned} (Y_{nj\pm}^t)_\phi &= -\frac{1}{4\pi} \int dt' T_j(t') \int_0^{2\pi} d\phi' \left(2\rho \cos v' \sin^2 \left(\frac{\phi' - \phi}{2} \right) \right. \\ &\left. + ((\rho - \rho') \cos v' - (z - z') \sin v') \cos(\phi' - \phi) \right) G'_\pm(R) e^{jn\phi'} \end{aligned} \quad (6.84)$$

$$(Y_{nj\pm}^t)_z = \frac{1}{4\pi} \int dt' T_j(t') \rho \sin v' \int_0^{2\pi} d\phi' \sin(\phi' - \phi) G'_\pm(R) e^{jn\phi'} \quad (6.85)$$

$$(Y_{nj\pm}^\phi)_\rho = -\frac{1}{4\pi} \int dt' T_j(t') (z - z') \int_0^{2\pi} d\phi' \cos(\phi' - \phi) G'_\pm(R) e^{jn\phi'} \quad (6.86)$$

$$(Y_{nj\pm}^\phi)_\phi = -\frac{1}{4\pi} \int dt' T_j(t') (z - z') \int_0^{2\pi} d\phi' \sin(\phi' - \phi) G'_\pm(R) e^{jn\phi'} \quad (6.87)$$

$$\begin{aligned} (Y_{nj\pm}^\phi)_z &= -\frac{1}{4\pi} \int dt' T_j(t') \int_0^{2\pi} d\phi' \left(2\rho' \sin^2 \left(\frac{\phi' - \phi}{2} \right) \right. \\ &\left. - (\rho - \rho') \cos(\phi' - \phi) \right) G'_\pm(R) e^{jn\phi'}. \end{aligned} \quad (6.88)$$

The integrands of the integrals with respect to ϕ' in (6.77)–(6.88) are periodic functions of ϕ' with the period 2π . Therefore, ϕ can be added to ϕ' in each integrand without changing the value of the integral. Doing this, integrating from $-\pi$ to π instead of from 0 to 2π , decomposing each integrand into an even function of ϕ' and an odd function of ϕ' , and then taking advantage of the even and odd properties of the resulting integrands to obtain integrals from 0 to π instead of from $-\pi$ to π , one obtains, for $q = t$ or ϕ ,

$$(Z_{nj\pm}^q)_\rho = \left(\check{Z}_{nj\pm}^q \right)_\rho \left(\frac{e^{jn\phi}}{2\pi} \right) \quad (6.89)$$

$$(Z_{nj\pm}^q)_\phi = \left(\check{Z}_{nj\pm}^q \right)_\phi \left(\frac{e^{jn\phi}}{2\pi} \right) \quad (6.90)$$

$$(Z_{nj\pm}^q)_z = \left(\check{Z}_{nj\pm}^q \right)_z \left(\frac{e^{jn\phi}}{2\pi} \right) \quad (6.91)$$

$$(Y_{nj\pm}^q)_\rho = \left(\check{Y}_{nj\pm}^q \right)_\rho \left(\frac{e^{jn\phi}}{2\pi} \right) \quad (6.92)$$

$$(Y_{nj\pm}^q)_\phi = (\check{Y}_{nj\pm}^q)_\phi \left(\frac{e^{jn\phi}}{2\pi} \right) \quad (6.93)$$

$$(Y_{nj\pm}^q)_z = (\check{Y}_{nj\pm}^q)_z \left(\frac{e^{jn\phi}}{2\pi} \right) \quad (6.94)$$

where

$$\left(\check{Z}_{nj\pm}^t \right)_\rho = jk_\pm \int dt' T_j(t') \sin v' G_{2\pm} - \frac{j}{k_\pm} \int dt' \left(\frac{P_j(t')}{d_j} - \frac{P_{j+1}(t')}{d_{j+1}} \right) (\rho G'_{1\pm} + (\rho - \rho') G'_{2\pm}) \quad (6.95)$$

$$\left(\check{Z}_{nj\pm}^t \right)_\phi = -k_\pm \int dt' T_j(t') \sin v' G_{3\pm} - \frac{1}{k_\pm} \int dt' \rho' \left(\frac{P_j(t')}{d_j} - \frac{P_{j+1}(t')}{d_{j+1}} \right) G'_{3\pm} \quad (6.96)$$

$$\left(\check{Z}_{nj\pm}^t \right)_z = jk_\pm \int dt' T_j(t') \cos v' G_{1\pm} - \frac{j}{k_\pm} \int dt' \left(\frac{P_j(t')}{d_j} - \frac{P_{j+1}(t')}{d_{j+1}} \right) (z - z') (G'_{1\pm} + G'_{2\pm}) \quad (6.97)$$

$$\left(\check{Z}_{nj\pm}^\phi \right)_\rho = k_\pm \int dt' T_j(t') G_{3\pm} + \frac{n}{k_\pm} \int dt' \frac{T_j(t')}{\rho'} (\rho G'_{1\pm} + (\rho - \rho') G'_{2\pm}) \quad (6.98)$$

$$\left(\check{Z}_{nj\pm}^\phi \right)_\phi = jk_\pm \int dt' T_j(t') G_{2\pm} - \frac{jn}{k_\pm} \int dt' T_j(t') G'_{3\pm} \quad (6.99)$$

$$\left(\check{Z}_{nj\pm}^\phi \right)_z = \frac{n}{k_\pm} \int dt' \frac{T_j(t')}{\rho'} (z - z') (G'_{1\pm} + G'_{2\pm}) \quad (6.100)$$

$$\left(\check{Y}_{nj\pm}^t \right)_\rho = -j \int dt' T_j(t') (\rho' \cos v' + (z - z') \sin v') G'_{3\pm} \quad (6.101)$$

$$\left(\check{Y}_{nj\pm}^t \right)_\phi = - \int dt' T_j(t') (\rho \cos v' G'_{1\pm} + ((\rho - \rho') \cos v' - (z - z') \sin v') G'_{2\pm}) \quad (6.102)$$

$$\left(\check{Y}_{nj\pm}^t \right)_z = j \int dt' T_j(t') \rho \sin v' G'_{3\pm} \quad (6.103)$$

$$\left(\check{Y}_{nj\pm}^\phi \right)_\rho = - \int dt' T_j(t') (z - z') G'_{2\pm} \quad (6.104)$$

$$\left(\check{Y}_{nj\pm}^\phi \right)_\phi = -j \int dt' T_j(t') (z - z') G'_{3\pm} \quad (6.105)$$

$$\left(\check{Y}_{nj\pm}^\phi \right)_z = - \int dt' T_j(t') (\rho' G'_{1\pm} - (\rho - \rho') G'_{2\pm}) \quad (6.106)$$

where, as in (3.66)–(3.71),

$$G_{1\pm} = \int_0^\pi G_\pm(\check{R}) \cos(n\phi') d\phi' \quad (6.107)$$

$$G_{2\pm} = \int_0^\pi G_\pm(\check{R}) \cos \phi' \cos(n\phi') d\phi' \quad (6.108)$$

$$G_{3\pm} = \int_0^\pi G_\pm(\check{R}) \sin \phi' \sin(n\phi') d\phi' \quad (6.109)$$

$$G'_{1\pm} = 2 \int_0^\pi G'_\pm(\check{R}) \sin^2\left(\frac{\phi'}{2}\right) \cos(n\phi') d\phi' \quad (6.110)$$

$$G'_{2\pm} = \int_0^\pi G'_\pm(\check{R}) \cos \phi' \cos(n\phi') d\phi' \quad (6.111)$$

$$G'_{3\pm} = \int_0^\pi G'_\pm(\check{R}) \sin \phi' \sin(n\phi') d\phi' \quad (6.112)$$

where, similar to (3.6), similar to (3.17), and identical to (3.72),

$$G_\pm(\check{R}) = \frac{e^{-jk_\pm\check{R}}}{\check{R}} \quad (6.113)$$

$$G'_\pm(\check{R}) = \frac{1 + jk_\pm\check{R}}{\check{R}^3} e^{-jk_\pm\check{R}} \quad (6.114)$$

$$\check{R} = \sqrt{(\rho - \rho')^2 + (z - z')^2 + 4\rho\rho' \sin^2\left(\frac{\phi'}{2}\right)}. \quad (6.115)$$

The integrals with respect to t' in (6.95)–(6.106) are approximated by sampling at the points $\{t' = \bar{t}_p, p = 1, 2, \dots\}$ given by (3.73) where the domain of $T_j(t')$ extends from $t' = t_{2j-1}$ to $t' = t_{j+2}$. Thus, (6.95)–(6.106) become

$$\left(\check{Z}_{nj\pm}^t\right)_\rho = jk_\pm \sum_{q=2j-1}^{2j+2} T_{q'} \sin v_q G_{2\pm}^q - \frac{j}{k_\pm} \sum_{q=2j-1}^{2j+2} T_{q'} (\rho G_{1\pm}^{q'} + (\rho - \bar{\rho}_q) G_{2\pm}^{q'}) \quad (6.116)$$

$$\left(\check{Z}_{nj\pm}^t\right)_\phi = -k_\pm \sum_{q=2j-1}^{2j+2} T_{q'} \sin v_q G_{3\pm}^q - \frac{1}{k_\pm} \sum_{q=2j-1}^{2j+2} T_{q'} \bar{\rho}_q G_{3\pm}^{q'} \quad (6.117)$$

$$\left(\check{Z}_{nj\pm}^t\right)_z = jk_\pm \sum_{q=2j-1}^{2j+2} T_{q'} \cos v_q G_{1\pm}^q - \frac{j}{k_\pm} \sum_{q=2j-1}^{2j+2} T_{q'} (z - \bar{z}_q) (G_{1\pm}^{q'} + G_{2\pm}^{q'}) \quad (6.118)$$

$$\left(\check{Z}_{nj\pm}^\phi\right)_\rho = k_\pm \sum_{q=2j-1}^{2j+2} T_{q'} G_{3\pm}^q + \frac{n}{k_\pm} \sum_{q=2j-1}^{2j+2} \frac{T_{q'}}{\bar{\rho}_q} (\rho G_{1\pm}^{q'} + (\rho - \bar{\rho}_q) G_{2\pm}^{q'}) \quad (6.119)$$

$$\left(\check{Z}_{nj\pm}^\phi\right)_\phi = jk_\pm \sum_{q=2j-1}^{2j+2} T_{q'} G_{2\pm}^q - \frac{jn}{k_\pm} \sum_{q=2j-1}^{2j+2} T_{q'} G_{3\pm}^{q'} \quad (6.120)$$

$$\left(\check{Z}_{nj\pm}^\phi\right)_z = \frac{n}{k_\pm} \sum_{q=2j-1}^{2j+2} \frac{T_{q'}}{\bar{\rho}_q} (z - \bar{z}_q) (G_{1\pm}^{\prime q} + G_{2\pm}^{\prime q}) \quad (6.121)$$

$$\left(\check{Y}_{nj\pm}^t\right)_\rho = -j \sum_{q=2j-1}^{2j+2} T_{q'} (\bar{\rho}_q \cos v_q + (z - \bar{z}_q) \sin v_q) G_{3\pm}^{\prime q} \quad (6.122)$$

$$\left(\check{Y}_{nj\pm}^t\right)_\phi = - \sum_{q=2j-1}^{2j+2} T_{q'} (\rho \cos v_q G_{1\pm}^{\prime q} + ((\rho - \bar{\rho}_q) \cos v_q - (z - \bar{z}_q) \sin v_q) G_{2\pm}^{\prime q}) \quad (6.123)$$

$$\left(\check{Y}_{nj\pm}^t\right)_z = j \sum_{q=2j-1}^{2j+2} T_{q'} \rho \sin v_q G_{3\pm}^{\prime q} \quad (6.124)$$

$$\left(\check{Y}_{nj\pm}^\phi\right)_\rho = - \sum_{q=2j-1}^{2j+2} T_{q'} (z - \bar{z}_q) G_{2\pm}^{\prime q} \quad (6.125)$$

$$\left(\check{Y}_{nj\pm}^\phi\right)_\phi = -j \sum_{q=2j-1}^{2j+2} T_{q'} (z - \bar{z}_q) G_{3\pm}^{\prime q} \quad (6.126)$$

$$\left(\check{Y}_{nj\pm}^\phi\right)_z = - \sum_{q=2j-1}^{2j+2} T_{q'} (\bar{\rho}_q G_{1\pm}^{\prime q} - (\rho - \bar{\rho}_q) G_{2\pm}^{\prime q}) \quad (6.127)$$

where, with reference to (3.85)–(3.93), (3.98)–(3.106), (3.6), (3.17), and (3.107),

$$q' = q + 2(j - 1) \quad (6.128)$$

$$T_{4j-3} = \frac{\Delta_{2j-1}^2}{2d_j} \quad (6.129)$$

$$T_{4j-2} = \frac{(\Delta_{2j-1} + \frac{1}{2}\Delta_{2j})\Delta_{2j}}{d_j} \quad (6.130)$$

$$T_{4j-1} = \frac{(\Delta_{2j+2} + \frac{1}{2}\Delta_{2j+1})\Delta_{2j+1}}{d_{j+1}} \quad (6.131)$$

$$T_{4j} = \frac{\Delta_{2j+2}^2}{2d_{j+1}} \quad (6.132)$$

$$T'_{4j-3} = \frac{\Delta_{2j-1}}{d_j} \quad (6.133)$$

$$T'_{4j-2} = \frac{\Delta_{2j}}{d_j} \quad (6.134)$$

$$T'_{4j-1} = -\frac{\Delta_{2j+1}}{d_{j+1}} \quad (6.135)$$

$$T'_{4j} = -\frac{\Delta_{2j+2}}{d_{j+1}} \quad (6.136)$$

$$\bar{\rho}_q = \rho(\bar{t}_q) \quad (6.137)$$

$$\bar{z}_q = z(\bar{t}_q) \quad (6.138)$$

$$v_q = v(t), \quad t_q \leq t < t_{q+1} \quad (6.139)$$

$$G'_{1\pm}{}^q = \int_0^\pi G_\pm(R^q) \cos(n\phi') d\phi' \quad (6.140)$$

$$G'_{2\pm}{}^q = \int_0^\pi G_\pm(R^q) \cos \phi' \cos(n\phi') d\phi' \quad (6.141)$$

$$G'_{3\pm}{}^q = \int_0^\pi G_\pm(R^q) \sin \phi' \sin(n\phi') d\phi' \quad (6.142)$$

$$G'_{1\pm}{}^{q'} = 2 \int_0^\pi G'_\pm(R^q) \sin^2\left(\frac{\phi'}{2}\right) \cos(n\phi') d\phi' \quad (6.143)$$

$$G'_{2\pm}{}^{q'} = \int_0^\pi G'_\pm(R^q) \cos \phi' \cos(n\phi') d\phi' \quad (6.144)$$

$$G'_{3\pm}{}^{q'} = \int_0^\pi G'_\pm(R^q) \sin \phi' \sin(n\phi') d\phi' \quad (6.145)$$

$$G_\pm(R^q) = \frac{e^{-jk_\pm R^q}}{R^q} \quad (6.146)$$

$$G'_\pm(R^q) = \frac{1 + jk_\pm R^q}{(R^q)^3} e^{-jk_\pm R^q} \quad (6.147)$$

$$R^q = \sqrt{(\rho - \bar{\rho}_q)^2 + (z - \bar{z}_q)^2 + 4\rho\bar{\rho}_q \sin^2\left(\frac{\phi'}{2}\right)}. \quad (6.148)$$

Equations (6.73)–(6.76) condense to

$$\mathbf{Z}_{nj\pm}^q = \hat{\boldsymbol{\rho}}(Z_{nj\pm}^q)_\rho + \hat{\boldsymbol{\phi}}(Z_{nj\pm}^q)_\phi + \hat{\mathbf{z}}(Z_{nj\pm}^q)_z \quad (6.149)$$

$$\mathbf{Y}_{nj\pm}^q = \hat{\boldsymbol{\rho}}(Y_{nj\pm}^q)_\rho + \hat{\boldsymbol{\phi}}(Y_{nj\pm}^q)_\phi + \hat{\mathbf{z}}(Y_{nj\pm}^q)_z \quad (6.150)$$

where $q = t$ or $q = \phi$. Substituting (6.89)–(6.91) into (6.149) and substituting (6.92)–(6.94) into (6.150), the \mathbf{Z} 's and \mathbf{Y} 's of (6.16) and (6.17) are evaluated as

$$\mathbf{Z}_{nj\pm}^q = \check{\mathbf{Z}}_{nj\pm}^q \left(\frac{e^{jn\phi}}{2\pi} \right) \quad (6.151)$$

$$\mathbf{Y}_{nj\pm}^q = \check{\mathbf{Y}}_{nj\pm}^q \left(\frac{e^{jn\phi}}{2\pi} \right). \quad (6.152)$$

where

$$\check{\mathbf{Z}}_{nj\pm}^q = \hat{\rho} \left(\check{Z}_{nj\pm}^q \right)_\rho + \hat{\phi} \left(\check{Z}_{nj\pm}^q \right)_\phi + \hat{z} \left(\check{Z}_{nj\pm}^q \right)_z \quad (6.153)$$

$$\check{\mathbf{Y}}_{nj\pm}^q = \hat{\rho} \left(\check{Y}_{nj\pm}^q \right)_\rho + \hat{\phi} \left(\check{Y}_{nj\pm}^q \right)_\phi + \hat{z} \left(\check{Y}_{nj\pm}^q \right)_z. \quad (6.154)$$

For $q = t$ or $q = \phi$, the \check{Z} 's and the \check{Y} 's on the right-hand sides of (6.153) and (6.154) are given by (6.116)–(6.127). The q in (6.116)–(6.127) is different from the q in (6.149)–(6.154). In (6.149)–(6.154), q is either t or ϕ but, in (6.116)–(6.127), q is a summation index which is an integer.

6.5 The Cylindrical and Rectangular Components of the Electromagnetic Field ($\mathbf{E}_i, \mathbf{H}_i$) Inside the Scatterer

First, the cylindrical components of the inside electromagnetic field will be obtained and then the rectangular components of the inside electromagnetic field will be obtained from the cylindrical components of the inside electromagnetic field.

6.5.1 The Cylindrical Components of the Inside Electromagnetic Field

Substituting (6.151) and (6.152) into (6.20) and (6.21), one obtains

$$\mathbf{Z}_{ny}^q = \check{\mathbf{Z}}_{ny}^q \left(\frac{e^{jn\phi}}{4\pi} \right), \quad q = t, \phi \quad (6.155)$$

$$\mathbf{Y}_{nz}^q = \check{\mathbf{Y}}_{nz}^q \left(\frac{e^{jn\phi}}{4\pi} \right), \quad q = t, \phi \quad (6.156)$$

where

$$\check{\mathbf{Z}}_{ny}^q = \check{\mathbf{Z}}_{nj+}^q + \check{\mathbf{Z}}_{nj-}^q - j(\check{\mathbf{Y}}_{nj+}^q - \check{\mathbf{Y}}_{nj-}^q), \quad q = t, \phi \quad (6.157)$$

$$\check{\mathbf{Y}}_{nz}^q = \check{\mathbf{Y}}_{nj+}^q + \check{\mathbf{Y}}_{nj-}^q + j(\check{\mathbf{Z}}_{nj+}^q - \check{\mathbf{Z}}_{nj-}^q), \quad q = t, \phi \quad (6.158)$$

Substitution of (6.155) and (6.156) into (6.18) and (6.19) produces

$$\mathbf{E}_i = \frac{1}{4\pi} \sum_{n=-N}^N e^{jn\phi} \sum_{j=1}^{N_t} \{ L'_j \eta_i (V_{nj}^t \check{\mathbf{Z}}_{ny}^t + V_{nj}^\phi \check{\mathbf{Z}}_{ny}^\phi) \}$$

$$+L_j\eta_i(I_{nj}^t\check{\mathbf{Z}}_{ny}^t + I_{nj}^\phi\check{\mathbf{Z}}_{ny}^\phi) - L_j\eta_e(V_{nj}^t\check{\mathbf{Y}}_{nz}^t + V_{nj}^\phi\check{\mathbf{Y}}_{nz}^\phi)\} \quad (6.159)$$

$$\begin{aligned} \mathbf{H}_i = & \frac{1}{4\pi} \sum_{n=-N}^N e^{jn\phi} \sum_{j=1}^{N_t} \{L'_j(V_{nj}^t\check{\mathbf{Y}}_{nz}^t + V_{nj}^\phi\check{\mathbf{Y}}_{nz}^\phi) \\ & + L_j(I_{nj}^t\check{\mathbf{Y}}_{nz}^t + I_{nj}^\phi\check{\mathbf{Y}}_{nz}^\phi) + \frac{L_j}{\eta_r}(V_{nj}^t\check{\mathbf{Z}}_{ny}^t + V_{nj}^\phi\check{\mathbf{Z}}_{ny}^\phi)\} \end{aligned} \quad (6.160)$$

The ρ -, ϕ -, and z -components of (6.159) are $E_{i\rho}$, $E_{i\phi}$, and E_{iz} given by

$$\begin{aligned} E_{i\rho} = & \frac{1}{4\pi} \sum_{n=-N}^N e^{jn\phi} \sum_{j=1}^{N_t} \left\{ L'_j\eta_i \left(V_{nj}^t \left(\check{Z}_{ny}^t \right)_\rho + V_{nj}^\phi \left(\check{Z}_{ny}^\phi \right)_\rho \right) \right. \\ & \left. + L_j\eta_i \left(I_{nj}^t \left(\check{Z}_{ny}^t \right)_\rho + I_{nj}^\phi \left(\check{Z}_{ny}^\phi \right)_\rho \right) - L_j\eta_e \left(V_{nj}^t \left(\check{Y}_{nz}^t \right)_\rho + V_{nj}^\phi \left(\check{Y}_{nz}^\phi \right)_\rho \right) \right\}. \end{aligned} \quad (6.161)$$

$$\begin{aligned} E_{i\phi} = & \frac{1}{4\pi} \sum_{n=-N}^N e^{jn\phi} \sum_{j=1}^{N_t} \left\{ L'_j\eta_i \left(V_{nj}^t \left(\check{Z}_{ny}^t \right)_\phi + V_{nj}^\phi \left(\check{Z}_{ny}^\phi \right)_\phi \right) \right. \\ & \left. + L_j\eta_i \left(I_{nj}^t \left(\check{Z}_{ny}^t \right)_\phi + I_{nj}^\phi \left(\check{Z}_{ny}^\phi \right)_\phi \right) - L_j\eta_e \left(V_{nj}^t \left(\check{Y}_{nz}^t \right)_\phi + V_{nj}^\phi \left(\check{Y}_{nz}^\phi \right)_\phi \right) \right\}. \end{aligned} \quad (6.162)$$

$$\begin{aligned} E_{iz} = & \frac{1}{4\pi} \sum_{n=-N}^N e^{jn\phi} \sum_{j=1}^{N_t} \left\{ L'_j\eta_i \left(V_{nj}^t \left(\check{Z}_{ny}^t \right)_z + V_{nj}^\phi \left(\check{Z}_{ny}^\phi \right)_z \right) \right. \\ & \left. + L_j\eta_i \left(I_{nj}^t \left(\check{Z}_{ny}^t \right)_z + I_{nj}^\phi \left(\check{Z}_{ny}^\phi \right)_z \right) - L_j\eta_e \left(V_{nj}^t \left(\check{Y}_{nz}^t \right)_z + V_{nj}^\phi \left(\check{Y}_{nz}^\phi \right)_z \right) \right\}. \end{aligned} \quad (6.163)$$

The ρ -, ϕ -, and z -components of (6.160) are $H_{i\rho}$, $H_{i\phi}$, and H_{iz} given by

$$\begin{aligned} H_{i\rho} = & \frac{1}{4\pi} \sum_{n=-N}^N e^{jn\phi} \sum_{j=1}^{N_t} \left\{ L'_j \left(V_{nj}^t \left(\check{Y}_{nz}^t \right)_\rho + V_{nj}^\phi \left(\check{Y}_{nz}^\phi \right)_\rho \right) \right. \\ & \left. + L_j \left(I_{nj}^t \left(\check{Y}_{nz}^t \right)_\rho + I_{nj}^\phi \left(\check{Y}_{nz}^\phi \right)_\rho \right) + \frac{L_j}{\eta_r} \left(V_{nj}^t \left(\check{Z}_{ny}^t \right)_\rho + V_{nj}^\phi \left(\check{Z}_{ny}^\phi \right)_\rho \right) \right\}. \end{aligned} \quad (6.164)$$

$$\begin{aligned} H_{i\phi} = & \frac{1}{4\pi} \sum_{n=-N}^N e^{jn\phi} \sum_{j=1}^{N_t} \left\{ L'_j \left(V_{nj}^t \left(\check{Y}_{nz}^t \right)_\phi + V_{nj}^\phi \left(\check{Y}_{nz}^\phi \right)_\phi \right) \right. \\ & \left. + L_j \left(I_{nj}^t \left(\check{Y}_{nz}^t \right)_\phi + I_{nj}^\phi \left(\check{Y}_{nz}^\phi \right)_\phi \right) + \frac{L_j}{\eta_r} \left(V_{nj}^t \left(\check{Z}_{ny}^t \right)_\phi + V_{nj}^\phi \left(\check{Z}_{ny}^\phi \right)_\phi \right) \right\}. \end{aligned} \quad (6.165)$$

$$H_{iz} = \frac{1}{4\pi} \sum_{n=-N}^N e^{jn\phi} \sum_{j=1}^{N_t} \left\{ L'_j \left(V_{nj}^t \left(\check{Y}_{nz}^t \right)_z + V_{nj}^\phi \left(\check{Y}_{nz}^\phi \right)_z \right) \right.$$

$$+L_j \left(I_{nj}^t \left(\check{Y}_{nz}^t \right)_z + I_{nj}^\phi \left(\check{Y}_{nz}^\phi \right)_z \right) + \frac{L_j}{\eta_r} \left(V_{nj}^t \left(\check{Z}_{ny}^t \right)_z + V_{nj}^\phi \left(\check{Z}_{ny}^\phi \right)_z \right) \}. \quad (6.166)$$

The \check{Z}_{ny} 's and \check{Y}_{nz} 's on the right-hand sides of (6.161)–(6.166) are obtained by taking the ρ -, ϕ -, and z -components of each of (6.157) with $q = t$, (6.157) with $q = \phi$, (6.158) with $q = t$, and (6.158) with $q = \phi$:

$$\left(\check{Z}_{ny}^t \right)_\rho = \left(\check{Z}_{nj+}^t \right)_\rho + \left(\check{Z}_{nj-}^t \right)_\rho - j \left(\left(\check{Y}_{nj+}^t \right)_\rho - \left(\check{Y}_{nj-}^t \right)_\rho \right) \quad (6.167)$$

$$\left(\check{Z}_{ny}^t \right)_\phi = \left(\check{Z}_{nj+}^t \right)_\phi + \left(\check{Z}_{nj-}^t \right)_\phi - j \left(\left(\check{Y}_{nj+}^t \right)_\phi - \left(\check{Y}_{nj-}^t \right)_\phi \right) \quad (6.168)$$

$$\left(\check{Z}_{ny}^t \right)_z = \left(\check{Z}_{nj+}^t \right)_z + \left(\check{Z}_{nj-}^t \right)_z - j \left(\left(\check{Y}_{nj+}^t \right)_z - \left(\check{Y}_{nj-}^t \right)_z \right) \quad (6.169)$$

$$\left(\check{Z}_{ny}^\phi \right)_\rho = \left(\check{Z}_{nj+}^\phi \right)_\rho + \left(\check{Z}_{nj-}^\phi \right)_\rho - j \left(\left(\check{Y}_{nj+}^\phi \right)_\rho - \left(\check{Y}_{nj-}^\phi \right)_\rho \right) \quad (6.170)$$

$$\left(\check{Z}_{ny}^\phi \right)_\phi = \left(\check{Z}_{nj+}^\phi \right)_\phi + \left(\check{Z}_{nj-}^\phi \right)_\phi - j \left(\left(\check{Y}_{nj+}^\phi \right)_\phi - \left(\check{Y}_{nj-}^\phi \right)_\phi \right) \quad (6.171)$$

$$\left(\check{Z}_{ny}^\phi \right)_z = \left(\check{Z}_{nj+}^\phi \right)_z + \left(\check{Z}_{nj-}^\phi \right)_z - j \left(\left(\check{Y}_{nj+}^\phi \right)_z - \left(\check{Y}_{nj-}^\phi \right)_z \right) \quad (6.172)$$

$$\left(\check{Y}_{nz}^t \right)_\rho = \left(\check{Y}_{nj+}^t \right)_\rho + \left(\check{Y}_{nj-}^t \right)_\rho + j \left(\left(\check{Z}_{nj+}^t \right)_\rho - \left(\check{Z}_{nj-}^t \right)_\rho \right) \quad (6.173)$$

$$\left(\check{Y}_{nz}^t \right)_\phi = \left(\check{Y}_{nj+}^t \right)_\phi + \left(\check{Y}_{nj-}^t \right)_\phi + j \left(\left(\check{Z}_{nj+}^t \right)_\phi - \left(\check{Z}_{nj-}^t \right)_\phi \right) \quad (6.174)$$

$$\left(\check{Y}_{nz}^t \right)_z = \left(\check{Y}_{nj+}^t \right)_z + \left(\check{Y}_{nj-}^t \right)_z + j \left(\left(\check{Z}_{nj+}^t \right)_z - \left(\check{Z}_{nj-}^t \right)_z \right) \quad (6.175)$$

$$\left(\check{Y}_{nz}^\phi \right)_\rho = \left(\check{Y}_{nj+}^\phi \right)_\rho + \left(\check{Y}_{nj-}^\phi \right)_\rho + j \left(\left(\check{Z}_{nj+}^\phi \right)_\rho - \left(\check{Z}_{nj-}^\phi \right)_\rho \right) \quad (6.176)$$

$$\left(\check{Y}_{nz}^\phi \right)_\phi = \left(\check{Y}_{nj+}^\phi \right)_\phi + \left(\check{Y}_{nj-}^\phi \right)_\phi + j \left(\left(\check{Z}_{nj+}^\phi \right)_\phi - \left(\check{Z}_{nj-}^\phi \right)_\phi \right) \quad (6.177)$$

$$\left(\check{Y}_{nz}^\phi \right)_z = \left(\check{Y}_{nj+}^\phi \right)_z + \left(\check{Y}_{nj-}^\phi \right)_z + j \left(\left(\check{Z}_{nj+}^\phi \right)_z - \left(\check{Z}_{nj-}^\phi \right)_z \right). \quad (6.178)$$

The cylindrical components ($E_{i\rho}$, $E_{i\phi}$, E_{iz} , $H_{i\rho}$, $H_{i\phi}$, H_{iz}) of the inside electromagnetic field are obtained by first substituting (6.116)–(6.127) into (6.167)–(6.178). The resulting \check{Z}_{ny} 's and \check{Y}_{nz} 's are then substituted into (6.161)–(6.166).

6.5.2 The Rectangular Components of the Inside Electromagnetic Field

The rectangular components of the inside electromagnetic field are E_{ix} , E_{iy} , E_{iz} , H_{ix} , H_{iy} , and H_{iz} given by

$$E_{ix} = \hat{\mathbf{x}} \cdot \left(\hat{\rho} E_{i\rho} + \hat{\phi} E_{i\phi} + \hat{\mathbf{z}} E_{iz} \right) \quad (6.179)$$

$$E_{iy} = \hat{\mathbf{y}} \cdot \left(\hat{\rho} E_{i\rho} + \hat{\phi} E_{i\phi} + \hat{\mathbf{z}} E_{iz} \right) \quad (6.180)$$

$$E_{iz} = \hat{\mathbf{z}} \cdot \left(\hat{\rho} E_{i\rho} + \hat{\phi} E_{i\phi} + \hat{\mathbf{z}} E_{iz} \right) \quad (6.181)$$

$$H_{ix} = \hat{\mathbf{x}} \cdot \left(\hat{\rho} H_{i\rho} + \hat{\phi} H_{i\phi} + \hat{\mathbf{z}} H_{iz} \right) \quad (6.182)$$

$$H_{iy} = \hat{\mathbf{y}} \cdot \left(\hat{\rho} H_{i\rho} + \hat{\phi} H_{i\phi} + \hat{\mathbf{z}} H_{iz} \right) \quad (6.183)$$

$$H_{iz} = \hat{\mathbf{z}} \cdot \left(\hat{\rho} H_{i\rho} + \hat{\phi} H_{i\phi} + \hat{\mathbf{z}} H_{iz} \right) \quad (6.184)$$

where $E_{i\rho}$, $E_{i\phi}$, E_{iz} , $H_{i\rho}$, $H_{i\phi}$, and H_{iz} are the cylindrical components of the inside electromagnetic field. Using

$$(\hat{\mathbf{x}} \cdot \hat{\rho}, \hat{\mathbf{x}} \cdot \hat{\phi}, \hat{\mathbf{x}} \cdot \hat{\mathbf{z}}) = (\cos \phi, -\sin \phi, 0) \quad (6.185)$$

$$(\hat{\mathbf{y}} \cdot \hat{\rho}, \hat{\mathbf{y}} \cdot \hat{\phi}, \hat{\mathbf{y}} \cdot \hat{\mathbf{z}}) = (\sin \phi, \cos \phi, 0) \quad (6.186)$$

$$(\hat{\mathbf{z}} \cdot \hat{\rho}, \hat{\mathbf{z}} \cdot \hat{\phi}, \hat{\mathbf{z}} \cdot \hat{\mathbf{z}}) = (0, 0, 1) \quad (6.187)$$

in (6.179)–(6.183), one obtains

$$E_{ix} = E_{i\rho} \cos \phi - E_{i\phi} \sin \phi \quad (6.188)$$

$$E_{iy} = E_{i\rho} \sin \phi + E_{i\phi} \cos \phi \quad (6.189)$$

$$E_{iz} = E_{iz} \quad (6.190)$$

$$H_{ix} = H_{i\rho} \cos \phi - H_{i\phi} \sin \phi \quad (6.191)$$

$$H_{iy} = H_{i\rho} \sin \phi + H_{i\phi} \cos \phi \quad (6.192)$$

$$H_{iz} = H_{iz}. \quad (6.193)$$

Equation (6.190) verifies that E_{iz} serves as both a rectangular and a cylindrical coordinate and (6.193) verifies that H_{iz} serves as both a rectangular and a cylindrical coordinate.

6.6 The Special Case Where the Electromagnetic Field Inside the Scatterer is Observed on the z -Axis

On the z -axis, the spatial position where the rectangular components of the inside electromagnetic field are evaluated does not depend on ϕ so that, if they vary continuously with spatial position, the rectangular components (6.188)–(6.193) on the z -axis do not depend on ϕ . On the z -axis, the value of ϕ on the right-hand sides of (6.188)–(6.193) is therefore arbitrary. It is suggested that ϕ be set equal to zero for evaluations of the field components (6.188)–(6.193) on the z -axis.

The G^q 's of (6.141)–(6.143) on the z -Axis and the G'^q 's of (6.45)–(6.47) on the z -Axis

On the z -axis, $\rho = 0$ so that R^q of (6.148) does not depend on ϕ' and therefore neither $G_{\pm}(R^q)$ of (6.146) nor $G'_{\pm}(R^q)$ of (6.147) depend on ϕ' . As a result, (6.140)–(6.145) and (6.148) become

$$G_{1\pm}^q = G_{\pm}(R^q) \int_0^{\pi} \cos(n\phi') d\phi' \quad (6.194)$$

$$G_{2\pm}^q = G_{\pm}(R^q) \int_0^{\pi} \cos \phi' \cos(n\phi') d\phi' \quad (6.195)$$

$$G_{3\pm}^q = G_{\pm}(R^q) \int_0^{\pi} \sin \phi' \sin(n\phi') d\phi' \quad (6.196)$$

$$G_{1\pm}^{\prime q} = 2G'_{\pm}(R^q) \int_0^{\pi} \sin^2\left(\frac{\phi'}{2}\right) \cos(n\phi') d\phi' \quad (6.197)$$

$$G_{2\pm}^{\prime q} = G'_{\pm}(R^q) \int_0^{\pi} \cos \phi' \cos(n\phi') d\phi' \quad (6.198)$$

$$G_{3\pm}^{\prime q} = G'_{\pm}(R^q) \int_0^{\pi} \sin \phi' \sin(n\phi') d\phi' \quad (6.199)$$

$$R^q = \sqrt{\bar{\rho}_q^2 + (z - \bar{z}_q)^2}. \quad (6.200)$$

The integrals in (6.194), (6.195), (6.197), and (6.198) are even functions of n and the integrals in (6.196) and (6.199) are odd functions on n . Therefore, the values of the integrals in (6.194)–(6.199) for negative integers n can easily be obtained from their values for positive integers n . In the rest of Section 6.4.1, the integrals in (6.194)–(6.199) are evaluated for nonnegative integers n .

The integrals in (6.194) and (6.195) are evaluated as

$$\int_0^\pi \cos(n\phi') d\phi' = \begin{cases} \pi, & n = 0 \\ 0, & n = 1, 2, \dots \end{cases} \quad (6.201)$$

$$\int_0^\pi \cos \phi' \cos(n\phi') d\phi' = \begin{cases} 0, & n = 0 \\ \frac{\pi}{2}, & n = 1 \end{cases} \quad (6.202)$$

$$\int_0^\pi \cos \phi' \cos(n\phi') d\phi' = \frac{1}{2} \int_0^\pi (\cos((n+1)\phi') + \cos((n-1)\phi')) d\phi', \quad n = 2, 3, \dots \quad (6.203)$$

$$\int_0^\pi \cos \phi' \cos(n\phi') d\phi' = \frac{1}{2} \left[\frac{\sin((n+1)\phi')}{n+1} + \frac{\sin((n-1)\phi')}{n-1} \right]_0^\pi = 0, \quad n = 2, 3, \dots \quad (6.204)$$

Equations (6.202) and (6.204) combine to give

$$\int_0^\pi \cos \phi' \cos(n\phi') d\phi' = \frac{\pi}{2} \begin{cases} 0, & n = 0 \\ 1, & n = 1 \\ 0, & n = 2, 3, \dots \end{cases} \quad (6.205)$$

The integral in (6.196) is evaluated as

$$\int_0^\pi \sin \phi' \sin(n\phi') d\phi' = \frac{\pi}{2} \begin{cases} 0, & n = 0 \\ 1, & n = 1. \end{cases} \quad (6.206)$$

$$\int_0^\pi \sin \phi' \sin(n\phi') d\phi' = \frac{1}{2} \int_0^\pi (\cos((n-1)\phi') - \cos((n+1)\phi')) d\phi', \quad n = 2, 3, \dots \quad (6.207)$$

$$\int_0^\pi \sin \phi' \sin(n\phi') d\phi' = \frac{1}{2} \left[\frac{\sin((n-1)\phi')}{n-1} - \frac{\sin((n+1)\phi')}{n+1} \right]_0^\pi = 0, \quad n = 2, 3, \dots \quad (6.208)$$

Equations (6.206) and (6.208) combine to give

$$\int_0^\pi \sin \phi' \sin(n\phi') d\phi' = \frac{\pi}{2} \begin{cases} 0, & n = 0 \\ 1, & n = 1 \\ 0, & n = 2, 3, \dots \end{cases} \quad (6.209)$$

For the integral in (6.197), use of (3.56) gives

$$\int_0^\pi \sin^2 \left(\frac{\phi'}{2} \right) \cos(n\phi') d\phi' = \frac{1}{2} \int_0^\pi (1 - \cos \phi') \cos(n\phi') d\phi'. \quad (6.210)$$

Using (6.201) and (6.205) to evaluate the integral on the right-hand side of (6.210), one obtains

$$\int_0^\pi \sin^2 \left(\frac{\phi'}{2} \right) \cos(n\phi') d\phi' = \frac{\pi}{4} \begin{cases} 2, & n = 0 \\ -1, & n = 1 \\ 0, & n = 2, 3, \dots \end{cases} \quad (6.211)$$

Substituting (6.201) into (6.194), (6.205) into (6.195), (6.209) into (6.196), (6.211) into (6.197), (6.205) into (6.198), and (6.209) into (6.199), one obtains

$$G_{1\pm}^q = \pi G_{\pm}(R^q) \begin{cases} 1, & n = 0 \\ 0, & n = 1, 2, \dots \end{cases} \quad (6.212)$$

$$G_{2\pm}^q = \frac{\pi G_{\pm}(R^q)}{2} \begin{cases} 0, & n = 0 \\ 1, & n = 1 \\ 0, & n = 2, 3, \dots \end{cases} \quad (6.213)$$

$$G_{3\pm}^q = \frac{\pi G_{\pm}(R^q)}{2} \begin{cases} 0, & n = 0 \\ 1, & n = 1 \\ 0, & n = 2, 3, \dots \end{cases} \quad (6.214)$$

$$G_{1\pm}'^q = \frac{\pi G_{\pm}'(R^q)}{2} \begin{cases} 2, & n = 0 \\ -1, & n = 1 \\ 0, & n = 2, 3, \dots \end{cases} \quad (6.215)$$

$$G_{2\pm}'^q = \frac{\pi G_{\pm}'(R^q)}{2} \begin{cases} 0, & n = 0 \\ 1, & n = 1 \\ 0, & n = 2, 3, \dots \end{cases} \quad (6.216)$$

$$G_{3\pm}'^q = \frac{\pi G_{\pm}'(R^q)}{2} \begin{cases} 0, & n = 0 \\ 1, & n = 1 \\ 0, & n = 2, 3, \dots \end{cases} \quad (6.217)$$

where R^q is given by (6.200).

6.6.1 Properties of the Fourier Coefficients of the Cylindrical and Rectangular Components of the Inside Electromagnetic Field on the z -Axis

Equations (6.161)–(6.166) are rewritten as

$$E_{i\rho} = \sum_{n=-N}^N A_n^{\rho} e^{jn\phi} \quad (6.218)$$

$$E_{i\phi} = \sum_{n=-N}^N A_n^{\phi} e^{jn\phi} \quad (6.219)$$

$$E_{iz} = \sum_{n=-N}^N A_n^z e^{jn\phi} \quad (6.220)$$

$$H_{i\rho} = \sum_{n=-N}^N B_n^\rho e^{jn\phi} \quad (6.221)$$

$$H_{i\phi} = \sum_{n=-N}^N B_n^\phi e^{jn\phi} \quad (6.222)$$

$$H_{iz} = \sum_{n=-N}^N B_n^z e^{jn\phi} \quad (6.223)$$

where the A 's and B 's are the quantities that multiply $e^{jn\phi}$ on the right-hand sides of (6.161)–(6.166). Because, as stated at the beginning of Section 6.6, the rectangular components of the inside electromagnetic field on the z -axis do not depend on ϕ , E_{iz} and H_{iz} do not depend on ϕ so that (6.220) and (6.223) reduce to

$$E_{iz} = A_0^z \quad (6.224)$$

$$H_{iz} = B_0^z. \quad (6.225)$$

Upon replacement of $\cos \phi$ and $\sin \phi$ by their complex exponential representations, (6.188) and (6.189) become

$$E_{ix} = \frac{1}{2} ((E_{i\rho} + jE_{i\phi})e^{j\phi} + (E_{i\rho} - jE_{i\phi})e^{-j\phi}) \quad (6.226)$$

$$E_{iy} = \frac{1}{2} ((E_{i\phi} - jE_{i\rho})e^{j\phi} + (E_{i\phi} + jE_{i\rho})e^{-j\phi}). \quad (6.227)$$

Substituting (6.218) and (6.219) into (6.226) and (6.227), one obtains

$$E_{ix} = \frac{1}{2} \left(\sum_{n=-N}^N (A_n^\rho + jA_n^\phi) e^{j(n+1)\phi} + \sum_{n=-N}^N (A_n^\rho - jA_n^\phi) e^{j(n-1)\phi} \right) \quad (6.228)$$

$$E_{iy} = \frac{1}{2} \left(\sum_{n=-N}^N (A_n^\phi - jA_n^\rho) e^{j(n+1)\phi} + \sum_{n=-N}^N (A_n^\phi + jA_n^\rho) e^{j(n-1)\phi} \right). \quad (6.229)$$

Equations (6.228) and (6.229) are recast as

$$E_{ix} = \frac{1}{2} \left(\sum_{n=-N+1}^{N+1} (A_{n-1}^\rho + jA_{n-1}^\phi) e^{jn\phi} + \sum_{n=-N-1}^{N-1} (A_{n+1}^\rho - jA_{n+1}^\phi) e^{jn\phi} \right) \quad (6.230)$$

$$E_{iy} = \frac{1}{2} \left(\sum_{n=-N+1}^{N+1} (A_{n-1}^\phi - jA_{n-1}^\rho) e^{jn\phi} + \sum_{n=-N-1}^{N-1} (A_{n+1}^\phi + jA_{n+1}^\rho) e^{jn\phi} \right) \quad (6.231)$$

which become

$$E_{ix} = \frac{1}{2} \left(\left(\sum_{n=-N}^N (A_{n-1}^\rho + jA_{n-1}^\phi + A_{n+1}^\rho - jA_{n+1}^\phi) e^{jn\phi} \right) - (A_{-N-1}^\rho + jA_{-N-1}^\phi) e^{-jN\phi} \right. \\ \left. + (A_N^\rho + jA_N^\phi) e^{j(N+1)\phi} + (A_{-N}^\rho - jA_{-N}^\phi) e^{-j(N+1)\phi} - (A_{N+1}^\rho - jA_{N+1}^\phi) e^{jN\phi} \right) \quad (6.232)$$

$$E_{iy} = \frac{1}{2} \left(\left(\sum_{n=-N}^N (A_{n-1}^\phi - jA_{n-1}^\rho + A_{n+1}^\phi + jA_{n+1}^\rho) e^{jn\phi} \right) - (A_{-N-1}^\phi - jA_{-N-1}^\rho) e^{-jN\phi} \right. \\ \left. + (A_N^\phi - jA_N^\rho) e^{j(N+1)\phi} + (A_{-N}^\phi + jA_{-N}^\rho) e^{-j(N+1)\phi} - (A_{N+1}^\phi + jA_{N+1}^\rho) e^{jN\phi} \right). \quad (6.233)$$

If N is extremely large, the terms outside the summations from $-N$ to N in (6.232) and (6.233) can be neglected so that (6.232) and (6.233) reduce to

$$E_{ix} = \frac{1}{2} \sum_{n=-N}^N (A_{n-1}^\rho + jA_{n-1}^\phi + A_{n+1}^\rho - jA_{n+1}^\phi) e^{jn\phi} \quad (6.234)$$

$$E_{iy} = \frac{1}{2} \sum_{n=-N}^N (A_{n-1}^\phi - jA_{n-1}^\rho + A_{n+1}^\phi + jA_{n+1}^\rho) e^{jn\phi}. \quad (6.235)$$

Two combinations of (6.234) and (6.235) are

$$E_{ix} + jE_{iy} = \sum_{n=-N}^N (A_{n-1}^\rho + jA_{n-1}^\phi) e^{jn\phi} \quad (6.236)$$

$$E_{ix} - jE_{iy} = \sum_{n=-N}^N (A_{n+1}^\rho - jA_{n+1}^\phi) e^{jn\phi}. \quad (6.237)$$

Because, as stated at the beginning of Section 6.4, the rectangular components of the inside electromagnetic field on the z -axis do not depend on ϕ , the right-hand sides of (6.236) and (6.237) do not depend on ϕ so that, because $\{e^{jn\phi}, n = -N, -N+1, \dots, N\}$ is a linearly independent set of functions of ϕ ,

$$A_{n-1}^\rho + jA_{n-1}^\phi = 0 \quad \text{for all integer values of } n \text{ except } 0 \quad (6.238)$$

$$A_{n+1}^\rho - jA_{n+1}^\phi = 0 \quad \text{for all integer values of } n \text{ except } 0. \quad (6.239)$$

Equations (6.238) and (6.239) are rewritten as

$$A_n^\rho + jA_n^\phi = 0 \quad \text{for all integer values of } n \text{ except } -1 \quad (6.240)$$

$$A_n^\rho - jA_n^\phi = 0 \quad \text{for all integer values of } n \text{ except } +1. \quad (6.241)$$

For all integer values of n except ± 1 , (6.240) and (6.241) are

$$A_n^\rho + jA_n^\phi = 0 \text{ for all integer values of } n \text{ except } \pm 1. \quad (6.242)$$

$$A_n^\rho - jA_n^\phi = 0 \text{ for all integer values of } n \text{ except } \pm 1. \quad (6.243)$$

For $n = +1$, only (6.240) holds:

$$A_1^\rho + jA_1^\phi = 0. \quad (6.244)$$

For $n = -1$, only (6.241) holds:

$$A_{-1}^\rho - jA_{-1}^\phi = 0. \quad (6.245)$$

Adding (6.243) to (6.242) and subtracting (6.243) from (6.242), it is seen that

$$A_n^\rho = A_n^\phi = 0 \text{ for all integer values of } n \text{ except } \pm 1. \quad (6.246)$$

Equation (6.246) reduces (6.218) and (6.219) to

$$E_{i\rho} = A_1^\rho e^{j\phi} + A_{-1}^\rho e^{-j\phi} \quad (6.247)$$

$$E_{i\phi} = A_1^\phi e^{j\phi} + A_{-1}^\phi e^{-j\phi}. \quad (6.248)$$

where A_1^ρ and A_1^ϕ are related by (6.244) and A_{-1}^ρ and A_{-1}^ϕ are related by (6.245). According to (6.224), E_{iz} does not depend on ϕ :

$$E_{iz} = A_0^z. \quad (6.249)$$

Similarly, it can be shown that (6.221) and (6.222) reduce to

$$H_{i\rho} = B_1^\rho e^{j\phi} + B_{-1}^\rho e^{-j\phi} \quad (6.250)$$

$$H_{i\phi} = B_1^\phi e^{j\phi} + B_{-1}^\phi e^{-j\phi} \quad (6.251)$$

where B_1^ρ and B_1^ϕ are related by

$$B_1^\rho + jB_1^\phi = 0 \quad (6.252)$$

and B_{-1}^ρ and B_{-1}^ϕ are related by

$$B_{-1}^\rho - jB_{-1}^\phi = 0. \quad (6.253)$$

According to (6.225), H_{iz} does not depend on ϕ :

$$H_{iz} = B_0^z. \quad (6.254)$$

Substitution of (6.212)–(6.217) into (6.116)–(6.127) gives $\left(\check{Z}_{nj\pm}\right)_\rho$'s, $\left(\check{Z}_{nj\pm}\right)_\phi$'s, $\left(\check{Y}_{nj\pm}\right)_\rho$'s, and $\left(\check{Y}_{nj\pm}\right)_\phi$'s that are not zero only for $n = \pm - 1$ and also gives $\left(\check{Z}_{nj\pm}\right)_z$'s and $\left(\check{Y}_{nj\pm}\right)_z$'s that are not zero only for $n = 0$. As given by (6.161)–(6.166), where the \check{Z}_{ny} 's and \check{Y}_{nz} 's are given by (6.167)–(6.178) where the $\left(\check{Z}_{nj\pm}\right)_\rho$'s, $\left(\check{Z}_{nj\pm}\right)_\phi$'s, $\left(\check{Z}_{nj\pm}\right)_z$'s, $\left(\check{Y}_{nj\pm}\right)_\rho$'s, $\left(\check{Y}_{nj\pm}\right)_\phi$'s, and $\left(\check{Y}_{nj\pm}\right)_z$'s are those described in the previous sentence, the cylindrical components $(E_{i\rho}, E_{i\phi}, E_{iz}, H_{i\rho}, H_{i\phi}, H_{iz})$ of the inside electromagnetic field on the z -axis satisfy (6.244), (6.245), (6.252) and (6.253). In numerical solutions, (6.244), (6.245), (6.252) and (6.253) were satisfied within roundoff error.

Chapter 7

Computed Results

7-1 Chiral Sphere

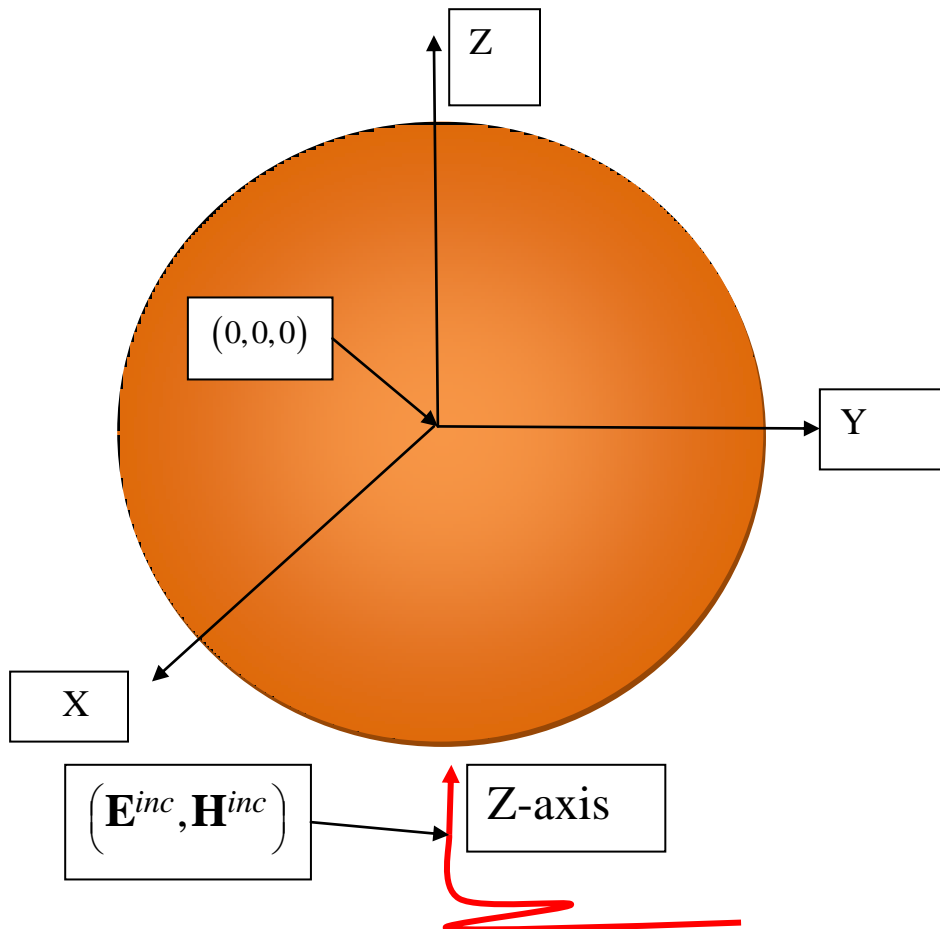


Figure 7-1.1 A chiral sphere is illuminated by a plane electromagnetic wave $(\mathbf{E}^{inc}, \mathbf{H}^{inc})$

(Figure 7-1.1 will be the frame of reference in relation to the results and the graphs that are obtained in the following sections).

7-2.1 Computed Results

In this section we will present and compare relevant characteristics of our results and graphs that are plotted in the following sections with the corresponding results and the graphs taken from Altunkilic [3]. We will also explain and clarify the results and the graphs wherever such elucidation is conducive in understanding the mapping of the graphs.

Figure 7-2.2.1 and the Figure 7-2.2.3 (taken from Altunkilic [3]) plot the $\sigma_{\theta\theta}$ (co-polarized bistatic radar cross section). Graphs of these two figure show striking almost one hundred percent resemblance to each other. Figure 7-2.2.2 and the Figure 7-2.2.4 (taken from Altunkilic [3]) plot the $\sigma_{\phi\theta}$ (cross-polarized bistatic radar cross section). Graphs of these two figures bear almost one hundred percent resemblance to each other. Figures 7-2.2.5–7-2.2.6 are the graphs of the magnitudes of the θ -component of the external and the internal equivalent electric currents in the $\phi=0$ plane. These two graphs of ours are compared with the graph of the Figure 7-2.2.7 (taken from Altunkilic [3]) that includes analytically computed exact graph representing magnitudes of the θ -components of external and internal equivalent electric currents in the $\phi=0$ plane. Our two graphs show almost one hundred percent pictorial conformability of graph mappings as well as graph readings with respect to the exact graph (shown in red color) of the graph of the Figure 7-2.2.7. Comparison of our graph of the Figure 7-2.2.8 with the graph of the Figure 7-2.2.9 (taken from Altunkilic [3]) that includes analytically computed exact graph representing magnitude of θ -component of the equivalent magnetic current in the $\phi=0$ plane show almost one hundred percent conformability in every respect with the exact graph of the Figure 7-2.2.9. Comparison of our graph of the Figure 7-2.2.10 with the graph of the Figure 7-2.2.11 (taken from Altunkilic [3]) that includes analytically computed exact graph representing magnitude of x-component of the field internal to chiral sphere along the z-axis show almost one hundred percent resemblance in every respect to the exact graph of the Figure 7-2.2.11. Comparison of our graph of the Figure 7-2.2.12 with the graph of the Figure 7-2.2.13 (taken from Altunkilic [3]) that includes analytically computed exact graph representing magnitude of y-component of the field internal to chiral sphere along the z-axis show almost one hundred percent pictorial conformability in every respect to the exact graph of the Figure 7-2.2.13.

7-2.2 Characteristic Graphs of the Chiral Sphere.

In most of the graphs we used the value of $ka=1.5$. Therefore with $\lambda=1m$, $ka=1.5 \rightarrow a=1.5/k \rightarrow a=1.5\lambda/2\pi=1.5/2\pi=0.2387\text{meter}$, here a is the radius of the sphere.

We will compare our results, wherever possible, with those of Altunkilic [3] and Denchai [57].

Figure 7-2.2.1 shows $\sigma_{\theta\theta}$ (co-polarized bistatic radar cross section) and Figure 7-2.2.2 shows $\sigma_{\phi\theta}$ (cross-polarized bistatic radar cross-section). Figure 7-2.2.3 and Figure 7-2.2.4 are inserts of Figure 3.7 and Figure 3.8 taken from the research work of Altunkilic [3]. One can

notice almost one hundred percent conformity of the Altunkilic's two figures with the figures produced by our programs (i.e., Figure 7-2.2.1 and Figure 7-2.2.2).

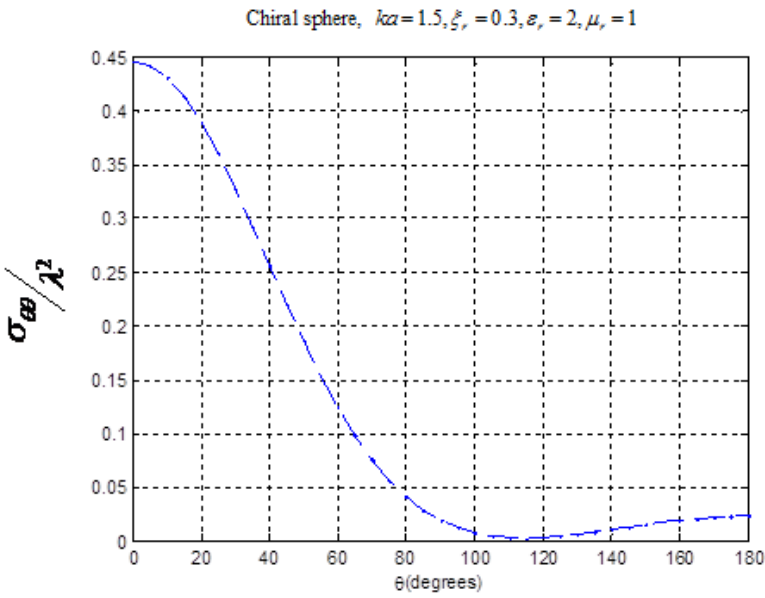


Figure 7-2.2.1 $\sigma_{\theta\theta}$ of the chiral sphere. The generating curve is approximated by 426 straight line segments.

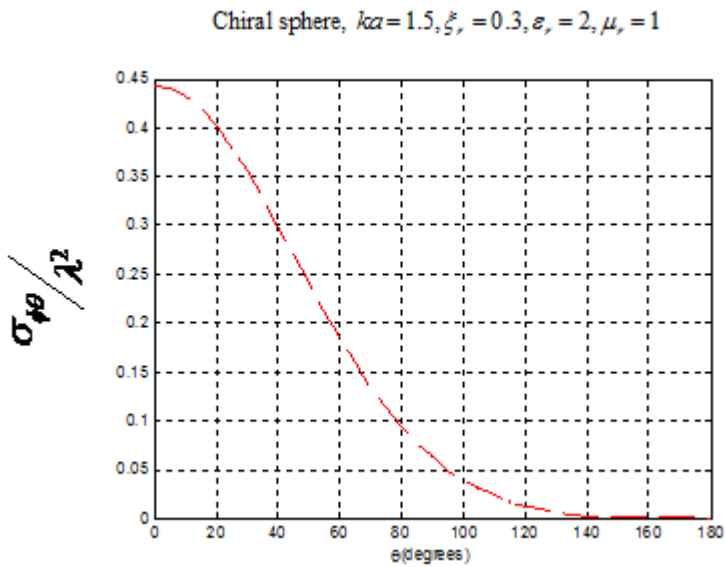


Figure 7-2.2.2 $\sigma_{\phi\theta}$ of the chiral sphere. The generating curve is approximated by 426 straight line segments.

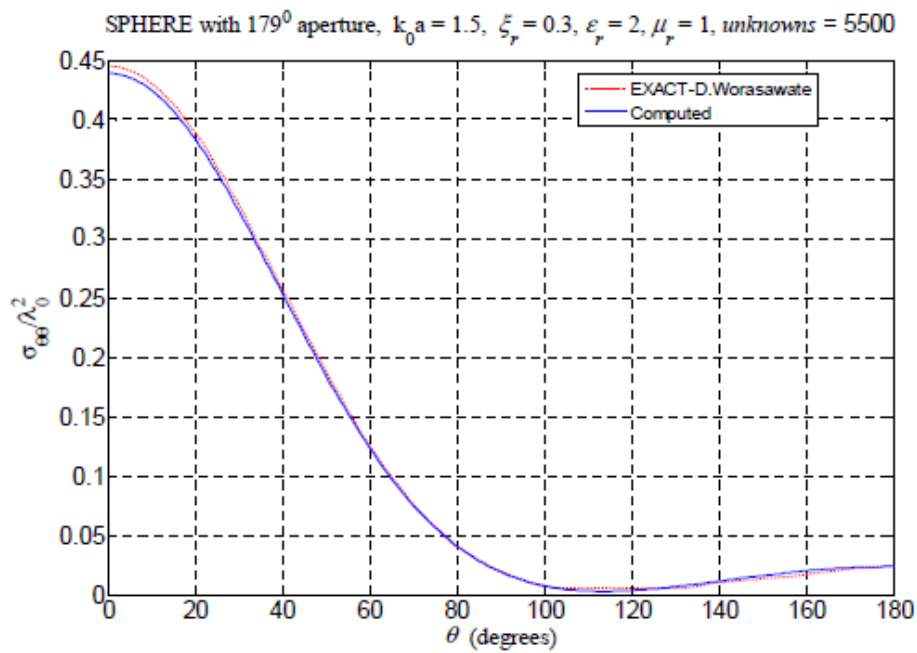


Figure 7-2.2.3 $\sigma_{\theta\theta}$ of the chiral sphere (Insert taken from Altunkilic [3]).

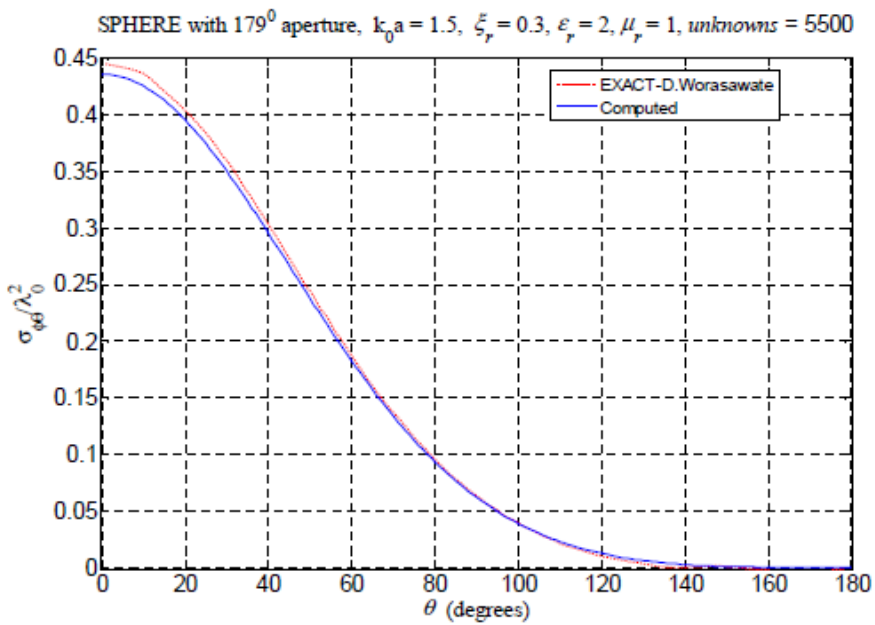


Figure 7-2.2.4 $\sigma_{\phi\theta}$ of the chiral sphere (Insert taken from Altunkilic [3]).

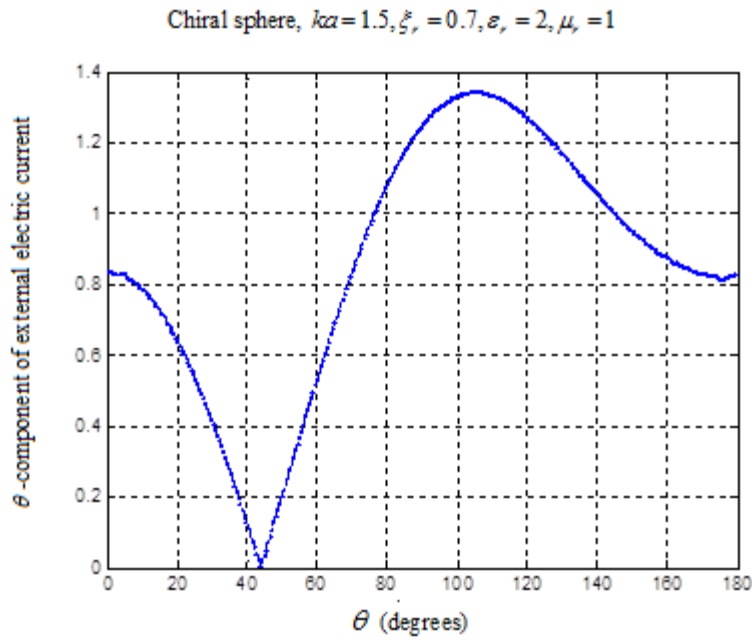


Figure 7-2.2.5 Magnitude of θ - component of the external equivalent electric current in the $\phi=0$ plane. The generating curve is approximated by 426 straight line segments.

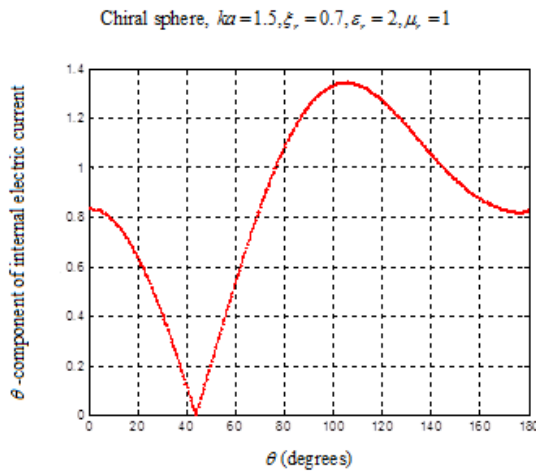


Figure 7-2.2.6 Magnitude of θ - component of internal equivalent electric current in the $\phi=0$ plane. The generating curve is approximated by 426 straight line segments.

Graph of Figure 7-2.2.7 is an insert taken from Altunkilic [3] that plots magnitude of θ -component of external and internal currents in the $\phi=0$ plane compared with the exact solution of a chiral sphere. Comparison of graph of Figure 7-2.2.7 with our graph of Figure 7-2.2.5 and that

of Figure 7-2.2.6 shows excellent pictorial conformability between these graphs, particularly, with the exact plot shown in red color [57] in Figure 7-2.2.7. *Altunkilic [3] had to use a very small perfectly conducting 1° circular metallic patch at the north pole (top) of the chiral sphere in order to run his program in Matlab code and to obtain the graph shown in blue color in the Figure 7-2.2.7. Because of the placement of the perfectly conducting metallic patch at the north pole at 0° external and internal equivalent currents show high value at 0° in the Altunkilic's graph (shown in the blue color). Altunkilic [3] refers this structure as a perfectly conducting sphere with 179° aperture that exposes the chiral material.*

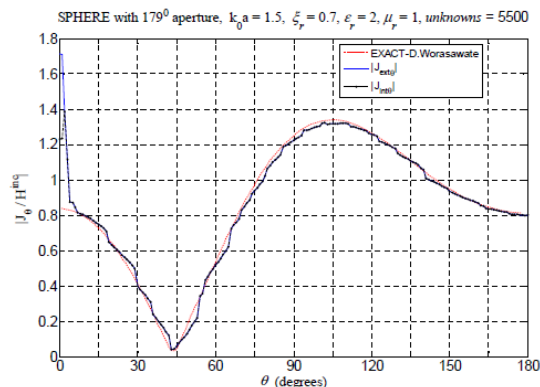


Figure 7-2.2.7 Magnitude of θ -component of external and internal equivalent electric currents in the $\phi = 0$ plane compared with the exact solution of a chiral sphere (Insert taken from Altunkilic [3]).

Figure 7-2.2.8, produced by our Matlab program, represents magnitude of of the equivalent magnetic current in the $\phi = 0$ plane. Figure 7-2.2.9 is an insert of the graph of Figure 3.13 taken from Altunkilic [3]. Figure 7-2.2.9 includes a red dotted line representing exact graph obtained by analytical solution by D. Warasawate [57]. Our graph of Figure 7-2.2.8, shows striking, almost one hundred percent, resemblance with the exact graph of D. Warasawate [57].

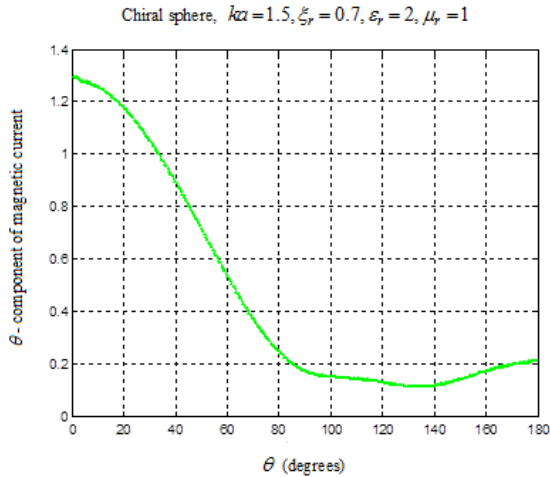


Figure 7-2.2.8 Magnitude of θ -component of the equivalent magnetic current in the $\phi = 0$ plane. The generating curve is approximated by 426 straight line segments.

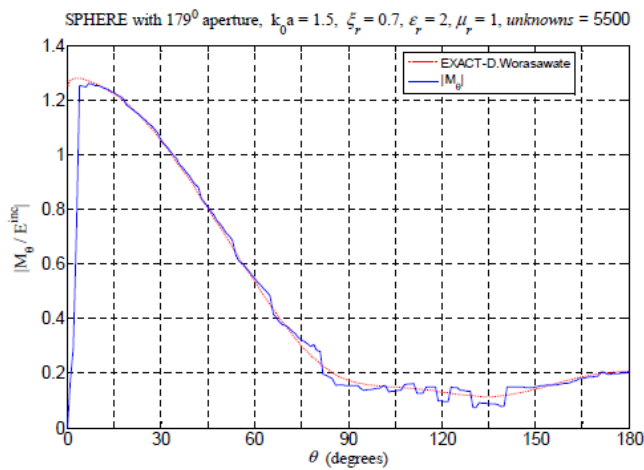


Figure 7-2.2.9 Magnitude of θ -component of equivalent magnetic current in $\phi = 0$ plane compared with exact solution of chiral sphere (Insert taken from Altunkilic [3]).

Altunkilic [3] had to use a very small perfectly conducting metallic patch at the north pole (top) of the chiral sphere in order to run his program in Matlab code and to obtain the graph shown in blue color in the Figure 7-2.2.9. Because of the placement of the perfectly conducting metallic patch at the north pole at 0° , equivalent magnetic current plunges to zero value at the north pole which is 0° in the Altunkilic's graph (shown in the blue color).

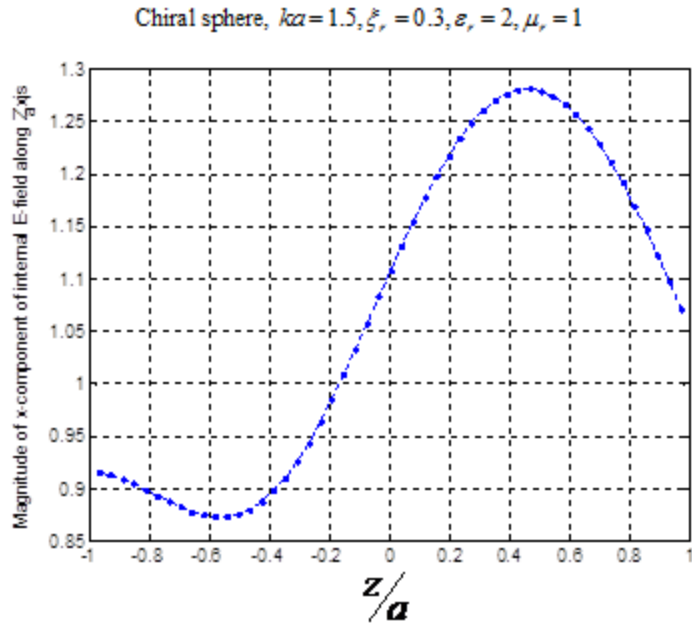


Figure 7-2.2.10 Magnitude of x-component of electric field internal to the Chiral sphere along z-axis. The generating curve is approximated by 426 straight line segments.

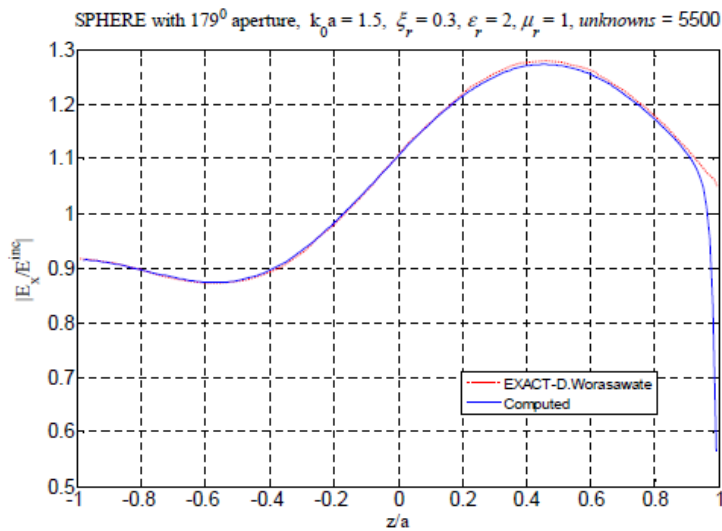


Figure 7-2.2.11 Magnitude of x-component of electric field internal to chiral sphere along the z-axis (taken from Altunkilic [3]).

Figure 7-2.2.10 represents magnitude of x-component of electric field internal to the chiral sphere along z-axis. Figure 7-2.2.11 (taken from Altunkilic [3]) plots magnitude of x-component of electric field internal to chiral sphere along the z-axis. Figure 7-2.2.11 includes exact graph obtained by analytical solution carried out by D. Worasawate [57]. Comparison of our graph of

Figure 7-2.2.10 with the exact graph of the Figure 7-2.2.11 shows excellent agreement between them.

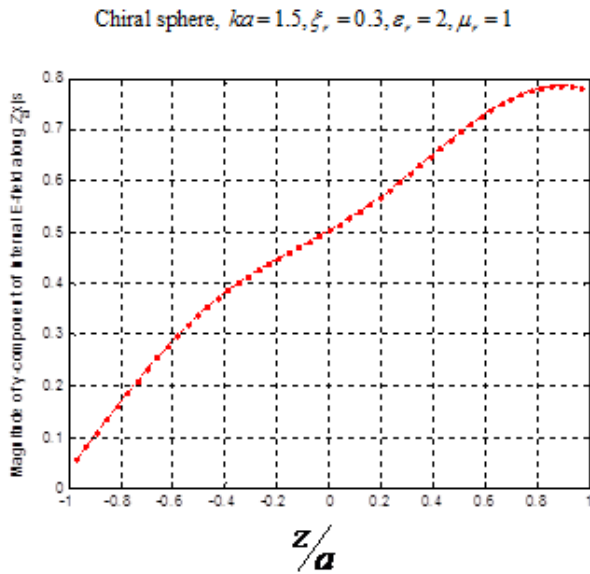


Figure 7-2.2.12 Magnitude of y-component of electric field internal to the Chiral sphere along z-axis. The generating curve is approximated by 426 straight line segments.

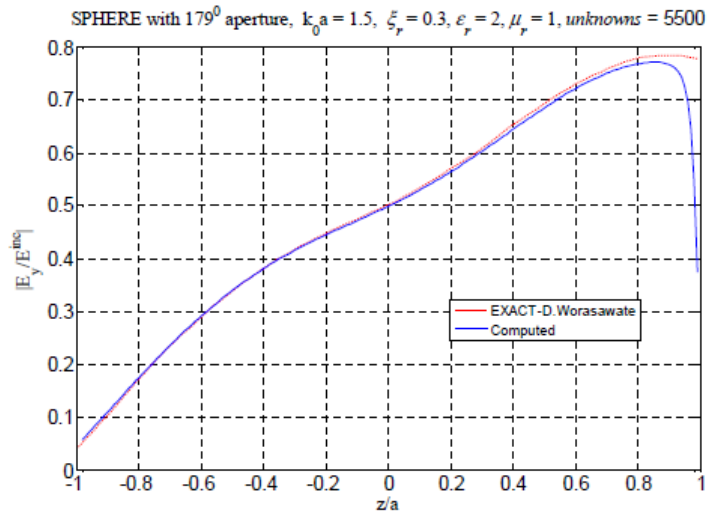


Figure 7-2.2.13 Magnitude of y-component of electric field internal to the chiral sphere along the z-axis (taken from Altunkilic [3]).

Figure 7-2.2.13 is an insert taken from Altunkilic [3]. Figure 7-2.2.13 includes exact graph obtained by analytical solution carried out by D. Worasawate [57]. Our graph of Figure 7-2.2.12 shows almost one hundred percent resemblance with the exact graph [57] of Figure 7-2.2.13.

7-3 Conducting Sphere

A conducting spherical shell, shown in Figure 7-3.1, is illuminated by a plane electromagnetic wave from the bottom of the sphere.

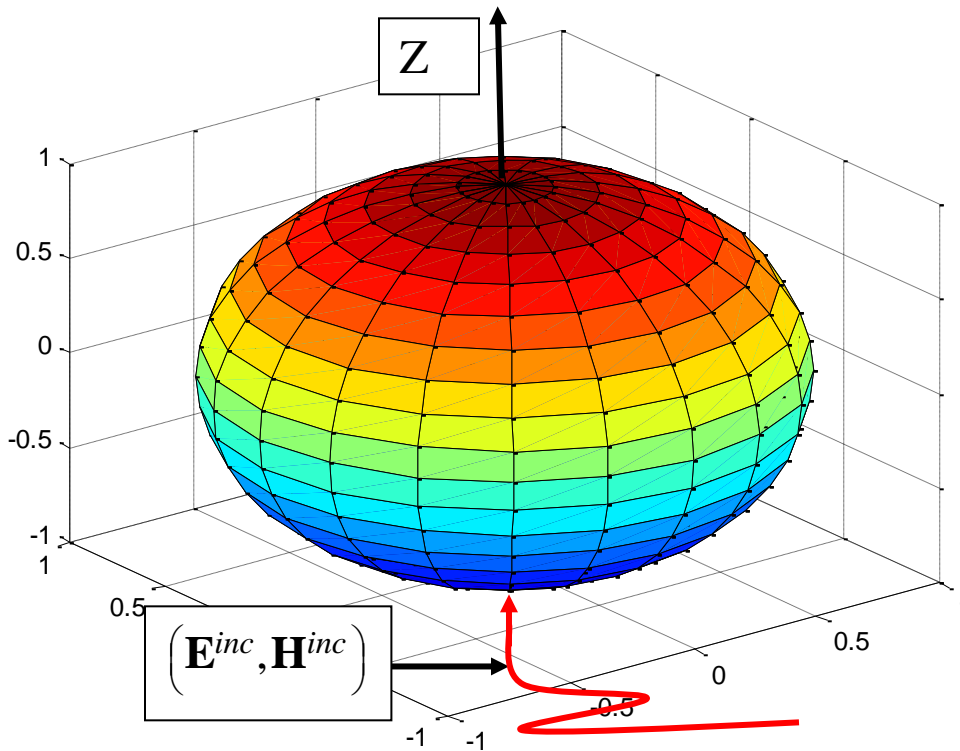


Figure 7-3.1 Perfectly conducting metallic spherical shell. This shell is illuminated by a plane electromagnetic wave.

(Figure 7-3.1 will be the frame of reference in relation to the results and the graphs that are obtained in the following section).

Figure 7-3.1 shows perfectly conducting metallic spherical shell showing t -directed or θ -directed (longitudinal) curves at 10^0 intervals as well as ϕ -directed (latitudinal) curves . This metallic shell is illuminated by a plane electromagnetic wave $(\mathbf{E}^{inc}, \mathbf{H}^{inc})$ from its bottom along the z-axis.

7-3.1 Characteristic Graphs of the Conducting Sphere

Figure below shows magnitude of θ -component of physical electric current produced when a plane electromagnetic wave impinges on the perfectly conducting sphere, shown in Figure 7-3.1.

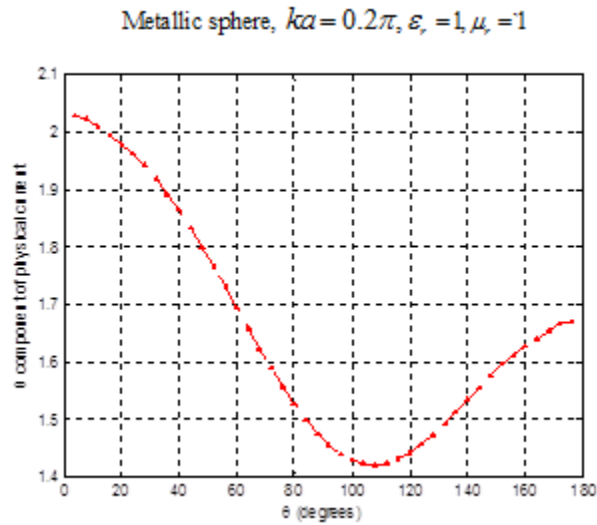


Figure 7-3.2 Magnitude of θ -component of physical electric current in the $\phi = 0$ plane. The generating curve is approximated by 426 straight line segments.

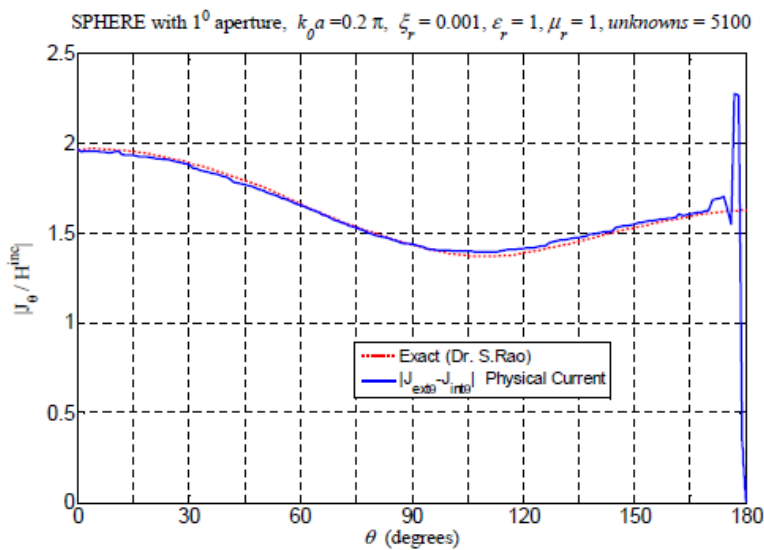


Figure 7-3.3 Magnitude of θ -component of physical electric current in the $\phi = 0$ plane compared with exact solution of conductor sphere (Insert taken from Altunkilic [3]).

We plotted a graph of the θ -component of physical current produced by the plane electromagnetic wave illuminating from the bottom of the perfectly conducting metallic spherical shell as shown in Figure 7-3.2. Figure 7-3.3 is an insert of the graph of Figure 3.19 taken from Altunkilic [3]. This inserted graph includes exact analytical graph, shown in red color, of Dr. S. Rao. Our graph of Figure 7-3.2 exhibits marked resemblance with the exact graph of Dr. S. Rao. The two graphs, shown above, originate around 2 along the y-axis and terminate at about 1.7 reading on the y-axis. Both of these graphs take a low ebb at about 1.4 reading on the y-axis corresponding to about 115 degrees on the x-axis. Aside from different scales of these two graphs, the readings of our graph conform almost one hundred percent with the readings of the graph of exact graph of S. Rao.

Figure 7-3.4, shown below, plots $\sigma_{\theta\theta}$ of the perfectly conducting metallic spherical shell which is impinged upon by a plane electromagnetic wave at its bottom as shown in Figure 7-3.1.

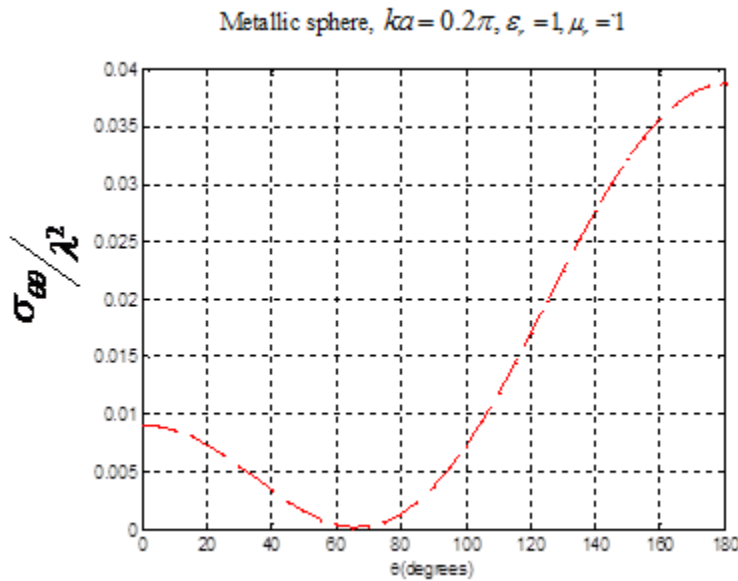


Figure 7-3.4 $\sigma_{\theta\theta}$ of the Metallic sphere. The generating curve is approximated by 426 straight line segments.

7-4 Spherical-Shaped Perfectly Conducting BOR Surface enclosing Chiral material with an Aperture of 30 degrees at its bottom.

In this section, we will treat, in particular, the case of a spherical-shaped chiral BOR contained in a perfectly conducting thin metallic spherical shell with a single aperture of 30° at its bottom that exposes the chiral material to the plane electromagnetic wave that illuminates the BOR along z-axis from the bottom of the spherical shell, as shown in Figure 7-4.1. The purpose of choosing a single apertured perfectly conducting thin metallic shell enclosing chiral material in it is to compare our results with early researchers, particularly with graphic results of Altunkilic [3].

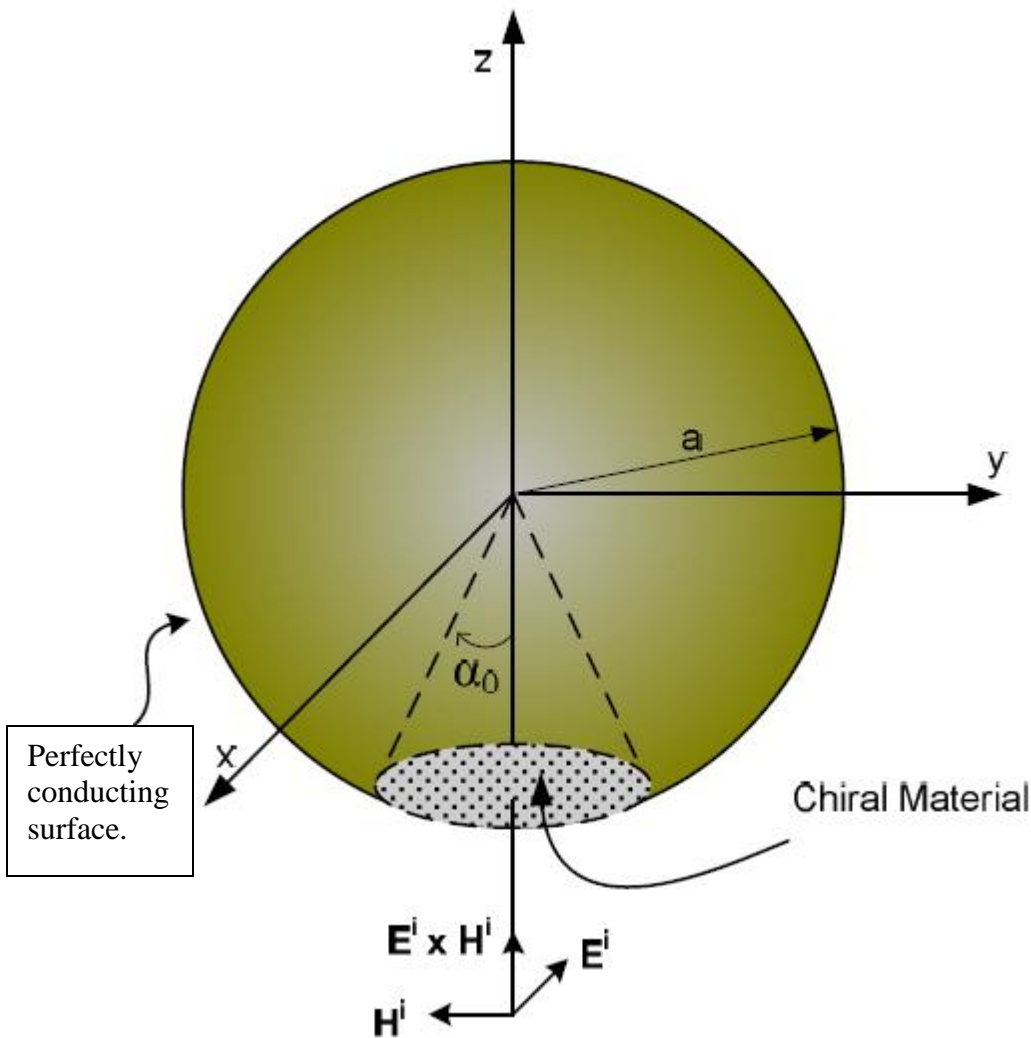


Figure 7-4.1 Plane wave incident from the bottom of a perfectly conducting thin metallic shell that encloses chiral material in it.

(Figure 7-4.1 will be the frame of reference in relation to the results and the graphs that are obtained in the following sections).

7-4.1 Computed Results

In this section we will present and compare relevant characteristics of our results and graphs that are plotted in the following section(s) with the corresponding results and the graphs taken from Altunkilic [3]. We will also explain and clarify the results and the graphs wherever such elucidation is conducive in understanding the mapping of the graphs.

Figure 7-4.2.2 and the Figure 7-4.2.3 (taken from Altunkilic [3]) plot the θ -component of external equivalent electric current of varying chiralities in $\phi=0$ plane. These two graphs show acceptable accuracy of graph readings on the conducting surface (almost 85% of the total sphere surface).

Our graph of the Figure 7-4.2.2 shows extreme smoothness on the conducting surface compared to the graph of the Figure 7-4.2.3 (taken from Altunkilic [3]). In the aperture area ($150^\circ - 180^\circ$), our graph shows sharp up and down swings averaging to a graph reading of 1. Transition from a conducting surface to an aperture exposing the chiral material is the cause of this up and down sharp fluctuations. Mautz and Harrington [36] have published theories regarding an improved E-Field Solution for a conducting body of revolution. Our case consists of the E-Field as well as the H-Field solution of the problem giving rise to such sharp upward and downward swings in the aperture space (about 15% of the total surface of the sphere). However, these fluctuations in the aperture space give an unmistakable average graph reading. In this case the average graph reading is 1. The graph of the Figure 7-4.2.3 (taken from Altunkilic [3]) produces abrupt upward and downward zigzagging in direction along the course of the graph mapping not only on the conducting surface but in the aperture space as well.

Figure 7-4.2.4 and the Figure 7-4.2.5 (taken from Altunkilic [3]) plot the θ -component of internal equivalent electric current of varying chiralities in $\phi=0$ plane. These two graphs show acceptable accuracy of graph readings on the conducting surface (almost 85% of the total sphere surface). The remarks in italics in the above paragraph are applicable in regard to these two graphs.

Figure 7-4.2.6 and the Figure 7-4.2.7 (taken from Altunkilic [3]) plot the θ -component of the physical electric current of varying chiralities in $\phi=0$ plane. These two graphs show acceptable accuracy of graph readings on the conducting surface (almost 85% of the total sphere surface). The remarks in italics in the above paragraph are applicable in regard to these two graphs on the conducting surface of the sphere. Both graphs, as expected, show zero values in the aperture space.

Figure 7-4.2.8 and the Figure 7-4.2.9 (taken from Altunkilic [3]) plot the θ -component of equivalent magnetic current of varying chiralities in $\phi=0$ plane. The remarks in bold italics above are applicable in regard to these two graphs on the aperture surface of the sphere. Both graphs, as expected, show zero values on the conducting surface.

Figure 7-4.2.10 and the Figure 7-4.2.11 (taken from Altunkilic [3]) plot the ϕ -component of external equivalent electric current of varying chiralities in $\phi = 0$ plane. The remarks in italics in the above paragraph are applicable in regard to these two graphs on the aperture surface of the sphere. Our graph, as expected, shows zero values on the conducting surface whereas graph of the Figure 7-4.2.11 (taken from Altunkilic [3]) keeps close to zero values on the conducting surface.

Figure 7-4.2.12 and the Figure 7-4.2.13 (taken from Altunkilic [3]) plot the ϕ -component of internal equivalent electric current of varying chiralities in $\phi = 0$ plane. The remarks in italics in the above paragraph are applicable in regard to these two graphs.

Figure 7-4.2.14 and the Figure 7-4.2.15 (taken from Altunkilic [3]) plot the ϕ -component of the physical electric current of varying chiralities in $\phi = 0$ plane. The remarks in italics in the above paragraph are applicable in regard to these two graphs on the conducting surface of the sphere. Both graphs, as expected, show zero values in the aperture space.

Figure 7-4.2.16 and the Figure 7-4.2.17 (taken from Altunkilic [3]) plot the ϕ -component of the equivalent magnetic current of varying chiralities in $\phi = 0$ plane. The remarks in italics in the above paragraph are applicable in regard to these two graphs on the aperture surface of the sphere. Both graphs, as expected, show zero values in the conducting surface.

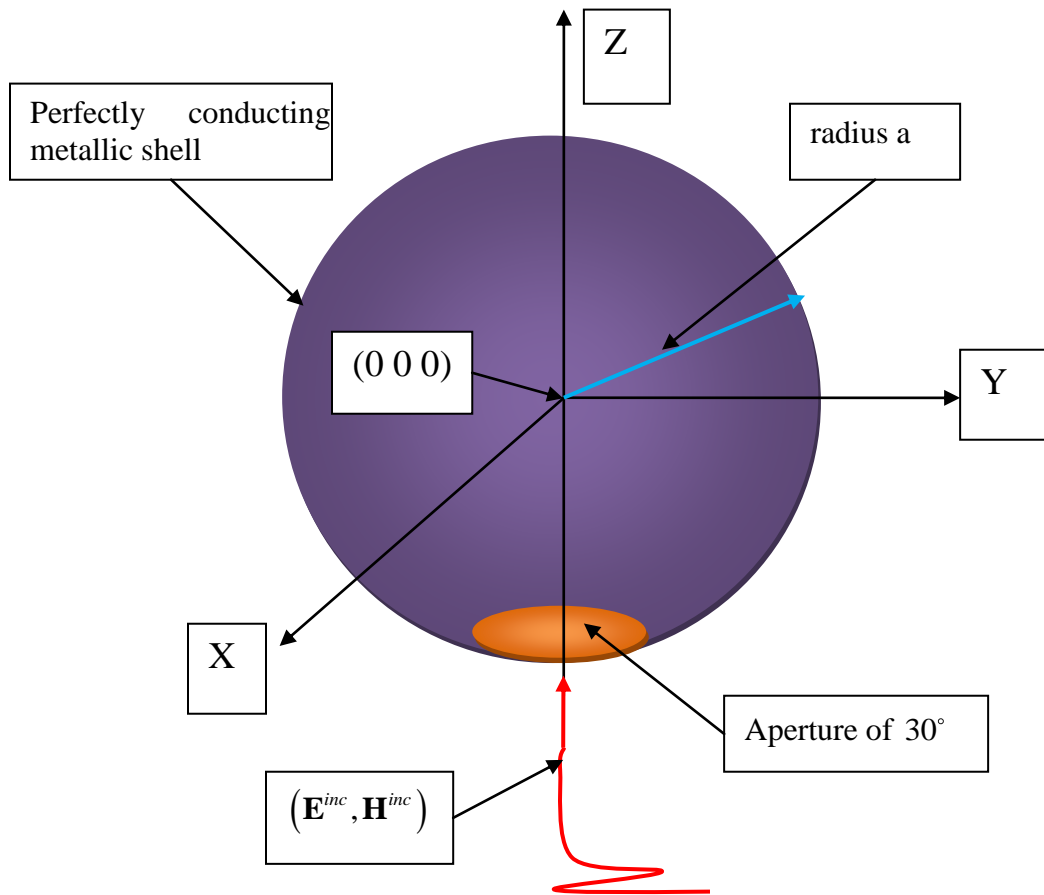


Figure 7-4.2.1 Perfectly conducting metallic shell with an aperture of 30° at its bottom.

In this section we will present and compare relevant characteristics of our results and graphs that are plotted in the following sections with the corresponding results and the graphs taken from Altunkilic [3]. We will also explain and clarify the results and the graphs wherever such elucidation is conducive in understanding the mapping of the graphs.

Equations developed in Chapters two through six are applied to obtain graphs of magnitudes of θ -component of external, internal and physical surface electric currents that are produced as a result of a plane electromagnetic wave impinging on the afore-mentioned spherical shell from its bottom. These graphs are shown below in Figure 7-4.2.2, Figure 7-4.2.4, Figure 7-4.2.6, and Figure 7-4.2.8. Inserts of graphs taken from Altunkilic [3] in Figure 7-4.2.3, Figure 7-4.2.5, Figure 7-4.2.7, and Figure 7-4.2.9 are placed below each of our four graphs for comparison purpose. Pictorial graph mappings of Altunkilic's and our graphs show marked conformability.

7-4.2 Chirality vs. Surface Currents

Figure 7-4.2.2 plots θ -component of external electric current in $\phi = 0$ plane.

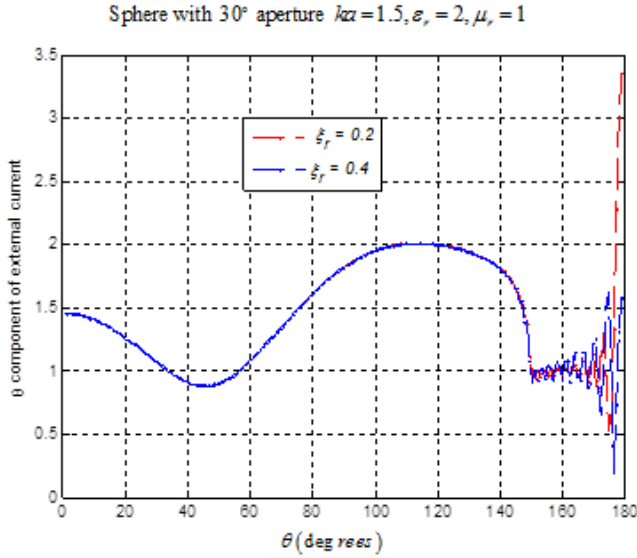


Figure 7-4.2.2 Magnitude of θ -component of external equivalent electric current in $\phi = 0$ plane (varying chiralities) . The generating curve is approximated by 426 straight line segments.

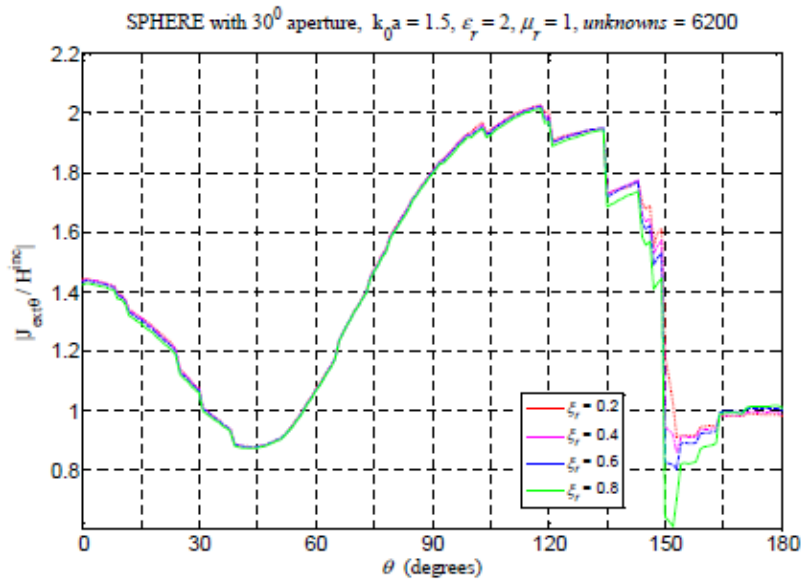


Figure 7-4.2.3 Magnitude of θ -component of external equivalent electric current in the $\phi = 0$ plane (varying chiralities) (taken from Altunkilic [3]).

Figure 7-4.2.4 plots θ -component of internal electric current in $\phi = 0$ plane.

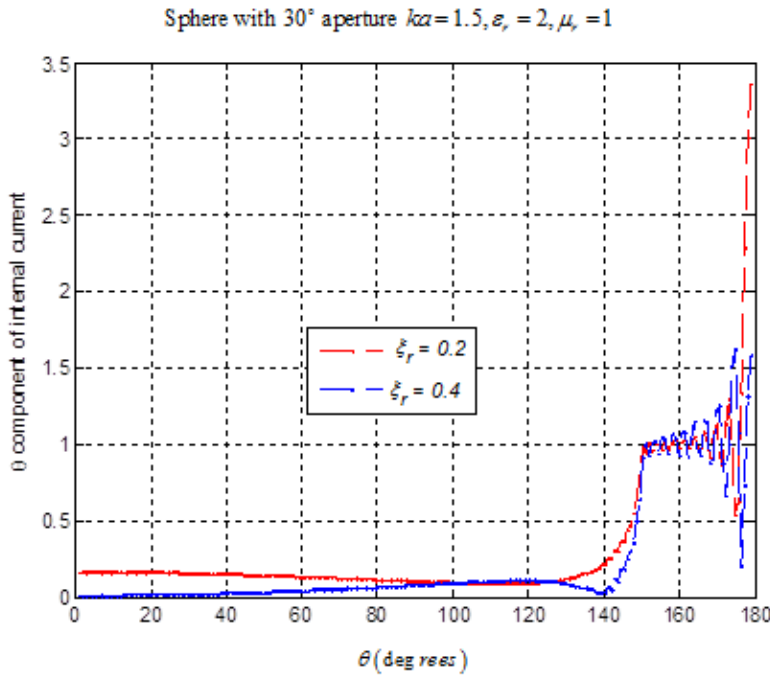


Figure 7-4.2.4 Magnitude of θ -component of internal equivalent electric current in $\phi = 0$ plane (varying chiralities). The generating curve is approximated by 426 straight line segments.

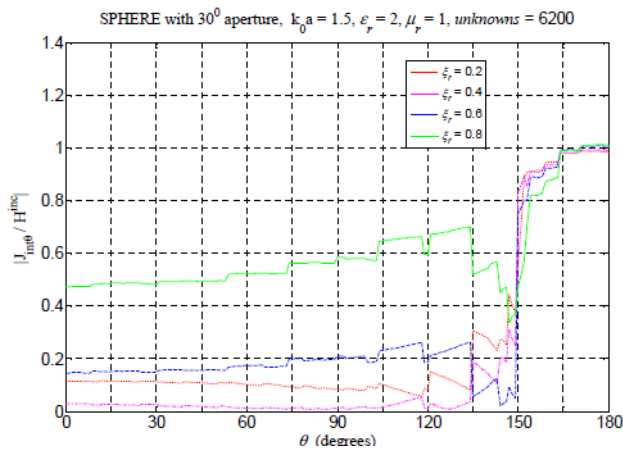


Figure 7-4.2.5 Magnitude of θ -component of internal equivalent electric current in $\phi = 0$ plane (varying chiralities) (Insert taken from Altunkilic [3]).

Our graph of the Figure 7-4.2.4 and Altunkilic's graph of the Figure 7-4.2.5 are obtained by using two distinctly different numerical approaches. Therefore variations in these two graphs cannot be evaluated and accuracy of the one graph with respect to the other cannot be established.

Figure 7-4.2.6 plots θ -component of physical current in $\phi = 0$ plane.

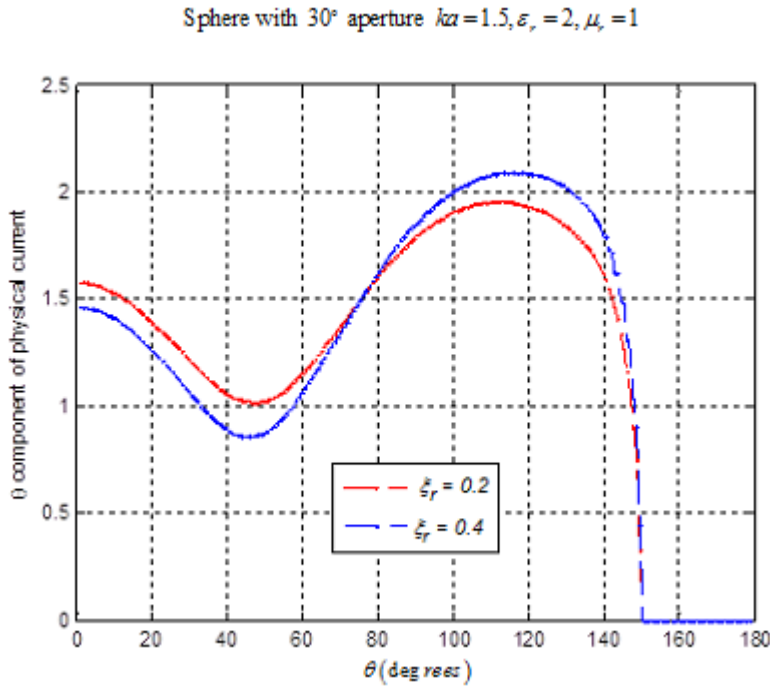


Figure 7-4.2.6 Magnitude of θ -component of physical electric current in the $\phi = 0$ plane (varying chiralities). Physical current shows zero values in the aperture space ($150^\circ - 180^\circ$). The generating curve is approximated by 426 straight line segments.

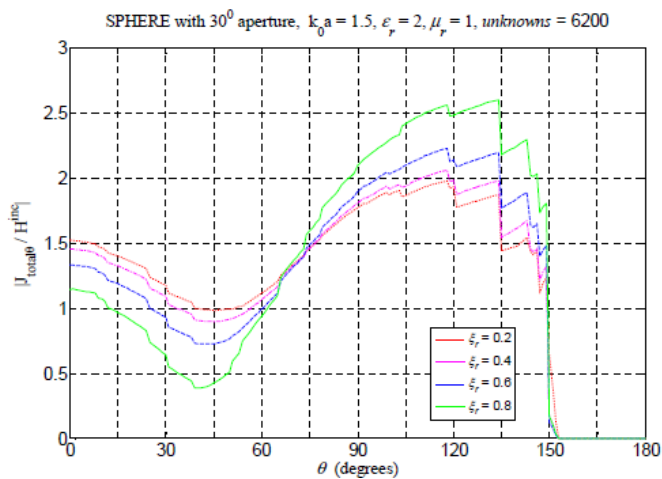


Figure 7-4.2.7 Magnitude of θ -component of physical electric current in the $\phi = 0$ plane (varying chiralities) (Insert taken from Altunkilic [3]).

.Both graphs of the Figures 7-4.2.6 –7-4.2.7 show zero values in the aperture space ($150^\circ - 180^\circ$). Our graph of the Figure 7-4.2.6 and Altunkilic's graph of the Figure 7-4.2.7 are obtained by using two distinctly different numerical approaches. Therefore variations in these two graphs cannot be evaluated and accuracy of the one graph with respect to the other cannot be established. However, graph readings of these two graphs for $\xi_r = 0.2$ and $\xi_r = 0.4$ are about the same. Graph mapping of our graph of the Figure 7-4.2.7 is smooth and free from zigzagging in up and down directions.

Figure 7-4.2.8 plots θ -component of magnetic current in $\phi = 0$ plane.

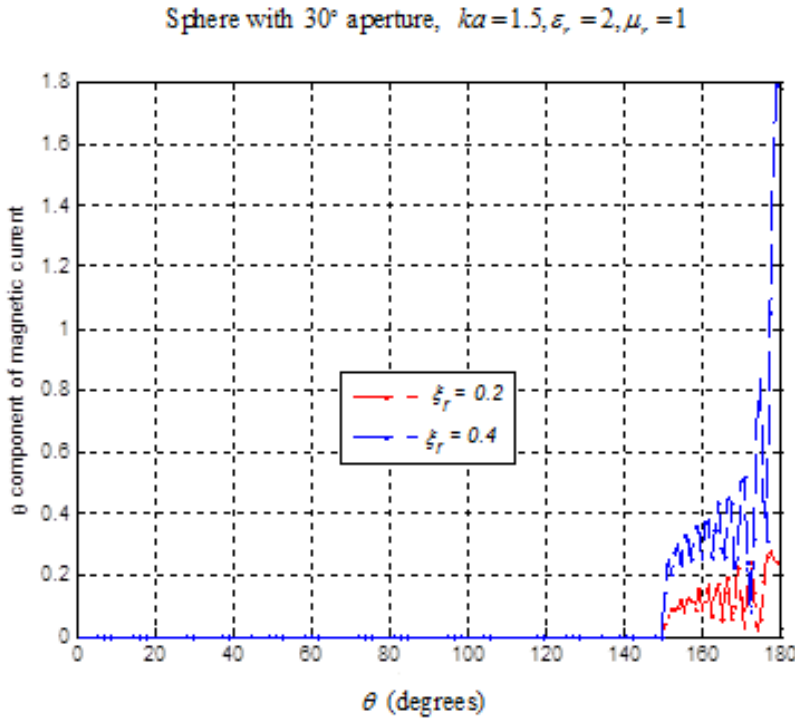


Figure 7-4.2.8 Magnitude of θ -component of equivalent magnetic current in the $\phi = 0$ plane (varying chiralities). The generating curve is approximated by 426 straight line segments.

Graph of the Figure 7-4.2.8 shows sharp up and down swings in the aperture space ($150^\circ - 180^\circ$). Transition from a perfectly conducting surface to an aperture which exposes chiral material to the advancing plane electromagnetic wave is observed to produce sharp up and down swings. Improvement in the E-field solution of this situation has been published. Our theory involves the E-field as well as the H-field solution of the problem, as such up and down fluctuations in the aperture space cannot be improved. However the average of these fluctuations agrees with the computed result.

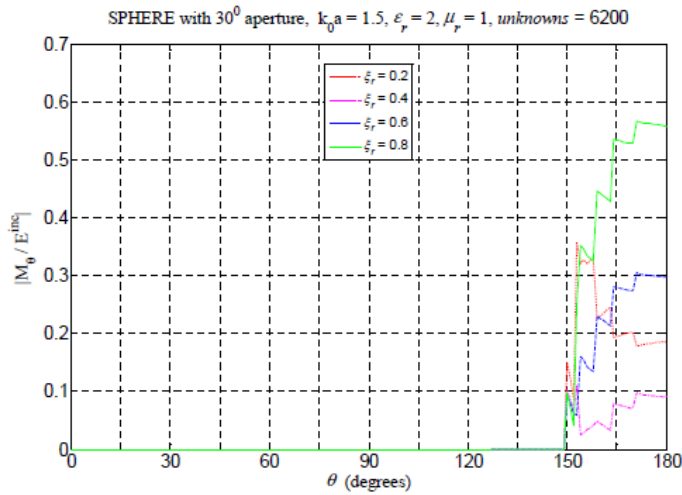


Figure 7-4.2.9 Magnitude of θ -component of equivalent magnetic current in the $\phi = 0$ plane (varying chiralities) (Insert taken from Altunkilic [3]).

Figure 7-4.2.10 plots ϕ -component of external electric current in $\phi = 0$ plane and Figure 7-4.2.11 plots ϕ -component of internal electric current in $\phi = 0$ plane.

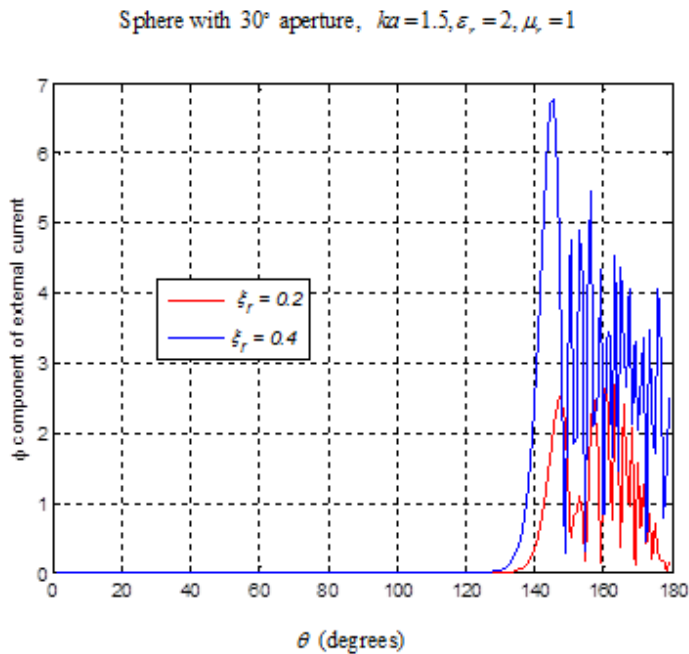


Figure 7-4.2.10 Magnitude of ϕ -component of external equivalent electric current in $\phi = 0$ plane (varying chiralities). The generating curve is approximated by 426 straight line segments.

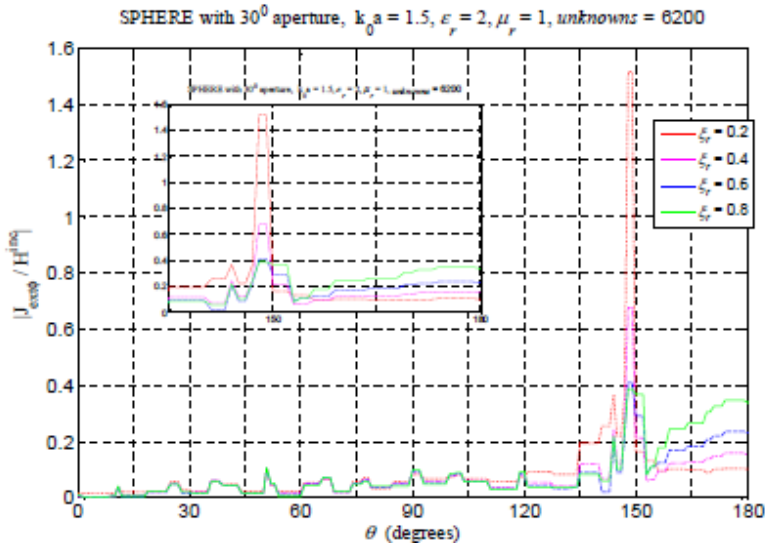


Figure 7-4.2.11 Magnitude of ϕ – component of external equivalent electric current in $\phi = 0$ plane (varying chiralities) (Insert taken from Altunkilic [3]).

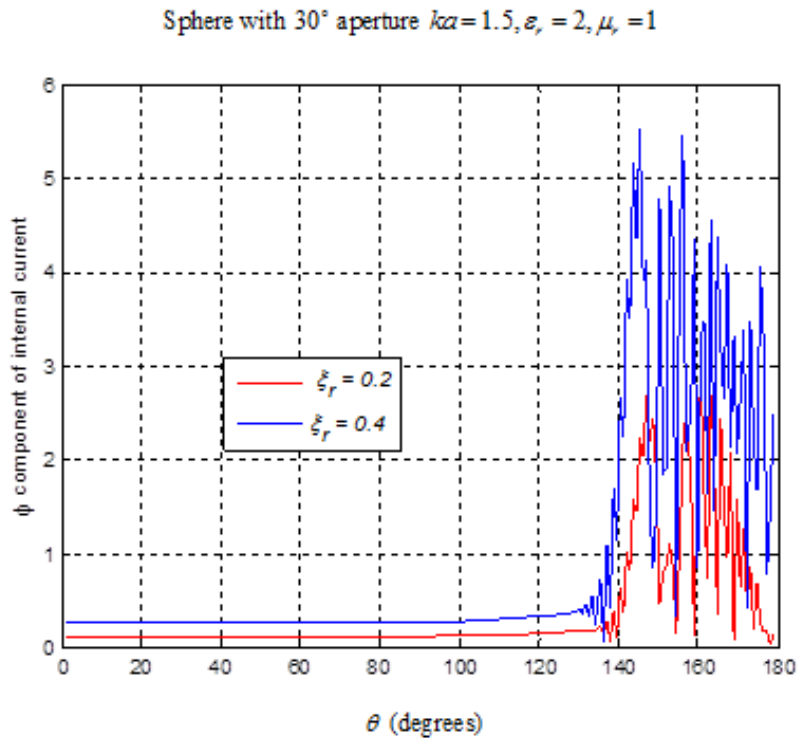


Figure 7-4.2.12 Magnitude of ϕ – component of internal equivalent electric current in $\phi = 0$ plane (varying chiralities). The generating curve is approximated by 426 straight line segments.

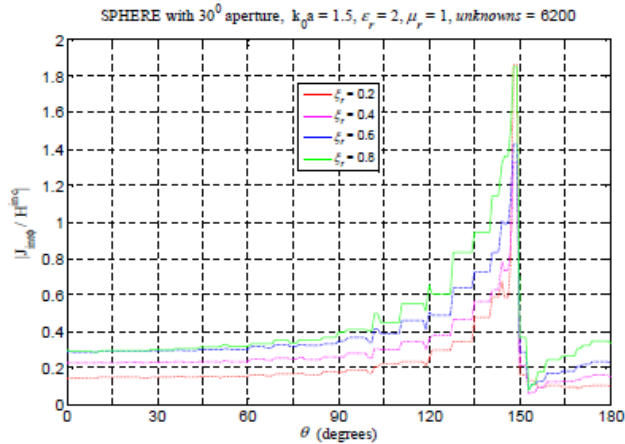


Figure 7-4.2.13 Magnitude of ϕ -component of internal equivalent electric current in $\phi = 0$ plane (varying chiralities). This graph is taken from Altunkilic [3].

Graph readings for $\xi_r = 0.2$ and $\xi_r = 0.4$ in the Figure 7-4.2.12 and the Figure 7-4.2.13 are about the same in the conducting space which is about 72% of the total sphere surface. Graph mapping of our graph of the Figure 7-4.2.12 is smooth and free from any zigzagging in direction in this space. However, in the aperture space which is about 28% of the total sphere surface our graph shows sharp and down swings compared to the graph of Altunkilic [3]. The reason for these up and down fluctuations are explained above.

Figure 7-4.2.14 plots ϕ -component of physical electric current in $\phi = 0$ plane and Figure 7-4.2.13 plots ϕ -component of magnetic current in $\phi = 0$ plane.

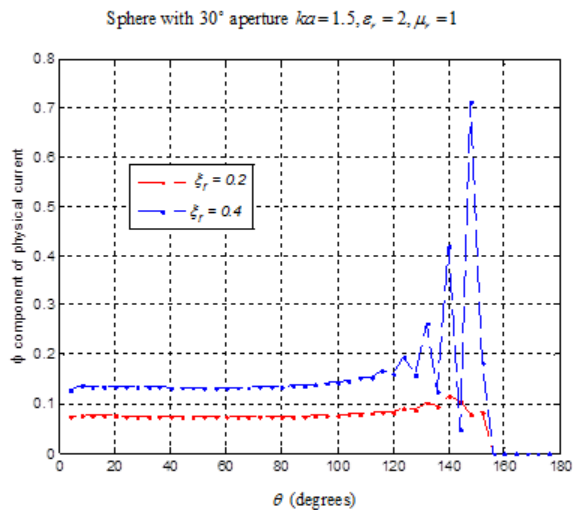


Figure 7-4.2.14 Magnitude of ϕ -component of physical electric current in the $\phi = 0$ plane (varying chiralities). The generating curve is approximated by 426 straight line segments.

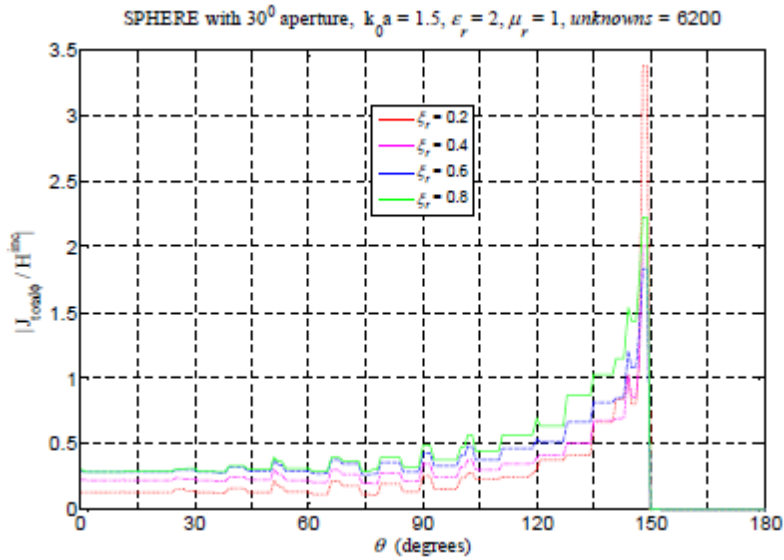


Figure 7-4.2.15 Magnitude of ϕ -component of physical electric current in the $\phi = 0$ plane (varying chiralities). This graph is taken from Altunkilic [3].

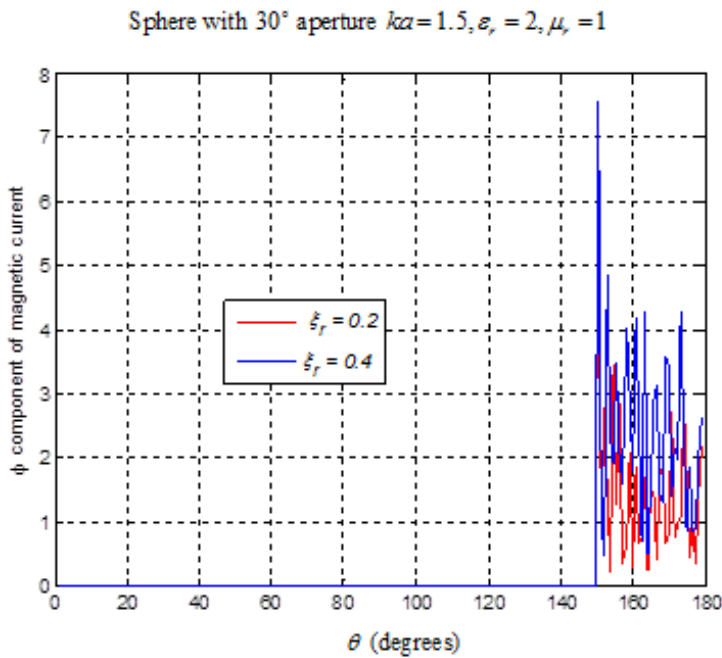


Figure 7-4.2.16 Magnitude of ϕ -component of equivalent magnetic current in the $\phi = 0$ plane (varying chiralities). The generating curve is approximated by 426 straight line segments.

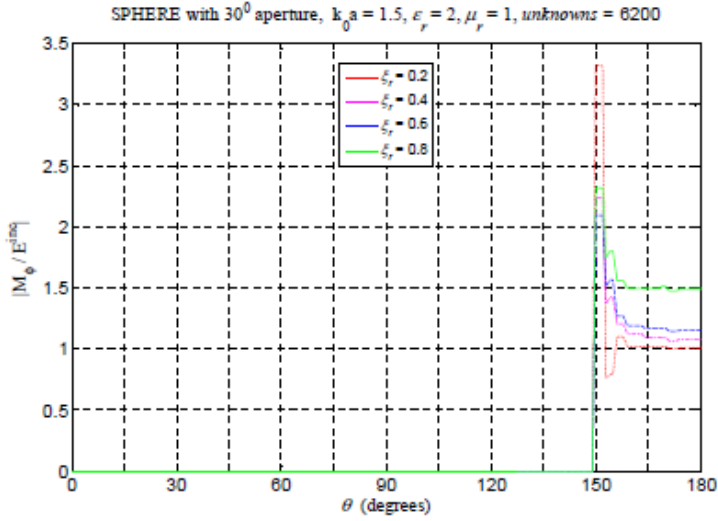


Figure 7-4.2.17 Magnitude of ϕ -component of equivalent magnetic current in the $\phi = 0$ plane (varying chiralities). This graph is taken from Altunkilic [3].

The graphs of the Figures 7-4.2.16 – 7-4.2.16, show zero values on the conducting surface. In the aperture space ($150^\circ - 180^\circ$) our graph of the Figure 7-4.2.16 shows sharp up and down swings. As explained above transition from the conducting surface to the chiral space produces sharp fluctuations in the graph. Suggestion for improved E-field solution of this problem has been published by Harrington and Mautz. Suggestion for improved E-field and H-field solution of this problem that pertains to our case has not been published. However, the average value of the graph readings in the aperture space agrees with the averaged computed result in this space.

7-4.3 Computed results of the Chirality vs. Bistatic RCS

Figure 7-4.4.1 and the Figure 7-4.4.2 (taken from Altunkilic [3]) plot the $\sigma_{\theta\theta}$ (co-polarized bistatic radar cross section) of varying chiralities. Our graphs of the Figure 7-4.4.1 show overlapping because of extremely small variations in the graph readings. Figure 7-4.4.3 produces graphs of the cross polarized $\sigma_{\phi\theta}$ of the obstacle for varying chiralities. Figure 7-4.4.4 and the Figure 7-4.4.5 (taken from Altunkilic [3]) plot the $\sigma_{\theta\theta}$ (co-polarized bistatic radar cross section) of varying wave numbers. Graphs of the Figure 7-4.4.4 and the graphs of the Figure 7-4.4.5 (taken from Altunkilic [3]) show markedly almost one hundred resemblance to each other. Figure 7-4.4.6 plots graphs of the cross polarized $\sigma_{\phi\theta}$ of the obstacle for varying wave numbers.

7-4.4 Chirality vs. Bistatic Radar Cross Sections (RCS)

Figure 7-4.4.1, shown below, indicates insignificant variations in the overall RCS values as chirality varies from $\xi_r = 0.2$ to $\xi_r = 0.9$ with parameters $k_e = 1.5$, $\epsilon_r = 2$, and $\mu_r = 1$.

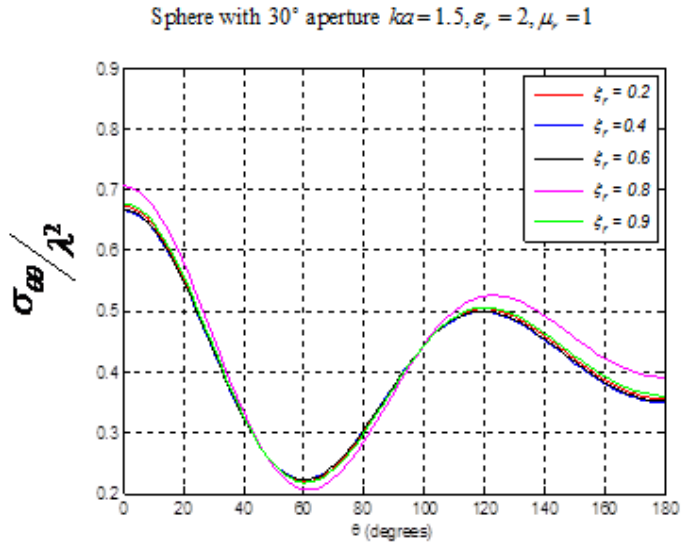


Figure 7-4.4.1 $\sigma_{\theta\theta}$ of the obstacle (varying chiralities) . Generating curve is approximated by 1200 straight line segments.

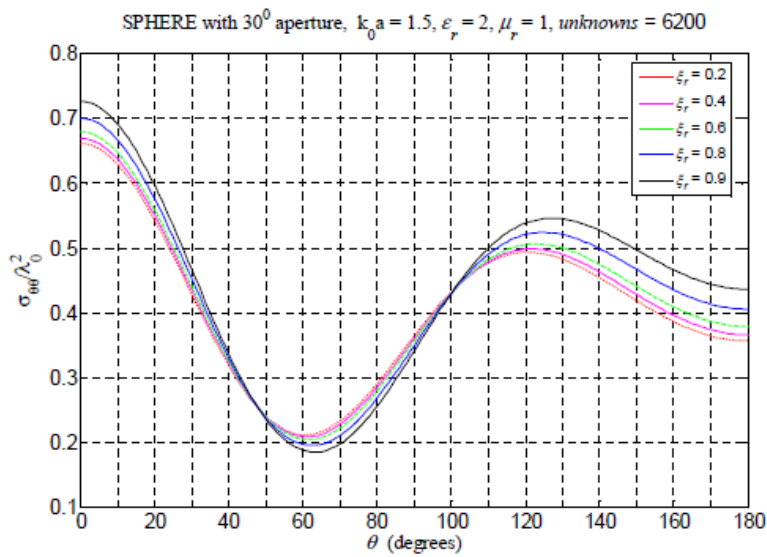


Figure 7-4.4.2 $\sigma_{\theta\theta}$ of the obstacle (varying chiralities) (Insert taken from Altunkilic [3]).

We see marked resemblance between our graph of Fig 7-4.4.1 and that of the insert of Altunkilic's graph of Figure 7-4.4.2 .

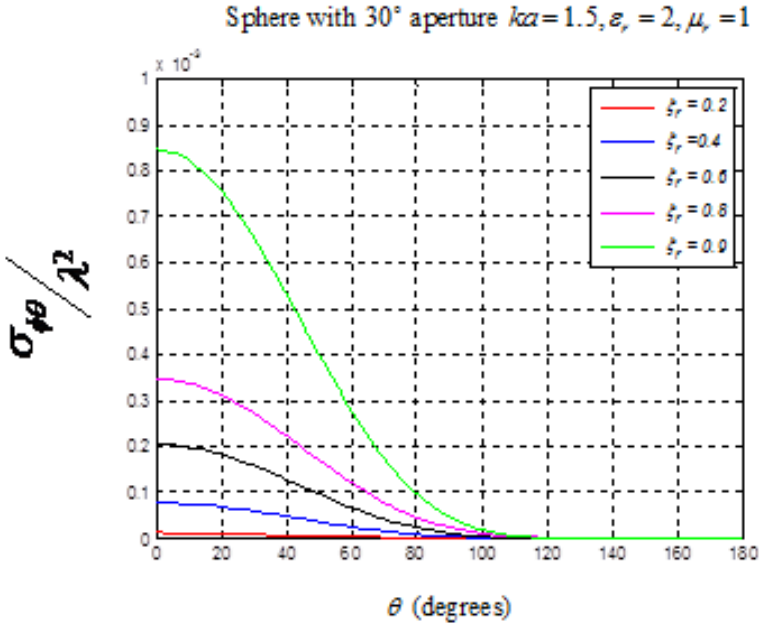


Figure 7-4.4.3 $\sigma_{\phi\theta}$ of the obstacle (varying chiralities) . Generating curve is approximated by 1200 straight line segments.

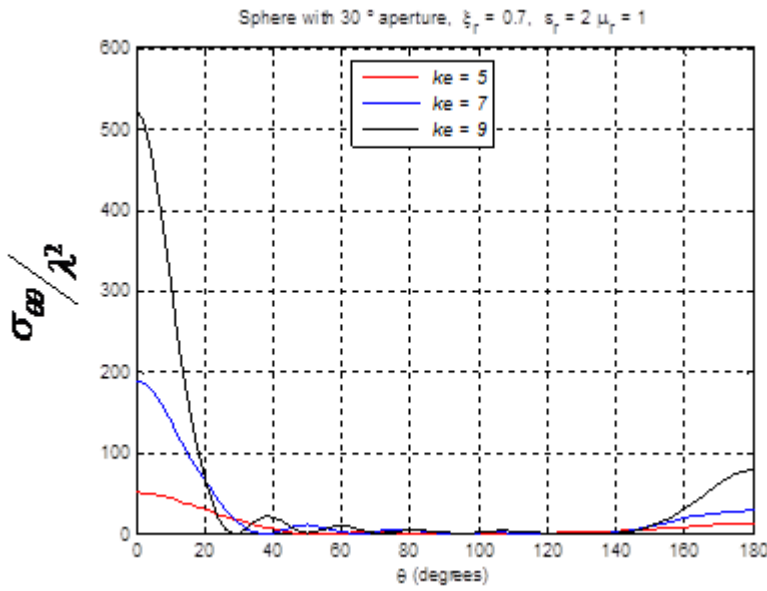


Figure 7-4.4.4 $\sigma_{\theta\theta}$ of the perfectly conducting spherical shell with 30° aperture at its bottom that exposes enclosed chiral material (varying wave numbers). Generating curve is approximated by 1200 straight line segments.

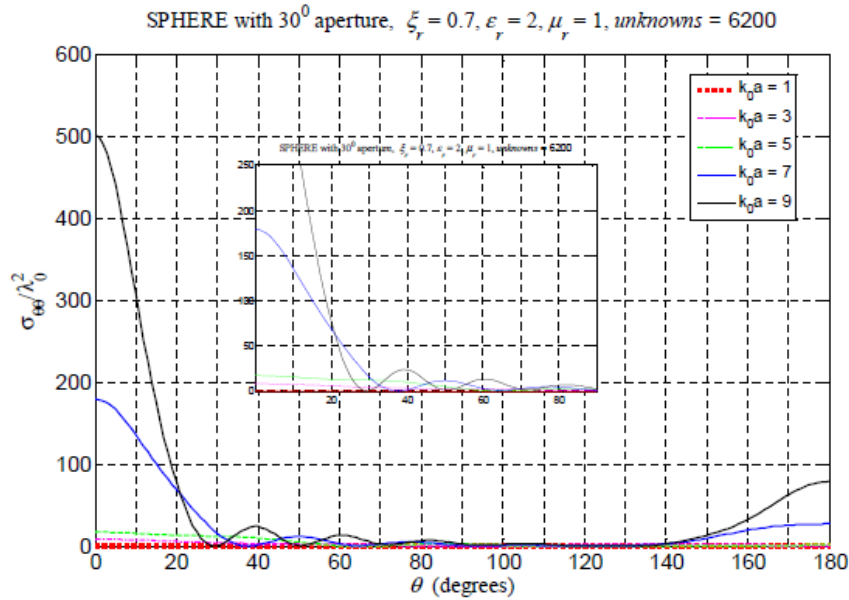


Figure 7-4.4.5 $\sigma_{\theta\theta}$ of the obstacle (varying wave numbers) (Insert taken from Altunkilic [3]).

We see marked resemblance between our graph of Fig 7-4.4.4 and that of the insert of Altunkilic's [3] graph of Figure 7-4.4.5 .

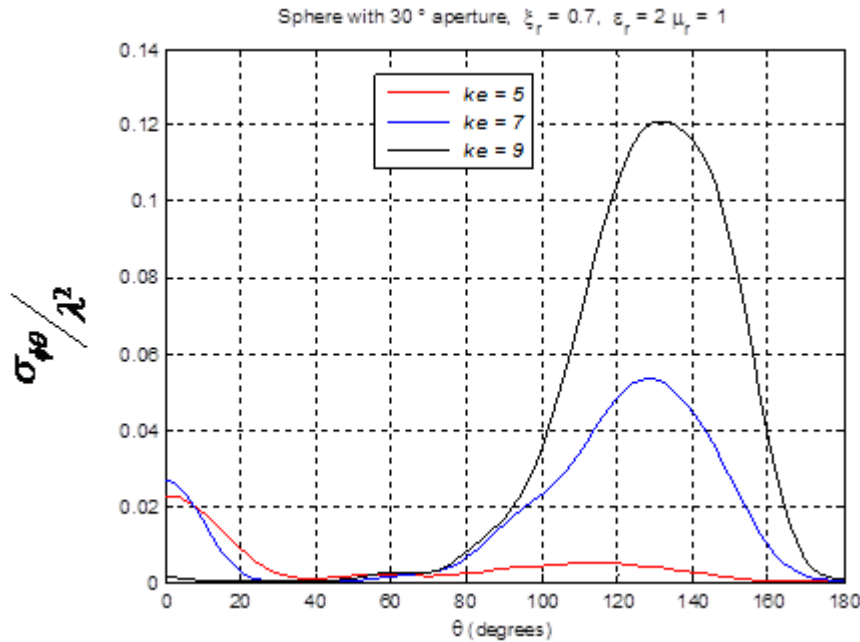


Figure 7-4.4.6 $\sigma_{\theta\theta}$ of the perfectly conducting spherical shell with 30° aperture at its bottom That exposes enclosed chiral materia l (varying wave numbers). Generating curve is approximated by 1200 straight line segments.

7-4.5 Computed Results of the Internal fields

At the end, we wanted to obtain the best results, therefore, we chose 102 points on the z-axis, in contrast with 52 points on the z-axis, which Alltunkilick [3] uses. In pursuit of our goal of attaining the utmost we divided the generating curve into 3132 straight line segments leading to two matrices of size 6260×6260 to produce each graph of the following section. We have been using 426 straight line segments leading to two matrices of size 848×848 to produce our earlier graphs. The graphs of the Figures 7-4.6.1 – 7-4.6.6 are the results of our great effort.

7-4.6 Internal fields

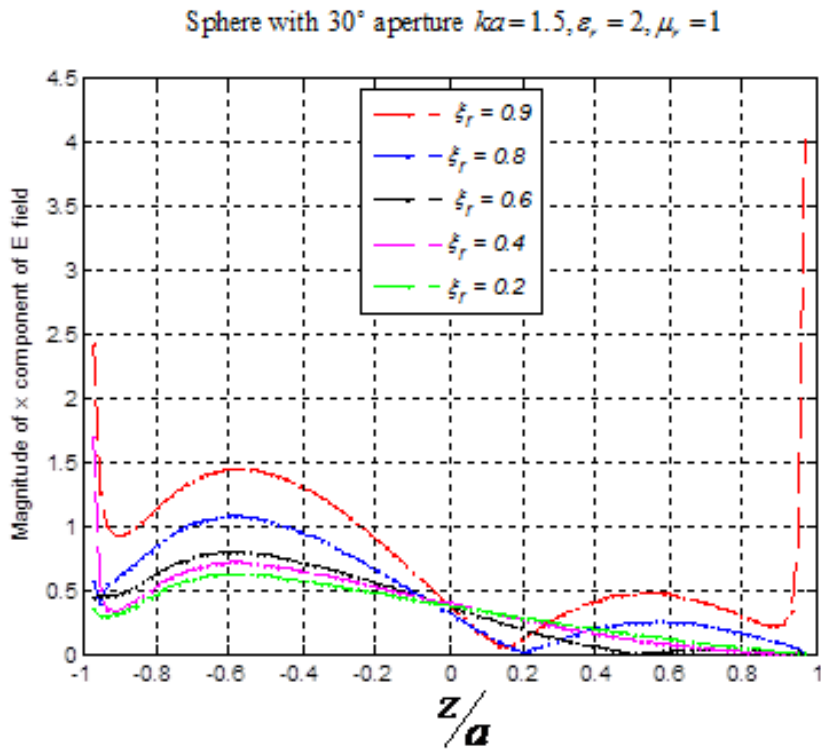


Figure 7-4.6.1 Magnitude of x-component of internal electric field along z-axis (varying chiralities). Generating curve is approximated by 3132 straight line segments and 102 points on z-axis were used to obtain the graph.

Sphere with 30° aperture, $ka = 1.5$, $\epsilon_r = 2$, $\mu_r = 1$

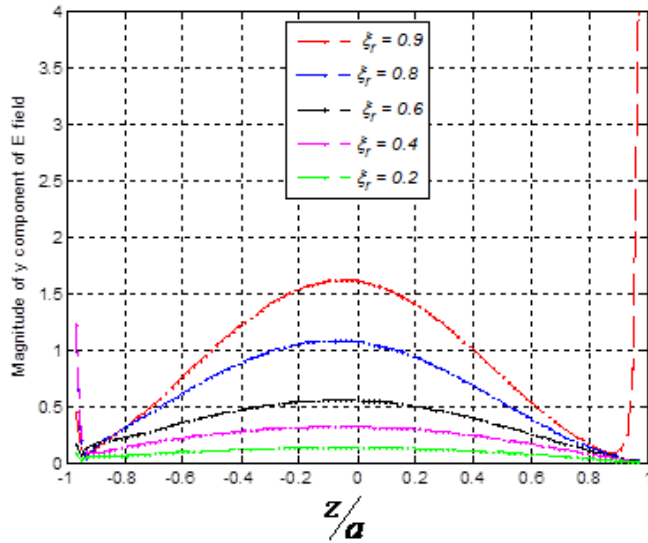


Figure 7-4.6.2 Magnitude of y-component of internal electric field along z-axis (varying chiralities). Generating curve is approximated by 3132 straight line segments and 102 points on z-axis were used to obtain the graph.

Sphere with 30° aperture, $\xi_r = 0.7$, $\epsilon_r = 2$, $\mu_r = 1$

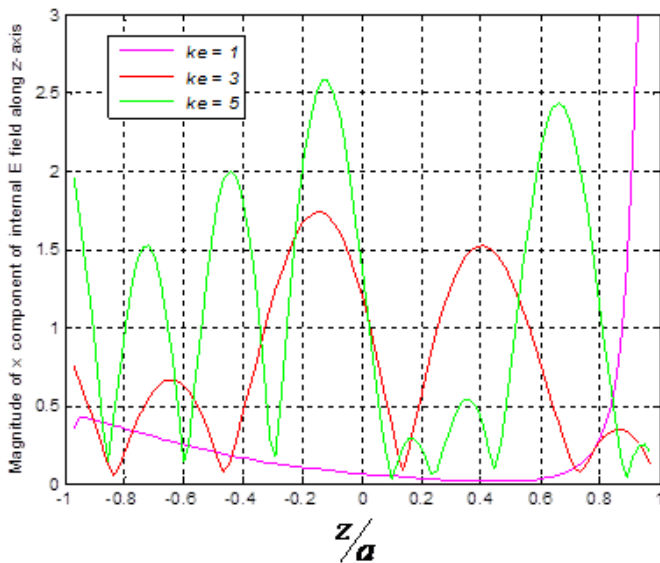


Figure 7-4.6.3 Magnitude of x-component of internal electric field along z-axis (varying wave numbers). Generating curve is approximated by 3132 straight line segments and 102 points on z-axis were used to obtain the graph.

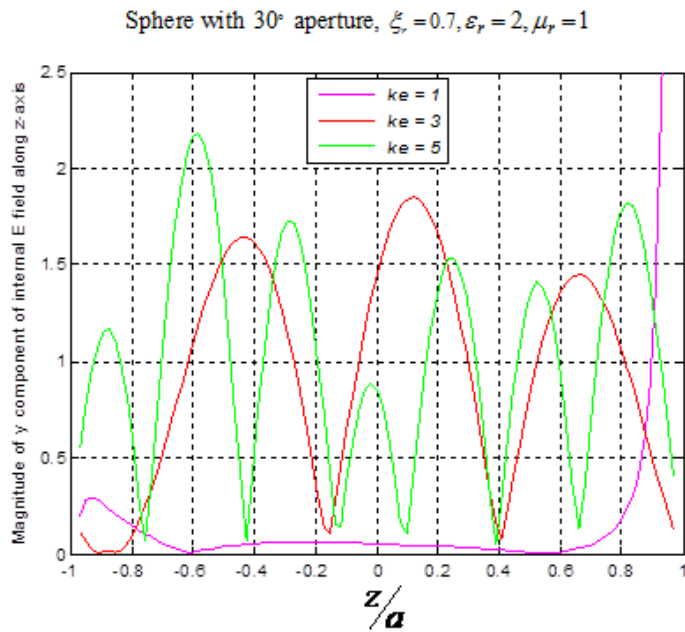


Figure 7-4.6.4 Magnitude of y-component of internal electric field along z-axis (varying wave numbers). Generating curve is approximated by 3132 straight line segments and 102 points on z-axis were used to obtain the graph.

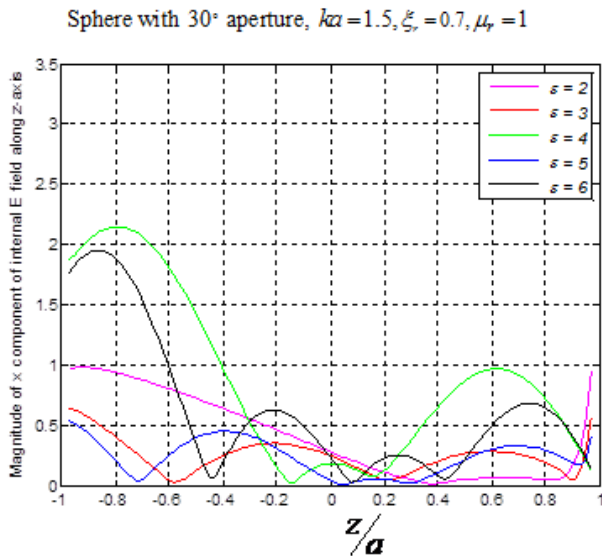


Figure 7-4.6.5 Magnitude of x-component of internal electric field along z-axis (varying permittivities). Generating curve is approximated by 3132 straight line segments and 102 points on z-axis were used to obtain the graph.

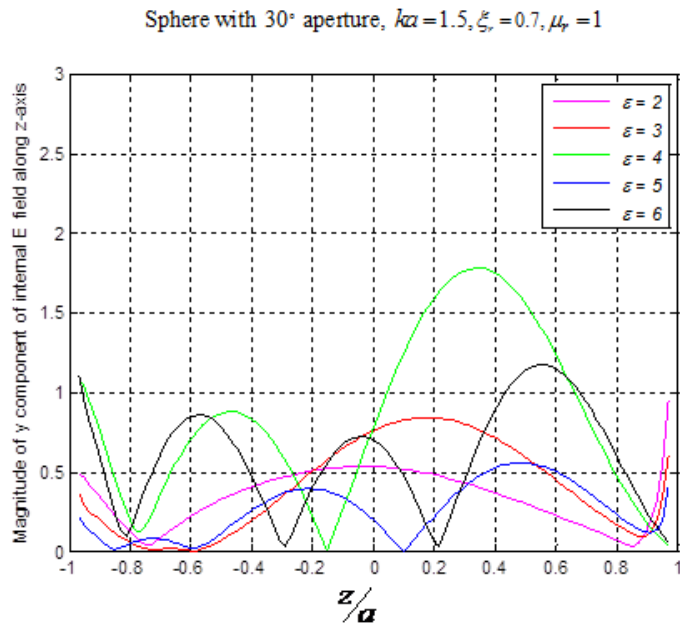
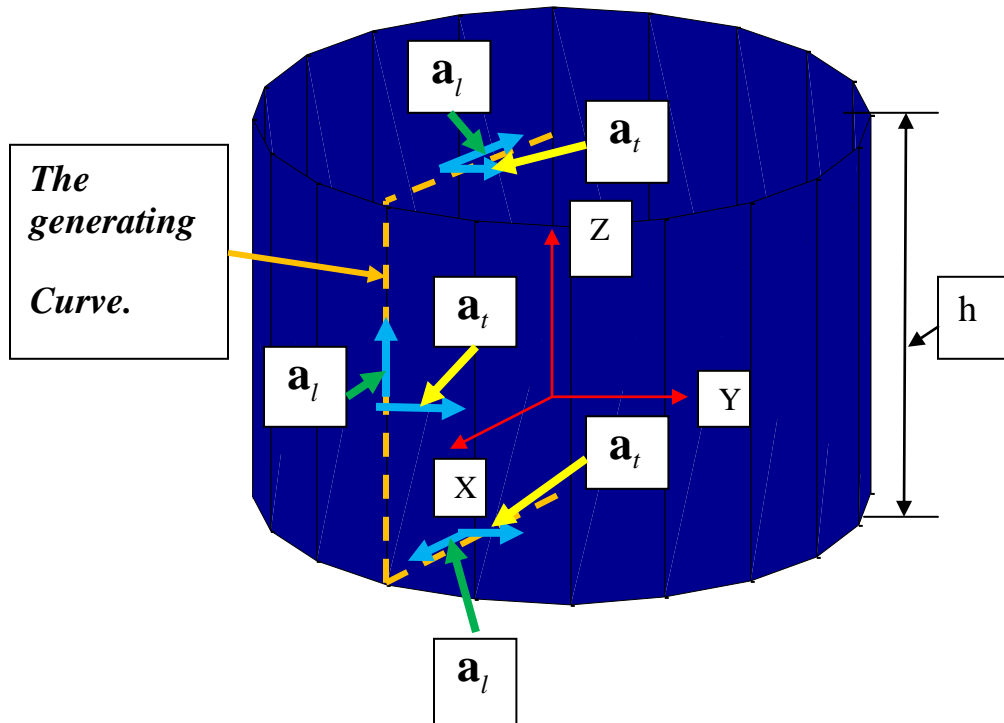


Figure 7-4.6.6 Magnitude of y-component of internal electric field along z-axis (varying permittivities). Generating curve is approximated by 3132 straight line segments and 102 points on z-axis were used to obtain the graph.

7-5 Cylinder

7-5.1 A Cylinder and its Generating Curve.



7-5.1 The generating curve of the cylinder in the $\phi = 0$ plane.

Figure 7-5.1 shows a cylinder shaped body of revolution (BOR) that illustrates the generating curve and the direction of unit vectors \mathbf{a}_l and \mathbf{a}_t placed on the generating curve. Unit vector \mathbf{a}_l traverses along the length of the generating curve as shown in the Figure 7-5.1 and unit vector \mathbf{a}_t provides transverse perpendicular direction along the length of the generating curve as shown in the Figure 7-5.1. This figure also shows the three dimensional coordinate axes as well height "h" of the cylinder. It also shows the length l along the perimeter of the cross section of the cylinder in the $\phi = 0$ plane. We will use the direction of unit vectors, perimeter length l and radius and height of the cylinder for computational purposes.

Figure 7-5 shows a plane electromagnetic wave incident from the bottom of the Chiral Cylinder. The cylinder is assumed to be illuminated by a θ -polarized plane wave incident from the

bottom of the chiral cylinder where $\theta^{inc} = 180^\circ, \phi^{inc} = 0^\circ$, $\mathbf{E}^{inc} = -\mathbf{a}_x E^{inc} e^{-jkz}$, and $\mathbf{H}^{inc} = -\mathbf{a}_y H^{inc} e^{-jkz}$. Here k is the wave number of free space.

7-6 A Chiral Cylinder

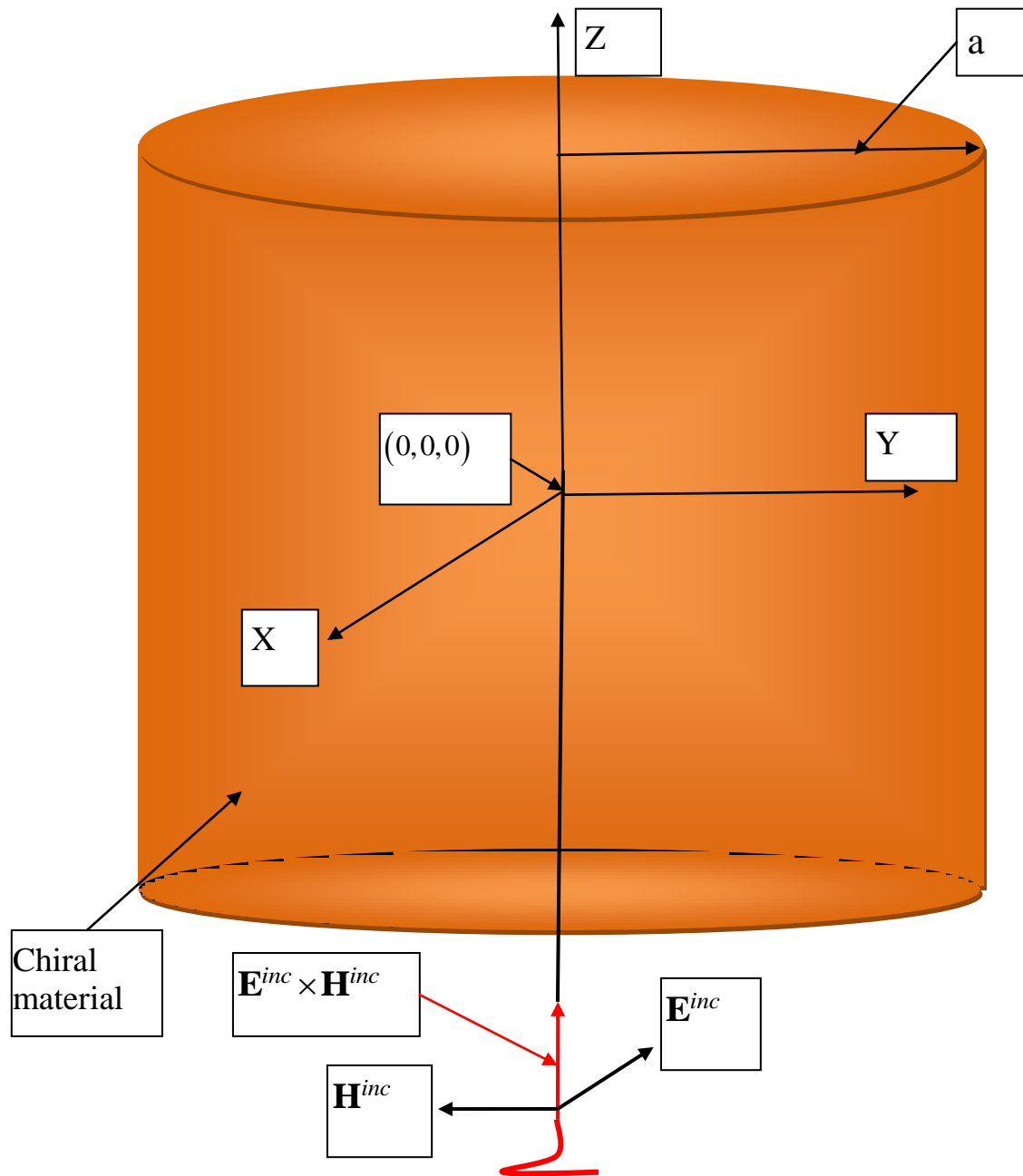


Figure 7-6 A chiral cylinder.

(Figure 7-12.1 will be the frame of reference in relation to the results and the graphs that are obtained in the following sections).

7-6.1 Computed Results of the Internal Fields

Figures in this section include figures of the graphs plotted by the application of our numerical approach and the figures of the corresponding graphs obtained by Altunkilic [3] by the application of a distinctly different numerical approach than ours. Graphs taken from Altunkilic [3] are included for comparison purpose.

Figures 7-6.2.1 – 7-6.2.4 that include the graphs taken from Altunkilic [3] for comparison purpose, deal with internal electric fields. Figure 7-6.3.1 – 7-6.3.4 that include the graphs taken from Altunkilic [3] for comparison purpose, plot $\sigma_{\theta\theta}$ (co-polarized) and $\sigma_{\phi\theta}$ (cross-polarized) bistatic RCS. Figures 7-6.4.1 – 7-6.4.7 that include the graphs taken from Altunkilic [3] for comparison purpose, plot t -transverse and l -longitudinal components of equivalent surface currents in the $\phi = 0$ plane.

Figure 7-7.1 and Figure 7-7.2 plot amplitude of the E -field along the axis of an open cylinder of perfectly conducting surface whose top surface is taken as aperture thereby filling it up with air.

Parameters shown as part of the title of each graph in this section are used in the plotting of that graph.

Characteristics of the graphs produced by the application of our numerical approach is compared and contrasted with the corresponding graphs produced by Altunkilic's numerical approach. Comments are properly placed below the graphs that are being compared and contrasted.

All the graphs produced in this section involve two matrices of 688×688 compared to the huge size matrix from a size of 5500×5500 up to a size of 6350×6350 used by Altunkilic [3] for producing each of his graphs. We thus save enormous amount of computer memory and computational time.

7-6.2 Internal Fields

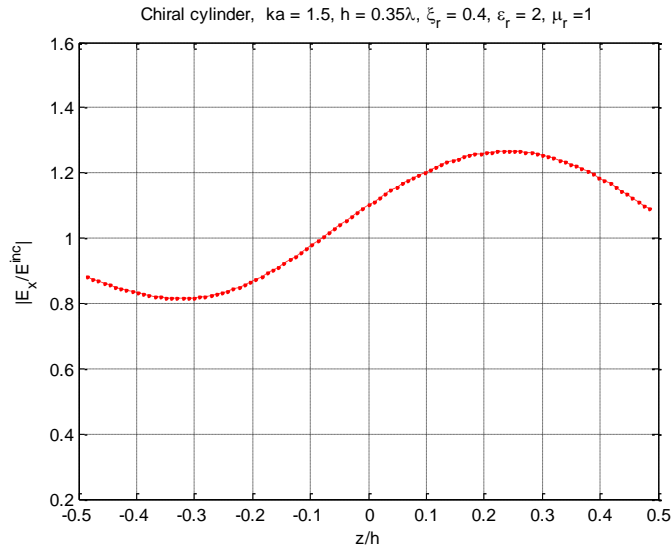


Figure 7-6.2.1 Magnitude of x-component of the internal E-field along z-axis.

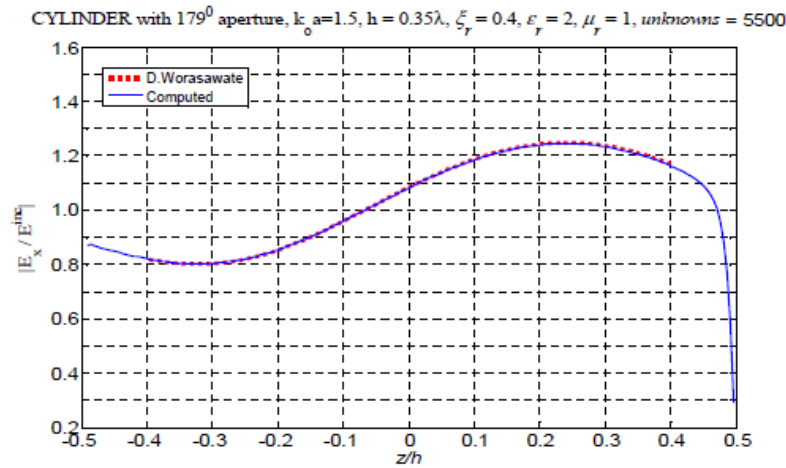


Figure 7-6.2.2 Magnitude of x-component of the internal E-field along z-axis (taken from Altunkilic [3]).

Figure 7-6.2.2 shows a graph (in red color) plotted from data computed by D. Worasawate. Our graph of Figure 7-6.2.1 shows striking almost one hundred percent resemblance to the exact graph of the Figure 7-6.2.2. In order to run his Matlab program Altunkilic [3] places a small circular perfectly conducting metallic patch of radius $0.01a$, where a is the radius of the sphere, at the top (north pole) of the chiral sphere. Because of the placement of the metallic patch the x-component of the internal E-field along z-axis, shown in the Figure 7-6.2.2 in blue color, plunges to zero at the north pole.

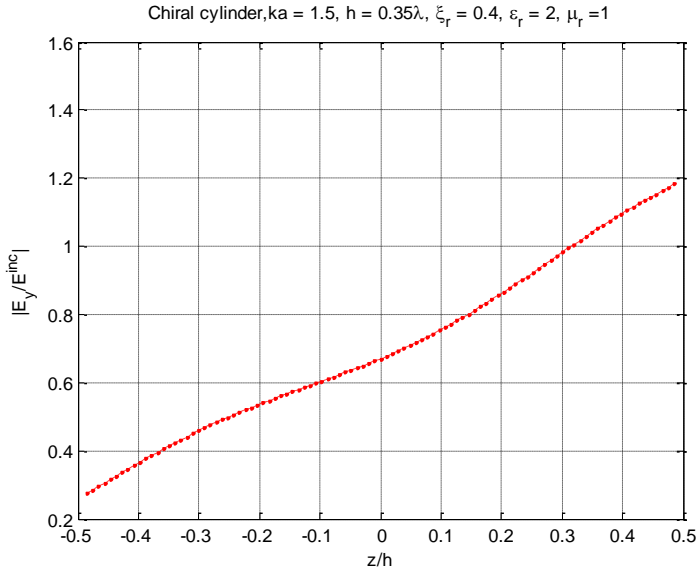


Figure 7-6.2.3 Magnitude of y-component of the internal E-field along z-axis.

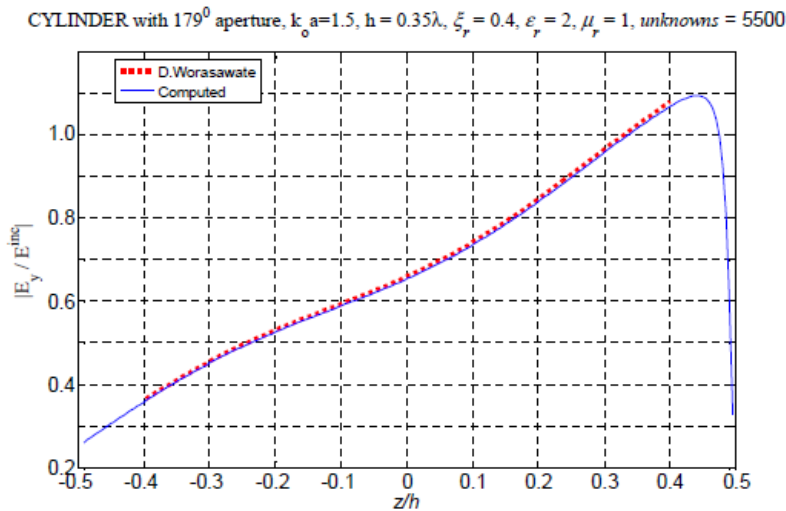


Figure 7-6.2.4 Magnitude of y-component of the internal E-field along z-axis (taken from Altunkilic [3]).

Figure 7-6.2.4 shows a graph (in red color) plotted from data computed by D. Worasawate. Our graph of Figure 7-6.2.3 shows remarkable almost one hundred percent resemblance to the exact graph of the Figure 7-6.2.4. In order to run his Matlab program Altunkilic [3] places a small circular perfectly conducting metallic patch of radius $0.01a$, where a is the radius of the sphere, at the top (north pole) of the chiral sphere. Because of the placement of the metallic patch the y-component of the internal E-field along z-axis, shown in the Figure 7-6.2.4 in blue color, plunges to zero at the north pole. Altunkilic [3] refers this structure as a perfectly conducting body of

revolution with an aperture of 179° that exposes the chiral material to the plane electromagnetic wave.

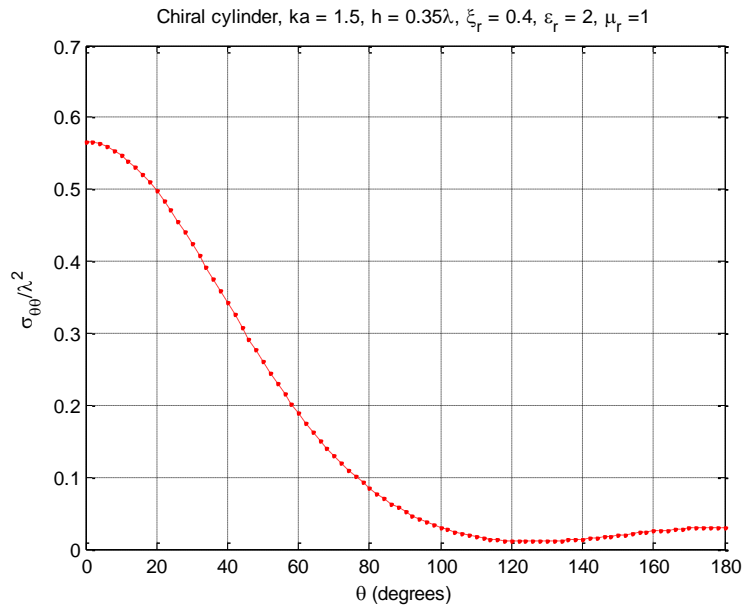


Figure 7-6.3.1 $\sigma_{\theta\theta}$ of the obstacle.

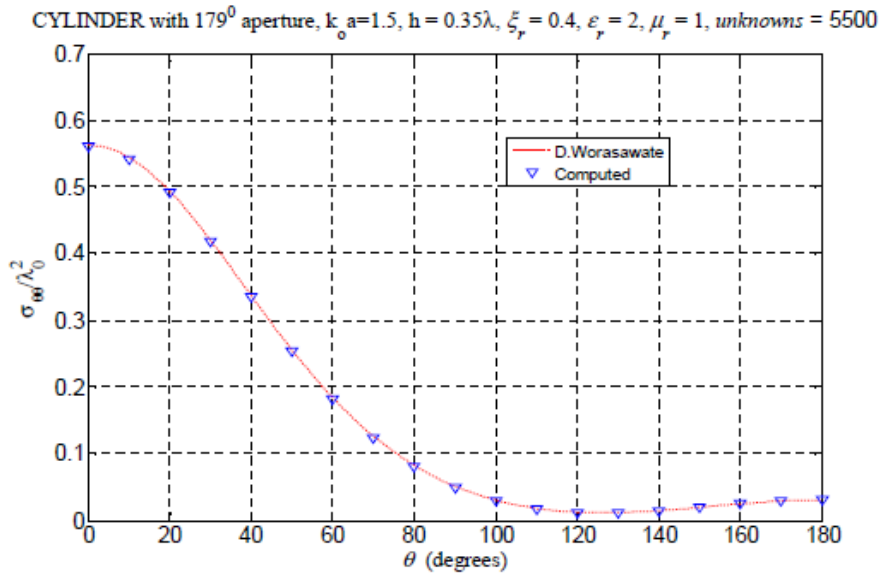


Figure 7-6.3.2 $\sigma_{\theta\theta}$ of the obstacle (taken from Altunkilic [3]).

Our graph of Figure 7-6.3.1 shows remarkable almost one hundred percent conformability with the graph (shown in red color) of data computed by D. Worasawate of the Figure 7-6.3.2.

7-6.3 Bistatic RCS

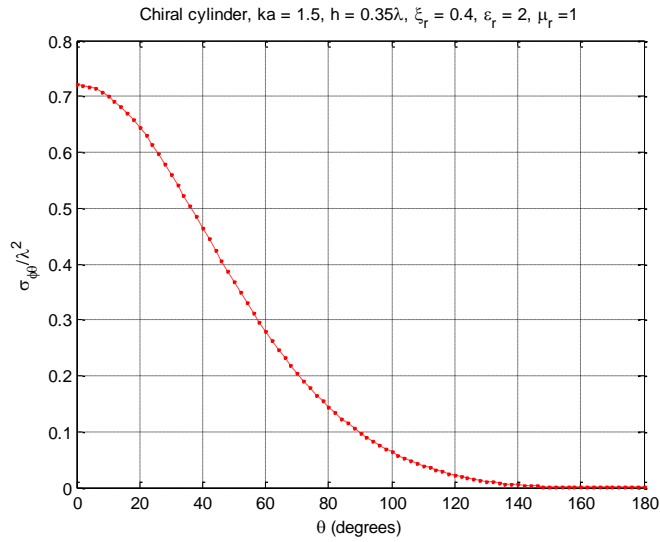


Figure 7-6.3.3 $\sigma_{\phi\theta}$ of the obstacle.

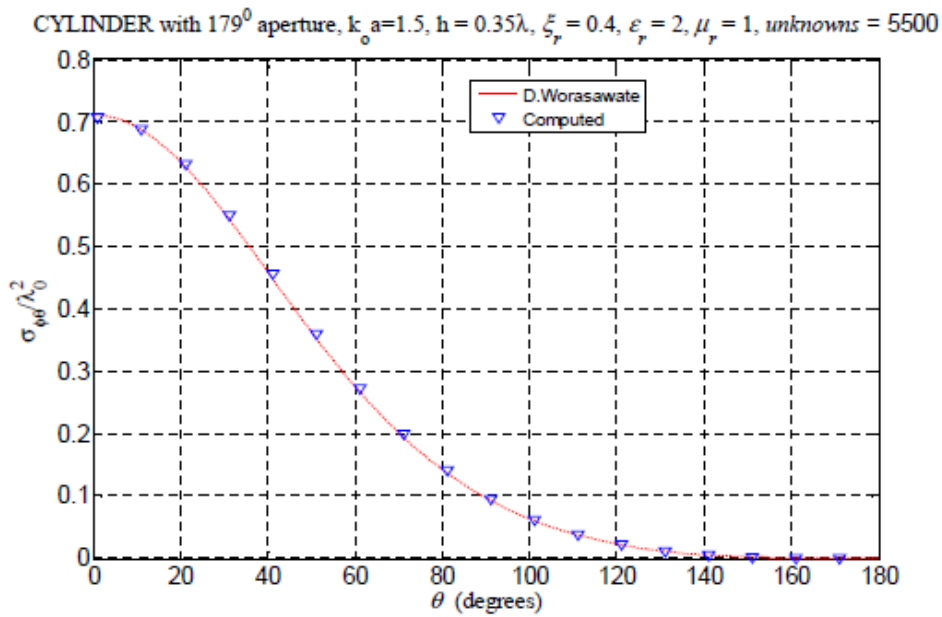


Figure 7-6.3.4 $\sigma_{\phi\theta}$ of the obstacle (taken from Altunkilic [3])

Again our graph of Figure 7-6.3.3 shows striking almost one hundred percent likeness with the graph (shown in red color) of data computed by D. Worasawate of the Figure 7-6.3.4.

7-6.4 Surface Currents

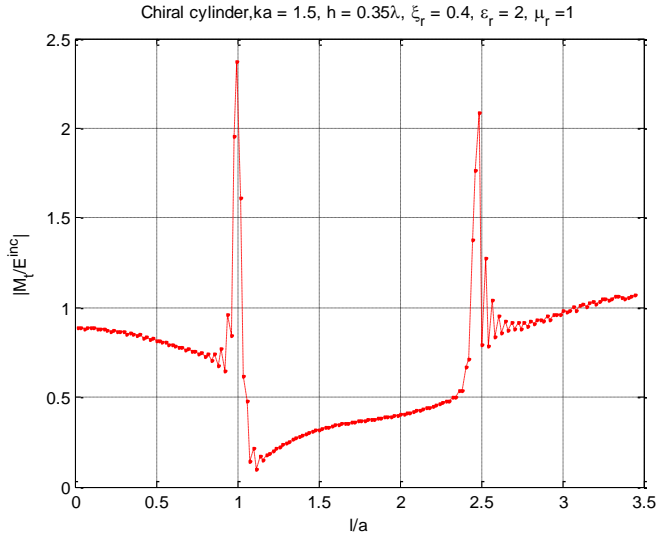


Figure 7-6.4.1 Magnitude of t -component of magnetic current in the $\phi = 0$ plane.

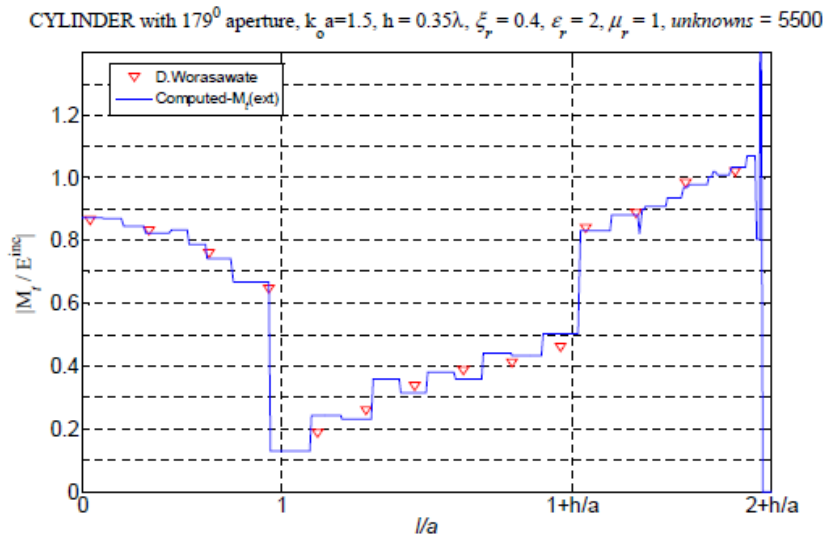


Figure 7-6.4.2 Magnitude of t -component of magnetic current in the $\phi = 0$ plane (taken from Altunkilic [3]).

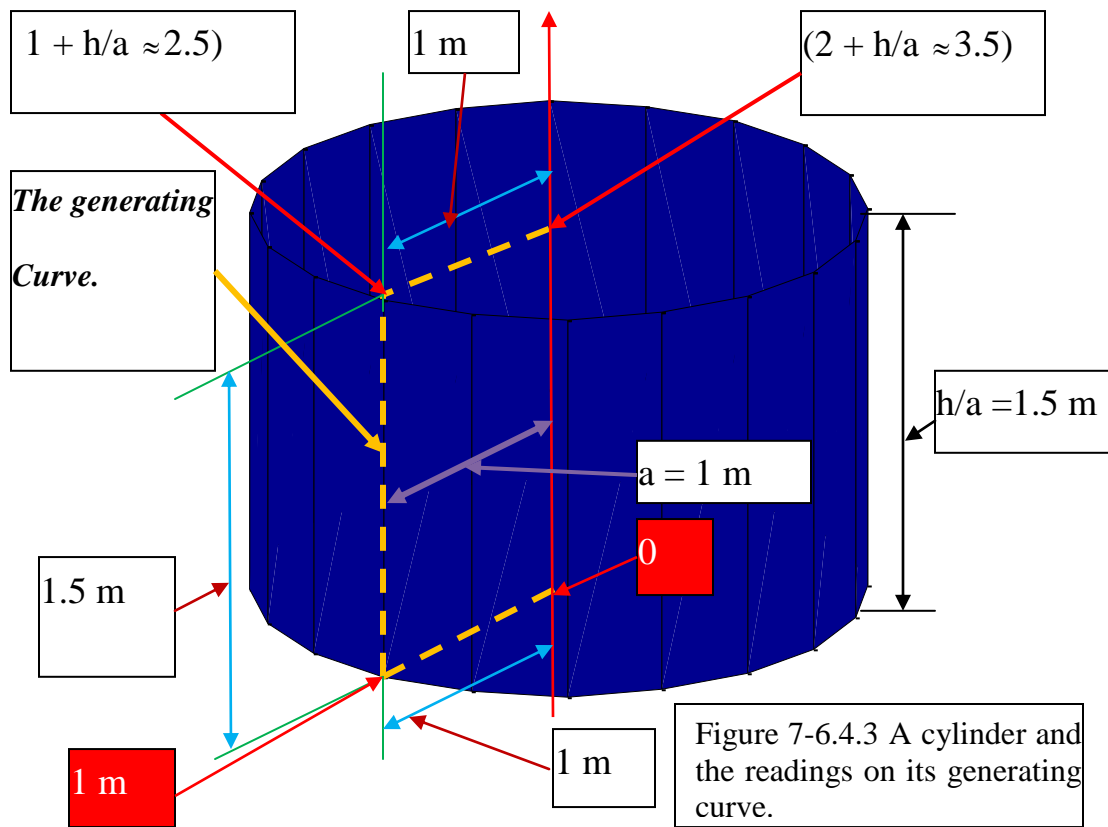
Our graph of the Figure 7-6.4.1 maps smooth curve from the start of the generating curve till it traverses the distance of 1 m on the generating curve where a sharp change in the geometry of the cylinder occurs as shown in the Figure 7-6.4.3. Our graph reacts to the abrupt change in the

geometry of the cylinder by producing sharp abrupt upward swing at this point. Thereafter graph mapping of our graph resumes its smooth course until it encounters another abrupt change in the geometry of the cylinder when it has traversed a distance of 2.5 meter on the generating curve as shown in the Figure 7-6.4.3. The graph, as expected, reacts to this abrupt change in the geometry of the cylinder as shown in the Figure 7-6.4.1 and resumes its almost smooth mapping thereafter. Noticing the sensitivity, and smoothness, as well as abrupt glitches that occur in our graph which correspond to the abrupt sharp changes in the geometry of the cylinder we assert that accuracy of the graph mapping of our graph stands to be more in the fitness of things than Altunkilic's graph of the Figure 7-6.4.2. The fact of the matter is that our and Altunkilic's graphs are produced by using two distinctly different numerical approaches and, therefore, in the absence of analytically calculated exact graph to compare with, it is just a matter of opinion as to which of the graph is correct. **One may notice that graph readings of our earlier graphs and Altunkilic's earlier graphs are about the same.** The caption at the top in Figure 7-6.4.2 reads $ka = 1.5$ and $h = 0.35\lambda$,

therefore, $h = 0.35\left(\frac{2\pi}{k}\right) \rightarrow kh = (0.35)(2\pi)$ so that, because $ka = 1.5$ and

$$\frac{kh}{ka} = \frac{h}{a} = \frac{(0.35)(2\pi)}{1.5} = 1.46607657. \quad \frac{kh}{ka} = \frac{h}{a} = \frac{(0.35)(2\pi)}{1.5} = 1.46607657 \rightarrow$$

$$2 + \frac{h}{a} = 2 + 1.46607657 = 3.46607657 \approx 3.5 \quad \text{and} \quad 1 + \frac{h}{a} = 1 + 1.46607657 = 2.46607657 \approx 2.5$$



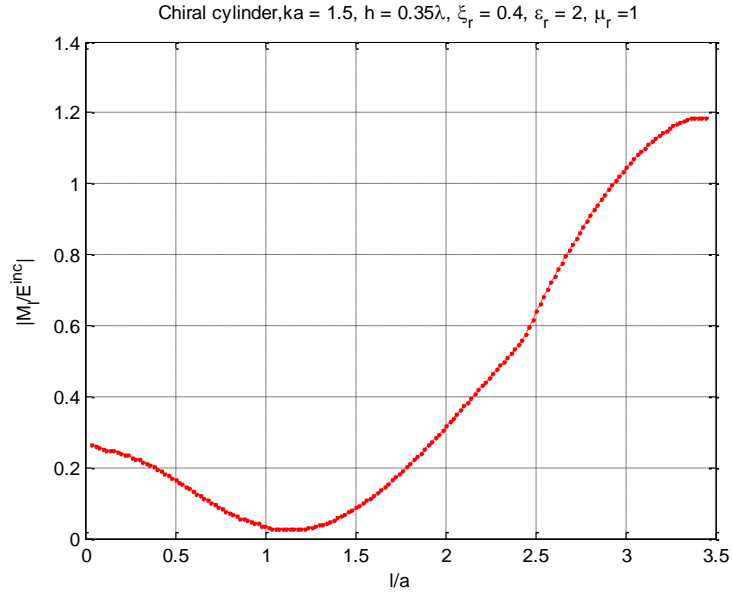


Figure 7-6.4.4 Magnitude of l -component of magnetic current in the $\phi = 0$ plane.

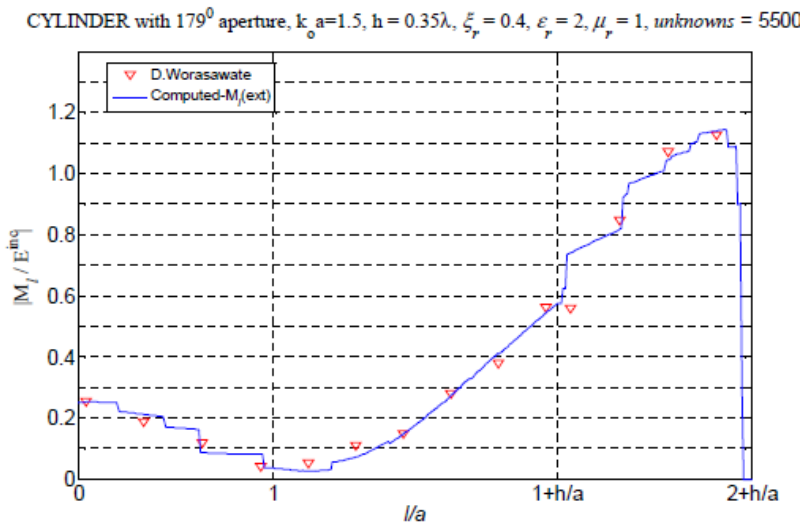


Figure 7-6.4.5 Magnitude of l -component of magnetic current in the $\phi = 0$ plane (taken from Altunkilic).

Graph readings of the Figure 7-6.4.4 and Figure 7-6.4.5 in which red markers represent the graph of D. warasawate show good agreement.

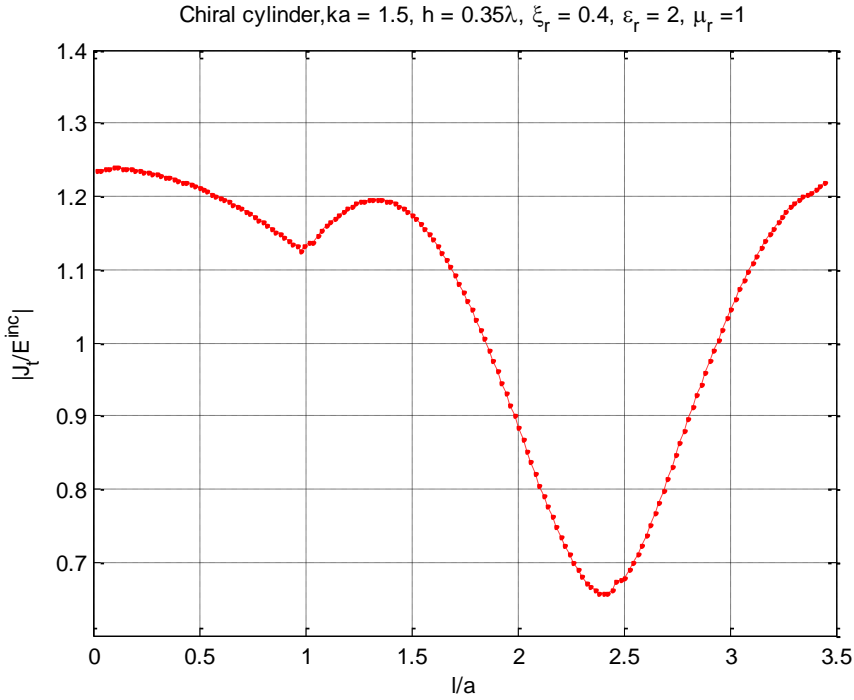


Figure 7-6.4.6 Magnitude of l -component of equivalent electric current in the $\phi = 0$ plane.

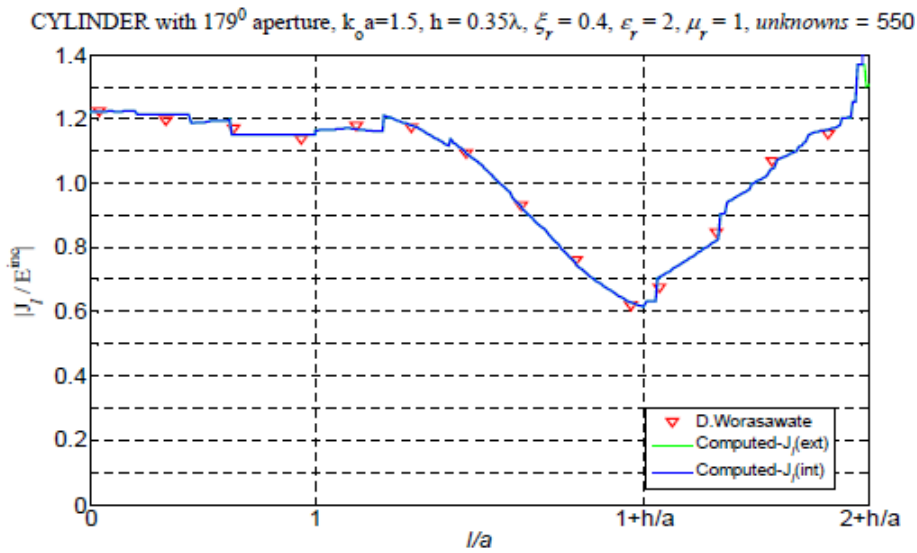


Figure 7-6.4.7 Magnitude of l -component of equivalent electric current in the $\phi = 0$ plane (taken from Altunkilic).

Graph readings of the Figure 7-6.4.6 and Figure 7-6.4.57 in which red markers represent the graph of D. warasawate show good agreement.

7-7 Empty Conducting Cylindrical Shell with an Aperture:

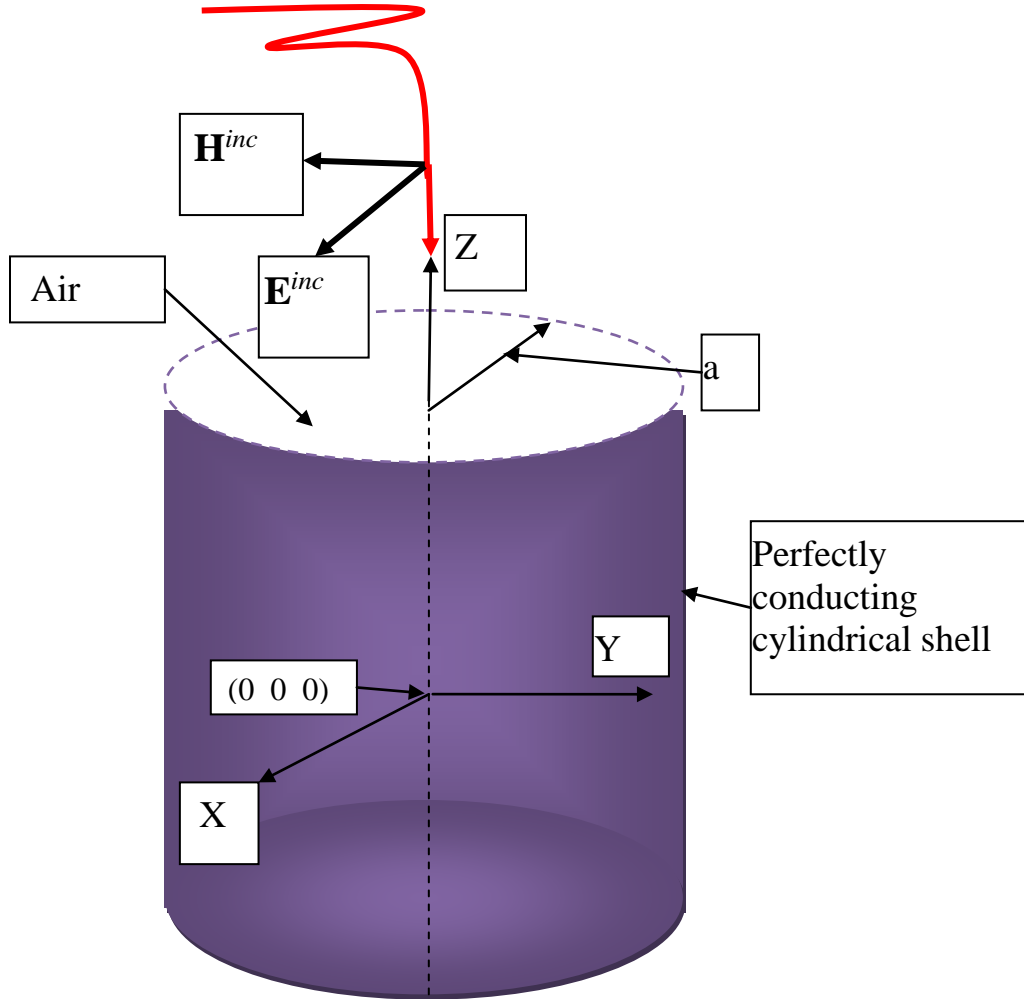


Figure 7-7 Plane wave incident on conducting shell of empty cylinder.

Figure 7-7 shows an empty conducting cylindrical shell top surface of which is open and has air ($\xi_r = 0, \epsilon_r = 1, \mu_r = 1$) inside it. Top surface of the cylinder is taken as aperture. Plane electromagnetic wave is illuminates from the top ($\theta^{inc} = 0^\circ$ and $\phi^{inc} = 0^\circ$) as shown in Figure 7-7.

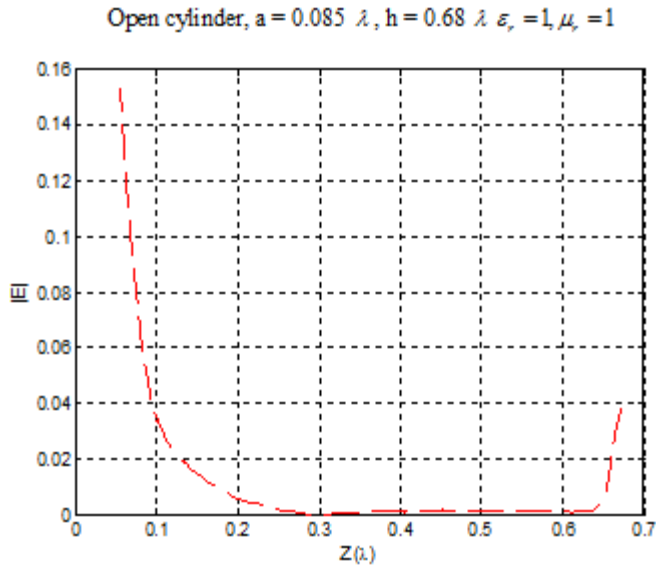


Figure 7-7.1 Amplitude of E -field on the axis of an open ended cylinder.

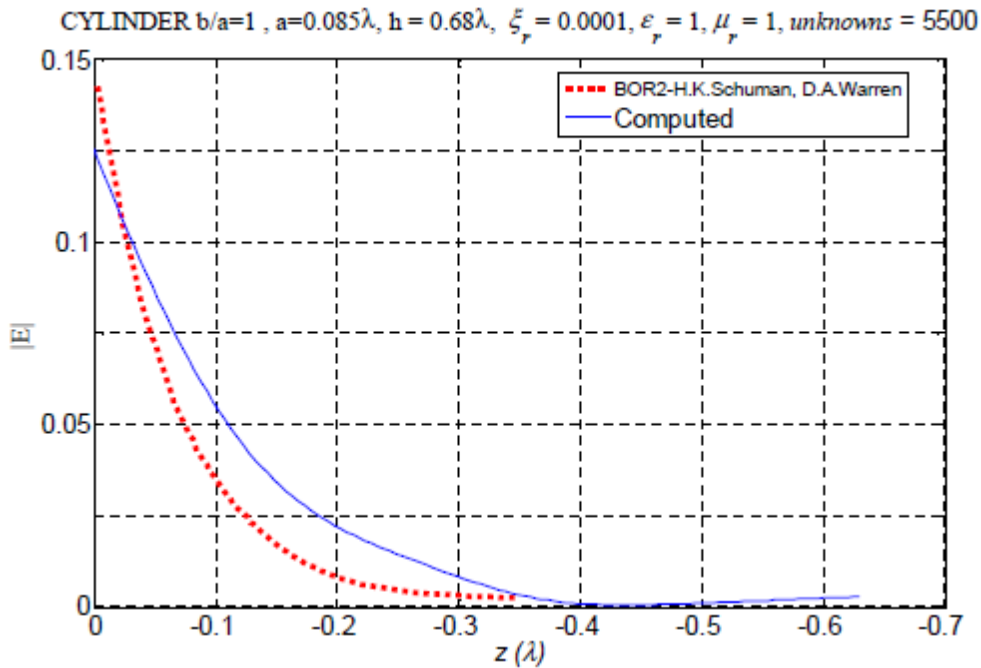


Figure 7-7.2 Amplitude of E -field on axis of an open ended cylinder (taken from Altunkilic).

Graphs of Figure 7-7.1 and Figure 7-7.2 show agreeable graph mapping.

7-8 Cylinder-shaped Perfectly Conducting Cylindrical Surface of Revolution enclosing Chiral material with $b/a = 0.5$ at its top.

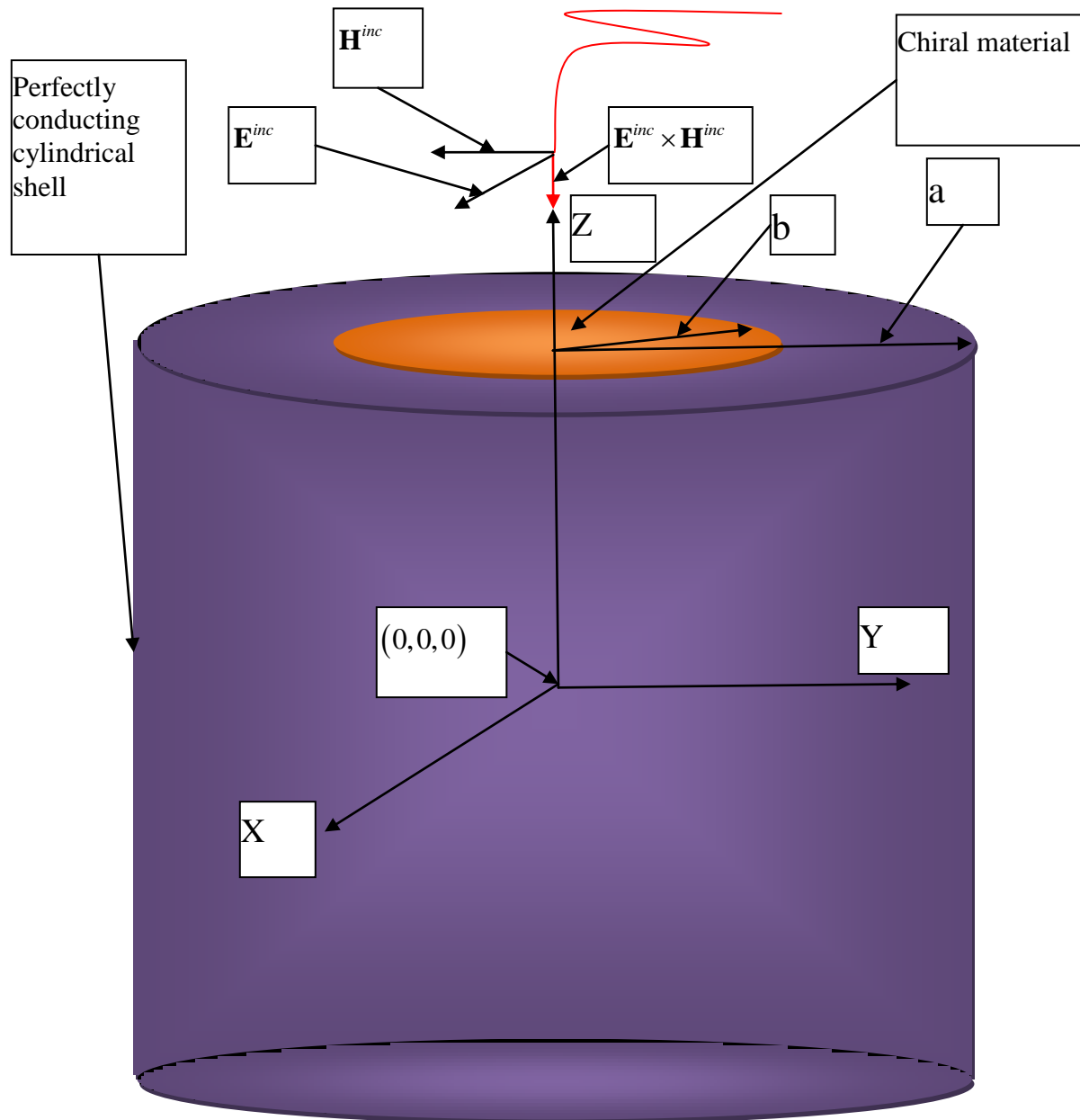


Figure 7-8 Plane electromagnetic wave impinges on the top of the cylinder.

7-8.1 Computed Results

Figures in this section include figures of the graphs plotted by the application of our numerical approach and the figures of the corresponding graphs obtained by Altunkilic [3] by the application of a distinctly different numerical approach than ours. Graphs taken from Altunkilic [3] are included for comparison purpose.

Figure 7-8.2.1 and the Figure 7-8.2.2 (taken from Altunkilic [3]), representing Magnitude of x-component of the internal E -field along z-axis, show close conformability of the graph mappings as well as the graph readings. Figure 7-8.2.3 and the Figure 7-8.2.4 (taken from Altunkilic [3]), representing Magnitude of y-component of the internal E -field along z-axis, also show close conformability of the graph mappings as well as the graph readings. Figure 7-8.3.1 and the Figure 7-8.3.2 (taken from Altunkilic [3]), representing bistatic co-polarized cross section $\sigma_{\theta\theta}$ of the obstacle, show close almost one hundred percent conformability of the graph mappings as well as the graph readings. Our graphs of the Figure 7-8.3.1 plotted for varying chiralities show overlapping of these graphs thereby pointing out clearly that chiralities of the chiral material do not affect $\sigma_{\theta\theta}$ of the obstacle in the far away zone. Figure 7-8.3.3 and the Figure 7-8.3.4 (taken from Altunkilic [3]), representing bistatic cross polarized cross section $\sigma_{\phi\theta}$ of the obstacle, show variance of the graph mappings as well as the graph readings. The graph readings of these two graphs are so extremely small that differences with respect to the pictorial conformability of these two graphs may be inconsequential. After all, the graphs of the Figure 7-8.3.3 and the Figure 7-8.3.4 (taken from Altunkilic [3]), are plotted using approximate values by applying two distinctly different numerical approaches.

Figure 7-8.4.1 and the Figure 7-8.4.2 (taken from Altunkilic [3]), representing magnitude of l -component of magnetic current in the $\phi = 0$ plane show one hundred percent conformability of the graph mappings as well as the graph readings on the conducting surface (about 85% of the total cylindrical surface). However, our graph of the Figure 7-8.4.1 shows sharp up and down swings in the aperture space (about 15% of the total cylinder surface). However, the red colored graph of the Figure 7-8.4.1 plotted for the chirality value of $\xi_r = 0.3$ gives the position of the average value of the graph reading in the aperture space as 0.15. The green colored graph of the Figure 7-8.4.1 plotted for the chirality value of $\xi_r = 0.7$ gives the position of the average value of the graph reading in the aperture space as 0.5. The reason for these fluctuation in the aperture space are thoroughly discussed and summarized above in a paragraph in *italic* in the the context of the surface current graphs of the sphere. The graph of the Figure 7-8.4.2 (taken from Altunkilic [3]) shows up and down zigzagging in direction along the course of the graph mapping in the aperture space.

Figure 7-8.4.3 and the Figure 7-8.4.4 (taken from Altunkilic [3]) representing magnitude of t -component of magnetic current in the $\phi = 0$ plane show one hundred percent conformability of the graph mappings as well as the graph readings on the conducting surface (about 85% of the total cylindrical surface). Reason for the variations of the graph mapping in the aperture space in our graph of the Figure 7-8.4.3 is the same as that explained above.

Our graphs of the Figure 7-8.4.5 representing magnitude of l -component of physical electric current in the $\phi=0$ plane show smooth graph mapping of both the graphs on the conducting surface of the cylinder (about 85% of the total cylindrical surface) and show correct zero values in the aperture space. Graphs of the Figure 7-8.4.6 (taken from Altunkilic [3]) representing magnitude of l -component of physical electric current in the $\phi=0$ plane show correct zero values in the aperture space. However, these graphs show up and down zigzagging in direction along the course of the graph mapping on the conducting surface. Graph readings of our graph of the Figure 7-8.4.5 differ slightly on the conducting surface from the graph readings of the Figure 7-8.4.6 (taken from Altunkilic [3]) on the conducting surface. The reason for the slight variations in the graph readings is due to the approximate values used, based on the different numerical approaches, in the compilation of ours and Altunkilic's graphs.

Our graphs of the Figure 7-8.4.7 representing magnitude of t -component of physical electric current in the $\phi=0$ plane show smooth graph mapping of both the graphs on the conducting surface of the cylinder (about 85% of the total cylindrical surface) and show correct zero values in the aperture space. In Matlab overlapping of the graphs is shown in a single color. Graphs of the Figure 7-8.4.8 (taken from Altunkilic [3]) representing magnitude of t -component of physical electric current in the $\phi=0$ plane do not show zero values in the aperture space. His graphs show up and down zigzagging in direction along the course of the graph mapping on the conducting surface as well as in the aperture space. Altunkilic's graphs of the Figure 7-8.4.8 incorrectly do not show zero values in the aperture space. Graph readings of our graph of the Figure 7-8.4.7 differ slightly on the conducting surface but sharply in the aperture space from the graph readings of the Figure 7-8.4.8 (taken from Altunkilic [3]). The reason for the variations in the graph readings is due to the approximate values used, based on the different numerical approaches, in the compilation of ours and Altunkilic's graphs.

All the graphs produced in this section involve two matrices of 688×688 compared to the huge size matrix from a size of 5500×5500 up to a size of 6350×6350 used by Altunkilic [3] for producing each of his graphs. We thus save enormous amount of computer memory and computational time.

7-8.2 Internal Fields

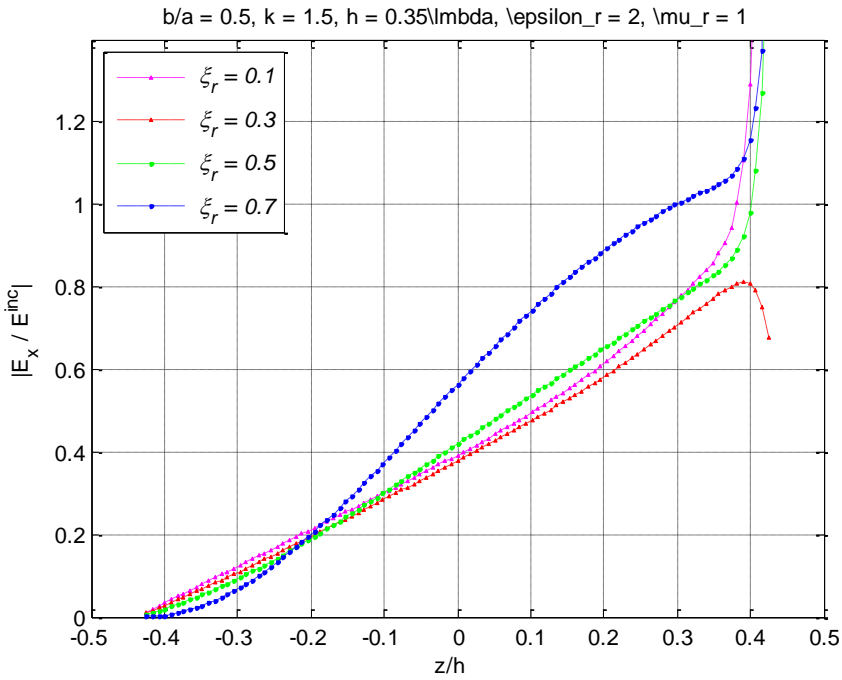


Figure 7-8.2.1 Magnitude of x-component of the internal E -field along z -axis.

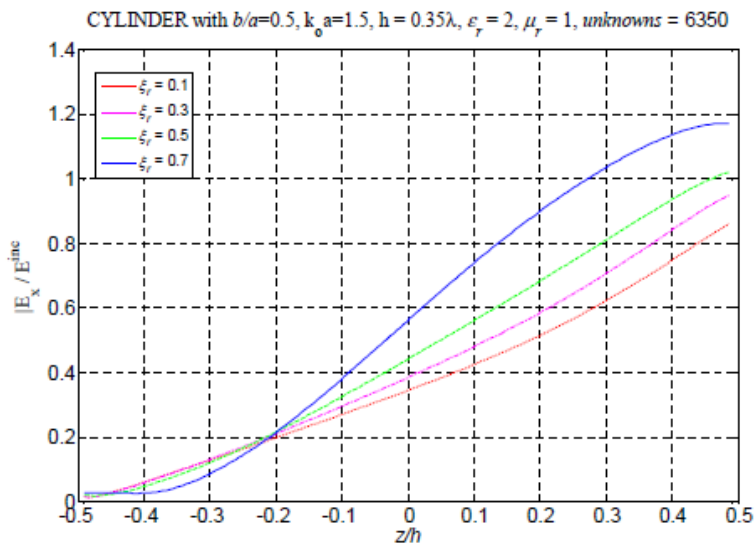


Figure 7-8.2.2 Magnitude of x-component of the internal E -field along z -axis (taken from Altunkilic [3]).

Our graph of Figure 7-8.2.1 is pictorially in good agreement to a great extent with the graph of Figure 7-8.2.2 (taken from Altunkilic [3]).

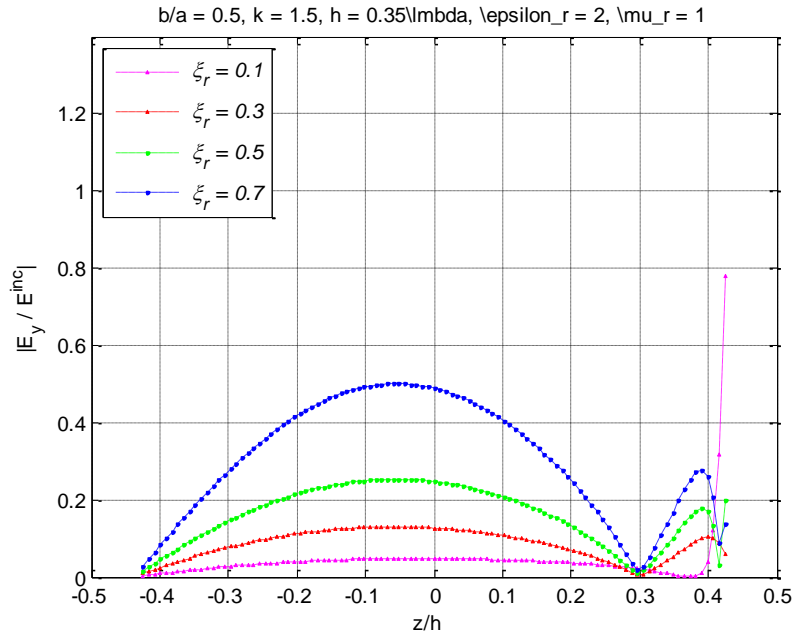


Figure 7-8.2.3 Magnitude of y-component of the internal E -field along z -axis.

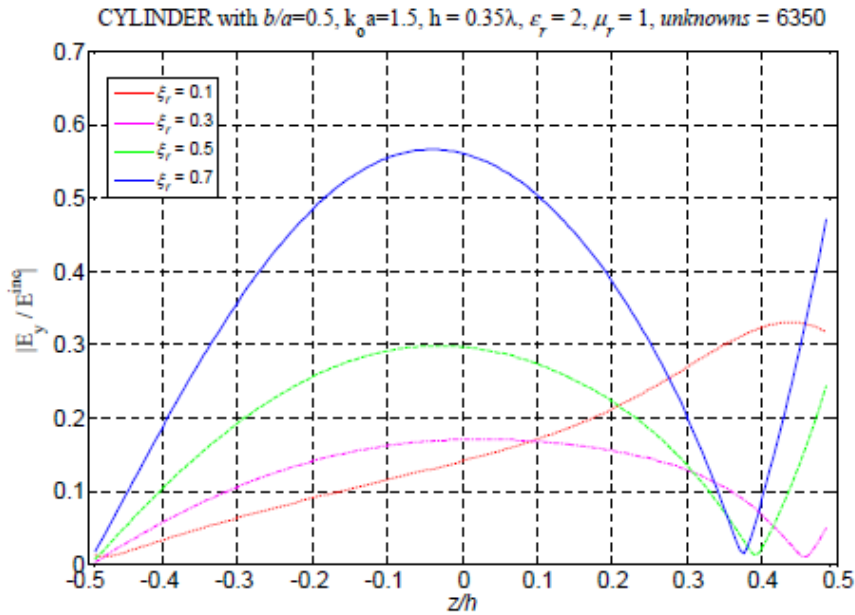


Figure 7-8.2.4 Magnitude of y-component of the internal E -field along the z -axis (taken from Altunkilic [3]).

Our graph of Figure 7-8.2.3 is pictorially in good agreement to a great extent with the graph of Figure 7-8.2.4 (taken from Altunkilic [3]).

7-8.3 Chirality versus Bistatic Radar Cross Sections (RCS)

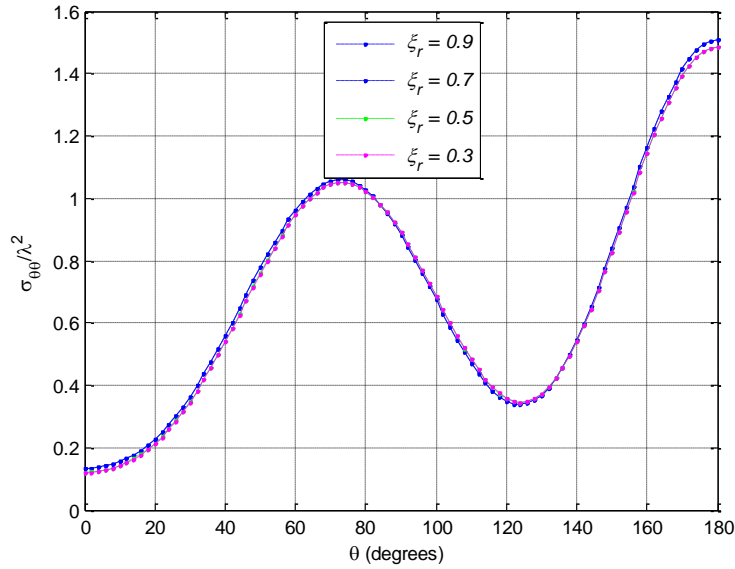


Figure 7-8.3.1 $\sigma_{\theta\theta}$ of the obstacle.

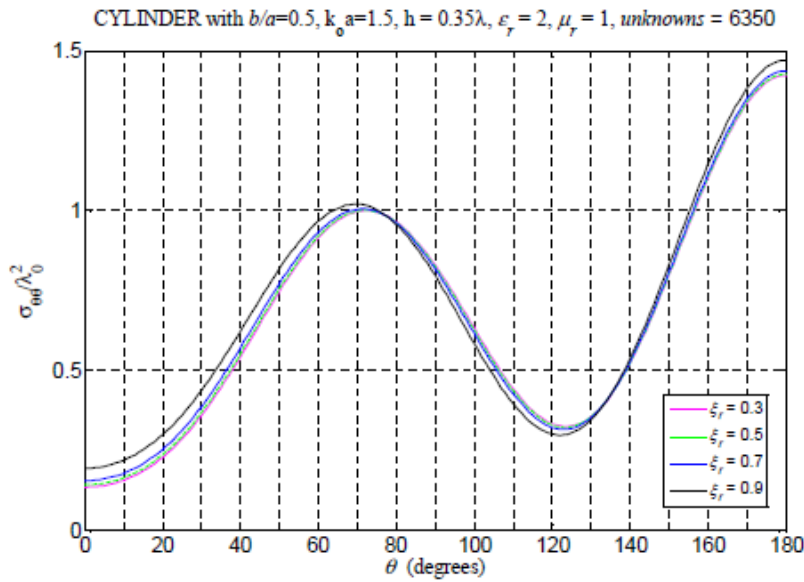


Figure 7-8.3.2 $\sigma_{\theta\theta}$ of the obstacle (taken from Altunkilic [3]).

Graphs of Figure 7-8.3.1 and Figure 7-8.3.2 show striking almost one hundred percent resemblance.

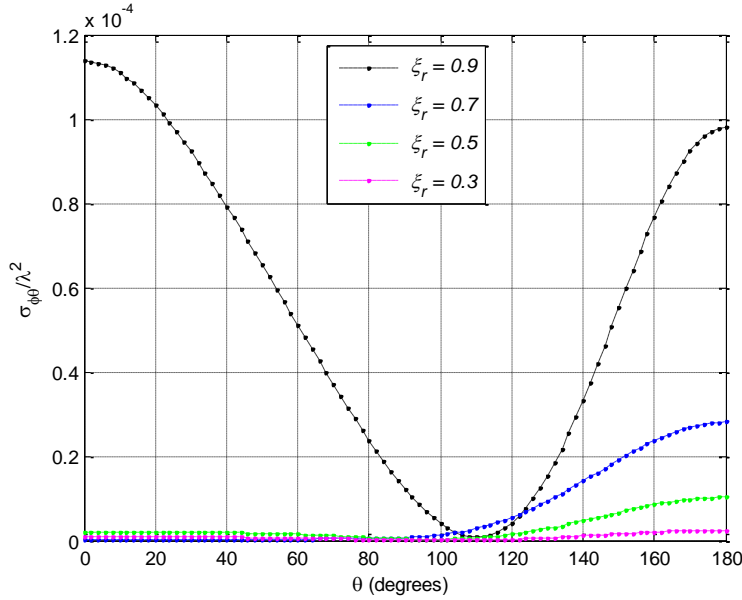


Figure 7-8.3.3 $\sigma_{\phi\theta}$ of the obstacle.

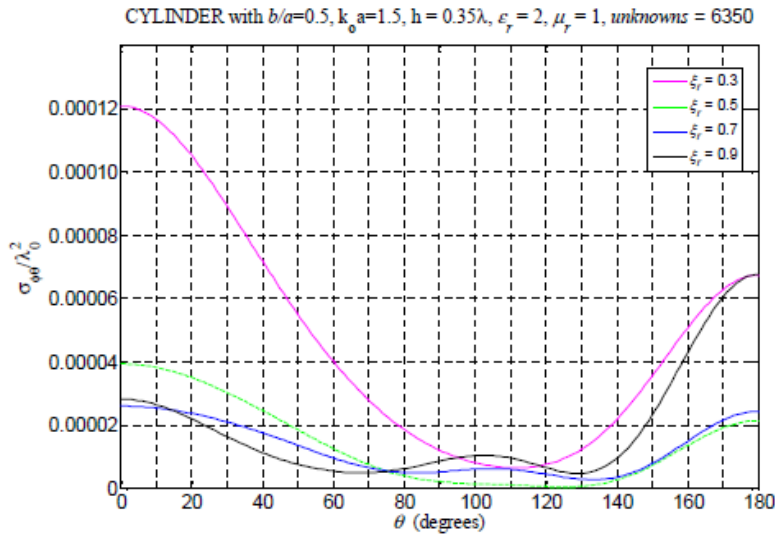


Figure 7-8.3.4 $\sigma_{\phi\theta}$ of the obstacle (taken from Altunkilic [3]).

Graphs of Figure 7-8.3.4 and Figure 7-8.3.4 represent cross polarization and as expected have insignificant graph readings. The accuracy of one graph relative to that of the other cannot be evaluated because both graphs are approximate.

7-8.4 Chirality versus Surface Currents

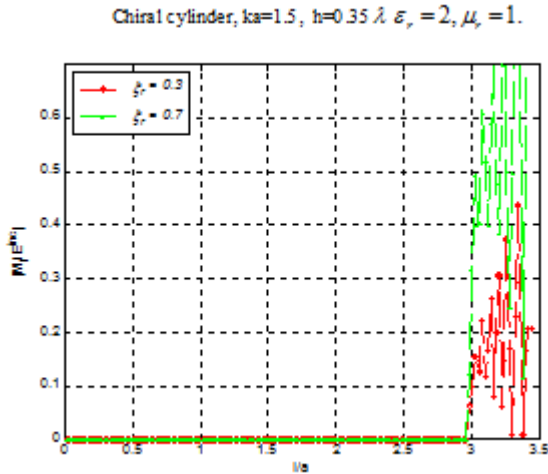


Figure 7-8.4.1 Magnitude of l -component of magnetic current in the $\phi = 0$ plane.

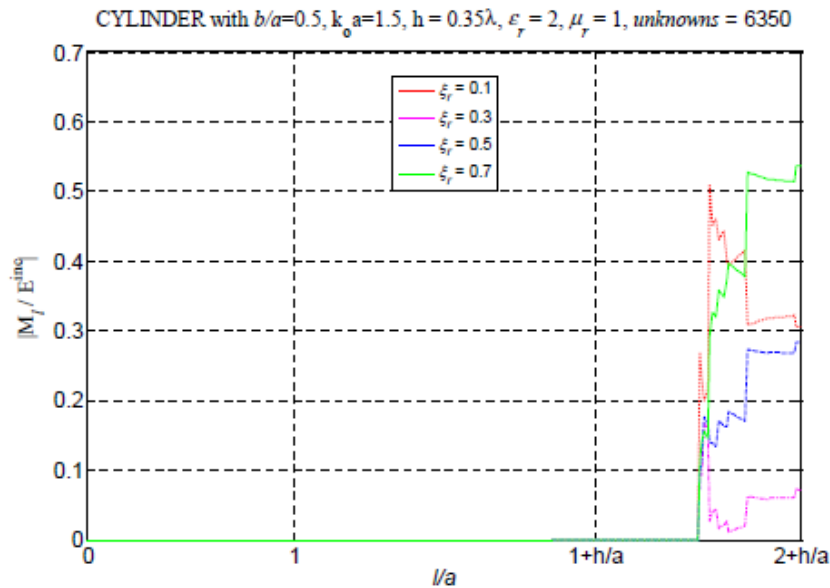


Figure 7-8.4.2 Magnitude of l -component of magnetic current in the $\phi = 0$ plane (taken from Altunkilic [3]).

Graphs of Figure 7-8.1.9 and Figure 7-8.1.10 as expected show zero values on the perfectly conducting surface. These graphs show different up and down variations in the chiral space. These variances shown in the chiral space of these two graphs cannot be evaluated because of the fact that both of these graphs are obtained by the application of two distinctly different numerical approaches.

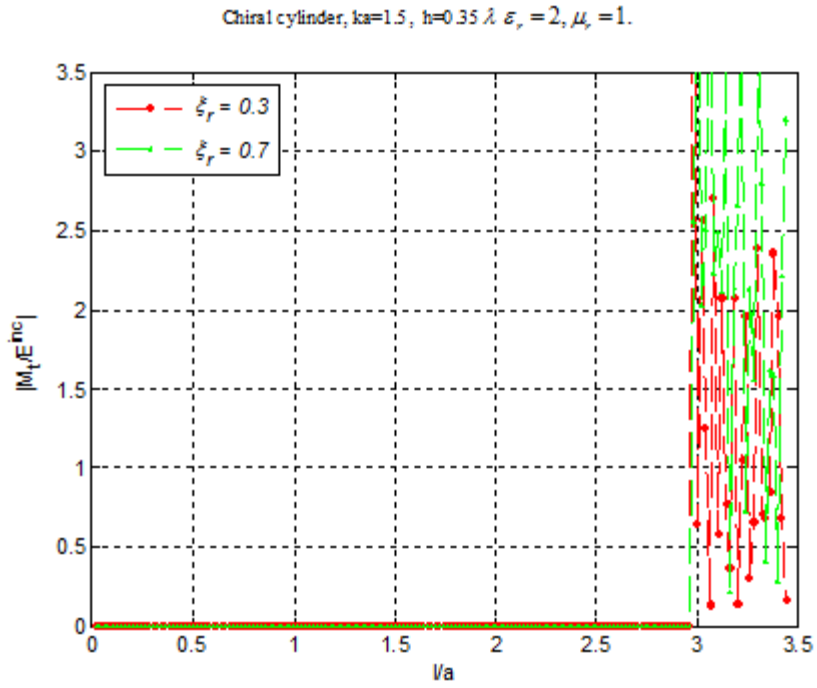


Figure 7-8.4.3 Magnitude of \hat{t} -component of magnetic current in the $\phi = 0$ plane.

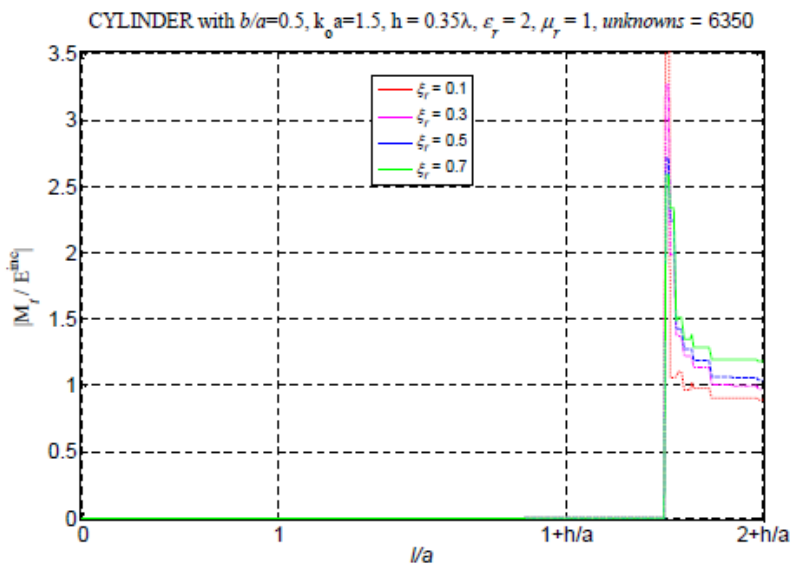


Figure 7-8.4.4 Magnitude of \hat{t} -component of magnetic current in the $\phi = 0$ plane (taken from Altunkilic [3]).

Graphs of Figure 7-8.4.3 and Figure 7-8.4.4 as expected show zero value on the perfectly conducting surface. These graphs show different up and down variations in the chiral space. These

variances shown in the chiral space of these two graphs cannot be evaluated because of the fact that both of these graphs are approximate graphs.

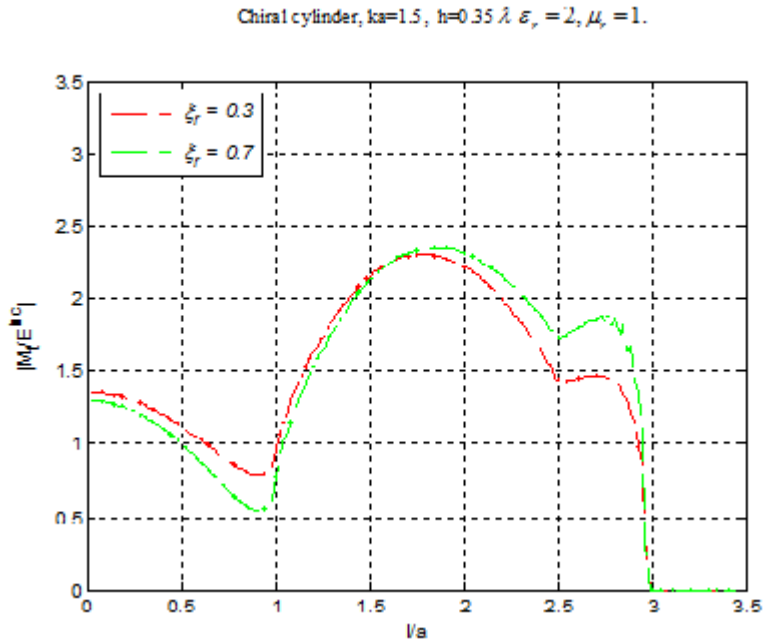


Figure 7-8.4.5 Magnitude of l -component of physical electric current in the $\phi=0$ plane.

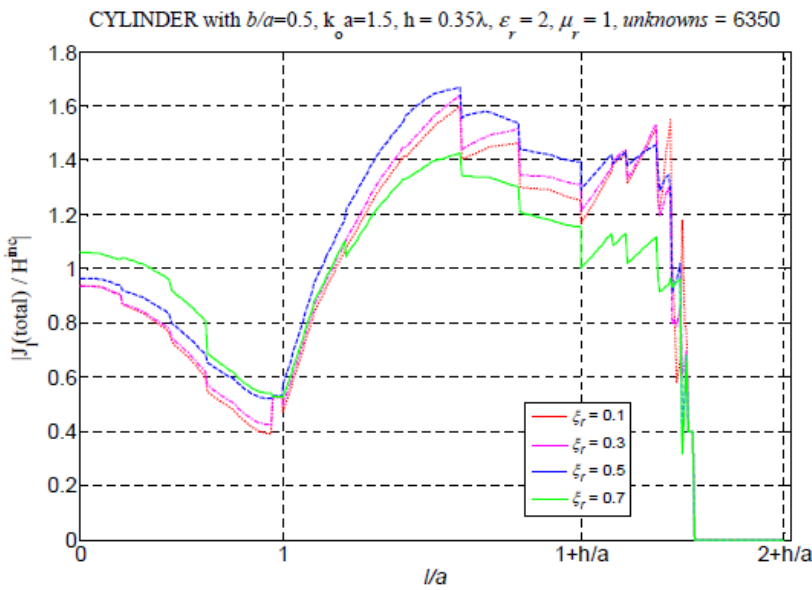


Figure 7-8.4.6 Magnitude of l -component of physical electric current in the $\phi=0$ plane (taken from Altunkilic [3]).

Graphs of Figure 7-8.4.5 and Figure 7-8.4.6 (taken from Altunkilic [3]), as expected, show zero values over the chiral surface. Our graph of Figure 7-8.4.5 is smooth and is free from any zigzag direction changes along the course of graph mapping in the conductor space. Variations in graph readings between these two graphs cannot be evaluated because of the fact that both of these graphs are produced by the application of two distinctly different numerical approaches.

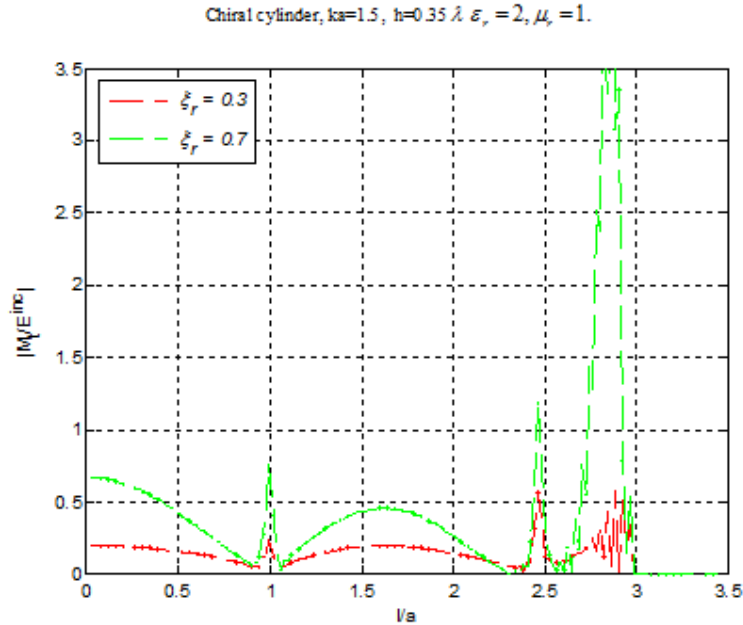


Figure 7-8.4.7 Magnitude of t -component of physical electric current in the $\phi = 0$ plane.

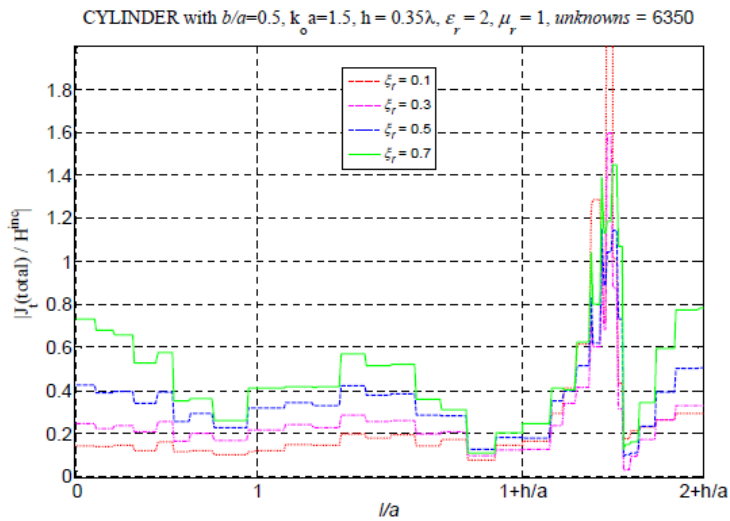


Figure 7-8.4.8 Magnitude of t -component of physical electric current in the $\phi = 0$ plane (taken from Altunkilic [3]).

Our graph of Figure 7-8.4.7 unlike the graph of Figure 7-8.4.8 (taken from Altunkilic [3]), as expected, shows zero values of physical current in the aperture space and is smooth and free from zigzagging in direction on the conducting surface except at the edge of the aperture.

7-9 Perfectly Conducting Cylindrical surface of revolution enclosing Chiral material with an Aperture ratio of $b/a = 1$ at its top.

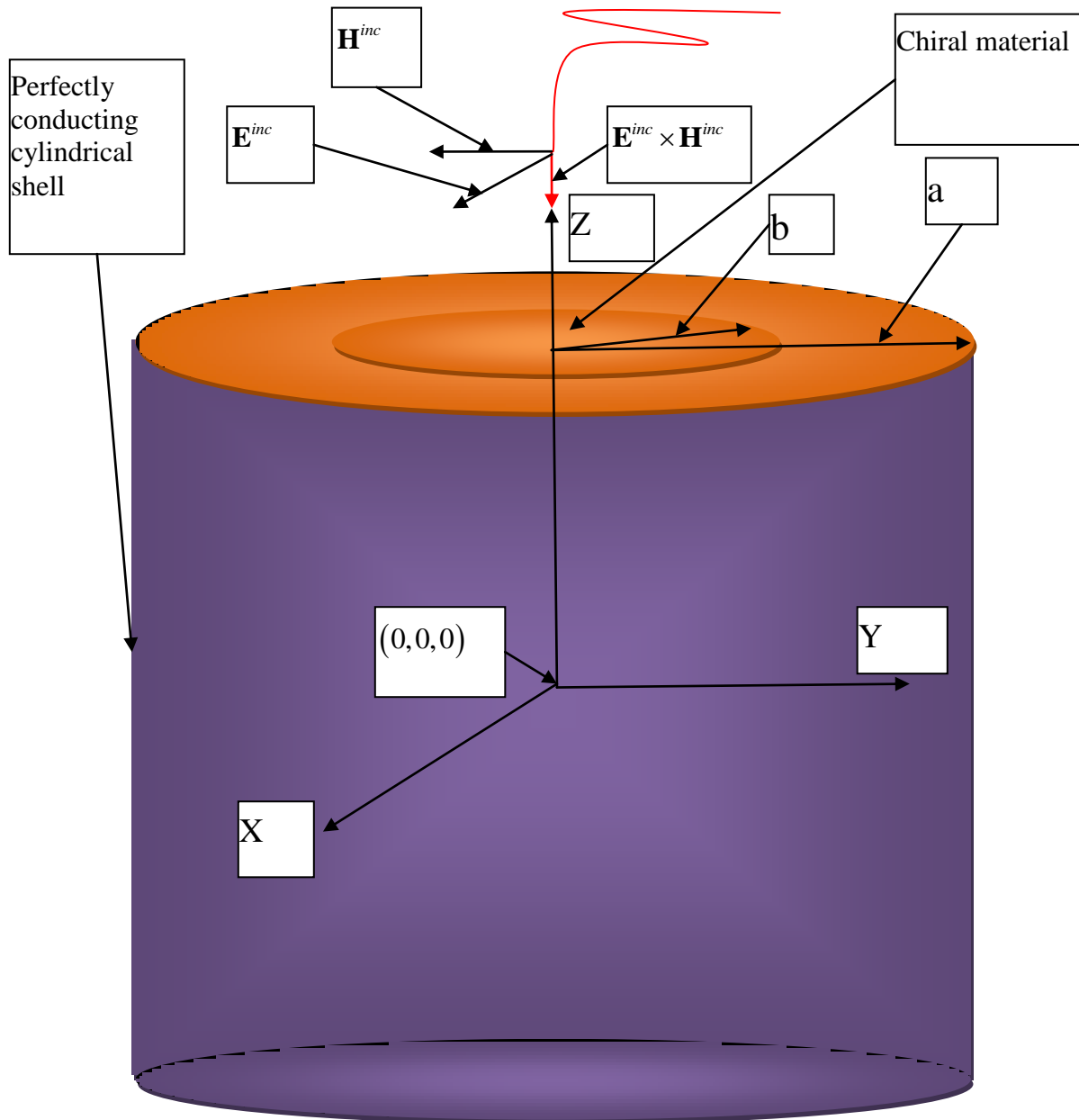


Figure 7-9 Plane electromagnetic wave impinges on the top of the cylinder.

(**Figure 7-9 will be the frame of reference in relation to the results and the graphs that are obtained in the following sections**).

7-9.1 Computed Results

Figures in this section include figures of the graphs plotted by the application of our numerical approach and the figures of the corresponding graphs obtained by Altunkilic [3] by the application of a distinctly different numerical approach than ours. Graphs taken from Altunkilic [3] are included for comparison purpose.

Figure 7-9.2.1 and the Figure 7-9.2.2 (taken from Altunkilic [3]), representing Magnitude of x-component of the internal E -field along z-axis, show close conformability of the graph mappings as well as the graph readings. Figure 7-9.2.3 and the Figure 7-9.2.4 (taken from Altunkilic [3]), representing Magnitude of y-component of the internal E -field along z-axis, also show close almost one hundred percent conformability of the graph mappings as well as the graph readings. Figure 7-9.3.1 and the Figure 7-9.3.2 (taken from Altunkilic [3]), representing bistatic co-polarized cross section $\sigma_{\theta\theta}$ of the obstacle, show striking almost one hundred percent conformability of the graph mappings as well as the graph readings. Figure 7-9.3.3 and the Figure 7-9.3.4 (taken from Altunkilic [3]), representing bistatic cross polarized cross section $\sigma_{\phi\theta}$ of the obstacle, show variance of the graph mappings as well as the graph readings. The graph readings of these two graphs are so extremely small that differences with respect to the pictorial conformability of these two graphs are not worthy of great weight. After all, the graphs of the Figure 7-9.3.3 and the Figure 7-9.3.4 (taken from Altunkilic [3]), are plotted using approximate values by applying two distinctly different numerical approaches.

Figure 7-9.4.1 and the Figure 7-9.4.2 (taken from Altunkilic [3]), representing magnitude of t -component of magnetic current in the $\phi = 0$ plane show one hundred percent conformability of the graph mappings as well as the graph readings on the conducting surface (about 85% of the total cylindrical surface). However, our graph of the Figure 7-9.4.1 shows sharp up and down swings in the aperture space (about 15% of the total cylinder surface). However, the red colored graph of the Figure 7-9.4.1 plotted for the chirality value of $\xi_r = 0.3$ gives the position of the average value of the graph reading in the aperture space approximately as 3.5. The blue colored graph of the Figure 7-9.4.1 plotted for the chirality value of $\xi_r = 0.5$ gives the position of the average value of the graph reading in the aperture space approximately as 3.5. The reason for these fluctuation in the aperture space are thoroughly discussed and summarized above in a paragraph in the context of the surface current graphs of the sphere. The graphs of the Figure 7-9.4.2 (taken from Altunkilic [3]) show up and down unexplainable zigzagging in direction along the course of the graph mapping in the aperture space.

Figure 7-9.4.3 and the Figure 7-9.4.4 (taken from Altunkilic [3]) representing magnitude of l -component of magnetic current in the $\phi = 0$ plane show one hundred percent conformability of the graph mappings as well as the graph readings on the conducting surface (about 85% of the total cylindrical surface). Our graph of the Figure 7-9.4.3 produces smooth curves in the aperture space.

The graph of the Figure 7-9.4.4 (taken from Altunkilic [3]) shows up and down unexplainable zigzagging in direction along the course of the graph mapping in the aperture space. Comparison of the graph readings between these two set of graphs in the aperture space is impossible.

Our graphs of the Figure 7-9.4.5 representing magnitude of t -component of physical electric current in the $\phi=0$ plane show smoothness on the conducting surface of the cylinder. The three graphs of the Figure 7-9.4.5 for the chiralities of $\xi_r = 0.1, \xi_r = 0.3$, and $\xi_r = 0.5$, as expected, show zero values in the aperture space. These three graphs overlap in the aperture space showing just one color representing zero values instead of the three colors. The graphs of the Figure 7-9.4.6 (taken from Altunkilic [3]) show up and down unexplainable zigzagging in direction along the course of the graph mapping not only on the conducting surface but in the aperture space as well. Only one of the graphs of the Figure 7-9.4.6 (taken from Altunkilic [3]) that corresponds to the chirality of $\xi_r = 0.1$ shows zero values in the aperture space.

Graphs of the Figure 7-9.4.7 and the Figure 7-9.4.8 (taken from Altunkilic [3]), representing magnitude of l -component of the physical current in the $\phi=0$ plane show zero values in the aperture space (about 15% of the total cylindrical surface). Our graphs of the Figure 7-9.4.7 show smooth curves on the conducting surface. The graphs of the Figure 7-9.4.2 (taken from Altunkilic [3]) show up and down unexplainable zigzagging in direction along the course of the graph mapping in the aperture space. It is difficult to compare the graph readings between these two set of graphs. The graph plotted for the chirality value of $\xi_r = 0.5$ shows a peak value of about 2.3 right at the left end of the graph in our graph as well as in the graph of Altunkilic [3]. However, graphs representing the chiralities of $\xi_r = 0.1$ and $\xi_r = 0.3$ show variance in the graph readings all along the graph mappings.

All the graphs produced in this section involve two matrices of 688×688 compared to the huge size matrix from a size of 5500×5500 up to a size of 6350×6350 used by Altunkilic [3] for producing each of his graphs. We thus save enormous amount of computer memory and computational time.

7-9.2 Internal Fields

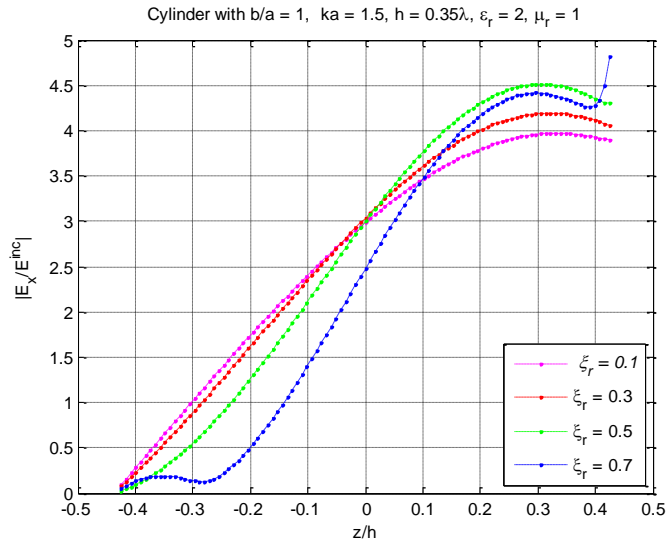


Figure 7-9.2.1 Magnitude of x-component of the internal E -field along z -axis.

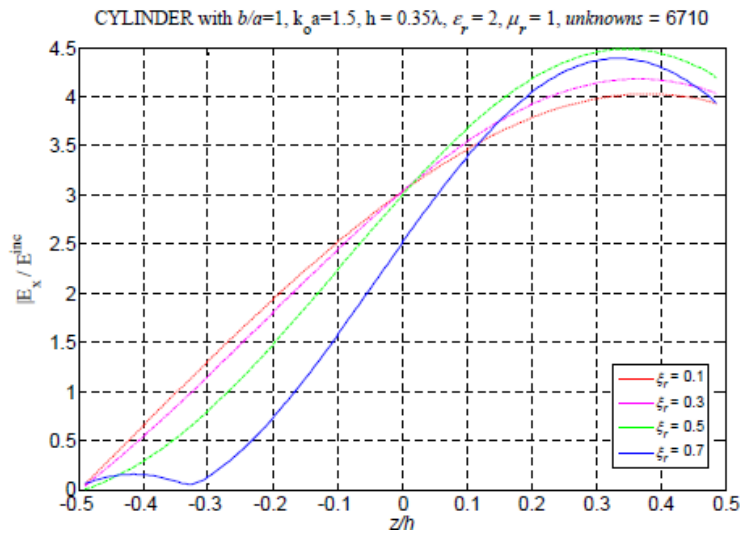


Figure 7-9.2.2 Magnitude of x-component of the internal E -field along z -axis (taken from Altunkilic).

Graph of the Figure 7-9.2.1 shows good agreement with the graph of Figure 7-9.2.2 (taken from Altunkilic).

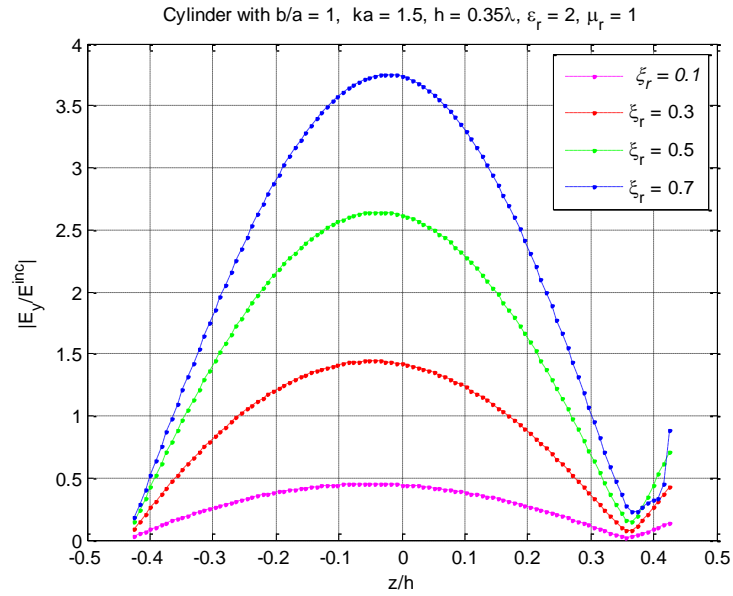


Figure 7-9.2.3 Magnitude of y-component of the internal E -field along z -axis

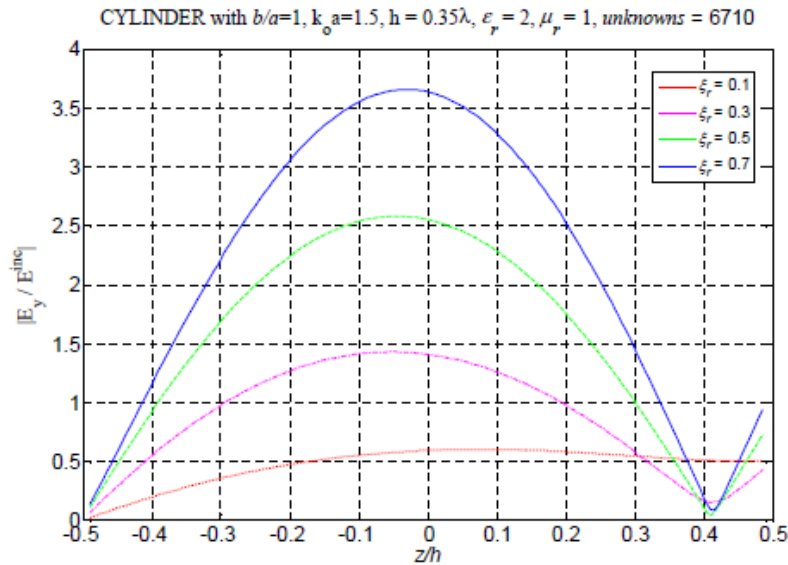


Figure 7-9.2.4 Magnitude of y-component of the internal E -field along z -axis (taken from Altunkilic).

Our graph of the Figure 7.9.2.3 shows striking resemblance with the graph of Figure 7.9.2.4 (taken from Altunkilic).

7-9.3 Chirality versus Bistatic Radar Cross Sections (RCS)

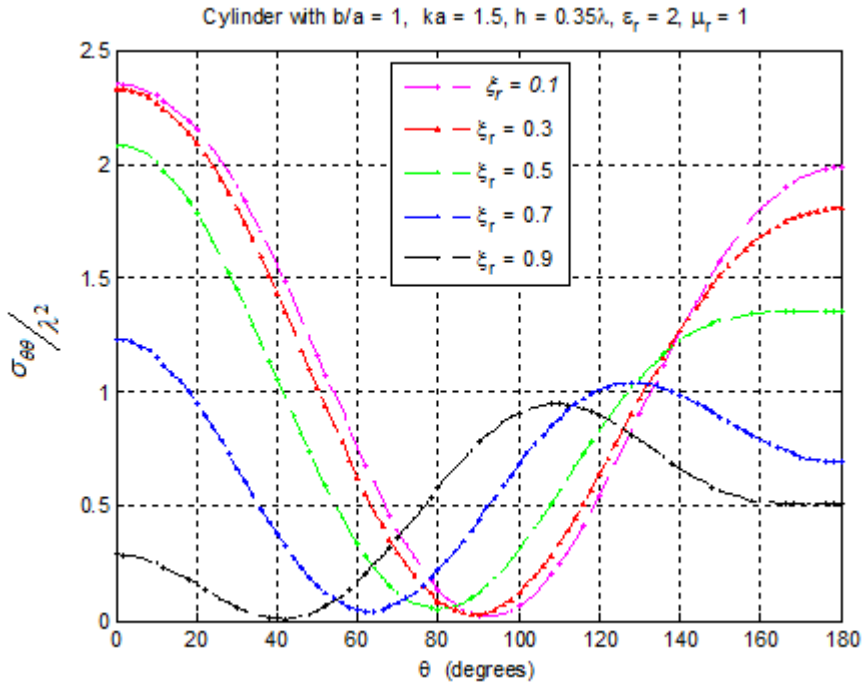


Figure 7-9.3.1 σ_{ee} of the obstacle.

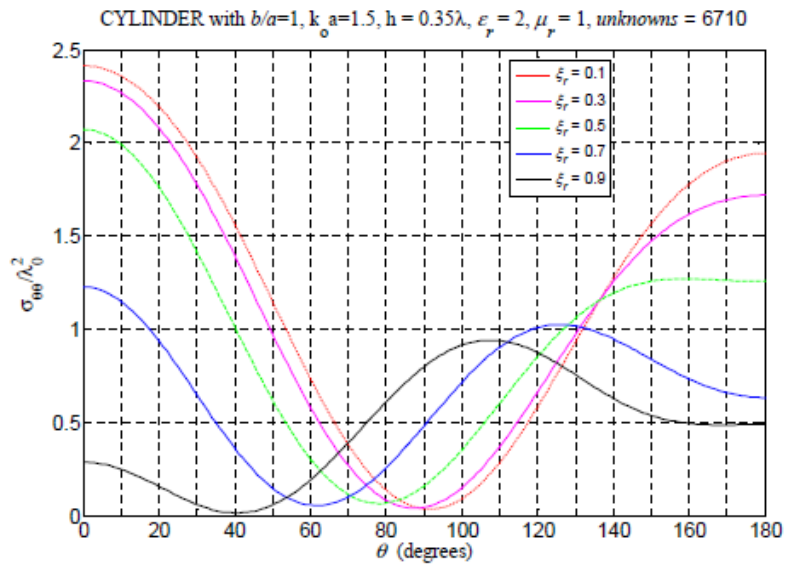


Figure 7-9.3.2 σ_{ee} of the obstacle (taken from Altunkilic).

Our graph of the Figure 7-9.3.1 shows marked almost one hundred percent resemblance to the graph of Figure 7-9.3.2 (taken from Altunklic).

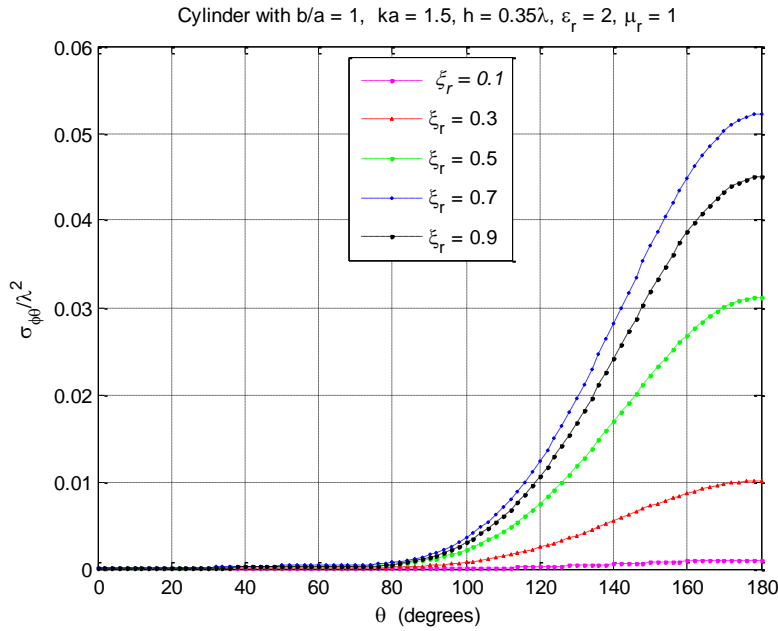


Figure 7-9.3.3 $\sigma_{\phi\theta}$ of the obstacle.

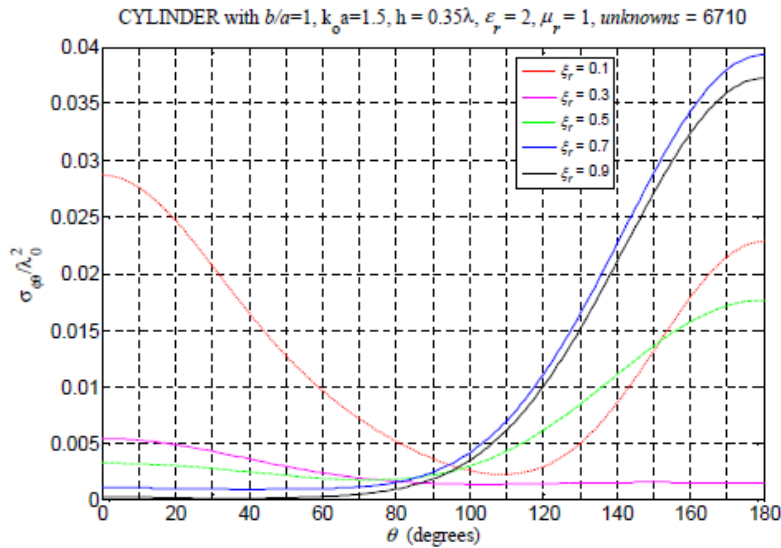


Figure 7-9.3.4 $\sigma_{\phi\theta}$ of the obstacle (taken from Altunklic).

Graph of the Figure 7-9.3.3 and the Figure 7-9.3.4 represent cross polarization and as expected have small graph readings. The accuracy of one graph relative to that of the other cannot be evaluated because both graphs are approximate.

7-9.4 Chirality versus Surface Currents

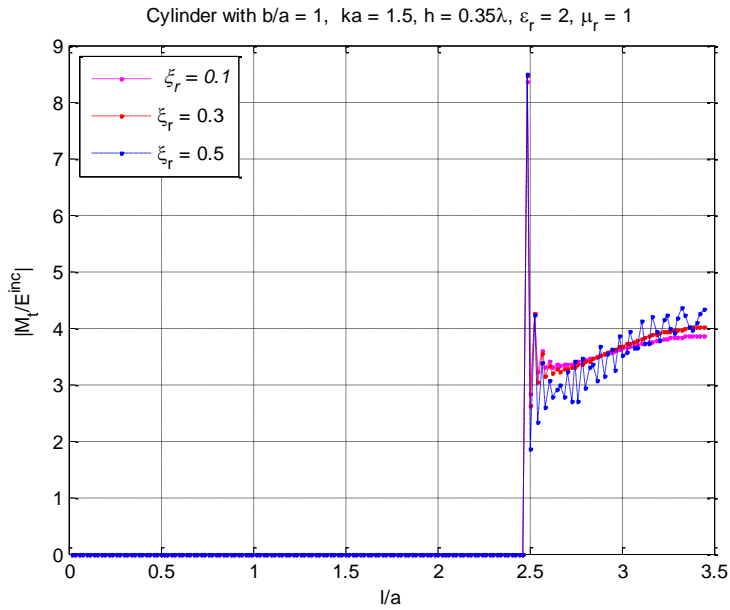


Figure 7-9.4.1 Magnitude of t -component of magnetic current in $\phi = 0$ plane.

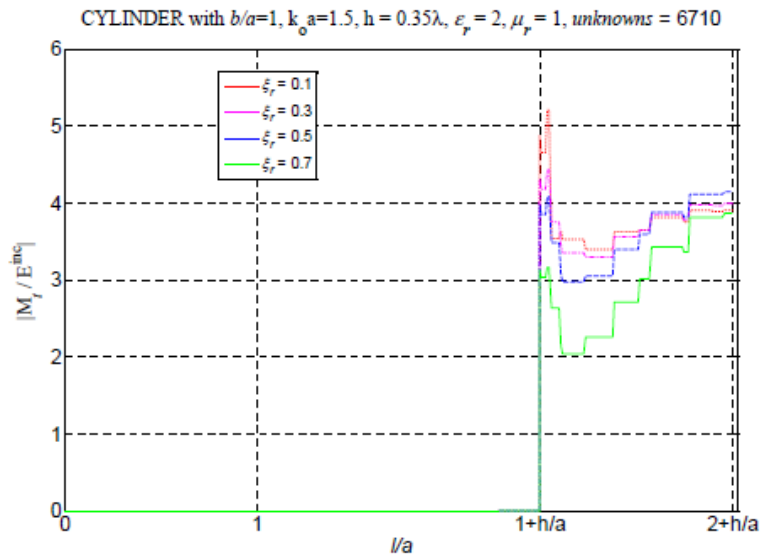


Figure 7-9.4.2 Magnitude of t -component of magnetic current in $\phi = 0$ plane (taken from Altunkilic).

Graph of the Figure 7-9.4.1 shows, as expected, is one hundred percent accurate with respect to the graph of the Figure 7-9.4.2 (taken from Altunkilic) on the conducting surface (both showing zero values) which is almost 85 % of the total conducting cylinder shaped BOR space which encloses

chiral material and exposes it through an aperture at its top. The up and down variations in these two graphs in the chiral space (about 15% of the total cylinder surface), with respect to each other, cannot be evaluated because both these graphs are produced by approximate numerical values. However, it is to be noted that in the chiral space both graphs give almost the same average value.

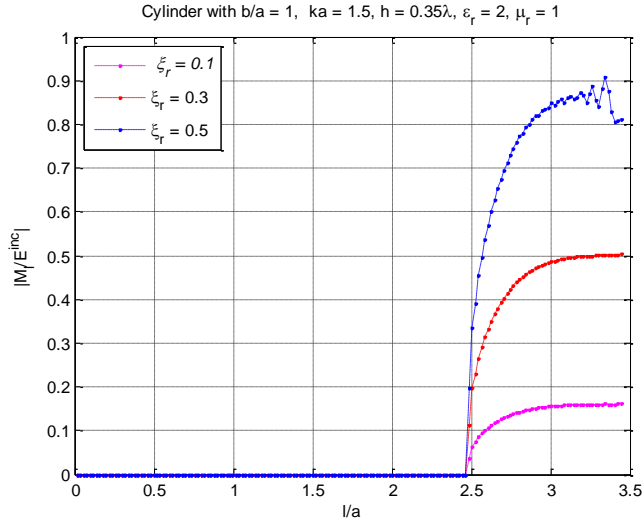


Figure 7-9.4.3 Magnitude of l -component of magnetic current in $\phi = 0$ plane.

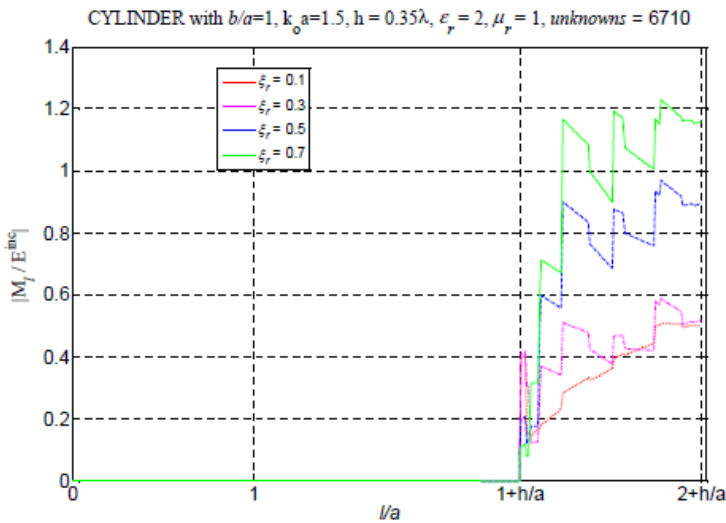


Figure 7-9.4.4 Magnitude of l -component of magnetic current in $\phi = 0$ plane (taken from Altunkilic).

Graph of the Figure 7.8.4.3 shows, as expected, one hundred percent accuracy with respect to the graph of the Figure 7-9.4.4 (taken from Altunkilic) on the conducting surface. Both graphs showing zero values in the conducting space which is almost 85 % of the total conducting cylinder surface

which encloses chiral material and exposes it through an aperture at its top. The up and down variations in these two graphs in the chiral space (about 15 % of the total cylinder surface) with respect to each other cannot be evaluated because both these graphs are produced by approximate numerical values. However, it is to be noted that in the chiral space both graphs give almost the same average value. It is also to be noted that our graph of the Figure 7-9.4.3, unlike the graph of the Figure 7-9.4.4, shows smooth curves in the chiral space.

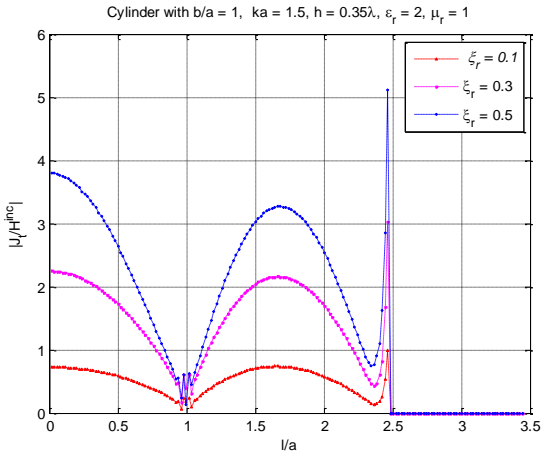


Figure 7-9.4.5 Magnitude of t -component of physical electric current in the $\phi = 0$ plane.

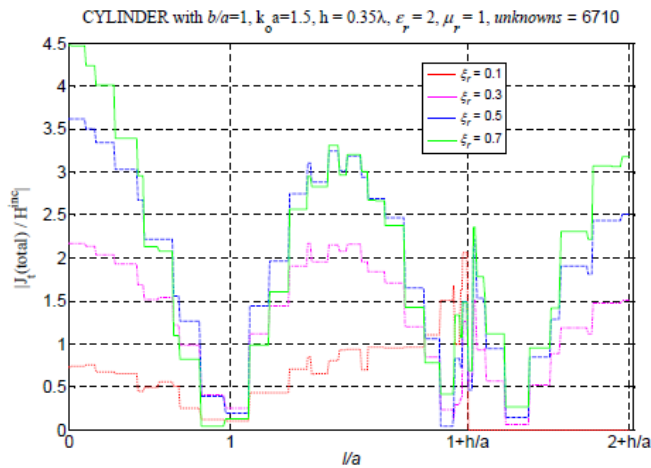


Figure 7-9.4.6 Magnitude of t -component of physical electric current in the $\phi = 0$ plane (taken from Altunkilic).

Graph of the Figure 7-9.4.5, unlike the graph of the Figure 7-9.4.6 (taken from Altunkilic), shows smooth curves joined with abrupt upward swings at 1 meter and $(1+h/a)$ meter. The reason for this abrupt changes is thoroughly explained above. Our graph of the Figure 7-9.4.5, unlike the graph of the Figure 7-9.4.6 (taken from Altunkilic), correctly shows zero values for all the chiralities in the aperture space. Correctness of our graph with respect to the graph taken from Altunkilic cannot be

evaluated because of the fact that both of these graphs are produced by different numerical approaches.

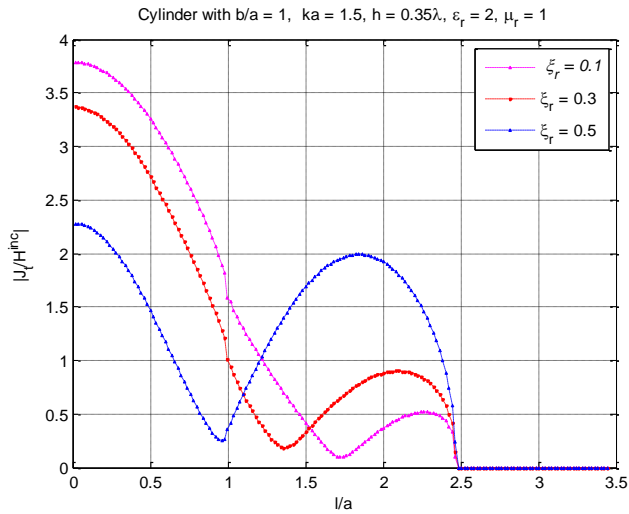


Figure 7-9.4.7 Magnitude of l -component of physical electric current in the $\phi = 0$ plane.

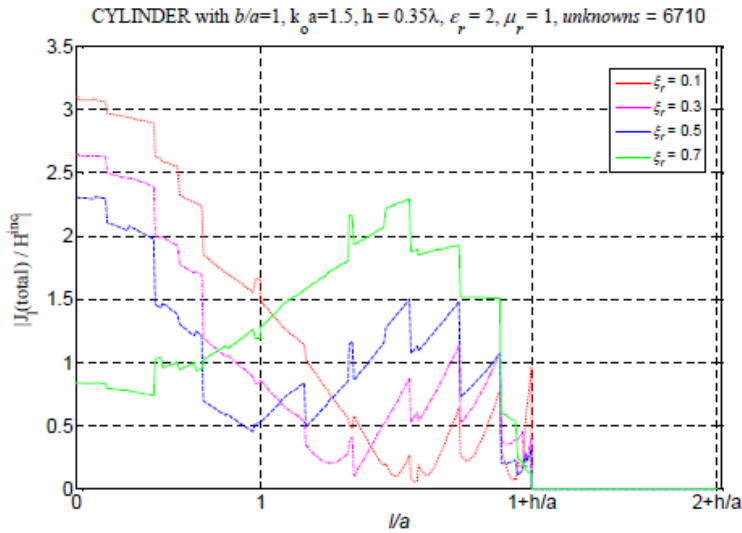


Figure 7-9.4.8 Magnitude of l -component of physical electric current in the $\phi = 0$ plane (taken from Altunkilic).

Both the graphs of the Figures 7-9.4.7 –7-9.4.8 show zero values in the aperture space. Graph of the Figure 7-9.4.7, unlike the graph of the Figure 7-9.4.8 (taken from Altunkilic), shows smooth curves. The graph taken from Altunkilic shows zigzagging in direction all over the mappings of the graph on the conducting surface.

7-10 Cone

7-10.1 Chiral Cone

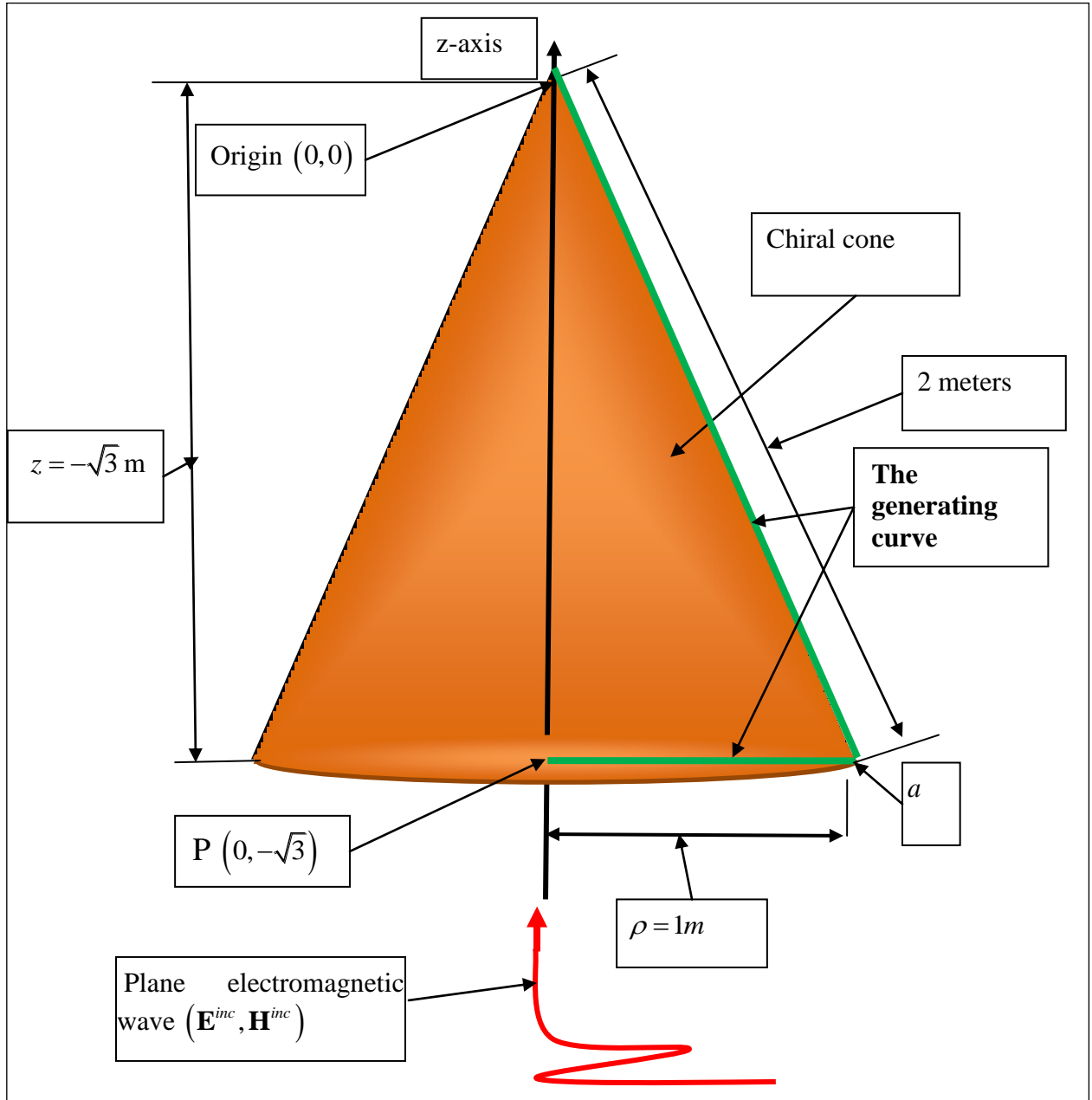


Figure 7-10.1 Chiral Cone

(Figure 7-10.1 will be the frame of reference in relation to the results and the graphs that are obtained in the following sections).

7-10.2 Computed Results.

In this section we will present relevant characteristics of our results and graphs that are plotted in the following section(s). We will also explain and clarify the results and the graphs wherever such elucidation is conducive in understanding the mapping of the graphs.

Figure 7-10.3.1 and the Figure 7-10.3.2 plot the graphs of the t -directed component of external and internal equivalent electric current (varying chiralities). Since the figure of reference is the chiral cone, therefore, we expect the graphs of the external and internal equivalent electric current (varying chiralities) to be exactly the same. The graphs of the Figure 7-10.3.1 and the Figure 7-10.3.2 met this expectation. We see in both graphs a glitch at 1 meter from the point P of the generating curve. In the Figure 7-10.1, this location is named 'a' which is precisely 1 meter to the right of P on the generating curve of the cone. At the point 'a' a sharp change in the geometry of the cone takes place. It is encouraging to note that a glitch in both the above-mentioned graphs and the graphs that follow occurs right at the point 'a' of the Figure 7-10.1. The graphs, therefore, have to be correct. Figure 7-10.3.3 represents magnitude of t -directed component of physical current (varying chiralities). In the case of a chiral cone magnitude of t -directed component of physical current (varying chiralities) is expected to be zero. The graph of the Figure 7-10.3.3 met this expectation. Figure 7-10.3.4 produces graphs of the magnitude of t -directed component of equivalent magnetic current (varying chiralities). Figure 7-10.3.5 produces magnitude of ϕ -directed component of equivalent external current (varying chiralities). Figure 7-10.3.6 plots graphs of the magnitude of ϕ -directed component of internal electric current (varying chiralities). Figure 7-10.3.7 plots graphs of the magnitude of ϕ -directed component of physical current (varying chiralities). Both the graphs of the Figure 7-10.3.7, as expected, show zero values and the overlap. Figure 7-10.3.8 plots the magnitude of ϕ -directed component of magnetic current (varying chiralities).

Figure 7-10.4.1 plots the co-polarized $\sigma_{\theta\theta}$ of the obstacle (varying chiralities) and the Figure 7-10.4.2 plots the cross polarized $\sigma_{\phi\theta}$ of the obstacle (varying chiralities).

Figure 7-11.2.1 plots the magnitude of t -component of equivalent external current of a perfectly conducting cone shell. Figure 7-11.2.2 plots the co-polarized $\sigma_{\theta\theta}$ of the perfectly conducting cone shell.

7-10.3 Surface currents

As expected graphs of Figure 7-10.3.1 and Figure 7-10.3.2 show that external and internal currents are the same giving rise to zero value of physical current shown in Figure 7-10.3.3. *As expected, graphs of Figure 7-10.3.1 and Figure 7-10.3.2 show a little deviation from their normal path at 1 meter from the origin. Point 'a', shown in Figure 7-10.1.1, where the base of the cone meets its hypotenuse precisely at a distance of one meter from the point P represents cause of the glitch*

in the graph. These graphs show variations as chirality of the chiral material changes from $\xi_r = 0.3$ to $\xi_r = 0.5$.

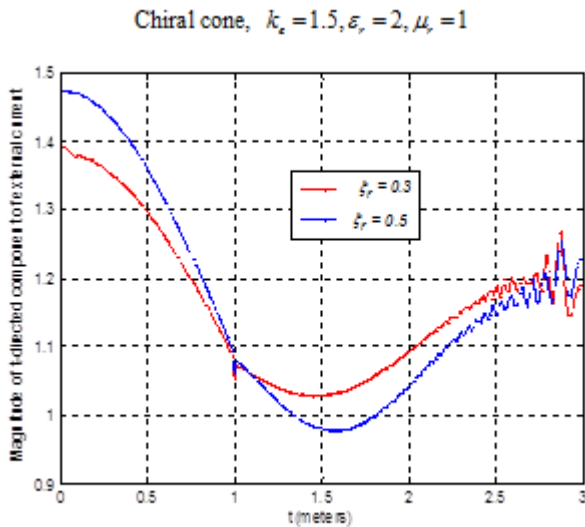


Figure 7-10.3.1 Magnitude of t-directed component of external equivalent electric current (varying chiralities). $k_e = 1.5$ is the free space wavenumber. The generating curve is approximated by 426 straight line segments.

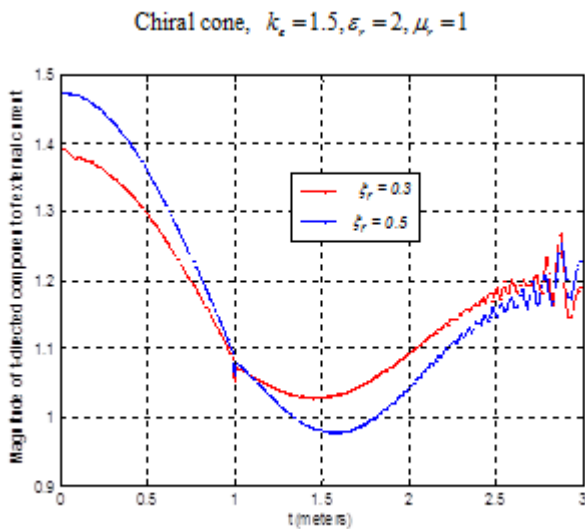


Figure 7-10.3.2 Magnitude of t-directed component of internal equivalent electric current (varying chiralities). The generating curve is approximated by 426 straight line segments.

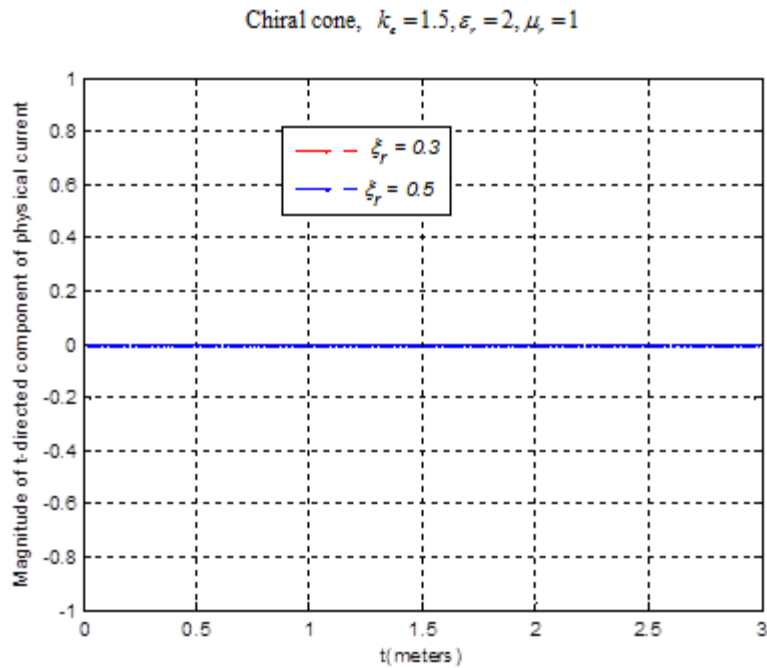


Figure 7-10.3.3 Magnitude of t-directed component of physical current (varying chiralities). The generating curve is approximated by 426 straight line segments.

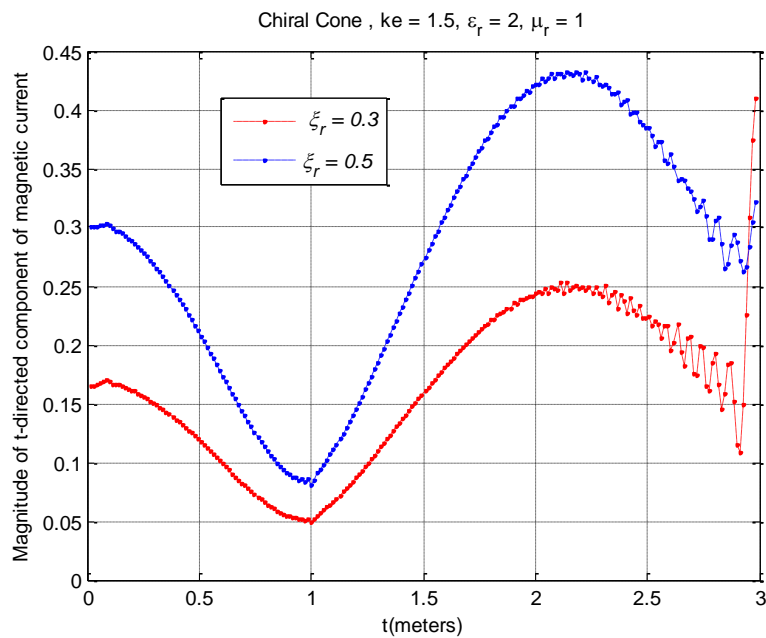


Figure 7-10.3.4 Magnitude of t-directed component of equivalent magnetic current (varying chiralities). The generating curve is approximated by 426 straight line segments.

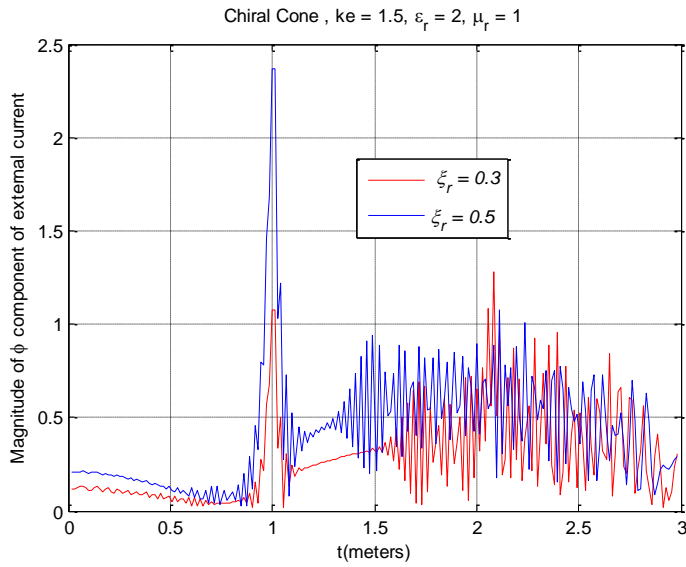


Figure 7-10.3.5 Magnitude of ϕ -directed component of equivalent external current (varying chiralities). The generating curve is approximated by 426 straight line segments.

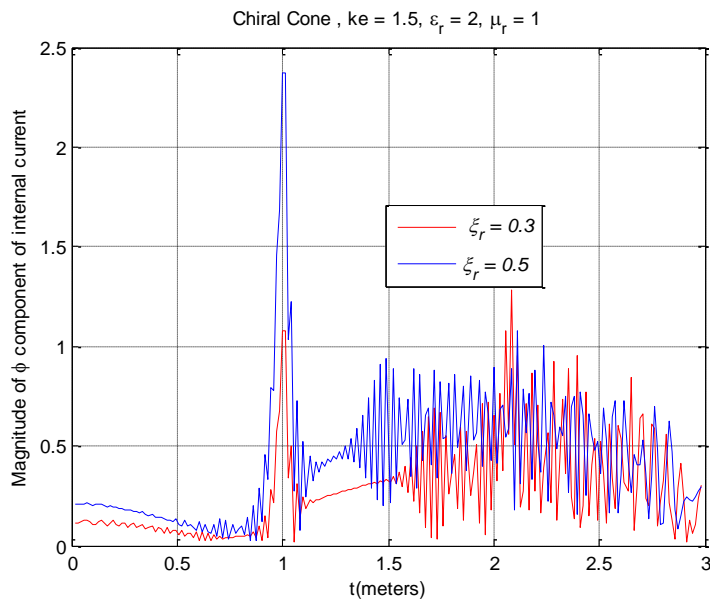


Figure 7-10.3.6 Magnitude of ϕ -directed component of internal electric current (varying chiralities). The generating curve is approximated by 426 straight line segments.

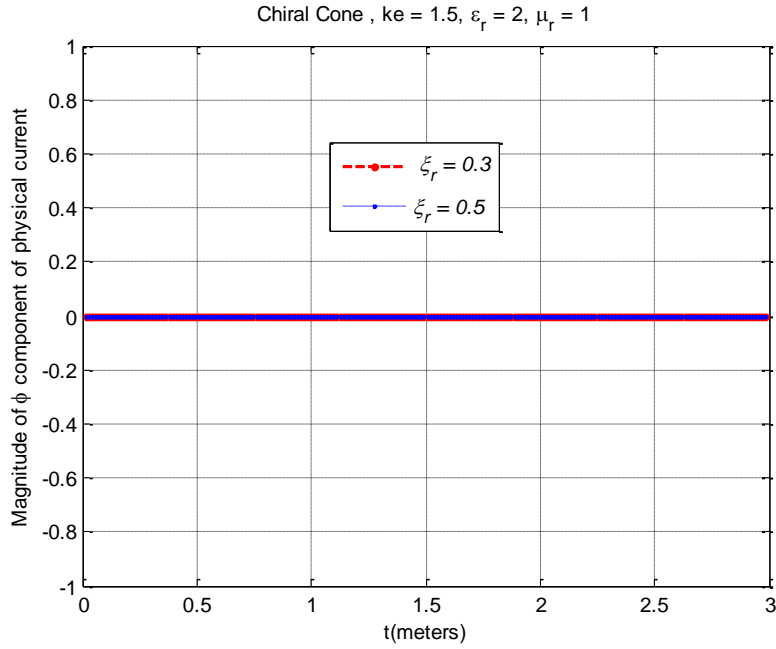


Figure 7-10.3.7 Magnitude of ϕ -directed component of physical current (varying chiralities). The generating curve is approximated by 426 straight line segments.

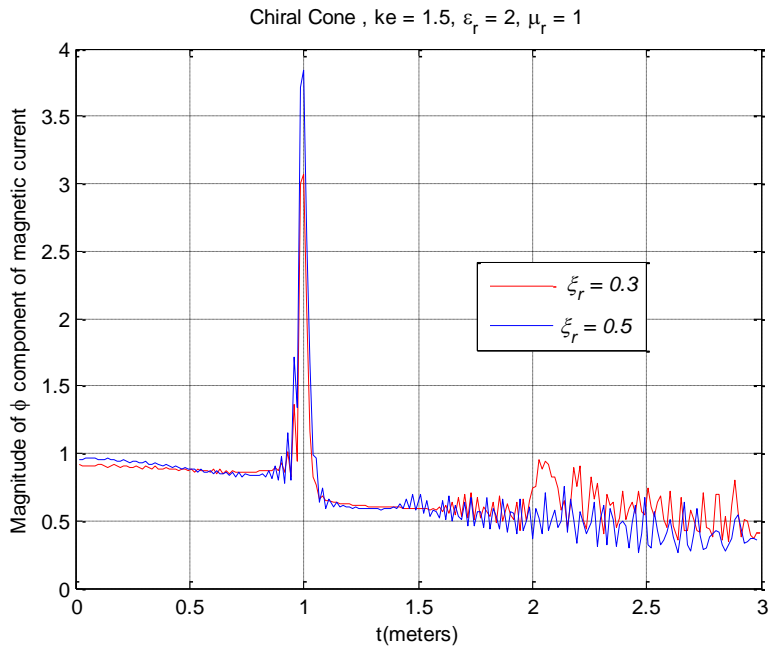


Figure 7-10.3.8 Magnitude of ϕ -directed component of magnetic current (varying chiralities). The Generating curve is approximated by 426 straight line segments.

7-10.4 Bistatic co-polarize and cross polarized RCS.

Radar cross sections of the chiral cone shown in Figure 7-10.1 are plotted in Figure 7-10.4.1 and Figure 7-10.4.2.

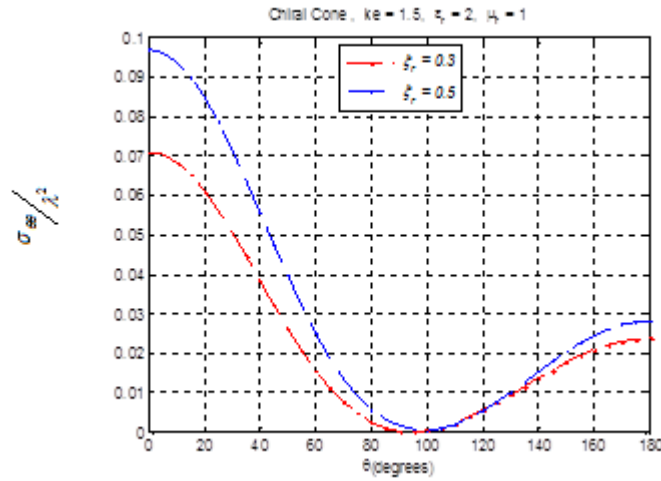


Figure 7-10.4.1 $\sigma_{\theta\theta}$ of the obstacle (varying chiralities) . Generating curve is approximated by 426 straight line segments

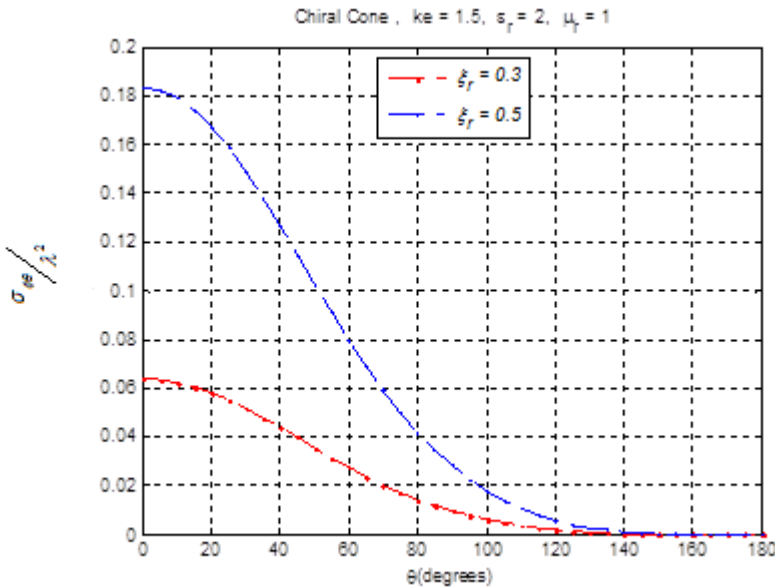


Figure 7-10.4.2 $\sigma_{\theta\theta}$ of the obstacle (varying chiralities). Generating curve is approximated by 426 straight line segments

7-11.1 Perfectly conducting metallic cone

Figure 7.11.1 shows a perfectly conducting metallic cone. A plane electromagnetic wave illuminates the cone at its bottom along the z-axis.

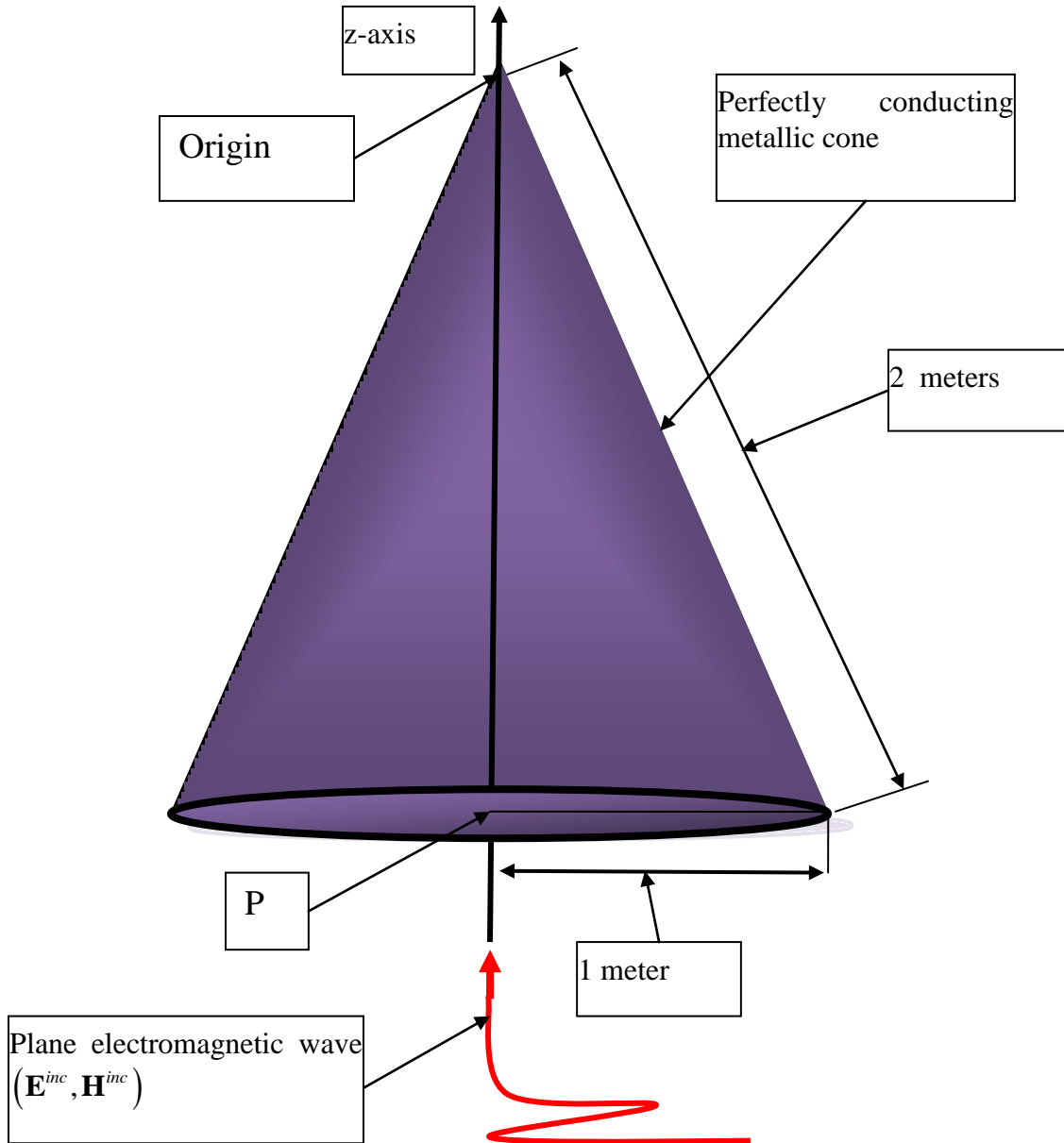


Figure 7-11.1 Perfectly conducting metallic cone

(Figure 7-11.1 will be the frame of reference in relation to the results and the graphs that are obtained in the following section).

7-11.2 Surface currents and a radar cross sections

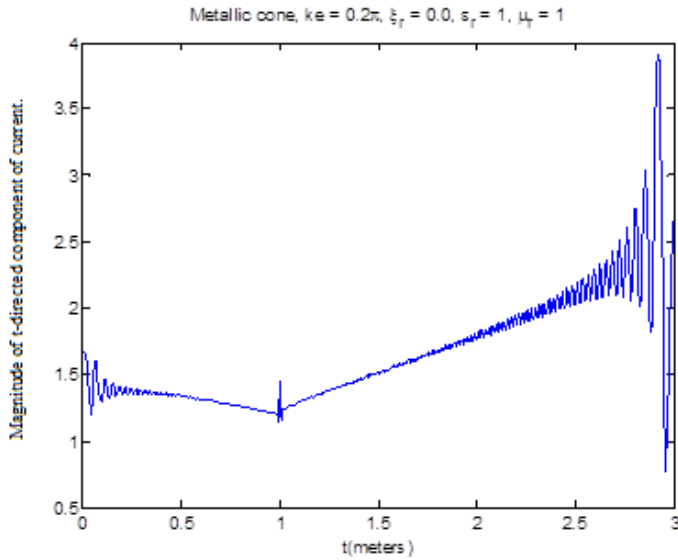


Figure 7-11.2.1 Magnitude of t -component of equivalent external current. Generating curve is approximated by 1200 straight line segments

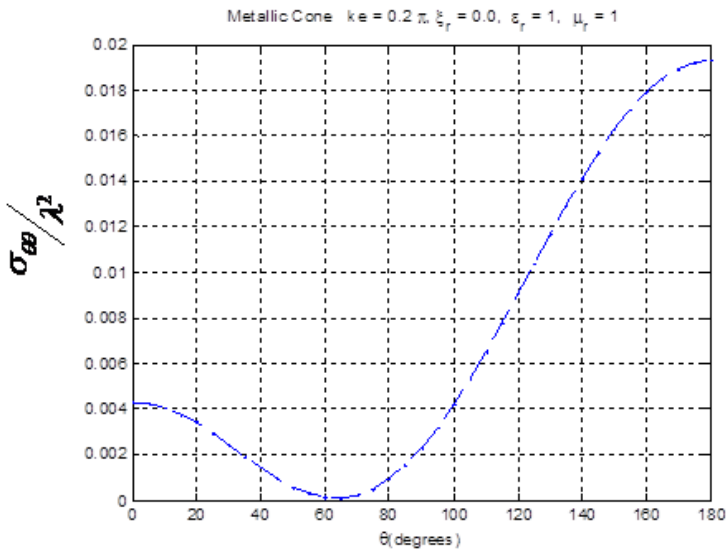


Figure 7-11.2.2 $\sigma_{\theta\theta}$ of the perfectly conducting cone shell. The generating curve is approximated by 1200 straight line segments.

7-12.1 Cone-shaped perfectly conducting metallic BOR surface enclosing chiral material with an aperture of radius 0.5 meter at its bottom.

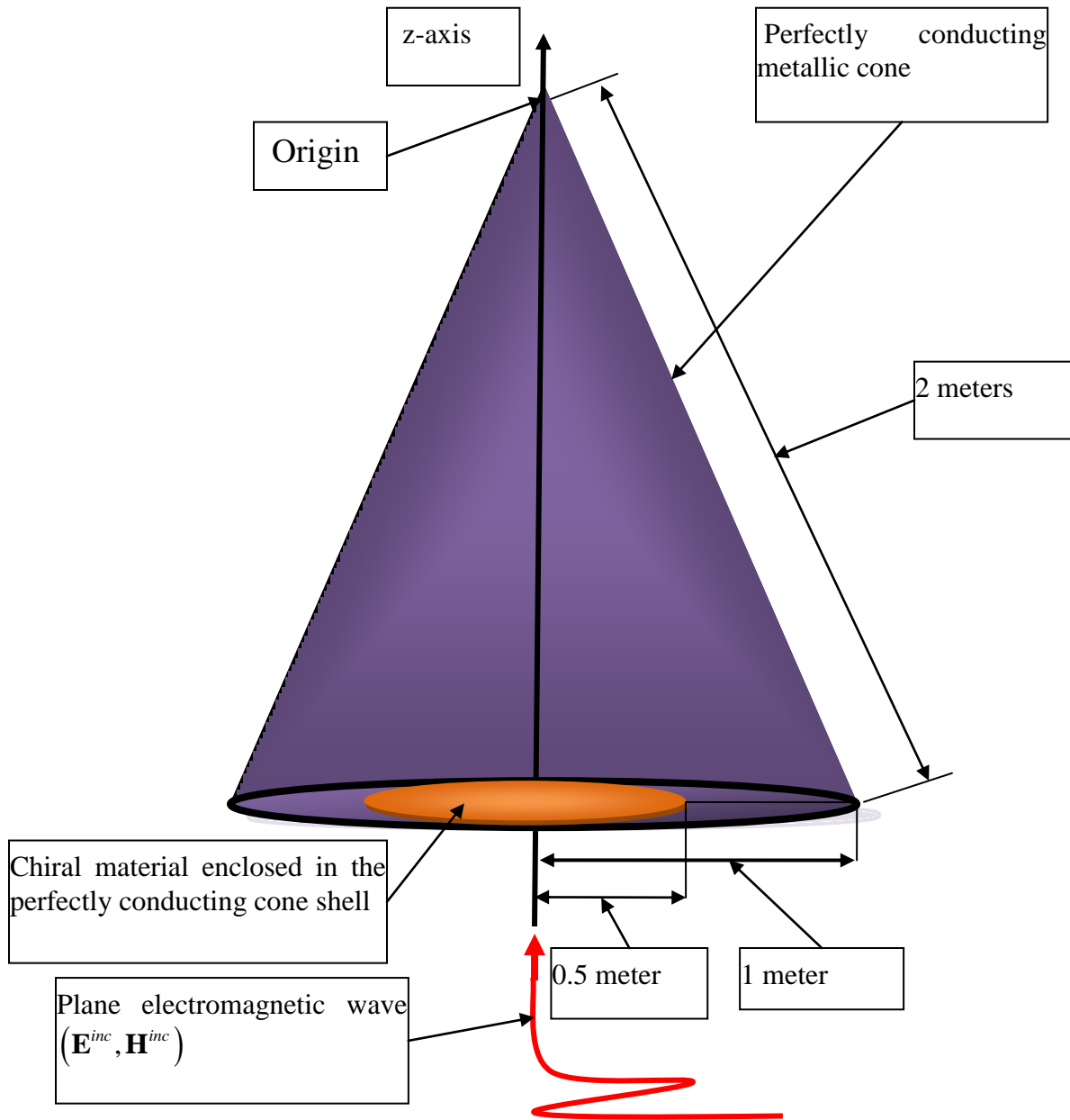


Figure 7-12.1.1 Perfectly conducting conical shell with an aperture enclosing chiral material

(Figure 7-12.1 will be the frame of reference in relation to the results and the graphs that are obtained in the following sections).

7-12.2 Computed Results.

In this section we will present relevant characteristics of our results and graphs that are plotted in the following section(s). We will also explain and clarify the results and the graphs wherever such elucidation is conducive in understanding the mapping of the graphs.

Figure 7-12.3.1 plots the magnitude of t-directed component of equivalent external current (varying chiralities). The graph shows up and down swings in the aperture space followed by smooth curve on the conducting surface of the shell cone. Figure 7-12.3.2 plots the magnitude of t-directed component of equivalent internal current (varying chiralities). The graph shows up and down swings in the aperture space followed by smooth curve on the conducting surface of the shell cone. Figure 7-12.3.4 plots the magnitude of t-directed component of equivalent magnetic current in $\phi = 0$ plane (varying chiralities). As expected, the graphs of the Figure 7-12.3.4 show zero values on the conducting surface. Figures 7-12.3.5–12.3.6 plot the magnitudes of ϕ -component of equivalent external and internal electric current in $\phi = 0$ plane. These graphs show sharp up and down fluctuations in the aperture space. We have discussed about it above in a paragraph (italics.). Figure 7-12.3.7 produces magnitude of ϕ -component of physical electric current in $\phi = 0$ plane (varying chiralities). The graphs of the Figure 7-12.3.7, as expected, show zero values in the aperture space. Figure 7-12.3.8 plots Magnitude of ϕ -component of equivalent magnetic current in $\phi = 0$ plane (varying chiralities). The two graphs of the Figure 7-12.3.8 show correctly zero values of equivalent magnetic currents on the conducting surface of the shell cone.

7-12.3 Surface currents

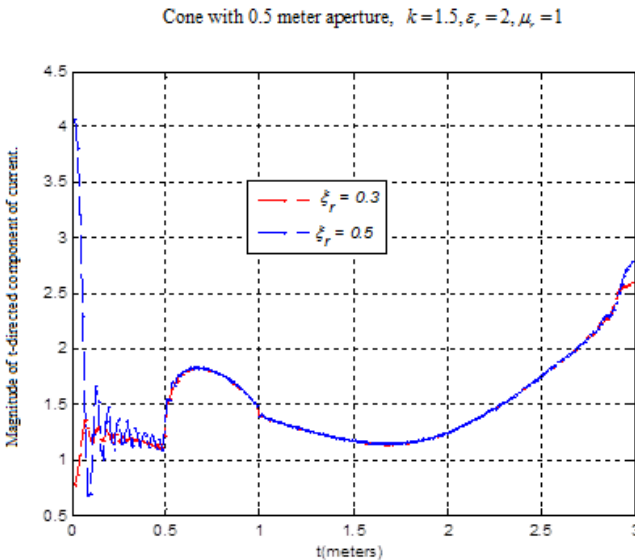


Figure 7-12.3.1 Magnitude of t-directed component of equivalent external current (varying chiralities). The generating curve is approximated by 426 straight line segments.

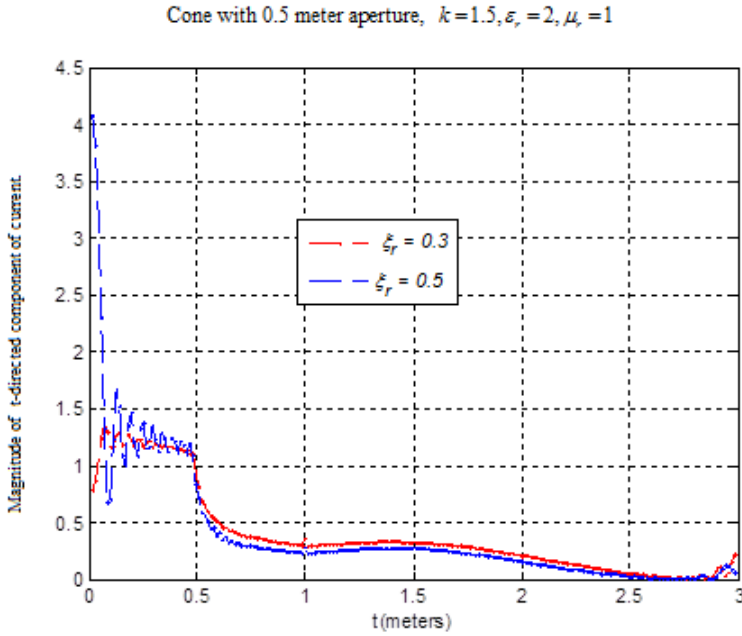


Figure 7-12.3.2 Magnitude of t-directed component of equivalent internal electric current (varying chiralities). The generating curve is approximated by 426 straight line segments.

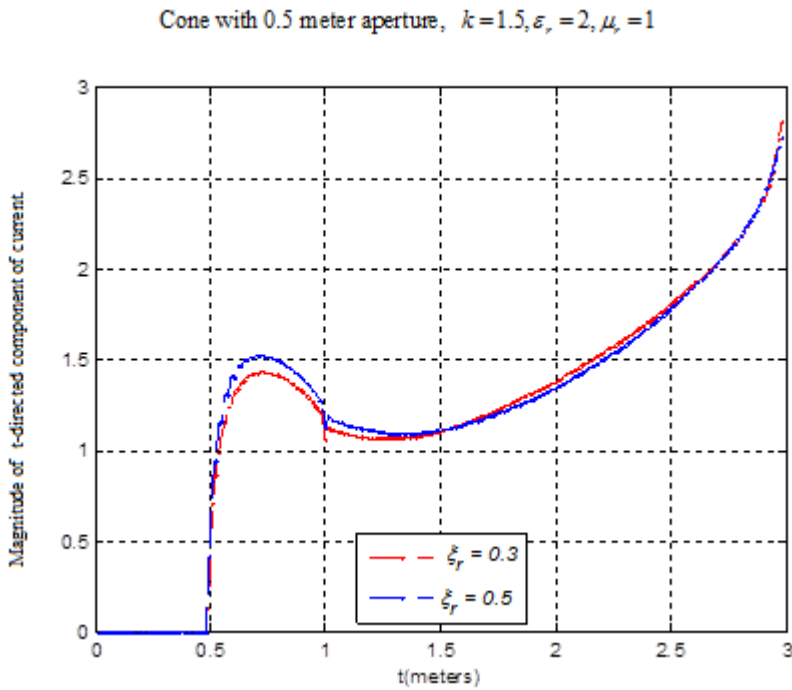


Figure 7-12.3.3 Magnitude of t-directed component of physical current (varying chiralities). The generating curve is approximated by 426 straight line segments

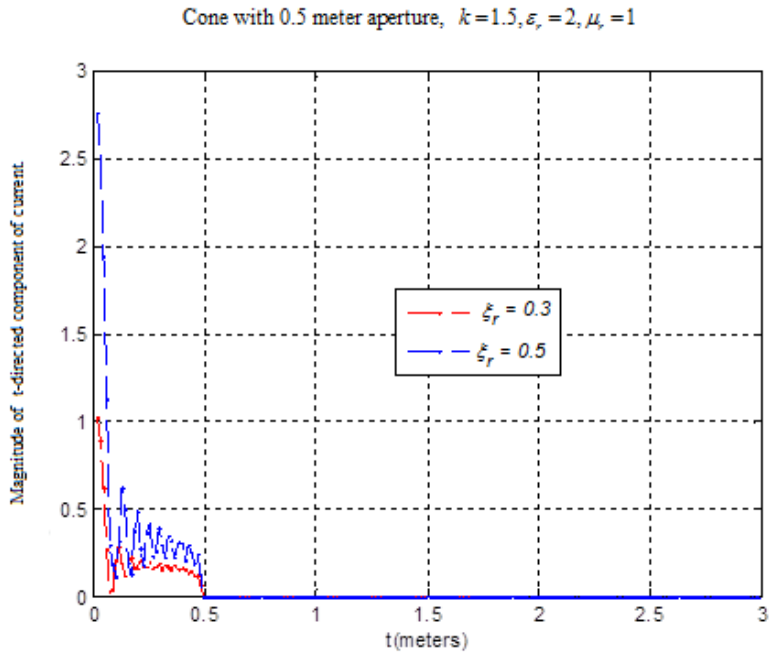


Figure 7-12.3.4 Magnitude of t -directed component of equivalent magnetic current in $\phi = 0$ plane (varying chiralities). The generating curve is approximated by 426 straight line segments.

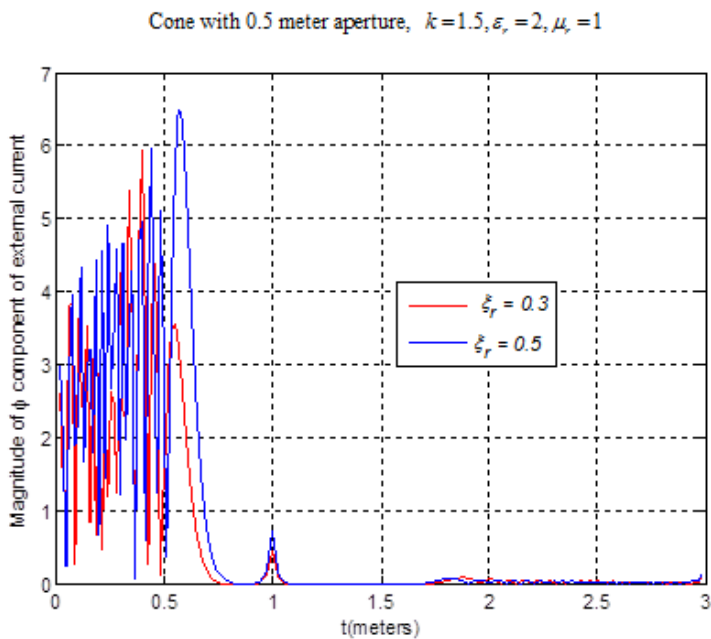


Figure 7-12.3.5 Magnitude of ϕ -component of equivalent external electric current in $\phi = 0$ plane (varying chiralities). The generating curve is approximated by 426 straight line segments.

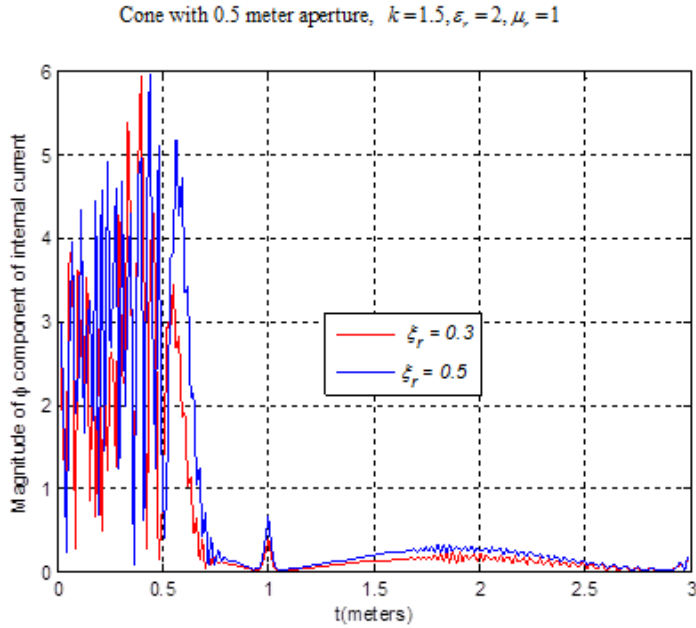


Figure 7-12.3.6 Magnitude of ϕ -component of equivalent internal electric current in $\phi=0$ plane (varying chiralities). The generating curve is approximated by 426 straight line segments.

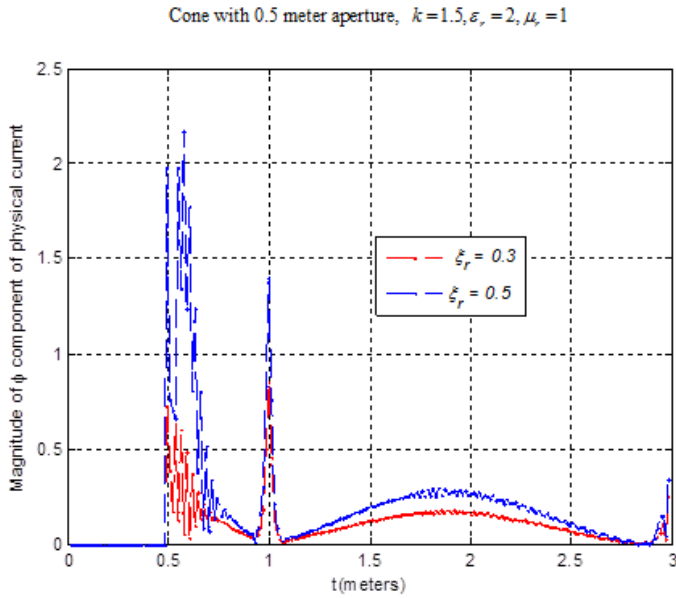


Figure 7-12.3.7 Magnitude of ϕ -component of physical electric current in $\phi=0$ plane (varying chiralities). The generating curve is approximated by 426 straight line segments.

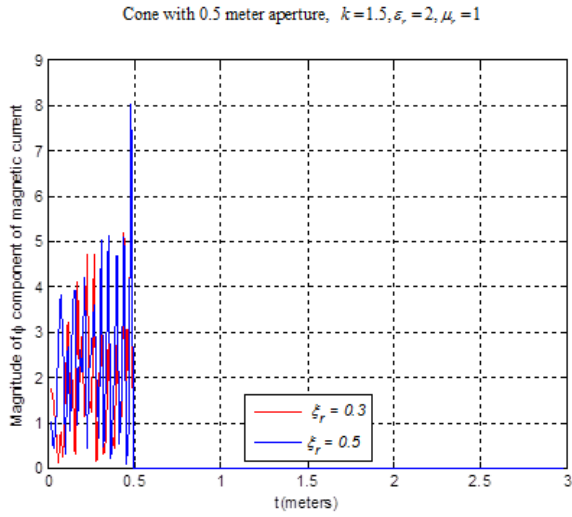


Figure 7-12.3.8 Magnitude of ϕ -component of equivalent magnetic current in $\phi=0$ plane (varying chiralities). The generating curve is approximated by 426 straight line segments.

7-12.4 Computed Results.

Figure 7-12.5.1 plots the bistatic co-polarized RCS $\sigma_{\theta\theta}$ of the obstacle (varying chiralities) and the Figure 7-12.5.2 plots the bistatic cross polarized RCS $\sigma_{\phi\theta}$ of the obstacle.

7-12.5 Radar cross sections

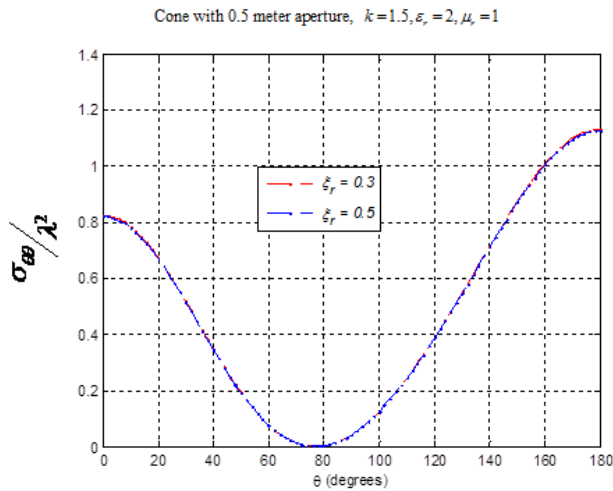


Figure 7-12.5.1 $\sigma_{\theta\theta}$ of the obstacle (varying chiralities). Generating curve is approximated by 3132 straight line segments.

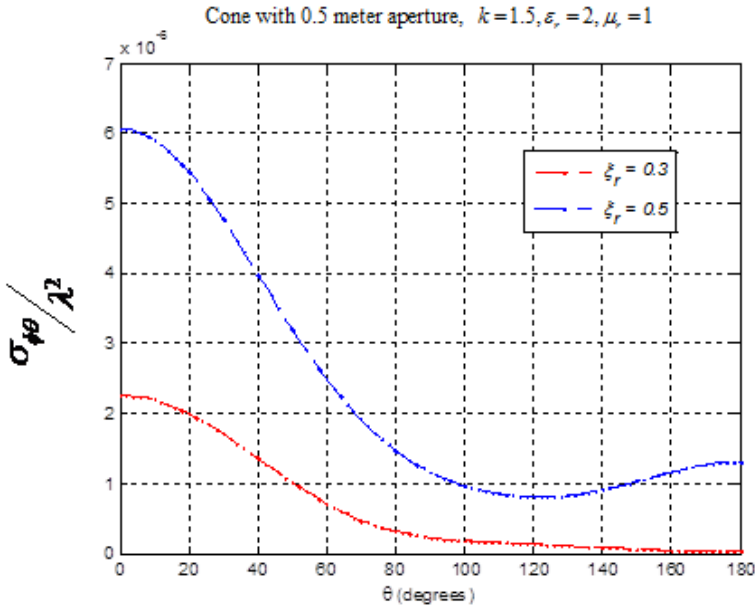


Figure 7-12.5.2 $\sigma_{\phi\theta}$ of the obstacle. The generating curve is approximated by 3132 straight line segments.

7-12.6 Computed Results.

Figures 7-12.7.1–7-12.7.2 plot the x- and y- components of the external electric fields, respectively along z-axis (varying chiralities). Figures 7-12.7.3–7-12.7.4 plot the x- and y- components of the internal electric fields, respectively along z-axis (varying chiralities). Figures 7-12.7.5–7-12.7.6 plot the x- and y- components of the internal electric fields, respectively along z-axis (varying wave numbers).

7-12.7 Internal fields

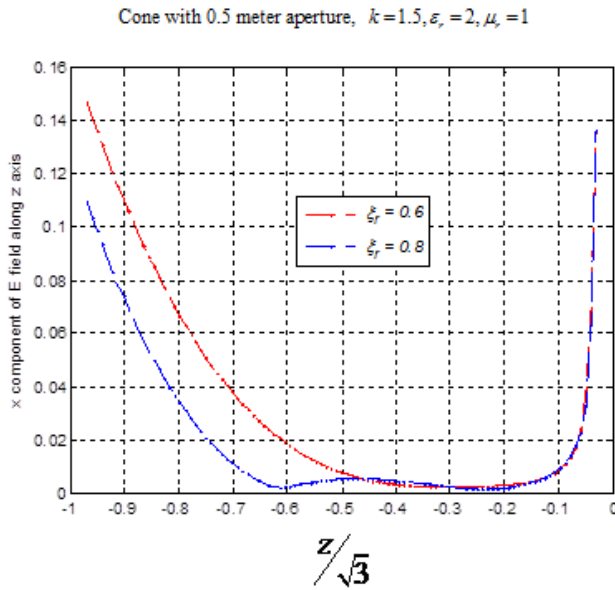


Figure 7-12.7.1 Magnitude of x-component of external electric field along z-axis (varying chiralities). Generating curve is approximated by 3132 straight line segments and 98 points on z-axis were used to obtain the graph.

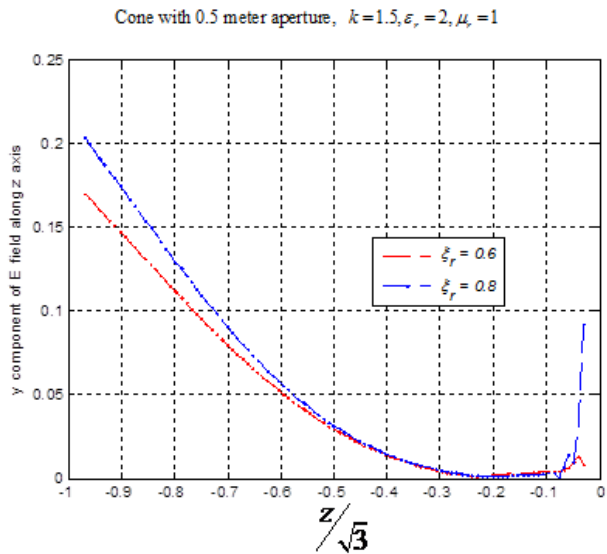


Figure 7-12.7.2 Magnitude of y-component of external electric field along z-axis (varying chiralities). Generating curve is approximated by 3132 straight line segments and 98 points on z-axis were used to obtain the graph.

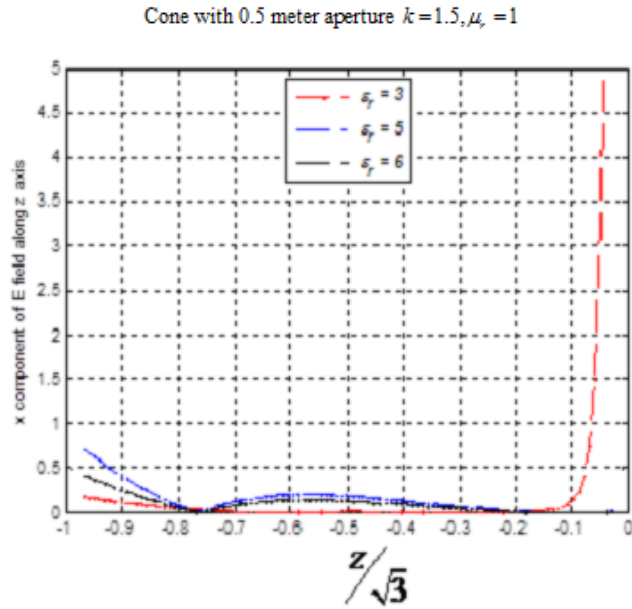


Figure 7-12.7.3 Magnitude of x-component of internal electric field along z-axis (varying permittivities). Generating curve is approximated by 3132 straight line segments and 98 points on z-axis were used to obtain the graph.

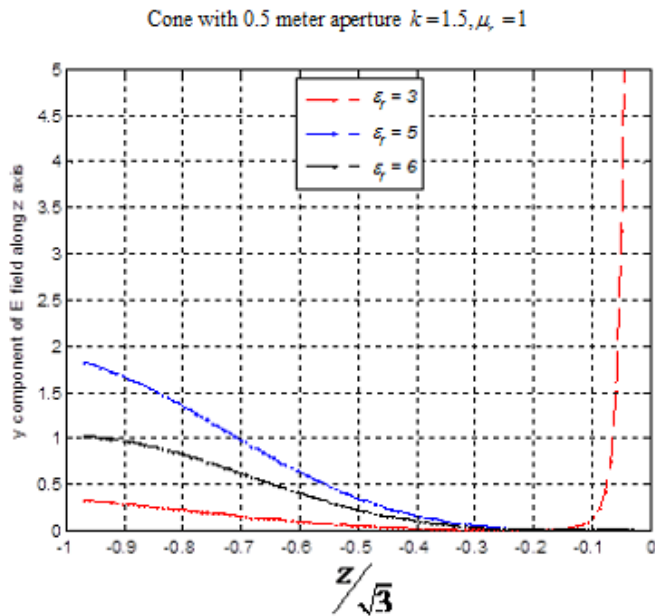


Figure 7-12.7.4 Magnitude of y-component of internal electric field along z-axis (varying chiralities). Generating curve is approximated by 3132 straight line segments and 98 points on z-axis were used to obtain the graph.

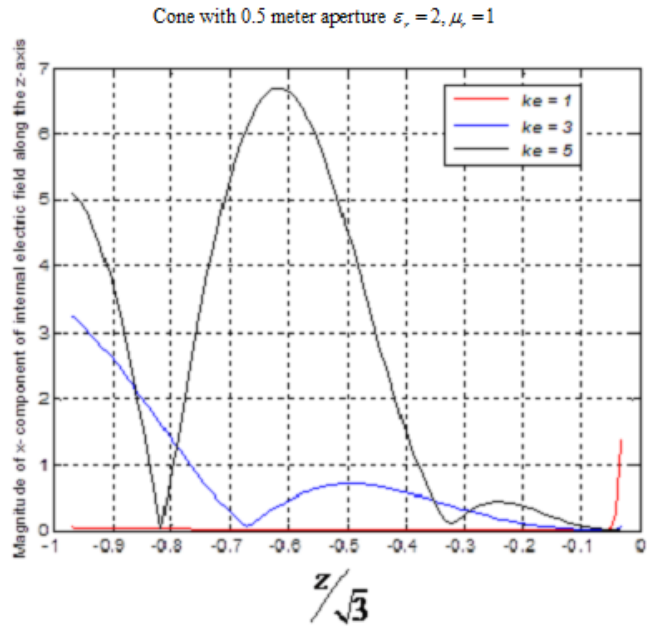


Figure 7-12.7.5 Magnitude of x-component of internal electric field along z-axis (varying wave numbers). Generating curve is approximated by 3132 straight line segments and 98 points on z-axis were used to obtain the graph.

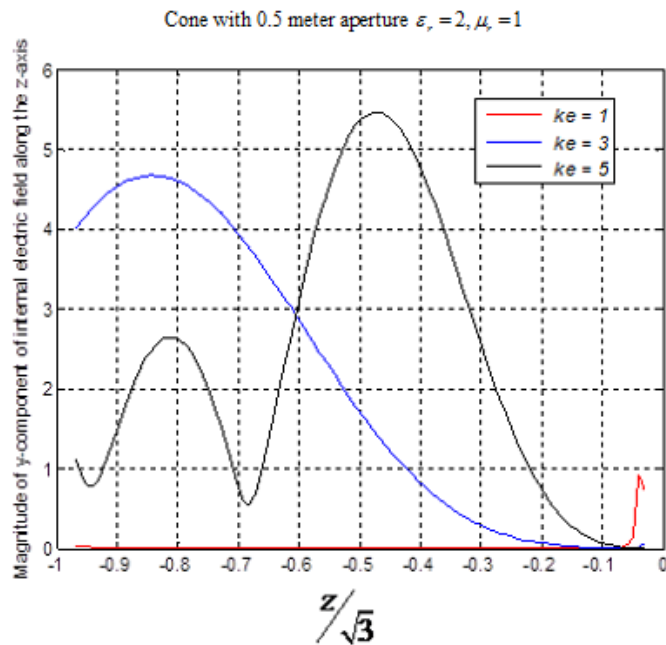


Figure 7-12.7.6 Magnitude of y-component of internal electric field along z-axis (varying wave numbers). Generating curve is approximated by 3132 straight line segments and 98 points on z-axis were used to obtain the graph.

Chapter 8

Conclusion.

We sum up in conclusion:

① The sound theoretical framework developed in chapters two through six was validated by comparison of our results for various BOR's with exact results and existing numerical results whenever available. We have proven that our graphs of Figure 7-1.1.1 and Figure 7-1.1.2, bear remarkable almost one hundred percent resemblance with the analytically calculated graphs of the Figure 7-1.1.3 and the Figure 7-1.1.4. Our graph of the Figure 7-1.1.5 bears striking almost one hundred percent likeness with analytically calculated graph of the Figure 7-1.1.7. Our graph of the Figure 7-1.1.10 bears noticeable almost one hundred percent likeness with analytically calculated graph of the Figure 7-1.1.11. Our graph of the Figure 7-1.1.12 bears striking almost one hundred percent likeness with analytically calculated graph of the Figure 7-1.1.13. Our graph of the Figure 7-2.2 bears striking almost one hundred percent resemblance with analytically calculated graph of the Figure 7-2.3. Our graph of the Figure 7-5.2.1 bears remarkable almost one hundred percent resemblance with analytically calculated graph of the Figure 7-5.2.2. Our graph of the Figure 7-5.2.3 bears striking almost one hundred percent resemblance with the analytically calculated graph of the Figure 7-5.2.4. Our graph of the Figure 7-5.3.1 bears striking almost one hundred percent likeness with analytically calculated graph of the Figure 7-5.3.2. Our graph of the Figure 7-5.3.3 bears noticeable almost one hundred percent resemblance with analytically calculated graph of the Figure 7-5.3.4. Due to good grounding and validity of our theoretical framework by reason of almost one hundred percent pictorial conformability of our graph mappings, our graph forms and accuracy of our graph readings with the exact graphs is established.

From comparisons, our graph mappings and our graph readings with respect to the graphs of Altunkilic [3] representing the same parameters vary in degrees from almost the same to being at variance primarily with respect to the smoothness of the graph mappings. His graph mappings veer along in a zigzag course moving up and down alternately thereby depriving meaningful comparison of his graph readings with ours. Our graphs are remarkably quick to detect and respond to sharp changes in the geometry of the cylinder and the cone with instant sharp surges that correspond to the sharp changes in the geometry of the figure. Altunkilic's graphs have shown lack of response to sharp changes in the geometry of the figure. It is assumed that the above-mentioned disadvantages in Altunkilic's graphs have to do with the basic numerical approach he uses in obtaining his graphs. Aside from these disadvantages in comparison of our graphs with his graphs, graph readings between ours and his graphs in most cases show about the same values. For example, our graph of the Figure 7-3.2.1 with Altunkilic's graph of the Figure 7-3.2.2 show remarkable likeness with respect to graph readings and the form of these two graphs. The graph of the Figure 7-3.2.1 bears striking almost one hundred percent resemblance with the graph of the Figure 7-3.2.2. Similarly our graph of the Figure 7-3.2.4 bears remarkable almost one hundred percent likeness with Altunkilic's graph of the Figure 7-3.2.5. Our graph of the Figure 7-7.3.1

bears striking almost one hundred percent resemblance with Altunkilic's graph of the Figure 7-7.3.2. Our graph of the Figure 7-8.3.1 bears remarkable almost one hundred percent likeness with Altunkilic's graph of the Figure 7-8.3.2.

② Our thesis primarily pertains to the case of a partially shielded chiral body of revolution (BOR) with rotationally symmetric aperture(s) that exposes chiral material and the shielded surface of the body to a plane electromagnetic wave that impinges upon the chiral material that is exposed through the aperture(s) as well as upon the shielded perfectly conducting surface. The method discussed and applied in our thesis is that of Harrington and Mautz [10], [38], one of the most commonly used methods of solving BOR problems using the method of moments (MoM) technique.

Our formulation involves surface currents on a BOR using triangular expansion functions that are sub-sectional and piecewise linear in the longitudinal $\hat{\mathbf{t}}$ -direction and a finite Fourier series in the azimuthal $\hat{\phi}$ -direction. The advantage of this method is that the expansion functions are one dimensional and its coefficients exist only on the generating curve that defines the BOR, resulting in a matrix equation of compact size for each Fourier mode.

Taking $e^{-jm\phi}$ dependent testing functions and $e^{jn\phi}$ dependent expansion functions where $\{m, n = 0, \pm 1, \pm 2, \dots\}$, the electromagnetic field of an $e^{jn\phi}$ dependent expansion function tested with an $e^{-jm\phi}$ testing function is because of the rotational symmetry of the BOR, zero for $m \neq n$ so that the moment matrix consists of diagonally arranged sub-matrices surrounded by sub-matrices all of whose elements are zero. We thus save enormous amount of computational time and computer memory.

Altunkilic's [3] formulation uses the method of moments (MoM) involving primarily the case of a perfectly conducting surface of arbitrary shape which encloses chiral material and has arbitrarily shaped aperture(s) that expose the chiral material as well as the perfectly conducting surface to a plane electromagnetic wave that impinges upon the chiral material that is exposed through the aperture(s) as well as upon the perfectly conducting arbitrary surface. Ours is a special case of Altunkilic's problem. For example our theory cannot handle the case of a cubic-shaped or square-shaped partially shielded chiral body with aperture(s) for the simple reason that cubes and squares are not bodies of revolution.

Altunkilic [3] uses computer aided design (CAD) software using planar triangles which have the ability to conform to an arbitrarily shaped surface. CAD programs have the ability to generate triangular meshes of exceptionally high quality. Altunkilic [3] uses Rao-Wilton_Glisson (RWG) triangular expansion and testing functions. His theoretical formulations, unlike ours, are deprived of rotational symmetry. Moreover using two dimensional expansion and testing functions leads to very huge size matrices. He uses matrices of size of 5500×5500 up to size 6200×6200 to produce the same graphs which we have produced by using two matrices of size 848×848 , thereby saving an enormous amount of computer memory and computational time.

The curves of our graphs were smooth and without zigzag changes of direction compared with the curves of Altunkilic [3]. Moreover our graphs demonstrated acute sensitivity to abrupt changes in the geometry of the cylinder and the cone by producing a sharp abrupt upward swing at points where changes in the geometry of the figure occur. Noticing the sensitivity, smoothness, as well as abrupt glitches in our graphs that correspond to the abrupt sharp changes in the geometry of the cylinder and the cone we assert that the accuracy of the graph mapping of our graphs stand out to be more in the fitness of things.

The fact of the matter is that ours and Altunkilic's graphs are produced by using two distinctly different numerical approaches. Therefore, in the absence of an analytically calculated exact graph to compare with, it is just a matter of opinion as to which graph is correct. It is to be noted that graph readings unlike the graph mappings of ours and Altunkilic's graphs are about the same.

③ If computer time and memory are limited, our BOR formulation can handle BORs that are much larger than those handled by Altunkilic's formulation [3]. For example, we analyzed and obtained, for the free space wavelength of $\frac{2\pi}{1.5}m \approx 4.2m$, graphs of surface currents induced on the two meter diameter and $\sqrt{3}$ meter high chiral cone covered by a perfectly conducting surface with an aperture at the bottom of the cone. We also obtained internal electromagnetic fields and radar cross sections of this object. Our theoretical framework is applicable to the rocket shaped BOR structure which encloses chiral material as shown in Figure 8 (a). We can obtain radar cross sections of this huge structure. Altunkilic [3] uses value of $ka = 1.5$ in most of his graphs. Hence, for a wavelength of 1 meter he uses a radius of length 0.2387 m and matrices of the size 6200×6200 to produce requisite graphs of the sphere. His theoretical framework, as such, cannot handle a huge structure shown in Figure 8(a) because of the extremely huge size unsolvable matrices this structure needs for producing graphs of radar cross sections.

Future research:

It is very tempting to suggest that our research work can produce the radar cross section of a rocket in flight such as shown in Figure 8(c). The main drawback in this suggestion is that our theory is based on the homogeneous case of a chiral material. However, if future research establishes that the flue gases emitted from the bottom aperture of a rocket in flight are homogeneous and also determines the constitutive parameters of the flue gases then MoM based integral formulations of our theory may go a long way in furthering the theoretical framework with respect to the flue gases.

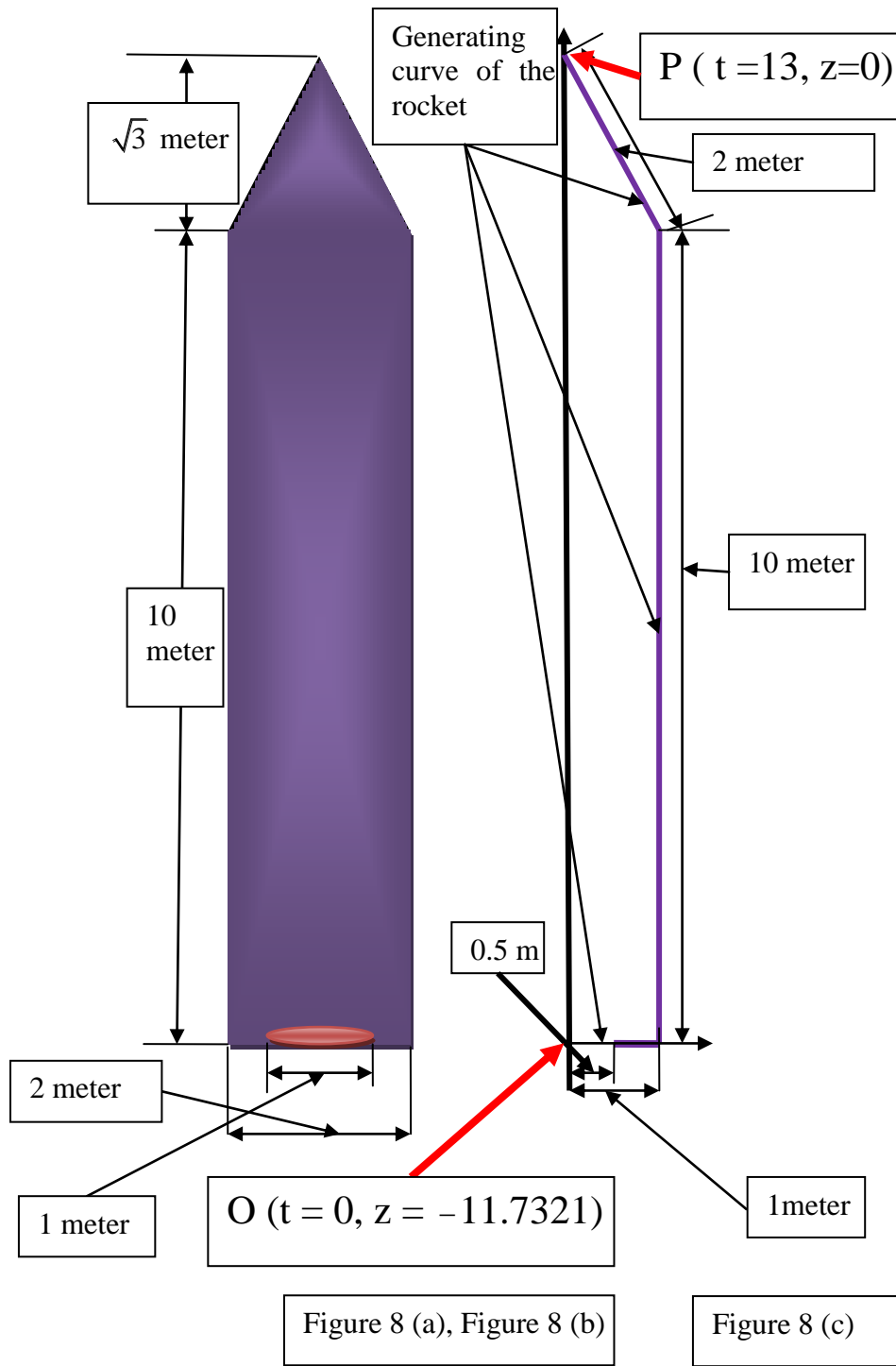


Figure 8(a) A rocket-shaped perfectly conducting body of revolution with a single aperture at its bottom which encloses chiral material.

Figure 8(b) Generating curve of the rocket of the Figure 8(a), Figure 8(c) A rocket in flight.

APPENDIX A

A_1.1 – Equivalence Principle

In the application of Equivalence Principle, we need to make sure that,

- Original impressed sources that existed in the original problem are preserved in the Equivalent problem.
- The same mediums that existed in the original problem are preserved.
- All boundary conditions that existed in the original problem are preserved.

A_1.1(a) – Original Problem

A pictorial representation of the original problem (Figure A_1.1.1) shows two regions separated by a bounding surface. The internal region has dielectric with parameters (ϵ_i, μ_i) and the external region has a different dielectric parameters (ϵ_e, μ_e) . A plane electromagnetic wave, generated by impressed sources, would produce in all space filled with the medium of region R_e the fields $(\mathbf{E}^{inc}, \mathbf{H}^{inc})$ in the both external region R_e and the internal region R_i . Now due to the presence of medium of region R_i bounded by S , the total electric and magnetic fields that come into play in the *external region* are

$$\mathbf{E}_1 = \mathbf{E}^{inc} + \mathbf{E}^s \quad (\text{A}_1.1.1)$$

$$\mathbf{H}_1 = \mathbf{H}^{inc} + \mathbf{H}^s \quad (\text{A}_1.1.2)$$

Here \mathbf{E}^s and \mathbf{H}^s are the scattered electric and magnetic fields in the external region. We are interested in finding \mathbf{E}^s and \mathbf{H}^s .

In order to find \mathbf{E}^s and \mathbf{H}^s conveniently, we formulate two equivalent problems namely *the External Equivalence* and *the Internal Equivalence*.

A_1.1(b) External Equivalence

In the External Equivalence we create an equivalent representation in the external region by replacing the bounding surface of the original problem by a fictitious surface S as shown in Figure A_1.1.2. We fill up the internal region of space with the external dielectric with parameters

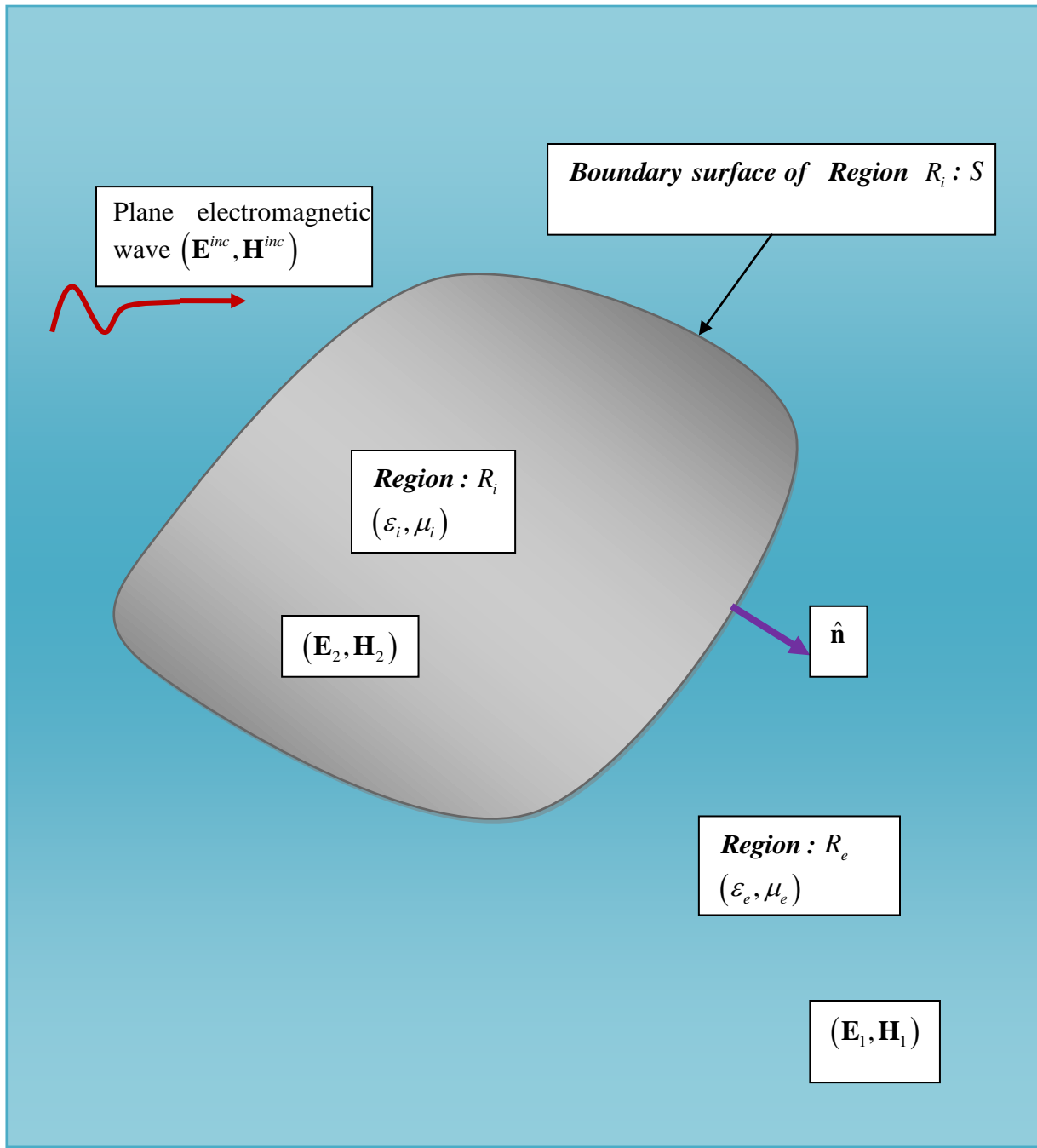


Figure A-1.1.1 Original problem.

(ϵ_e, μ_e) thereby creating an unbounded space filled with the dielectric (ϵ_e, μ_e) that existed in the external region of the original problem. We denote the region R_i of the original problem as the *region of no interest or excluded region*. As such, we choose the internal fields in this region as we please. In this case we will choose the fields in the region R_i to be $\mathbf{E} = \mathbf{0} = \mathbf{H}$. Now with

$\mathbf{E}=0=\mathbf{H}$ in the region R_i and fields $(\mathbf{E}_1, \mathbf{H}_1)$ in the external region R_e , the jump from the external electric field \mathbf{E}_1 to the internal electric field $\mathbf{E}=0$ and the jump from the external magnetic field \mathbf{H}_1 to the internal magnetic field $\mathbf{H}=0$ can only be obtained by placing on the fictitious boundary surface S the equivalent currents,

$$\mathbf{J}_e = \hat{\mathbf{n}} \times \mathbf{H}_1 \quad (\text{A}_1.1.3)$$

$$\mathbf{M} = -\hat{\mathbf{n}} \times \mathbf{E}_1 \quad (\text{A}_1.1.4)$$

$\mathbf{J}_e = \hat{\mathbf{n}} \times \mathbf{H}_1$ and $\mathbf{M} = -\hat{\mathbf{n}} \times \mathbf{E}_1$ are the equivalent sources on S which radiating all over the space in the external region R_e produce the *scattered* electric and magnetic fields $\mathbf{E}_e(\mathbf{J}_e, \mathbf{M})$ and $\mathbf{H}_e(\mathbf{J}_e, \mathbf{M})$ all over the region R_e . From these equivalent currents (Figure A_1.1.2) we can compute the far away fields in the external region. With reference to (A_1.1.1) and (A_1.1.2), we can deduce that

$$\mathbf{E}^s = \mathbf{E}_e(\mathbf{J}_e, \mathbf{M}) \quad (\text{A}_1.1.5)$$

$$\mathbf{H}^s = \mathbf{H}_e(\mathbf{J}_e, \mathbf{M}) \quad (\text{A}_1.1.6)$$

The internal face of S that is S^- does not belong to the region R_e . Since $\mathbf{E}=0=\mathbf{H}$ in the internal region R_i , we can deduce that

$$\left[\mathbf{E}_1 \Big|_{\tan} \right]_{S^-} = 0 \quad (\text{A}_1.1.7)$$

$$\left[\mathbf{H}_1 \Big|_{\tan} \right]_{S^-} = 0 \quad (\text{A}_1.1.8)$$

We can write (A_1.1.1) and (A_1.1.2), with reference to (A_1.1.5) and (A_1.1.6) as:

$$\mathbf{E}_1 = \mathbf{E}^{inc} + \mathbf{E}^s \Rightarrow$$

$$\mathbf{E}_1 = \mathbf{E}^{inc} + \mathbf{E}_e(\mathbf{J}_e, \mathbf{M}) \quad (\text{A}_1.1.9)$$

$$\mathbf{H}_1 = \mathbf{H}^{inc} + \mathbf{H}^s \Rightarrow$$

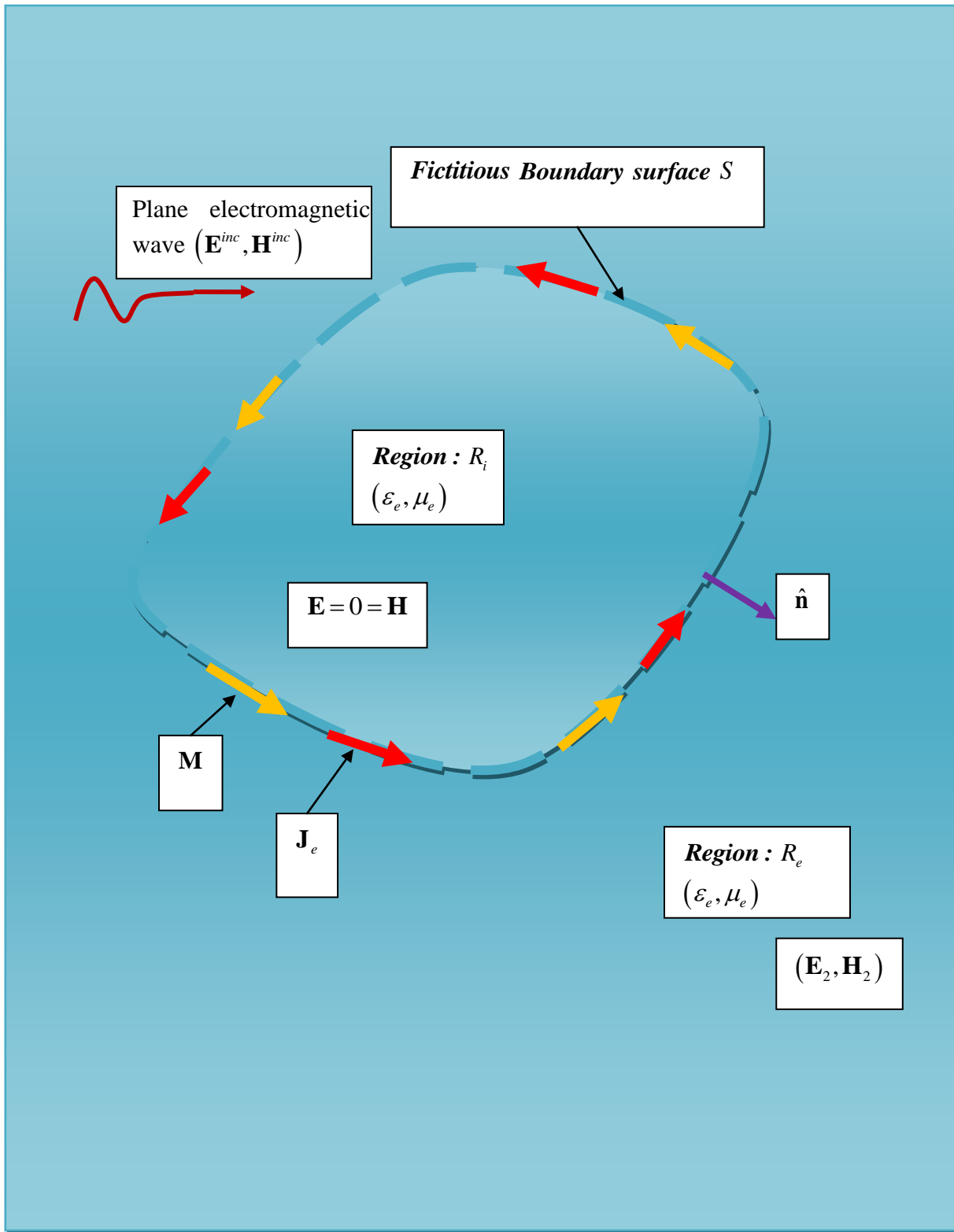


Figure A-1.1.2 External equivalence.

$$\mathbf{H}_1 = \mathbf{H}^{inc} + \mathbf{H}_e(\mathbf{J}_e, \mathbf{M}) \quad (\text{A}_1.1.10)$$

Substituting (A_1.3.9) into (A_1.3.7), we obtain

$$\begin{aligned} \left[(\mathbf{E}^{inc} + \mathbf{E}_e(\mathbf{J}_e, \mathbf{M})) \Big|_{\text{tan}} \right]_{S^-} &= \left[\mathbf{E}^{inc} \Big|_{\text{tan}} + \mathbf{E}_e(\mathbf{J}_e, \mathbf{M}) \Big|_{\text{tan}} \right]_{S^-} = 0 \Rightarrow \\ -\left[\mathbf{E}_e(\mathbf{J}_e, \mathbf{M}) \Big|_{\text{tan}} \right]_{S^-} &= \left[\mathbf{E}^{inc} \Big|_{\text{tan}} \right]_{S^-} \end{aligned} \quad (\text{A}_1.1.11)$$

Eq. (A_1.1.11) implies

$$-\left[\mathbf{E}_e(\mathbf{J}_e, \mathbf{M}) \right]_{S^-} = \left[\mathbf{E}^{inc} \right]_{S^-}$$

Since \mathbf{E}^{inc} remains unchanged taken either tangential to S or tangential to S^- , as such, we can write

$$-\left[\mathbf{E}_e(\mathbf{J}_e, \mathbf{M}) \right]_{S^-} = \left[\mathbf{E}^{inc} \right]_S \quad (\text{A}_1.1.12)$$

or

$$-\frac{1}{\eta_e} \left[\mathbf{E}_e(\mathbf{J}_e, \mathbf{M}) \right]_{S^-} = \frac{1}{\eta_e} \left[\mathbf{E}^{inc} \right]_S \quad (\text{A}_1.1.13)$$

Substituting (A_1.1.10) in (A_1.1.8), we obtain

$$\begin{aligned} \left[(\mathbf{H}^{inc} + \mathbf{H}_e(\mathbf{J}_e, \mathbf{M})) \Big|_{\text{tan}} \right]_{S^-} &= \left[\mathbf{H}^{inc} \Big|_{\text{tan}} + \mathbf{H}_e(\mathbf{J}_e, \mathbf{M}) \Big|_{\text{tan}} \right]_{S^-} = 0 \Rightarrow \\ -\left[\mathbf{H}_e(\mathbf{J}_e, \mathbf{M}) \Big|_{\text{tan}} \right]_{S^-} &= \left[\mathbf{H}^{inc} \Big|_{\text{tan}} \right]_{S^-} \end{aligned}$$

Since \mathbf{H}^{inc} remains unchanged taken either tangential to S or tangential to S^- , as such, we can write

$$-\left[\mathbf{H}_e(\mathbf{J}_e, \mathbf{M}) \right]_{S^-} = \left[\mathbf{H}^{inc} \right]_S \quad (\text{A}_1.1.14)$$

A_1.1(c) Internal Equivalence

In the Internal Equivalence we fill up the whole space, including the external region, with the

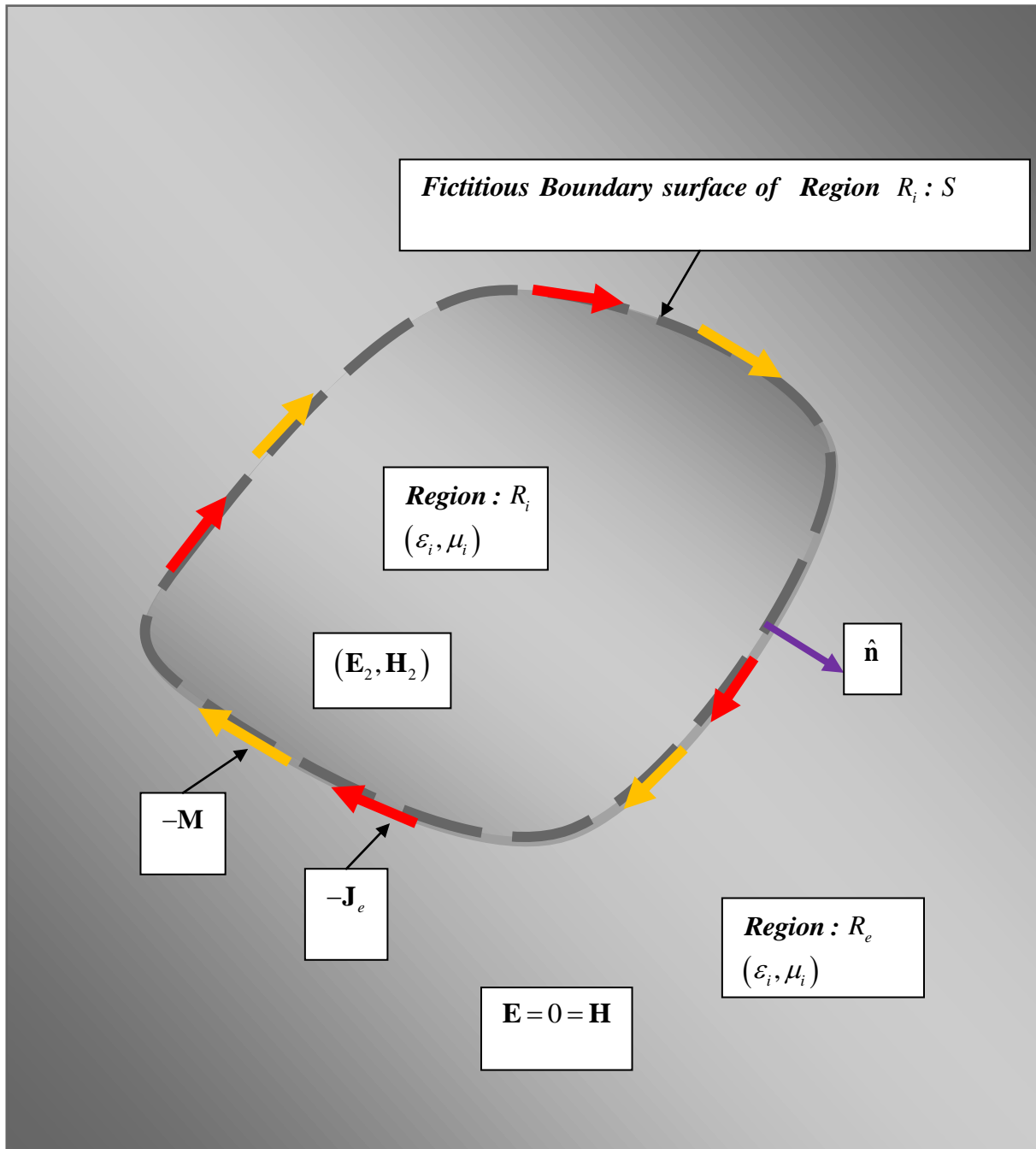


Figure A-1.1.3 Internal equivalence.

filled with the dielectric that existed in the internal region of the original problem. This time, the external region R_e is designated as the *region of no interest* in which we are free to choose whatever fields we desire. It will be convenient to choose $\mathbf{E}=0=\mathbf{H}$ in the region R_e . The internal region of the original problem had no impressed source. Therefore the whole unbounded space has no impressed source.

Now we have fields $(\mathbf{E}_2, \mathbf{H}_2)$ in the internal region and $\mathbf{E}=0=\mathbf{H}$ in the external region. As a result a jump in electric field from \mathbf{E}_2 in the internal region to $\mathbf{E}=0$ in the external region occurs. Similarly a jump in magnetic field from \mathbf{H}_2 in the internal region to $\mathbf{H}=0$ in the external region takes place. These jumps in the electric and magnetic fields are supported by placing equivalent electric and magnetic currents on the fictitious boundary. In this case the equivalent currents are

$$-\mathbf{J}_e = \hat{\mathbf{n}} \times (0 - \mathbf{H}_2) \Rightarrow$$

$$-\mathbf{J}_e = -\hat{\mathbf{n}} \times \mathbf{H}_2 \tag{A_1.1.15}$$

$$-\mathbf{M} = -\hat{\mathbf{n}} \times (-\mathbf{E}_2) \Rightarrow$$

$$-\mathbf{M} = \hat{\mathbf{n}} \times \mathbf{E}_2 \tag{A_1.1.16}$$

The derivations of (A_1.1.15) and (A_1.1.16) accord with the direction of unit vector $\hat{\mathbf{n}}$ which points into the external region.

The equivalent surface currents thus placed on the fictitious bounding surface radiate in unbounded space filled with the dielectric which existed only in the interior region of the original problem. These surface currents produce electric and magnetic fields at every point in the unbounded space. These electric and magnetic fields brought about by the equivalent surface currents $-\mathbf{J}_e$ and $-\mathbf{M}$ placed on the fictitious bounding surface are denoted as

$$\mathbf{E}_i(-\mathbf{J}_e, -\mathbf{M}) \tag{A_1.1.17}$$

$$\mathbf{H}_i(-\mathbf{J}_e, -\mathbf{M}) \tag{A_1.1.18}$$

$\mathbf{E}=0=\mathbf{H}$ exists in the external region. We meet this situation with the knowledge that zero tangential components of $\mathbf{E}_i(-\mathbf{J}_e, -\mathbf{M})$ and $\mathbf{H}_i(-\mathbf{J}_e, -\mathbf{M})$ on S^+ guarantee that $\mathbf{E}=0=\mathbf{H}$ in the external region. S^+ is the side that faces the external region. The statement that the tangential field components are zero on S^+ is expressed by the following two equations.

$$\left[\mathbf{E}_i(-\mathbf{J}_e, -\mathbf{M}) \Big|_{\tan} \right]_{S^+} = 0 \tag{A_1.1.19}$$

$$\left[\mathbf{H}_i(-\mathbf{J}_e, -\mathbf{M}) \Big|_{\text{tan}} \right]_{S^+} = 0 \quad (\text{A}_1.1.20)$$

Eqs. (A_1.1.19) and (A_1.1.20) imply

$$\left[\mathbf{E}_i(-\mathbf{J}_e, -\mathbf{M}) \right]_{S^+} = 0 \quad (\text{A}_1.1.21)$$

$$\left[\mathbf{H}_i(-\mathbf{J}_e, -\mathbf{M}) \right]_{S^+} = 0 \quad (\text{A}_1.1.22)$$

Multiplying (A_1.1.21) by an arbitrary constant α and adding it to (A_1.1.13) gives

$$-\frac{1}{\eta_e} \left(\left[\mathbf{E}_e(\mathbf{J}_e, \mathbf{M}) \right]_{S^-} + \alpha \left[\mathbf{E}_i(-\mathbf{J}_e, -\mathbf{M}) \right]_{S^+} \right) = \frac{1}{\eta_e} \left[\mathbf{E}^{inc} \right]_S \quad (\text{A}_1.1.23)$$

Multiplying (A_1.1.22) by an arbitrary constant β and adding it to (A_1.1.14) gives

$$-\left(\left[\mathbf{H}_e(\mathbf{J}_e, \mathbf{M}) \right]_{S^-} + \beta \left[\mathbf{H}_i(-\mathbf{J}_e, -\mathbf{M}) \right]_{S^+} \right) = \left[\mathbf{H}^{inc} \right]_S \quad (\text{A}_1.1.24)$$

The unknowns in (A_1.1.23) and (A_1.1.24) are \mathbf{J}_e and \mathbf{M} on S . Therefore (A_1.1.23) and (A_1.1.24) can be solved by the Method of Moments (MoM). The equations that can be solved by the method of moments are the tangential components of (A_1.1.23) and (A_1.1.24).

APPENDIX B

B_1.1 The Method of Moments (MoM)

Electromagnetic problems usually involve solution of linear partial differential or integral equations. The general form of such a linear equation is the operator equation.

$$\mathbf{L}\mathbf{f}(x) = \mathbf{g}(x) \quad a \leq x \leq b \quad (\text{B}_1.1.1)$$

where \mathbf{L} is a linear operator

\mathbf{f} is the function to be calculated

\mathbf{g} is a known function

To solve (B_1.1.1), the method of moments begins by approximating the unknown function $\mathbf{f}(x)$ by a linear combination of known functions $\Phi_n(x)$ referred to as *basis functions (expansion functions)*. Let us choose a set of N basis functions $\Phi_n(x)$ and expand the unknown function $\mathbf{f}(x)$ as a linear combination of these:

$$\mathbf{f}(x) \approx \bar{\mathbf{f}}(x) = \sum_{n=1}^N \alpha_n \Phi_n(x) \quad (\text{B}_1.1.2)$$

Here α_n are expansion coefficients to be determined. These basis functions are so selected that with appropriate values for the parameters α_n , the right side of (B_1.1.2) is exact as $N \rightarrow \infty$. In other words, we want to make

$$\mathbf{L}\bar{\mathbf{f}}(x) \approx \mathbf{g}(x) \quad (\text{B}_1.1.3)$$

Substituting (B_1.1.2) into (B_1.1.3) results in the following equation,

$$\mathbf{L}\bar{\mathbf{f}}(x) = \mathbf{L}\left(\sum_{n=1}^N \alpha_n \Phi_n(x)\right) \approx \mathbf{g}(x) \quad a \leq x \leq b \quad (\text{B}_1.1.4)$$

By subtracting (B_1.1.1) from $\mathbf{L}\bar{\mathbf{f}}(x)$ of (B_1.1.4), we obtain a residual \mathfrak{R} equal to

$$\mathfrak{R}(x) = \mathbf{L}\left(\sum_{n=1}^N \alpha_n \Phi_n(x)\right) - \mathbf{L}\mathbf{f}(x) = \mathbf{L}\left(\sum_{n=1}^N \alpha_n \Phi_n(x)\right) - \mathbf{g}(x) \quad (\text{B}_1.1.5)$$

We would like to force the residual to zero, that is

$$\mathfrak{R}(x) = \sum_{n=1}^N \alpha_n \mathbf{L}\Phi_n(x) - \mathbf{g}(x) \approx 0 \quad a \leq x \leq b \quad (\text{B}_1.1.6)$$

If we can find coefficients α_n that make the residual small for all x , $a \leq x \leq b$, then we take $\bar{\mathbf{f}}(x)$ to be a good approximation for $\mathbf{f}(x)$.

To determine α_n , one of two methods is generally used.

B_1.2 Method of collocation (Point matching)

Rather than seeking α_n that require the residual \mathfrak{R} to be small for all x in $[a, b]$, we set the residual \mathfrak{R} identically zero at N discrete *match points* x_m as many as *basis functions* $\Phi_n(x)$ that lie within this interval.

$$\mathfrak{R}(x = x_m) = 0 \quad m = 1, 2, \dots, N \quad (\text{B}_1.2.1)$$

Therefore, from (B_1.1.6), we deduce that

$$\mathfrak{R}(x) = \sum_{n=1}^N \alpha_n [\mathbf{L}\Phi_n(x)]_{x=x_m} - \mathbf{g}(x_m) = 0 \quad (\text{B}_1.2.2)$$

$$\sum_{n=1}^N \alpha_n [\mathbf{L}\Phi_n(x)]_{x=x_m} = \mathbf{g}(x_m) \quad (\text{B}_1.2.3)$$

For the *point matching* solution, we can choose N equidistant points defined as

$$x_m = a + \frac{(b-a)m}{N+1} \quad m = 1, 2, \dots, N \quad (\text{B}_1.2.4)$$

The point matching solution process can be implemented by satisfying (B_1.2.2) at the points x_m . This approach results in the following matrix equation

$$[l_{mm}][\alpha_n] = [b_m] \quad m = 1, 2, \dots, N \quad (\text{B}_1.2.5)$$

$$\text{and} \quad b_m = \mathbf{g}(x_m) \quad m = 1, 2, \dots, N \quad (\text{B}_1.2.6)$$

Once the α_n have been determined, they can be used in (B_1.1.2) to obtain approximation $\bar{\mathbf{f}}(x)$ to $\mathbf{f}(x)$.

B_1.3 Method of Weighted residuals

An alternative to Collocation (or *point matching*) is to set the N weighted averages of the residual to zero. In the weighted residual method, the *weighting functions* or *testing functions* w_m (which, in general, are not the same as the expansion functions) are chosen as many as expansion functions such that the integral of a weighted residual of the approximation is zero, i.e.,

$$\int_a^b w_m(x) \mathfrak{R}(x) dx = 0 \quad m = 1, 2, \dots, N \quad (\text{B}_1.3.1)$$

or

$$\langle w_m, \mathfrak{R} \rangle = 0 \quad (\text{B}_1.3.2)$$

where $\int_a^b w_m(x) \mathfrak{R}(x) dx$ or $\langle w_m, \mathfrak{R} \rangle$ are referred to as the *inner product*.

Substituting (B_1.1.6) in (B_1.3.1), we get

$$\int_a^b \left(\sum_{n=1}^N \alpha_n \mathbf{L}[\Phi_n(x)] - \mathbf{g}(x) \right) w_m(x) dx = 0 \Rightarrow$$

$$\sum_{n=1}^N \alpha_n \int_a^b \mathbf{L}[\Phi_n(x)] w_m(x) dx = \int_a^b \mathbf{g}(x) w_m(x) dx \quad m = 1, 2, \dots, N \quad (\text{B}_1.3.3)$$

The system of linear equations (B_1.3.3) can be cast into matrix form

$$[l_{mn}][\alpha_n] = [b_m] \quad m = 1, 2, \dots, N \quad (\text{B}_1.3.4)$$

Here

$$l_{mn} = \int_a^b \mathbf{L}[\Phi_n(x)] w_m(x) dx \quad (\text{B}_1.3.5)$$

and

$$b_m = \int_a^b \mathbf{g}(x) w_m(x) dx \quad (\text{B}_1.3.6)$$

Solving for α_n in (B_1.3.4) and substituting these values in (B_1.1.2), we get an approximate solution to (B_1.1.1). Collocation is a special case of the weighting function method with

$$w_m(x) = \delta(x - x_m) \quad m = 1, 2, \dots, N \quad (\text{B}_1.3.7)$$

here $\delta(x - x_m)$ is called the *dirac delta function*.

B_1.4 Choice of basis (expansion) and weighting(testing) functions.

Basis and weighting functions can be broadly classed as follows

1. **subdomain functions** are defined only over part of the domain of the unknown function. Included in this category are:

B-1.4(a). Piecewise uniform or pulse functions:

Let us consider the range of interest or domain size as $0 \leq x \leq 1$, and divide this range into $N + 1$ equal subintervals (subdomains) of width

$$\Delta_x = \frac{1}{N + 1} \quad (\text{B}_1.4.1)$$

The m^{th} subinterval extends from $x = x_{m-1}$ to x_m where

$$x_m = \frac{m}{N + 1}, \quad m = 0, 1, 2, 3, \dots, N + 1 \quad (\text{B}_1.4.2)$$

The subintervals and points x_m are shown in Figure B_1.4.1 for $N = 4$. A pulse function which is centered about x_m is defined as

$$P(x - x_m) = \begin{cases} 1 & \text{for } x_m - \frac{\Delta_x}{2} \leq x \leq x_m + \frac{\Delta_x}{2}, \\ 0 & \text{elsewhere} \end{cases} \quad m = 1, 2, 3, \dots, N \quad \text{where } \Delta = \frac{1}{N + 1} \quad (\text{B}_1.4.3)$$

A linear combination of pulse functions according to $f(x) = \sum_{n=1}^N \alpha_n P(x - x_m)$ gives a step or staircase approximation as shown in Figure B_1.4.2. It may be noted that Pulse functions are

orthogonal in nature because they do not overlap with others. The derivative of a pulse function consists of two Dirac delta functions.

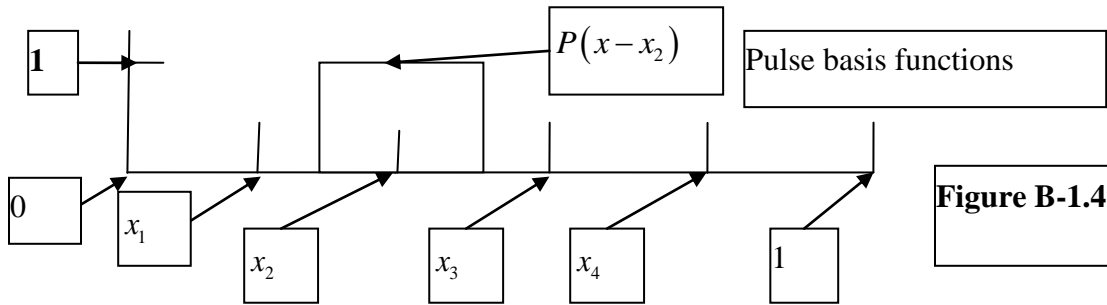


Figure B-1.4.1

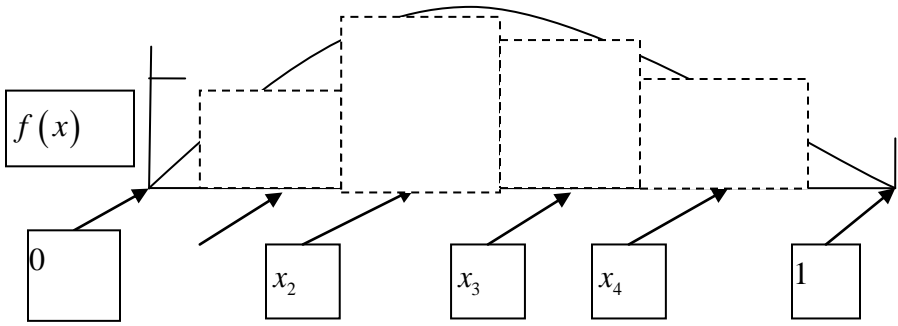


Figure B_1.4.2

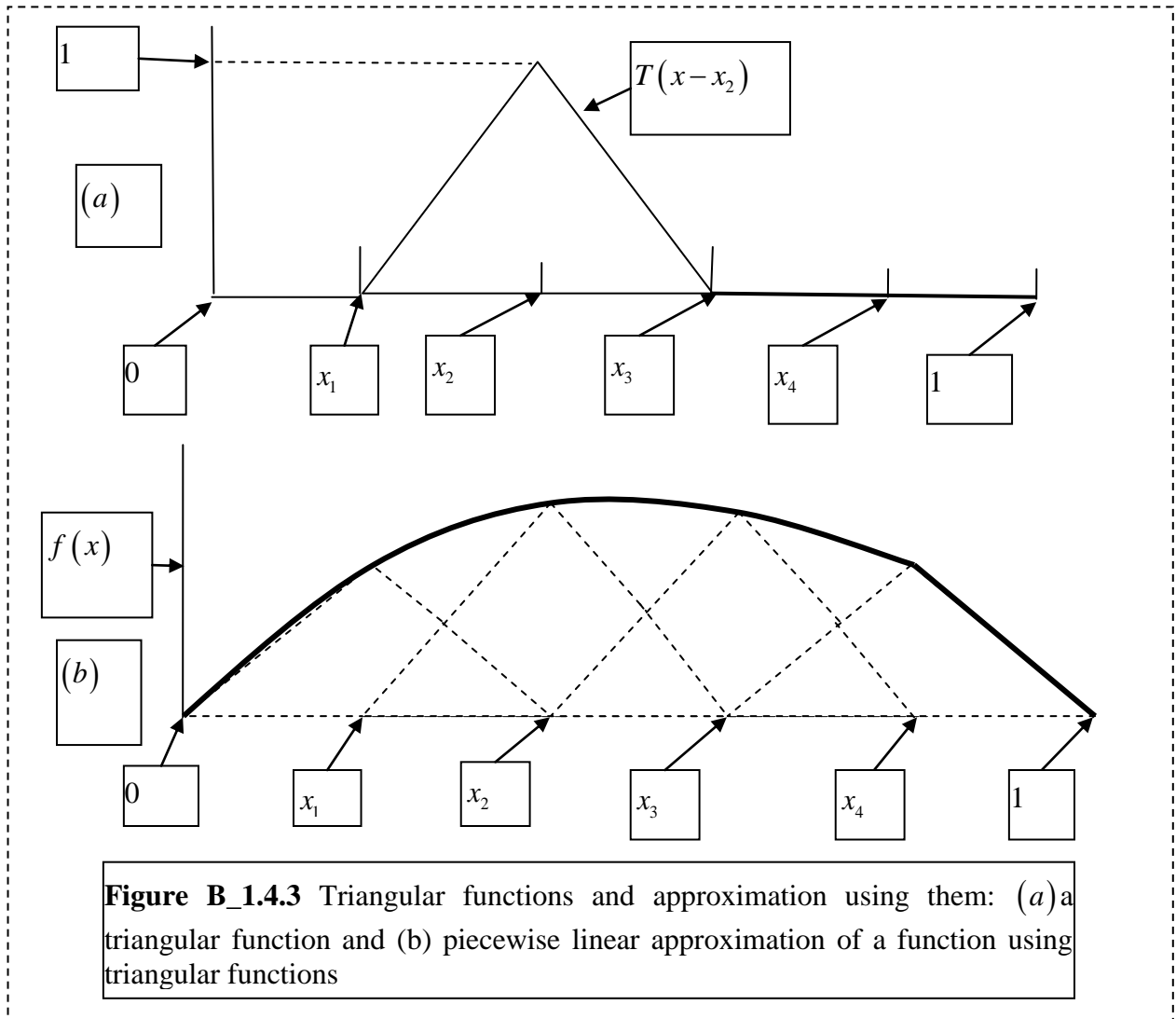
Step approximation of a function using pulse functions

B_1.4 (b). Triangular basis functions

A triangular function or piecewise linear function is defined as

$$T(x - x_m) = \begin{cases} \frac{x - x_{m-1}}{x_m - x_{m-1}} & \text{for } x_{m-1} \leq x \leq x_m \\ \frac{x_{m+1} - x}{x_{m+1} - x_m} & \text{for } x_m \leq x \leq x_{m+1} \\ 0 & \text{elsewhere} \end{cases} \quad (\text{B}_1.4.4)$$

For $N=4$, the function $T(x-x_2)$ is shown in Figure B_1.4.3(a). Figure B_1.4.3 shows a piecewise linear approximation to f .



How does one select the "best" testing functions for a choice of basis functions? Equation (B_1.1.1) is tested the best by any set of testing functions that is a basis for the range of the operator \mathbf{L} . the range of \mathbf{L} is the space of $\sum_{n=1}^N \alpha_n \mathbf{L}[\Phi_n(x)]$ where α_n is arbitrary. A basis for a space is a linearly independent functions that are in the space and are such that any function in the space can be

written as a linear combination of them. As far as forcing the residual to zero, the best we can do is to require the residual to be orthogonal to each basis function in the sense.

$$\int_a^b w_m(x) \mathfrak{R}(x) dx = 0 \quad m = 1, 2, 3, \dots, N \quad (\text{B}_1.4.5)$$

Substituting (B_1.1.5) in (B_1.4.5), we get

$$\int_a^b w_m(x) \left(\sum_{n=1}^N \alpha_n \mathbf{L}[\Phi_n(x)] - \mathbf{g}(x) \right) dx = 0 \Rightarrow$$

$$\sum_{n=1}^N \alpha_n \int_a^b \mathbf{L}[\Phi_n(x)] w_m(x) dx = \int_a^b \mathbf{g}(x) w_m(x) dx \quad (\text{B}_1.4.6)$$

Equation (B_1.4.6) is identical to (B_1.3.3).

Consider

$$w_m(x) = \Phi_m(x), \quad m = 1, 2, 3, \dots, N \quad (\text{B}_1.4.7)$$

This special case of the MoM in which basis and weighting functions are identical is called Galerkin's method.

B_1.5 – Galerkin's method

We will illustrate application of Galerkin's method by an example [24].

Example(B1.5) – Consider the following differential equation

$$-\frac{d^2 f}{dx^2} = 1 + 4x^2 \quad (\text{B}_1.5.1)$$

subject to $f(0) = f(1) = 0$. The analytical solution of (2.5.1) is

$$f(x) = \frac{5x}{6} - \frac{x^2}{2} - \frac{x^4}{3} \quad (\text{B}_1.5.2)$$

We will use method of moments to solve (B_1.5.1), compare results with the exact solution (B_1.5.2) and plot graphs of both exact solution and MoM solution.

With reference to the theoretical framework developed in above paragraphs, we have

$$\mathbf{L} = -\frac{d^2}{dx^2} \quad (\text{B}_1.5.3)$$

and

$$\mathbf{g}(x) = 1 + 4x^2 \quad (\text{B}_1.5.4)$$

We will choose basis function $\Phi_n(x)$ to be

$$\Phi_n(x) = x - x^{n+1}, \quad n = 1, 2, 3, \dots, N \quad (\text{B}_1.5.5)$$

and, therefore from (B_1.5.3) and (B_1.1.2),

$$\mathbf{L}\bar{\mathbf{f}}(x) = \mathbf{L}\left(\sum_{n=1}^N \alpha_n \Phi_n(x)\right) = -\frac{d^2}{dx^2}\left(\sum_{n=1}^N \alpha_n \Phi_n(x)\right) \quad (\text{B}_1.5.6)$$

Substituting (B_1.5.5) into (B_1.5.6), we get

$$\begin{aligned} \mathbf{L}\bar{\mathbf{f}}(x) &= \mathbf{L}\left(\sum_{n=1}^N \alpha_n \Phi_n(x)\right) = -\frac{d^2}{dx^2}\left(\sum_{n=1}^N \alpha_n (x - x^{n+1})\right) \quad (\text{B}_1.5.7) \\ &= -\left(\frac{d}{dx}(x - x^{n+1})\right) = -(1 - (n+1)x^n) \Rightarrow \\ &= -\left(\frac{d^2}{dx^2}(x - x^{n+1})\right) = -(0 - (n+1)(n)x^{n-1}) \Rightarrow \\ &= -\left(\frac{d^2}{dx^2}(x - x^{n+1})\right) = n(n+1)x^{n-1} \quad (\text{B}_1.5.8) \end{aligned}$$

Galerkin's approach requires replacement of weighting function $w_m(x)$ with $\Phi_m(x)$ according to (B_1.4.7). We will now use (B_1.3.3) replacing in it $w_m(x)$ with $\Phi_m(x)$ thus obtaining

$$\sum_{n=1}^N \alpha_n \int_0^1 \mathbf{L}[\Phi_n(x)] \Phi_m(x) dx = \int_0^1 \mathbf{g}(x) \Phi_m(x) dx \quad m = 1, 2, 3, \dots, N \quad (\text{B}_1.5.9)$$

Eq. (B_1.5.9) can, according to (B_1.3.4) be cast in matrix form

$$[l_{mn}][\alpha_n] = [b_m] \quad m = 1, 2, 3, \dots, N \quad (\text{B}_1.5.10)$$

Here, unlike (B_1.3.5) and (B_1.3.6), we have

$$l_{mn} = \int_0^1 \mathbf{L}[\Phi_n(x)] \Phi_m(x) dx \quad m = 1, 2, 3, \dots, N \quad (\text{B}_1.5.11)$$

$$b_m = \int_0^1 \mathbf{g}(x) \Phi_m(x) dx \quad (\text{B}_1.5.12)$$

$$\Phi_m(x) = x - x^{m+1} \quad (\text{B}_1.5.13)$$

Substituting (B_1.5.13), (B_1.5.5) and (B_1.5.3) into (B_1.5.11), we obtain

$$l_{mn} = \int_0^1 \mathbf{L}[\Phi_n(x)] \Phi_m(x) dx = \int_0^1 \left(-\frac{d^2}{dx^2} (x - x^{n+1}) \right) (x - x^{m+1}) dx \quad (\text{B}_1.5.14)$$

Substituting (B_1.5.8) into (B_1.5.14), we get

$$l_{mn} = \int_0^1 \mathbf{L}[\Phi_n(x)] \Phi_m(x) dx = n(n+1) \int_0^1 (x^{n-1}) (x - x^{m+1}) dx \quad (\text{B}_1.5.15)$$

$$l_{mn} = n(n+1) \left(\int_0^1 x^n dx - \int_0^1 x^{m+n} dx \right) = n(n+1) \left(\frac{x^{n+1}}{n+1} \Big|_0^1 - \frac{x^{m+n+1}}{m+n+1} \Big|_0^1 \right) \Rightarrow$$

$$l_{mn} = n(n+1) \left(\frac{1}{n+1} - \frac{1}{m+n+1} \right) = n(n+1) \left(\frac{m+n+1-n-1}{(n+1)(m+n+1)} \right) \Rightarrow$$

$$l_{mn} = \frac{mn}{(m+n+1)} \quad (\text{B}_1.5.16)$$

We substitute (B_1.5.4) and (B_1.5.13) into (B_1.5.12) and obtain

$$b_m = \int_0^1 (1+4x^2)(x - x^{m+1}) dx = \int_0^1 x(1+4x^2) dx - \int_0^1 x^{m+1}(1+4x^2) dx \quad (\text{B}_1.5.17)$$

$$\int_0^1 x(1+4x^2) dx = \left[\frac{x^2}{2} \Big|_0^1 \right] + 4 \left[\frac{x^4}{4} \Big|_0^1 \right] = \frac{1}{2} + 1 = \frac{3}{2} \quad (\text{B}_1.5.18)$$

$$-\int_0^1 x^{m+1} (1+4x^2) dx = -\left[\frac{x^{m+2}}{(m+2)} \right]_0^1 - 4 \left[\frac{x^{m+4}}{(m+4)} \right]_0^1 = -\frac{1}{(m+2)} - \frac{4}{(m+4)} = -\frac{(m+4+4m+8)}{(m+2)(m+4)} \quad (\text{B}_1.5.19)$$

Substituting (B_1.5.17) and (B_1.5.18) into (B_1.5.17), we obtain

$$b_m = \frac{(3m^2 + 18m + 24) - (10m + 24)}{2(m+2)(m+4)} = \frac{3m^2 + 8m}{2(m+2)(m+4)} \Rightarrow$$

$$b_m = \frac{m(3m+8)}{2(m+2)(m+4)} \quad (\text{B}_1.5.20)$$

We will rewrite (B_1.5.16) and (B_1.5.20) as

$$l_{mn} = \langle \Phi_m(x), \mathbf{L}\Phi_n(x) \rangle = \frac{mn}{(m+n+1)} \quad (\text{B}_1.5.21)$$

$$b_m = \langle \Phi_m(x), \mathbf{g}(x) \rangle = \frac{m(3m+8)}{2(m+2)(m+4)} \quad (\text{B}_1.5.22)$$

Galerkin method

In the matlab script L(m,n) stands for l_{mn} and N stands for number of expansion and weighting functions and g(m) stands for b_m .

Using Matlab program, we obtained the following results including graph of f and \bar{f} .

```
=====
N
=====
1
=====
```

L(m,n)

0.3333

g(m)

0.3667

alpha =

1.1000

Galerkin method

=====

N

=====

2

=====

L(m,n)

0.3333 0.5000

0.5000 0.8000

g(m)

0.3667

0.5833

alpha =

0.1000

0.6667

Galerkin method

=====

N

=====

3

=====

L(m,n)

0.3333 0.5000 0.6000

0.5000 0.8000 1.0000

0.6000 1.0000 1.2857

g(m)

0.3667

0.5833

0.7286

alpha =

0.5000

0.0000

0.3333

Galerkin method

=====

N

=====

10

=====

L(m,n)

0.3333	0.5000	0.6000	0.6667	0.7143	0.7500	0.7778	0.8000	0.8182	0.8333
0.5000	0.8000	1.0000	1.1429	1.2500	1.3333	1.4000	1.4545	1.5000	1.5385
0.6000	1.0000	1.2857	1.5000	1.6667	1.8000	1.9091	2.0000	2.0769	2.1429
0.6667	1.1429	1.5000	1.7778	2.0000	2.1818	2.3333	2.4615	2.5714	2.6667
0.7143	1.2500	1.6667	2.0000	2.2727	2.5000	2.6923	2.8571	3.0000	3.1250
0.7500	1.3333	1.8000	2.1818	2.5000	2.7692	3.0000	3.2000	3.3750	3.5294
0.7778	1.4000	1.9091	2.3333	2.6923	3.0000	3.2667	3.5000	3.7059	3.8889
0.8000	1.4545	2.0000	2.4615	2.8571	3.2000	3.5000	3.7647	4.0000	4.2105

0.8182 1.5000 2.0769 2.5714 3.0000 3.3750 3.7059 4.0000 4.2632 4.5000
0.8333 1.5385 2.1429 2.6667 3.1250 3.5294 3.8889 4.2105 4.5000 4.7619

g(m)

0.3667

0.5833

0.7286

0.8333

0.9127

0.9750

1.0253

1.0667

1.1014

1.1310

alpha =

0.5000

0.0000

0.3333

-0.0001

0.0001

-0.0003

0.0005

-0.0002
 0.0000
 -0.0000

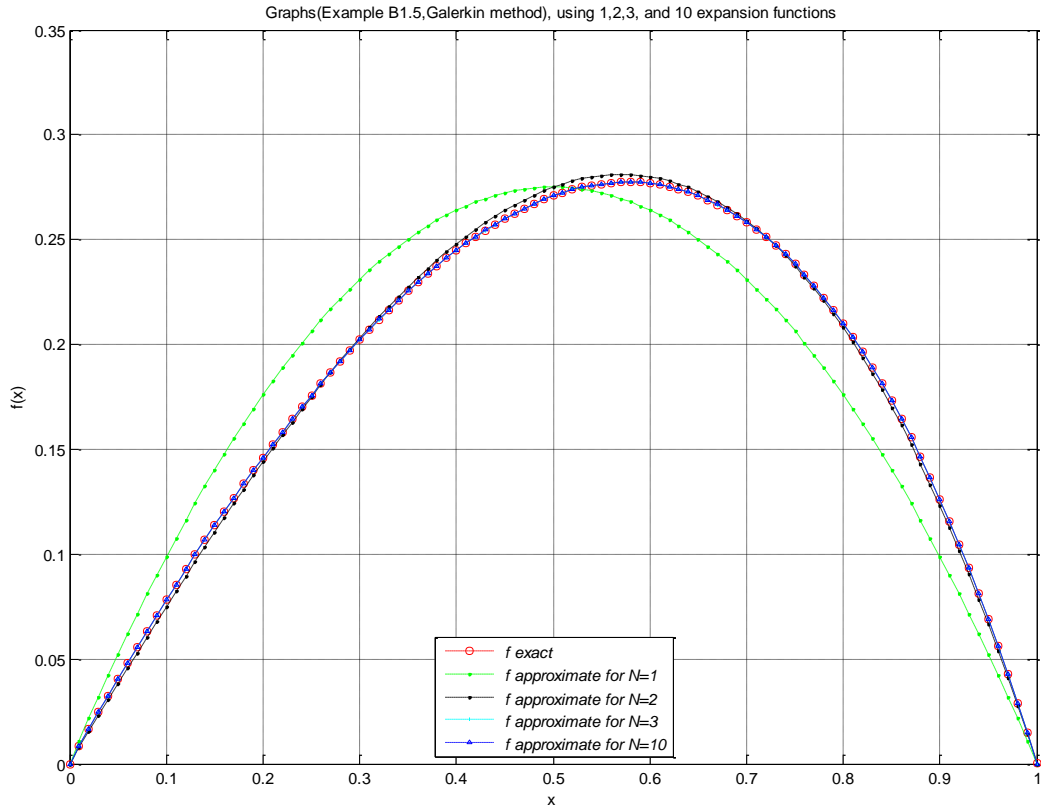


Figure B_1.5.1 Graph of Exact and Approximate solution (Galerkin's method).

B_1.6 – Point Matching method

We will illustrate application of the Point Matching method by an example [24].

Example(B1.6) – Consider the following differential equation

$$-\frac{d^2 f}{dx^2} = 1 + 4x^2 \tag{B_1.6.1}$$

subject to $f(0) = f(1) = 0$. The analytical solution of (B_2.6.1) is

$$f(x) = \frac{5x}{6} - \frac{x^2}{2} - \frac{x^4}{3} \quad (\text{B}_1.6.2)$$

We will use method of moments to solve (B_1.6.1), compare results with the exact solution (B_1.6.2) and plot graphs of both exact solution and MoM solution.

With reference to the theoretical framework developed in above paragraphs, we have

$$\mathbf{L} = -\frac{d^2}{dx^2} \quad (\text{B}_1.6.3)$$

and

$$\mathbf{g}(x) = 1 + 4x^2 \quad (\text{B}_1.6.4)$$

We will choose basis function $\Phi_n(x)$ to be

$$\Phi_n(x) = x - x^{n+1} \quad (\text{B}_1.6.5)$$

and, therefore from (B_1.6.3)

$$\mathbf{L}\bar{\mathbf{f}}(x) = \mathbf{L}\left(\sum_{n=1}^N \alpha_n \Phi_n(x)\right) = -\frac{d^2}{dx^2}\left(\sum_{n=1}^N \alpha_n \Phi_n(x)\right) \quad (\text{B}_1.6.6)$$

Substituting (B_1.6.5) into (B_1.6.6), we get

$$\mathbf{L}\bar{\mathbf{f}}(x) = \mathbf{L}\left(\sum_{n=1}^N \alpha_n \Phi_n(x)\right) = -\frac{d^2}{dx^2}\left(\sum_{n=1}^N \alpha_n (x - x^{n+1})\right) \quad (\text{B}_1.6.7)$$

$$-\left(\frac{d}{dx}(x - x^{n+1})\right) = -(1 - (n+1)x^n) \Rightarrow$$

$$-\left(\frac{d^2}{dx^2}(x - x^{n+1})\right) = -(0 - (n+1)(n)x^{n-1}) \Rightarrow$$

$$-\left(\frac{d^2}{dx^2}(x - x^{n+1})\right) = n(n+1)x^{n-1} \quad (\text{B}_1.6.8)$$

For the Point Matching solution, we choose N equidistant points defined as

$$x_m = \frac{m}{N+1} \quad m = 1, 2, 3, \dots, N \quad (\text{B}_1.6.9)$$

Matching (B_1.6.7) and (B_1.6.4) at x_m , we obtain

$$l_{mn} = \left[n(n+1)x^{n-1} \right]_{x=x_m} \quad m = 1, 2, 3, \dots, N, \quad n = 1, 2, 3, \dots, N \quad (\text{B}_1.6.10)$$

$$g(x_m) = \left[1 + 4x^2 \right]_{x=x_m} \quad m = 1, 2, 3, \dots, N \quad (\text{B}_1.6.11)$$

we can cast (B_2.6.9) – (2.6.11) into a matrix form as

$$[l_{mn}][\alpha_n] = [g_m] \quad m = 1, 2, 3, \dots, N \quad (\text{B}_1.6.12)$$

Point Matching method

In the matlab script L(m,n) stands for l_{mn} and N stands for number of expansion and weighting functions and g(m) stands for b_m .

Using Matlab program, we obtained the following results including graph of f and \bar{f} .

=====

N

=====

1

=====

L(m,n)

9.8696

g(m)

2

alpha =

0.2026

=====

N

=====

2

=====

L(m,n)

8.5473 34.1893

8.5473 -34.1893

g(m)

1.4444 2.7778

alpha =

0.2470

-0.0195

=====

N

=====

3

=====

L

6.9789 39.4784 62.8098

9.8696 0.0000 -88.8264

6.9789 -39.4784 62.8098

g

1.2500

2.0000

3.2500

alpha =

0.2625

-0.0253

0.0067

=====

N

=====

10

=====

L

2.7806 21.3436 67.1305 143.6433 244.2287 351.6893 439.9077 477.3728 432.2088 278.0589
5.3359 35.9108 87.9223 119.3432 69.5147 -100.1012 -365.4885 -625.2253 -727.1943 -533.5911
7.4589 39.0766 48.0232 -44.4894 -224.4427 -323.1975 -136.2489 341.4983 791.3008 745.8949
8.9777 29.8358 -25.0253 -156.3063 -133.3978 192.0928 478.6882 177.9577 -604.1749 -897.7708
9.7691 11.1224 -80.7994 -85.3746 186.4737 268.5222 -261.4596 -574.5733 225.2277 976.9146
9.7691 -11.1224 -80.7994 85.3746 186.4737 -268.5222 -261.4596 574.5733 225.2277 -976.9146
8.9777 -29.8358 -25.0253 156.3063 -133.3978 -192.0928 478.6882 -177.9577 -604.1749 897.7708
7.4589 -39.0766 48.0232 44.4894 -224.4427 323.1975 -136.2489 -341.4983 791.3008 -745.8949
5.3359 -35.9108 87.9223 -119.3432 69.5147 100.1012 -365.4885 625.2253 -727.1943 533.5911
2.7806 -21.3436 67.1305 -143.6433 244.2287 -351.6893 439.9077 -477.3728 432.2088 -278.0589

g

1.0331
1.1322
1.2975
1.5289
1.8264
2.1901
2.6198
3.1157
3.6777
4.3058

alpha =

0.2798

-0.0314

0.0130

-0.0036

0.0025

-0.0009

0.0007

-0.0003

0.0002

-0.0001

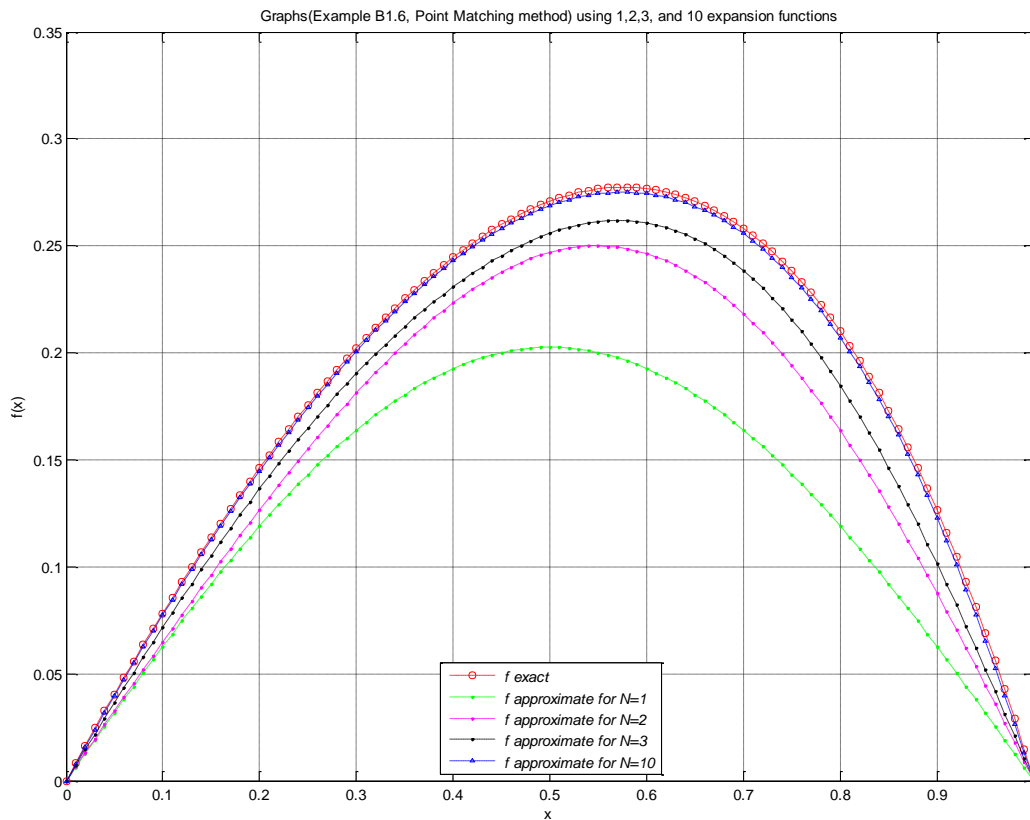


Figure B_1.6.1 Graph of Exact and Approximate solution (Point Matching method).

B_1.7 – Triangular function

We will illustrate application of Triangular function or piecewise linear function application by an example [24]. Both basis and triangular functions are triangular functions.

Example(B1.7) – Consider the following differential equation [24].

$$-\frac{d^2 f}{dx^2} = 1 + 4x^2 \tag{B_1.7.1}$$

subject to $f(0) = f(1) = 0$. The analytical solution of (B_1.7.1) is

$$f(x) = \frac{5x}{6} - \frac{x^2}{2} - \frac{x^4}{3} \tag{B_1.7.2}$$

We will use the method of moments to solve (B_1.7.1), compare results with the exact solution (B_1.7.2) and plot graphs of both exact solution and MoM solution.

We will choose basis function $\Phi_n(x)$ to be

$$\Phi_n(x) = \begin{cases} \frac{x - x_{n-1}}{x_n - x_{n-1}}, & x_{n-1} \leq x_n \\ \frac{x_{n+1} - x}{x_{n+1} - x_n}, & x_n \leq x_{n+1} \end{cases}$$

With reference to theoretical framework developed in above paragraphs, we have

$$\mathbf{L} = -\frac{d^2}{dx^2} \tag{B_1.7.3}$$

and

$$\mathbf{g}(x) = 1 + 4x^2 \tag{B_1.7.4}$$

Here

$$l_{mm} = \begin{cases} 2(N+1) & m = n \\ -(N+1) & |m - n| = 1 \\ 0 & |m - n| > 1 \end{cases} \tag{B_1.7.5}$$

$$g_m = \int_{x_{m-1}}^{x_m} (1 + 4x^2) \frac{(x - x_{m-1})}{x_m - x_{m-1}} dx + \int_{x_m}^{x_{m+1}} (1 + 4x^2) \frac{(x_{m+1} - x)}{x_{m+1} - x_m} dx$$

$$x_m - x_{m-1} = x_{m+1} - x_m = \frac{1}{N+1} = \Delta$$

let

$$u = x - x_{m-1}$$

$$v = x_{m+1} - x$$

then

$$g_m = \frac{1}{\Delta} \int_0^{\Delta} (1 + 4(u + x_{m-1})^2) u du - \frac{1}{\Delta} \int_{\Delta}^0 (1 + 4(x_{m+1} - v)^2) v dv$$

$$g_m = \frac{1}{\Delta} \int_0^{\Delta} 1 + 4(u + x_{m-1})^2 u du + \frac{1}{\Delta} \int_0^{\Delta} (1 + 4(x_{m+1} - v)^2) v dv$$

$$g_m = \frac{1}{\Delta} \int_0^{\Delta} \{1 + 4(u + x_{m-1})^2 + 1 + 4(x_{m+1} - u)^2\} u du$$

$$g_m = \frac{1}{\Delta} \int_0^{\Delta} \{2 + 4(u^2 + 2ux_{m-1} + x_{m-1}^2 + x_{m+1}^2 - 2ux_{m+1} + u^2)\} u du$$

$$g_m = \frac{1}{\Delta} \int_0^{\Delta} \{2 + 4(2u^2 - 2u(x_{m+1} - x_{m-1}) + x_{m-1}^2 + x_{m+1}^2)\} u du$$

$$g_m = \frac{1}{\Delta} \int_0^{\Delta} \{2 + 4(2u^2 - 4u\Delta + (m-1)^2 \Delta^2 + (m+1)^2 \Delta^2)\} u du$$

$$g_m = \frac{1}{\Delta} \int_0^{\Delta} \{2 + 4(2u^2 - 4u\Delta + (m^2 - 2m + 1)\Delta^2 + (m^2 + 2m + 1)\Delta^2)\} u du$$

$$g_m = \frac{1}{\Delta} \int_0^{\Delta} \{2 + 4(2u^2 - 4u\Delta + (2m^2 + 2)\Delta^2)\} u du$$

$$g_m = \frac{2}{\Delta} \int_0^{\Delta} \{1 + 4u^2 - 8u\Delta + (4m^2 + 4)\Delta^2\} u du$$

$$g_m = \frac{2}{\Delta} \int_0^{\Delta} \{u + 4u^3 - 8u^2\Delta + (4m^2 + 4)\Delta^2 u\} du$$

$$g_m = \frac{2}{\Delta} \left[\frac{u^2}{2} + u^4 - \frac{8}{3} u^3 \Delta + (4m^2 + 4) \frac{u^2}{2} \Delta^2 \right]_0^{\Delta}$$

$$g_m = \frac{2}{\Delta} \left[\frac{\Delta^2}{2} + \Delta^4 - \frac{8}{3} \Delta^4 + (4m^2 + 4) \frac{\Delta^4}{2} \right]$$

$$g_m = \frac{2}{\Delta} \left[\frac{\Delta^2}{2} + \Delta^4 \left(2m^2 + 1 - \frac{8}{3} + 2 \right) \right]$$

$$g_m = \frac{2}{\Delta} \left[\frac{\Delta^2}{2} + \Delta^4 \left(2m^2 + \frac{1}{3} \right) \right]$$

$$g_m = \left[\Delta + 2\Delta^3 \left(2m^2 + \frac{1}{3} \right) \right]$$

$$g_m = \Delta \left[1 + \left(4m^2 + \frac{2}{3} \right) \Delta^2 \right]$$

$$g_m = \frac{1}{N+1} \left[1 + \frac{4m^2 + (2/3)}{(N+1)^2} \right] \quad (\text{B}_-1.7.6)$$

Triangle function method

In the matlab script L(m,n) stands for l_{mn} and N stands for number of expansion and weighting functions and g(m) stands for b_m . Five triangle functions are used.

Using Matlab program, we obtained the following results including graph of f and \bar{f} .

L

```

12  -6  0  0  0
-6  12 -6  0  0
0   -6 12 -6  0
0   0  -6 12 -6
0   0  0  -6 12

```

g

0.1867

0.2423

0.3349

0.4645

0.6312

alpha =

0.1241

0.2171

0.2697

0.2665

0.1858

L

12 -6 0 0 0

-6 12 -6 0 0

0 -6 12 -6 0

0 0 -6 12 -6

0 0 0 -6 12

g

0.1867

0.2423

0.3349
 0.4645
 0.6312
 alpha =
 0.1241
 0.2171
 0.2697
 0.2665
 0.1858

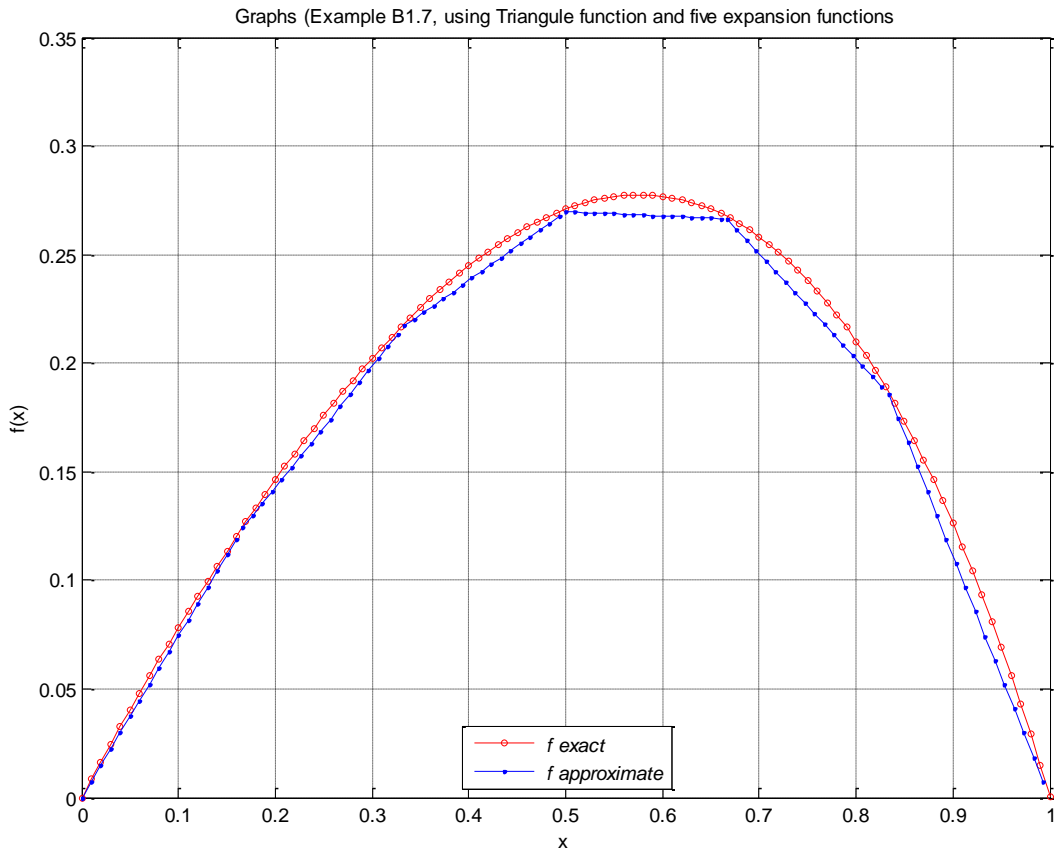


Figure B-1.7.1 Graph of Exact and Approximate solution (Triangle function method), using five expansion functions

Triangle function method

In the matlab script $L(m,n)$ stands for l_{mn} and N stands for number of expansion and weighting functions and $g(m)$ stands for b_m . Ten triangle functions are used.

Using Matlab program, we obtained the following results including graph of f and \bar{f} .

L

```
22 -11  0  0  0  0  0  0  0  0
-11 22 -11  0  0  0  0  0  0  0
 0 -11 22 -11  0  0  0  0  0  0
 0  0 -11 22 -11  0  0  0  0  0
 0  0  0 -11 22 -11  0  0  0  0
 0  0  0  0 -11 22 -11  0  0  0
 0  0  0  0  0 -11 22 -11  0  0
 0  0  0  0  0  0 -11 22 -11  0
 0  0  0  0  0  0  0 -11 22 -11
 0  0  0  0  0  0  0  0 -11 22
```

g

0.0942

0.1032

0.1182

0.1392

0.1663

0.1993

0.2384

0.2835

0.3346

0.3917

alpha =

0.0715

0.1344

0.1880

0.2308

0.2609

0.2759

0.2728

0.2481

0.1975

0.1166

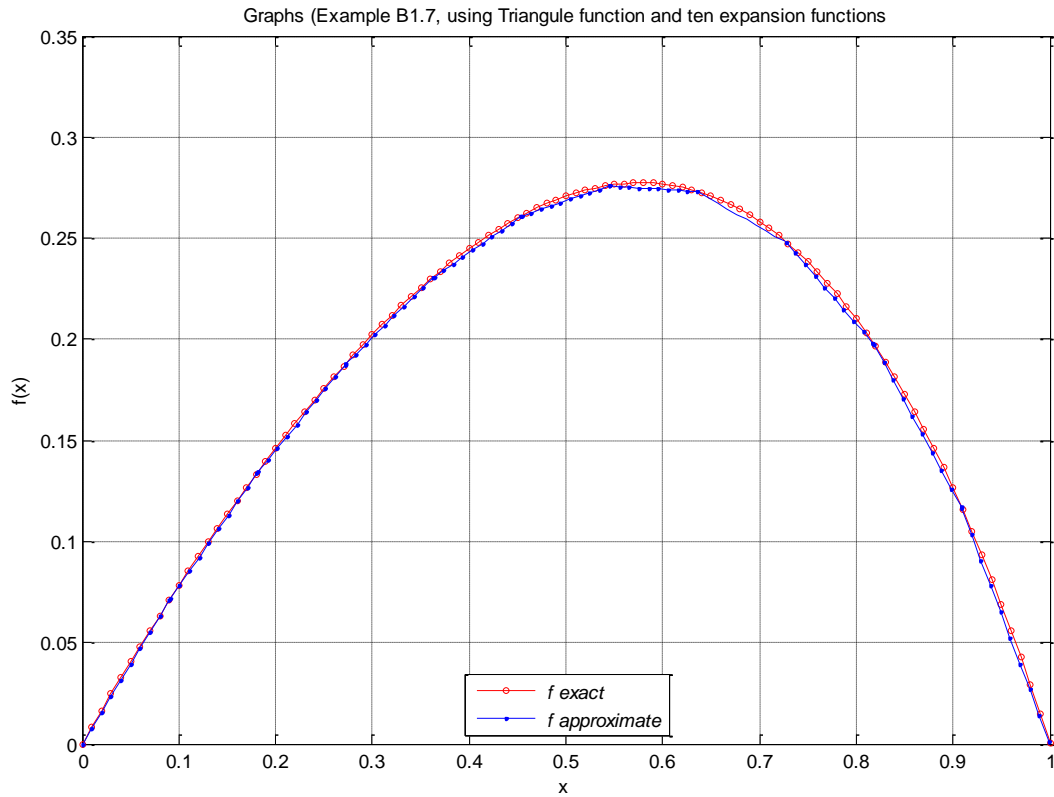


Figure B-1.7.2 Graph of Exact and Approximate solution (Triangle function method), using ten expansion functions.

Triangle function method

In the matlab script $L(m,n)$ stands for l_{mn} and N stands for number of expansion and weighting functions and $g(m)$ stands for b_m . Fifteen triangle functions are used.

Using Matlab program, we obtained the following results including graph of f and \bar{f} .

L

32	-16	0	0	0	0	0	0	0	0	0	0	0	0	0
-16	32	-16	0	0	0	0	0	0	0	0	0	0	0	0
0	-16	32	-16	0	0	0	0	0	0	0	0	0	0	0

0	0	-16	32	-16	0	0	0	0	0	0	0	0	0	0
0	0	0	-16	32	-16	0	0	0	0	0	0	0	0	0
0	0	0	0	-16	32	-16	0	0	0	0	0	0	0	0
0	0	0	0	0	-16	32	-16	0	0	0	0	0	0	0
0	0	0	0	0	0	-16	32	-16	0	0	0	0	0	0
0	0	0	0	0	0	0	-16	32	-16	0	0	0	0	0
0	0	0	0	0	0	0	0	-16	32	-16	0	0	0	0
0	0	0	0	0	0	0	0	0	-16	32	-16	0	0	0
0	0	0	0	0	0	0	0	0	0	-16	32	-16	0	0
0	0	0	0	0	0	0	0	0	0	0	-16	32	-16	0
0	0	0	0	0	0	0	0	0	0	0	0	-16	32	-16
0	0	0	0	0	0	0	0	0	0	0	0	0	-16	32

g

0.0636

0.0665

0.0714

0.0782

0.0870

0.0977

0.1104

0.1251

0.1417

0.1602

0.1807

0.2032

0.2276

0.2540

0.2823

alpha =

0.0501

0.0962

0.1382

0.1757

0.2083

0.2354

0.2565

0.2707

0.2770

0.2745

0.2620

0.2382

0.2016

0.1509

0.0843

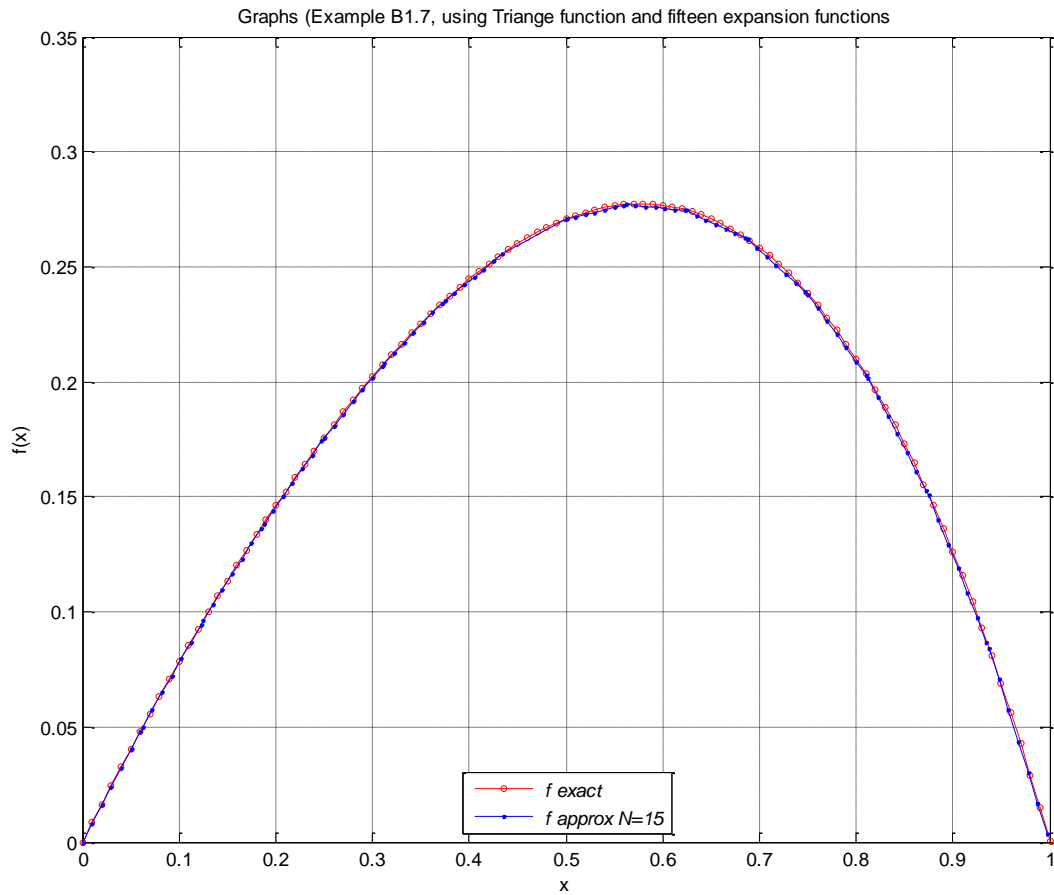


Figure B-1.7.3 Graph of Exact and Approximate solution (Triangle function method), using fifteen expansion functions.

Example(B1.8) – Consider the following differential equation [24].

$$-\frac{d^2 f}{dx^2} = 1 + 4x^2 \quad (\text{B}_1.8.1)$$

subject to $f(0) = f(1) = 0$. The analytical solution of (B_1.7.1) is

$$f(x) = \frac{5x}{6} - \frac{x^2}{2} - \frac{x^4}{3} \quad (\text{B}_1.8.2)$$

We will use the method of moments to solve (B_1.8.1), compare results with the exact solution (B_1.8.2) and plot graphs of both exact solution and MoM solution.

Solution

$$\mathbf{L}\bar{f}(x) = \mathbf{L}\left(\sum_{n=1}^N \alpha_n \Phi_n(x)\right) = -\frac{d^2}{dx^2}\left(\sum_{n=1}^N \alpha_n \Phi_n(x)\right) \quad (\text{B}_1.8.3)$$

$$\mathbf{L} = -\frac{d^2}{dx^2} \quad (\text{B}_1.8.4)$$

$$\mathbf{g} = 1 + 4x^2 \quad (\text{B}_1.8.5)$$

We will choose basis function $\Phi_n(x)$ to be

$$\Phi_n(x) = \sin(n\pi x) \quad (\text{B}_1.8.6)$$

$$\mathbf{L}[\Phi_n(x)] = -\frac{d^2\Phi_n(x)}{dx^2} = (n\pi)^2 \sin(n\pi x) \quad (\text{B}_1.8.7)$$

$$l_{mn} = \int_0^1 \mathbf{L}[\Phi_n(x)]\Phi_m(x) dx \quad (\text{B}_1.8.8)$$

$$l_{mn} = \int_0^1 \left((n\pi)^2 \sin(n\pi x)\right) \sin(m\pi x) dx \Rightarrow$$

$$l_{mn} = (n\pi)^2 \int_0^1 \sin(n\pi x) \sin(m\pi x) dx \Rightarrow$$

For $m = n$

$$l_{nn} = (n\pi)^2 \int_0^1 \sin^2(n\pi x) dx \quad (\text{B}_1.8.9)$$

Let

$$\pi x = u \quad (\text{B}_1.8.10)$$

hence

$$\pi dx = du \quad (\text{B}_1.8.11)$$

substituting (B_1.8.10) and (B_1.8.11) into (B_1.8.9), one obtains

$$l_{mn}|_{m=n} = (n\pi)^2 \int_0^\pi \sin^2(nu) \left(\frac{du}{\pi} \right) \quad (\text{B}_1.8.12)$$

$$l_{mn}|_{m=n} = \frac{(n\pi)^2}{\pi} \int_0^\pi \sin^2(nu) du \Rightarrow$$

$$l_{mn}|_{m=n} = \frac{(n\pi)^2}{\pi} \int_0^\pi \left(\frac{1 - \cos(2nu)}{2} \right) du \Rightarrow$$

$$l_{mn}|_{m=n} = \frac{(n\pi)^2}{2\pi} \int_0^\pi (1 - \cos 2nu) du \Rightarrow$$

$$l_{mn}|_{m=n} = \frac{(n\pi)^2}{2\pi} \left\{ \int_0^\pi du - \int_0^\pi (\cos(2nu)) du \right\} \Rightarrow$$

$$l_{mn}|_{m=n} = \frac{(n\pi)^2}{2\pi} \left\{ \pi - \frac{\sin(2nu)}{2n} \Big|_0^\pi \right\} \Rightarrow$$

$$l_{mn}|_{m=n} = \frac{(n\pi)^2}{2\pi} (\pi) \Rightarrow$$

$$l_{mn}|_{m=n} = \frac{(n\pi)^2}{2} \quad (\text{B}_1.8.13)$$

$$b_m = \int_0^1 (1 + 4x^2) \sin(m\pi x) dx \quad (\text{B}_1.8.14)$$

$$b_m = \int_0^1 \sin(m\pi x) dx + 4 \int_0^1 x^2 \sin(m\pi x) dx \quad (\text{B}_1.8.15)$$

$$\int_0^1 \sin(m\pi x) dx = \left[-\frac{\cos(m\pi x)}{m\pi} \Big|_0^1 \right] \Rightarrow$$

$$\int_0^1 \sin(m\pi x) dx = -\left(\frac{1}{m\pi} \right) \left[\cos(m\pi x) \Big|_0^1 \right] \Rightarrow$$

$$\int_0^1 \sin(m\pi x) dx = \left(\frac{1}{m\pi} \right) [1 - \cos m\pi] \quad (\text{B}_1.8.16)$$

$$\int x^2 \sin(m\pi x) dx = (x^2) \left[-\frac{\cos(m\pi x)}{m\pi} \right] - \int (2x) \left[-\frac{\cos(m\pi x)}{m\pi} \right] dx \Rightarrow$$

$$\int x^2 \sin(m\pi x) dx = (x^2) \left[-\frac{\cos(m\pi x)}{m\pi} \right] + \left(\frac{2}{m\pi} \right) \int (x) \cos(m\pi x) dx \Rightarrow$$

$$\int x^2 \sin(m\pi x) dx = (x^2) \left[-\frac{\cos(m\pi x)}{m\pi} \right] + \left(\frac{2}{m\pi} \right) \left\{ x \left[\frac{\sin(m\pi x)}{(m\pi)} \right] - \frac{1}{m\pi} \int \sin(m\pi x) dx \right\} \Rightarrow$$

$$\int x^2 \sin(m\pi x) dx = (x^2) \left[-\frac{\cos(m\pi x)}{m\pi} \right] + \left(\frac{2}{m\pi} \right) \left\{ x \left[\frac{\sin(m\pi x)}{(m\pi)} \right] - \frac{1}{m\pi} \left[-\frac{\cos(m\pi x)}{m\pi} \right] \right\} \Rightarrow$$

$$\int x^2 \sin(m\pi x) dx = \left[-\frac{(x^2) \cos(m\pi x)}{m\pi} \right] + \left(\frac{2}{m\pi} \right) \left(\frac{1}{m\pi} \right) \left\{ x \sin(m\pi x) + \frac{1}{m\pi} \cos(m\pi x) \right\} \Rightarrow$$

$$\int x^2 \sin(m\pi x) dx = -\frac{(x^2) \cos(m\pi x)}{m\pi} + \frac{2}{(m\pi)^2} x \sin(m\pi x) + \frac{2}{(m\pi)^3} \cos(m\pi x) \quad (\text{B}_1.8.17)$$

and

$$\int_0^1 x^2 \sin(m\pi x) dx = \left(-\frac{(x^2) \cos(m\pi x)}{m\pi} + \frac{2}{(m\pi)^2} x \sin(m\pi x) + \frac{2}{(m\pi)^3} \cos(m\pi x) \right) \Bigg|_0^1 \Rightarrow$$

$$\int_0^1 x^2 \sin(m\pi x) dx = \left(-\frac{\cos(m\pi)}{m\pi} + \frac{2}{(m\pi)^3} \cos(m\pi) \right) - \left(\frac{2}{(m\pi)^3} \right) \Bigg|_0^1 \Rightarrow$$

$$\int_0^1 x^2 \sin(m\pi x) dx = \left\{ \left(-\frac{\cos(m\pi)}{m\pi} + \frac{2}{(m\pi)^3} \cos(m\pi) \right) - \frac{2}{(m\pi)^3} \right\} \Rightarrow$$

$$\int_0^1 x^2 \sin(m\pi x) dx = \frac{1}{m\pi} \left\{ \left(-\cos(m\pi) + \frac{2}{(m\pi)^2} \cos(m\pi) - \frac{2}{(m\pi)^2} \right) - \frac{2}{(m\pi)^2} \right\} \quad (\text{B}_1.8.18)$$

$$4 \int_0^1 x^2 \sin(m\pi x) dx = \frac{1}{m\pi} \left\{ \left(-4 \cos(m\pi) + \frac{8}{(m\pi)^2} \cos(m\pi) - \frac{8}{(m\pi)^2} \right) \right\} \quad (\text{B}_1.8.19)$$

Substituting (B_1.8.16) and (B_1.8.19) into (B_1.8.15), one obtains

$$b_m = \int_0^1 \sin(m\pi x) dx + 4 \int_0^1 x^2 \sin(m\pi x) dx = \left(\frac{1}{m\pi} \right) \left[1 - \cos m\pi - 4 \cos(m\pi) + \frac{8}{(m\pi)^2} \cos(m\pi) - \frac{8}{(m\pi)^2} \right] \quad (\text{B}_1.8.20)$$

Using Matlab program, we obtained the following results including graph of f and \bar{f} .

Galerkin method

In the matlab script L(m,n) stands for l_{mn} and N stands for number of expansion and weighting functions and g(m) stands for b_m .

Galerkin method

=====

N

=====

1

=====

L(m,n)

4.9348

g(m)

1.3938

alpha =

0.2824

=====

N

=====

2

=====

L(m,n)

4.9348 0

0 19.7392

g(m)

1.3938 -0.6366

alpha =

0.2824

-0.0323

=====

N

=====

3

=====

L

4.9348 0 0
0 19.7392 0
0 0 44.4132

g

1.3938
-0.6366
0.6175

alpha =

0.2824
-0.0323
0.0139

=====

N

=====

5

=====

L

4.9348 0 0 0 0

0	19.7392	0	0	0
0	0	44.4132	0	0
0	0	0	78.9568	0
0	0	0	0	123.3701

g

1.3938

-0.6366

0.6175

-0.3183

0.3778

alpha =

0.2824

-0.0323

0.0139

-0.0040

0.0031

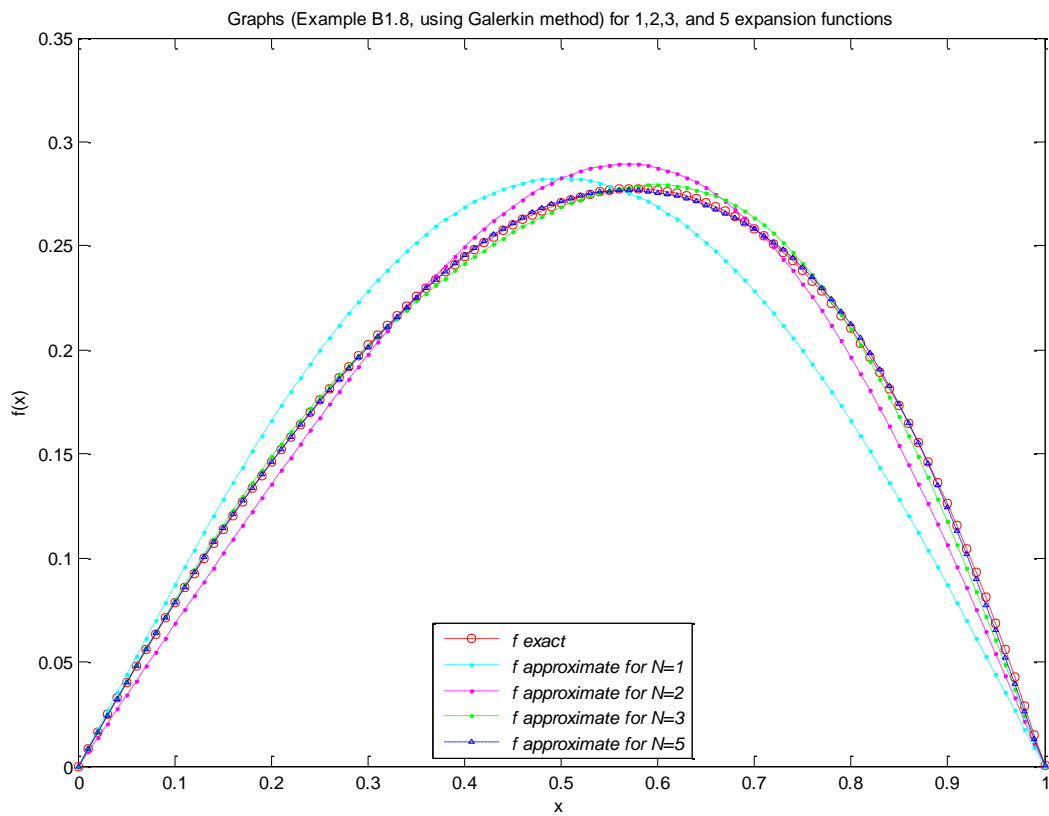


Figure B-1.8.1 Graph of Exact and Approximate solution (Galerkin method), using 1, 2, 3, and 5 expansion functions. $\Phi_n(x) = \sin(n\pi x)$ is the expansion function .

APPENDIX C

C 3.1 Chiral media

Because of *novel features* of chiral media, we have chosen our research field to be a chiral BOR enclosed within a perfectly conducting thin metallic BOR with apertures which is exactly similar in form and symmetrical around z-axis with the chiral BOR.

Chiral media exhibit electromagnetic chirality which embraces optical activity and circular dichroism. Optical activity refers to the rotation of the plane of polarization of optical waves by a medium while circular dichroism indicates a change in the polarization ellipticity of optical waves medium. Chiral media has been known in optics under the more common name of optically active materials. Such materials are characterized by an intrinsic left- or right-handedness at optical frequencies, due to a helical natural structure. Consequently, waves of different circular polarization propagate in these media at different velocities. As a result linearly polarized electromagnetic wave incident on a chiral medium emerges with its plane of polarization rotated about its direction.

A chiral medium is a particular case of bi-isotropic medium, characterized by linear constitutive relations which couple the electric and magnetic field by three scalars (ϵ, μ, ξ) . Beside the potential application of chiral media in optical and sub-optical frequencies [58]–[61], considerable interest has been generated in isotropic chiral media. This interest is based on the existence of one additional parameter, the chirality admittance ξ , that could make the practical design more flexible. Chirality means a lack of bilateral symmetry. The most outstanding properties of chiral media concerning the propagation of electromagnetic fields are their ability for rotating the plane of polarization of an electromagnetic wave. Electromagnetic properties of unbounded chiral media have been investigated and published [62]–[65].

Electromagnetic plane wave scattering and Maxwell's Equations

The twentieth century has been the century of electromagnetic waves. With Maxwell's electromagnetic theory and Hertz's experiments in the nineteenth century, as the point of departure, Marconi's "wireless" communication systems have been running and various types of electromagnetic waves in the form of radio and television are now criss-crossing the earth, endlessly carrying information.

The wireless systems using the propagation of electromagnetic waves in space include other applications such as satellite communication systems, cell phones, automobile telephones, radar and GPS systems. Waveguides and strip lines use the propagation of electromagnetic waves over long tubes and strip conductors. Optical fibers guide waves along thin dielectric wires called cores.

The aforementioned phenomena or devices are all treated as electromagnetic wave problems in which Maxwell's equations are to be solved under some boundary, media, or excitation conditions. Maxwell's equations form an intellectual edifice in this thesis.

C_3.3 ELECTRIC AND MAGNETIC FIELD EQUATIONS AND FIELD SOURCES IN CHIRAL MEDIA

In the past few years, the attention paid to the study of electromagnetic wave propagation in biisotropic and bianisotropic chiral media has increased notably. This increasing interest is raised by the potential applications of the chiral material. A chiral object is one that can not be brought into congruence with its mirror image by translation or rotation. A collection of such objects is then characterized by right or left-handedness and, therefore, chirality means a lack of bilateral symmetry. The most outstanding properties of chiral media concerning the propagation of electromagnetic fields are their ability for rotating the plane of polarization of an electromagnetic wave.

The description of chiral media is contained in the material parameters of the constitutive relations. The literature contains several ways of writing the constitutive relations for chiral media. We will use the following commonly used set of constitutive relations:

$$\mathbf{D} = \varepsilon \mathbf{E} - j\xi \mathbf{H} \quad (\text{C}_3.1.1)$$

$$\mathbf{B} = \mu \mathbf{H} + j\xi \mathbf{E} \quad (\text{C}_3.1.2)$$

where ε, μ and ξ are permittivity, permeability and chirality of the chiral media. Equations (C_3.1.1) and (C_3.1.2) can be cast into matrix form as

$$\begin{bmatrix} \mathbf{D} \\ \mathbf{B} \end{bmatrix} = \begin{bmatrix} \varepsilon & -j\xi \\ j\xi & \mu \end{bmatrix} \begin{bmatrix} \mathbf{E} \\ \mathbf{H} \end{bmatrix} \quad (\text{C}_3.1.3)$$

We define the relative chirality ξ_r as

$$\xi_r = \frac{\xi}{\sqrt{\mu\varepsilon}} \quad (\text{C}_3.1.4)$$

The Maxwell equations in frequency domain can be written as

$$\nabla \times \mathbf{E} = -j\omega \mathbf{B} - \mathbf{M} \quad (\text{C}_3.1.5)$$

$$\nabla \times \mathbf{H} = j\omega \mathbf{D} + \mathbf{J} \quad (\text{C}_3.1.6)$$

where $\mathbf{E}, \mathbf{B}, \mathbf{D}$ and \mathbf{H} are the electromagnetic field vectors and \mathbf{J} and \mathbf{M} are the electric and magnetic current source vectors.

Substituting (C_3.1.2) and (C_3.1.1), in (C_3.1.5) and (C_3.1.6), respectively, we obtain

$$\nabla \times \mathbf{E} = -j\omega[\mu\mathbf{H} + j\xi\mathbf{E}] - \mathbf{M} = j\omega[-\mu\mathbf{H} - j\xi\mathbf{E}] - \mathbf{M} = j\omega[-j\xi\mathbf{E} - \mu\mathbf{H}] - \mathbf{M} \quad (\text{C}_3.1.7)$$

$$\nabla \times \mathbf{H} = j\omega[\varepsilon\mathbf{E} - j\xi\mathbf{H}] + \mathbf{J} \quad (\text{C}_3.1.8)$$

Equations (C_3.1.7) and (C_3.1.8) can be cast in matrix form as

$$\nabla \times \begin{bmatrix} \mathbf{E} \\ \mathbf{H} \end{bmatrix} = j\omega \begin{bmatrix} -j\xi & -\mu \\ \varepsilon & -j\xi \end{bmatrix} \begin{bmatrix} \mathbf{E} \\ \mathbf{H} \end{bmatrix} + \begin{bmatrix} -\mathbf{M} \\ \mathbf{J} \end{bmatrix} \quad (\text{C}_3.1.9)$$

We denote

$$K = j\omega \begin{bmatrix} -j\xi & -\mu \\ \varepsilon & -j\xi \end{bmatrix} \quad (\text{C}_3.1.10)$$

and write (C_3.1.9) as

$$\nabla \times \begin{bmatrix} \mathbf{E} \\ \mathbf{H} \end{bmatrix} = K \begin{bmatrix} \mathbf{E} \\ \mathbf{H} \end{bmatrix} + \begin{bmatrix} -\mathbf{M} \\ \mathbf{J} \end{bmatrix} \quad (\text{C}_3.1.11)$$

Choose a matrix

$$A = \begin{bmatrix} 1 & 1 \\ \frac{j}{\eta} & \frac{-j}{\eta} \end{bmatrix} \quad (\text{C}_3.1.12)$$

The inverse of matrix A is

$$A^{-1} = \frac{1}{2} \begin{bmatrix} 1 & -j\eta \\ 1 & j\eta \end{bmatrix} \quad (\text{C}_3.1.13)$$

We can bring about diagonalization of matrix A

i.e.,

$$A^{-1}KA = \begin{bmatrix} k_+ & 0 \\ 0 & -k_- \end{bmatrix} \quad (\text{C}_3.1.14)$$

where

$$k_+ = \omega(\sqrt{\mu\varepsilon} + \xi) = \omega\sqrt{\mu\varepsilon} \left(1 + \frac{\xi}{\sqrt{\mu\varepsilon}} \right) = \omega\sqrt{\mu\varepsilon} (1 + \xi_r) = k(1 + \xi_r) \quad (\text{C}_3.1.15)$$

and

$$k_- = \omega(\sqrt{\mu\varepsilon} - \xi) = \omega\sqrt{\mu\varepsilon} \left(1 - \frac{\xi}{\sqrt{\mu\varepsilon}} \right) = \omega\sqrt{\mu\varepsilon} (1 - \xi_r) = k(1 - \xi_r) \quad (\text{C}_3.1.16)$$

where

k and η are given by

$$k = \omega\sqrt{\mu\varepsilon} \quad (\text{C}_3.1.17)$$

$$\eta = \sqrt{\frac{\mu}{\varepsilon}} \quad (\text{C}_3.1.18)$$

The right-handed (+) and left-handed (-) fields and currents are defined by

$$\begin{bmatrix} \mathbf{E}_+ \\ \mathbf{E}_- \end{bmatrix} = A^{-1} \begin{bmatrix} \mathbf{E} \\ \mathbf{H} \end{bmatrix} \quad (\text{C}_3.1.19)$$

$$\begin{bmatrix} \mathbf{M}_+ \\ \mathbf{M}_- \end{bmatrix} = -A^{-1} \begin{bmatrix} \mathbf{M} \\ \mathbf{J} \end{bmatrix} \quad (\text{C}_3.1.20)$$

$$\mathbf{H}_+ = +j \frac{\mathbf{E}_+}{\eta} \quad (\text{C}_3.1.21)$$

$$\mathbf{H}_- = -j \frac{\mathbf{E}_-}{\eta} \quad (\text{C}_3.1.22)$$

$$\mathbf{J}_+ = -j \frac{\mathbf{M}_+}{\eta} \quad (\text{C}_3.1.23)$$

$$\mathbf{J}_- = +j \frac{\mathbf{M}_-}{\eta} \quad (\text{C}_3.1.24)$$

Substituting (C_3.1.13) into (C_3.1.19), we obtain

$$\begin{bmatrix} \mathbf{E}_+ \\ \mathbf{E}_- \end{bmatrix} = \frac{1}{2} \begin{bmatrix} 1 & -j\eta \\ 1 & j\eta \end{bmatrix} \begin{bmatrix} \mathbf{E} \\ \mathbf{H} \end{bmatrix} = \frac{1}{2} \begin{bmatrix} \mathbf{E} - j\eta\mathbf{H} \\ \mathbf{E} + j\eta\mathbf{H} \end{bmatrix} \quad (\text{C}_3.1.25)$$

i.e.,

$$\mathbf{E}_+ = \frac{1}{2} [\mathbf{E} - j\eta\mathbf{H}] \quad (\text{C}_3.1.26)$$

$$\mathbf{E}_- = \frac{1}{2} [\mathbf{E} + j\eta\mathbf{H}] \quad (\text{C}_3.1.27)$$

Adding (C_3.1.26) and (C_3.1.27), we get

$$\mathbf{E} = \mathbf{E}_+ + \mathbf{E}_- \quad (\text{C}_3.1.28)$$

Substituting (C_3.1.26) into (C_3.1.21) and (C_3.1.27) into (C_3.1.22), we get

$$\mathbf{H}_+ = +j \frac{1}{2} \frac{[\mathbf{E} - j\eta\mathbf{H}]}{\eta} = \frac{1}{2} \left[\mathbf{H} + \frac{j\mathbf{E}}{\eta} \right] \quad (\text{C}_3.1.29)$$

and

$$\mathbf{H}_- = -j \frac{1}{2} \frac{[\mathbf{E} + j\eta\mathbf{H}]}{\eta} = \frac{1}{2} \left[\mathbf{H} - \frac{j\mathbf{E}}{\eta} \right] \quad (\text{C}_3.1.30)$$

Adding (C_3.1.29) and (C_3.1.30), we get

$$\mathbf{H} = \mathbf{H}_+ + \mathbf{H}_- \quad (\text{C}_3.1.31)$$

Similarly, substituting (C_3.1.13) into (C_3.1.20), we get

$$\begin{bmatrix} \mathbf{M}_+ \\ \mathbf{M}_- \end{bmatrix} = -A^{-1} \begin{bmatrix} -\mathbf{M} \\ \mathbf{J} \end{bmatrix} = -\frac{1}{2} \begin{bmatrix} 1 & -j\eta \\ 1 & j\eta \end{bmatrix} \begin{bmatrix} -\mathbf{M} \\ \mathbf{J} \end{bmatrix} = \frac{1}{2} \begin{bmatrix} \mathbf{M} + j\eta\mathbf{J} \\ \mathbf{M} - j\eta\mathbf{J} \end{bmatrix}$$

i.e.,

$$\mathbf{M}_+ = \frac{1}{2}[\mathbf{M} + j\eta\mathbf{J}] \quad (\text{C}_3.1.32)$$

and

$$\mathbf{M}_- = \frac{1}{2}[\mathbf{M} - j\eta\mathbf{J}] \quad (\text{C}_3.1.33)$$

Adding (C_3.1.32) and (C_3.1.33), we get

$$\mathbf{M} = \mathbf{M}_+ + \mathbf{M}_- \quad (\text{C}_3.1.34)$$

Substituting (C_3.1.32) and (C_3.1.33) respectively into equations (C_3.1.23) and (C_3.1.24), we get

$$\mathbf{J}_+ = -j \frac{\frac{1}{2}[\mathbf{M} + j\eta\mathbf{J}]}{\eta} = \frac{1}{2} \left[\mathbf{J} - \frac{j}{\eta} \mathbf{M} \right] \quad (\text{C}_3.1.35)$$

and

$$\mathbf{J}_- = +j \frac{\frac{1}{2}[\mathbf{M} - j\eta\mathbf{J}]}{\eta} = \frac{1}{2} \left[\mathbf{J} + \frac{j}{\eta} \mathbf{M} \right] \quad (\text{C}_3.1.36)$$

or

$$\mathbf{J}_\pm = \frac{1}{2} \left[\mathbf{J} \mp \frac{j}{\eta} \mathbf{M} \right] \quad (\text{C}_3.1.36a)$$

Adding (C_3.1.35) and (C_3.1.36), we get

$$\mathbf{J} = \mathbf{J}_+ + \mathbf{J}_- \quad (\text{C}_3.1.37)$$

From Equation (C_3.1.3), we get

$$\mathbf{D} = \varepsilon\mathbf{E} - j\xi\mathbf{H} \quad (\text{C}_3.1.38)$$

and

$$\mathbf{B} = j\xi\mathbf{E} + \mu\mathbf{H} \quad (\text{C}_3.1.39)$$

By using Equations (C_3.1.21), (C_3.1.22), (C_3.1.28), and (C_3.1.31), we can write Equation (C_3.1.38) as

$$\begin{aligned} \mathbf{D} &= \varepsilon\mathbf{E}_+ + \varepsilon\mathbf{E}_- - j\xi\mathbf{H}_+ - j\xi\mathbf{H}_- = \varepsilon\mathbf{E}_+ + \varepsilon\mathbf{E}_- - j\xi\left(j\frac{\mathbf{E}_+}{\eta}\right) - j\xi\left(-j\frac{\mathbf{E}_-}{\eta}\right) \\ \mathbf{D} &= \varepsilon\mathbf{E}_+ + \varepsilon\mathbf{E}_- - j\xi\left(j\frac{\mathbf{E}_+}{\eta}\right) - j\xi\left(-j\frac{\mathbf{E}_-}{\eta}\right) = \left(\varepsilon + \frac{\xi}{\eta}\right)\mathbf{E}_+ + \left(\varepsilon - \frac{\xi}{\eta}\right)\mathbf{E}_- \end{aligned} \quad (\text{C}_3.1.40)$$

Similarly from Equation (C_3.1.39), we obtain

$$\begin{aligned} \mathbf{B} &= j\xi\mathbf{E} + \mu\mathbf{H} = j\xi(\mathbf{E}_+ + \mathbf{E}_-) + \mu(\mathbf{H}_+ + \mathbf{H}_-) = j\xi(\mathbf{E}_+ + \mathbf{E}_-) + \mu\left(j\frac{\mathbf{E}_+}{\eta} - j\frac{\mathbf{E}_-}{\eta}\right) \\ \mathbf{B} &= j\xi(\mathbf{E}_+ + \mathbf{E}_-) + \mu\left(j\frac{\mathbf{E}_+}{\eta} - j\frac{\mathbf{E}_-}{\eta}\right) = \left(j\xi + \frac{j\mu}{\eta}\right)\mathbf{E}_+ + \left(j\xi - \frac{j\mu}{\eta}\right)\mathbf{E}_- \\ \mathbf{B} &= \left(j\xi + \frac{j\mu}{\eta}\right)\mathbf{E}_+ + \left(j\xi - \frac{j\mu}{\eta}\right)\mathbf{E}_- = \left(\frac{j(\mu + \xi\eta)}{\eta}\right)\mathbf{E}_+ + \left(\frac{-j(\mu - \xi\eta)}{\eta}\right)\mathbf{E}_- \end{aligned} \quad (\text{C}_3.1.41)$$

We can cast Equations (C_3.1.40) and (C_3.1.41) into matrix form as

$$\begin{bmatrix} \mathbf{D} \\ \mathbf{B} \end{bmatrix} = \begin{bmatrix} \varepsilon + \frac{\xi}{\eta} & \varepsilon - \frac{\xi}{\eta} \\ \frac{j(\mu + \xi\eta)}{\eta} & \frac{-j(\mu - \xi\eta)}{\eta} \end{bmatrix} \begin{bmatrix} \mathbf{E}_+ \\ \mathbf{E}_- \end{bmatrix} \quad (\text{C}_3.1.42)$$

We define the right-handed (+) and left-handed (-) electric displacement and magnetic flux density vectors \mathbf{D}_\pm and \mathbf{B}_\pm as

$$\mathbf{D}_+ = \varepsilon_+ \mathbf{E}_+ \quad (\text{C}_3.1.43)$$

$$\mathbf{D}_- = \varepsilon_- \mathbf{E}_- \quad (\text{C}_3.1.44)$$

$$\mathbf{B}_+ = \mu_+ \mathbf{H}_+ \quad (\text{C}_3.1.45)$$

$$\mathbf{B}_- = \mu_- \mathbf{H}_- \quad (\text{C}_3.1.46)$$

where

$$\varepsilon_+ = \varepsilon + \frac{\xi}{\eta} \quad (\text{C}_3.1.47)$$

$$\varepsilon_- = \varepsilon - \frac{\xi}{\eta} \quad (\text{C}_3.1.48)$$

$$\mu_+ = \mu + \xi\eta \quad (\text{C}_3.1.49)$$

$$\mu_- = \mu - \xi\eta \quad (\text{C}_3.1.50)$$

Use of (C_3.1.40), (C_3.1.47), (C_3.1.48), (C_3.1.43), (C_3.1.26), and (C_3.1.44) gives

$$D = D_+ + D_- \quad (\text{C}_3.1.51)$$

Use of (C_3.1.41), (C_3.1.21), (C_3.1.22), (C_3.1.49), (C_3.1.50), and (C_3.1.46) gives

$$B = B_+ + B_- \quad (\text{C}_3.1.52)$$

From (C_3.1.15)

$$k_+ = \omega \sqrt{\mu\varepsilon \left(1 + \frac{\xi}{\sqrt{\mu\varepsilon}}\right) \left(1 + \frac{\xi}{\sqrt{\mu\varepsilon}}\right)} \quad (\text{C}_3.1.53)$$

Equation (C_3.1.53) is rewritten as

$$k_+ = \omega \sqrt{(\mu + \xi\eta) \left(\varepsilon + \frac{\xi}{\eta}\right)} \quad (\text{C}_3.1.54)$$

Equations (C_3.1.49) and (C_3.1.47) simplify (C_3.1.54) to

$$k_+ = \sqrt{\mu_+ \varepsilon_+} \quad (\text{C}_3.1.55)$$

From (C_3.1.16)

$$k_- = \omega \sqrt{\mu \varepsilon \left(1 - \frac{\xi}{\sqrt{\mu \varepsilon}}\right) \left(1 - \frac{\xi}{\sqrt{\mu \varepsilon}}\right)} \quad (\text{C}_3.1.56)$$

Equation (C_3.1.56) is rewritten as

$$k_- = \omega \sqrt{(\mu - \xi \eta) \left(\varepsilon - \frac{\xi}{\eta}\right)} \quad (\text{C}_3.1.57)$$

Equations (C_3.1.50) and (C_3.1.48) simplify (C_3.1.57) to

$$k_- = \sqrt{\mu_- \varepsilon_-} \quad (\text{C}_3.1.58)$$

So far, we have formulated the values of

$\mathbf{E}_+, \mathbf{E}_-, \mathbf{H}_+, \mathbf{H}_-, \mathbf{M}_+, \mathbf{M}_-, \mathbf{J}_+, \mathbf{J}_-, \mathbf{D}_+, \mathbf{D}_-, \mathbf{B}_+, \mathbf{B}_-, \varepsilon_+, \varepsilon_-, \mu_+$ and μ_- . Now, we will formulate the values of $\nabla \times \mathbf{E}_+$, $\nabla \times \mathbf{E}_-$, $\nabla \times \mathbf{H}_+$ and $\nabla \times \mathbf{H}_-$ in the following way;

From Equation (C_3.1.19), we get

$$\begin{bmatrix} \mathbf{E} \\ \mathbf{H} \end{bmatrix} = A \begin{bmatrix} \mathbf{E}_+ \\ \mathbf{E}_- \end{bmatrix} \quad (\text{C}_3.1.59)$$

We now manipulate (C_3.1.11), and (C_3.1.59)

to obtain

$$\nabla \times \begin{bmatrix} \mathbf{E} \\ \mathbf{H} \end{bmatrix} = \nabla \times A \begin{bmatrix} \mathbf{E}_+ \\ \mathbf{E}_- \end{bmatrix} = K \begin{bmatrix} \mathbf{E} \\ \mathbf{H} \end{bmatrix} + \begin{bmatrix} -\mathbf{M} \\ \mathbf{J} \end{bmatrix} \quad (\text{C}_3.1.60)$$

$$\nabla \times A \begin{bmatrix} \mathbf{E}_+ \\ \mathbf{E}_- \end{bmatrix} = K \begin{bmatrix} \mathbf{E} \\ \mathbf{H} \end{bmatrix} + \begin{bmatrix} -\mathbf{M} \\ \mathbf{J} \end{bmatrix} = KA \begin{bmatrix} \mathbf{E}_+ \\ \mathbf{E}_- \end{bmatrix} + \begin{bmatrix} -\mathbf{M} \\ \mathbf{J} \end{bmatrix}$$

i.e.,

$$\nabla \times A \begin{bmatrix} \mathbf{E}_+ \\ \mathbf{E}_- \end{bmatrix} = KA \begin{bmatrix} \mathbf{E}_+ \\ \mathbf{E}_- \end{bmatrix} + \begin{bmatrix} -\mathbf{M} \\ \mathbf{J} \end{bmatrix} \quad (\text{C}_3.1.61)$$

Substituting values of A^{-1} and $A^{-1}KA$ from (C_3.1.13) and (C_3.1.14) into the above Equation

we obtain

$$\nabla \times \begin{bmatrix} \mathbf{E}_+ \\ \mathbf{E}_- \end{bmatrix} = \begin{bmatrix} k_+ & 0 \\ 0 & -k_- \end{bmatrix} \begin{bmatrix} \mathbf{E}_+ \\ \mathbf{E}_- \end{bmatrix} + \frac{1}{2} \begin{bmatrix} 1 & -j\eta \\ 1 & j\eta \end{bmatrix} \begin{bmatrix} -\mathbf{M} \\ \mathbf{J} \end{bmatrix}$$

i.e.,

$$\nabla \times \begin{bmatrix} \mathbf{E}_+ \\ \mathbf{E}_- \end{bmatrix} = \begin{bmatrix} k_+ \mathbf{E}_+ \\ -k_- \mathbf{E}_- \end{bmatrix} + \frac{1}{2} \begin{bmatrix} -\mathbf{M} - j\eta \mathbf{J} \\ -\mathbf{M} + j\eta \mathbf{J} \end{bmatrix} \quad (\text{C}_3.1.62)$$

From (C_3.1.32) and (C_3.1.33),

$$\frac{1}{2} [-\mathbf{M} - j\eta \mathbf{J}] = -\mathbf{M}_+ \quad (\text{C}_3.1.63)$$

$$\frac{1}{2} [-\mathbf{M} + j\eta \mathbf{J}] = -\mathbf{M}_- \quad (\text{C}_3.1.64)$$

Substituting (C_3.1.63) and (C_3.1.64) into (C_3.1.62), we obtain

$$\nabla \times \begin{bmatrix} \mathbf{E}_+ \\ \mathbf{E}_- \end{bmatrix} = \begin{bmatrix} k_+ \mathbf{E}_+ \\ -k_- \mathbf{E}_- \end{bmatrix} + \begin{bmatrix} -\mathbf{M}_+ \\ -\mathbf{M}_- \end{bmatrix}$$

i.e.,

$$\nabla \times \mathbf{E}_+ = k_+ \mathbf{E}_+ - \mathbf{M}_+ \quad (\text{C}_3.1.65)$$

$$\nabla \times \mathbf{E}_- = -k_- \mathbf{E}_- - \mathbf{M}_- \quad (\text{C}_3.1.66)$$

From (C_3.1.21),

$$\mathbf{E}_+ = -j\eta \mathbf{H}_+ \quad (\text{C}_3.1.67)$$

From (C_3.1.22),

$$\mathbf{E}_- = j\eta \mathbf{H}_- \quad (\text{C}_3.1.68)$$

From (C_3.1.23),

$$\mathbf{M}_+ = jn\mathbf{J}_+ \quad (\text{C}_3.1.69)$$

From (C_3.1.24),

$$\mathbf{M}_- = -jn\mathbf{J}_- \quad (\text{C}_3.1.70)$$

Substituting (C_3.1.67) – (C_3.1.70) into (C_3.1.65) and (C_3.1.66), we obtain

$$\nabla \times \mathbf{H}_+ = k_+ \mathbf{H}_+ + \mathbf{J}_+ \quad (\text{C}_3.1.71)$$

and

$$\nabla \times \mathbf{H}_- = -k_- \mathbf{H}_- + \mathbf{J}_- \quad (\text{C}_3.1.72)$$

Substituting (C_3.1.67) into (C_3.1.65) and substituting (C_3.1.21) into (C_3.1.71), we obtain

$$\nabla \times \mathbf{E}_+ = -jk_+ \eta \mathbf{H}_+ - \mathbf{M}_+ \quad (\text{C}_3.1.73)$$

$$\nabla \times \mathbf{H}_+ = j \frac{k_+}{\eta} \mathbf{E}_+ + \mathbf{J}_+ \quad (\text{C}_3.1.74)$$

Substituting (C_3.1.68) into (C_3.1.66) and substituting (C_3.1.22) into (C_3.1.72), we obtain

$$\nabla \times \mathbf{E}_- = -jk_- \eta \mathbf{H}_- - \mathbf{M}_- \quad (\text{C}_3.1.75)$$

$$\nabla \times \mathbf{H}_- = j \frac{k_-}{\eta} \mathbf{E}_- + \mathbf{J}_- \quad (\text{C}_3.1.76)$$

Wave impedance η_+ and η_- are defined by

$$\eta_{\pm} = \sqrt{\frac{\mu_{\pm}}{\varepsilon_{\pm}}} \quad (\text{C}_3.1.77)$$

Substituting (C_3.1.47) – (C_3.1.50) into (C_3.1.77), we obtain

$$\eta_{\pm} = \sqrt{\frac{\mu_{\pm} \xi \eta}{\varepsilon_{\pm} \xi / \eta}} \quad (\text{C}_3.1.78)$$

Equation (C_3.1.78) is rewritten as

$$\eta_{\pm} = \eta \sqrt{\frac{1 \pm \xi \eta / \mu}{1 \pm \xi / (\eta \varepsilon)}} \quad (\text{C}_3.1.79)$$

where η is given by (C_3.1.18). In view of (C_3.1.18),

$$\frac{\eta}{\mu} = \frac{1}{\eta \varepsilon} = \frac{1}{\sqrt{\mu \varepsilon}} \quad (\text{C}_3.1.80)$$

Equation (C_3.1.80) reduces (C_3.1.79) to

$$\eta_{\pm} = \eta \quad (\text{C}_3.1.81)$$

Using (C_3.1.81), (C_3.1.77), (C_3.1.55), and (C_3.1.58), we cast (C_3.1.73) – (C_3.1.76) as

$$\nabla \times \mathbf{E}_+ = -j\omega\mu_+ \mathbf{H}_+ - \mathbf{M}_+ \quad (\text{C}_3.1.82)$$

$$\nabla \times \mathbf{H}_+ = j\omega\varepsilon_+ \mathbf{E}_+ + \mathbf{J}_+ \quad (\text{C}_3.1.83)$$

$$\nabla \times \mathbf{E}_- = -j\omega\mu_- \mathbf{H}_- - \mathbf{M}_- \quad (\text{C}_3.1.84)$$

$$\nabla \times \mathbf{H}_- = j\omega\varepsilon_- \mathbf{E}_- + \mathbf{J}_- \quad (\text{C}_3.1.85)$$

Equations (C_3.1.82) and (C_3.1.83) are the *Maxwell equations* for the hypothetical medium characterized by (ε_+, μ_+) . Equations (C_3.1.84) and (C_3.1.85) are the *Maxwell equations* for the hypothetical medium characterized by (ε_-, μ_-) . The electric and magnetic fields \mathbf{E} and \mathbf{H} in the chiral medium are given by (C_3.1.28) and (C_3.1.31) where \mathbf{E}_+ and \mathbf{H}_+ are obtained by using vector and scalar potentials to solve (C_3.1.82) and (C_3.1.83), and \mathbf{E}_- and \mathbf{H}_- are obtained by similarly solving (C_3.1.84) and (C_3.1.85).

The (+) subscripts appearing in all the above equations represent right-handed fields and waves and their constitutive parameters. The right-handed fields are due to the right-handed sources radiating into a homogeneous isotropic medium characterized by (ε_+, μ_+) .

The (–) subscripts appearing in all the above equations represent left-handed fields and waves and their constitutive parameters. The left-handed fields are due to the left-handed sources radiating into a homogeneous isotropic medium characterized by (ε_-, μ_-) .

C 3.2 The vector potential \mathbf{A} for an electric current source \mathbf{J} in a homogeneous medium

For a vector field \mathbf{A} we will prove in the following steps that $\nabla \cdot \nabla \times \mathbf{A} = 0$; that is the divergence of the curl of any vector field is zero.

$$\nabla \cdot \nabla \times \mathbf{A} = \left(\frac{\partial}{\partial x}, \frac{\partial}{\partial y}, \frac{\partial}{\partial z} \right) \cdot \begin{vmatrix} \hat{\mathbf{x}} & \hat{\mathbf{y}} & \hat{\mathbf{z}} \\ \frac{\partial}{\partial x} & \frac{\partial}{\partial y} & \frac{\partial}{\partial z} \\ A_x & A_y & A_z \end{vmatrix}$$

$$\nabla \cdot \nabla \times \mathbf{A} = \left(\frac{\partial}{\partial x}, \frac{\partial}{\partial y}, \frac{\partial}{\partial z} \right) \cdot \left[\left(\frac{\partial A_z}{\partial y} - \frac{\partial A_y}{\partial z} \right), - \left(\frac{\partial A_z}{\partial x} - \frac{\partial A_x}{\partial z} \right), \left(\frac{\partial A_y}{\partial x} - \frac{\partial A_x}{\partial y} \right) \right]$$

$$\nabla \cdot \nabla \times \mathbf{A} = \frac{\partial}{\partial x} \left(\frac{\partial A_z}{\partial y} - \frac{\partial A_y}{\partial z} \right) - \frac{\partial}{\partial y} \left(\frac{\partial A_z}{\partial x} - \frac{\partial A_x}{\partial z} \right) + \frac{\partial}{\partial z} \left(\frac{\partial A_y}{\partial x} - \frac{\partial A_x}{\partial y} \right)$$

$$\nabla \cdot \nabla \times \mathbf{A} = \frac{\partial^2 A_z}{\partial x \partial y} - \frac{\partial^2 A_y}{\partial x \partial z} - \frac{\partial^2 A_z}{\partial y \partial x} + \frac{\partial^2 A_x}{\partial y \partial z} + \frac{\partial^2 A_y}{\partial z \partial x} - \frac{\partial^2 A_x}{\partial z \partial y}$$

$$\nabla \cdot \nabla \times \mathbf{A} = 0$$

$$\text{because } \frac{\partial^2 A_z}{\partial x \partial y} = \frac{\partial^2 A_z}{\partial y \partial x}, \frac{\partial^2 A_y}{\partial x \partial z} = \frac{\partial^2 A_y}{\partial z \partial x}, \text{ and } \frac{\partial^2 A_x}{\partial y \partial z} = \frac{\partial^2 A_x}{\partial z \partial y}$$

One of the Maxwell's equations for time harmonic fields is $\nabla \cdot \mathbf{B} = 0$ (the magnetic flux \mathbf{B} is always solenoidal)

Any solenoidal vector is the curl of some other vector. Hence

$$\nabla \cdot \mathbf{B} = 0 \Rightarrow \mathbf{B} = \nabla \times \mathbf{A} \quad (\text{C}_3.2.1)$$

We will refer to \mathbf{A} , vector potential. \mathbf{A} is useful in solving for the electromagnetic field generated by a given harmonic electric current \mathbf{J} . We will particularize (C_3.2.1) as

$$\mathbf{B}_A = \mu \mathbf{H}_A = \nabla \times \mathbf{A} \quad (\text{C}_3.2.2)$$

or

$$\mathbf{H}_A = \frac{1}{\mu} \nabla \times \mathbf{A} \quad (\text{C}_3.2.3)$$

where subscript *A* indicates the field due to the *A* potential.

The time-harmonic Maxwell's equations in terms of vector fields \mathbf{E} and \mathbf{H} and sources (ρ_e, \mathbf{J}) in a simple (linear, isotropic, and homogeneous) medium are

$$\nabla \times \mathbf{E} = -j\omega\mu\mathbf{H} \quad (\text{C}_3.2.3a)$$

$$\nabla \times \mathbf{H} = \mathbf{J} + j\omega\varepsilon\mathbf{E} \quad (\text{C}_3.2.3b)$$

$$\nabla \cdot \mathbf{E} = \frac{\rho_e}{\varepsilon} \quad (\text{C}_3.2.3c)$$

$$\nabla \cdot \mathbf{H} = 0 \quad (\text{C}_3.2.3d)$$

Substituting (C_3.2.2) into Maxwell's curl equation (C_3.2.3a), we obtain

$$\nabla \times \mathbf{E}_A = -j\omega\mu\mathbf{H}_A = -j\omega\mu \left(\frac{\nabla \times \mathbf{A}}{\mu} \right) = -j\omega\nabla \times \mathbf{A} \quad (\text{C}_3.2.4a)$$

We can write the above equation as

$$\nabla \times \mathbf{E}_A + j\omega\nabla \times \mathbf{A} = 0$$

or

$$\nabla \times [\mathbf{E}_A + j\omega\mathbf{A}] = 0 \quad (\text{C}_3.2.4b)$$

In general, as shown below, the curl of a gradient of a scalar is always zero.

$$\begin{aligned} \nabla \times (-\nabla\phi_e) &= -\nabla \times \left(\frac{\partial\phi_e}{\partial x}, \frac{\partial\phi_e}{\partial y}, \frac{\partial\phi_e}{\partial z} \right) \\ \nabla \times (-\nabla\phi_e) &= - \begin{vmatrix} \hat{\mathbf{x}} & \hat{\mathbf{y}} & \hat{\mathbf{z}} \\ \frac{\partial}{\partial x} & \frac{\partial}{\partial y} & \frac{\partial}{\partial z} \\ \frac{\partial\phi_e}{\partial x} & \frac{\partial\phi_e}{\partial y} & \frac{\partial\phi_e}{\partial z} \end{vmatrix} = - \left[\hat{\mathbf{x}} \left(\frac{\partial^2\phi_e}{\partial y\partial z} - \frac{\partial^2\phi_e}{\partial y\partial z} \right) - \hat{\mathbf{y}} \left(\frac{\partial^2\phi_e}{\partial x\partial z} - \frac{\partial^2\phi_e}{\partial x\partial z} \right) + \hat{\mathbf{z}} \left(\frac{\partial^2\phi_e}{\partial x\partial y} - \frac{\partial^2\phi_e}{\partial x\partial y} \right) \right] = 0 \end{aligned}$$

$$\nabla \times -\nabla \phi_e = 0$$

Furthermore, any curl-free vector is the gradient of some scalar so that (C_3.2.4b) implies that

$$[\mathbf{E}_A + j\omega\mathbf{A}] = -\nabla \phi_e \quad (\text{C}_3.2.5)$$

or

$$\mathbf{E}_A = -\nabla \phi_e - j\omega\mathbf{A} \quad (\text{C}_3.2.6)$$

The scalar function ϕ_e represents an arbitrary electric scalar potential which is a function of position.

Taking the curl of both sides of (C_3.2.2),

$$\text{we get } \mathbf{H}_A = \frac{1}{\mu} \nabla \times \mathbf{A} \Rightarrow$$

$$\mu \nabla \times \mathbf{H}_A = \nabla \times \nabla \times \mathbf{A} \quad (\text{C}_3.2.7)$$

Now we will use the following vector identity and the above equation

$$\nabla \times \nabla \times \mathbf{A} = \nabla(\nabla \cdot \mathbf{A}) - \nabla^2 \mathbf{A} \quad (\text{C}_3.2.8)$$

to obtain

$$\nabla \times \mu \mathbf{H}_A = \nabla(\nabla \cdot \mathbf{A}) - \nabla^2 \mathbf{A} \quad (\text{C}_3.2.9)$$

We will now use Maxwell's Equation (C_3.2.3b) with fields subscripted with A to obtain

$$\nabla \times \mathbf{H}_A = \mathbf{J} + j\omega\epsilon\mathbf{E}_A \quad (\text{C}_3.2.10a)$$

or

$$\nabla \times \mu \mathbf{H}_A = \mu \mathbf{J} + j\omega\mu\epsilon\mathbf{E}_A \quad (\text{C}_3.2.10b)$$

Substituting Equation (C_3.2.10b) into (C_3.2.9), we get

$$\nabla \times \mu \mathbf{H}_A = \mu \mathbf{J} + j\omega\mu\epsilon\mathbf{E}_A = \nabla(\nabla \cdot \mathbf{A}) - \nabla^2 \mathbf{A}$$

i.e.,

$$\mu\mathbf{J} + j\omega\mu\epsilon\mathbf{E}_A = \nabla(\nabla \cdot \mathbf{A}) - \nabla^2\mathbf{A} \quad (\text{C}_3.2.11)$$

Substituting (C_3.2.6) into the above equation we get

$$\mu\mathbf{J} + j\omega\mu\epsilon(-\nabla\phi_e - j\omega\mathbf{A}) = \nabla(\nabla \cdot \mathbf{A}) - \nabla^2\mathbf{A}$$

i.e.,

$$\mu\mathbf{J} + j\omega\mu\epsilon(-\nabla\phi_e - j\omega\mathbf{A}) = \nabla(\nabla \cdot \mathbf{A}) - \nabla^2\mathbf{A} \Rightarrow \mu\mathbf{J} - \nabla(j\omega\mu\epsilon\phi_e) + \omega^2\mu\epsilon\mathbf{A} = \nabla(\nabla \cdot \mathbf{A}) - \nabla^2\mathbf{A}$$

or

$$\mu\mathbf{J} - \nabla(j\omega\mu\epsilon\phi_e) + k^2\mathbf{A} = \nabla(\nabla \cdot \mathbf{A}) - \nabla^2\mathbf{A} \Rightarrow \nabla^2\mathbf{A} + k^2\mathbf{A} = -\mu\mathbf{J} + \nabla(\nabla \cdot \mathbf{A} + j\omega\mu\epsilon\phi_e)$$

or

$$\nabla^2\mathbf{A} + k^2\mathbf{A} = -\mu\mathbf{J} + \nabla(\nabla \cdot \mathbf{A} + j\omega\mu\epsilon\phi_e) \quad (\text{C}_3.2.12)$$

where

$$k^2 = \omega^2\mu\epsilon$$

A vector is uniquely determined by its curl and divergence . In (C_3.2.1), we specified the curl of \mathbf{A} . We are still free to choose the divergence of \mathbf{A} . In order to simplify (C_3.2.12), let

$$\nabla \cdot \mathbf{A} = -j\omega\mu\epsilon\phi_e \Rightarrow \phi_e = -\frac{1}{j\omega\mu\epsilon} \nabla \cdot \mathbf{A} \quad (\text{C}_3.2.13)$$

which is known as the *Lorentz condition*. Before (C_3.2.13) is applied ϕ_e is arbitrary but after (C_3.2.13) is applied ϕ_e is no longer arbitrary. Substituting (C_3.2.13) into (C_3.2.12), we get

$$\nabla^2\mathbf{A} + k^2\mathbf{A} = -\mu\mathbf{J} + \nabla\left(\nabla \cdot \mathbf{A} + j\omega\mu\epsilon\left(-\frac{1}{j\omega\mu\epsilon} \nabla \cdot \mathbf{A}\right)\right) \Rightarrow \nabla^2\mathbf{A} + k^2\mathbf{A} = -\mu\mathbf{J} + \nabla(\nabla \cdot \mathbf{A} - \nabla \cdot \mathbf{A})$$

i.e.,

$$\nabla^2\mathbf{A} + k^2\mathbf{A} = -\mu\mathbf{J} \quad (\text{C}_3.2.14)$$

Now substituting (C_3.2.13) into (C_3.2.6), we get

$$\mathbf{E}_A = -\nabla\phi_e - j\omega\mathbf{A} \Rightarrow \mathbf{E}_A = -\nabla\left(-\frac{1}{j\omega\mu\varepsilon}\nabla\cdot\mathbf{A}\right) - j\omega\mathbf{A} \Rightarrow \mathbf{E}_A = -j\omega\mathbf{A} + \frac{1}{j\omega\mu\varepsilon}\nabla(\nabla\cdot\mathbf{A})$$

$$\mathbf{E}_A = -j\omega\mathbf{A} - j\frac{1}{\omega\mu\varepsilon}\nabla(\nabla\cdot\mathbf{A}) \quad (\text{C}_3.2.15)$$

That is,

once \mathbf{A} and ϕ_e are known, \mathbf{H}_A can be found from (C_3.2.2) and \mathbf{E}_A from either (C_3.2.6) or (C_3.2.15).

3.3 The vector potential \mathbf{F} for a magnetic current source \mathbf{M} in a homogeneous medium

Although magnetic currents appear to be physically unrealizable, equivalent magnetic currents arise when we use the volume or surface equivalence theorems. The fields generated by a harmonic magnetic current in a homogeneous region, with $\mathbf{J} = 0$ but $\mathbf{M} \neq 0$ must satisfy $\nabla\cdot\mathbf{D} = 0$. Therefore \mathbf{E}_F can be expressed as the curl of the vector potential \mathbf{F} by

$$\mathbf{E}_F = -\frac{1}{\varepsilon}\nabla\times\mathbf{F} \quad (\text{C}_3.3.1)$$

We can particularize Maxwell's curl equation $\nabla\times\mathbf{H} = \mathbf{J} + j\omega\varepsilon\mathbf{E}$ as

$$\nabla\times\mathbf{H}_F = j\omega\varepsilon\mathbf{E}_F \quad (\text{as } \mathbf{J} = 0) \quad (\text{C}_3.3.2)$$

Substituting (C_3.3.1) into (C_3.3.2), we get

$$\nabla\times\mathbf{H}_F = j\omega\varepsilon\left(-\frac{1}{\varepsilon}\nabla\times\mathbf{F}\right) = -j\omega\nabla\times\mathbf{F}$$

i.e.,

$$\nabla\times(\mathbf{H}_F + j\omega\mathbf{F}) = 0 \quad (\text{C}_3.3.3)$$

Because a vector whose curl is zero can be written as the gradient of a scalar, it follows that

$$\mathbf{H}_F = -\nabla\phi_m - j\omega\mathbf{F} \quad (\text{C}_3.3.4)$$

where ϕ_m represents an arbitrary magnetic scalar potential which is a function of position.

Taking the curl of (C_3.3.1), we get

$$\nabla \times \mathbf{E}_F = -\frac{1}{\varepsilon} \nabla \times \nabla \times \mathbf{F}$$

Now we will use the following vector identity to simplify the above equation

$$\nabla \times \nabla \times \mathbf{F} = \nabla(\nabla \cdot \mathbf{F}) - \nabla^2 \mathbf{F} \quad (\text{C}_3.3.5)$$

as

$$\nabla \times \mathbf{E}_F = -\frac{1}{\varepsilon} [\nabla \nabla \cdot \mathbf{F} - \nabla^2 \mathbf{F}] \quad (\text{C}_3.3.6)$$

We will now particularize the Maxwell's equation

$$\nabla \times \mathbf{E} = -\mathbf{M} - j\omega\mu\mathbf{H}$$

as

$$\nabla \times \mathbf{E}_F = -\mathbf{M} - j\omega\mu\mathbf{H}_F \quad (\text{C}_3.3.7)$$

Now substituting (C_3.3.7) into (C_3.3.6), we get

$$\nabla \times \mathbf{E}_F = -\frac{1}{\varepsilon} [\nabla \nabla \cdot \mathbf{F} - \nabla^2 \mathbf{F}] \Rightarrow -\mathbf{M} - j\omega\mu\mathbf{H}_F = -\frac{1}{\varepsilon} [\nabla \nabla \cdot \mathbf{F} - \nabla^2 \mathbf{F}]$$

The above can be simplified as

$$-\mathbf{M} - j\omega\mu\mathbf{H}_F = -\frac{1}{\varepsilon} [\nabla \nabla \cdot \mathbf{F} - \nabla^2 \mathbf{F}] \Rightarrow \varepsilon(\mathbf{M} + j\omega\mu\mathbf{H}_F) = [\nabla \nabla \cdot \mathbf{F} - \nabla^2 \mathbf{F}]$$

i.e.,

$$\nabla^2 \mathbf{F} + j\omega\mu\varepsilon\mathbf{H}_F = \nabla \nabla \cdot \mathbf{F} - \varepsilon\mathbf{M} \quad (\text{C}_3.3.8)$$

Substituting (C_3.3.4) into (C_3.3.8), we get

$$\nabla^2 \mathbf{F} + j\omega\mu\varepsilon(-\nabla\phi_m - j\omega\mathbf{F}) = \nabla \nabla \cdot \mathbf{F} - \varepsilon\mathbf{M} \Rightarrow \nabla^2 \mathbf{F} - \nabla(j\omega\mu\varepsilon\phi_m) + k^2\mathbf{F} = \nabla \nabla \cdot \mathbf{F} - \varepsilon\mathbf{M}$$

i.e.,

$$\nabla^2 \mathbf{F} + k^2 \mathbf{F} = -\varepsilon \mathbf{M} + \nabla(\nabla \cdot \mathbf{F}) + \nabla(j\omega\mu\varepsilon\phi_m) \quad (\text{C}_3.3.9)$$

By letting

$$\nabla \cdot \mathbf{F} = -j\omega\mu\varepsilon\phi_m \Rightarrow \phi_m = -\frac{1}{j\omega\mu\varepsilon} \nabla \cdot \mathbf{F} \quad (\text{C}_3.3.10)$$

and substituting the above equation into (C_3.3.9), we get

$$\nabla^2 \mathbf{F} + k^2 \mathbf{F} = -\varepsilon \mathbf{M} + \nabla(\nabla \cdot \mathbf{F}) + \nabla\left(j\omega\mu\varepsilon\left(-\frac{1}{j\omega\mu\varepsilon}(\nabla \cdot \mathbf{F})\right)\right) = -\varepsilon \mathbf{M} + \nabla(\nabla \cdot \mathbf{F}) - \nabla(\nabla \cdot \mathbf{F})$$

i.e.,

$$\nabla^2 \mathbf{F} + k^2 \mathbf{F} = -\varepsilon \mathbf{M} \quad (\text{C}_3.3.11)$$

Now substituting (C_3.3.10) into (C_3.3.4), we get

$$\mathbf{H}_F = -\nabla\left(-\frac{1}{j\omega\mu\varepsilon} \nabla \cdot \mathbf{F}\right) - j\omega\mathbf{F} \Rightarrow \mathbf{H}_F = -j\omega\mathbf{F} + \left(\frac{1}{j\omega\mu\varepsilon} \nabla(\nabla \cdot \mathbf{F})\right)$$

i.e.,

$$\mathbf{H}_F = -j\omega\mathbf{F} - \frac{j}{\omega\mu\varepsilon} \nabla(\nabla \cdot \mathbf{F}) \quad (\text{C}_3.3.12)$$

Once \mathbf{F} and ϕ_e are known \mathbf{E}_F can be found from (C_3.3.1) and \mathbf{H}_F from either (C_3.3.4) or (C_3.3.12)

C 3.4 Electric and magnetic fields for electric (J) and magnetic (M) current sources

In Sections 3.2 and 3.3 we developed equations that can be used to find the electric and magnetic fields generated by an electric current source \mathbf{J} and a magnetic current source \mathbf{M} . The procedure requires that the potential functions \mathbf{A} and \mathbf{F} generated, respectively, by \mathbf{J} and \mathbf{M} are found first. In turn, the corresponding electric and magnetic fields are then determined ($\mathbf{E}_A, \mathbf{H}_A$ due to \mathbf{A} and $\mathbf{E}_F, \mathbf{H}_F$ due to \mathbf{F}). The total fields are then obtained by superposition of the individual fields due to \mathbf{A} and \mathbf{F} (\mathbf{J} and \mathbf{M}).

In summary form, the procedure that can be used to find the fields is as follows:

Summary

1. Specify \mathbf{J} and \mathbf{M} (electric and magnetic current source).
2. a. Find \mathbf{A} (due to \mathbf{J}) using

$$\mathbf{A} = \frac{\mu}{4\pi} \iiint_V \mathbf{J} \frac{e^{-jkR}}{R} dv' \quad (\text{C}_3.4.1)$$

which is the solution of the inhomogeneous vector wave equation of (C_3.2.14)

- b. Find \mathbf{F} (due to \mathbf{M}) using

$$\mathbf{F} = \frac{\varepsilon}{4\pi} \iiint_V \mathbf{M} \frac{e^{-jkR}}{R} dv' \quad (\text{C}_3.4.2)$$

which is the solution of the inhomogeneous vector wave equation of (C_3.3.11).

In (C_3.4.1) and (C_3.4.2), $k^2 = \omega^2 \mu \varepsilon$ and R is the distance from any point in the source to the observation point.

- a. Find \mathbf{H}_A using (C_3.2.2) and \mathbf{E}_A using either (C_3.2.6) or (C_3.2.15).

- b. Find \mathbf{E}_F using (C_3.3.1) and \mathbf{H}_F using either (C_3.3.4) or (C_3.3.12).

3. The total fields are then given by

$$\mathbf{E} = \mathbf{E}_A + \mathbf{E}_F = -j\omega\mathbf{A} - \nabla\phi_e - \frac{1}{\varepsilon}\nabla\times\mathbf{F} \quad (\text{C}_3.4.3a)$$

$$\mathbf{E} = \mathbf{E}_A + \mathbf{E}_F = -j\omega\mathbf{A} - j\frac{1}{\omega\mu\varepsilon}\nabla(\nabla\cdot\mathbf{A}) - \frac{1}{\varepsilon}\nabla\times\mathbf{F} \quad (\text{C}_3.4.3b)$$

$$\mathbf{H} = \mathbf{H}_A + \mathbf{H}_F = \frac{1}{\mu}\nabla\times\mathbf{A} - j\omega\mathbf{F} - \nabla\phi_m \quad (\text{C}_3.4.4a)$$

or

$$\mathbf{H} = \mathbf{H}_A + \mathbf{H}_F = \frac{1}{\mu} \nabla \times \mathbf{A} - j\omega \mathbf{F} - j \frac{1}{\omega \mu \varepsilon} \nabla (\nabla \cdot \mathbf{F}) \quad (\text{C}_3.4.4\text{b})$$

C 3.5 Equivalent representations in chiral media of equations (C_3.4.3a) and (C_3.4.4a)

Equivalent representations in chiral media of equations (C_3.4.3a) and (C_3.4.4a), which are reproduced below are the following equations:

$$\mathbf{E}_\pm = \mathbf{E}_A + \mathbf{E}_F = -j\omega \mathbf{A}_\pm - \nabla \phi_{e_\pm} - \frac{1}{\varepsilon_\pm} \nabla \times \mathbf{F}_\pm$$

$$\mathbf{H}_\pm = \mathbf{H}_A + \mathbf{H}_F = \frac{1}{\mu_\pm} \nabla \times \mathbf{A}_\pm - j\omega \mathbf{F}_\pm - \nabla \phi_{m_\pm}$$

We will replace ϕ_e , which represents an electric scalar potential which is a function of position, with V' and replace ϕ_m , which represents a magnetic scalar potential which is a function of position, with U' and write the above two equations as

$$\mathbf{E}_\pm(\mathbf{r}) = -j\omega \mathbf{A}'_\pm(\mathbf{r}) - \nabla V'_\pm(\mathbf{r}) - \nabla \times \frac{\mathbf{F}'_\pm(\mathbf{r})}{\varepsilon_\pm} \quad (\text{C}_3.5.1)$$

$$\mathbf{H}_\pm(\mathbf{r}) = -j\omega \mathbf{F}'_\pm(\mathbf{r}) - \nabla U'_\pm(\mathbf{r}) + \nabla \times \frac{\mathbf{A}'_\pm(\mathbf{r})}{\mu_\pm} \quad (\text{C}_3.5.2)$$

where

$(\mathbf{E}_+, \mathbf{H}_+)$ represents the right handed electromagnetic field in the chiral media, and $(\mathbf{E}_-, \mathbf{H}_-)$ represents the left-handed electromagnetic field in the chiral media.

In (C_3.5.1) and (C_3.5.2),

$$\mathbf{A}'_\pm(\mathbf{r}) = \frac{\mu_\pm}{4\pi} \int \mathbf{J}_\pm(\mathbf{r}') G_\pm(\mathbf{r}, \mathbf{r}') ds' \quad (\text{C}_3.5.3)$$

$$\mathbf{F}'_\pm(\mathbf{r}) = \frac{\varepsilon_\pm}{4\pi} \int \mathbf{M}_\pm(\mathbf{r}') G_\pm(\mathbf{r}, \mathbf{r}') ds' \quad (\text{C}_3.5.4)$$

$$V'_\pm(\mathbf{r}) = \frac{1}{4\pi \varepsilon_\pm} \int \rho_{e_\pm}(\mathbf{r}') G_\pm(\mathbf{r}, \mathbf{r}') ds' \quad (\text{C}_3.5.5)$$

$$U'_{\pm}(\mathbf{r}) = \frac{1}{4\pi\mu_{\pm}} \int \rho_{m\pm}(\mathbf{r}') G_{\pm}(\mathbf{r}, \mathbf{r}') ds' \quad (\text{C}_3.5.6)$$

$$G_{\pm}(\mathbf{r}, \mathbf{r}') = \frac{1}{|\mathbf{r} - \mathbf{r}'|} e^{-jk_{\pm}|\mathbf{r} - \mathbf{r}'|} \quad (\text{C}_3.5.7)$$

The electric surface charge density $\rho_{e\pm}$ and the magnetic surface charge density $\rho_{m\pm}$ are given in terms of \mathbf{J}_{\pm} and \mathbf{M}_{\pm} as

$$\rho_{e\pm}(\mathbf{r}') = -\frac{1}{j\omega} \nabla'_s \cdot \mathbf{J}_{\pm}(\mathbf{r}') \quad (\text{C}_3.5.8)$$

$$\rho_{m\pm}(\mathbf{r}') = -\frac{1}{j\omega} \nabla'_s \cdot \mathbf{M}_{\pm}(\mathbf{r}') \quad (\text{C}_3.5.9)$$

The scattering problem will be formulated with \mathbf{J} and \mathbf{M} as independent unknowns. For this purpose we will substitute Equations (C_3.1.35) and (C_3.1.36), which are reproduced below

$$\mathbf{J}_+ = -j \frac{1}{2} \frac{[\mathbf{M} + j\eta\mathbf{J}]}{\eta} = \frac{1}{2} \left[\mathbf{J} - \frac{j}{\eta} \mathbf{M} \right] \quad (\text{C}_3.5.10)$$

and

$$\mathbf{J}_- = +j \frac{1}{2} \frac{[\mathbf{M} - j\eta\mathbf{J}]}{\eta} = \frac{1}{2} \left[\mathbf{J} + \frac{j}{\eta} \mathbf{M} \right] \quad (\text{C}_3.5.11)$$

i.e., substituting

$$\mathbf{J}_{\pm} = \frac{1}{2} \left[\mathbf{J} \mp \frac{j}{\eta} \mathbf{M} \right] \quad (\text{C}_3.5.12)$$

into (C_3.5.3), we get

$$\mathbf{A}'_{\pm}(\mathbf{r}) = \frac{\mu_{\pm}}{4\pi} \int \mathbf{J}_{\pm}(\mathbf{r}') G_{\pm}(\mathbf{r}, \mathbf{r}') ds' = \frac{\mu_{\pm}}{4\pi} \int \frac{1}{2} \left[\mathbf{J} \mp \frac{j}{\eta} \mathbf{M} \right] G_{\pm}(\mathbf{r}, \mathbf{r}') ds'$$

i.e.,

$$\mathbf{A}'_{\pm}(\mathbf{r}) = \frac{\mu_{\pm}}{4\pi} \int \frac{1}{2} \mathbf{J}(\mathbf{r}') G_{\pm}(\mathbf{r}, \mathbf{r}') ds' \mp \frac{\mu_{\pm}}{4\pi} \int \frac{1}{2} \left[\frac{j}{\eta} \mathbf{M} \right] G_{\pm}(\mathbf{r}, \mathbf{r}') ds' \quad (\text{C}_3.5.13)$$

From (C_3.1.81), (C_3.1.77), we obtain

$$\eta = \eta_{\pm} = \sqrt{\frac{\mu_{\pm}}{\varepsilon_{\pm}}} \quad (\text{C}_3.5.14)$$

Substituting (C_3.5.14) into (C_3.5.13), we get

$$\mathbf{A}'_{\pm}(\mathbf{r}) = \frac{\mu_{\pm}}{4\pi} \int \frac{1}{2} \mathbf{J}(\mathbf{r}') G_{\pm}(\mathbf{r}, \mathbf{r}') ds' \mp \frac{\mu_{\pm}}{4\pi} \int \frac{1}{2} \left[\frac{j}{\sqrt{\frac{\mu_{\pm}}{\varepsilon_{\pm}}}} \mathbf{M} \right] G_{\pm}(\mathbf{r}, \mathbf{r}') ds'$$

i.e.,

$$\mathbf{A}'_{\pm}(\mathbf{r}) = \frac{\mu_{\pm}}{4\pi} \int \frac{1}{2} \mathbf{J}(\mathbf{r}') G_{\pm}(\mathbf{r}, \mathbf{r}') ds' \mp \frac{\mu_{\pm}}{4\pi} \left(\sqrt{\frac{\varepsilon_{\pm}}{\mu_{\pm}}} \right) \int \frac{1}{2} [j\mathbf{M}] G_{\pm}(\mathbf{r}, \mathbf{r}') ds'$$

i.e.,

$$\mathbf{A}'_{\pm}(\mathbf{r}) = \frac{\mu_{\pm}}{4\pi} \int \frac{1}{2} \mathbf{J}(\mathbf{r}') G_{\pm}(\mathbf{r}, \mathbf{r}') ds' \mp \frac{\varepsilon_{\pm}}{4\pi} \left(\frac{\mu_{\pm}}{\varepsilon_{\pm}} \right) \left(\sqrt{\frac{\varepsilon_{\pm}}{\mu_{\pm}}} \right) \int \frac{1}{2} [j\mathbf{M}] G_{\pm}(\mathbf{r}, \mathbf{r}') ds'$$

i.e.,

$$\mathbf{A}'_{\pm}(\mathbf{r}) = \frac{\mu_{\pm}}{4\pi} \int \frac{1}{2} \mathbf{J}(\mathbf{r}') G_{\pm}(\mathbf{r}, \mathbf{r}') ds' \mp \frac{\varepsilon_{\pm}}{4\pi} \left(\sqrt{\frac{\mu_{\pm}}{\varepsilon_{\pm}}} \right) \int \frac{1}{2} [j\mathbf{M}] G_{\pm}(\mathbf{r}, \mathbf{r}') ds'$$

i.e.,

$$\mathbf{A}'_{\pm}(\mathbf{r}) = \frac{\mu_{\pm}}{4\pi} \int \frac{1}{2} \mathbf{J}(\mathbf{r}') G_{\pm}(\mathbf{r}, \mathbf{r}') ds' \mp \frac{\varepsilon_{\pm}}{4\pi} \eta \int \frac{1}{2} [j\mathbf{M}] G_{\pm}(\mathbf{r}, \mathbf{r}') ds' \quad (\text{C}_3.5.15)$$

with

$$\mathbf{A}_{\pm}(\mathbf{r}) = \frac{\mu_{\pm}}{4\pi} \int \mathbf{J}(\mathbf{r}') G_{\pm}(\mathbf{r}, \mathbf{r}') ds' \quad (\text{C}_3.5.16)$$

and

$$\mathbf{F}_{\pm}(\mathbf{r}) = \frac{\varepsilon_{\pm}}{4\pi} \int \mathbf{M}(\mathbf{r}') G_{\pm}(\mathbf{r}, \mathbf{r}') ds' \quad (\text{C}_3.5.17)$$

we can write Equation (C_3.5.15) as

$$\mathbf{A}'_{\pm}(\mathbf{r}) = \frac{1}{2} (\mathbf{A}_{\pm}(\mathbf{r}) \mp j\eta \mathbf{F}_{\pm}(\mathbf{r})) \quad (\text{C}_3.5.18)$$

Similarly combining (C_3.1.32) and (C_3.1.33), which are,

$$\mathbf{M}_{+} = \frac{1}{2} [\mathbf{M} + j\eta \mathbf{J}] \quad (\text{C}_3.5.19)$$

$$\mathbf{M}_{-} = \frac{1}{2} [\mathbf{M} - j\eta \mathbf{J}] \quad (\text{C}_3.5.20)$$

as

$$\mathbf{M}_{\pm} = \frac{1}{2} [\mathbf{M} \pm j\eta \mathbf{J}] \quad (\text{C}_3.5.21)$$

and substituting the above equation into (C_3.5.4), we get

$$\mathbf{F}'_{\pm}(\mathbf{r}) = \frac{\varepsilon_{\pm}}{4\pi} \int \left[\frac{1}{2} (\mathbf{M} \pm j\eta \mathbf{J}) \right] G_{\pm}(\mathbf{r}, \mathbf{r}') ds' = \frac{\varepsilon_{\pm}}{4\pi} \int \frac{1}{2} \mathbf{M} G_{\pm}(\mathbf{r}, \mathbf{r}') ds' + \frac{\varepsilon_{\pm}}{4\pi} \int \frac{1}{2} (j\eta) \mathbf{J} G_{\pm}(\mathbf{r}, \mathbf{r}') ds'$$

now substituting Equation (C_3.5.14) into the above equation, we get

$$\mathbf{F}'_{\pm}(\mathbf{r}) = \frac{\varepsilon_{\pm}}{4\pi} \int \frac{1}{2} \mathbf{M} G_{\pm}(\mathbf{r}, \mathbf{r}') ds' \pm \frac{\varepsilon_{\pm}}{4\pi} \int \frac{1}{2} \left(j \sqrt{\frac{\mu_{\pm}}{\varepsilon_{\pm}}} \right) \mathbf{J} G_{\pm}(\mathbf{r}, \mathbf{r}') ds'$$

i.e.,

$$\mathbf{F}'_{\pm}(\mathbf{r}) = \frac{\varepsilon_{\pm}}{4\pi} \int \frac{1}{2} \mathbf{M} G_{\pm}(\mathbf{r}, \mathbf{r}') ds' \pm \frac{\mu_{\pm}}{4\pi} \left(\frac{\varepsilon_{\pm}}{\mu_{\pm}} \right) \left(\sqrt{\frac{\mu_{\pm}}{\varepsilon_{\pm}}} \right) \int \frac{1}{2} (j) \mathbf{J} G_{\pm}(\mathbf{r}, \mathbf{r}') ds'$$

i.e.,

$$\mathbf{F}'_{\pm}(\mathbf{r}) = \frac{\epsilon_{\pm}}{4\pi} \int \frac{1}{2} \mathbf{M} G_{\pm}(\mathbf{r}, \mathbf{r}') ds' \pm \frac{\mu_{\pm}}{4\pi} \left(\sqrt{\frac{\epsilon_{\pm}}{\mu_{\pm}}} \right) \int \frac{1}{2} (j) \mathbf{J} G_{\pm}(\mathbf{r}, \mathbf{r}') ds'$$

i.e.,

$$\mathbf{F}'_{\pm}(\mathbf{r}) = \frac{\epsilon_{\pm}}{4\pi} \int \frac{1}{2} \mathbf{M} G_{\pm}(\mathbf{r}, \mathbf{r}') ds' \pm \frac{\mu_{\pm}}{4\pi} \left(\frac{1}{\eta} \right) \int \frac{1}{2} (j) \mathbf{J} G_{\pm}(\mathbf{r}, \mathbf{r}') ds' \quad (\text{C}_3.5.22)$$

Equation (C_3.5.17) is rewritten as

$$\mathbf{F}'_{\pm}(\mathbf{r}) = \frac{1}{2} \left(\mathbf{F}_{\pm}(\mathbf{r}) \pm \left(\frac{j}{\eta} \right) \mathbf{A}_{\pm}(\mathbf{r}) \right) \quad (\text{C}_3.5.23)$$

where $\mathbf{A}_{\pm}(\mathbf{r})$ and $\mathbf{F}_{\pm}(\mathbf{r})$ are defined by (C_3.5.16) and (C_3.5.17), respectively

In a similar way , we derive the following two equations

$$\mathbf{V}'_{\pm}(\mathbf{r}) = \frac{1}{2} \left(\mathbf{V}_{\pm}(\mathbf{r}) \mp j\eta U_{\pm}(\mathbf{r}) \right) \quad (\text{C}_3.5.24)$$

and

$$U'_{\pm}(\mathbf{r}) = \frac{1}{2} \left(U_{\pm}(\mathbf{r}) \pm \frac{j}{\eta} \mathbf{V}_{\pm}(\mathbf{r}) \right) \quad (\text{C}_3.5.25)$$

where

$$\mathbf{V}_{\pm}(\mathbf{r}) = \frac{1}{4\pi\epsilon_{\pm}} \int \rho_e(\mathbf{r}') G_{\pm}(\mathbf{r}, \mathbf{r}') ds' \quad (\text{C}_3.5.26)$$

and

$$U_{\pm}(\mathbf{r}) = \frac{1}{4\pi\mu_{\pm}} \int \rho_m(\mathbf{r}') G_{\pm}(\mathbf{r}, \mathbf{r}') ds' \quad (\text{C}_3.5.27)$$

The electric surface charge density and the magnetic surface charge density are given in terms of \mathbf{J} and \mathbf{M} as

$$\rho_e(\mathbf{r}') = -\frac{1}{j\omega} \nabla'_s \cdot \mathbf{J}(\mathbf{r}') \quad (\text{C}_3.5.28)$$

$$\rho_m(\mathbf{r}') = -\frac{1}{j\omega} \nabla'_s \cdot \mathbf{M}(\mathbf{r}') \quad (\text{C}_3.5.29)$$

Now, we expand (C_3.5.1), reproduced below

$$\mathbf{E}_\pm(\mathbf{r}) = -j\omega \mathbf{A}'_\pm(\mathbf{r}) - \nabla V'_\pm(\mathbf{r}) - \nabla \times \frac{\mathbf{F}'_\pm(\mathbf{r})}{\varepsilon_\pm} \quad (\text{C}_3.5.30)$$

as

$$\mathbf{E}_+(\mathbf{r}) = -j\omega \mathbf{A}'_+(\mathbf{r}) - \nabla V'_+(\mathbf{r}) - \nabla \times \frac{\mathbf{F}'_+(\mathbf{r})}{\varepsilon_+} \quad (\text{C}_3.5.31)$$

and

$$\mathbf{E}_-(\mathbf{r}) = -j\omega \mathbf{A}'_-(\mathbf{r}) - \nabla V'_-(\mathbf{r}) - \nabla \times \frac{\mathbf{F}'_-(\mathbf{r})}{\varepsilon_-} \quad (\text{C}_3.5.32)$$

In (C_3.5.31) and (C_3.5.32), $\mathbf{A}'_\pm(\mathbf{r})$, $\mathbf{F}'_\pm(\mathbf{r})$, and $V'_\pm(\mathbf{r})$ are, according to (C_3.5.18), (C_3.5.23), and (C_3.5.24), respectively, given by

$$\mathbf{A}'_\pm(\mathbf{r}) = \frac{1}{2} (\mathbf{A}_\pm(\mathbf{r}) \mp j\eta \mathbf{F}_\pm(\mathbf{r})) \quad (\text{C}_3.5.33)$$

$$\mathbf{F}'_\pm(\mathbf{r}) = \frac{1}{2} \left(\mathbf{F}_\pm(\mathbf{r}) \pm \left(\frac{j}{\eta} \right) \mathbf{A}_\pm(\mathbf{r}) \right) \quad (\text{C}_3.5.34)$$

$$V'_\pm(\mathbf{r}) = \frac{1}{2} (V_\pm(\mathbf{r}) \mp j\eta U_\pm(\mathbf{r})) \quad (\text{C}_3.5.35)$$

Equation (C_3.1.28), reproduced below, is

$$\mathbf{E}(\mathbf{r}) = \mathbf{E}_+(\mathbf{r}) + \mathbf{E}_-(\mathbf{r}) \quad (\text{C}_3.5.36)$$

First, we substitute (C_3.5.31) and (C_3.5.32) into (C_3.5.36) to get

$$\mathbf{E}(\mathbf{r}) = \mathbf{E}_+(\mathbf{r}) + \mathbf{E}_-(\mathbf{r}) = -j\omega\mathbf{A}'_+(\mathbf{r}) - \nabla V'_+(\mathbf{r}) - \nabla \times \frac{\mathbf{F}'_+(\mathbf{r})}{\varepsilon_+} - j\omega\mathbf{A}'_-(\mathbf{r}) - \nabla V'_-(\mathbf{r}) - \nabla \times \frac{\mathbf{F}'_-(\mathbf{r})}{\varepsilon_-}$$

$$\mathbf{E}(\mathbf{r}) = -j\omega\mathbf{A}'_+(\mathbf{r}) - j\omega\mathbf{A}'_-(\mathbf{r}) - \nabla \times \frac{\mathbf{F}'_+(\mathbf{r})}{\varepsilon_+} - \nabla \times \frac{\mathbf{F}'_-(\mathbf{r})}{\varepsilon_-} - \nabla V'_+(\mathbf{r}) - \nabla V'_-(\mathbf{r})$$

$$\mathbf{E}(\mathbf{r}) = \left\{ -j\omega[\mathbf{A}'_+(\mathbf{r}) + \mathbf{A}'_-(\mathbf{r})] - \nabla \times \left[\frac{\mathbf{F}'_+(\mathbf{r})}{\varepsilon_+} + \frac{\mathbf{F}'_-(\mathbf{r})}{\varepsilon_-} \right] - \nabla[V'_+(\mathbf{r}) + V'_-(\mathbf{r})] \right\}$$

Substituting (C_3.5.33) – (C_3.5.35) into the above equation, we obtain

$$\mathbf{E}(\mathbf{r}) = \left\{ -j\omega \left[\frac{1}{2}(\mathbf{A}_+(\mathbf{r}) - j\eta\mathbf{F}_+(\mathbf{r})) + \frac{1}{2}(\mathbf{A}_-(\mathbf{r}) + j\eta\mathbf{F}_-(\mathbf{r})) \right] - \nabla \times \left[\frac{1}{\varepsilon_+} \frac{1}{2} \left(\mathbf{F}_+(\mathbf{r}) + \left(\frac{j}{\eta} \right) \mathbf{A}_+(\mathbf{r}) \right) \right] \right. \\ \left. - \nabla \times \left[\frac{1}{\varepsilon_-} \frac{1}{2} \left(\mathbf{F}_-(\mathbf{r}) - \left(\frac{j}{\eta} \right) \mathbf{A}_-(\mathbf{r}) \right) \right] - \nabla \left[\frac{1}{2}(V_+(\mathbf{r}) - j\eta U_+(\mathbf{r})) + \frac{1}{2}(V_-(\mathbf{r}) + j\eta U_-(\mathbf{r})) \right] \right\} \quad (\text{C}_3.5.37)$$

Knowing that $\eta = \sqrt{\frac{\mu}{\varepsilon}} = \sqrt{\frac{\mu_+}{\varepsilon_+}} = \sqrt{\frac{\mu_-}{\varepsilon_-}}$, we can obtain

$$-j\nabla \times \left[\frac{\mathbf{A}_+(\mathbf{r})}{\varepsilon_+ \eta} - \frac{\mathbf{A}_-(\mathbf{r})}{\varepsilon_- \eta} \right] = -j\nabla \times \left[\frac{\mathbf{A}_+(\mathbf{r})}{\varepsilon_+ \sqrt{\frac{\mu_+}{\varepsilon_+}}} - \frac{\mathbf{A}_-(\mathbf{r})}{\varepsilon_- \sqrt{\frac{\mu_-}{\varepsilon_-}}} \right] = -j\omega \nabla \times \left[\frac{\mathbf{A}_+(\mathbf{r})}{\omega \sqrt{\mu_+ \varepsilon_+}} - \frac{\mathbf{A}_-(\mathbf{r})}{\omega \sqrt{\mu_- \varepsilon_-}} \right] = \\ -j\omega \nabla \times \left[\frac{\mathbf{A}_+(\mathbf{r})}{k_+} - \frac{\mathbf{A}_-(\mathbf{r})}{k_-} \right] \quad (\text{C}_3.5.38)$$

Substituting (C_3.5.38) into (C_3.5.37), we get

$$\mathbf{E}(\mathbf{r}) = \frac{1}{2} \left\{ -j\omega [\mathbf{A}_+(\mathbf{r}) + \mathbf{A}_-(\mathbf{r})] - \nabla [V_+(\mathbf{r}) + V_-(\mathbf{r})] - \nabla \times \left[\frac{\mathbf{F}_+(\mathbf{r})}{\varepsilon_+} + \frac{\mathbf{F}_-(\mathbf{r})}{\varepsilon_-} \right] \right. \\ \left. - \omega\eta [\mathbf{F}_+(\mathbf{r}) - \mathbf{F}_-(\mathbf{r})] + j\eta \nabla [U_+(\mathbf{r}) - U_-(\mathbf{r})] - j\omega \nabla \times \left[\frac{\mathbf{A}_+(\mathbf{r})}{k_+} - \frac{\mathbf{A}_-(\mathbf{r})}{k_-} \right] \right\} \quad (\text{C}_3.5.39)$$

Now, we expand (C_3.5.2), reproduced below,

$$\mathbf{H}_\pm(\mathbf{r}) = -j\omega \mathbf{F}'_\pm(\mathbf{r}) - \nabla U'_\pm(\mathbf{r}) + \nabla \times \frac{\mathbf{A}'_\pm(\mathbf{r})}{\mu_\pm} \quad (\text{C}_3.5.40)$$

$$\mathbf{H}_+(\mathbf{r}) = -j\omega \mathbf{F}'_+(\mathbf{r}) - \nabla U'_+(\mathbf{r}) + \nabla \times \frac{\mathbf{A}'_+(\mathbf{r})}{\mu_+} \quad (\text{C}_3.5.41)$$

$$\mathbf{H}_-(\mathbf{r}) = -j\omega \mathbf{F}'_-(\mathbf{r}) - \nabla U'_-(\mathbf{r}) + \nabla \times \frac{\mathbf{A}'_-(\mathbf{r})}{\mu_-} \quad (\text{C}_3.5.42)$$

In (C_3.5.41) and (C_3.5.42), \mathbf{A}'_\pm , \mathbf{F}'_\pm , and U'_\pm are, according to (C_3.5.18), (C_3.5.23), and (C_3.5.25), respectively given by

$$\mathbf{A}'_\pm(\mathbf{r}) = \frac{1}{2} (\mathbf{A}_\pm(\mathbf{r}) \mp j\eta \mathbf{F}_\pm(\mathbf{r})) \quad (\text{C}_3.5.43)$$

$$\mathbf{F}'_\pm(\mathbf{r}) = \frac{1}{2} \left(\mathbf{F}_\pm(\mathbf{r}) \pm \left(\frac{j}{\eta} \right) \mathbf{A}_\pm(\mathbf{r}) \right) \quad (\text{C}_3.5.44)$$

$$U'_\pm(\mathbf{r}) = \frac{1}{2} \left(U_\pm(\mathbf{r}) \pm \frac{j}{\eta} V_\pm(\mathbf{r}) \right) \quad (\text{C}_3.5.45)$$

Equation (C_3.1.31), reproduced below, is

$$\mathbf{H} = \mathbf{H}_+ + \mathbf{H}_- \quad (\text{C}_3.4.46)$$

First, we substitute (C_3.5.41) and (C_3.5.42) into (C_3.5.46) to get

$$\mathbf{H}(\mathbf{r}) = -j\omega\mathbf{F}'_+(\mathbf{r}) - \nabla U'_+(\mathbf{r}) + \nabla \times \frac{\mathbf{A}'_+(\mathbf{r})}{\mu_+} - j\omega\mathbf{F}'_-(\mathbf{r}) - \nabla U'_-(\mathbf{r}) + \nabla \times \frac{\mathbf{A}'_-(\mathbf{r})}{\mu_-}$$

$$\mathbf{H}(\mathbf{r}) = -j\omega[\mathbf{F}'_+(\mathbf{r}) + \mathbf{F}'_-(\mathbf{r})] + \nabla \times \left[\frac{\mathbf{A}'_+(\mathbf{r})}{\mu_+} + \frac{\mathbf{A}'_-(\mathbf{r})}{\mu_-} \right] - \nabla[U'_+(\mathbf{r}) + U'_-(\mathbf{r})]$$

Substituting (C_3.5.43) – (C_3.5.45) into the above equation, we obtain

$$\begin{aligned} \mathbf{H}(\mathbf{r}) = & \left\{ -j\omega \left[\frac{1}{2} \left(\mathbf{F}_+(\mathbf{r}) + \left(\frac{j}{\eta} \right) \mathbf{A}_+(\mathbf{r}) \right) + \frac{1}{2} \left(\mathbf{F}_-(\mathbf{r}) - \left(\frac{j}{\eta} \right) \mathbf{A}_-(\mathbf{r}) \right) \right] \right. \\ & \left. + \nabla \times \left[\frac{\frac{1}{2}(\mathbf{A}_+(\mathbf{r}) - j\eta\mathbf{F}_+(\mathbf{r}))}{\mu_+} + \frac{\frac{1}{2}(\mathbf{A}_-(\mathbf{r}) + j\eta\mathbf{F}_-(\mathbf{r}))}{\mu_-} \right] \right. \\ & \left. - \nabla \left[\frac{1}{2} \left(U_+(\mathbf{r}) + \frac{j}{\eta} V_+(\mathbf{r}) \right) + \frac{1}{2} \left(U_-(\mathbf{r}) - \frac{j}{\eta} V_-(\mathbf{r}) \right) \right] \right\} \Rightarrow \\ \mathbf{H}(\mathbf{r}) = & \left\{ -j\omega \left[\frac{1}{2} \left(\mathbf{F}_+(\mathbf{r}) + \left(\frac{j}{\eta} \right) \mathbf{A}_+(\mathbf{r}) \right) + \frac{1}{2} \left(\mathbf{F}_-(\mathbf{r}) - \left(\frac{j}{\eta} \right) \mathbf{A}_-(\mathbf{r}) \right) \right] \right. \\ & \left. + \nabla \times \left[\frac{1}{\mu_+} \frac{1}{2} (\mathbf{A}_+(\mathbf{r}) - j\eta\mathbf{F}_+(\mathbf{r})) \right] + \nabla \times \left[\frac{1}{\mu_-} \frac{1}{2} (\mathbf{A}_-(\mathbf{r}) + j\eta\mathbf{F}_-(\mathbf{r})) \right] \right\} \end{aligned}$$

$$\left. -\nabla \left[\frac{1}{2} \left(U_+(\mathbf{r}) + \frac{j}{\eta} \mathbf{V}_+(\mathbf{r}) \right) + \frac{1}{2} \left(U_-(\mathbf{r}) - \frac{j}{\eta} \mathbf{V}_-(\mathbf{r}) \right) \right] \right\} \quad (\text{C}_3.5.47)$$

knowing that $\eta = \sqrt{\frac{\mu}{\varepsilon}} = \sqrt{\frac{\mu_+}{\varepsilon_+}} = \sqrt{\frac{\mu_-}{\varepsilon_-}}$, we will simplify the middle two terms in (C_3.5.47)

$$\begin{aligned} & \nabla \times \left[\frac{1}{\mu_+} \frac{1}{2} (\mathbf{A}_+(\mathbf{r}) - j\eta \mathbf{F}_+(\mathbf{r})) \right] + \nabla \times \left[\frac{1}{\mu_-} \frac{1}{2} (\mathbf{A}_-(\mathbf{r}) + j\eta \mathbf{F}_-(\mathbf{r})) \right] \\ &= -j \nabla \times \left[\frac{\eta \mathbf{F}_+(\mathbf{r})}{2\mu_+} - \frac{\eta \mathbf{F}_-(\mathbf{r})}{2\mu_-} \right] + \nabla \times \left[\frac{1}{\mu_+} \frac{1}{2} \mathbf{A}_+(\mathbf{r}) + \frac{1}{\mu_-} \frac{1}{2} \mathbf{A}_-(\mathbf{r}) \right] \end{aligned}$$

$$\begin{aligned} & \nabla \times \left[\frac{1}{\mu_+} \frac{1}{2} (\mathbf{A}_+(\mathbf{r}) - j\eta \mathbf{F}_+(\mathbf{r})) \right] + \nabla \times \left[\frac{1}{\mu_-} \frac{1}{2} (\mathbf{A}_-(\mathbf{r}) + j\eta \mathbf{F}_-(\mathbf{r})) \right] \\ &= -j \nabla \times \left[\frac{\sqrt{\frac{\mu_+}{\varepsilon_+}} \mathbf{F}_+(\mathbf{r})}{2\mu_+} - \frac{\sqrt{\frac{\mu_-}{\varepsilon_-}} \mathbf{F}_-(\mathbf{r})}{2\mu_-} \right] + \nabla \times \left[\frac{1}{\mu_+} \frac{1}{2} \mathbf{A}_+(\mathbf{r}) + \frac{1}{\mu_-} \frac{1}{2} \mathbf{A}_-(\mathbf{r}) \right] \end{aligned}$$

$$\begin{aligned} & \nabla \times \left[\frac{1}{\mu_+} \frac{1}{2} (\mathbf{A}_+(\mathbf{r}) - j\eta \mathbf{F}_+(\mathbf{r})) \right] + \nabla \times \left[\frac{1}{\mu_-} \frac{1}{2} (\mathbf{A}_-(\mathbf{r}) + j\eta \mathbf{F}_-(\mathbf{r})) \right] \\ &= -j \nabla \times \left[\frac{\mathbf{F}_+(\mathbf{r})}{2\sqrt{\mu_+ \varepsilon_+}} - \frac{\mathbf{F}_-(\mathbf{r})}{2\sqrt{\mu_- \varepsilon_-}} \right] + \nabla \times \left[\frac{1}{\mu_+} \frac{1}{2} \mathbf{A}_+(\mathbf{r}) + \frac{1}{\mu_-} \frac{1}{2} \mathbf{A}_-(\mathbf{r}) \right] \end{aligned}$$

$$\begin{aligned} & \nabla \times \left[\frac{1}{\mu_+} \frac{1}{2} (\mathbf{A}_+(\mathbf{r}) - j\eta \mathbf{F}_+(\mathbf{r})) \right] + \nabla \times \left[\frac{1}{\mu_-} \frac{1}{2} (\mathbf{A}_-(\mathbf{r}) + j\eta \mathbf{F}_-(\mathbf{r})) \right] \\ &= -j\omega \nabla \times \left[\frac{\mathbf{F}_+(\mathbf{r})}{2\omega\sqrt{\mu_+ \varepsilon_+}} - \frac{\mathbf{F}_-(\mathbf{r})}{2\omega\sqrt{\mu_- \varepsilon_-}} \right] + \nabla \times \left[\frac{1}{\mu_+} \frac{1}{2} \mathbf{A}_+(\mathbf{r}) + \frac{1}{\mu_-} \frac{1}{2} \mathbf{A}_-(\mathbf{r}) \right] \end{aligned}$$

$$\nabla \times \left[\frac{1}{\mu_+} \frac{1}{2} (\mathbf{A}_+(\mathbf{r}) - j\eta \mathbf{F}_+(\mathbf{r})) \right] + \nabla \times \left[\frac{1}{\mu_-} \frac{1}{2} (\mathbf{A}_-(\mathbf{r}) + j\eta \mathbf{F}_-(\mathbf{r})) \right]$$

$$= -j\omega\nabla \times \left[\frac{\mathbf{F}_+(\mathbf{r})}{2k_+} - \frac{\mathbf{F}_-(\mathbf{r})}{2k_-} \right] + \nabla \times \left[\frac{1}{\mu_+} \frac{1}{2} \mathbf{A}_+(\mathbf{r}) + \frac{1}{\mu_-} \frac{1}{2} \mathbf{A}_-(\mathbf{r}) \right] \quad (\text{C}_3.5.48)$$

Substituting (C_3.5.48) into (C_3.5.47), we get

$$\mathbf{H}(\mathbf{r}) = \left\{ -j\omega \left[\frac{1}{2} \left(\mathbf{F}_+(\mathbf{r}) + \left(\frac{j}{\eta} \right) \mathbf{A}_+(\mathbf{r}) \right) + \frac{1}{2} \left(\mathbf{F}_-(\mathbf{r}) - \left(\frac{j}{\eta} \right) \mathbf{A}_-(\mathbf{r}) \right) \right] \right. \\ \left. -j\omega\nabla \times \left[\frac{\mathbf{F}_+(\mathbf{r})}{2k_+} - \frac{\mathbf{F}_-(\mathbf{r})}{2k_-} \right] + \nabla \times \left[\frac{1}{\mu_+} \frac{1}{2} \mathbf{A}_+(\mathbf{r}) + \frac{1}{\mu_-} \frac{1}{2} \mathbf{A}_-(\mathbf{r}) \right] \right. \\ \left. -\nabla \left[\frac{1}{2} \left(U_+(\mathbf{r}) + \frac{j}{\eta} \mathbf{V}_+(\mathbf{r}) \right) + \frac{1}{2} \left(U_-(\mathbf{r}) - \frac{j}{\eta} \mathbf{V}_-(\mathbf{r}) \right) \right] \right\} \Rightarrow \\ \mathbf{H}(\mathbf{r}) = \frac{1}{2} \left\{ -j\omega \left[\left(\mathbf{F}_+(\mathbf{r}) + \mathbf{F}_-(\mathbf{r}) \right) \right] + \left(\frac{-j\omega \times j}{\eta} \right) \left[\mathbf{A}_+(\mathbf{r}) - \mathbf{A}_-(\mathbf{r}) \right] \right. \\ \left. -j\omega\nabla \times \left[\frac{\mathbf{F}_+(\mathbf{r})}{k_+} - \frac{\mathbf{F}_-(\mathbf{r})}{k_-} \right] + \nabla \times \left[\frac{1}{\mu_+} \mathbf{A}_+(\mathbf{r}) + \frac{1}{\mu_-} \mathbf{A}_-(\mathbf{r}) \right] \right. \\ \left. -\nabla \left[\left(U_+(\mathbf{r}) + U_-(\mathbf{r}) \right) + \left(\frac{j}{\eta} \mathbf{V}_+(\mathbf{r}) - \frac{j}{\eta} \mathbf{V}_-(\mathbf{r}) \right) \right] \right\} \Rightarrow \\ \mathbf{H}(\mathbf{r}) = \frac{1}{2} \left\{ -j\omega \left[\left(\mathbf{F}_+(\mathbf{r}) + \mathbf{F}_-(\mathbf{r}) \right) \right] - \nabla \left[U_+(\mathbf{r}) + U_-(\mathbf{r}) \right] \right. \\ \left. + \nabla \times \left[\frac{1}{\mu_+} \mathbf{A}_+(\mathbf{r}) + \frac{1}{\mu_-} \mathbf{A}_-(\mathbf{r}) \right] + \frac{\omega}{\eta} \left[\mathbf{A}_+(\mathbf{r}) - \mathbf{A}_-(\mathbf{r}) \right] \right\}$$

$$\left. \begin{aligned} & -\frac{j}{\eta} \nabla [\mathbf{V}_+(\mathbf{r}) - \mathbf{V}_-(\mathbf{r})] - j\omega \nabla \times \left[\frac{\mathbf{F}_+(\mathbf{r})}{k_+} - \frac{\mathbf{F}_-(\mathbf{r})}{k_-} \right] \end{aligned} \right\} \quad (\text{C}_3.5.49)$$

THE FOLLOWING SET OF EQUATIONS REPRESENT THE ELECTRIC AND MAGNETIC FIELDS OF ELECTRIC AND MAGNETIC CURRENT SOURCES IN CHIRAL MEDIA

$$\mathbf{E}(\mathbf{r}) = \frac{1}{2} \left\{ -j\omega [\mathbf{A}_+(\mathbf{r}) + \mathbf{A}_-(\mathbf{r})] - \nabla [V_+(\mathbf{r}) + V_-(\mathbf{r})] - \nabla \times \left[\frac{\mathbf{F}_+(\mathbf{r})}{\epsilon_+} + \frac{\mathbf{F}_-(\mathbf{r})}{\epsilon_-} \right] \right. \\ \left. - \omega\eta [\mathbf{F}_+(\mathbf{r}) - \mathbf{F}_-(\mathbf{r})] + j\eta \nabla [U_+(\mathbf{r}) - U_-(\mathbf{r})] - j\omega \nabla \times \left[\frac{\mathbf{A}_+(\mathbf{r})}{k_+} - \frac{\mathbf{A}_-(\mathbf{r})}{k_-} \right] \right\} \quad (\text{C}_3.5.50)$$

$$\mathbf{H}(\mathbf{r}) = \frac{1}{2} \left\{ -j\omega [\mathbf{F}_+(\mathbf{r}) + \mathbf{F}_-(\mathbf{r})] - \nabla [U_+(\mathbf{r}) + U_-(\mathbf{r})] + \nabla \times \left[\frac{\mathbf{A}_+(\mathbf{r})}{\mu_+} + \frac{\mathbf{A}_-(\mathbf{r})}{\mu_-} \right] \right. \\ \left. + \frac{\omega}{\eta} [\mathbf{A}_+(\mathbf{r}) - \mathbf{A}_-(\mathbf{r})] - \frac{j}{\eta} \nabla [V_+(\mathbf{r}) - V_-(\mathbf{r})] - j\omega \nabla \times \left[\frac{\mathbf{F}_+(\mathbf{r})}{k_+} - \frac{\mathbf{F}_-(\mathbf{r})}{k_-} \right] \right\} \quad (\text{C}_3.5.51)$$

Where (see (C_3.5.16), (C_3.5.17), (C_3.5.26), (C_3.5.27), (C_3.5.7), (C3.5.28), and (C_3.5.29), respectively)

$$\mathbf{A}_\pm(\mathbf{r}) = \frac{\mu_\pm}{4\pi} \int \mathbf{J}(\mathbf{r}') G_\pm(\mathbf{r}, \mathbf{r}') ds' \quad (\text{C}_3.5.52)$$

$$\mathbf{F}_\pm(\mathbf{r}) = \frac{\epsilon_\pm}{4\pi} \int \mathbf{M}(\mathbf{r}') G_\pm(\mathbf{r}, \mathbf{r}') ds' \quad (\text{C}_3.5.53)$$

$$V_{\pm}(\mathbf{r}) = \frac{1}{4\pi\epsilon_{\pm}} \int \rho_e(\mathbf{r}') G_{\pm}(\mathbf{r}, \mathbf{r}') ds' \quad (\text{C}_3.5.54)$$

$$U_{\pm}(\mathbf{r}) = \frac{1}{4\pi\mu_{\pm}} \int \rho_m(\mathbf{r}') G_{\pm}(\mathbf{r}, \mathbf{r}') ds' \quad (\text{C}_3.5.55)$$

$$G_{\pm}(\mathbf{r}, \mathbf{r}') = \frac{1}{|\mathbf{r} - \mathbf{r}'|} e^{-jk_{\pm}|\mathbf{r} - \mathbf{r}'|} \quad (\text{C}_3.5.56)$$

$$\rho_e(r') = -\frac{1}{j\omega} \nabla'_s \cdot \mathbf{J}(r') \quad (\text{C}_3.5.57)$$

$$\rho_m(r') = -\frac{1}{j\omega} \nabla'_s \cdot \mathbf{M}(r') \quad (\text{C}_3.5.58)$$

When the chirality $\zeta = 0$,

$$\mathbf{A}_+(\mathbf{r}) = \mathbf{A}_-(\mathbf{r}) = \mathbf{A}(\mathbf{r}),$$

$$\mathbf{F}_+(\mathbf{r}) = \mathbf{F}_-(\mathbf{r}) = \mathbf{F}(\mathbf{r})$$

$$V_+(\mathbf{r}) = V_-(\mathbf{r}) = V(\mathbf{r})$$

$$U_+(\mathbf{r}) = U_-(\mathbf{r}) = U(\mathbf{r})$$

$$\epsilon_+ = \epsilon_- = \epsilon$$

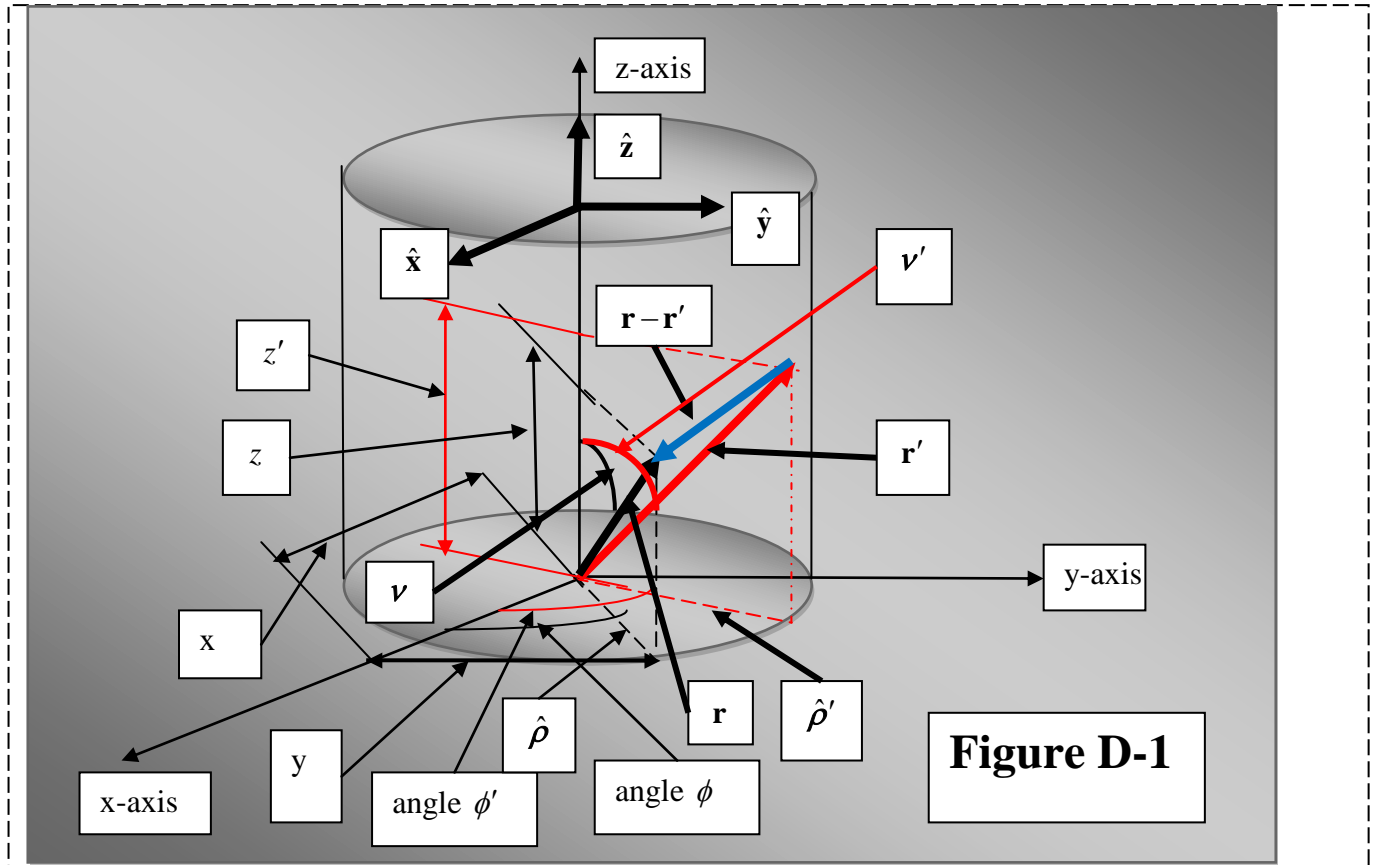
$$\mu_+ = \mu_- = \mu$$

With the above substitutions (3.5.50) and (3.5.51) reduce to:

$$\mathbf{E}(\mathbf{r}) = -j\omega\mathbf{A}(\mathbf{r}) - \nabla V(\mathbf{r}) - \frac{1}{\epsilon} \nabla \times \mathbf{F}(\mathbf{r}) \quad (\text{C}_3.5.59)$$

$$\mathbf{H}(\mathbf{r}) = -j\omega\mathbf{F}(\mathbf{r}) - \nabla U(\mathbf{r}) + \frac{1}{\mu} \nabla \times \mathbf{A}(\mathbf{r}) \quad (\text{C}_3.5.60)$$

APPENDIX D



with reference to the above Figure, we deduce:

$$\mathbf{r} = \hat{\mathbf{x}}x + \hat{\mathbf{y}}y + \hat{\mathbf{z}}z \dots\dots (1)$$

$$\mathbf{r}' = \hat{\mathbf{x}}'x' + \hat{\mathbf{y}}'y' + \hat{\mathbf{z}}'z' \dots\dots (2)$$

$$\mathbf{r} - \mathbf{r}' = \hat{\mathbf{x}}(x - x') + \hat{\mathbf{y}}(y - y') + \hat{\mathbf{z}}(z - z') \dots\dots (3)$$

$$|\mathbf{r} - \mathbf{r}'| = \sqrt{(x - x')^2 + (y - y')^2 + (z - z')^2} \dots\dots (4)$$

$$\hat{\rho}' = \cos \phi' \hat{\mathbf{x}} + \sin \phi' \hat{\mathbf{y}} \dots\dots (5)$$

$$\hat{\rho} = \cos \phi \hat{\mathbf{x}} + \sin \phi \hat{\mathbf{y}} \dots\dots (6)$$

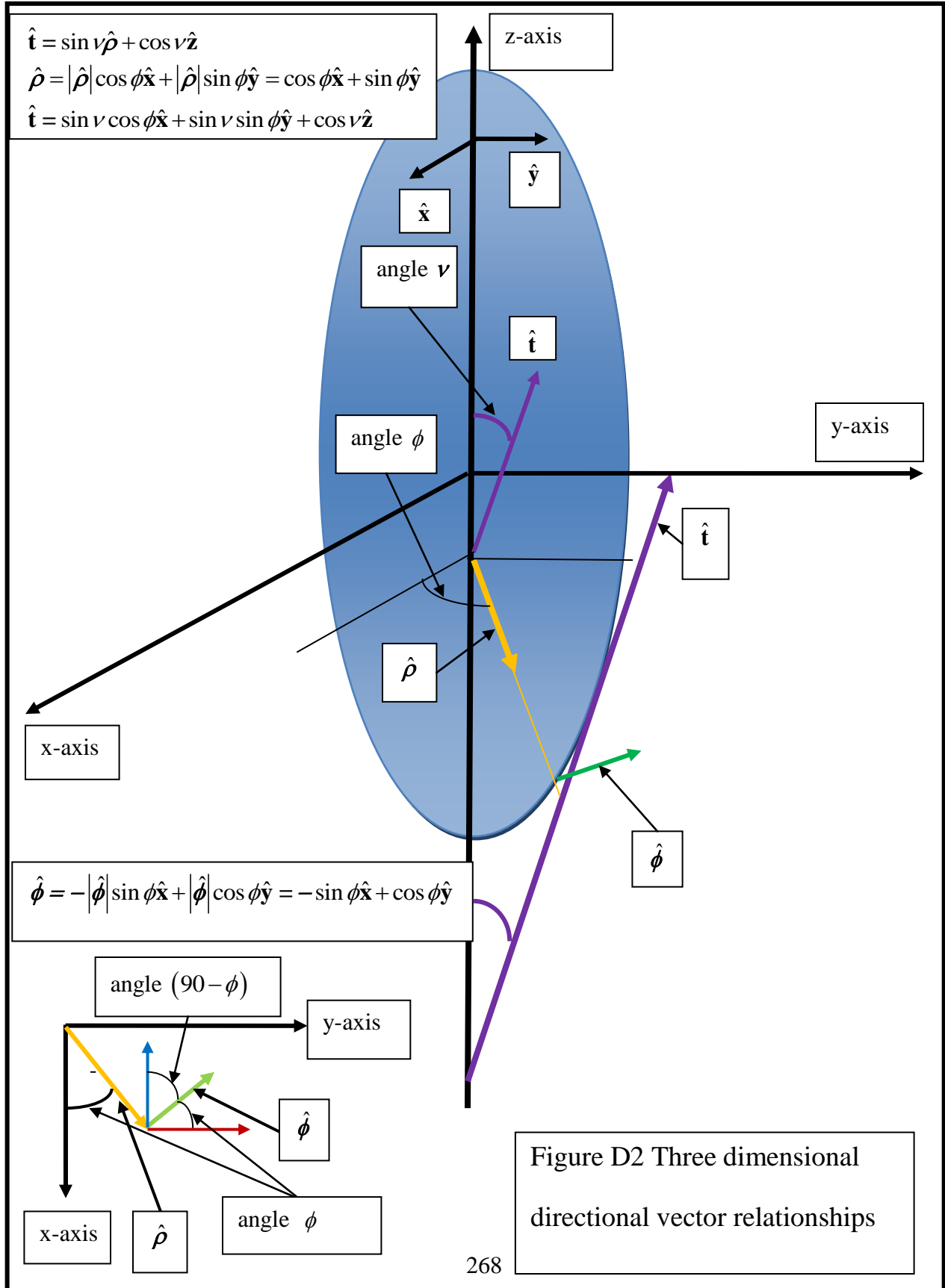
$$\mathbf{r} = \rho \hat{\boldsymbol{\rho}} + z \hat{\mathbf{z}} = \rho \cos \phi \hat{\mathbf{x}} + \rho \sin \phi \hat{\mathbf{y}} + z \hat{\mathbf{z}} \dots (7)$$

$$\mathbf{r}' = \rho' \hat{\boldsymbol{\rho}}' + z' \hat{\mathbf{z}} = \rho' \cos \phi' \hat{\mathbf{x}} + \rho' \sin \phi' \hat{\mathbf{y}} + z' \hat{\mathbf{z}} \dots (8)$$

$$\mathbf{r} - \mathbf{r}' = (\rho \cos \phi - \rho' \cos \phi') \hat{\mathbf{x}} + (\rho \sin \phi - \rho' \sin \phi') \hat{\mathbf{y}} + (z - z') \hat{\mathbf{z}} \dots (9)$$

$$|\mathbf{r} - \mathbf{r}'| = \sqrt{(\rho \cos \phi - \rho' \cos \phi')^2 + (\rho \sin \phi - \rho' \sin \phi')^2 + (z - z')^2} \dots (10)$$

Figure D-1 Rectangular and Cylindrical Coordinates



From Figure D 2, we deduce:

$$\hat{\mathbf{t}} = \sin \nu \hat{\boldsymbol{\rho}} + \cos \nu \hat{\mathbf{z}} \quad (\text{D.1})$$

$$\hat{\boldsymbol{\rho}} = \cos \phi \hat{\mathbf{x}} + \sin \phi \hat{\mathbf{y}} \quad (\text{D.2})$$

$$\hat{\mathbf{t}} = \sin \nu \cos \phi \hat{\mathbf{x}} + \sin \nu \sin \phi \hat{\mathbf{y}} + \cos \nu \hat{\mathbf{z}} \quad (\text{D.3})$$

$$\hat{\boldsymbol{\phi}} = -\sin \phi \hat{\mathbf{x}} + \cos \phi \hat{\mathbf{y}} \quad (\text{D.4})$$

Following the same steps as applied in the derivation of vectors $\hat{\mathbf{t}}$, $\hat{\boldsymbol{\rho}}$ and $\hat{\boldsymbol{\phi}}$, we can derive the following: $\hat{\mathbf{t}}' = \sin \nu' \hat{\boldsymbol{\rho}}' + \cos \nu' \hat{\mathbf{z}}$ (D.5)

$$\hat{\boldsymbol{\rho}}' = |\hat{\boldsymbol{\rho}}'| \cos \phi' \hat{\mathbf{x}} + |\hat{\boldsymbol{\rho}}'| \sin \phi' \hat{\mathbf{y}} = \cos \phi' \hat{\mathbf{x}} + \sin \phi' \hat{\mathbf{y}} \quad (\text{D.6})$$

$$\hat{\mathbf{t}}' = \sin \nu' \cos \phi' \hat{\mathbf{x}} + \sin \nu' \sin \phi' \hat{\mathbf{y}} + \cos \nu' \hat{\mathbf{z}} \quad (\text{D.7})$$

$$\hat{\boldsymbol{\phi}}' = -|\hat{\boldsymbol{\phi}}'| \sin \phi' \hat{\mathbf{x}} + |\hat{\boldsymbol{\phi}}'| \cos \phi' \hat{\mathbf{y}} = -\sin \phi' \hat{\mathbf{x}} + \cos \phi' \hat{\mathbf{y}} \quad (\text{D.8})$$

From Figure D1, we obtain

$$\mathbf{r} - \mathbf{r}' = (\rho \cos \phi - \rho' \cos \phi') \hat{\mathbf{x}} + (\rho \sin \phi - \rho' \sin \phi') \hat{\mathbf{y}} + (z - z') \hat{\mathbf{z}} \quad (\text{D.9})$$

$$|\mathbf{r} - \mathbf{r}'| = \sqrt{(\rho \cos \phi - \rho' \cos \phi')^2 + (\rho \sin \phi - \rho' \sin \phi')^2 + (z - z')^2} \quad (\text{D.10})$$

$$\mathbf{r} - \mathbf{r}' = \hat{\mathbf{x}}(x - x') + \hat{\mathbf{y}}(y - y') + \hat{\mathbf{z}}(z - z') \quad (\text{D.11})$$

$$|\mathbf{r} - \mathbf{r}'| = \sqrt{(x - x')^2 + (y - y')^2 + (z - z')^2} \quad (\text{D.12})$$

From (A.7) and (A.9), we get

$$\hat{\mathbf{t}}' \times (\mathbf{r} - \mathbf{r}') = \begin{vmatrix} \hat{\mathbf{x}} & \hat{\mathbf{y}} & \hat{\mathbf{z}} \\ \sin \nu' \cos \phi' & \sin \nu' \sin \phi' & \cos \nu' \\ (\rho \cos \phi - \rho' \cos \phi') & (\rho \sin \phi - \rho' \sin \phi') & (z - z') \end{vmatrix} \quad (\text{D.13})$$

from (D.3) and (D.13), we get

$$\hat{\mathbf{t}} \cdot (\hat{\mathbf{t}}' \times (\mathbf{r} - \mathbf{r}')) = \begin{vmatrix} \cos \phi \sin \nu & \sin \phi \sin \nu & \cos \nu \\ \sin \nu' \cos \phi' & \sin \nu' \sin \phi' & \cos \nu' \\ (\rho \cos \phi - \rho' \cos \phi') & (\rho \sin \phi - \rho' \sin \phi') & (z - z') \end{vmatrix} \quad (\text{D.14})$$

We will expand the above matrix equation in the following steps:

$$\begin{aligned} \hat{\mathbf{t}} \cdot (\hat{\mathbf{t}}' \times (\mathbf{r} - \mathbf{r}')) &= \cos \phi \sin \nu [(z - z') \sin \nu' \sin \phi' - \cos \nu' (\rho \sin \phi - \rho' \sin \phi')] \\ &\quad - \sin \phi \sin \nu [(z - z') \sin \nu' \cos \phi' - \cos \nu' (\rho \cos \phi - \rho' \cos \phi')] \\ &\quad + \cos \nu [\sin \nu' \cos \phi' (\rho \sin \phi - \rho' \sin \phi') - \sin \nu' \sin \phi' (\rho \cos \phi - \rho' \cos \phi')] \\ \hat{\mathbf{t}} \cdot (\hat{\mathbf{t}} \times (\mathbf{r} - \mathbf{r}')) &= (z - z') \sin \nu \sin \nu' (\sin \phi' \cos \phi - \sin \phi \cos \phi') \\ &\quad + \sin \nu' \cos \nu (\cos \phi' (\rho \sin \phi - \rho' \sin \phi') - \sin \phi' (\rho \cos \phi - \rho' \cos \phi')) \\ &\quad + \sin \nu \cos \nu' (-\cos \phi (\rho \sin \phi - \rho' \sin \phi') + \sin \phi (\rho \cos \phi - \rho' \cos \phi')) \\ \hat{\mathbf{t}} \cdot (\hat{\mathbf{t}} \times (\mathbf{r} - \mathbf{r}')) &= (z - z') \sin \nu \sin \nu' (\sin \phi' \cos \phi - \sin \phi \cos \phi') \\ &\quad + \sin \nu' \cos \nu (\rho (\sin \phi \cos \phi' - \sin \phi' \cos \phi) + \rho' (\sin \phi' \cos \phi' - \sin \phi \cos \phi')) \\ &\quad + \sin \nu \cos \nu' (\rho (\sin \phi \cos \phi - \sin \phi \cos \phi) + \rho' (\sin \phi' \cos \phi - \sin \phi \cos \phi')) \end{aligned} \quad (\text{D.15})$$

$$\begin{aligned} \hat{\mathbf{t}} \cdot (\hat{\mathbf{t}} \times (\mathbf{r} - \mathbf{r}')) &= (z - z') \sin \nu \sin \nu' \sin(\phi' - \phi) - \rho \sin \nu' \cos \nu \sin(\phi' - \phi) \\ &\quad + \sin \nu \cos \nu' (\rho' \sin(\phi' - \phi)) \\ \hat{\mathbf{t}} \cdot (\hat{\mathbf{t}} \times (\mathbf{r} - \mathbf{r}')) &= (-\rho \sin \nu' \cos \nu + \rho' \sin \nu \cos \nu' + (z - z') \sin \nu \sin \nu') \sin(\phi' - \phi) \end{aligned} \quad (\text{D.16})$$

From (D.3), (D.7), and (D.12), we get

$$\hat{\mathbf{t}} \cdot \hat{\mathbf{t}}' = (\hat{\mathbf{x}} \cos \phi \sin \nu + \hat{\mathbf{y}} \sin \phi \sin \nu + \hat{\mathbf{z}} \cos \nu) \cdot (\hat{\mathbf{x}} \sin \nu' \cos \phi' + \hat{\mathbf{y}} \sin \nu' \sin \phi' + \hat{\mathbf{z}} \cos \nu')$$

$$\hat{\mathbf{t}} \cdot \hat{\mathbf{t}}' = \cos \phi \sin \nu \sin \nu' \cos \phi' + \sin \phi \sin \nu \sin \nu' \sin \phi' + \cos \nu \cos \nu'$$

$$\hat{\mathbf{t}} \cdot \hat{\mathbf{t}}' = \sin \nu \sin \nu' (\cos \phi \cos \phi' + \sin \phi \sin \phi') + \cos \nu \cos \nu'$$

$$\hat{\mathbf{t}} \cdot \hat{\mathbf{t}}' = \sin \nu \sin \nu' \cos(\phi' - \phi) + \cos \nu \cos \nu' \quad (\text{D.17})$$

From (D.4) and (D.7), we obtain

$$\hat{\phi} \cdot \hat{\mathbf{t}}' = (-\sin \phi \hat{\mathbf{x}} + \cos \phi \hat{\mathbf{y}}) \cdot (\sin \nu' \cos \phi' \hat{\mathbf{x}} + \sin \nu' \sin \phi' \hat{\mathbf{y}} + \cos \nu' \hat{\mathbf{z}}) \Rightarrow$$

$$\hat{\phi} \cdot \hat{\mathbf{t}}' = -\sin \phi \sin \nu' \cos \phi' + \cos \phi \sin \nu' \sin \phi' \Rightarrow$$

$$\hat{\phi} \cdot \hat{\mathbf{t}}' = \sin \nu' (\cos \phi \sin \phi' - \sin \phi \cos \phi') \Rightarrow$$

$$\hat{\phi} \cdot \hat{\mathbf{t}}' = \sin \nu' \sin(\phi' - \phi) \quad (\text{D.18})$$

From (D.4) and (D.8), we obtain

$$\hat{\phi} \cdot \hat{\phi}' = (-\sin \phi \hat{\mathbf{x}} + \cos \phi \hat{\mathbf{y}}) \cdot (-\sin \phi' \hat{\mathbf{x}} + \cos \phi' \hat{\mathbf{y}}) \Rightarrow$$

$$\hat{\phi} \cdot \hat{\phi}' = (-\sin \phi \hat{\mathbf{x}} + \cos \phi \hat{\mathbf{y}}) \cdot (-\sin \phi' \hat{\mathbf{x}} + \cos \phi' \hat{\mathbf{y}}) \Rightarrow$$

$$\hat{\phi} \cdot \hat{\phi}' = \sin \phi \sin \phi' + \cos \phi \cos \phi' \Rightarrow$$

$$\hat{\phi} \cdot \hat{\phi}' = \cos(\phi' - \phi) \quad (\text{D}_19)$$

$$|\mathbf{r} - \mathbf{r}'| = \sqrt{(x - x')^2 + (y - y')^2 + (z - z')^2} \quad (\text{D.20})$$

$$\nabla' G_{\pm}(|\mathbf{r} - \mathbf{r}'|) = \left(\hat{\mathbf{x}} \frac{\partial}{\partial x'} + \hat{\mathbf{y}} \frac{\partial}{\partial y'} + \hat{\mathbf{z}} \frac{\partial}{\partial z'} \right) \frac{e^{-jk_{\pm}|\mathbf{r} - \mathbf{r}'|}}{|\mathbf{r} - \mathbf{r}'|} \quad (\text{D.21})$$

And

$$\begin{aligned}\nabla G_{\pm}(|\mathbf{r}-\mathbf{r}'|) &= \left(\hat{\mathbf{x}} \frac{\partial}{\partial x} + \hat{\mathbf{y}} \frac{\partial}{\partial y} + \hat{\mathbf{z}} \frac{\partial}{\partial z} \right) \frac{e^{-jk_{\pm}|\mathbf{r}-\mathbf{r}'|}}{|\mathbf{r}-\mathbf{r}'|} \\ \frac{\partial}{\partial x'} \frac{e^{-jk_{\pm}|\mathbf{r}-\mathbf{r}'|}}{|\mathbf{r}-\mathbf{r}'|} &= \frac{\partial}{\partial x'} \left(\frac{e^{-jk_{\pm}[(x-x')^2+(y-y')^2+(z-z')^2]^{\frac{1}{2}}}}{\left[(x-x')^2+(y-y')^2+(z-z')^2 \right]^{\frac{1}{2}}} \right)\end{aligned}\quad (\text{D.22})$$

And

$$\begin{aligned}\frac{\partial}{\partial x} \frac{e^{-jk_{\pm}|\mathbf{r}-\mathbf{r}'|}}{|\mathbf{r}-\mathbf{r}'|} &= \frac{\partial}{\partial x} \left(\frac{e^{-jk_{\pm}[(x-x')^2+(y-y')^2+(z-z')^2]^{\frac{1}{2}}}}{\left[(x-x')^2+(y-y')^2+(z-z')^2 \right]^{\frac{1}{2}}} \right) \\ \frac{\partial}{\partial x'} \frac{e^{-jk_{\pm}|\mathbf{r}-\mathbf{r}'|}}{|\mathbf{r}-\mathbf{r}'|} &= \frac{\partial}{\partial x'} \left(\left(e^{-jk_{\pm}[(x-x')^2+(y-y')^2+(z-z')^2]^{\frac{1}{2}}} \right) \left(\left[(x-x')^2+(y-y')^2+(z-z')^2 \right]^{-\frac{1}{2}} \right) \right)\end{aligned}$$

And

$$\begin{aligned}\frac{\partial}{\partial x} \frac{e^{-jk_{\pm}|\mathbf{r}-\mathbf{r}'|}}{|\mathbf{r}-\mathbf{r}'|} &= \frac{\partial}{\partial x} \left(\left(e^{-jk_{\pm}[(x-x')^2+(y-y')^2+(z-z')^2]^{\frac{1}{2}}} \right) \left(\left[(x-x')^2+(y-y')^2+(z-z')^2 \right]^{-\frac{1}{2}} \right) \right) \\ \frac{\partial}{\partial x'} \frac{e^{-jk_{\pm}|\mathbf{r}-\mathbf{r}'|}}{|\mathbf{r}-\mathbf{r}'|} &= \left\{ \begin{aligned} &(-jk_{\pm}) \left(\frac{1}{2} \left[(x-x')^2+(y-y')^2+(z-z')^2 \right]^{\frac{1}{2}} \right) e^{-jk_{\pm}[(x-x')^2+(y-y')^2+(z-z')^2]^{\frac{1}{2}}} \\ &(2(x-x')(-1)) \left(\left[(x-x')^2+(y-y')^2+(z-z')^2 \right]^{-\frac{1}{2}} \right) \\ &+ e^{-jk_{\pm}[(x-x')^2+(y-y')^2+(z-z')^2]^{\frac{1}{2}}} \left(-\frac{1}{2} \left[(x-x')^2+(y-y')^2+(z-z')^2 \right]^{\frac{3}{2}} (2(x-x')(-1)) \right) \end{aligned} \right\}\end{aligned}$$

And

$$\frac{\partial}{\partial x} \frac{e^{-jk_{\pm}|\mathbf{r}-\mathbf{r}'|}}{|\mathbf{r}-\mathbf{r}'|} = \left\{ \begin{aligned} &(-jk_{\pm}) \left(\frac{1}{2} \left[(x-x')^2 + (y-y')^2 + (z-z')^2 \right]^{\frac{1}{2}} \right) e^{-jk_{\pm} \left[(x-x')^2 + (y-y')^2 + (z-z')^2 \right]^{\frac{1}{2}}} \\ &\left(2(x-x')(1) \right) \left(\left[(x-x')^2 + (y-y')^2 + (z-z')^2 \right]^{\frac{1}{2}} \right) \\ &+ e^{-jk_{\pm} \left[(x-x')^2 + (y-y')^2 + (z-z')^2 \right]^{\frac{1}{2}}} \left(-\frac{1}{2} \left[(x-x')^2 + (y-y')^2 + (z-z')^2 \right]^{\frac{3}{2}} (2(x-x')(1)) \right) \end{aligned} \right\}$$

$$\frac{\partial}{\partial x'} \frac{e^{-jk_{\pm}|\mathbf{r}-\mathbf{r}'|}}{|\mathbf{r}-\mathbf{r}'|} = \left\{ -jk_{\pm} \frac{1}{2|\mathbf{r}-\mathbf{r}'|} e^{-jk_{\pm}|\mathbf{r}-\mathbf{r}'|} \frac{-2(x-x')}{|\mathbf{r}-\mathbf{r}'|} + e^{-jk_{\pm}|\mathbf{r}-\mathbf{r}'|} \left(-\frac{1}{2|\mathbf{r}-\mathbf{r}'|^3} \right) (-2(x-x')) \right\}$$

And

$$\frac{\partial}{\partial x} \frac{e^{-jk_{\pm}|\mathbf{r}-\mathbf{r}'|}}{|\mathbf{r}-\mathbf{r}'|} = \left\{ -jk_{\pm} \frac{1}{2|\mathbf{r}-\mathbf{r}'|} e^{-jk_{\pm}|\mathbf{r}-\mathbf{r}'|} \frac{2(x-x')}{|\mathbf{r}-\mathbf{r}'|} + e^{-jk_{\pm}|\mathbf{r}-\mathbf{r}'|} \left(-\frac{1}{2|\mathbf{r}-\mathbf{r}'|^3} \right) (2(x-x')) \right\}$$

$$\frac{\partial}{\partial x'} \frac{e^{-jk_{\pm}|\mathbf{r}-\mathbf{r}'|}}{|\mathbf{r}-\mathbf{r}'|} = \left\{ \frac{jk_{\pm}}{|\mathbf{r}-\mathbf{r}'|^2} + \frac{1}{|\mathbf{r}-\mathbf{r}'|^3} \right\} (x-x') e^{-jk_{\pm}|\mathbf{r}-\mathbf{r}'|}$$

And

$$\frac{\partial}{\partial x} \frac{e^{-jk_{\pm}|\mathbf{r}-\mathbf{r}'|}}{|\mathbf{r}-\mathbf{r}'|} = - \left\{ \frac{jk_{\pm}}{|\mathbf{r}-\mathbf{r}'|^2} + \frac{1}{|\mathbf{r}-\mathbf{r}'|^3} \right\} (x-x') e^{-jk_{\pm}|\mathbf{r}-\mathbf{r}'|}$$

$$\frac{\partial}{\partial x'} \frac{e^{-jk_{\pm}|\mathbf{r}-\mathbf{r}'|}}{|\mathbf{r}-\mathbf{r}'|} = \left\{ \frac{1 + jk_{\pm}|\mathbf{r}-\mathbf{r}'|}{|\mathbf{r}-\mathbf{r}'|^3} \right\} (x-x') e^{-jk_{\pm}|\mathbf{r}-\mathbf{r}'|} \quad (\text{D.23})$$

And

$$\frac{\partial}{\partial x} \frac{e^{-jk_{\pm}|\mathbf{r}-\mathbf{r}'|}}{|\mathbf{r}-\mathbf{r}'|} = - \left\{ \frac{1 + jk_{\pm}|\mathbf{r}-\mathbf{r}'|}{|\mathbf{r}-\mathbf{r}'|^3} \right\} (x-x') e^{-jk_{\pm}|\mathbf{r}-\mathbf{r}'|} \quad (\text{D.24})$$

Carrying out the same steps as done in the derivation of (D.23) and (D.24), we get

$$\frac{\partial}{\partial y'} \frac{e^{-jk_{\pm}|\mathbf{r}-\mathbf{r}'|}}{|\mathbf{r}-\mathbf{r}'|} = \left\{ \frac{1 + jk_{\pm}|\mathbf{r}-\mathbf{r}'|}{|\mathbf{r}-\mathbf{r}'|^3} \right\} (y - y') e^{-jk_{\pm}|\mathbf{r}-\mathbf{r}'|} \quad (\text{D.25})$$

And

$$\frac{\partial}{\partial y} \frac{e^{-jk_{\pm}|\mathbf{r}-\mathbf{r}'|}}{|\mathbf{r}-\mathbf{r}'|} = - \left\{ \frac{1 + jk_{\pm}|\mathbf{r}-\mathbf{r}'|}{|\mathbf{r}-\mathbf{r}'|^3} \right\} (y - y') e^{-jk_{\pm}|\mathbf{r}-\mathbf{r}'|} \quad (\text{D.26})$$

$$\frac{\partial}{\partial z'} \frac{e^{-jk_{\pm}|\mathbf{r}-\mathbf{r}'|}}{|\mathbf{r}-\mathbf{r}'|} = \left\{ \frac{1 + jk_{\pm}|\mathbf{r}-\mathbf{r}'|}{|\mathbf{r}-\mathbf{r}'|^3} \right\} (z - z') e^{-jk_{\pm}|\mathbf{r}-\mathbf{r}'|} \quad (\text{D.27})$$

And

$$\frac{\partial}{\partial z} \frac{e^{-jk_{\pm}|\mathbf{r}-\mathbf{r}'|}}{|\mathbf{r}-\mathbf{r}'|} = - \left\{ \frac{1 + jk_{\pm}|\mathbf{r}-\mathbf{r}'|}{|\mathbf{r}-\mathbf{r}'|^3} \right\} (z - z') e^{-jk_{\pm}|\mathbf{r}-\mathbf{r}'|} \quad (\text{D.28})$$

Substituting (D.23), (D.25), and (D.27) into (D.21), we get

$$\nabla' G_{\pm}(|\mathbf{r}-\mathbf{r}'|) = \left\{ \hat{\mathbf{x}} \frac{1 + jk_{\pm}|\mathbf{r}-\mathbf{r}'|}{|\mathbf{r}-\mathbf{r}'|^3} (x - x') + \hat{\mathbf{y}} \frac{1 + jk_{\pm}|\mathbf{r}-\mathbf{r}'|}{|\mathbf{r}-\mathbf{r}'|^3} (y - y') + \hat{\mathbf{z}} \frac{1 + jk_{\pm}|\mathbf{r}-\mathbf{r}'|}{|\mathbf{r}-\mathbf{r}'|^3} (z - z') \right\} e^{-jk_{\pm}|\mathbf{r}-\mathbf{r}'|}$$

$$\nabla' G_{\pm}(|\mathbf{r}-\mathbf{r}'|) = \left\{ \frac{1 + jk_{\pm}|\mathbf{r}-\mathbf{r}'|}{|\mathbf{r}-\mathbf{r}'|^3} [\hat{\mathbf{x}}(x - x') + \hat{\mathbf{y}}(y - y') + \hat{\mathbf{z}}(z - z')] e^{-jk_{\pm}|\mathbf{r}-\mathbf{r}'|} \right\}$$

$$\nabla' G_{\pm}(|\mathbf{r}-\mathbf{r}'|) = \left\{ \frac{1 + jk_{\pm}|\mathbf{r}-\mathbf{r}'|}{|\mathbf{r}-\mathbf{r}'|^3} (\mathbf{r} - \mathbf{r}') e^{-jk_{\pm}|\mathbf{r}-\mathbf{r}'|} \right\}$$

$$\nabla' G_{\pm}(|\mathbf{r}-\mathbf{r}'|) = \left\{ \frac{1 + jk_{\pm}|\mathbf{r}-\mathbf{r}'|}{|\mathbf{r}-\mathbf{r}'|^3} e^{-jk_{\pm}|\mathbf{r}-\mathbf{r}'|} \right\} (\mathbf{r} - \mathbf{r}') \quad (\text{D.29})$$

We can write (D.29) as

$$\nabla' G_{\pm}(R) = G'_{\pm}(R)(\mathbf{r} - \mathbf{r}') \quad (\text{D.30})$$

where

$$G'_\pm(R) = \frac{1 + jk_\pm R}{R^3} e^{-jk_\pm R} \quad (\text{D.31})$$

In a similar way, we can derive

$$\nabla' G_e(R) = \left(\frac{1 + jk_e R}{R^3} e^{-jk_e R} \right) (\mathbf{r} - \mathbf{r}') \quad (\text{D.32})$$

We can write (D.33) as

$$\nabla' G_e(R) = G'_e(R) (\mathbf{r} - \mathbf{r}') \quad (\text{D.33})$$

where

$$G'_e(R) = \frac{1 + jk_e R}{R^3} e^{-jk_e R} \quad (\text{D.34})$$

Substituting (D.24), (D.26), and (D.28) into (D.22), we get

$$\nabla G_\pm(|\mathbf{r} - \mathbf{r}'|) = - \left(\frac{1 + jk_\pm |\mathbf{r} - \mathbf{r}'|}{|\mathbf{r} - \mathbf{r}'|^3} \right) \{ \hat{\mathbf{x}}(x - x) + \hat{\mathbf{y}}(y - y') + \hat{\mathbf{z}}(z - z') \} e^{-jk_\pm |\mathbf{r} - \mathbf{r}'|} \Rightarrow$$

$$\nabla G_\pm(|\mathbf{r} - \mathbf{r}'|) = - \left\{ \frac{1 + jk_\pm |\mathbf{r} - \mathbf{r}'|}{|\mathbf{r} - \mathbf{r}'|^3} \right\} (\mathbf{r} - \mathbf{r}') e^{-jk_\pm |\mathbf{r} - \mathbf{r}'|} \quad (\text{D.35})$$

From (D.29) and (D.35), we conclude

$$\nabla G_\pm(|\mathbf{r} - \mathbf{r}'|) = -\nabla' G_\pm(|\mathbf{r} - \mathbf{r}'|) \quad (\text{D.36})$$

that is, the gradient of $G_\pm(|\mathbf{r} - \mathbf{r}'|)$ with respect to the primed variables equals the negative of the gradient of $G_\pm(|\mathbf{r} - \mathbf{r}'|)$ with respect to the unprimed variables.

Since the term $\frac{1 + jk_\pm |\mathbf{r} - \mathbf{r}'|}{|\mathbf{r} - \mathbf{r}'|^3} e^{-jk_\pm |\mathbf{r} - \mathbf{r}'|}$ in (D.29) is a scalar term, hence we can write

$$\hat{\mathbf{t}} \cdot (\hat{\mathbf{t}}' \times \nabla' G_{\pm}(|\mathbf{r} - \mathbf{r}'|)) = \left\{ \frac{1 + jk_{\pm} |\mathbf{r} - \mathbf{r}'|}{|\mathbf{r} - \mathbf{r}'|^3} e^{-jk_{\pm} |\mathbf{r} - \mathbf{r}'|} \right\} \hat{\mathbf{t}} \cdot (\hat{\mathbf{t}}' \times (\mathbf{r} - \mathbf{r}')) \quad (\text{D.37})$$

substituting (D.16) in (D.37), we get

$$\hat{\mathbf{t}} \cdot (\hat{\mathbf{t}}' \times \nabla' G_{\pm}(|\mathbf{r} - \mathbf{r}'|)) = \left\{ \frac{1 + jk_{\pm} |\mathbf{r} - \mathbf{r}'|}{|\mathbf{r} - \mathbf{r}'|^3} e^{-jk_{\pm} |\mathbf{r} - \mathbf{r}'|} \right\} (-\rho \sin \nu \cos \nu + \rho' \sin \nu \cos \nu' + (z - z') \sin \nu \sin \nu') \sin(\phi' - \phi) \quad (\text{D.38})$$

Equations (D.8), and (D.3) are recalled as

$$\hat{\boldsymbol{\phi}}' = -\hat{\mathbf{x}} \sin \phi' + \hat{\mathbf{y}} \cos \phi' \quad (\text{D.39})$$

$$\hat{\mathbf{t}} = \hat{\mathbf{x}} \sin \nu \cos \phi + \hat{\mathbf{y}} \sin \nu \sin \phi + \hat{\mathbf{z}} \cos \nu \quad (\text{D.40})$$

$$\hat{\mathbf{t}} \cdot \hat{\boldsymbol{\phi}}' = -\sin \nu \sin \phi' \cos \phi + \sin \nu \cos \phi' \sin \phi \Rightarrow$$

$$\hat{\mathbf{t}} \cdot \hat{\boldsymbol{\phi}}' = -\sin \nu [\sin \phi' \cos \phi - \cos \phi' \sin \phi] \Rightarrow$$

$$\hat{\mathbf{t}} \cdot \hat{\boldsymbol{\phi}}' = -\sin \nu \sin(\phi' - \phi) \quad (\text{D.41})$$

Equation (D.9) is repeated as

$$(\mathbf{r} - \mathbf{r}') = \hat{\mathbf{x}}(\rho \cos \phi - \rho' \cos \phi') + \hat{\mathbf{y}}(\rho \sin \phi - \rho' \sin \phi') + \hat{\mathbf{z}}(z - z') \quad (\text{D.42})$$

$$\hat{\boldsymbol{\phi}}' = -\hat{\mathbf{x}} \sin \phi' + \hat{\mathbf{y}} \cos \phi' \quad (\text{D.43})$$

Using (D.35), (D.34), and (D.37), we get

$$\hat{\mathbf{t}} \cdot (\hat{\boldsymbol{\phi}}' \times (\mathbf{r} - \mathbf{r}')) = \begin{vmatrix} \sin \nu \cos \phi & \sin \nu \sin \phi & \cos \nu \\ -\sin \phi' & \cos \phi' & 0 \\ (\rho \cos \phi - \rho' \cos \phi') & (\rho \sin \phi - \rho' \sin \phi') & (z - z') \end{vmatrix}$$

$$\hat{\mathbf{t}} \cdot (\hat{\boldsymbol{\phi}}' \times (\mathbf{r} - \mathbf{r}')) = \left\{ \begin{aligned} &(\sin \nu \cos \phi) \cos \phi' (z - z') - (\sin \nu \sin \phi) (-\sin \phi') (z - z') \\ &+ (\cos \nu) [-\sin \phi' (\rho \sin \phi - \rho' \sin \phi') - \cos \phi' (\rho \cos \phi - \rho' \cos \phi')] \end{aligned} \right\}$$

$$\hat{\mathbf{t}} \cdot (\hat{\boldsymbol{\phi}}' \times (\mathbf{r} - \mathbf{r}')) = \left\{ \begin{array}{l} \sin \nu (z - z') [\cos \phi' \cos \phi + \sin \phi' \sin \phi] \\ + \cos \nu [-\rho \sin \phi' \sin \phi + \rho' \sin^2 \phi' + \rho' \cos^2 \phi' - \rho \cos \phi' \cos \phi] \end{array} \right\}$$

$$\hat{\mathbf{t}} \cdot (\hat{\boldsymbol{\phi}}' \times (\mathbf{r} - \mathbf{r}')) = \left\{ \begin{array}{l} \sin \nu (z - z') \cos(\phi' - \phi) \\ + \cos \nu [-\rho (\cos \phi' \cos \phi + \sin \phi' \sin \phi) + \rho'] \end{array} \right\}$$

$$\hat{\mathbf{t}} \cdot (\hat{\boldsymbol{\phi}}' \times (\mathbf{r} - \mathbf{r}')) = \left\{ \begin{array}{l} \sin \nu (z - z') \cos(\phi' - \phi) \\ + \cos \nu [-\rho \cos(\phi' - \phi) + \rho'] \end{array} \right\}$$

$$\hat{\mathbf{t}} \cdot (\hat{\boldsymbol{\phi}}' \times (\mathbf{r} - \mathbf{r}')) = \rho' \cos \nu - \rho \cos \nu \cos(\phi' - \phi) + \sin \nu (z - z') \cos(\phi' - \phi)$$

$$\hat{\mathbf{t}} \cdot (\hat{\boldsymbol{\phi}}' \times (\mathbf{r} - \mathbf{r}')) = \rho' \cos \nu - (\rho \cos \nu + (z' - z) \sin \nu) \cos(\phi' - \phi) \quad (\text{D.44})$$

From (D.4), (D.7), and (D.9), we derive

$$\hat{\boldsymbol{\phi}} \cdot (\hat{\mathbf{t}}' \times (\hat{\mathbf{r}} - \hat{\mathbf{r}}')) = \left| \begin{array}{ccc} -\sin \phi & \cos \phi & 0 \\ \sin \nu' \cos \phi' & \sin \nu' \sin \phi' & \cos \nu' \\ (\rho \cos \phi - \rho' \cos \phi') & (\rho \sin \phi - \rho' \sin \phi') & (z - z') \end{array} \right|$$

$$\hat{\boldsymbol{\phi}} \cdot (\hat{\mathbf{t}}' \times (\hat{\mathbf{r}} - \hat{\mathbf{r}}')) = (-\sin \phi) [\sin \nu' \sin \phi' (z - z') - (\rho \sin \phi - \rho' \sin \phi') \cos \nu']$$

$$- (\cos \phi) [\sin \nu' \cos \phi' (z - z') - (\rho \cos \phi - \rho' \cos \phi') \cos \nu'] \Rightarrow$$

$$\hat{\boldsymbol{\phi}} \cdot (\hat{\mathbf{t}}' \times (\hat{\mathbf{r}} - \hat{\mathbf{r}}')) = -\sin \phi \sin \nu' \sin \phi' (z - z') + \sin \phi (\rho \sin \phi - \rho' \sin \phi') \cos \nu'$$

$$- \cos \phi \sin \nu' \cos \phi' (z - z') + \cos \phi (\rho \cos \phi - \rho' \cos \phi') \cos \nu' \Rightarrow$$

$$\hat{\boldsymbol{\phi}} \cdot (\hat{\mathbf{t}}' \times (\hat{\mathbf{r}} - \hat{\mathbf{r}}')) = -\sin \nu' (z - z') [\sin \phi \sin \phi' + \cos \phi \cos \phi'] + \rho \sin^2 \phi \cos \nu'$$

$$- \rho' \sin \phi \sin \phi' \cos \nu' + \rho \cos^2 \phi \cos \nu' - \rho' \cos \phi \cos \phi' \cos \nu' \Rightarrow$$

$$\hat{\boldsymbol{\phi}} \cdot (\hat{\mathbf{t}}' \times (\hat{\mathbf{r}} - \hat{\mathbf{r}}')) = -\sin \nu' (z - z') \cos(\phi' - \phi) + \rho (\sin^2 \phi + \cos^2 \phi) \cos \nu'$$

$$- \rho' (\sin \phi \sin \phi' + \cos \phi \cos \phi') \cos \nu' \Rightarrow$$

$$\begin{aligned}
\hat{\phi} \cdot (\hat{\mathbf{t}}' \times (\hat{\mathbf{r}} - \hat{\mathbf{r}}')) &= -\sin v' (z - z') \cos(\phi' - \phi) + \rho \cos v' - \rho' \cos(\phi' - \phi) \cos v' \Rightarrow \\
\hat{\phi} \cdot (\hat{\mathbf{t}}' \times (\hat{\mathbf{r}} - \hat{\mathbf{r}}')) &= \rho \cos v' + [-\rho' \cos v' - \sin v' (z - z')] \cos(\phi' - \phi) \Rightarrow \\
\hat{\phi} \cdot (\hat{\mathbf{t}}' \times (\hat{\mathbf{r}} - \hat{\mathbf{r}}')) &= \rho \cos v' + [-\rho' \cos v' + (z' - z) \sin v'] \cos(\phi' - \phi) \tag{D.45}
\end{aligned}$$

From (D.4), (D.7), and (D.38), we obtain

$$\begin{aligned}
\hat{\phi} \cdot (\hat{\phi}' \times (\hat{\mathbf{r}} - \hat{\mathbf{r}}')) &= \begin{vmatrix} -\sin \phi & \cos \phi & 0 \\ -\sin \phi' & \cos \phi' & 0 \\ (\rho \cos \phi - \rho' \cos \phi') & (\rho \sin \phi - \rho' \sin \phi') & (z - z') \end{vmatrix} \\
\hat{\phi} \cdot (\hat{\phi}' \times (\hat{\mathbf{r}} - \hat{\mathbf{r}}')) &= (-\sin \phi) [\cos \phi' (z - z')] - \cos \phi [-\sin \phi' (z - z')] \Rightarrow \\
\hat{\phi} \cdot (\hat{\phi}' \times (\hat{\mathbf{r}} - \hat{\mathbf{r}}')) &= (z - z') [\sin \phi' \cos \phi - \cos \phi' \sin \phi] \Rightarrow \\
\hat{\phi} \cdot (\hat{\phi}' \times (\hat{\mathbf{r}} - \hat{\mathbf{r}}')) &= (z - z') \sin(\phi' - \phi) \Rightarrow \\
\hat{\phi} \cdot (\hat{\phi}' \times (\hat{\mathbf{r}} - \hat{\mathbf{r}}')) &= -(z' - z) \sin(\phi' - \phi) \tag{D.46}
\end{aligned}$$

Trigonometric identities:

$$\sin(mx) \sin(nx) = \frac{1}{2} (\cos[(m-n)x] - \cos[(m+n)x]) \tag{D.47}$$

$$\sin(mx) \cos(nx) = \frac{1}{2} (\sin[(m-n)x] + \sin[(m+n)x]) \tag{D.48}$$

$$\cos(mx) \cos(nx) = \frac{1}{2} (\cos[(m-n)x] + \cos[(m+n)x]) \tag{D.49}$$

Bibliography

- [1] H. K. Schuman and D. E. Warren, “Coupling through rotationally symmetric apertures in cavities of revolution,” Rome Air Development Center, RADC-TR-77-214, Phase report, June 1977.
- [2] H. K. Schuman, and D. E. Warren, “Aperture coupling in bodies of revolution,” *IEEE Trans. Antennas Propagat.*, vol. AP-26, no. 6, pp. 778–773, Nov. 1978.
- [3] F. Altunkilic, “Transmission through an arbitrary aperture in an arbitrary 3-D conducting surface Enclosing chiral material,” Ph.D. Dissertation, Syracuse University, June 2007.
- [4] J. R. Mautz and R. F. Harrington, “Radiation and scattering from bodies of revolution,” *Appl. Sci. Res.*, vol. 20, no. 6, pp. 405–435, June 1969.
- [5] R. Larson, R. P. Hostetler, B. H. Edwards, “*Calculus with Analytic Geometry*,” *Eighth Edition*, Boston : Houghton Mifflin Company, Boston, 2005.
- [6] C. M. Butler and K. R. Umashankar, “Electromagnetic penetration through an aperture in an infinite, planar screen separating two half spaces of different electromagnetic properties,” *Radio Sci.*, vol. 11, no. 7, pp. 611–619, New York, 206619, July 1976.
- [7] S. T. Imeci, F. Altunkilic, J. R. Mautz, and E. Arvas, “Transmission through an arbitrarily shaped aperture in a conducting plane separating air and a chiral medium,” *ACES Journal*, vol. 25, no. 7, pp. 587–599, July 2010.
- [8] T. Wang, R. F. Harrington, and J. R. Mautz, “Electromagnetic scattering from and transmission through arbitrary apertures in conducting bodies,” *IEEE Trans. Antennas Propagat.*, vol. 38, no. 11, pp. 1805–1814, Nov. 1990.
- [9] R. F. Harrington, and J. R. Mautz, “Electromagnetic transmission through an aperture in a conducting plane,” *AEÜ*, vol. 31, pp. 81–87, 1977.
- [10] J. R. Mautz and R. F. Harrington, “Electromagnetic scattering from a homogeneous material body of revolution,” *AEÜ*, vol. 33, pp. 71–80, 1979.
- [11] H. K. Schuman and B. J. Strait, “Aperture coupling in bodies of revolution,” *IEEE Int. Antennas Propagat. Symp. Dig.* vol. 14, pp. 507–510, Oct. 1976.

- [12] D. Worasawate, J. R. Mautz, and E. Arvas, "Electromagnetic scattering from an arbitrarily shaped three-dimensional homogeneous chiral body," *IEEE Trans. Antennas Propag.*, vol. 51, no. 5, pp. 1077–1084, May 2003.
- [13] M. Yuceer, J. R. Mautz, and E. Arvas, "Method of moments solution for the radar cross section of a chiral body of revolution," *IEEE Trans. Antennas Propag.*, vol. 53, No. 3, pp. 1163–1167, Mar. 2005.
- [14] M. G. Andreasen, "Scattering from bodies of revolution," *IEEE Trans. Antennas Propag.*, vol. AP-13, pp. 303–310, Mar. 1965.
- [15] B. Cranganu-Cretu and R. Hiptmair, "Scattering from apertures: A general boundary integral equations based approach," *Rev. Roum. Sci. Techn. – Electrotechn.*, vol. 49, no. 4, pp. 1–20, 2004.
- [16] P. Barber and C. Yeh, "Scattering of electromagnetic waves by arbitrarily shaped dielectric bodies," *Appl. Opt.*, vol. 14, no. 12, pp. 2864–2872, Dec. 1975.
- [17] A. W. Glisson and D. R. Wilton, "Simple and efficient numerical methods for problems of electromagnetic radiation and scattering from surfaces," *IEEE Trans. Antennas Propag.*, vol. AP-28, no. 5, pp. 593–603, Sept. 1980.
- [18] K. Hongo and H. Serizawa, "Diffraction of electromagnetic plane wave by a rectangular plate and a rectangular hole in the conducting plate," *IEEE Trans. Antennas propag.*, vol. 47, no. 6, pp. 1029–1041, June 1999.
- [19] K. Hongo, and Q. A. Naqvi, "Diffraction of electromagnetic wave by disk and circular hole in a perfectly conducting plane," *Progress in Electromagnetics Research, PIER*, vol. 68, pp. 113–150, 2007.
- [20] D. T. Auckland, and R. F. Harrington, "A nonmodal formulation for electromagnetic transmission through a filled slot of arbitrary cross section in a thick conducting screen," *IEEE Trans. Microwave Theory Tech.*, vol. MTT-28, no. 6, pp. 548–555, June 1980.
- [21] J.-M. Jin, and J. L. Volakis, "Electromagnetic scattering by and transmission through a three-dimensional slot in a thick conducting plane," *IEEE Trans. Antennas Propag.*, vol. 39, no. 4, pp. 543–550, Apr. 1991.
- [22] J. R. Mautz and R. F. Harrington, "Boundary formulations for aperture coupling problems," *AEÜ*, vol. 34, no. 9, pp. 377–384, 1980.
- [23] R. F. Harrington, *Time-Harmonic Electromagnetic Fields*. New York: McGraw-Hill, 1961.

- [24] R. F. Harrington, *Field Computation by Moment Methods*. Piscataway, NJ: IEEE Press, 1993
- [25] Jin Au Kong, *Electromagnetic Wave Theory*. Cambridge, Mass.: EMW Publishing, 2008.
- [26] H. K. Schuman and B. J. Strait, “Coupling through apertures of arbitrary shape in bodies of revolution,” *IEEE Int. Antenna Propag. Symp. Dig.* vol. 13, pp. 85–88, June 1975.
- [27] R. W. Ziolkowski and W. A. Johnson, “Electromagnetic scattering of an arbitrary plane wave from a spherical shell with a circular aperture,” *J. Math. Phys.* vol. 28, no. 6, pp. 1293–1314, June 1987.
- [28] V. Demir, A. Elsherbeni, D. Worasawate, and E. Arvas, “A graphical user interface (GUI) for plane-wave scattering from a conducting, dielectric, or chiral sphere,” *IEEE Antennas Propagat., Mag.*, vol. 46, no. 5, pp. 94–99, Oct. 2004.
- [29] T. B. A. Senior and G. A. Desjardins, “Electromagnetic field penetration into a spherical cavity,” *IEEE Trans. Electromagn. Compat.*, vol. EMC–16, no. 4, pp. 205–208, Nov. 1974.
- [30] Y. Hua, Q. Z. Liu, Y. L. Zou, and L. Sun, “A hybrid FE-BI method for electromagnetic scattering from dielectric bodies partially covered by conductors,” *J. Electromagnetic Waves and Appl.*, vol. 22, pp. 423–430, 2008.
- [31] B. Cranganu-Cretu and R. Hiptmair, “Direct boundary integral equation method for electromagnetic scattering by partly coated dielectric objects,” *Comput. Visual Sci.*, vol. 8, nos. 3–4, pp. 145–158, 2005.
- [32] W. M. Yu, D. G. Fang, and T. J. Cui, “Closed form modal Green's functions for accelerated computation of bodies of revolution,” *IEEE Trans. Antennas Propag.*, vol. 56, pp. 3452–3461, Nov. 2008.
- [33] C. M. Butler, Y. Rahmat-Samii, and R. Mittra, “Electromagnetic penetration through apertures in conducting surfaces,” *IEEE Trans. Antennas Propag.*, vol. AP–26, no. 1, pp. 82–93, Jan. 1978.
- [34] J. Bao, D. Wang, and E. K. N. Yung, “Radiation and scattering from bi-isotropic bodies of revolution,” *IEEE Antennas and Propagat.*, pp. 5023–5026, June 2007.
- [35] S. S. Vinogradov and A. V. Sulima, “Calculation of the absorption cross section of a partially shielded dielectric sphere,” Translated from *Izvestiya Vysshikh Uchebnykh Zavedenii, Radiofizika, Radio Physics and Quantum Electronics*, vol. 26, no. 10, pp. 927–931, 1984.

- [36] J. R. Mautz and R. F. Harrington, "An Improved E-Field Solution for a conducting body of revolution," *AEÜ*, vol. 36, pp. 198-206, 1982..
- [37] P. C. Waterman, "Matrix Formulation of Electromagnetic Scattering," *Proc. IEEE*, vol. 53, no. 8, pp. 805–812, Aug. 1965.
- [38] J. R. Mautz, R. F. Harrington, "H-field, E-field, and combined field solutions for bodies of revolution," Interim Technical Report, RADC-TR-77-109, Mar. 1977.
- [39] M. G. Andreasen, "Scattering from cylinders with arbitrary surface impedance," *Proc. IEEE*, vol. 53, no. 8, pp. 812–817, Aug. 1965.
- [40] Jack H. Richmond, "Digital computer solutions of the rigorous equations for scattering problems," *Proc. IEEE*, vol. 53, no.8, pp. 796–805, Aug. 1965.
- [41] X. Yuan, R. F. Harrington, and S. S. Lee, "Electromagnetic scattering by a dielectric cylinder partially covered by conductors," *J. Electromag. Waves Appl.*, vol. 2, no. 1, pp. 21–44, 1988.
- [42] L. N. Medgyesi-Mitschang, and C. Eftimiu, "Scattering from wires and open circular cylinders of finite length using entire domain Galerkin expansions," *IEEE Trans. Antennas Propag.*, vol. AP-30, no. 4, pp. 628–636, July 1982.
- [43] D. S. Wang, and L. N. Medgyesi-Mitschang, "Electromagnetic scattering from finite circular and elliptic cones," *IEEE Trans. Antennas Propag.*, vol. AP-33, no. 5, pp. 488–497, May 1985.
- [44] J. Meixner, "The behavior of electromagnetic fields at edges," *IEEE Trans. Antennas Propag.*, vol. AP-20, no. 4, pp. 442–446, July 1972
- [45] D. K. Cheng, *Field and Wave Electromagnetics*, Second Edition. Reading, MA: Addison Wesley, 1989.
- [46] D. H. Staelin, A. W. Morgenthaler, and J. A. Kong, *Electromagnetic Waves*. Englewood Cliffs, N.J. : Prentice Hall.
- [47] C. A. Balanis, *Advanced Engineering Electromagnetics*. New York : John Wiley & Sons, 1989.
- [48] M. N. O. Sadiku, *Numerical Techniques in Electromagnetics with Matlab, Third Edition*. Boca Raton, London, New York: CRC Press, 2011.

- [49] A. Serdyukov, I. Semchenko, S. Tretyakov and A. Sihvola, *Electromagnetics of Bi-anisotropic Materials, Theory and Applications*. Amsterdam: Gordon And Breach Science Publishers, 2001.
- [50] H. Mustacoglu, J. R. Mautz, and E. Arvas, "Method of moments analysis of an axisymmetric Chiral Radome," General Assenbly and Scientific Symposium 2011 XXXth URSI, Oct. 2011.
- [51] Moamer Hasanovic, Chong Mei, Joseph R. Mautz, and Ercument Arvas, "Scattering from 3-D Inhomogeneous Chiral Bodies of Arbitrary Shape by The Method of Moments," *IEEE Trans. Antennas Propag.*, vol. 55, No. 6, June 2007.
- [52] S. M. Rao, D. R. Wilton, and A. W. Glisson, "Electromagnetic scattering by surfaces of arbitrary shapes," *IEEE Trans. Antennas Propag.*, vol. AP-30, no. 3, pp. 409–418, May 1982.
- [53] C. M. Butler, "The equivalent radius of a narrow conducting strip," *IEEE Trans. Antennas Propag.*, vol. AP-30, no. 7, pp. 755–758, July 1982.
- [54] N. Mouta, N. kunagai, and J. R. Mautz, *Integral Equation methods for Electromagnetics*. Boston: Artech House, 1990.
- [55] H. B. Dwight, *Tables of Integrals and other mathematical data*. New York: Macmillan, 1961.
- [56] M. Abramowitz and I. A. Stegun, Eds., *Handbook of mathematical Functions*. Washington, D.C. : U.S. Government Printing Office, 1964.
- [57] Denchai Worasawate, "*Electromagnetic scattering from an arbitrarily shaped three-dimensional chiral body*," Ph.D. Dissertation, Syracuse University, August 2002.
- [58] T. Guire, V. V. Varadan, and V. K. Varadan, "Influence of chirality on the reflection of EM waves by planar dielectric slabs," *IEEE Trans. Electromagn. Compat.*, vol. 32, no. 4, pp. 300-303, Nov. 1990.
- [59] A. Lakhtakia, V. V. Varadan, and V. K. Varadan, "What Happens to Plane Waves at the Planar Interfaces of Mirror-Conjugated Chiral Media," *J. Opt. Soc. Am. A*, vol. 6, pp. 23-26, Jan. 1989.
- [60] N. Engheta, M. W. Kowarz, and D. L. Jaggard, "Effect of Chirality on the Doppler Shift and Aberration of Light Waves," *J. Appl. Phys.*, vol. 66, pp. 2274-2277, Sept. 15, 1989.

- [61] A. Lakhtakia, V. V. Varadan, and V. K. Varadan, "Reflection of Plane Waves at Planar Achiral- Chiral Interfaces: Independence of the Reflected Polarization State from the Incident Polarization State," *J. Opt. Soc. Amer. A*, vol. 7, pp. 1654-1656, Sept. 1990.
- [62] M. P. Silverman, "Reflection and Refraction at the Surface of a Chiral Medium: Computation of Gyrotropic Constitutive Relations Invariant or Noninvariant Under a Duality Transformation," *J. Opt. Soc. Am. A*, vol. 3, pp. 830-837, June 1986.
- [63] I. V. Lindell, A. H. Sihvola, S. A. Tretyakov, and A. J. Viitanen, *Electromagnetic Waves in Chiral and Bi-Isotropic Media*. Boston: Artech House, 1994.
- [64] D. L. Jaggard, A. R. Mickelson, and C. H. Papas, "On electromagnetic waves in chiral media," *Appl. Phys.*, vol. 18, pp. 211-216, 1979.
- [65] W. S. Weiglhofer, "Electromagnetic field representation in (inhomogeneous) isotropic chiral media," *Electromagnetics*, vol. 10, pp. 271-278, July-Sept. 1990.

VITA

Name : Khaja Qutubuddin

Date of Birth : June 10, 1937

Date of Place : Hyderabad, A.P., India.

Bachelor's Degrees : B.Sc. (Mathematics), Osmania University, India, 1958.
: B.E. (Mechanical Eng.), Osmania university, India, 1963.

Master's Degree
(Engineering Science
Department) : Florida State University, Tallahassee, Florida, May, 1968.
Computer Engineer
Degree (Computer Eng.
Department) : Syracuse University, Syracuse, New York, May, 2002.